

# **Functional Materials from Nanostructured Block Polymers Prepared via Ring-opening Metathesis Polymerization**

**A DISSERTATION  
SUBMITTED TO THE FACULTY OF THE GRADUATE SCHOOL  
OF THE UNIVERSITY OF MINNESOTA  
BY**

Louis Marcel Pitet

**IN PARTIAL FULFILLMENT OF THE REQUIREMENTS  
FOR THE DEGREE OF  
Doctor of Philosophy**

Marc A. Hillmyer, Advisor

August, 2011

© Louis Marcel Pitet 2011  
ALL RIGHTS RESERVED

## Acknowledgements

First and foremost, I would like to thank my advisor Marc Hillmyer. His guidance throughout my graduate school experience has helped me improve tremendously as a scientist and as a member of the scientific community. I have learned a great deal about scientific conduct and graceful articulation of results. Special gratitude is bestowed on several undergraduate researchers I have mentored throughout my time here, which has resulted in lasting friendships and several publications. These people are Sarah Wegwerth (St. Cloud State University), Adam Hauser (UMN), Peter Lawrence (UMN), and Cory Thomas (UMN). Additionally, Prof. Bradley Chamberlain (Luther College) deserves recognition for a fruitful collaboration during his sabbatical leave spent in our laboratories.

The graduate students and post-doctoral associates with whom I have shared time and lab space while performing research have made my stay here enjoyable, and have contributed considerably to my flourishing. In particular, several people deserve special acknowledgement: Dr. Nathaniel Lynd, Dr. Liang Chen, Dr. Mark Amendt, Dr. Shingo Kobayashi, Dr. Bryan Boudouris, Dr. John Zupancich, Dr. Carolyn Wanamaker, Dr. Megan Robertson, Dr. Feng Jing, Dr. Monique Roerdink, Dr. Agostino Pietrangelo, Dr. Yang Qin, Dr. Jennifer Lowe, Dr. Chun Liu, Grayce Theryo, Mark Martello, Josh Speros, Elizabeth Jackson, Ligeng Yin, Jihoon Shin, Will Gramlich, and Maria Miranda.

I have benefited in many ways from the collaboration and correspondence with several astounding researchers both in and outside of the University of Minnesota. These people include: Aruna Ramkrishnan, Huiyong Chen, and Prof. Michael Tsapatsis (UMN); Henry Kostalik IV and Prof. Geoff Coates (Cornell University); Dr. Zhaokang Hu, Dr. Yapei Wang, and Prof. Joseph DeSimone (University of North Carolina, Chapel Hill); Dr. Patrick Brant (Exxon-Mobil Chemical Company).

---

The opportunity to visit Argonne National Laboratories on ten occasions was facilitated by close collaboration with Prof. Timothy Lodge and Prof. Frank Bates, and several students within their research groups helped to make the visits both fun and productive (Ameara Mansour, Dr. Mike Bluemle, Prof. Chris Ellison, Dr. Guillaume Fleury, Dr. Adam Meuler, Dr. Feng Zuo, Dr. Soohyung Choi, Dr. Sangwoo Lee, Dr. Peter Simone, Brian Habersberger, Brad Jones, Erica Redline).

Financial support from several sources is gratefully acknowledged. Two fellowships were awarded by the Department of Chemistry and the Doctoral Dissertation Fellowship was awarded by the University of Minnesota Graduate School, granting me the resources to devote substantial effort toward preparing my dissertation. The National Science Foundation provided the necessary financial resources to conduct the research described herein.

## Dedication

To my parents and brother.

## Abstract

The structural and molecular versatility afforded to polymeric materials by ruthenium catalysts during ring-opening metathesis polymerization (ROMP) cannot be exaggerated. This dissertation describes the synthesis of functionalized polyolefins via ROMP with particular emphasis on designing straightforward approaches to materials in which the molecular structure is meticulously controlled. Moreover, large portions of the body are dedicated to describing functionalized polyolefins as precursors to more complex multicomponent block copolymers. Block copolymers having various components derived from mechanistically incompatible feedstocks were designed with translational targets in mind, including toughening agents for brittle plastics, and free-standing nanoporous membranes. Several fundamental structure-property relationships were also explored for the newly synthesized materials.

---

# Table of Contents

<b>Acknowledgements</b>	<b>i</b>
<b>Dedication</b>	<b>iii</b>
<b>Abstract</b>	<b>iv</b>
<b>Table of Contents</b>	<b>v</b>
<b>List of Tables</b>	<b>ix</b>
<b>List of Figures</b>	<b>x</b>
<b>List of Schemes</b>	<b>xv</b>
<b>1 Background: Ring-opening Metathesis Polymerization with Chain-Transfer</b>	<b>1</b>
1.1 Introduction.....	2
1.1.1 Metathesis Reaction Overview .....	2
1.1.2 Metathesis Catalyst Development.....	4
1.2 Ring-opening Metathesis Polymerization.....	9
1.2.1 ROMP Mechanism and Scope .....	9
1.2.2 End-functionalization by ROMP Termination .....	13
1.2.3 Telechelic Polymers by ROMP with Chain Transfer Agents .....	16
1.3 Block Copolymers from Telechelic Polymers Prepared by ROMP .....	25
1.3.1 Coordinating Telechelic Polymers .....	25
1.3.2 Mechanistic Transformations for Linear Block Copolymer Syntheses.....	30
1.4 Conclusions.....	46
1.5 References .....	47
<b>2 Linear Block Copolymers by Tandem Ring-opening Polymerizations</b>	<b>59</b>
2.1 Introduction.....	60

---

2.2	LCL Triblock Copolymers.....	62
2.2.1	Synthesis of Triblock Copolymers.....	63
2.2.2	Thermal Analysis of LCL Triblock Copolymers.....	67
2.2.3	Morphological Characteristics of LCL Triblock Copolymers .....	69
2.2.4	Mechanical Properties of LCL Triblock Copolymers .....	75
2.3	Poly[D,L-lactide- <i>b</i> -(cyclooctene- <i>s</i> -norbornene)- <i>b</i> -D,L-lactide] triblock copolymers.....	77
2.3.1	Synthesis of Statistical Telechelic poly(COE- <i>s</i> -NB) Copolymers..	79
2.3.2	Thermal Properties of poly(COE- <i>s</i> -NB) Statistical Copolymers ...	85
2.3.3	Synthesis of L-CN-L Triblock Copolymers.....	88
2.3.4	Thermal Properties of L-CN-L Triblock Copolymers .....	92
2.3.5	Morphological Characteristics of L-CN-L Triblock Copolymers ...	94
2.4	Multiblock Copolymers from Linear Triblock Copolymers.....	96
2.4.1	Synthesis of Multiblock (LCL) <sub>n</sub> Copolymers .....	99
2.4.2	Thermal Properties of Multiblock Copolymers .....	107
2.4.3	Morphological Characteristics of Multiblock Copolymers.....	109
2.4.4	Tensile Properties of Multiblock Copolymers .....	111
2.5	Conclusions.....	113
2.6	Experimental Details.....	114
2.6.1	Materials .....	114
2.6.2	Synthetic Details .....	114
2.7	References .....	116

### **3 Complex Molecular Architectures in Block Copolymers from Tandem Ring-opening Polymerizations** **123**

3.1	Introduction.....	124
3.2	Results and Discussion .....	128
3.2.1	Synthesis of Chain Transfer Agents.....	128
3.2.2	ROMP of COE with CTAs <b>1</b> , <b>3</b> , and <b>5</b> .....	130
3.2.3	Synthesis of PCOE–PLA block copolymers.....	135
3.2.4	Phase Behavior of Branched Block Copolymers .....	143
3.2.4	Thermal Properties of PCOE–PLA Block Copolymers .....	161
3.4	Conclusions.....	170
3.5	Experimental Details.....	172
3.5.1	Materials .....	172
3.5.2	Synthetic details .....	172
3.6	References .....	188



---

<b>4 Nanoporous Linear Polyethylene Templated from Triblock Copolymers</b>	<b>198</b>
4.1 Introduction.....	199
4.1.1 Nanoporous Materials from Block Copolymer Templates.....	199
4.1.2 Linear Polyethylene Block Copolymers by ROMP.....	208
4.1.3 Design of Nanoporous Linear Polyethylene.....	219
4.2 Results.....	224
4.2.1 Synthesis and Molecular Characterization.....	224
4.2.2 Thermal Analysis Polymers.....	232
4.2.3 Preparation of Nanoporous LPE.....	237
4.2.4 X-ray Scattering from Block Copolymers.....	244
4.2.5 Imaging of Nanoporous Materials by SEM.....	252
4.2.6 Nitrogen Sorption.....	262
4.2.7 Performance Characteristics of Nanoporous LPE Membranes..	271
4.3 Conclusions.....	274
4.4 Experimental Details.....	276
4.5 References.....	279
<b>5 Linear Polyethylene Copolymers from Sequential ROMP</b>	<b>290</b>
5.1 Introduction.....	291
5.2 Results and Discussion.....	296
5.2.1 Synthesis and Molecular Characterization.....	296
5.2.2 Hydrogenation of Copolymers.....	317
5.2.3 Thermal Properties of Hydrogenated Polymers.....	320
5.2.4 X-ray Scattering of Hydrogenated Block Copolymers.....	323
5.2.5 Sulfonation of hydrogenated poly(3PC-COE) copolymers.....	329
5.2.6 Thermal Properties of sulfonated <i>h</i> -poly(3PC-COE) copolymers	332
5.2.7 Scattering from sulfonated <i>h</i> -poly(3PC-COE) copolymers.....	334
5.2.8 Mechanical properties of copolymers.....	337
5.3 Conclusions and Outlook.....	339
5.4 Experimental Details.....	341
5.4.1 Materials.....	341
5.4.2 Synthetic Details.....	341
5.5 References.....	351
<b>6 Carboxy-telechelic Polyolefins from ROMP with Maleic Acid as Chain Transfer Agent</b>	<b>355</b>
6.1 Introduction.....	356

---

6.2	Results and Discussion .....	358
6.3	Conclusions.....	370
6.4	Experimental Details.....	370
6.4.1	Materials .....	370
6.4.2	Synthetic Details .....	371
6.5	References .....	373
<b>Bibliography</b>		<b>378</b>
<b>Appendix A</b>		<b>406</b>
<b>Characterization Methods</b>		<b>406</b>
A.1	Nuclear Magnetic Resonance Spectroscopy.....	407
A.2	IR Spectroscopy .....	407
A.3	Elemental Analysis .....	408
A.4	Differential Scanning Calorimetry .....	408
A.5	Size Exclusion Chromatography .....	409
A.6	Small Angle X-ray Scattering.....	410
A.7	Wide Angle X-ray Scattering.....	411
A.8	Scanning Electron Microscopy .....	411
A.9	Transmission Electron Microscopy .....	412
A.10	Nitrogen Sorption .....	412
<b>Appendix B</b>		<b>415</b>
<b>Functional Polymers from Ring-opening Metathesis Polymerization of 3-substituted cyclooct-1-enes</b>		<b>415</b>
B.1	Substituted Cyclooctenes.....	416
B.1.1	3-bromo- <i>cis</i> -cyclooct-1-ene.....	417
B.1.2	3-hydroxy- <i>cis</i> -cyclooct-1-ene.....	420
B.1.3	3-acetoxycyclooct-1-ene .....	423
B.1.4	3-oxocyclooct-1-ene .....	429
B.1.5	3-(2-bromo-2-methyl prionate)cyclooct-1-ene.....	434

---

## List of Tables

Table 2.1 .....	66
Table 2.2 .....	76
Table 2.3 .....	82
Table 2.4 .....	87
Table 2.5 .....	89
Table 2.6 .....	101
Table 2.7 .....	102
Table 3.1 .....	132
Table 3.2 .....	137
Table 3.3 .....	151
Table 3.4 .....	169
Table 4.1 .....	225
Table 4.2 .....	231
Table 4.3 .....	236
Table 4.4 .....	270
Table 5.1 .....	307
Table 5.2 .....	313
Table 5.3 .....	331
Table 5.4 .....	339
Table 6.1 .....	358
Table A.1 .....	407

---

## List of Figures

Figure 1.1.....	3
Figure 1.2.....	3
Figure 1.3.....	5
Figure 1.4.....	8
Figure 1.5.....	12
Figure 1.6.....	14
Figure 1.7.....	17
Figure 1.8.....	18
Figure 1.9.....	19
Figure 1.10.....	24
Figure 1.11.....	26
Figure 1.12.....	27
Figure 1.13.....	29
Figure 2.1.....	65
Figure 2.2.....	67
Figure 2.3.....	68
Figure 2.4.....	70
Figure 2.5.....	72
Figure 2.6.....	74
Figure 2.7.....	76
Figure 2.8.....	81
Figure 2.9.....	83
Figure 2.10.....	84
Figure 2.11.....	86
Figure 2.12.....	90
Figure 2.13.....	91
Figure 2.14.....	93

---

Figure 2.15.....	94
Figure 2.16.....	97
Figure 2.17.....	104
Figure 2.18.....	105
Figure 2.19.....	106
Figure 2.20.....	108
Figure 2.21.....	110
Figure 2.22.....	112
Figure 3.1.....	127
Figure 3.2.....	134
Figure 3.3.....	139
Figure 3.4.....	142
Figure 3.5.....	146
Figure 3.6.....	152
Figure 3.7.....	155
Figure 3.8.....	156
Figure 3.10.....	160
Figure 3.11.....	163
Figure 3.12.....	166
Figure 3.13.....	174
Figure 3.14.....	175
Figure 3.15.....	175
Figure 3.16.....	176
Figure 3.17.....	177
Figure 3.18.....	179
Figure 3.19.....	180
Figure 3.20.....	181
Figure 3.21.....	183
Figure 3.22.....	184
Figure 3.23.....	185
Figure 4.1.....	200
Figure 4.2.....	203

---

Figure 4.3.....	204
Figure 4.4.....	205
Figure 4.5.....	206
Figure 4.6.....	209
Figure 4.7.....	211
Figure 4.9.....	220
Figure 4.10.....	226
Figure 4.11.....	227
Figure 4.12.....	229
Figure 4.13.....	232
Figure 4.14.....	233
Figure 4.15.....	234
Figure 4.16.....	240
Figure 4.17.....	241
Figure 4.18.....	243
Figure 4.19.....	244
Figure 4.20.....	245
Figure 4.21.....	247
Figure 4.22.....	250
Figure 4.23.....	251
Figure 4.24.....	253
Figure 4.25.....	254
Figure 4.26.....	256
Figure 4.27.....	257
Figure 4.28.....	258
Figure 4.29.....	259
Figure 4.30.....	260
Figure 4.31.....	261
Figure 4.32.....	263
Figure 4.33.....	266
Figure 4.34.....	267
Figure 4.35.....	269

---

Figure 4.36.....	271
Figure 4.37.....	272
Figure 4.38.....	274
Figure 5.1.....	291
Figure 5.2.....	293
Figure 5.3.....	298
Figure 5.4.....	300
Figure 5.5.....	303
Figure 5.6.....	307
Figure 5.7.....	308
Figure 5.8.....	309
Figure 5.9.....	311
Figure 5.10.....	314
Figure 5.11.....	315
Figure 5.12.....	316
Figure 5.13.....	319
Figure 5.14.....	320
Figure 5.15.....	322
Figure 5.16.....	324
Figure 5.17.....	326
Figure 5.18.....	328
Figure 5.19.....	329
Figure 5.20.....	333
Figure 5.21.....	335
Figure 5.22.....	336
Figure 5.23.....	337
Figure 5.24.....	338
Figure 5.25.....	342
Figure 5.26.....	343
Figure 5.27.....	345
Figure 5.28.....	346
Figure 5.29.....	347

---

Figure 5.30.....	348
Figure 6.2.....	361
Figure 6.3.....	362
Figure 6.4.....	364
Figure 6.5.....	365
Figure 6.6.....	366
Figure 6.7.....	367
Figure 6.8.....	368
Figure 6.9.....	369
Figure B.1.....	418
Figure B.2.....	419
Figure B.3.....	421
Figure B.4.....	422
Figure B.5.....	424
Figure B.6.....	425
Figure B.7.....	427
Figure B.8.....	428
Figure B.10.....	430
Figure B.11.....	431
Figure B.12.....	433
Figure B.13.....	435
Figure B.14.....	436
Figure B.15.....	438
Figure B.16.....	439



---

## List of Schemes

Scheme 1.1.....	6
Scheme 1.2.....	10
Scheme 1.3.....	15
Scheme 1.4.....	32
Scheme 1.5.....	33
Scheme 1.6.....	34
Scheme 1.7.....	36
Scheme 1.8.....	37
Scheme 1.9.....	37
Scheme 1.10.....	38
Scheme 1.11.....	39
Scheme 1.12.....	40
Scheme 1.13.....	41
Scheme 1.14.....	42
Scheme 1.15.....	43
Scheme 1.16.....	45
Scheme 2.1.....	62
Scheme 2.2.....	79
Scheme 2.3.....	88
Scheme 2.4.....	100
Scheme 3.1.....	129
Scheme 3.2.....	131
Scheme 3.3.....	135
Scheme 4.1.....	216
Scheme 4.2.....	217
Scheme 4.3.....	218

---

Scheme 4.4.....	219
Scheme 4.5.....	221
Scheme 4.6.....	222
Scheme 4.7.....	223
Scheme 5.1.....	295
Scheme 5.2.....	297
Scheme 5.3.....	313
Scheme 5.4.....	318
Scheme 6.1.....	357
Scheme 6.2.....	363

# Chapter 1

## Background: Ring-opening Metathesis

## Polymerization with Chain-Transfer

This chapter provides a summary of previous reports that describe using ring-opening metathesis polymerization (ROMP) to synthesize end-functional (telechelic) polymers. Telechellicity is conveniently achieved by using an acyclic chain transfer agent during ROMP, and hemi-telechellicity is likewise achieved by termination with an analogous compound. Special attention is paid to the desired utility of the end-functionality, with particular emphasis on mechanistic transformations intended to produce block copolymers.

## 1.1 Introduction

Polymeric materials having functional end-groups prepared by ring-opening metathesis polymerization (ROMP) are explored in this dissertation. The telechelic polyolefins derived from cyclic olefin monomers were investigated as precursors to linear and branched block copolymers. Block copolymers are long-chain macromolecules characterized by segments of different repeating units connected at a single molecular junction. Block copolymers have often been observed to undergo phase separation, self-assembling into microstructures with domain sizes commensurate with the length of individual polymer chains (*i.e.*, 5–50 nm).<sup>1–4</sup> There are four equilibrium structures that can be adopted for two component systems, for which ample theoretical<sup>5–12</sup> and experimental<sup>4,13,14</sup> substantiation has been established. The nanoscopic structures generated by block copolymer self-assembly often embody physical characteristics that are unique compared with conventional homopolymers or polymer blends. The implications of these behaviors are explored in the systems described throughout the dissertation, with particular emphasis being placed on applications in polymer toughening and templating nanoporous membranes. Block copolymers are prepared by methods that represent novel contributions to the current polymer community, and as such, the syntheses are described in great detail.

Ring-opening metathesis polymerization (ROMP) forms the basis for preparation of block copolymers containing mechanistically incompatible components. Therefore, the historical development of metathesis as it pertains to polymerization is briefly summarized. Additionally, previous examples that help provide guidance in systematic design of tandem polymerizations involving ROMP are also reviewed.

### 1.1.1 Metathesis Reaction Overview

Metathesis stems from the Greek word meaning "changing places". The term metathesis was first disclosed to describe a particular isodesmic chemical

transformation that was observed with a variety of different unsaturated compounds.<sup>15</sup> It was initially assumed that sigma bond cleavage was responsible for the transformation. However, it was soon clear that the double bond of the reacting alkenes was rearranging.<sup>16,17</sup> The transformation involves the rearrangement of alkenes in a substituent swap that mechanistically was initially proposed to involve a "quasicyclobutane" intermediate, with the exact role of the original complex catalyst mixtures (*e.g.*,  $\text{WCl}_6 + \text{C}_2\text{H}_5\text{OH} + \text{C}_2\text{H}_5\text{AlCl}_2$ ) not well understood (Figure 1.1).<sup>18,19</sup>

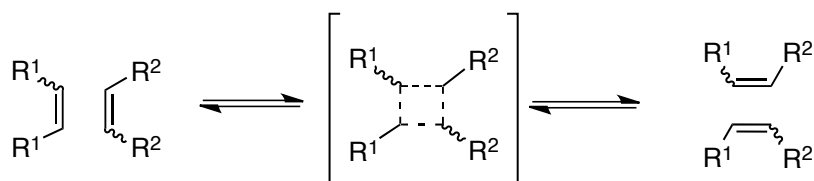


**Figure 1.1**

Initially proposed cross metathesis reaction with "quasicyclobutane" intermediate formed upon reversible exchange reactions ("dismutation") between substituted alkenes.

Although the initially described mechanism and the role of the catalyst in the transition states and intermediates were unclear, profound insight was gained from which plethoric quantities of research ultimately burgeoned. The description of the metathetical redistribution mechanism among alkenes was refined upon further analysis, and the agreed upon transformation involves a metal-alkylidene ( $\text{L}_n\text{M}=\text{CHR}$ ; M→metal; L→ligand) as the crucial component.<sup>20,21</sup> The metal-alkylidene double bond is the location of electron redistribution, with the reversible formation of a metallocyclobutane comprising the intermediate (Figure 1.2).<sup>22</sup>

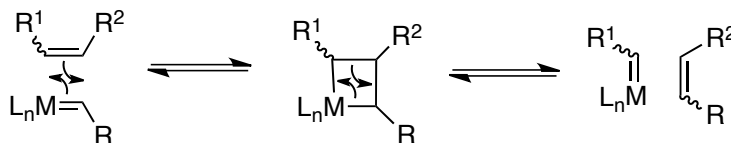


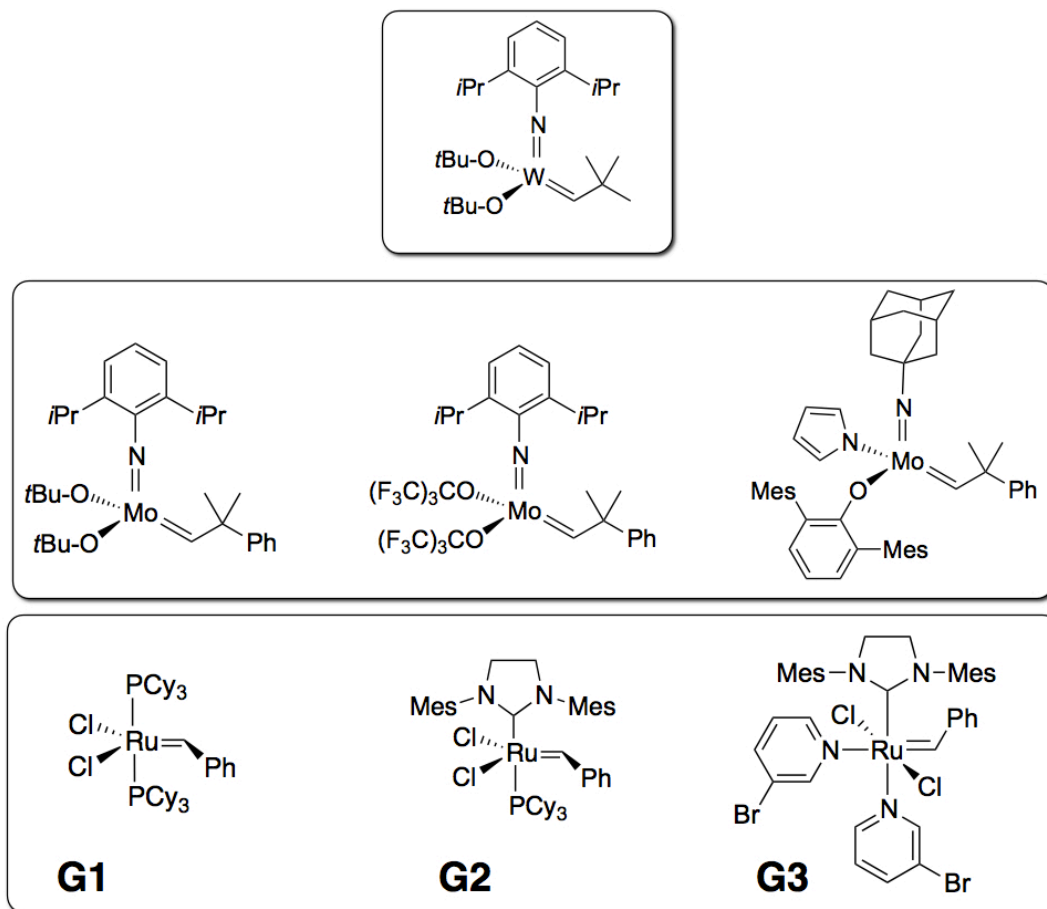
**Figure 1.2**

Mechanism for olefin metathesis proposed by Chauvin.

---

### 1.1.2 Metathesis Catalyst Development

Well-defined catalysts quickly emerged based on transition metals including titanium (Ti),<sup>23,24</sup> tungsten (W),<sup>25-27</sup> molybdenum (Mo),<sup>28-30</sup> and ruthenium (Ru)<sup>31-36</sup> (Figure 1.3). The metal-alkylidene bond, the site at which the redistribution occurs, signifies the crucial characteristic of each successful example. The intermediate metallocyclobutane forms by 2+2 addition between the metal-alkylidene and another olefin. The catalysts are adorned with ligands that play an indirect role in moderating the efficacy of the reactive center. The nucleophilicity and basicity of the ligands influences the electronic environment about the reactive alkylidene. A multitude of different ligands have been attached to the catalytic metal-centers to modulate the reactivity and tailor the regio/stereo selectivity and resilience to various reaction conditions. The Ru-based catalysts are further discussed, based on the importance throughout the experimental sections of the dissertation.

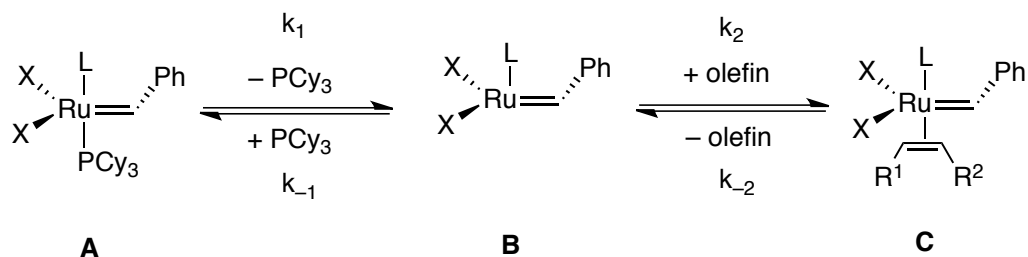
**Figure 1.3**

Several efficient metathesis catalysts based on the transition metals tungsten (*top*), molybdenum (*middle*), and ruthenium (*bottom*).

The mechanism of olefin metathesis using Ru-based catalysts having broadly ranging basic ligands and alkylidene substituents is well documented.<sup>31,37–43</sup> Briefly, the overall mechanism is described by a dissociative pathway for the ruthenium centered "precatalyst" having a tricyclohexylphosphine (PCy<sub>3</sub>) ligand and halides (X = Cl, Br, I) (Scheme 1.1). The PCy<sub>3</sub> initially dissociates reversibly with a rate constant of  $k_1$  representing the initiation step. The four coordinate ruthenium species **B** can bind with the PCy<sub>3</sub> in the reverse reaction ( $k_{-1}$ ) or reversibly coordinate with an olefin to enter the catalytic cycle with rate constant  $k_2$  (Scheme 1.1).

## Scheme 1.1

Olefin metathesis mechanism and rate constant description for ruthenium based catalysts having X = halide, L = generic ligand, and PCy<sub>3</sub> ligands. Dissociation of PCy<sub>3</sub> is followed by olefin binding.



Notably, substantially enhanced reactivity was observed when one tricyclohexylphosphine ligand was substituted for an N-heterocyclic carbene, which is strongly electron donating.<sup>44–46</sup> This relatively new class of catalysts, termed the second generation Grubbs catalyst (**G2**), showed astonishing reactivity toward metathesis even on tri- and tetrasubstituted double bonds<sup>47,48</sup> with the same dependable tolerance to many hetero-atomic functional groups.<sup>49</sup> Further modification with substituted pyridinyl ligands (*e.g.*, 3-bromopyridinyl, **G3**) proved to enhance the initiation rate associated with the first ligand dissociation step, while maintaining astounding reactivity and turnover numbers; the catalysts proceed to high conversion during ROMP of 1,5-cyclooctadiene in several minutes at ambient temperatures and catalyst loading as low as 0.0001 mol%.<sup>38</sup>

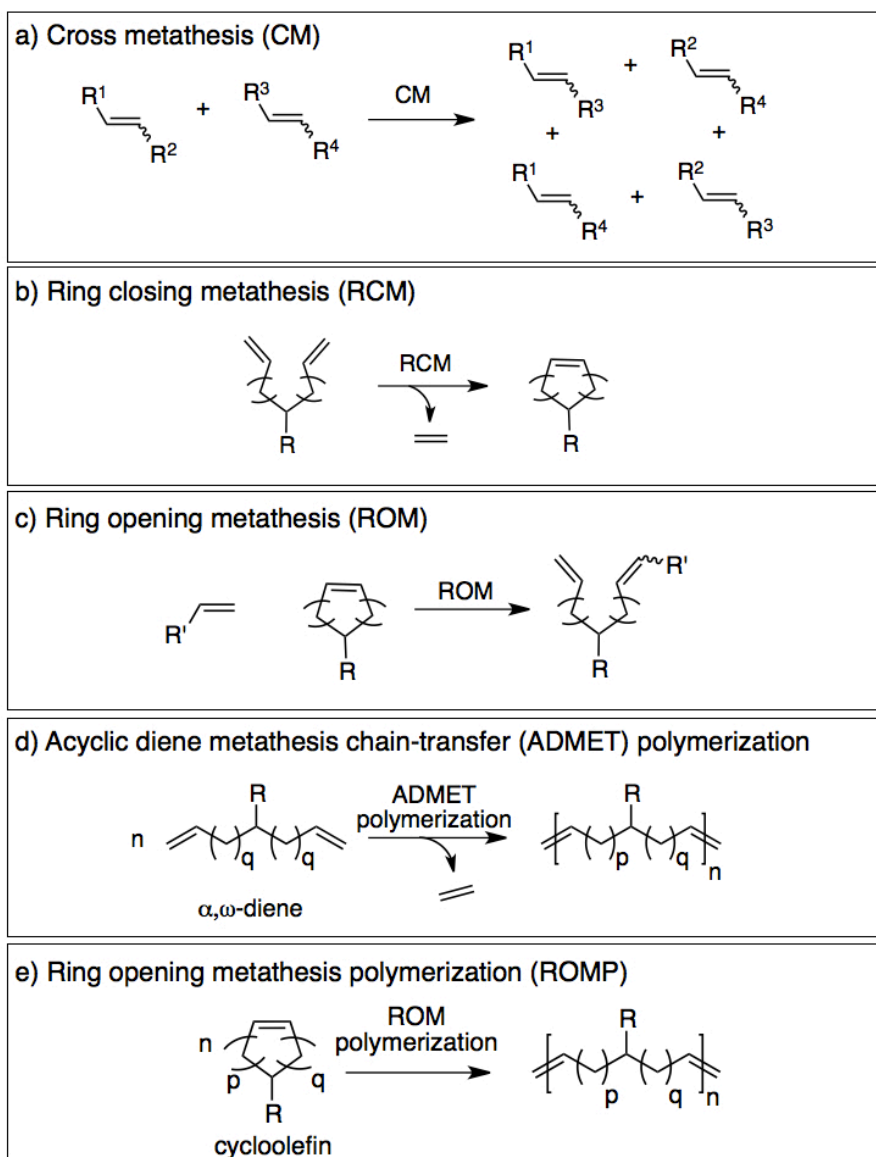
Olefin metathesis can be performed to achieve three different but closely related types of transformations, as summarized in Figure 1.4. The first is cross metathesis (CM) between two acyclic olefins; secondly, ring-closing metathesis (RCM) involves intramolecular cross metathesis to cyclize an olefin; lastly, ring-opening metathesis (ROM) can be performed with a cyclic olefin having substantial ring-strain. Polymerization may proceed using CM with a single starting compound having multiple vinylic termini (often two, termed  $\alpha,\omega$ -divinyl compounds) to promote a step-growth polymerization termed acyclic diene metathesis (ADMET) polymerization. Polymerization is also often observed in ROM, correspondingly termed ring-opening metathesis polymerization (ROMP). The latter ROMP



---

procedure forms the basis for all of the topics described throughout the remainder of this dissertation.

Since the first reports of successful cross-metathesis and detailed structural characterization of rearranged products, sophisticated catalyst structures have been developed with extremely high activity, tolerance to wide variety of functional groups, and superb chemo- and stereo selectivity. The usefulness of metathesis across nearly every facet of synthetic chemistry has earned immense praise, and the 2005 Nobel prize was awarded to those pioneering chemists who described the mechanism<sup>50</sup> and led catalyst development teams.<sup>51,52</sup> In particular, Mo-based and Ru-based catalysts have undergone extensive structural tailoring to enhance the activity and tune initiation rates and selectivity. Though not alone as practical systems for synthesizing well-defined polymers, ruthenium catalysts offer unprecedented functional group tolerance among the library of metathetical initiators. Large portions of the strategies described within this dissertation rely on the ability to precisely functionalize macromolecules in positions that allow access to various architectures through tandem polymerization mechanisms. In other words, ROMP-derived macromolecules are designed to have functionality from which additional polymerizations may be initiated to form hybrid materials utilizing multiple mechanisms. For reference, readers may refer to the many published reviews that summarize nearly every aspect of metathesis reactions, from catalyst design<sup>26,53-64</sup> to CM<sup>65</sup>, to RCM<sup>66</sup> and organic synthesis<sup>55,67-72</sup>, to polymer science.<sup>53,73-82</sup>

**Figure 1.4**

Generic synthetic depictions of olefin metathesis variations: (a) Cross-metathesis, (b) ring-closing metathesis (RCM), (c) ring-opening metathesis (ROM), (d) acyclic diene metathesis chain-transfer polymerization (ADMET), and (e) ring-opening metathesis polymerization (ROMP).

## 1.2 Ring-opening Metathesis Polymerization

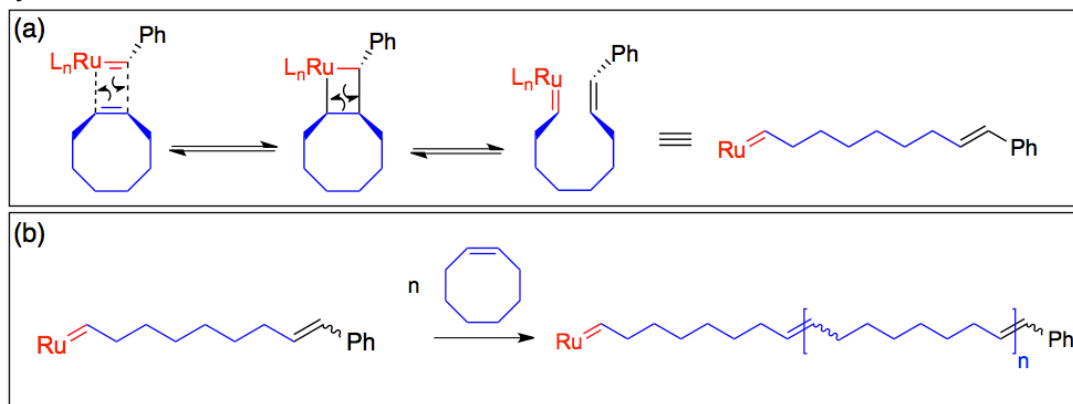
### 1.2.1 ROMP Mechanism and Scope

The mechanistic redistribution of electrons at an olefinic site is identical in all the metathetical transformations, and ROM is no exception (Scheme 1.2). The discovery that cyclic olefins bicyclo[2.2.1]hept-2-ene (norbornene, NB)<sup>83</sup> and cyclopentene<sup>84</sup> could be polymerized to unsaturated chains brought about intense exploration of details involving polymer microstructure using various monomers.<sup>85,86</sup> On the basis of considerable ring-strain ( $> 5$  kcal mol<sup>-1</sup>), cyclic olefins with 4-, 5-, 7-, and 8-carbon rings, as well as NB can be polymerized by several highly active metathesis catalysts in a living manner.<sup>75</sup> Complexity can be added with ring-substituents on these examples to tailor the properties; accordingly, innumerable examples of monomers to date that have been metathetically polymerized. No single catalyst is universally superior to all others; each catalyst offers strengths, and inherently has vulnerabilities.<sup>87</sup> For example, several derivatives of the molybdenum catalysts exhibit attractive living polymerization characteristics; very narrow molecular weight distributions were observed and block copolymers were readily prepared by sequential addition of different cyclic olefins.<sup>88</sup> Furthermore, the Mo-based catalysts have astounding activity and polymerization rates, though they are typically extremely sensitive to air, water, and heteroatomic substituents on monomers. On the other hand, Ru-based catalysts can often be used in air and are typically resilient to heteroatomic species like acids, bases, esters, ethers etc. For this latter reason, Ru-centered catalysts form the foundation upon which all the work in this dissertation is built. The direct functionalization of polymers with various heteroatoms lies at the heart of the investigated research projects.

As an example referred to extensively throughout the dissertation, and often serving as a standard for measuring the activity of new catalysts, the ROMP of *cis*-cyclooctene (COE) undergoes ring-opening polymerization due to substantial ring-strain, leading to a linear unsaturated polyolefin (Scheme 1.2).

## Scheme 1.2

(a) Mechanism of olefin ring-opening metathesis with *cis*-cyclooctene as an example and (b) additional monomer metathesis to perform ring-opening metathesis polymerization.



The reactive ruthenium alkylidene remains at the end of a growing polymer chain and can rapidly undergo subsequent metathetical based ring-opening cycles to consume monomer, representing a chain-growth polymerization. High molecular weight materials are realized at relatively low conversions, and the number average degree of polymerization ( $N_n$ ), and thus molecular weight ( $M_n$ ) is established by the concentration of monomer relative to Ru (*i.e.*, initiator) (eq 1.1).

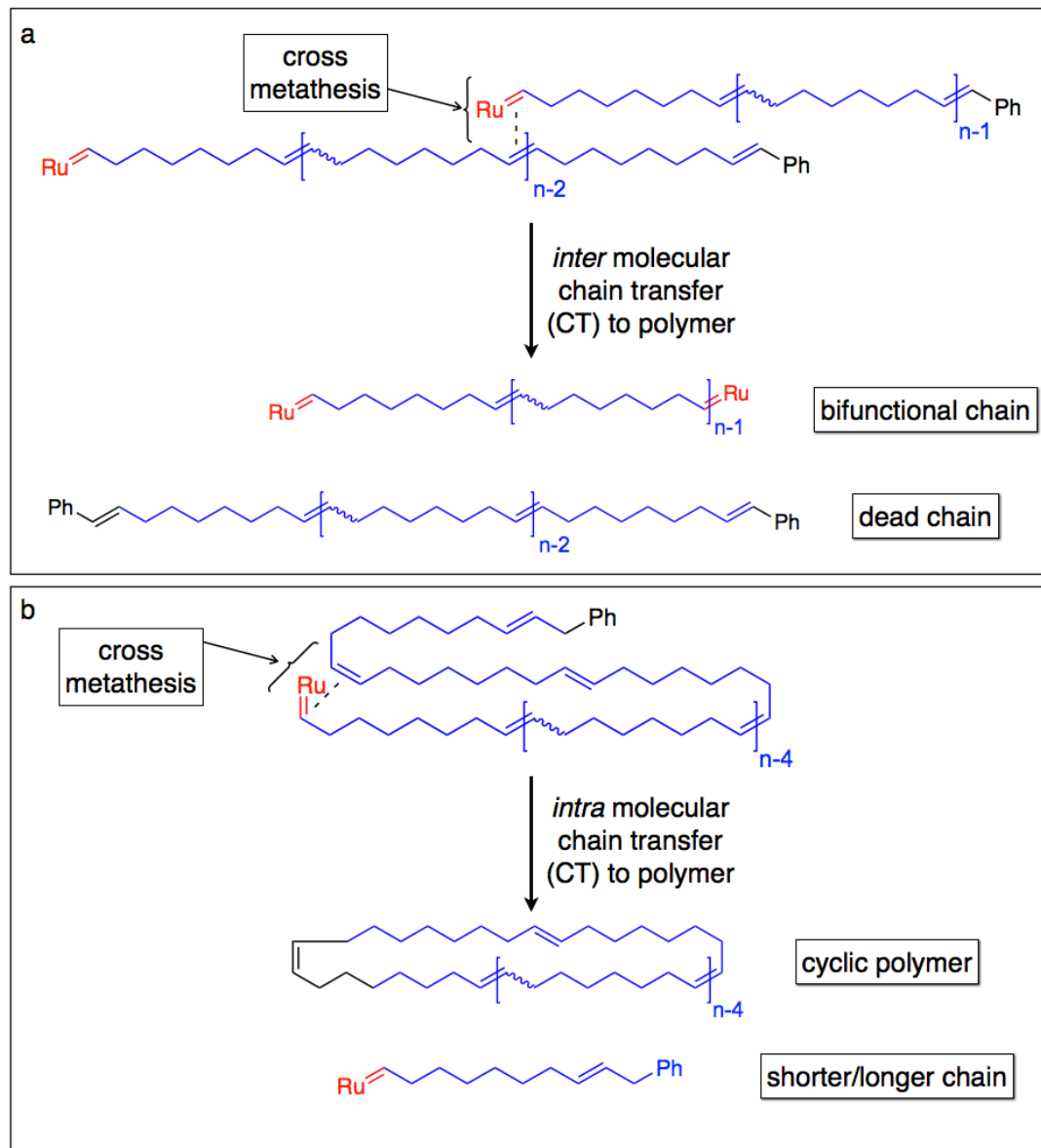
$$M_n = \frac{[monomer]}{[Ru]} \cdot m_o \cdot x \quad (1.1)$$

where  $M_n$  is the number average molecular weight of the polymer,  $m_o$  is the monomer molar mass and  $x$  is fractional conversion of monomer to polymer. Under most circumstances, the polymerization of cyclic olefins is considered living when effected by all the generations of Grubbs Ru-based catalysts.<sup>\*74</sup>

\* 1<sup>st</sup> generation, **G1** [(PCy<sub>3</sub>)<sub>2</sub>(Cl)<sub>2</sub>Ru=CHPh]; 2<sup>nd</sup>, **G2** [(IMesH<sub>2</sub>)(PCy<sub>3</sub>)(Cl)<sub>2</sub>Ru=CHPh]; 3<sup>rd</sup>, **G3** [(IMesH<sub>2</sub>)(pyBr)<sub>2</sub>(Cl)<sub>2</sub>Ru=CHPh]

---

However, certain catalysts combined with uncrowded olefins are prone to undergo extensive chain transfer (CT) reactions. The CT can occur via intermolecular cross-metathesis or intramolecular cross-metathesis (*e.g.*, chain transfer to polymer) (Figure 1.5). The former can lead to cyclic species and a redistribution of chain length to cause deviation from the weight average molecular weight associated with a living system. This is promoted by dilute conditions, and can therefore be minimized by conducting polymerization at the maximal concentration. The latter mechanism can lead to dead chains and chains with dual active termini. Both situations dramatically influence the polydispersity (PDI) and cause broadening of molecular weight distribution (MWD) as it approaches the most probable distribution ( $\text{PDI} \rightarrow 2$ ).<sup>89</sup> Although the extensive CT is to the detriment of narrow PDI, advantage can ultimately be salvaged from the inherent behavior. Particularly, the feature of continually active chain ends allows the addition of functional chain terminators and acyclic chain-transfer agents (CTA), which can ultimately endow the polymers with desirable attributes.

**Figure 1.5**

Chain transfer to polymer during ROMP of *cis*-cyclooctene by (a) intramolecular and (b) intermolecular pathways to afford cyclic, bifunctional chain growth, and dead polymer chain contaminants while broadening the molecular weight distribution.

### 1.2.2 End-functionalization by ROMP Termination

Living polymerizations have continually active species residing on the chain ends, even after all of the initially added monomer has been consumed. By this route, hybrid macromolecules with well-defined sequence distributions (*e.g.*, block copolymers) can easily be prepared through consecutive monomer addition. Multiple components can be added consecutively to prepare exotic multiblock architectures (*e.g.*, ABA, ABC). Although an active metal-alkylidene is convenient for further modification by metathesis, it is appealing to functionalize the chain ends with a variety of chemical constituents exhibiting a range of reactivity. A polymer chain having a single functional end group is termed hemi-telechelic, while telechelic refers to functionality on both termini of a linear chain. Heterotelechelic further specifies that *different* functional groups be on each of two ends. Telechelic polymers have long been valuable synthetic targets owing to the useful properties afforded by terminal functionality, with which additional chemical reactions are often performed. Telechelics are important components in polyurethane production; through strict modification, the length and identity of the telechelic chains allows foam softness to be finely tuned.

The primary Ru and Mo based metathesis catalysts that polymerize in a living fashion can be rendered inactive by adding vinyl ethers<sup>36</sup> or aldehydes, respectively. Particularly, the reaction of an active  $[L_nRu=CHR-]$  chain end with a vinyl ether ultimately leads to a metathesis species having substantially reduced reactivities,  $[L_nRu=CHOR]$ .<sup>90</sup> This termination leads to chain end functionalization with a vinyl group or substituted alkene. This offers the opportunity to functionalize a chain end with different moieties exhibiting a range of chemical characteristics by employing, for example, a specifically designed functional vinyl ether (Figure 1.6).

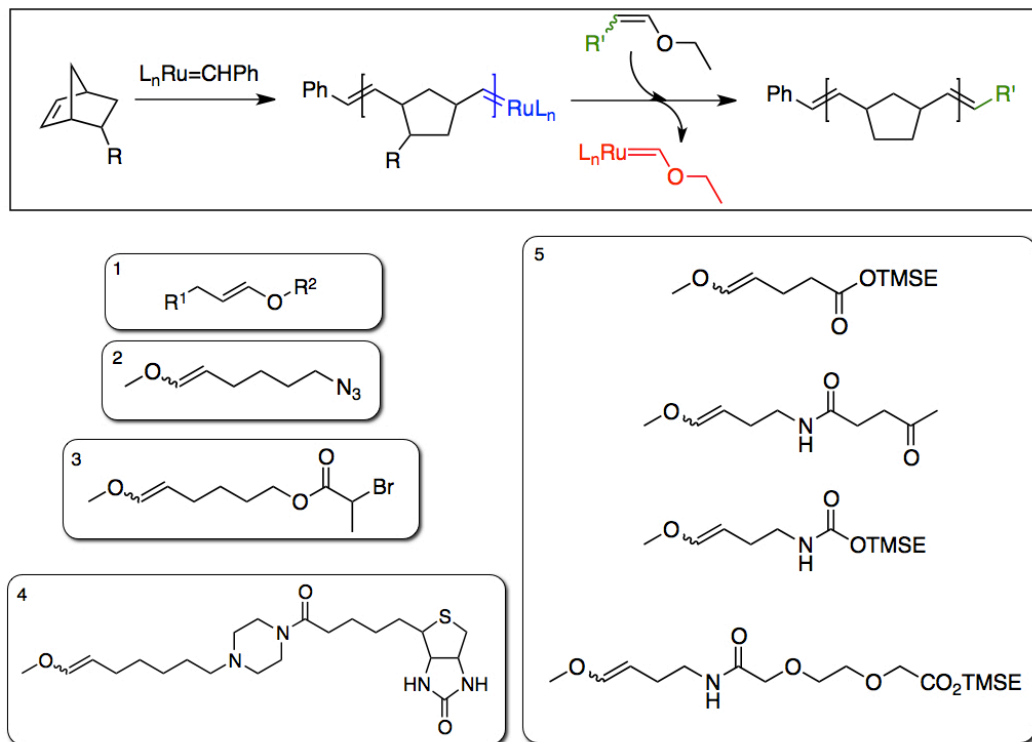


Figure 1.6

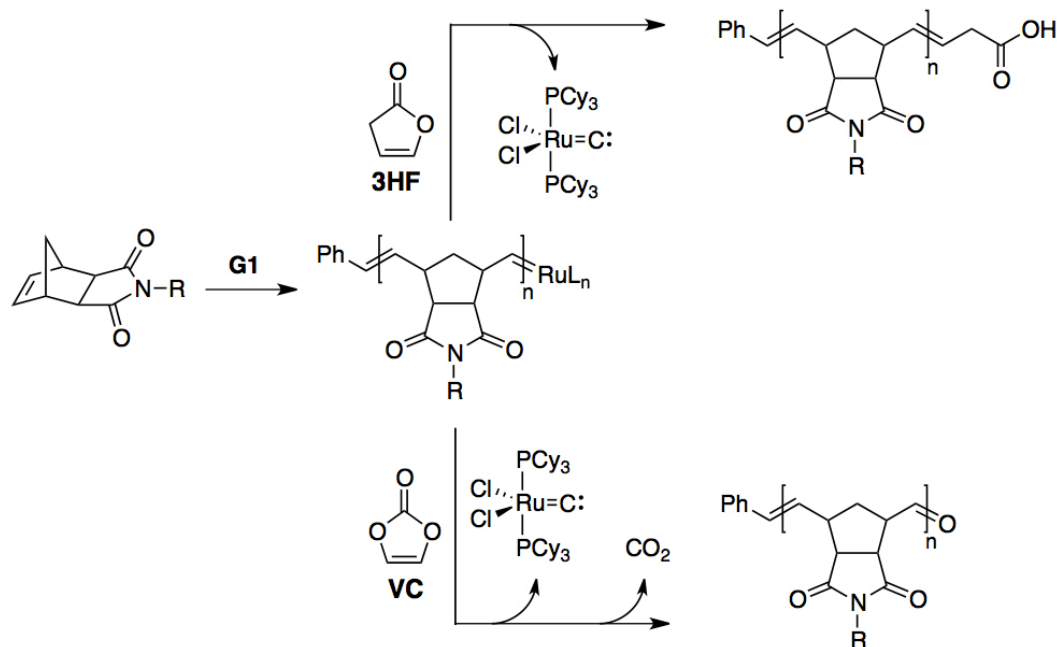
Examples illustrating termination of a generic living ROMP of substituted norbornene monomer with an ethyl alkenyl ether (green  $R'$  alkenyl substituent) to give metathesis inactive  $Ru=COCH_2H_5$  and  $R'$ -terminated poly(norbornene). Substituents **1**, **2**, **3**, **4**, and **5** reproduced from references <sup>(91,92)</sup>, <sup>(93)</sup>, <sup>(94)</sup>, <sup>(95)</sup>, and <sup>(96)</sup>, respectively.

Alternatively, it was recently disclosed that other terminating agents could render the propagating Ru alkylidene inactive while selectively functionalizing the polymer chain end. For example, the vinyl lactones 3*H*-furanone (3HF) or vinylene carbonate (VC) were shown to undergo a single ring-opening metathesis turnover when added after complete monomer consumption to give hemitelechelic poly(norbornene)s having carboxylic acid and aldehyde chain ends, respectively (Scheme 1.3).<sup>97-99</sup>



Scheme 1.3

ROMP termination with 3*H*-furanone (3HF) or vinylene carbonate (VC) to end-functionalize the poly(norbornenedicarboximide) with carboxylic acid or aldehyde, respectively.

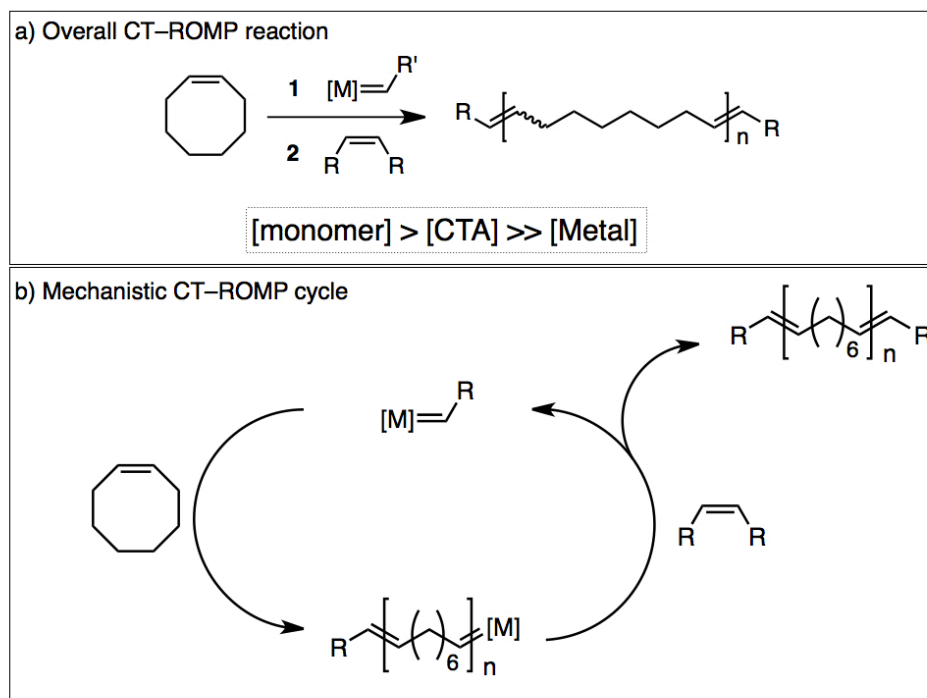


One challenge encountered in the end-functionalization of ROMP polymers to form hemi-telechelic chains is difficulty in achieving highly efficient termination. Likewise, the asymmetric vinyl (or alkenyl) ethers are often not completely regio-specific during termination, giving rise to chains with different functionality. This is a substantial disadvantage, particularly if the intended functionality represents a mechanistic transformation to an initiating species for a subsequent chain extension to form block copolymers; ROMP homopolymer contaminant is essentially unavoidable.<sup>94</sup>

### 1.2.3 Telechelic Polymers by ROMP with Chain Transfer Agents

One particularly attractive approach to introduce functional end-groups into macromolecules prepared by ROMP is to introduce an acyclic olefin designed to undergo cross metathesis. When a symmetric chain transfer agent (CTA) is added ( $R-C=C-R$  in Figure 1.7) during ROMP of a sterically unencumbered monomer (*e.g.*, *cis*-cyclooctene), catalysts may undergo extensive inter-chain metathesis. Inter-chain cross-metathesis between polymer chains and the symmetric CTA will ultimately place the R group at the ends of most polymer chains to give a telechelic sample. The average number of functional groups per chain,  $F_n$ , approaches two under infinitely dilute concentration of initiator (*i.e.*,  $[Ru] \rightarrow 0$ ), and can generally be expressed as in eq 1.2. The concentrations given in eq 1.2 represent the catalyst and CTA amounts reacted.

$$\frac{1}{F_n} = \left[ \frac{1}{2} + \frac{[catalyst]}{[CTA]} \right] \quad (1.2)$$

**Figure 1.7**

Chain Transfer–Ring opening metathesis polymerization (CT–ROMP) strategy for synthesizing telechelic polymers with (a) the overall reaction result and (b) the mechanistic cycle illustrated with the cyclic olefin *cis*-cyclooctene.

Early studies involving the classic metathesis catalyst  $\text{WCl}_6$  with a Lewis acid showed that acyclic CTAs with certain functionality could be incorporated at chain termini when co-metathesized with a cyclic olefin. Symmetric alkyl olefins like *cis*-4-octene (**1**) and alkyl dicarboxylates were shown to cross metathesize with unsaturated linear polyolefin chains during ROMP of cyclopentene or cyclooctene (Figure 1.8).<sup>100–102</sup> In particular, the unsaturated methyl carboxylate **2**<sup>101,102</sup> and the ethyl carboxylate **3**<sup>100</sup> both led to carboxylate terminal PCOE, with the extent of CTA incorporation dependent on several factors (*e.g.*, polymerization conditions). The ROMP–CT strategy applied to the highly strained bicyclic NB also resulted in intermolecular chain transfer to yield telechelic polymers with carboxylate ends.<sup>103,104</sup> Development of the highly tolerant Ru-based catalyst derivatives widened the realm of accessible functional groups, enhanced reactivity and therefore control over the physical behavior.

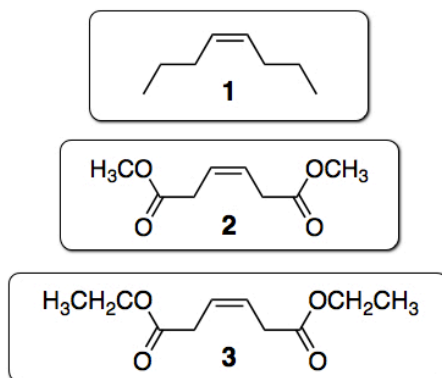


**Figure 1.8**

Symmetric acyclic CTAs *cis*-4-octene **1**, dimethyl hex-3-enedioate **2** and diethyl hex-3-enedioate **3** used in early telechelic metathesis polymer preparations with WCl<sub>6</sub>/Lewis acid catalyst systems.

Specifically, hydroxy-telechelic (HO–polymer–OH) polyolefins are attractive targets as they are crucial components in polyurethane foams, for example. For this reason, ROMP has been used to make polyolefins and other hybrid polymers having telechelic architecture because of the ease with which functional groups are precisely placed and chain length is controlled. Using this strategy, the ultimate mechanical properties (*e.g.*, foam hardness) can be specifically tailored to a desired application. Through scrupulous selection of the highly versatile monomer pool accessible with ROMP and copolymerizations, thermal characteristics and degradation properties of hydroxyl-telechelic polymers are easily tailored.<sup>105</sup> One simple, commercially available CTA that will theoretically give hydroxy-telechelic polymers by the ROMP–CT strategy is *cis*-2-butene-1,4-diol (**4a** in Figure 1.9). However, the position of the functional group with respect to the double bond has substantial influence on the reactivity of the CTA toward metathesis,<sup>103,104</sup> as do a handful of other factors including solvent, temperature, and concentration. Initial attempts to perform ROMP–CT with **4** and NB did not generate any end-functional polymer or oligomer using the classical WCl<sub>6</sub>/Sn(CH<sub>3</sub>)<sub>4</sub> system.<sup>103</sup> In order to alleviate the general incompatibility of the tungsten catalyst system with O, S, and N containing compounds, a protected CTA was designed having borane

substituents, which are known to be stable in transition metal/lewis acid reactions. Compound **7** was synthesized and polymerized with 1,5-cyclooctadiene (COD) catalyzed by  $WCl_6/Sn(CH_3)_4$ .<sup>106</sup> The catalyst subsumed the CTA to give telechelic chains; the 9-borabicyclononane (9BBN) derivatives were easily transformed to hydroxyl groups by a mild oxidation with NaOH and  $H_2O_2$ .

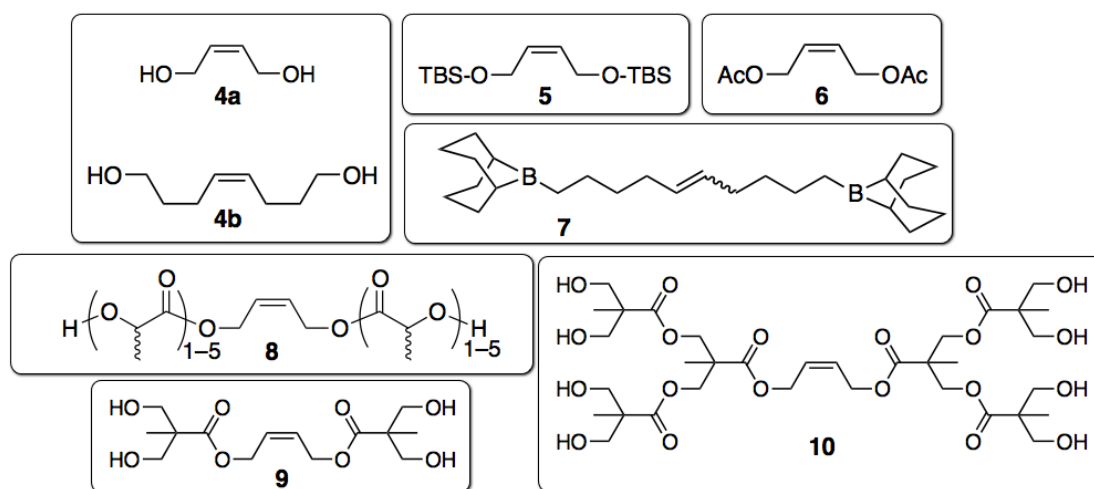


**Figure 1.9**

Symmetric CTAs that provide hydroxyl telechelic polymers by ROMP.

Alternative protected CTAs that yield hydroxyl groups upon deprotection have been reported with discrete metal-alkylidene catalysts. The first example of an alkylidene being employed for telechelic polymer synthesis via ROMP described using 1,5-cyclooctadiene (COD) monomer,  $W(CHAR)(NPh)[OCCH_3(CF_3)_2]_2$  and a *tert*-butyl dimethylsilyl (TBS) protected CTA **5**.<sup>107</sup> Polymerization proceeded readily to give the analog of perfectly linear 1,4-polybutadiene (PBD) having a high functionality ( $F_n \rightarrow 2$ ) owing to the highly active tungsten alkylidene, such that  $[W] \ll [CTA]$ . Subsequent deprotection with tetra-*n*-butylammonium fluoride provided the sought-after hydroxyl telechelic polyolefin. Difficulty was encountered targeting  $N$  by adjusting [monomer]:[CTA] ratios, especially at low molecular weights. This was attributed to deactivation of the allyl-TBS metal alkylidene, which was exacerbated as monomer depletion transpired during polymerization.

Low yields were consistently observed. Circumventing these difficulties required that the TBS group was placed further from the reactive double bond using a methylene spacer; the phenomenon of increased spatial distance enhancing the reactivity was observed with the classical Lewis acid systems as well. Additionally, a Mo-based alkylidene precatalyst was employed because of the purportedly enhanced activity compared with the W-system. Indeed, improved yields and molecular weight control were achieved.<sup>108</sup> Contrasting the simultaneous inclusion of monomer and CTA during metathesis polymerization, metathetical depolymerization of an unsaturated chain in the presence of CTA was also demonstrated to give telechelic polymers having  $F_n \approx 2$ . For example, polyalkenamers prepared by ADMET were subjected to metathetical depolymerization using a W-based catalyst and a TBS-functionalized CTA related to **5**.<sup>109–111</sup>

The synthesis of CTAs with at least 2 methylene spacers between the functional group and the double bond can be tedious. Development of the highly permissive and reactive Ru based catalysts allowed meticulous control of the molecular attributes without the necessity of preparing CTA molecules requiring complicated procedures. Indeed, nominally high yields combined with control of  $N$  was achieved when the commercially available *cis*-1,4-diacetoxy-2-butene **6** was employed as CTA during ROMP of COD catalyzed by **G1** [(PCy<sub>3</sub>)<sub>2</sub>(Cl)<sub>2</sub>Ru=CHPh]. This CTA contains only one methylene group between the COOCH<sub>3</sub> and the double bond, while basic hydrolysis to hydroxyl groups proceeds quantitatively. Extension of this concept was demonstrated with the **G2** catalyst with equally controlled molecular characteristics and significantly enhanced polymerization rates.<sup>112</sup> Additionally, both the CTAs **5** and **6** could be used to prepare a telechelic poly(acetylene) analog from polymerization of cyclooctetraene (COT) with the highly active **G2** catalyst.<sup>113</sup> The unprotected CTA derivative **4** with the relatively stable and robust Ru catalysts **G1** and **G2** were not reliably high yielding under any of various polymerization conditions with COD or COT.<sup>112,114</sup> However, the protected CTA **6** was applied to ROMP with NB and COD monomers using both **G1** and **G2** catalysts, achieving targeted chain lengths with impressive precision;

subsequent hydrolysis illustrated the ease with which ROMP can be applied to prepare hydroxy-telechelic polymers having various hydrocarbon backbone skeletons.<sup>115</sup> Other substituted NB monomers have also led to hydroxy telechelic polymers using a pulsed monomer addition technique with the acetoxy protected CTA **6**.<sup>116</sup> Furthermore, acetal substituted COE was polymerized in one instance, with a high level of precision; post-polymerization deprotection afforded simultaneous acetal and acetoxy hydrolysis to give pendant hydroxyl and end-group hydroxyl functionality.<sup>117</sup> Similarly, polymerization of 1,5-dimethylcyclooctadiene (DMCOD) in the presence of CTA **6** gave the analog of completely 1,4-polyisoprene with acetoxy end-groups; chain transfer proceeded readily using several ruthenium catalyst derivatives, despite the sterically obstructive trisubstituted double bond of the monomer.<sup>118</sup> Hydrolysis of the acetoxy end groups provided the first demonstration of hydroxy-telechelic polyisoprene from ROMP.

Metathetical depolymerization, as discussed briefly in relation to another CTA, has also been used to prepare hydroxyl telechelic polymers having unsaturated backbone structures that are essentially inaccessible using ROMP. A geminal dimethyl substituted polyalkenamer prepared by ADMET was depolymerized with a Ru-based Grubbs catalyst in the presence of CTA **6**.<sup>119</sup> Unsaturated polymers prepared by non-metathetical protocols are also susceptible to metathesis depolymerization if they contain backbone double bonds. In this manner, hydroxy-telechelic polymers could be ultimately derived from metallocene copolymerization of ethylene and 1,3-butadiene<sup>120,121</sup> followed by metathetical depolymerization and acetoxy hydrolysis.<sup>122</sup>

Solving the challenge of directly preparing hydroxy-telechelic polyolefins by using an unprotected CTA is desirable. The post-polymerization hydrolysis and other deprotection techniques previously described are advantageous in certain respects. However, the typical procedure requires solutions with low concentrations due to viscosity issues, which is exponentially exacerbated as molecular weight increases. One method for addressing this challenge was illustrated by preparing a CTA from reaction of compound **4a** with stoichiometric quantity of D,L-lactide (*i.e.*,

[OH]  $\approx$  [D,L-lactide].<sup>123</sup> This procedure gives a mixture of acyclic alkenes from ring-opening of the D,L-lactide and simultaneous transesterification, ultimately having oligomeric lactic acid units tethered on either side of the double bond (compound **8**). This small molecule was prepared from commercially available sources and represents a non-protected hydroxyl CTA that averts tedious post-polymerization deprotection. The hydroxyl groups are located adequately far from the metathetical reaction site to prevent substantial catalyst deactivation. In the same report, the authors describe using symmetric hydroxylated CTAs bearing either four or eight functional groups per double bond with CTAs **9** and **10**, respectively. Again, the hydroxyl groups are adequately far from the reactive site to allow accurate targeting of N by adjusting [monomer]:[CTA].<sup>123</sup>

Telechelic polyolefins and functionalized polyNBs are continually sought with end-groups of various chemical reactivity. Certain functional groups can impart unique physical attributes, and are often designed with the intent of conducting additional transformations. For example, carboxylic esters, carboxamides, carbamides, epoxides, vinyl groups (*e.g.*, methacrylates), halogens, cyanates and particularly carboxylic acids represent valuable synthetic targets for their inherent properties (*e.g.*, hydrogen bonding, hydrophilicity) and reactivities (Figure 1.10).

CTA **11a** was prepared as the diglycidyl ether derivative of *cis*-2-butene-1,4-diol, and polymerized with COD monomer using **G1** catalyst to give an epoxy-telechelic analog of 1,4-polybutadiene. Networks were subsequently prepared by crosslinking via epoxide ring-opening with H<sub>2</sub>SO<sub>4</sub>.<sup>124</sup> Similarly, simultaneous cross-metathesis of a vinyl epoxide to give CTA **11b** and ADMET of 1,9-decadiene purportedly gave the corresponding telechelic polyolefin.<sup>125</sup> Approaches to PCOD networks were also explored with the dimethacrylate of *cis*-2-butene-1,4-diol CTA **12**, with which radical crosslinking was achieved by uv-radiation.<sup>124</sup> A similar crosslinkable CTA **13** with terminal vinyl groups was polymerized with a substituted NB monomer. It was shown that crosslinking could be prevented if **G1** was the catalyst, giving linear vinyl telechelic poly(norbornene). Polymerization with **G2**, however, induced simultaneous crosslinking and ROMP to give networks with crosslink density controllable through the ratio [monomer]:[**13**].<sup>126</sup>



Amino-telechelic PCOD was prepared by polymerizing COD with the protected CTA **14**, followed by post-polymerization deprotection with formic acid.<sup>127</sup> Likewise, the synthesis of carboxyl telechelic PCOD was demonstrated using the same tandem polymerization–deprotection protocol with CTA **15** and formic acid.<sup>127</sup> Telechelic polyolefins derived from halogenated symmetric CTAs have also been reported. The CTA **16** (cis-1,4-dichloro-2-butene) gave chlorinated PCOD<sup>128</sup> while several additional methylene spacers were necessary to achieve well-controlled synthesis of bromo-telechelic PCOD derived from CTA **17**.<sup>129</sup> The bromo end groups were readily converted to azides by nucleophilic substitution using sodium azide. The azide-telechelic PCOE s were subsequently crosslinked by azide-alkyne click chemistry. The synthesis of poly(cyclododecene) with alkyl perfluorinated end-groups with different lengths (either  $-(CF_2)_9CF_3$  or  $-(CF_2)_3CF_3$ ) was illustrated from ROMP of cyclododecene with a classical  $WCl_6$  catalyst system in the presence of acyclic fluorinated CTAs **18a** and **18b**, respectively.<sup>130</sup> Polymerizations of NB derivatives catalyzed by Ru-based **G2** can alternatively be terminated with a symmetric CTA to provide hemitelechelic ( $F_n \approx 1$ ) polymers. The bulky backbone of polynorbornenes compared with completely linear chains of PCOD, PCOE and PCOT render them less susceptible to extensive cross metathesis. In this manner, hemi-telechelics were synthesized with perfluorinated aryl end-groups using CTAs **19a** and **19b** as terminating agents after ROMP of NB derivatives.<sup>131</sup>

Cyano-telechelic and chloro-telechelic high molecular weight PCOD samples were prepared with the respective CTAs **20a** and **16** when catalyzed by **G2**.<sup>128</sup> The allyl position of the cyano electron-withdrawing group (EWG) presented the obstacle of premature catalyst deactivation. Two additional methylene spacers between the  $-CN$  and double bond, however, remedied the difficulty in molecular weight control and high yields.<sup>132</sup> Subsequent reduction with  $LiAlH_4$  gave amino telechelic PCOD, with which coupling reactions were performed to prepare block copolymers with polystyrene.

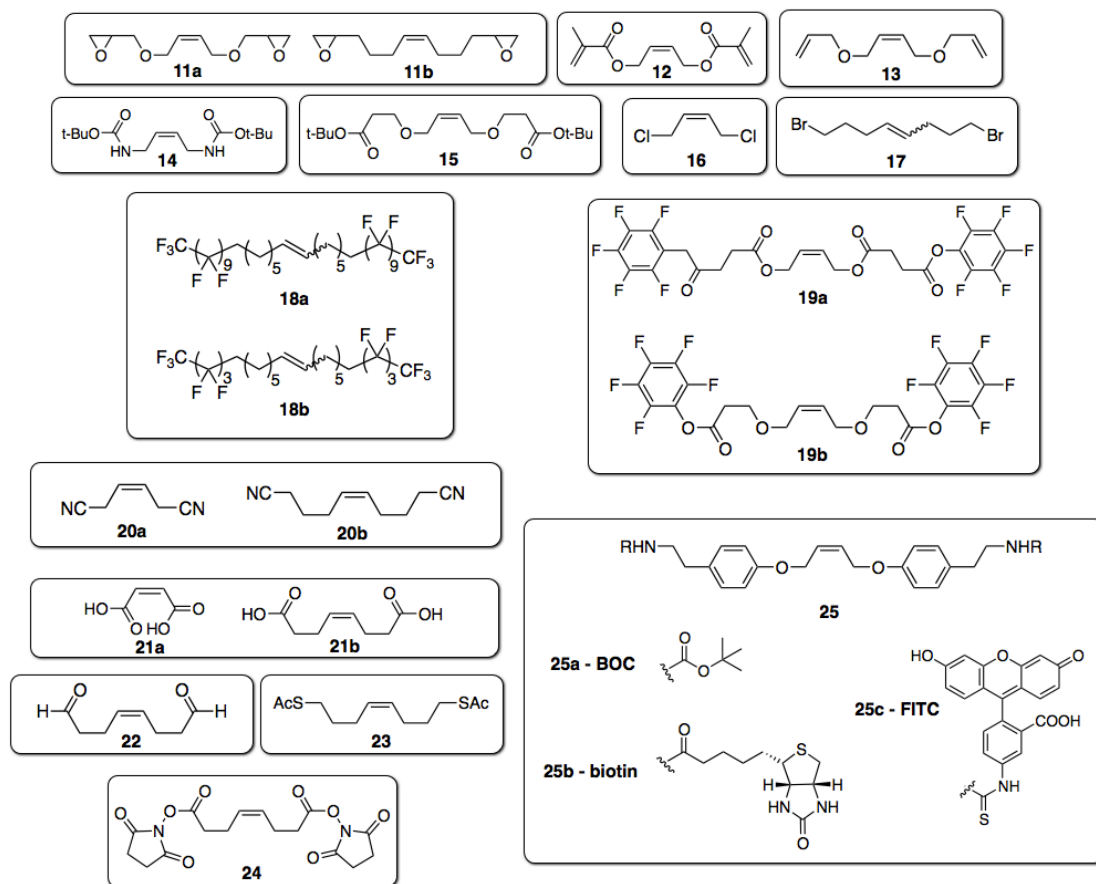


Figure 1.10

Symmetric CTAs for synthesis of telechelic polymers having reactive end-groups: epoxides **11a** and **11b**, methacrylate **12**, *t*-Butyl diamidate **13**, *t*-Butyl dioate **14**, dicyano **15**, dichloro **16** derivative of *cis*-2-butene and maleic acid **17**.

The classical catalyst  $WCl_6$  was unsuccessfully employed for ROMP-CT with maleic acid/fumaric acid and norbornene. Likewise, an additional methylene spacer ( $HOOC-CH_2-CH=CH-CH_2-COOH$ ) did not improve the outcome. The successful ROMP under identical conditions using CTA **2** (*i.e.*, with  $-COOCH_3$  methyl ester substitution) suggests an incompatibility between the catalyst and the  $-COOH$  functionality. Nonetheless, the protected polymeric analogs from polymerization of NB with CTA **2** could be modified by reduction with  $LiAlH_4$  to afford hydroxyl groups or hydrolysis with  $NaOH$  to afford carboxyl groups.<sup>103</sup> More recent attempts to directly functionalize polyolefins with carboxylic acid ( $-COOH$ ) groups via direct end-capping in the presence of CTA **21b** and catalyzed by a pyridinyl substituted

**G2** analog met with little success.<sup>133</sup> The authors attributed the lack of reactivity to presumed coordination of the COOH group with the metal center. However, the direct contrast with this supposition, it was demonstrated that maleic acid underwent nearly quantitative cross metathesis during the polymerization of COE monomer; control over molar mass through the ratio [COE]:[maleic acid] was demonstrated. The ROMP of COE gave carboxyl telechelic polymers in high yield when conducted in the polar solvent THF. This report represented the first such demonstration of the controlled use of an  $\alpha$ -substituted alkene with EWGs as CTA during ROMP and the first report of direct and controlled functionalization using a carboxy-functionalized CTA.<sup>134</sup>

## 1.3 Block Copolymers from Telechelic Polymers Prepared by ROMP

### 1.3.1 Coordinating Telechelic Polymers

Polyolefins have been prepared using ROMP to produce polymers with end-groups exhibiting strong/multiple hydrogen bonding characteristics and other functionalities with potential for strong intermolecular non-covalent interactions. Different end-group identities can be combined to create hybrid materials with very strongly linked molecular junctions, mimicking conventional block copolymers. The mechanical properties can be equivalent to the conventional, covalently bound counterparts. However, a non-covalent partnership is traditionally reversible by changing solvent or temperature, for example. This provides the potential for eased processing, while maintaining the desirable nanoscopic self-assembly behavior associated with conventional block copolymers. Figure 1.11 illustrates the possible combinations of some generic end-functionalized polymer materials that possess complementary end-groups to form various block polymer architectures.

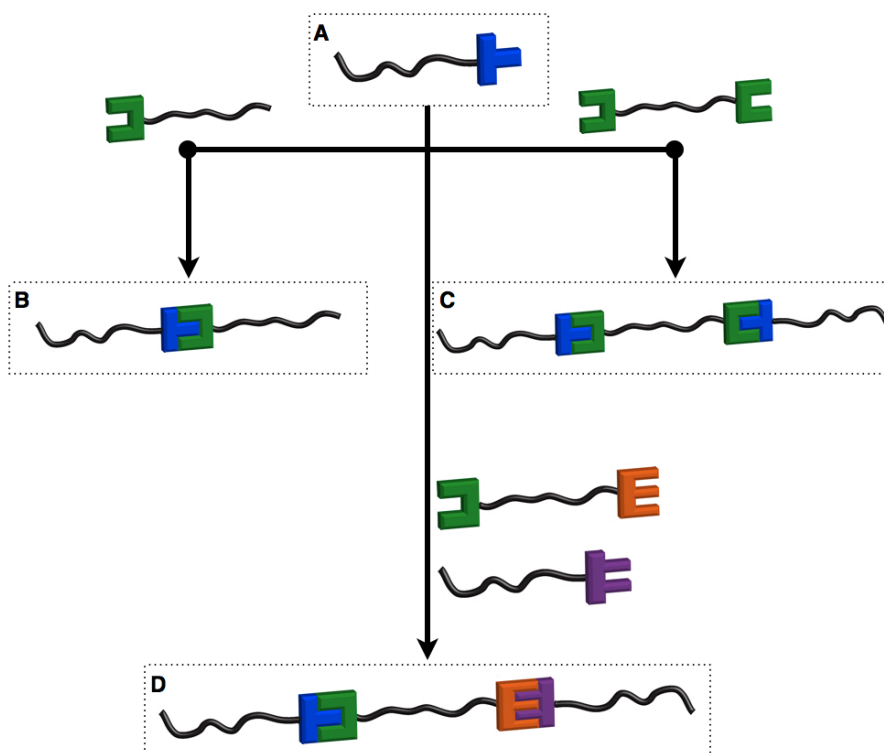


**Figure 1.11**

Non-covalent partnerships to form hybrid block copolymer mimics from end-group interactions between complementary components. Starting with hemi-telechelic "blue"-functional chain **A** to form: **B**, diblock from monofunctional "green" chain; **C**, triblock copolymer from telechelic "green" chain; **D**, triblock terpolymer from hetero-telechelic "green–orange" and hemi-telechelic "purple" chains

One early demonstration of symmetric CTAs with moieties capable of non-covalent molecular recognition and coordination being used to prepare telechelic polymers by ROMP was by Meijer and coworkers.<sup>135</sup> The strong, quadruple hydrogen bonding motif based on 2-ureido-pyrimidinone (UPy) is capable of self-complementary homo-dimerization. Indeed, the CTA **U2** (Figure 1.12) was prepared and used for telechelic polyoctenamer synthesis. The self-complementary coordination was indicated by intrinsic viscosity measurements. Additionally, telechelic polymers from ROMP using 2,7-diamido-1,8-naphthyridine (Napy) functionalized CTA **N2** are capable of quadruple hydrogen bonding in a heterodimerization with UPy end-groups. In this manner, block copolymers were

prepared by mixing differently functionalized polymers; self-assembly and microphase separation were verified using atomic-force microscopy, providing unambiguous evidence for molecular recognition and coordination using non-covalent interactions. Combining two telechelic polymers with complementary end-groups represents a step-growth polymerization between macromonomers X-X and Y-Y, where the ultimate molar mass after coordination is dictated by the stoichiometry between the end-groups. The multiblock formation was monitored by viscometric measurements, comparing the multiblock behavior with the respective homopolymer precursors.

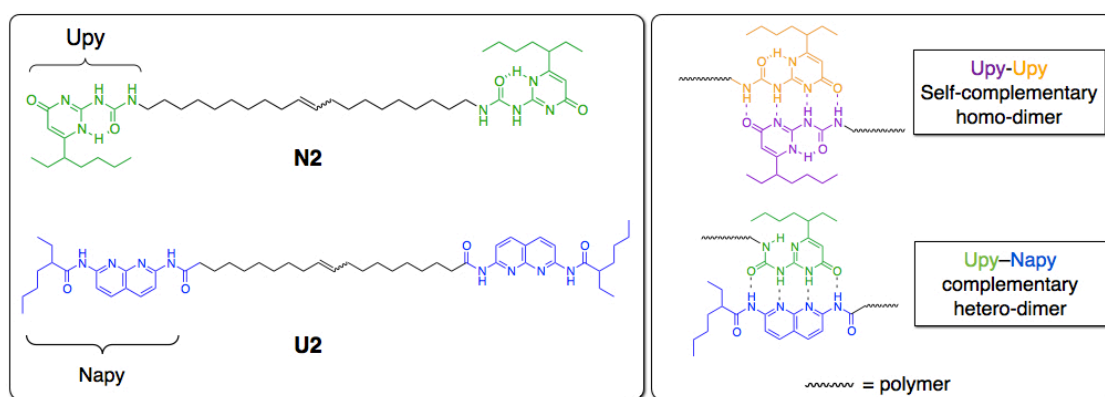


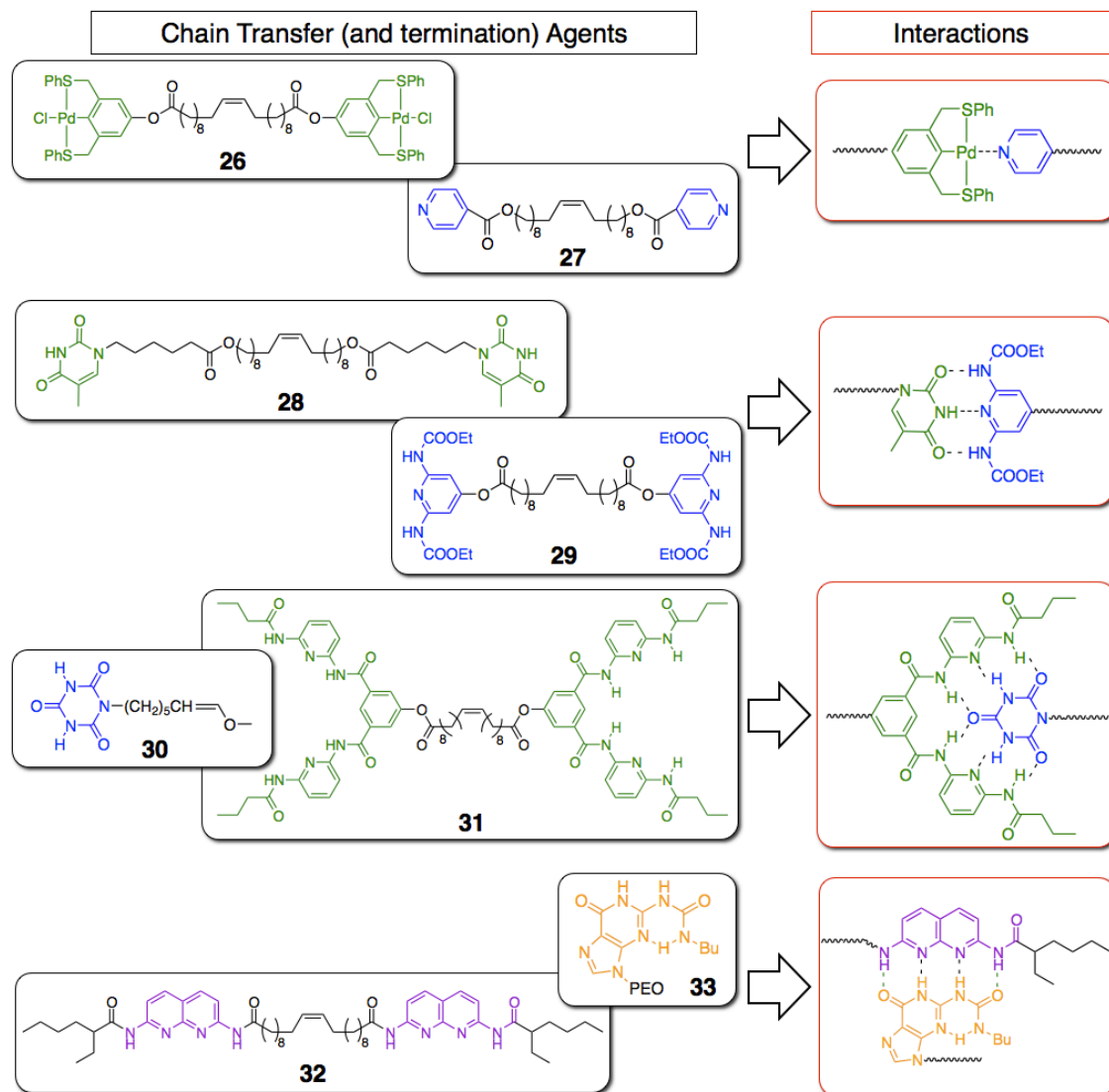
**Figure 1.12**

Symmetric CTAs for ROMP-CT with UPy and Napy end-group functionalities. Homo-dimerization of two UPy motifs (one orange, one violet) and heterodimerization between UPy and Napy is illustrated showing the quadruple hydrogen bonding.

The architectures illustrated in Figure 1.12 do not represent all of the possible combinations of end-functional polymers. It is straightforward to envision branched analogs leading ultimately to more complex architectures, including reversibly crosslinked networks based on dynamic complementary, non-covalent interactions. Several clever approaches to this self-assembly technique have been attempted (Figure 1.13). A symmetric CTA was devised having Lewis acidic transition metal (palladium) pincer-type complexes **26**; ROMP with a 5-substituted cyclooct-1-ene monomer provided telechelic PCOE capable of coordinating a

---

pyridinyl-telechelic polymer **27**.<sup>136</sup> Successful coordination between homopolymers prepared from CTAs **26** and **27** was monitored by the relative chemical shifts in <sup>1</sup>H NMR spectroscopy before and after mixing. Mixing two telechelic coordinating macromonomers is essentially analogous to a step growth polymerization with X-X and Y-Y type species, leading to multiblock copolymers. This modular approach to multiblock copolymers is ideal, embodying the access to a broadly diverse array of monomers afforded by ROMP with Ru-centered catalysts, and the convenience of well controlled molecular characteristics associated with the ROMP-CT technique. Components can be independently selected and prepared before the final matching through coordination.<sup>137</sup>

**Figure 1.13**

Several examples of symmetric chain transfer agents and vinyl-ether terminating agents that contain functionalities amenable to complementary, non-covalent interactions including multiply hydrogen-bonding motifs and transition metal–pyridine complexes.

Several components capable of complementary molecular recognition via hydrogen bonding have been attached to acyclic alkenes, thereby furnishing CTAs for end-functionalization by ROMP–CT. Symmetric CTA **28** with amide linkages are capable of triple hydrogen bonding with the CTA **29** having diamino pyridine

functionalities. In this manner, multiblock copolymers may be prepared after ROMP using the respective CTAs and mixing of the homopolymers. Again, the chemical shift of the amide protons in  $^1\text{H}$  NMR spectroscopy strongly indicates the absence or presence of coordination through hydrogen bonding.<sup>136</sup> The strength of coordination is tunable with alternate motifs, as demonstrated with CTA **31** having six possible sites for hydrogen bonding (two times the diamino pyridine end-groups from CTA **29**). Weck and coworkers creatively designed both symmetric CTAs with the moieties in addition to Ru-alkylidene derivatives<sup>138</sup> and vinyl ether derivatives like the cyclic triamide **30**.<sup>138–140</sup> The symmetric CTAs afford access to telechelic polymers, while the Ru-alkylidene initiates ROMP to give hemi-telechelic polymers (*e.g.*, Figure 1.11, part **A**). As previously discussed, terminating a living ROM polymerization with a vinyl ether (*e.g.*, **30**) offers an alternative route to hemi-telechelic polymers (Figure 1.6). Multiple end-group identities capable of coordinating could be strategically combined into a complex system, giving access to all the different architectures in Figure 1.11, including triblock copolymers, and triblock terpolymers.<sup>137</sup> Similarly, the quadruple hydrogen bonding CTA **32** was used in ROMP to give telechelic chains and combined with hemi-telechelic functionalized PEO **33** to give symmetric triblock copolymers.<sup>141</sup> Hemi-telechelic substituted polyNBs may also be prepared by termination with symmetric CTAs; the sterically crowded backbone essentially prevents extensive chain-transfer between polymer chains. Triamide end-functional CTAs (*e.g.*, **30**) and CTA **28** were used to prepare hemi-telechelic polyNBs.<sup>142</sup>

### 1.3.2 Mechanistic Transformations for Linear Block Copolymer Syntheses

Interest abounds in precise synthesis of block copolymers and other hybrid materials having various components, each of which contribute some unique physical property to the overall responsiveness of a material. The ease with which a broad variety of functional end-groups can be incorporated into polymers using ROMP has been demonstrably proven. As such, the polymerization strategy



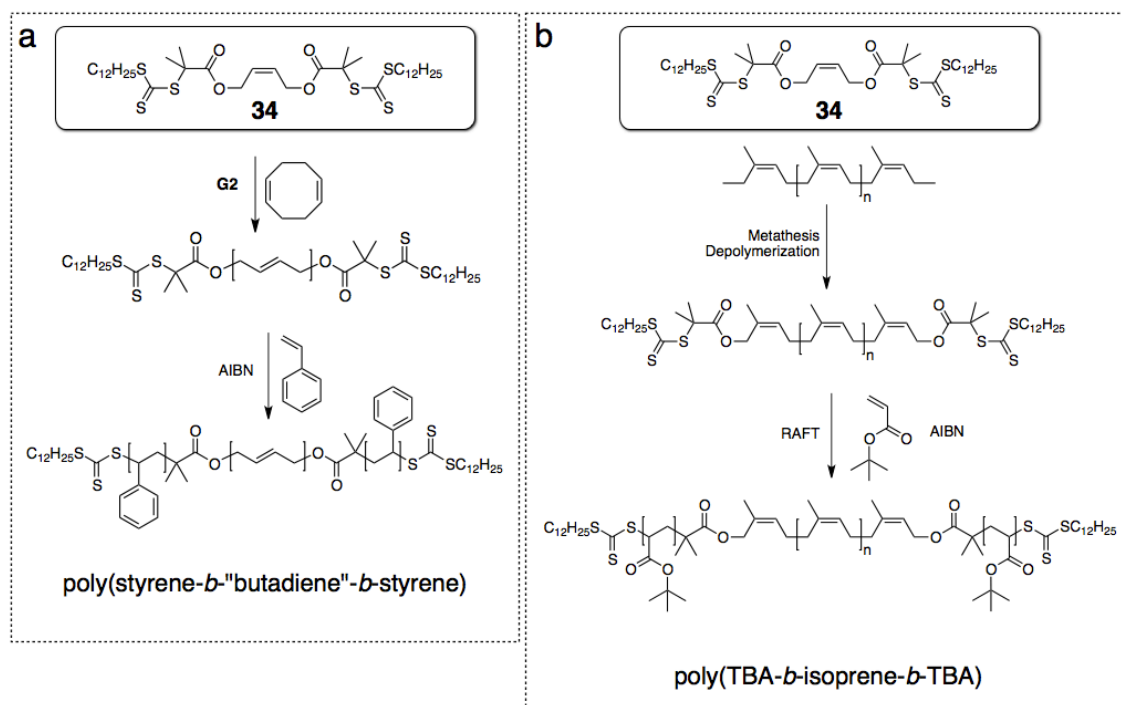
provides profound opportunities to prepare block copolymers by a mechanistic transformation through judiciously chosen end-group functionalization.<sup>143</sup> For example, hydroxyl-telechelic polymers prepared by ROMP have served as macroinitiators for cyclic ester ring-opening polymerization, creating a straightforward route toward BAB-type symmetric block copolymers. Analogously, this mechanistic transformation has been adapted for ROMP-derived polymers to be macroinitiators in atom-transfer radical polymerization (ATRP), reversible addition–fragmentation chain-transfer (RAFT) polymerization, nitroxide mediated polymerization (NMP), and anionic polymerization.

A trithiocarbonate functionalized CTA (**34**) derived from *cis*-2-butene-1,4-diol was prepared using standard esterification procedures. Mahanthappa and coauthors report only modest incorporation of the CTA (~ 50%) during ROMP of COD with **G2** catalyst, giving the analog of 1,4-polybutadiene with trithiocarbonate functionalized chain termini having degree of polymerization higher than the targeted value ( $N_{\text{target}} = 42$ ).<sup>144</sup> Nonetheless, subsequent polymerization of either styrene or *tert*-butyl acrylate (TBA) by controlled radical polymerization (CRP) mediated by the trithiocarbonate RAFT chain transfer motif provided BAB-type triblock poly(styrene-*b*-butadiene-*b*-styrene) and poly(TBA-*b*-butadiene-*b*-TBA) after chain extension, respectively (Scheme 1.4).

Alternatively, unsaturated polyisoprene chains prepared by anionic polymerization were rendered telechelic by metathetical depolymerization in the presence of CTA **34**.<sup>145</sup> BAB-type triblock copolymers resulted after the RAFT polymerization of TBA mediated by the trithiocarbonate chain termini that embody free-radical chain transfer agents.

## Scheme 1.4

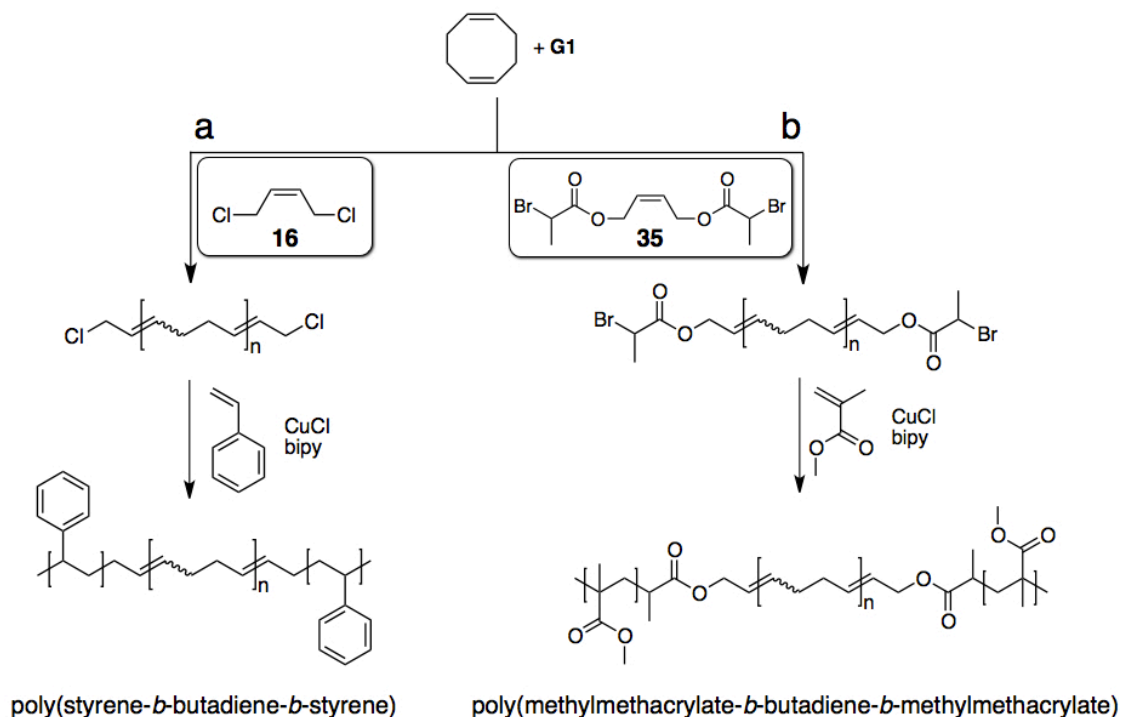
Combining metathesis with reversible addition–fragmentation chain–transfer (RAFT) polymerization to form BAB type triblock copolymers after (a) sequential ROMP of COD with CTA **34** and RAFT polymerization of styrene<sup>144</sup> or (b) metathetical depolymerization of polyisoprene with CTA **34** followed by RAFT polymerization of *tert*-butyl acrylate.<sup>145</sup>



Halide end-groups have been generated on PCOD after ROMP of COE in the presence of chloride CTA **16** or 2-bromopropionyl CTA **35** (Scheme 1.5).<sup>146</sup> The resulting telechelic PCOD were used as macroinitiators for ATRP of styrene (S) or methyl methacrylate (M), respectively, to generate thermoplastic triblock copolymers having glassy end-blocks and low  $T_g$  midblocks (defined as **B** blocks in the original report). Notably, this tandem polymerization strategy provided access to MBM thermoplastic elastomers for which the PBD block is defined by a microstructure consistent with perfect 1,4 addition; an analogous microstructure was unattainable using a conventional anionic polymerization approach.

## Scheme 1.5

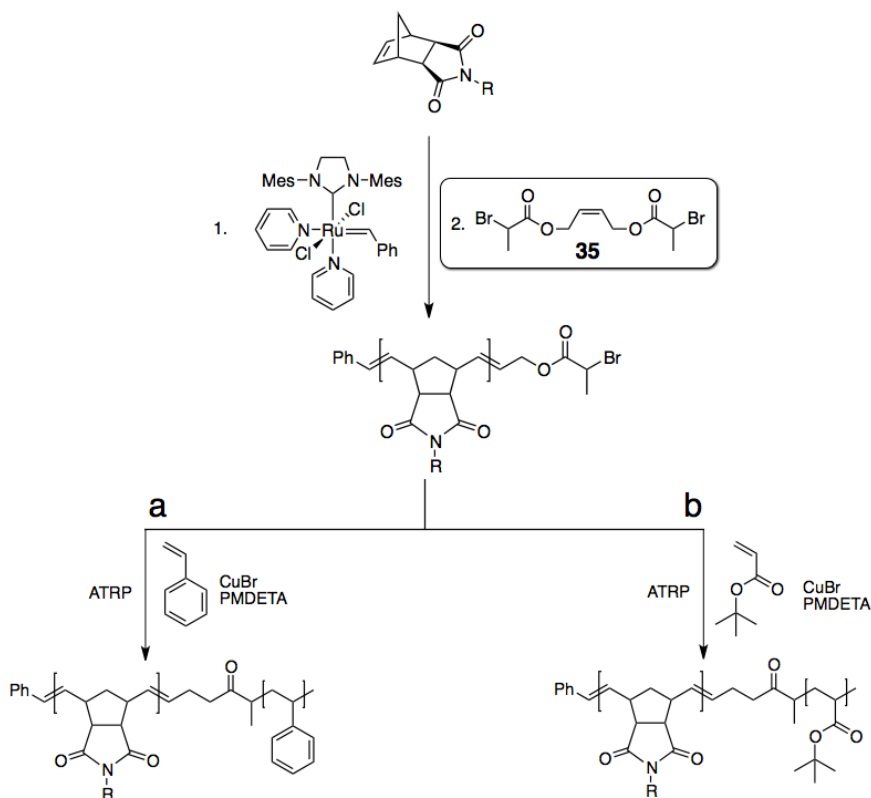
Demonstration of sequential polymerizations: ROMP of COD with (a) dichloro CTA **16** following ATRP of styrene to form triblock SBS and (b) dibromo CTA **35** following ATRP of methyl methacrylate to form triblock MBM.<sup>146</sup>



More recently, the bromopropionyl CTA **35** was used to generate asymmetric, hemi-telechelic polymers by a direct end-capping strategy (Scheme 1.6).<sup>94</sup> The living polymerization of several oxanorbornene monomers followed by termination and end-capping with **35** gave monofunctional bromopropionyl endowed chains, with which the successive ATRP of either styrene or MMA was managed. This alternative strategy of end-capping with the same symmetric, easily accessible CTA **35** represents an innovative path to block copolymers in which all blocks are characterized by narrow molecular weight distributions. The ROMP-CT approach to telechelic polymers generates inherently broad distributions (PDI  $\rightarrow$  2).

## Scheme 1.6

Demonstration of sequential polymerizations: Living ROMP of substituted norbornenes and oxo-norbornenes with pyridinyl ligated Grubbs **G2** catalyst followed by termination with symmetric dibromo CTA **31** followed by sequential ATRP of (a) styrene or (b) *tert*-butyl acrylate to form diblock copolymers.<sup>94</sup>



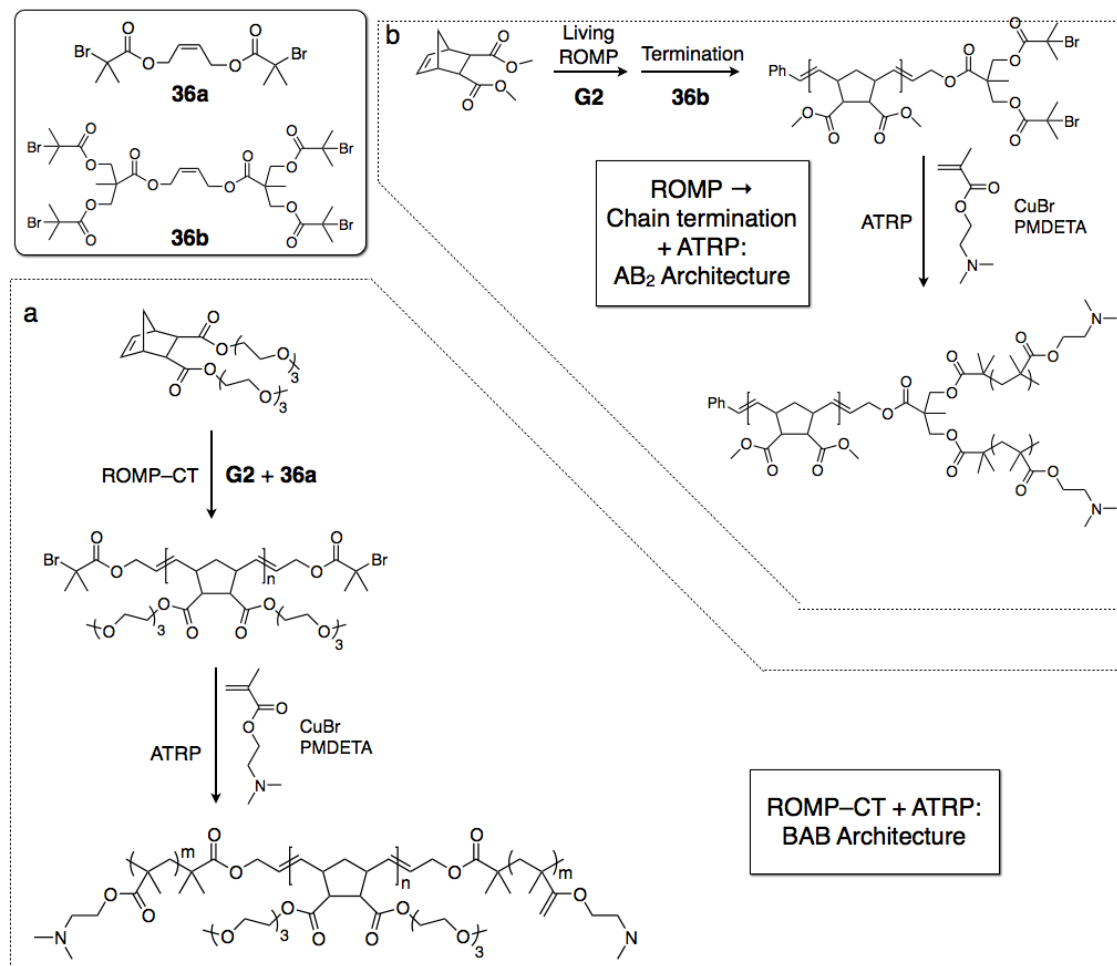
Linear-linear and linear-branched hybrid block copolymers were prepared using tandem ROMP-ATRP by employing a multifunctional bromo-propionyl CTA **36a** or **36b**, respectively (Scheme 1.7). Xie and coworkers described combining CTA **36a** during the polymerization of a poly(ethylene glycol)-substituted, water soluble NB derivative to provide telechelic macroinitiator.<sup>147</sup> Amphiphilic linear BAB block copolymers resulted after the ATRP of 2-(dimethylamino) ethyl methacrylate) (DMAEMA) monomer. Asymmetric branched B<sub>2</sub>A block copolymers were also prepared, but by utilizing a multifunctional CTA **36b** and the direct end-capping method. Low end-capping efficiency was reported, and therefore substantial

homopolymer contaminant was observed by GPC after subsequent polymerization of DMAEMA.<sup>148</sup> Polymers having the desired B<sub>2</sub>A architecture and pristine block copolymer formulation were obtained by end-capping the polymerization with *cis*-2-butene-1,4-diol (CTA **4a**) followed by esterification with a difunctional bis(bromoisobutyryl) bromide. The multifunctional CTA demonstrates a relatively straightforward approach to preparing branched block copolymers which embody unique mechanical characteristics compared to the linear counterparts. The CTA **36b** was prepared in two steps from commercially available starting materials. Improving the efficiency with which sterically demanding CTAs participate in cross-metathesis provides the basis for which syntheses discussed in Chapter 3 were designed.

Linear diblock copolymers were reported from a tandem ROMP–ATRP method after termination of the ROMP of NB monomer with several vinyl ethers with halide functionality: chlorophenyl (**37**), dimethylbromo (**38**), or dichloro (**39**) groups attached to the ethyl ester of vinyl ether (Scheme 1.8).<sup>149</sup> Katayama and coworkers developed vinylidene ruthenium complexes as derivatives of the classical Grubbs **G1** catalyst that were reportedly highly selective in chain transfer reactions with vinyl ethers, giving rise to hemi-telechelic polymers upon ROMP–CT.<sup>150–152</sup> The resulting mono-functional polyNBs were suitable as macroinitiators for ATRP of styrene or MMA, with the appropriately halide-functional chain ends. The vinylidene ruthenium complexes could foreseeably be used to selectively functionalize only one chain end with other moieties, and the vinyl ether synthesis described is amenable to various high-yielding synthetic transformations.

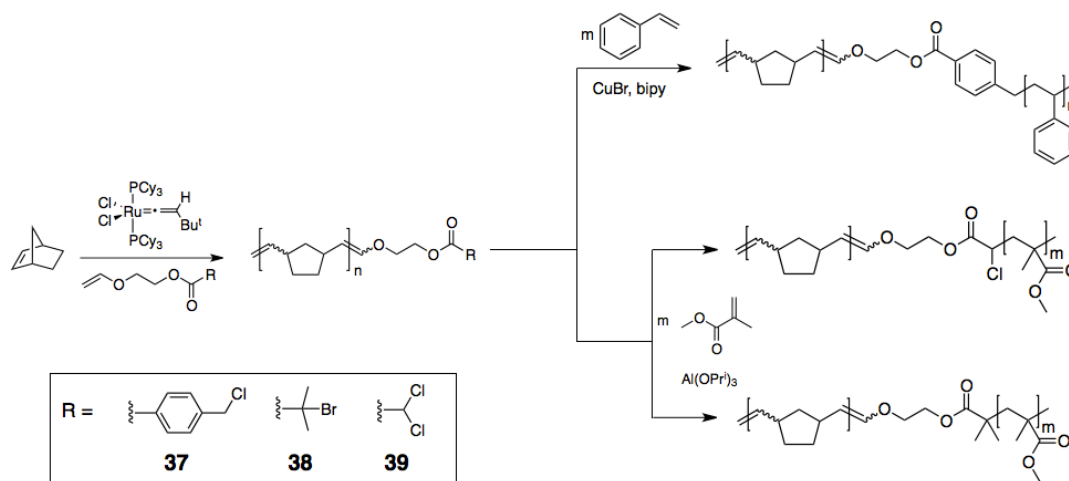
## Scheme 1.7

Tandem ROMP–ATRP polymerizations to form (a) BAB-type linear amphiphilic block copolymers utilizing CTA **36a**<sup>147</sup> and (b) B<sub>2</sub>A star-branched block copolymers by direct end-capping with CTA **36b**.<sup>148</sup>



Scheme 1.8

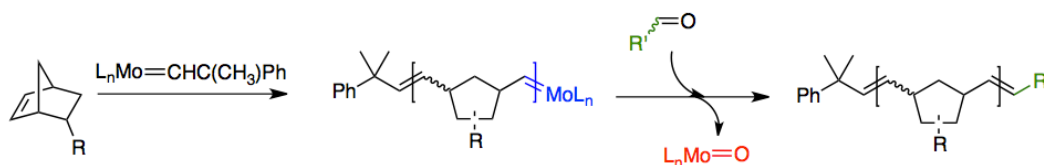
Tandem ROMP–ATRP strategy to form linear AB diblock copolymers by terminating ROMP of norbornylene with vinyl ethers **37**, **38**, and **39** followed by ATRP of either styrene (for **37**) or methyl methacrylate (for **38** and **39**).<sup>149</sup>



It is of particular relevance to introduce an alternative strategy for selective chain-end functionalization with Mo-based catalysts, in contrast to the vinyl-ether strategy employed with Ru-based systems. It has been shown that living Mo-catalyzed ROMP with several derivatives can be terminated in a highly efficient manner using aldehydes, upon which the polymer chain assimilates the attached functionality after a Wittig-type reaction between the carbonyl and the propagating Mo-alkylidene (Scheme 1.9).<sup>153</sup>

Scheme 1.9

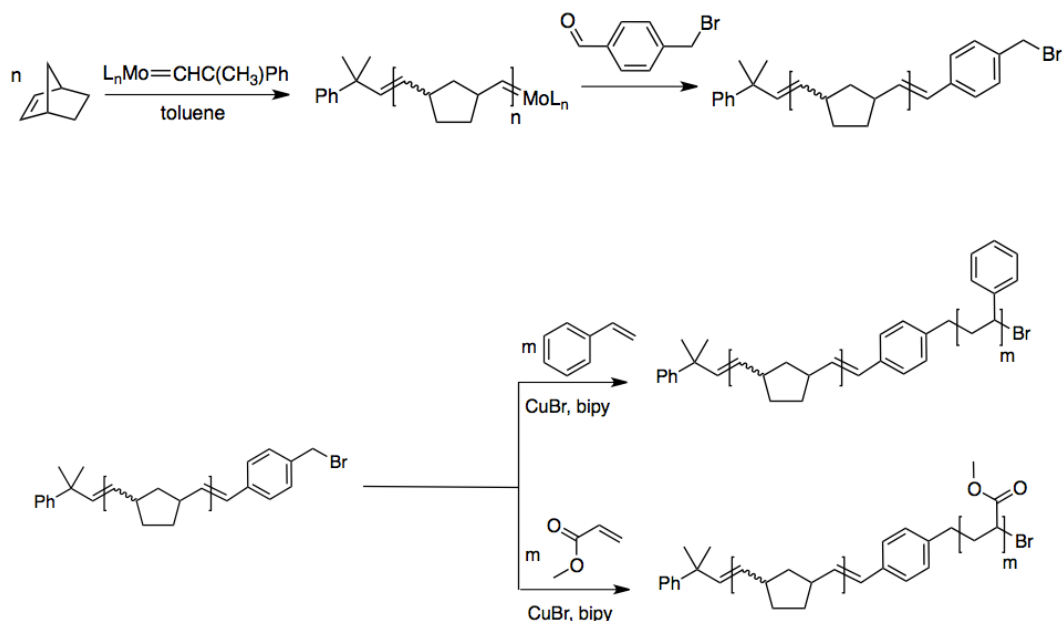
Termination and associated end-functionalizing of ROM polymerization mediated by Mo-based catalyst.<sup>153</sup>



Tandem ROMP–ATRP has been demonstrated after the termination of the Mo-catalyzed polymerization of NB with 4-(bromomethyl)benzaldehyde to yield bromobenzyl terminal polyNB (Scheme 1.10, *top*).<sup>154</sup> Block copolymers were prepared in a controlled fashion by using the polyNB as macroinitiator for ATRP of either styrene or MMA.

### Scheme 1.10

Demonstration of tandem ROMP–ATRP from (*top*) termination of Mo-catalyzed ROMP of NB with 4-(bromomethyl)benzaldehyde and (*bottom*) ATRP from macroinitiator with either styrene or MMA.<sup>154</sup>



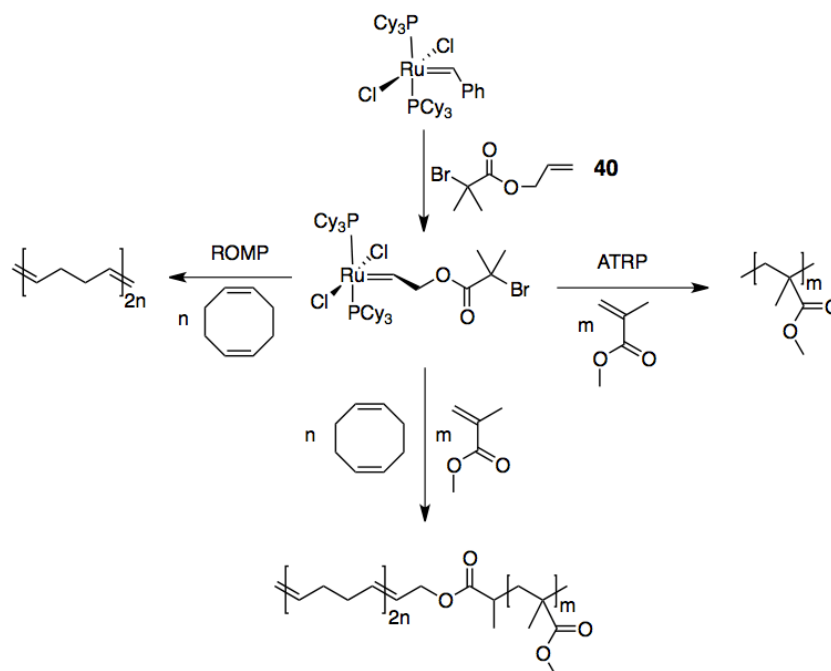
Specific functionalization of a metathesis catalyst prior to ROMP represents an alternative strategy for tandem polymerizations. Reaction of a bromo-isobutyryl vinyl ether with **G1** was reported to generate a Ru-based alkylidene with an initiating fragment bearing the corresponding bromo functionality (Scheme 1.11).<sup>155</sup> It was shown that the doubly reactive ruthenium complex could independently either polymerize COD monomer via the ROM mechanism or MMA via the ATR mechanism. Likewise, simultaneous polymerization of the two monomers was achieved to form well-defined block copolymers in a single pot



reaction setup. This report represented the first such polymerization, with which ATRP and ROMP were simultaneously mediated by the Ru-based catalyst system in a pseudo-living fashion.

### Scheme 1.11

Independent and simultaneous tandem ROMP-ATRP of COD and MMA using a bromoisobutyryl functionalized complex derived from conventional metathesis catalyst **G1**.<sup>155</sup>



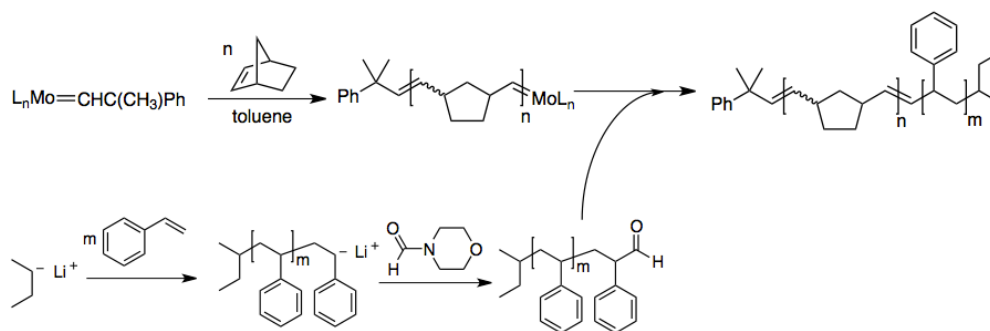
Combining polymers conventionally prepared by anionic polymerization with those prepared by ROMP offers access to potentially valuable hybrid materials. Neither polymerization method grants any overlap in microstructures, with the exception of 1,4-polybutadiene. However, the unsaturated PBD accessible by ROMP and anionic are not identical. Therefore, combining these two methods is useful.

One viable strategy employed involves the independent polymerization of two different polymers with the corresponding mechanism followed by chain end coupling. The respective chain ends were rendered compatible by (1) terminating a

living anionic polymerization of styrene with N-formyl morpholine to give hemi-telechelic aldehyde according to the method of Quirk<sup>156</sup> and (2) terminating a Mo-catalyzed ROMP of NB with the aldehyde in a Wittig-like manner (Scheme 1.12).<sup>157</sup>

### Scheme 1.12

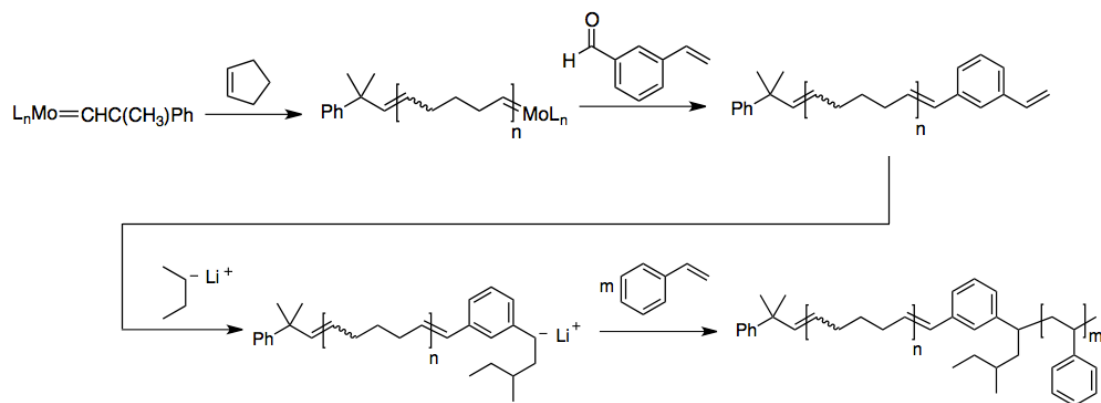
Independent anionic polymerization of styrene to form aldehyde capped chains, with which Mo-catalyzed NB ROMP was terminated to generate block copolymers.<sup>157</sup>



Mo-catalyzed ROMP of cyclopentene was terminated with a small molecule 3-vinylbenzaldehyde to provide vinyl terminated hemi-telechelic poly(cyclopentene) (Scheme 1.13).<sup>158</sup> The styrenyl end-group was subsequently ionized after reaction with *sec*-butyl lithium, rendering the macroinitiator suitable for styrene polymerization via anionic mechanism. The block copolymer underwent microphase separation, which suggests the reinitiation was efficient and block architecture was achieved. Furthermore, the blocks were fully hydrogenated to give block copolymers with linear polyethylene segments and high  $T_g$  poly(vinylcyclohexane) segments that are mechanically robust.<sup>159</sup>

Scheme 1.13

Tandem sequential polymerization of cyclopentene by ROM followed by termination with 3-vinylbenzaldehyde and subsequent chain end ionization with *sec*-butyl lithium to reinitiate polymerization of styrene.<sup>158</sup>



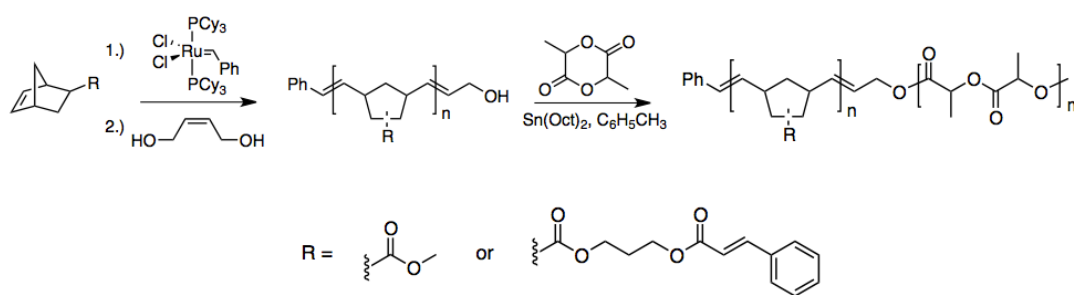
Combining the ROMP of cycloolefins with yet another mechanism, ring-opening transesterification polymerization (ROTEP), provides access to even more hybrid materials that contain incompatible segments inaccessible by any other method. ROTEP of cyclic esters such as D,L-lactide or  $\epsilon$ -caprolactone are often initiated by hydroxyl groups in the presence of metal-complexes such as  $Sn(Oct)_2$  or by transition metal alkoxides such as  $Al(i\text{-PrO})$ . Mechanistically, it has been shown with several systems that small molecules or macromolecules adorned with hydroxyl groups initiate polymerization and form ester bonds at the site of initiation. In this manner, block copolymers of various shapes and sizes are readily produced with appropriately functionalized starting materials.

Functionalization of polymers prepared by ROMP can be achieved with CTAs bearing hydroxyl groups, taking into consideration the nuances associated with such CTAs as **4a** with respect to reactivity. Nonetheless, Weck and coworkers reported direct end-capping of two different functionalized norbornylene monomers with *cis*-2-butene-1,4-diol (CTA **4a**) to form hemi-telechelic monofunctionalized chains (Scheme 1.14).<sup>160</sup> Subsequent  $Sn(Oct)_2$  catalyzed ROTEP of D,L-lactide generated diblock copolymers. The diblock copolymers were swelled with benzene

and freeze-dried to form porous structures with pore-sizes ranging from 20–300  $\mu\text{m}$ . The porous materials were photocrosslinked using the cinnamate side groups on the norbornylene monomers, leading to potentially biocompatible porous polymers intended as bone-grafting materials.

### Scheme 1.14

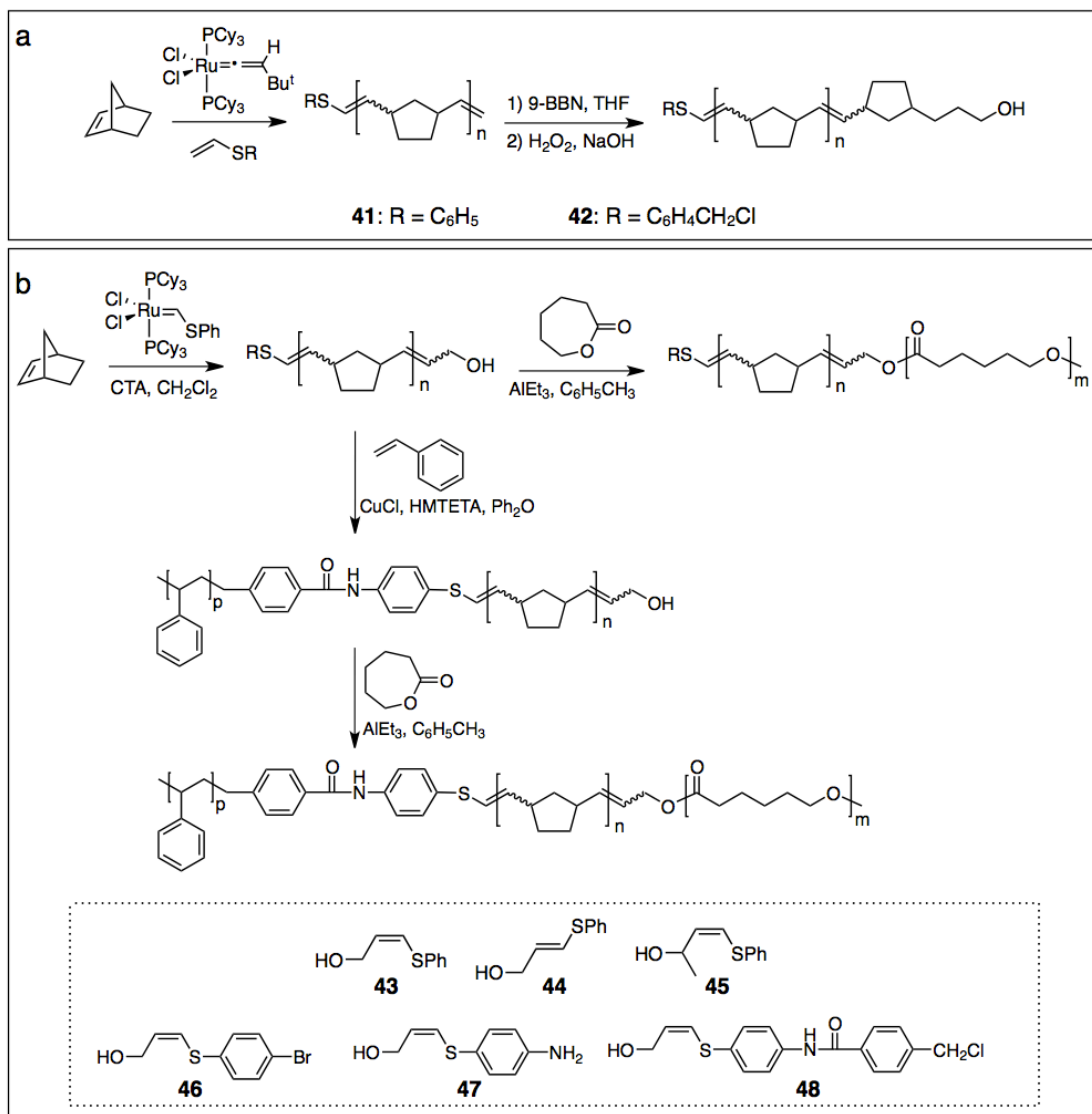
Diblock copolymers formed from tandem ROMP of cinnamate functionalized norbornylenes and ROTEP of D,L-lactide.<sup>160</sup>



There is only one additional previously reported combination of ROMP and ROTEP to form linear block copolymers to date. Katayama and coworkers initially reported polymerization of NB with a ruthenium complex derived from **G1** in the presence of vinyl thioether chain transfer agents (Scheme 1.15).<sup>161</sup> The resulting hemitelechelic polyNB reportedly contained vinyl ends, which were subsequently oxidized using 9-borabicyclo[3.3.1]nonane (9-BBN) and hydrogen peroxide to yield hydroxyl functionalized chains.

Scheme 1.15

Depiction of ROMP using a modified ruthenium complex to undergo chain transfer with asymmetric CTAs for generating hydroxyl terminal polyNB, followed by ROTEP of  $\epsilon$ -caprolactone or ATRP of styrene.<sup>161</sup>



A less tedious method for generating hemi-telechelic hydroxyl end-functionalized polyNB was disclosed in the same report by using asymmetric *cis* substituted CTAs having allyl hydroxyl groups and various thiols (CTAs **43–48**). The CTAs were reportedly incorporated with high efficiency during ROMP using the modified vinylidene ruthenium complex. The utility of the hydroxyl groups as initiators for ROTEP of the cyclic ester  $\epsilon$ -caprolactone was demonstrated to form diblock

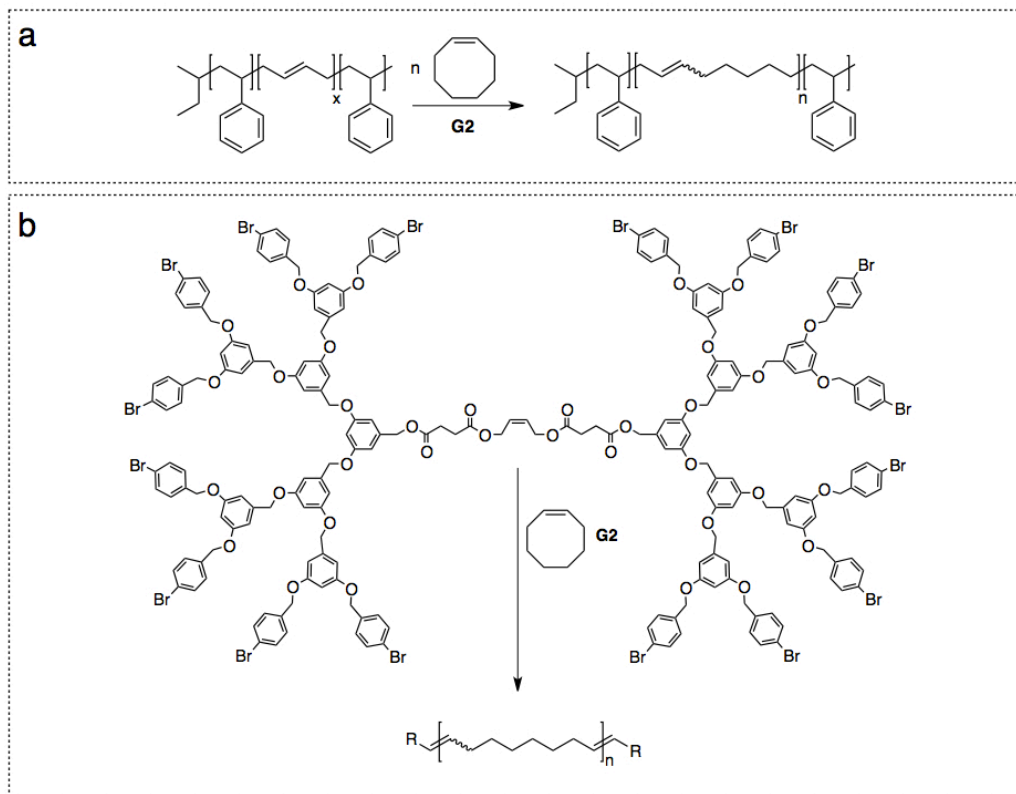
---

copolymers. Furthermore, the other chain end, bearing a chlorobenzyl group after using CTA 48, was used to initiate ATRP of styrene prior to chain extension with  $\epsilon$ -caprolactone, successfully demonstrating the combination of three different mechanisms to form ABC triblock copolymers.<sup>161</sup>

In addition to the previously described examples combining mechanistically incompatible monomers, the sequence of polymerization can ultimately be reversed, whereby ROMP does not constitute the first step. Macromolecular CTAs have been utilized to form symmetric triblock copolymers. This route represents a reversal of the polymerization order in which two consecutive polymerizations are conducted in comparison to the previously discussed examples. A macromolecular CTA is prepared by first employing one type of polymerization. The resulting macromolecules were designed to contain one (or several) point(s) of unsaturation that can partake in subsequent cross-metathesis during ROMP of a cyclic olefin. The mono-functional (or oligo-functional) point(s) of unsaturation then undergo chain transfer during ROMP of a cyclic olefin to give symmetric block copolymers (Scheme 1.16).

Scheme 1.16

Macromolecular CTAs demonstrated for (a) initial sequential anionic polymerization of styrene, 1,3-butadiene, and styrene to form symmetric macromolecular CTA followed by ROMP of COE<sup>162</sup> and (b) 3<sup>rd</sup> generation dendrimer preparation with a centrally located unsaturation for subsequent ROMP of COE.<sup>163</sup>



Bates and coworkers described the formation of nearly symmetric poly(styrene-*b*-butadiene-*b*-styrene) by anionic polymerization with only oligomeric quantities of butadiene. The butadiene unsaturation served as a CTA during subsequent ROMP of *cis*-cyclooctene, in the first such macromolecular CTA report (Scheme 1.16a).<sup>162</sup> However, the poorly defined stereochemical configuration of the butadiene segments led to somewhat inefficient chain transfer and therefore some homopolymer contaminant. Nonetheless, the resulting triblock copolymers were hydrogenated to provide cyclohexylethylene end blocks flanking a linear polyethylene midblock, which were proven to be microphase separated and exhibited impressive toughness. Sill and Emrick had previously described a macromolecular CTA bearing poly(phenyl ether) dendrimeric moieties with a

single, cis-olefinic component (Scheme 1.16b).<sup>163</sup> The discrete macromolecules proved efficient in modulating molecular weight during ROMP–CT to give linear-dendritic hybrid block copolymers. The midblock was formed from ROMP of COE, and similarly, chemical hydrogenation preserved the end-blocks while providing linear polyethylene midblock segments.

Collectively, these examples reveal the extraordinary versatility offered by metathesis CTAs. Telechelic chains or hemi-telechelic chains are afforded by ROMP–CT or chain termination, respectively. Metathetical depolymerization using CTA and polymers containing unsaturated backbones also provides a route to telechelic chains. Furthermore, there exists a diverse set of potential chain-end identities that offer the potential for transformation to alternate mechanisms, opening the door to an essentially infinite array of block copolymers exhibiting corresponding diversity of mechanical, thermal, and optical properties.

## 1.4 Conclusions

Examples of mechanistic transformations involving ROMP as one step have been briefly reviewed. The transformative strategy generates block copolymers having an astounding variety of chemical components, as several different mechanisms allows access to many monomers. The survey of combinations provide examples utilizing several controlled polymerization pathways that include RAFT polymerization, ATRP, anionic polymerization, and ROTEP, which convincingly establishes the potential power of mechanistic combinations with ROMP. Many challenges ranging from specialty to commodity applications could foreseeably be addressed by employing these strategies, owing to the vast chemical variability that could be realized. Particularly, the sparsity of examples combining ROMP with ROTEP leaves a void that could be thoroughly exploited and therefore deserves substantial attention. A substantial portion of the dissertation is focused on addressing this void and contains details of different polymerization design strategies that aim to extend the general utility of tandem polymerizations including ROMP.



---

## 1.5 References

- [1] Abetz, V.; Simon, P. F. W. *Adv. Polym. Sci.* **2005**, *189*, 125–212.
- [2] Li, M.; Coenjarts, C. A.; Ober, C. K. *Adv. Polym. Sci.* **2005**, *190*, 183–226.
- [3] Bates, F. S.; Fredrickson, G. H. *Annu. Rev. Phys. Chem.* **1990**, *41*, 525–557.
- [4] Bates, F. S. *Science (Washington, DC, United States)* **1991**, *251*, 898–905.
- [5] Matsen, M. W.; Schick, M. *Phys. Rev. Lett.* **1994**, *72*, 2660–2663.
- [6] Matsen, M. W.; Schick, M. *Macromolecules* **1994**, *27*, 4014–4015.
- [7] Matsen, M. W.; Bates, F. S. *Macromolecules* **1996**, *29*, 1091–1098.
- [8] Matsen, M. W.; Bates, F. S. *Macromolecules* **1996**, *29*, 7641–7644.
- [9] Matsen, M. W.; Bates, F. S. *J. Chem. Phys.* **1997**, *106*, 2436–2448.
- [10] Matsen, M. W.; Thompson, R. B. *J. Chem. Phys.* **1999**, *111*, 7139–7146.
- [11] Mai, S.-M.; Mingvanish, W.; Turner, S. C.; Chaibundit, C.; Fairclough, J. P. A.; Heatley, F.; Matsen, M. W.; Ryan, A. J.; Booth, C. *Macromolecules* **2000**, *33*, 5124–5130.
- [12] Matsen, M. W. *J. Chem. Phys.* **2001**, *114*, 10528–10530.
- [13] Khandpur, A. K.; Foerster, S.; Bates, F. S.; Hamley, I. W.; Ryan, A. J.; Bras, W.; Almdal, K.; Mortensen, K. *Macromolecules* **1995**, *28*, 8796–8806.
- [14] Schulz, M. F.; Khandpur, A. K.; Bates, F. S.; Almdal, K.; Mortensen, K.; Hajduk, D. A.; Gruner, S. M. *Macromolecules* **1996**, *29*, 2857–2867.
- [15] Calderon, N.; Chen, H. Y.; Scott, K. W. *Tetrahedron Lett.* **1967**, 3327–3329.
- [16] Calderon, N. *Acc. Chem. Res.* **1972**, *5*, 127–132.

- 
- [17] Calderon, N.; Ofstead, E. A.; Judy, W. A. *Angew. Chem.* **1976**, *88*, 433–442.
- [18] Bradshaw, C. P. C.; Howman, E. J.; Turner, L. *J. Catal.* **1967**, *7*, 269–276.
- [19] Calderon, N.; Ofstead, E. A.; Ward, J. P.; Judy, W. A.; Scott, K. W. *J. Am. Chem. Soc.* **1968**, *90*, 4133–4140.
- [20] Herisson, J. L.; Chauvin, Y. *Makromol. Chem.* **1971**, *141*, 161–176.
- [21] Kress, J.; Osborn, J. A.; Greene, R. M. E.; Ivin, K. J.; Rooney, J. J. *J. Am. Chem. Soc.* **1987**, *109*, 899–901.
- [22] Katz, T. J.; McGinnis, J. *J. Am. Chem. Soc.* **1975**, *97*, 1592–1594.
- [23] Howard, T. R.; Lee, J. B.; Grubbs, R. H. *J. Am. Chem. Soc.* **1980**, *102*, 6876–6878.
- [24] Gilliom, L. R.; Grubbs, R. H. *J. Am. Chem. Soc.* **1986**, *108*, 733–742.
- [25] Feldman, J.; Davis, W. M.; Thomas, J. K.; Schrock, R. R. *Organometallics* **1990**, *9*, 2535–2548.
- [26] Schrock, R. R.; DePue, R. T.; Feldman, J.; Yap, K. B.; Yang, D. C.; Davis, W. M.; Park, L.; DiMare, M.; Schofield, M.; et, a. *Organometallics* **1990**, *9*, 2262–2275.
- [27] Schrock, R. R.; Feldman, J.; Cannizzo, L. F.; Grubbs, R. H. *Macromolecules* **1987**, *20*, 1169–1172.
- [28] Bazan, G. C.; Khosravi, E.; Schrock, R. R.; Feast, W. J.; Gibson, V. C.; O'Regan, M. B.; Thomas, J. K.; Davis, W. M. *J. Am. Chem. Soc.* **1990**, *112*, 8378–8387.
- [29] Schrock, R. R.; Murdzek, J. S.; Bazan, G. C.; Robbins, J.; DiMare, M.; O'Regan, M. *J. Am. Chem. Soc.* **1990**, *112*, 3875–3886.

- 
- [30] Bazan, G. C.; Oskam, J. H.; Cho, H. N.; Park, L. Y.; Schrock, R. R. *J. Am. Chem. Soc.* **1991**, *113*, 6899–6907.
- [31] Dias, E. L.; Nguyen, S. T.; Grubbs, R. H. *J. Am. Chem. Soc.* **1997**, *119*, 3887–3897.
- [32] Nguyen, S. T.; Johnson, L. K.; Grubbs, R. H.; Ziller, J. W. *J. Am. Chem. Soc.* **1992**, *114*, 3974–3975.
- [33] Nguyen, S. T.; Grubbs, R. H.; Ziller, J. W. *J. Am. Chem. Soc.* **1993**, *115*, 9858–9859.
- [34] Wu, Z.; Nguyen, S. T.; Grubbs, R. H.; Ziller, J. W. *J. Am. Chem. Soc.* **1995**, *117*, 5503–5511.
- [35] Schwab, P.; France, M. B.; Ziller, J. W.; Grubbs, R. H. *Angew. Chem., Int. Ed.* **1995**, *34*, 2039–2041.
- [36] Schwab, P.; Grubbs, R. H.; Ziller, J. W. *J. Am. Chem. Soc.* **1996**, *118*, 100–110.
- [37] Sanford, M. S.; Love, J. A.; Grubbs, R. H. *J. Am. Chem. Soc.* **2001**, *123*, 6543–6554.
- [38] Love, J. A.; Sanford, M. S.; Day, M. W.; Grubbs, R. H. *J. Am. Chem. Soc.* **2003**, *125*, 10103–10109.
- [39] Love, J. A.; Morgan, J. P.; Trnka, T. M.; Grubbs, R. H. *Angew. Chem., Int. Ed.* **2002**, *41*, 4035–4037.
- [40] Sanford, M. S.; Ulman, M.; Grubbs, R. H. *J. Am. Chem. Soc.* **2001**, *123*, 749–750.
- [41] Hinderling, C.; Adlhart, C.; Chen, P. *Angew. Chem., Int. Ed.* **1998**, *37*, 2685–2689.

- 
- [42] Adlhart, C.; Hinderling, C.; Baumann, H.; Chen, P. *J. Am. Chem. Soc.* **2000**, *122*, 8204–8214.
- [43] Adlhart, C.; Chen, P. *J. Am. Chem. Soc.* **2004**, *126*, 3496–3510.
- [44] Trnka, T. M.; Morgan, J. P.; Sanford, M. S.; Wilhelm, T. E.; Scholl, M.; Choi, T. L.; Ding, S.; Day, M. W.; Grubbs, R. H. *J. Am. Chem. Soc.* **2003**, *125*, 2546–2558.
- [45] Scholl, M.; Trnka, T. M.; Morgan, J. P.; Grubbs, R. H. *Tetrahedron Lett.* **1999**, *40*, 2247–2250.
- [46] Scholl, M.; Ding, S.; Lee, C. W.; Grubbs, R. H. *Org. Lett.* **1999**, *1*, 953–956.
- [47] Ackermann, L.; Furstner, A.; Weskamp, T.; Kohl, F. J.; Herrmann, W. A. *Tetrahedron Lett.* **1999**, *40*, 4787–4790.
- [48] Furstner, A.; Thiel, O. R.; Ackermann, L. *Org. Lett.* **2001**, *3*, 449–451.
- [49] Bielawski, C. W.; Grubbs, R. H. *Angew. Chem., Int. Ed.* **2000**, *39*, 2903–2906.
- [50] Chauvin, Y. *Angew. Chem., Int. Ed.* **2006**, *45*, 3740–3747.
- [51] Grubbs, R. H. *Angew. Chem., Int. Ed.* **2006**, *45*, 3760–3765.
- [52] Schrock, R. R. *Angew. Chem., Int. Ed.* **2006**, *45*, 3748–3759.
- [53] Novak, B. M.; Risse, W.; Grubbs, R. H. *Adv. Polym. Sci.* **1992**, *102*, 47–72.
- [54] Pariya, C.; Jayaprakash, K. N.; Sarkar, A. *Coord. Chem. Rev.* **1998**, *168*, 1–48.
- [55] Randall, M. L.; Snapper, M. L. *J. Mol. Catal. A: Chem.* **1998**, *133*, 29–40.
- [56] Schrock, R. R.; Hoveyda, A. H. *Angew. Chem., Int. Ed.* **2003**, *42*, 4592–4633.

- 
- [57] Grubbs, R. H.; Trnka, T. M. *Ruthenium in Organic Synthesis* **2004**, 153–177.
- [58] Vougioukalakis, G. C.; Grubbs, R. H. *Chem. Rev.* **2010**, *110*, 1746–1787.
- [59] Frenzel, U.; Nuyken, O. *J. Polym. Sci., Part A: Polym. Chem.* **2002**, *40*, 2895–2916.
- [60] Frenzel, U.; Weskamp, T.; Kohl, F. J.; Schattenman, W. C.; Nuyken, O.; Herrmann, W. A. *J. Organomet. Chem.* **1999**, *586*, 263–265.
- [61] Schrock, R. R. *Tetrahedron* **1999**, *55*, 8141–8153.
- [62] Trnka, T. M.; Grubbs, R. H. *Acc. Chem. Res.* **2001**, *34*, 18–29.
- [63] Zaman, S.; Curnow, O. J.; Abell, A. D. *Aust. J. Chem.* **2009**, *62*, 91–100.
- [64] Bieniek, M.; Michrowska, A.; Usanov, D. L.; Grela, K. *Chem. Eur. J.* **2008**, *14*, 806–818.
- [65] Blackwell, H. E.; O'Leary, D. J.; Chatterjee, A. K.; Washenfelder, R. A.; Bussmann, D. A.; Grubbs, R. H. *J. Am. Chem. Soc.* **2000**, *122*, 58–71.
- [66] Deiters, A.; Martin, S. F. *Chem. Rev.* **2004**, *104*, 2199–2238.
- [67] Fürstner, A. *Angew. Chem., Int. Ed.* **2000**, *39*, 3012–3043.
- [68] Grubbs, R. H.; Chang, S. *Tetrahedron* **1998**, *54*, 4413–4450.
- [69] Grubbs, R. H.; Miller, S. J.; Fu, G. C. *Acc. Chem. Res.* **1995**, *28*, 446–452.
- [70] Schuster, M.; Blechert, S. *Angew. Chem., Int. Ed.* **1997**, *36*, 2036–2056.
- [71] Nolan, S. P.; Clavier, H. *Chem. Soc. Rev.* **2010**, *39*, 3305–3316.
- [72] Clavier, H.; Grela, K.; Kirschning, A.; Mauduit, M.; Nolan, S. P. *Angew. Chem., Int. Ed.* **2007**, *46*, 6786–6801.

- 
- [73] Baughman, T. W.; Wagener, K. B. *Adv. Polym. Sci.* **2005**, *176*, 1–42.
- [74] Bielawski, C. W.; Grubbs, R. H. *Prog. Polym. Sci.* **2007**, *32*, 1–29.
- [75] Breslow, D. S. *Prog. Polym. Sci.* **1993**, *18*, 1141–1195.
- [76] Buchmeiser, M. R. *Chem. Rev.* **2000**, *100*, 1565–1604.
- [77] Grubbs, R. H.; Tumas, W. *Science (Washington, DC, United States)* **1989**, *243*, 907–915.
- [78] Slugovc, C. *Macromol. Rapid Commun.* **2004**, *25*, 1283–1297.
- [79] Sutthasupa, S.; Shiotsuki, M.; Sanda, F. *Polym. J.* **2010**, *42*, 905–915.
- [80] Leitgeb, A.; Wappel, J.; Slugovc, C. *Polymer* **2010**, *51*, 2927–2946.
- [81] Riegler, S.; Slugovc, C.; Trimmel, G.; Stelzer, F. *Macromol. Symp.* **2004**, *217*, 231–246.
- [82] Smith, D.; Pentzer, E. B.; Nguyen, S. T. *Polym. Rev.* **2007**, *47*, 419–459.
- [83] Truett, W. L.; Johnson, D. R.; Robinson, I. M.; Montague, B. A. *J. Am. Chem. Soc.* **1960**, *82*, 2337–2340.
- [84] Natta, G.; Dall'Asta, G.; Mazzanti, G. *Angewandte Chemie International Edition in English* **1964**, *3*, 723–729.
- [85] Calderon, N. *Journal of Macromolecular Science, Reviews in Macromolecular Chemistry* **1972**, *7*, 105–159.
- [86] Calderon, N.; Ofstead, E. A.; Judy, W. A. *J. Polym. Sci., Part A: Polym. Chem.* **1967**, *5*, 2209–2217.
- [87] Ritter, T.; Hejl, A.; Wenzel, A. G.; Funk, T. W.; Grubbs, R. H. *Organometallics* **2006**, *25*, 5740–5745.

- 
- [88] Park, L. Y.; Schrock, R. R.; Stieglitz, S. G.; Crowe, W. E. *Macromolecules* **1991**, *24*, 3489–3495.
- [89] Benedicto, A. D.; Claverie, J. P.; Grubbs, R. H. *Macromolecules* **1995**, *28*, 500–511.
- [90] Louie, J.; Grubbs, R. H. *Organometallics* **2002**, *21*, 2153–2164.
- [91] Maynard, H. D.; Grubbs, R. H. *Macromolecules* **1999**, *32*, 6917–6924.
- [92] Weck, M.; Mohr, B.; Maughon, B. R.; Grubbs, R. H. *Macromolecules* **1997**, *30*, 6430–6437.
- [93] Mangold, S. L.; Carpenter, R. T.; Kiessling, L. L. *Org. Lett.* **2008**, *10*, 2997–3000.
- [94] Matson, J. B.; Grubbs, R. H. *Macromolecules* **2008**, *41*, 5626–5631.
- [95] Chen, B.; Metera, K.; Sleiman, H. F. *Macromolecules* **2005**, *38*, 1084–1090.
- [96] Owen, R. M.; Gestwicki, J. E.; Young, T.; Kiessling, L. L. *Org. Lett.* **2002**, *4*, 2293–2296.
- [97] Hilf, S.; Grubbs, R. H.; Kilbinger, A. F. M. *J. Am. Chem. Soc.* **2008**, *130*, 11040–11048.
- [98] Hilf, S.; Kilbinger, A. F. M. *Macromolecules* **2010**, *43*, 208–212.
- [99] Hilf, S.; Wurm, F.; Kilbinger, A. F. M. *J. Polym. Sci., Part A: Polym. Chem.* **2009**, *47*, 6932–6940.
- [100] Otton, J.; Colleuille, Y.; Varagnat, J. *J. Mol. Catal.* **1980**, *8*, 313–324.
- [101] Pinazzi, C. P.; Campistron, I.; Croissandeau, M. C.; Reyx, D. *J. Mol. Catal.* **1980**, *8*, 325–328.
- [102] Reyx, D.; Hamza, M.; Campistron, I. *J. Mol. Catal.* **1987**, *42*, 289–299.

- 
- [103] Cramail, H.; Fontanille, M.; Soum, A. *Journal of Molecular Catalysis* **1991**, *65*, 193–203.
- [104] Cramail, H.; Fontanille, M.; Soum, A. *Makromol. Chem.–M. Symp.* **1991**, *42/43*, 281–292.
- [105] Gascon, C.; Lucas, F.; Carlotti, S.; Deffieux, A. *J. Appl. Polym. Sci.* **2010**, *118*, 1830–1836.
- [106] Chung, T. C.; Chasmawala, M. *Macromolecules* **1992**, *25*, 5137–5144.
- [107] Hillmyer, M. A.; Grubbs, R. H. *Macromolecules* **1993**, *26*, 872–874.
- [108] Hillmyer, M. A.; Grubbs, R. H. *Macromolecules* **1995**, *28*, 8662–8667.
- [109] Marmo, J. C.; Wagener, K. B. *Macromolecules* **1993**, *26*, 2137–2138.
- [110] Marmo, J. C.; Wagener, K. B. *Macromolecules* **1995**, *28*, 2602–2606.
- [111] Marmo, J. C.; Wagener, k. B. *Rubber Chem. Technol.* **1997**, *70*, 519–529.
- [112] Bielawski, C. W.; Scherman, O. A.; Grubbs, R. H. *Polymer* **2001**, *42*, 4939–4945.
- [113] Scherman, O. A.; Rutenberg, I. M.; Grubbs, R. H. *J. Am. Chem. Soc.* **2003**, *125*, 8515–8522.
- [114] Scherman, O. A.; Rutenberg, I. M.; Grubbs, R. H. *J. Am. Chem. Soc.* **2003**, *125*, 8515–8522.
- [115] Bielawski, C. W.; Benitez, D.; Morita, T.; Grubbs, R. H. *Macromolecules* **2001**, *34*, 8610–8618.
- [116] Gibson, V. C.; Okada, T. *Macromolecules* **2000**, *33*, 655–656.
- [117] Scherman, O. A.; Walker, R.; Grubbs, R. H. *Macromolecules* **2005**, *38*, 9009–9014.



- 
- [118] Thomas, R. M.; Grubbs, R. H. *Macromolecules* **2010**, *43*, 3705–3709.
- [119] Schwendeman, J. E.; Wagener, K. B. *Macromol. Chem. Phys.* **2009**, *210*, 1818–1833.
- [120] Barbotin, F.; Monteil, V.; Llauro, M.-F.; Boisson, C.; Spitz, R. *Macromolecules* **2000**, *33*, 8521–8523.
- [121] Thuilliez, J.; Monteil, V.; Spitz, R.; Boisson, C. *Angew. Chem., Int. Ed.* **2005**, *44*, 2593–2596.
- [122] Lucas, F.; Peruch, F.; Carlotti, S.; Deffieux, A.; Leblanc, A.; Boisson, C. *Polymer* **2008**, *49*, 4935–4941.
- [123] Pitet, L. M.; Chamberlain, B. M.; Hauser, A. W.; Hillmyer, M. A. *Macromolecules* **2010**, *43*, 8018–8025.
- [124] Maughon, B. R.; Morita, T.; Bielawski, C. W.; Grubbs, R. H. *Macromolecules* **2000**, *33*, 1929–1935.
- [125] Tamura, H.; Nakayama, A. *Journal of Macromolecular Science, Pure and Applied Chemistry* **2002**, *A39*, 745–758.
- [126] Ding, L.; Xie, M.; Yang, D.; Song, C. *Macromolecules* **2010**, *43*, 10336–10342.
- [127] Morita, T.; Maughon, B. R.; Bielawski, C. W.; Grubbs, R. H. *Macromolecules* **2000**, *33*, 6621–6623.
- [128] Ji, S.; Hoye, T. R.; Macosko, C. W. *Macromolecules* **2004**, *37*, 5485–5489.
- [129] Xia, Y.; Verduzco, R.; Grubbs, R. H.; Kornfield, J. A. *J. Am. Chem. Soc.* **2008**, *130*, 1735–1740.
- [130] McLain, S. J.; Sauer, B. B.; Firment, L. E. *Macromolecules* **1996**, *29*, 8211–8219.

- 
- [131] Madkour, A. E.; Koch, A. H. R.; Lienkamp, K.; Tew, G. N. *Macromolecules* **2010**, *43*, 4557–4561.
- [132] Ji, S. X.; Hoye, T. R.; Macosko, C. W. *Polymer* **2008**, *49*, 5307–5313.
- [133] Matson, J. B.; Grubbs, R. H. *Macromolecules* **2010**, *43*, 213–221.
- [134] Pitet, L. M.; Hillmyer, M. A. *Macromolecules* **2011**, *44*, 2378–2381.
- [135] Scherman, O. A.; Ligthart, G. B. W. L.; Ohkawa, H.; Sijbesma, R. P.; Meijer, E. W. *Proc. Natl. Acad. Sci.* **2006**, *103*, 11850–11855.
- [136] Higley, M. N.; Pollino, J. M.; Hollembeak, E.; Weck, M. *Chem. Eur. J.* **2005**, *11*, 2946–2953.
- [137] Yang, S. K.; Ambade, A. V.; Weck, M. *Chem. Soc. Rev.* **2011**, *40*, 129–137.
- [138] Ambade, A. V.; Yang, S. K.; Weck, M. *Angew. Chem., Int. Ed.* **2009**, *48*, 2894–2898.
- [139] Yang, S. K.; Ambade, A. V.; Weck, M. *Chem. Eur. J.* **2009**, *15*, 6605–6611.
- [140] Ambade, A. V.; Burd, C.; Higley, M. N.; Nair, K. P.; Weck, M. *Chem. Eur. J.* **2009**, *15*, 11904–11911.
- [141] Yang, S. K.; Ambade, A. V.; Weck, M. *J. Am. Chem. Soc.* **2010**, *132*, 1637–1645.
- [142] Kurzhals, S.; Binder, W. H. *J. Polym. Sci., Part A: Polym. Chem.* **2010**, *48*, 5522–5532.
- [143] Yagci, Y.; Tasdelen, M. A. *Prog. Polym. Sci.* **2006**, *31*, 1133–1170.
- [144] Mahanthappa, M. K.; Bates, F. S.; Hillmyer, M. A. *Macromolecules* **2005**, *38*, 7890–7894.

- 
- [145] Saetung, N.; Campistrone, I.; Pascual, S.; Pilard, J. F.; Fontaine, L. *Macromolecules* **2011**, *44*, 784–794.
- [146] Bielawski, C. W.; Morita, T.; Grubbs, R. H. *Macromolecules* **2000**, *33*, 678–680.
- [147] Xie, M. R.; Kong, Y.; Han, H. J.; Shi, J. X.; Ding, L.; Song, C. N.; Zhang, Y. Q. *React. Funct. Polym.* **2008**, *68*, 1601–1608.
- [148] Liu, J. W.; Li, J. X.; Xie, M. R.; Ding, L.; Yang, D.; Zhang, L. Y. *Polymer* **2009**, *50*, 5228–5235.
- [149] Katayama, H.; Yonezawa, F.; Nagao, M.; Ozawa, F. *Macromolecules* **2002**, *35*, 1133–1136.
- [150] Katayama, H.; Urushima, H.; Nishioka, T.; Wada, C.; Nagao, M.; Ozawa, F. *Angew. Chem., Int. Ed.* **2000**, *39*, 4513–+.
- [151] Katayama, H.; Urushima, H.; Ozawa, F. *Chem. Lett.* **1999**, 369–370.
- [152] Katayama, H.; Urushima, H.; Ozawa, F. *J. Organomet. Chem.* **2000**, *606*, 16–25.
- [153] Mitchell, J. P.; Gibson, V. C.; Schrock, R. R. *Macromolecules* **1991**, *24*, 1220–1221.
- [154] Coca, S.; Paik, H.-j.; Matyjaszewski, K. *Macromolecules* **1997**, *30*, 6513–6516.
- [155] Bielawski, C. W.; Louie, J.; Grubbs, R. H. *J. Am. Chem. Soc.* **2000**, *122*, 12872–12873.
- [156] Quirk, R. P.; Kuang, J. *Polym. Int.* **1994**, *33*, 181–186.
- [157] Notestein, J. M.; Lee, L.-B. W.; Register, R. A. *Macromolecules* **2002**, *35*, 1985–1987.

- 
- [158] Myers, S. B.; Register, R. A. *Macromolecules* **2008**, *41*, 5283–5288.
- [159] Myers, S. B.; Register, R. A. *Macromolecules* **2010**, *43*, 393–401.
- [160] Wang, Y. Q.; Noga, D. E.; Yoon, K.; Wojtowicz, A. M.; Lin, A. S. P.; Garcia, A. J.; Collard, D. M.; Weck, M. *Adv. Funct. Mater.* **2008**, *18*, 3638–3644.
- [161] Katayama, H.; Fukuse, Y.; Nobuto, Y.; Akamatsu, K.; Ozawa, F. *Macromolecules* **2003**, *36*, 7020–7026.
- [162] Switek, K. A.; Chang, K.; Bates, F. S.; Hillmyer, M. A. *J. Polym. Sci., Part A: Polym. Chem.* **2006**, *45*, 361–373.
- [163] Sill, K.; Emrick, T. *J. Polym. Sci., Part A: Polym. Chem.* **2005**, *43*, 5429–5439.

## Chapter 2

# Linear Block Copolymers by Tandem Ring-opening Polymerizations\*

This chapter describes the design and synthesis of telechelic macromolecular initiators prepared by ring-opening metathesis polymerization of 1,5-cyclooctadiene. Subsequent ring-opening polymerization of D,L-lactide provided linear triblock copolymers with glassy ends and rubbery/semicrystalline midblocks. In addition to introducing the fundamental building blocks upon which all other chapters build, the triblock copolymers described in this chapter were explored as potential agents for toughening the brittle polyester poly(D,L-lactide). The synthesis of the triblock copolymers required combining mechanistically incompatible monomers; ring-opening metathesis polymerization is combined with ring-opening transesterification polymerization in a controlled manner.

---

\* Reproduced in part with permission from Pitet, L. M.; Hillmyer, M. A. *Macromolecules* **2009**, *42*, 3674–3680. Copyright 2009 American Chemical Society.

## 2.1 Introduction

The recent development and commercialization of ring-opening metathesis polymerization (ROMP) catalysts exhibiting unprecedented thermal and functional group tolerance have enabled the ready preparation of a versatile array of polymeric materials<sup>1–3</sup> including both telechelic and hemi-telechelic polymers that have functionality on either both or one chain terminus, respectively. Telechelics are an important class of polymeric materials in adhesive technology, polyurethane chemistry, and as precursors for the preparation of block copolymers.<sup>4</sup> Utilizing ROMP, end-functionalized macromolecular precursors for block copolymer synthesis may be prepared by (1) using functionalized metathesis catalysts,<sup>5–7</sup> (2) terminating a living ROMP reaction with an appropriately functionalized reagent (e.g., ethyl vinyl ether derivatives for Ru-based catalysts)<sup>8–10</sup> or (3) introducing a functionalized acyclic chain transfer agent (CTA) with a cyclic monomer.<sup>11</sup>

Linear block copolymers have been prepared from mechanistically incompatible monomers by combining ROMP of cyclic olefins with atom-transfer radical polymerization (ATRP),<sup>9,10,12–15</sup> reversible addition–fragmentation chain–transfer (RAFT) polymerization,<sup>16</sup> and anionic polymerization.<sup>17</sup> Likewise, hydroxyl terminal polymers are effective initiators for the ring-opening transesterification polymerization (ROTEP) of cyclic esters to produce block polymers. Combining ROMP with ROP was described by Katayama and coworkers, in which the vinyl termini of hemi-telechelic polynorbornene (PNB) were converted to hydroxyl groups that were subsequently used to initiate the ring-opening polymerization of  $\epsilon$ -caprolactone yielding diblock copolymers.<sup>14</sup>

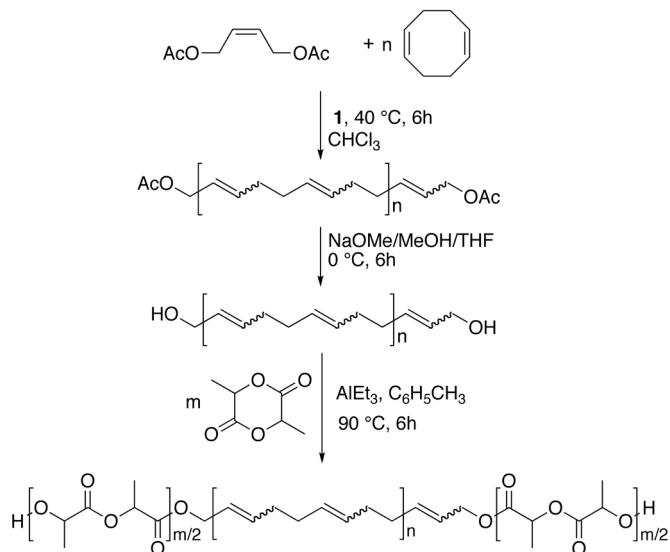
In the face of rising oil prices and voluminous landfills, increasing scrutiny is falling on petroleum-based plastic commodities, which has shifted the limelight towards materials comprising, for example, polylactide (PLA). This polymer boasts a renewable feedstock, biocompatibility and biodegradability and has proven suitable for a number of packaging and food containment applications.<sup>18–20</sup> Looming economic challenges and resource scarcity have inspired the use of PLA in an increasing array of commodity products, which has required specific tailoring of the

mechanical properties.<sup>20,21</sup> Amorphous PLA homopolymer has a high tensile modulus but suffers low toughness, a deficiency that may be addressed by exploiting some fundamental characteristics of block copolymers.<sup>22</sup> As an example, soft components that are tethered in triblock copolymers with an ABA architecture may impart elasticity and/or toughness to brittle materials as in the case of poly(styrene)-*b*-poly(butadiene)-*b*-poly(styrene) copolymers. Alternatively, triblocks may be introduced in two component blends to manipulate the dispersion, demonstrated in PLA blends with tougher materials such as polyethylene; block copolymers comprising the two components were introduced to improve the compatibilization.<sup>23–26</sup> The volume of literature exploring the synthesis and properties of PLA in the last decade<sup>27,28</sup> illustrates the growing importance of this environmentally friendly material.<sup>29</sup>

In this report, the synthesis of symmetric ABA triblock copolymers containing PCOD midblocks and PLA endblocks is described with the aim of enhancing the toughness of PLA-based copolymers. The synthesis requires a two-step process utilizing ROMP of 1,5-cyclooctadiene (COD) by the second generation Grubbs catalyst (1; benzylidene [1,3-bis(2,4,6-trimethylphenyl)-2-imidazolidinylidene]dichloro(tricyclohexylphosphine) ruthenium) in the presence of a CTA first, followed by ROP of D,L-lactide initiated by the terminal hydroxyl functionality in the PCOD precursor (Scheme 2.1). The morphological characteristics of these triblocks were examined using small-angle x-ray scattering (SAXS) and were compared with the theoretical phase behavior of linear triblock copolymers exhibiting narrow molecular weight distributions. The tensile properties of a series of triblocks with variable composition were examined and compared with those of the respective homopolymers.

Scheme 2.1

Synthesis of LCL triblock copolymers by sequential ring-opening polymerizations.



## 2.2 LCL Triblock Copolymers

The results of various aspects of synthesizing and characterizing the intended copolymer targets are presented here. This section is intended to convince the reader that the structures represented in Scheme 2.1 have been achieved. Moreover, the tensile properties are presented for triblock copolymers with a range of compositions. Finally, the thermal properties of the triblock copolymers are provided as measured by differential scanning calorimetry (DSC).



### 2.2.1 Synthesis of Triblock Copolymers

Preparation of hydroxy telechelic PCOD and PNB have been reported previously using a variety of methods including via addition of an acyclic CTA during ROMP of COD.<sup>30–37</sup> For example, basic hydrolysis of acetoxy groups at chain termini yields hydroxyl functional chains by using the appropriately substituted CTA.<sup>30,38,39</sup> Samples prepared by this approach exhibit high conversions and well-controlled degrees of polymerization; as such, this was chosen as the synthetic route for preparing the precursor macroinitiators leading to the triblock copolymers described in this study.

A single hydroxy telechelic PCOD sample was prepared. We employed low catalyst loadings ( $[\text{COD}]/[\text{catalyst}] = 15,000$ ), and thus the ratio of  $[\text{COD}]$  to  $[\text{CTA}]$  determines the final molecular weight of the PCOD homopolymer according to equation 2.1.

$$M_n = \frac{[\text{COD}]}{[\text{CTA}]} \cdot m_{\text{COD}} \cdot x_{\text{COD}} \quad (2.1)$$

where  $m_{\text{COD}}$  is the molar mass of the monomer and  $x_{\text{COD}}$  is the fractional conversion of COD, which was essentially quantitative ( $\approx 1$ ) based on  $^1\text{H}$  NMR spectroscopy of our reaction mixtures. The contribution of the CTA mass to the overall molecular weight is considered negligible in calculating theoretical  $M_n$  as it constitutes approximately 1.3 wt % of the resulting PCOD. The functional CTA we used was *cis*-1,4-diacetoxy-2-butene (DAB). Additionally, commercially available and freshly distilled COD monomer contain the isomer vinylcyclohexene (VCH), which acts as adventitious CTA.<sup>40</sup> A ratio of  $[\text{COD}]:[\text{DAB}] = 150$  was employed, making the DAB concentration equal to 0.67 mol%, while  $^1\text{H}$  NMR spectroscopy showed 0.16 mol% of VCH in the freshly distilled monomer. The combined concentrations of CTAs applied to equation 2.1 provided a theoretical  $M_n = 13.0 \text{ kg mol}^{-1}$ . The  $^1\text{H}$  NMR spectrum of AcO-PCOD-OAc revealed signals from both acetoxy and vinyl

endgroups, which were derived from the DAB and VCH, respectively. The calculated  $M_n$  of this precursor was  $16.4 \text{ kg mol}^{-1}$ , which suggests incomplete incorporation of CTA in the polymer. The molar ratio of [DAB] to [VCH] calculated before polymerization was equal to 4.2, compared to a value of 3.5 from the relative signals in the  $^1\text{H}$  NMR spectrum of the polymer, which suggests that VCH reacts more readily than does DAB. Using these quantities, the average number of functional end groups per polymer chain ( $F_n$ ) is calculated as  $F_n = 1.5$ . Therefore, there are substantial quantities of both monofunctional and non-functional chains that bear vinyl and/or cyclohexenyl moieties resulting from rapid secondary metathesis reactions throughout polymerization, although difunctional chains arguably constitute the majority of molecules. It is possible to attain  $F_n$  values approaching 2 with extensive purification of COD feedstock.<sup>40</sup> However, we forwent the procedure, being motivated by potential for practical applications using readily available starting materials.

Deprotection of the acetoxy termini using a solution of NaOMe in methanol/THF gave hydroxy telechelic PCOD (HO-PCOD-OH). Figures 2.1a and 2.1b show the size-exclusion chromatography (SEC) chromatograms for the telechelic PCOD samples before and after hydrolysis, respectively. The overlap between the two traces demonstrates the preservation of the overall characteristics. The  $M_n$  determined by  $^1\text{H}$  NMR spectroscopy after hydrolysis was  $15.6 \text{ kg mol}^{-1}$  in agreement with the acetoxy precursor molecular weight. The PDI values for the telechelic PCOD samples before and after hydrolysis were 1.80 and 1.72, respectively, as measured by SEC relative to polystyrene standards. There is a broad peak eluting between 23–25 mL in both samples presumably associated with a low level of low molecular weight cyclic oligomers.

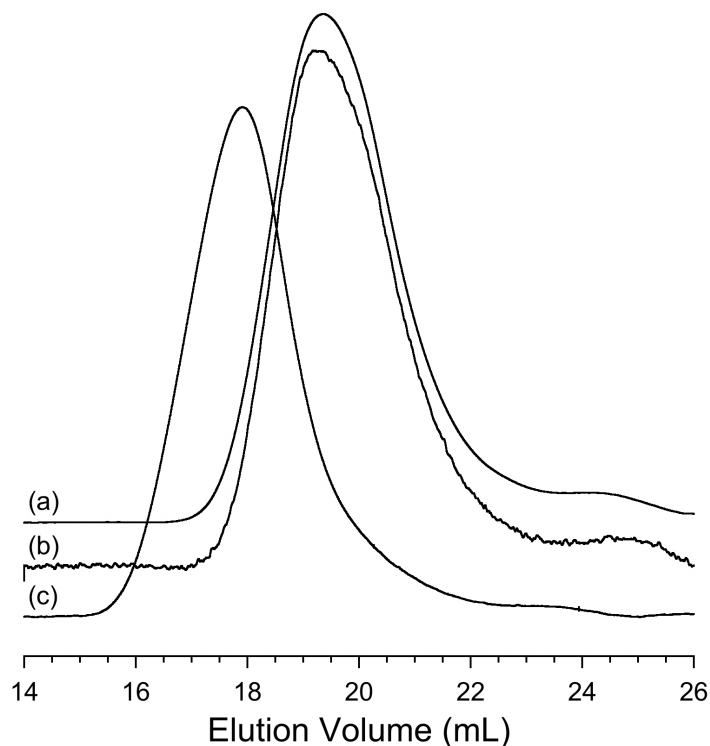


**Figure 2.1**

SEC chromatograms: (a) AcO-PCOD-OAc, (b) HO-PCOD-OH, (c) LCL (35-16-35) illustrating the incorporation of D,L-lactide into the polymer chains. The data in (c) are consistent with the absence of significant HO-PCOD-OH.

Poly(D,L-lactide)-poly(cyclooctadiene)-poly(D,L-lactide) [LCL] triblock copolymers were prepared by growing poly(D,L-lactide) from the telechelic PCOD precursor (Scheme 2.1). Triethyl aluminum was used to prepare macromolecular aluminum alkoxide species that effect initiation of ROP of various lactones and lactide.<sup>41-43</sup> The SEC chromatogram for sample LCL (35-16-35) [the numbers correspond to the number average molecular weights of each block in  $\text{kg mol}^{-1}$ ] is shown as a representative example in Figure 2.1c. Distinct peaks associated with unreacted PCOD were absent in all samples. The molecular characteristics of the LCL copolymers are summarized in Table 2.1.

**Table 2.1**

Molecular characteristics of telechelic PCOD precursors and LCL triblock copolymers.

Sample ID <sup>a</sup>	$f_{\text{PLA}}^{\text{b}}$	$M_n^{\text{c}}$ kg mol <sup>-1</sup>	PDI <sup>d</sup>	$T_m$ °C	$\Delta H_m^{\text{e}}$ J g <sup>-1</sup>	$X_{\text{(PCOD)}}^{\text{f}}$ %	$D^{\text{g}}$ nm	
							150 °C	35 °C
AcO-C-OAc	0.00	16.4	1.80					
HO-C-OH	0.00	15.6	1.72	26	69	80		
LCL (3.4-16-3.4)	0.24	22.5	1.55	22	40	68	32.4	32.0
LCL (5.6-16-5.6)	0.34	26.8	1.50	22	27	53	33.2	34.5
LCL (8.6-16-8.6)	0.44	32.9	1.60	24	20	49	38.5	38.5
LCL (13-16-13)	0.54	41.0	1.53	23	15	47	44.6	44.7
LCL (20-16-20)	0.65	56.4	1.70	21	6.6	28	49.1	53.9
LCL (35-16-35)	0.76	85.7	1.87	21	3.4	23	36.5	37.3
LCL (90-16-90)	0.89	195	1.40	19	1.3	19	43.6	44.3

(a) Sample ID corresponds to molecular weights of the respective blocks calculated by <sup>1</sup>H NMR spectroscopy (b) Volume fraction of PLA were calculated using the densities for the polymers at 25 °C;  $\rho_{\text{PLA}} = 1.25 \text{ g cm}^{-3}$  and  $\rho_{\text{PCOD}} = 0.89 \text{ g cm}^{-3}$  from references <sup>44</sup> and <sup>45</sup>, respectively. (c) Determined from integration of the corresponding repeat unit protons in <sup>1</sup>H NMR spectra relative to end-group signals of the precursor macromolecular initiator (d) Determined from SEC with CHCl<sub>3</sub> as the eluent at 35 °C, relative to narrow distribution polystyrene standards (e) Determined from integration of the melting endotherm on the second heat during DSC analysis (f) Crystallinity ( $X$ ) Calculated using  $\Delta H_m^0 = 85.2 \text{ J g}^{-1}$  for completely linear all *trans* poly(1,4-butadiene) and normalized to the midblock using weight fractions ( $w$ ) calculated from <sup>1</sup>H NMR spectroscopy [ $X_{\text{PCOD}} = \Delta H_m / (\Delta H_m^0 \cdot w_{\text{PCOD}})$ ] (g) Principle domain spacing determined by SAXS using the relation  $D^* = 2\pi/q^*$ .

Figure 2.2a shows the region of the <sup>1</sup>H NMR spectrum corresponding to the end-group methylene protons for the protected PCOD associated with AcO-PCOD-OAc. After hydrolysis of the acetate groups, the end-group methylene protons shift upfield. Complete hydrolysis is indicated by disappearance of signals at  $\delta = 4.1$  ppm (Figure 2b). The ring-opening polymerization of D,L-lactide using the hydroxyl groups as initiating moieties leads to a shift of the signal associated with the same protons to  $\delta = 4.50\text{--}4.70$  ppm as exemplified for LCL (13-16-13) in Figure 2c. An additional signal associated with the methine protons on the lactide chain ends is present at  $\delta = 4.31\text{--}4.41$  ppm. The full spectrum for LCL (13-16-13) is also shown in Figure 2. The integration ratio of the mid-methylene and end-group methine

protons is 2.07 (theoretically the ratio should be 2), consistent with the absence of adventitious initiator for the lactide polymerization, the absence of significant PLA homopolymer, and a high initiation efficiency.

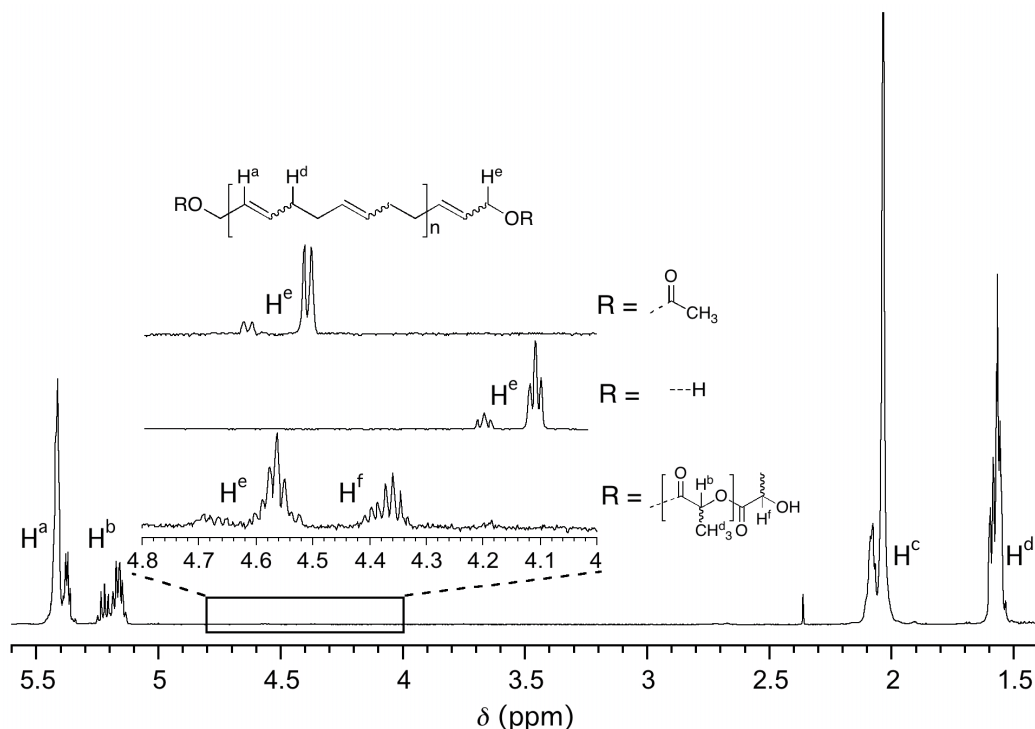


**Figure 2.2.**

$^1\text{H}$  NMR spectra for telechelic PCOD homopolymer precursors before (AcO-PCOD-OAc, top) and after (HO-PCOD-OH, middle) hydrolysis with signals corresponding to the *cis* and *trans* methylene end-group protons. The spectrum for sample LCL (13-16-13) is shown in full with the bottom inset region corresponding to the *cis* and *trans* mid methylene protons and the end-group methine protons on the PLA chains,  $\text{H}^f$ .

The ratio of *cis* to *trans* configuration for the double bonds in the precursors and triblocks is equal to 0.19 (84% *trans*), which is characteristic of ROMP polymerizations with extensive intermolecular chain transfer.

### 2.2.2 Thermal Analysis of LCL Triblock Copolymers

Samples in Table 2.1 were analyzed by DSC by first heating to 160 °C, annealing for 5 minutes at 160 °C, cooling to -100 °C at 10 °C  $\text{min}^{-1}$  and reheating

to 120 °C at 10 °C min<sup>-1</sup>. The data for the final reheating is shown in Figure 2.3. Consistent with microphase separation, glass transition signatures around 47 °C for the PLA blocks and -90 °C for the PCOD blocks were observed for all but highly compositionally asymmetric LCL samples. High *trans* PCOD is semi-crystalline and the melting temperature ( $T_m$ ) of the PCOD blocks was observed between 20 and 25 °C. The breadth of this transition is likely due to a distribution of crystallite sizes. The  $T_m$  values and percent crystallinities ( $X_{\text{PCOD}}$ ) are provided in Table 2.1.

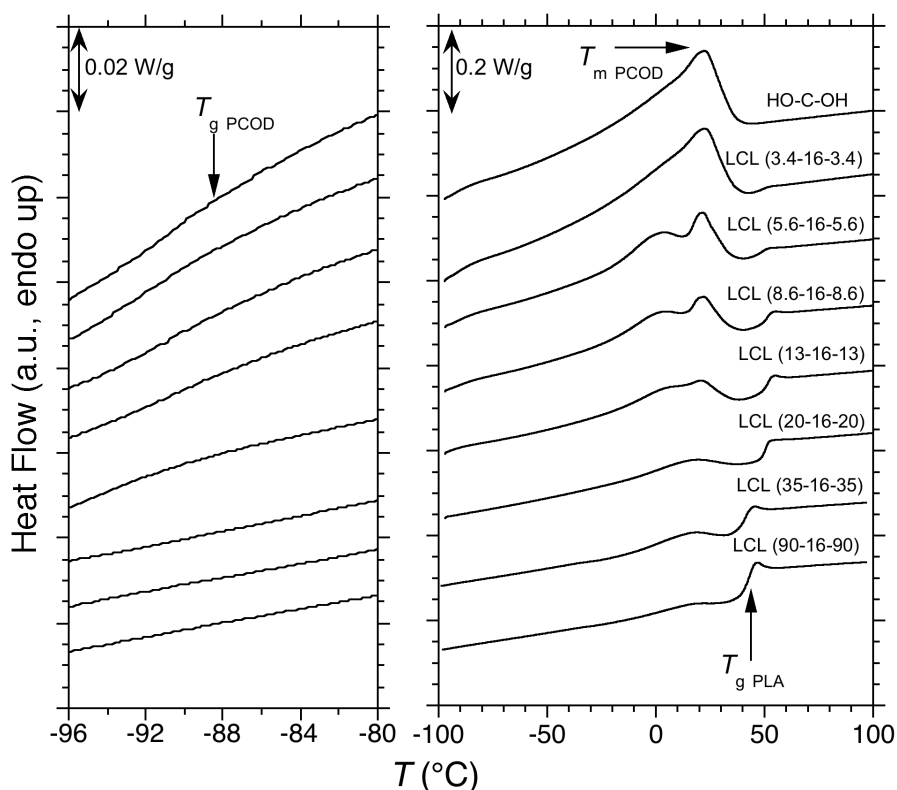


**Figure 2.3**

DSC traces for the LCL triblocks. The temperatures associated with characteristic transitions are indicated. Traces represent the second heat after annealing at 160 °C with a heating rate of 10 °C min<sup>-1</sup>.

A monotonic decrease in both crystallinity and  $T_m$  with increasing PLA content was observed. This could arise from the topological restriction imposed by the glassy PLA forcing confined crystallization in samples with majority PLA. Also, bimodality in the PCOD melting endotherm is clearly evident in samples LCL (13-

16-13), LCL (8.6-16-8.6), and LCL (5.6-16-5.6). There are two possible factors that contribute to this behavior. The relatively wide breadth of the peaks likely results from a broad distribution of trans-sequence lengths in the PCOD block.<sup>46</sup> Additionally, the large number of microdomains in the phase separated material causes crystallization during cooling by different mechanisms (i.e., hetero- vs. homogeneous nucleation).<sup>47,48</sup> Crystallites of two distinct size distributions likely exist, which manifests as multiple melting endotherms. This hypothesis is supported by the apparent absence of distinct endotherms in sample LCL (3.4-16-3.4), in which the crystalline PCOD occupies a continuous domain.

### 2.2.3 Morphological Characteristics of LCL Triblock Copolymers

Diblock copolymers can self-assemble into four classical equilibrium structures [lamellar (L), bicontinuous gyroid (G), hexagonally packed cylinders (C), and spheres on a body centered cubic lattice (S)], dependent on the composition and the degree of segregation, which is the product of the degree of polymerization,  $N$ , and the relative incompatibility of the species represented by the Flory-Huggins interaction parameter,  $\chi$ .<sup>49-54</sup> These structures may be identified by small-angle x-ray scattering.

One-dimensional SAXS patterns at both 150 °C and 35 °C for the triblock copolymers are illustrated in Figures 2.4a and 2.4b, respectively. The plots are presented as scattered intensity with respect to the scattering momentum vector  $q = 4\pi/\lambda(\sin \theta/2)$  where  $\theta$  is the scattering angle and  $\lambda$  is the wavelength of incident radiation. All LCL samples exhibited microphase separation as evidenced by a sharp principal peak ( $q^*$ ) at low scattering angle (Figure 2.4a). The predicted peak positions are indicated by arrows and correspond to the theoretically expected morphology at the specific volume fractions taking into consideration the architecture and the somewhat polydisperse nature of the samples.<sup>55</sup> The principal domain spacing ( $D^* = 2\pi/q^*$ ) values (Table 2.1) are consistent with variation in molecular weight, temperature, and morphological transitions.<sup>56</sup>

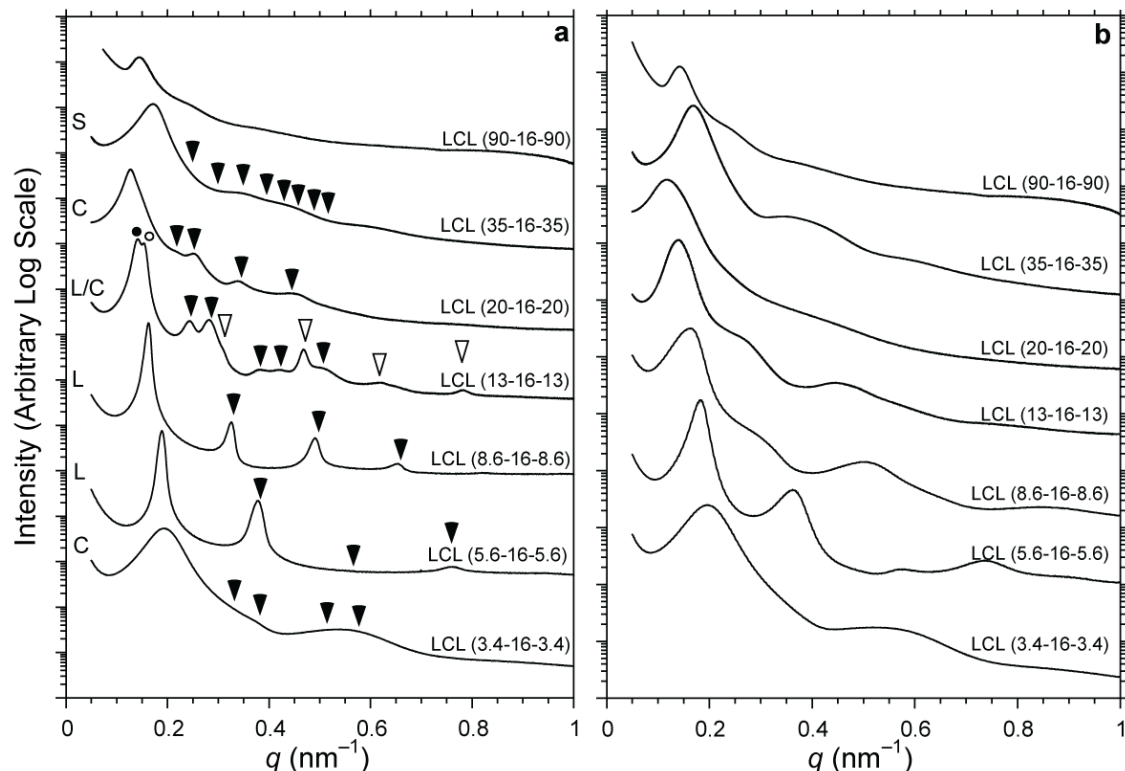


**Figure 2.4**

One-dimensional SAXS profiles for representative LCL triblock copolymers measured at (a) 150 °C after 5 min annealing times with the arrows indicating the predicted peak positions for the indicated morphologies [L = lamellae; C = cylinders; G = gyroid; S = spheres]. Sample LCL (13-16-13) exhibits coexisting morphologies with empty arrows indicating (L) and full arrows indicating (C), and (b) at 35 °C after cooling from 150 °C.

For the majority of samples, the principal spacing measured at 35 °C is larger than at 150 °C, consistent with increasing  $\chi$  with decreasing temperature.<sup>57,58</sup> The lowest molecular weight sample LCL (3.4-16-3.4) exhibits the smallest domain spacing at 32.4 nm (150 °C) and a SAXS profile consistent with hexagonally packed cylinders of PLA in a PCOD matrix. Both samples LCL (5.6-16-5.6) and LCL (8.6-16-8.6) have SAXS profiles consistent with a lamellar morphology. Sample LCL (13-16-13) appears to have coexisting lamellar and cylindrical morphologies at 150 °C. This is consistent with calculations that predict relatively large windows of coexisting C and L phases at large segregation strengths and when the minority component (PCOD) is the more polydisperse block.<sup>59</sup> The SAXS profile for sample



LCL (20-16-20) is consistent with a matrix of PLA with cylinders of PCOD, while that of both LCL (35-16-35) and LCL (90-16-90) are consistent with being dispersions of PCOD spheres in a PLA matrix.

$D^*$  increases monotonically with  $M_n$  until the apparent transition from cylinders of PCOD in a PLA matrix [LCL (20-16-20)] to spheres of PCOD in a PLA matrix [LCL (35-16-35)]. The decrease in  $D^*$  with increasing  $M_n$  going from LCL (20-16-20) to LCL (35-16-35) is consistent with the established dependence of domain spacing on morphology;<sup>56</sup> decrease in  $D^*$  associated with traversing the C  $\rightarrow$  S phase boundary apparently outweighs the opposing increase in  $D^*$  with increasing molecular weight.

The morphologies of LCL (35-16-35) and LCL (90-16-90) are believed to be an array of PCOD spheres embedded in a PLA matrix despite the relatively ill-resolved high order reflections in Figure 4 for these samples. LCL (90-16-90) exhibits a sharp primary peak at  $q^* = 0.149$  ( $D^* = 42$  nm) with several additional broad peaks at higher  $q$ -values. This is typical of a disordered array of micelles in which the minority component is dispersed in a “solution” of the majority component. We analyzed the scattering for LCL (90-16-90) using the spherical form factor shown in equation 2.2.

$$P(q) = \left( \frac{3}{(qR)^3} \right)^2 (\sin qR - qR \cos qR)^2 \quad (2.2)$$

The cylinder radius ( $R_c$ ) was initially calculated for samples LCL (20-16-20) ( $R_c = 17.6$  nm) and LCL (13-16-13) ( $R_c = 18.3$  nm) and it was assumed that this value would be approximately equal to the radii of the spheres in samples LCL (35-16-35) and LCL (90-16-90). The value  $R_c$  was extracted for these two cylindrical samples using  $D^*$  from SAXS, the volume fraction of PCOD ( $f_c$ ), and the expression  $R_c = (2f_c D^{*2} / \sqrt{3\pi})^{1/2}$ . The simulated form factor scattering corresponding to eq 2.2 with  $R = 16$  nm is provided with the actual scattering pattern obtained for sample LCL

(90-16-90) in Figure 2.5. This value ( $R = 16$  nm) provided the best match to the experimental pattern, suggesting the sphere radii are slightly smaller than the cylinder radii. This observation is consistent with a larger interfacial curvature and thus increased stretching experienced by the minority component in spheres compared to cylinders.<sup>56</sup> The minima in the fit correspond reasonably well with several peak minima in the actual scattering in agreement with the implicated morphology. Sample LCL (35-16-35) also exhibited form-factor scattering consistent with the indicated block size and proposed morphology.

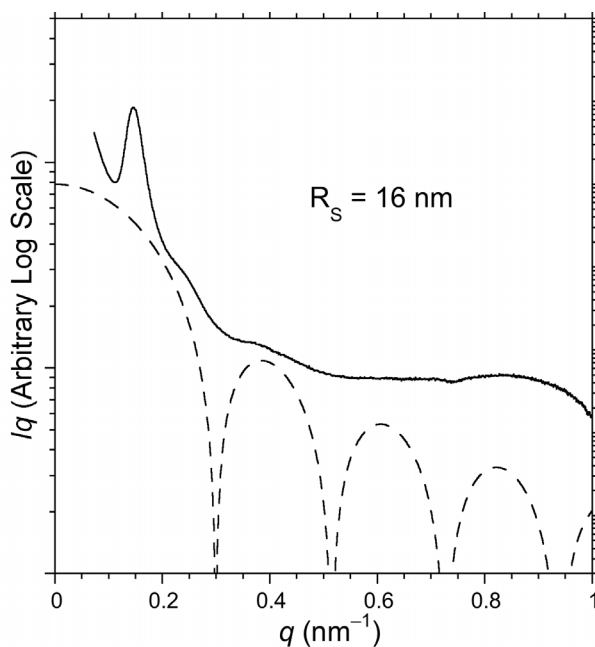


**Figure 2.5.**

Form factor scattering simulation (---) correlated with actual scattering data (—) for sample LCL (90-16-90). The form-factor fit utilizes 16 nm sphere radius based on the actual domain spacing from samples adopting the cylindrical morphology.

Transmission electron microscopy (TEM) images for samples LCL (8.6-16-8.6) and LCL (90-16-90) were acquired to corroborate the SAXS data (Figure 2.6). The sample LCL (8.6-16-8.6) was aligned using a channel-die as described previously,<sup>60,61</sup> and microtoming was performed perpendicular to the flow direction at cryogenic temperature ( $-140$  °C). The lamellar spacing from TEM (34 nm)

---

agrees reasonably well with  $D^*$  from the SAXS data (38.5 nm). Sample LCL (90-16-90) appears to consist of a disorganized array of spherical PCOD domains (dark) surrounded by the unstained PLA (light). The sphere diameter is approximately 30 nm, agreeing reasonably well with the value obtained from form factor modeling in the SAXS (see Figure 2.5 and equation 2.2).

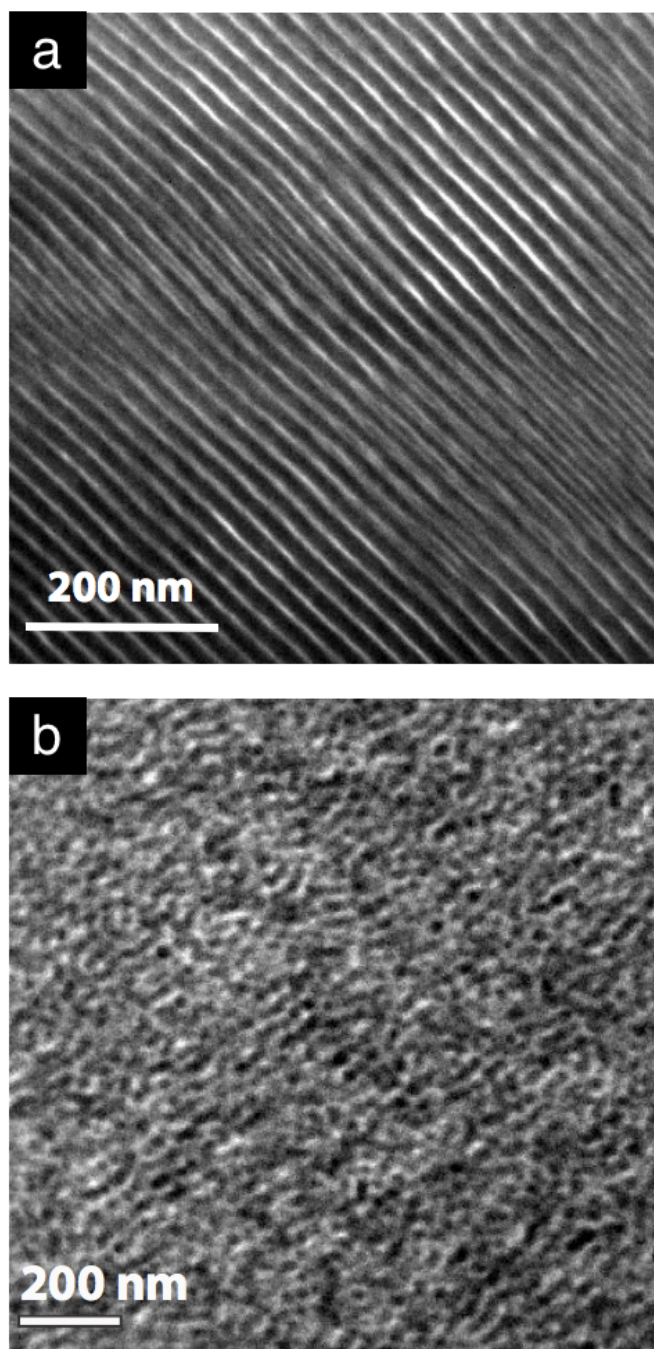


**Figure 2.6**

TEM images (stained with  $\text{OsO}_4$ ) at different magnifications for (a) sample LCL (8.6-16-8.6) showing lamellae of PCOD (dark) and PLA (light) and (b) LCL (90-16-90) showing a disordered array of PCOD (dark) spheres in a matrix of PLA (light).

### 2.2.4 Mechanical Properties of LCL Triblock Copolymers

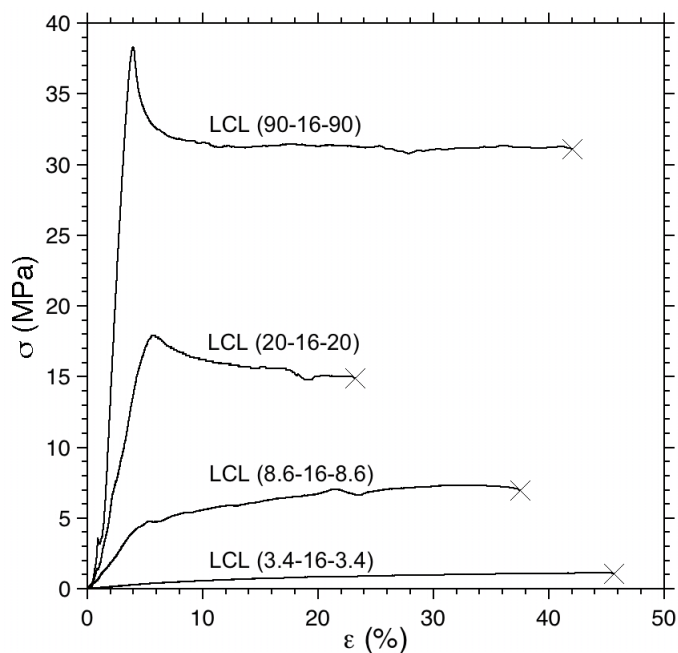
PLA property modification is the focus of many research efforts, the more recent of which have been thoroughly reviewed.<sup>22</sup> This study exploits a soft ( $T_g = -90$  °C;  $T_m = 20$  °C), semi-crystalline component tethered on either end by PLA to improve the toughness while attempting to maintain a high yield strength and modulus compared to PLA homopolymer. This method has proven successful as exemplified in the case of poly(cyclohexylethylene)-*b*-polyethylene-*b*-poly(cyclohexylethylene), in which a semi-crystalline midblock is flanked by glassy endblocks.<sup>62,63</sup>

The LCL tensile properties are summarized in Table 2.2. In each experiment, dogbones were prepared by melt pressing at 160 °C and 1000 psi followed by rapid cooling to 25 °C (ca. 30 °C min<sup>-1</sup>) and then uniaxial extension was applied at a rate of 2 mm min<sup>-1</sup> until the samples fractured. A representative set of tensile results is illustrated in Figure 2.7 for samples LCL (3.4-16-3.4), LCL (8.6-16-8.6), LCL (20-16-20) and LCL (90-16-90). The tensile modulus of amorphous PLA ranges from 2 to 4 GPa depending on processing conditions and molecular weight.<sup>64,65</sup> For amorphous PLA having molecular weights between 50 and 200 kg mol<sup>-1</sup>, the tensile strength was measured in the range of 40 to 50 MPa. However, typical elongation when fracture occurs ranges from approximately 3 to 10% for amorphous PLA homopolymer.<sup>22,66</sup>

**Table 2.2**

Mechanical properties from tensile testing of triblock LCL copolymers

Sample ID	Modulus	$\sigma_b$	$\epsilon_b$
	MPa	MPa	%
LCL (3.4-16-3.4)	$5.6 \pm 2.0$	$0.9 \pm 0.2$	$43 \pm 7$
LCL (5.6-16-5.6)	$50.7 \pm 5.2$	$2.7 \pm 0.3$	$18 \pm 6$
LCL (8.6-16-8.6)	$89 \pm 30$	$6.8 \pm 0.5$	$36 \pm 5$
LCL (13-16-13)	$308 \pm 48$	$11 \pm 2$	$33 \pm 27$
LCL (20-16-20)	$448 \pm 170$	$17 \pm 3$	$32 \pm 41$
LCL (35-16-35)	$864 \pm 224$	$20 \pm 4$	$180 \pm 170$
LCL (90-16-90)	$1270 \pm 380$	$33 \pm 1$	$42 \pm 17$

**Figure 2.7.**

Tensile measurements for selected LCL triblock copolymers presented as engineering stress ( $\sigma = F/A$ ) as a function of engineering strain percent ( $\epsilon = 100 \times \Delta L/L_0$ ), showing the progression of tensile modulus, yield strength, and tensile strength. The fracture point is represented by ( $\times$ ).

The modulus, tensile strength, and yield strength all increase monotonically with increasing molecular weight of the LCL samples. This can be attributed to increasing PLA content and molecular weight. Interestingly, neither the yield strain nor strain at break exhibited noticeable dependence on composition or molecular weight. Of notable exception is sample LCL (35-16-35) having an average  $\epsilon_b$  value of 180%, with an uncertainty of equal magnitude. This feature stems from three of the measurements having strain beyond 600%, while the remaining samples behaved similarly to the representative examples shown in Figure 2.8 with elongations between 30–50%. The samples with the highest PLA content exhibit the largest modulus, tensile strength, and yield strength values with ultimate elongations an order of magnitude greater than typical values for PLA homopolymer. Most notably, the sample LCL (90-16-90) has a modulus of 1.3 GPa, an average elongation of 42%, a yield strength of 38 MPa, and tensile strength of 33 MPa. These values are consistent with significant toughness in a sample of PLA containing less than 10 wt% of a rubbery component.

### 2.3 Poly[D,L-lactide-*b*-(cyclooctene-*s*-norbornene)-*b*-D,L-lactide] triblock copolymers

It is desirable to have ultimate control of each characteristic in the triblock system derived from the transformative polymerization from ROMP to ROTEP. Keeping the biorenewable component PLA, great advantage could be gained from tailoring the physical behavior of the midblock in the symmetric triblock. It was demonstrated that triblocks containing the glassy PLA end-blocks hold tremendous promise for creating partially renewable resource materials with enhanced toughness compared with pure PLA homopolymer. Therefore, the protocol for tandem ring-opening polymerizations was investigated further. The challenge of increasing the toughness demands the molecular design of new systems. The protocol offers a great deal of freedom with respect to component selection; the Ru-based ROMP reaction has been shown suitable for countless different monomers,

each embodying unique physical characteristics. For example, the thermal properties may be fine-tuned by appropriate monomers selection.

Indeed, architectural control can be improved by enriching the content of triblock copolymer, which was compromised by the adventitious CTA vinylcyclohexene contained in the COD feedstock. This contaminant proves difficult to remove with conventional purification techniques such as distillation or column chromatography. The non-functional CTA acts detrimentally toward achieving perfectly difunctional macro-initiator (i.e., HO–polymer–OH;  $F_n = 2$ ). This hurdle can be easily addressed by changing to a monomer that is easily purified, and free of isomers that may act as CTA. One such monomer is *cis*-cyclooctene (COE), which is nearly identical to COD, having one fewer unsaturation per molecule. The replacement of COD with COE under identical polymerization conditions has been successfully demonstrated, leading to essentially pristine triblocks after subsequent ROTEP of the biorenewable lactide monomer. These molecules are discussed extensively in Chapter 3 and in reference 67.<sup>67</sup>

Precise tailoring of thermal properties was illustrated by designing an ROM copolymerization between two commercially available cycloolefins. Extensive chain-transfer forms the basis for which the telechelic architecture is accessible. As such, statistical distributions might be expected for certain monomers in an ROM copolymerization when two components have reactive sites (i.e., alkenes) in the backbone with equal accessibility; sterically imposing substituents might cause substantial deviation from perfectly statistical distributions. Accessibility to statistically random copolymers for tailoring the physical characteristics in the PLA-containing block copolymers is fascinating, and the distribution is therefore of paramount importance. The copolymerization was designed to have components with considerably different (1) spatial arrangement about the reactive site to evaluate the propensity toward chain-transfer and (2) thermal characteristics between the respective homopolymers.

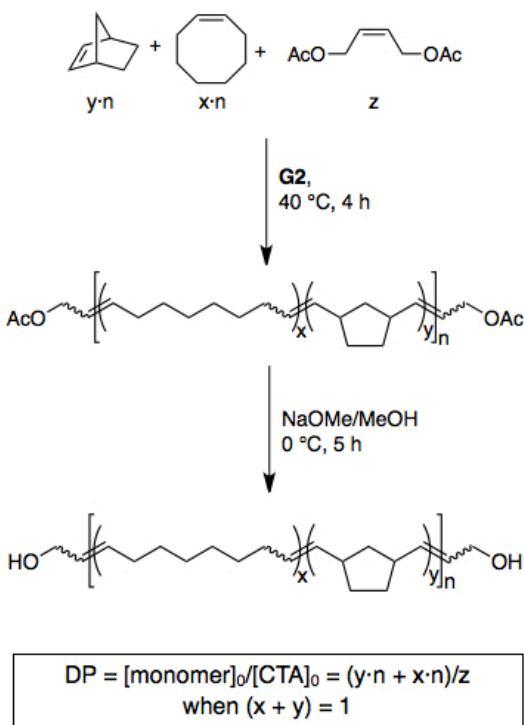


### 2.3.1 Synthesis of Statistical Telechelic poly(COE-s-NB) Copolymers

Considering the requirements initially set forth to efficiently investigate the copolymerization, two commercially available monomers *cis*-cyclooctene (COE) and norbornylene (NB; bicyclo[2.2.1]-hept-2-ene) were chosen. The statistical copolymerization was conducted under conditions identical to the COD ROP previously discussed (Scheme 2.2).

#### Scheme 2.2

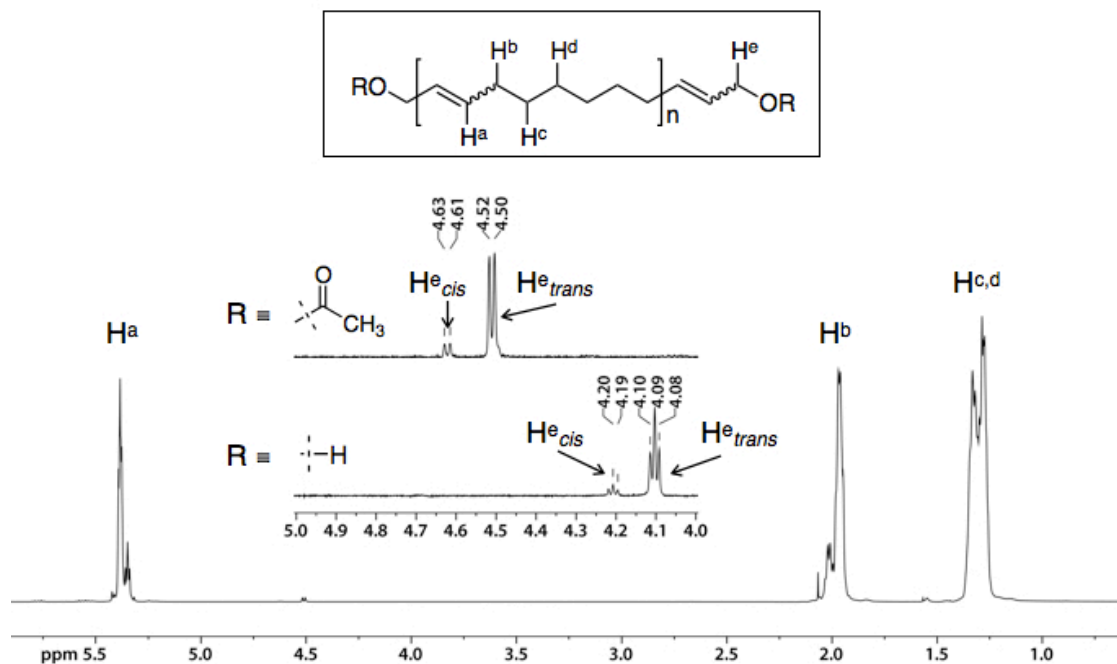
Statistical copolymerization of COE and NB by ROP-CT with 1,4-diacetoxy-2-butene CTA followed by hydrolysis of end-groups to give hydroxy-telechelic copolymer.



Poly(*cis*-cyclooctene) (PCOE) homopolymer has a completely linear hydrocarbon backbone, which results in semi-crystallinity owing to the highly regular structure (see thermal characteristics section below). Connoting substantial flexibility, PCOE has a low  $T_g$  that is commensurate with similar linear (largely methylene repeating units) hydrocarbon polymers like polyethylene ( $T_g \approx -120$  °C), 1,4-polybutadiene ( $T_g \approx -100$  °C) and polyisobutylene ( $T_g \approx -75$  °C), for example. Poly(norbornene) (PNB) homopolymer is a hydrocarbon with cyclopentane rings within the backbone structure, which instills significant rigidity to the structure. The cycle-containing backbone structure results in an amorphous polymer having  $T_{g,NB} \approx 45$  °C.<sup>38</sup>

Several statistical copolymers were synthesized and investigated for the monomer distribution by evaluating the thermal transitions. Functionality of the chain termini was monitored to evaluate the efficacy of molar mass control (e.g., degree of polymerization,  $N_{total}$ ) using a functional CTA. Ultimately, functionalization analogous to the LCL triblock copolymers was desired to perform subsequent polymerization of D,L-lactide initiated by the hydroxyl termini. Identical protocol conducted with the acetoxy-protect CTA provides an ideal situation for comparing molecular characteristics by <sup>1</sup>H NMR spectroscopy and examining the relative efficacy of incorporating two components with contrasting steric features.

Homopolymer PCOE was prepared by the ROMP–chain-transfer (ROMP–CT) protocol using 1,4-diacetoxy-2-butene CTA, followed by hydrolysis to afford hydroxyl functionality. The target  $N_{total}$  was 150, while the measured  $N$  was 140 before hydrolysis and 147 after. The <sup>1</sup>H NMR spectrum of homopolymer PCOE is shown in Figure 2.8 with the inset accentuating the same methylene protons associated with the end-group both before and after hydrolysis. The end-group signals are identical to the PCOD analogs previously reported (Figure 2.8).

**Figure 2.8**

Molecular structure and  $^1\text{H}$  NMR spectrum for PCOE homopolymer from ROMP-CT of COE with DAB CTA both before (*top* inset) and after (*bottom* inset) basic hydrolysis to afford hydroxyl telechelic PCOE.

Each hydroxyl-telechelic copolymer was synthesized with a target  $N_{\text{total}} = 200$ . The molar masses of the monomers ( $m_i$ )<sup>†</sup> are comparable, and the overall molecular weight targeted for each copolymer therefore fluctuates by less than 10 % across the entire potential composition spectrum (i.e., from 100% PCOE to 100% PNB). Statistical copolymers were synthesized with targeted mole fractions of PNB equal to 0.30, 0.50, 0.60 and 0.70 (Table 2.3). The polymers are identified by the nomenclature poly(COE<sub>x</sub>-s-NB<sub>y</sub>), where the quantities  $x$  and  $y$  refer to the mole percent of the respective blocks (i.e.,  $x + y = 100$ ) as measured by  $^1\text{H}$  NMR spectroscopy.

<sup>†</sup>  $m_{\text{COE}} = 110 \text{ g mol}^{-1}$ ;  $m_{\text{NB}} = 94 \text{ g mol}^{-1}$

**Table 2.3**Molecular characteristics of statistical copolymers poly(COE<sub>x</sub>-*s*-NB<sub>y</sub>)

Sample ID	N <sub>target</sub> <sup>a</sup>	NMR			n <sub>NB</sub> <sup>c</sup>
		N <sub>COE</sub> <sup>b</sup>	N <sub>NB</sub> <sup>b</sup>	N <sub>total</sub> <sup>b</sup>	
PCOE	150	147	0	147	0
poly(COE <sub>70</sub> - <i>s</i> -NB <sub>30</sub> )	200	152	66	218	0.30
poly(COE <sub>50</sub> - <i>s</i> -NB <sub>50</sub> )	200	111	115	226	0.51
poly(COE <sub>40</sub> - <i>s</i> -NB <sub>60</sub> )	200	87	137	224	0.61
poly(COE <sub>30</sub> - <i>s</i> -NB <sub>70</sub> )	200	64	161	226	0.71

<sup>a</sup> calculated from the molar ratio of the combined monomer to the CTA *cis*-1,4-diacetoxy-2-butene. <sup>b</sup> degrees of polymerization calculated from the integration of the respective signals associated with the different repeat units accessed by <sup>1</sup>H NMR spectroscopy. <sup>c</sup> mol fraction of PNB calculated from the degrees of polymerization of the respective repeating units determined by <sup>1</sup>H NMR spectroscopy (n<sub>NB</sub> = N<sub>NB</sub>/N<sub>total</sub>).

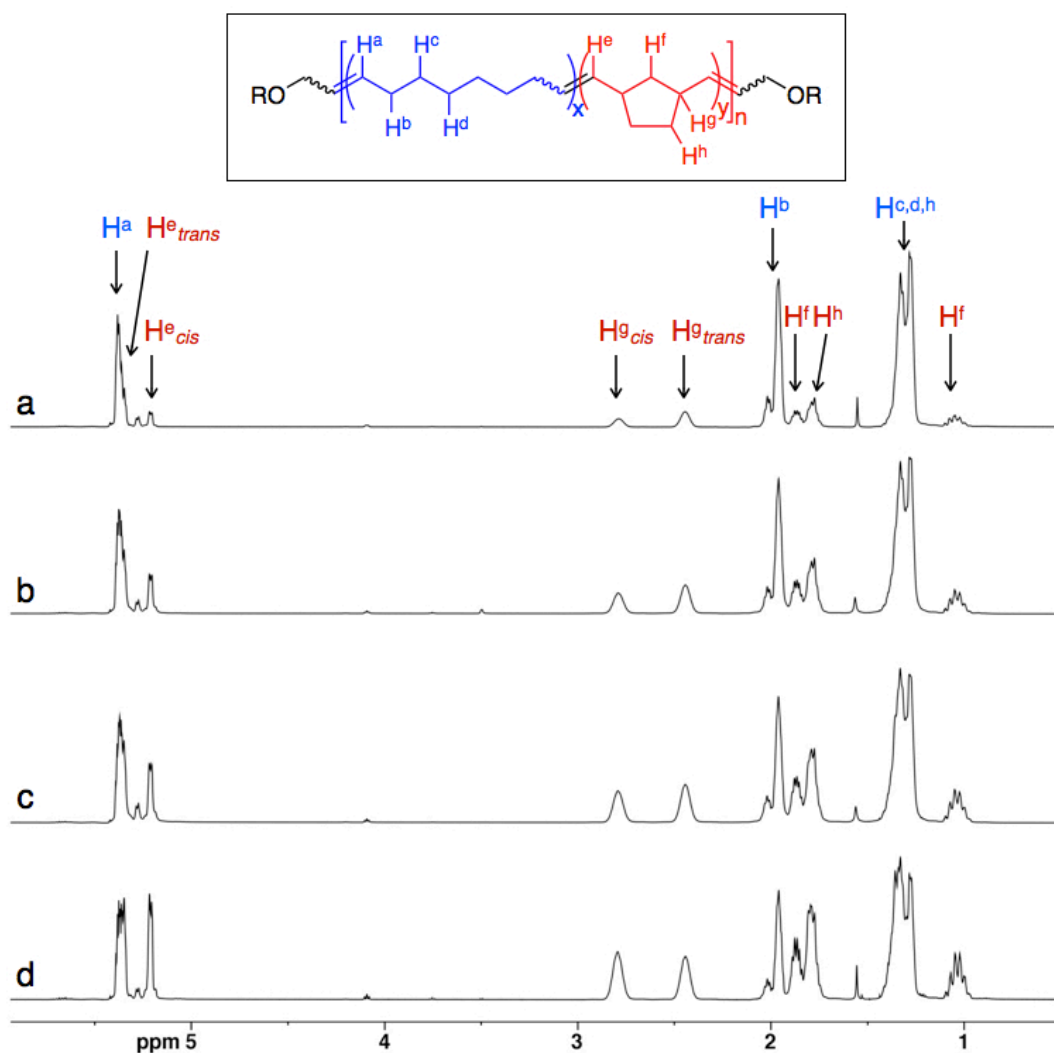


**Figure 2.9**

Stacked <sup>1</sup>H NMR spectra for four statistical copolymers poly(COE<sub>x</sub>-s-NB<sub>y</sub>) showing the relative intensity changes for characteristics signals from PCOE (blue) and PNB (red), corresponding to composition targets (a)  $x = 70$ ,  $y = 30$ ; (b)  $x = 50$ ,  $y = 50$ ; (c)  $x = 40$ ,  $y = 60$ ; (d)  $x = 30$ ,  $y = 70$ .

Compositions were determined by comparing the integration of signals from protons associated with the different repeat units (Figure 2.9). The intensities of proton signals associated with PNB clearly increase with the NB monomer feedstock concentration. Values of  $N_{\text{COE}}$  and  $N_{\text{NB}}$ , the sum of which is equal to  $N_{\text{total}}$ , agree quite closely with the targeted values  $N_{\text{target}}$  (Table 2.3). The molar masses were targeted assuming quantitative monomer consumption, and equal incorporation of the two monomeric species. Indeed, the quantities measured from

$^1\text{H}$  NMR spectroscopy all agree within 1% of the targeted compositions, and the experimentally determined molar masses are each within 15% of the  $N_{\text{target}}$  of 200. These results confirm high cross-metathesis reactivity between the polymer chains and the CTA, and nearly complete monomer consumption.

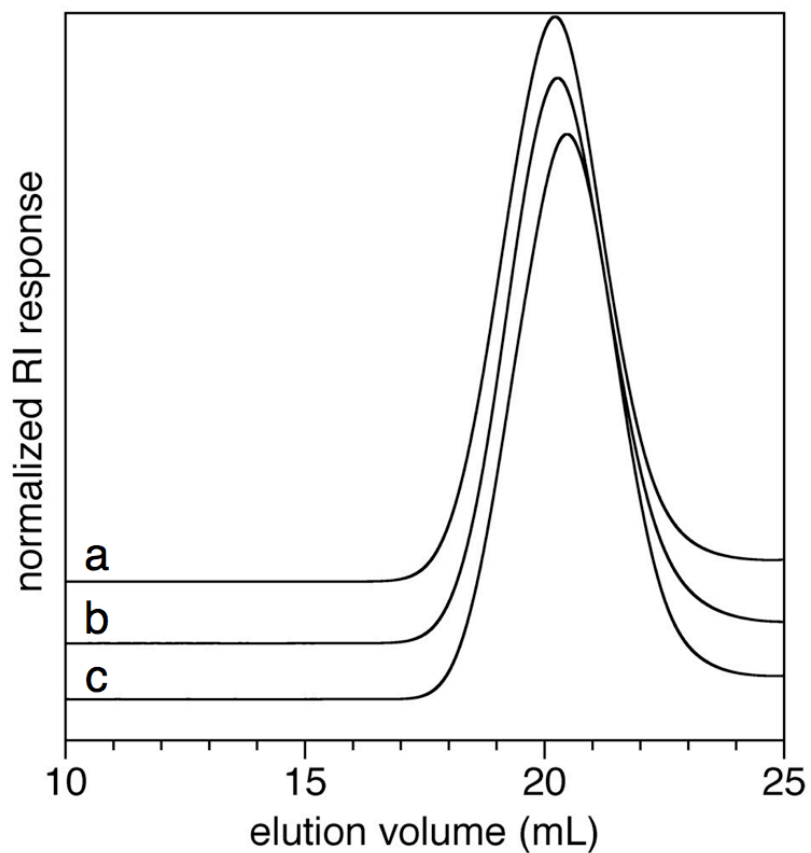


**Figure 2.10**

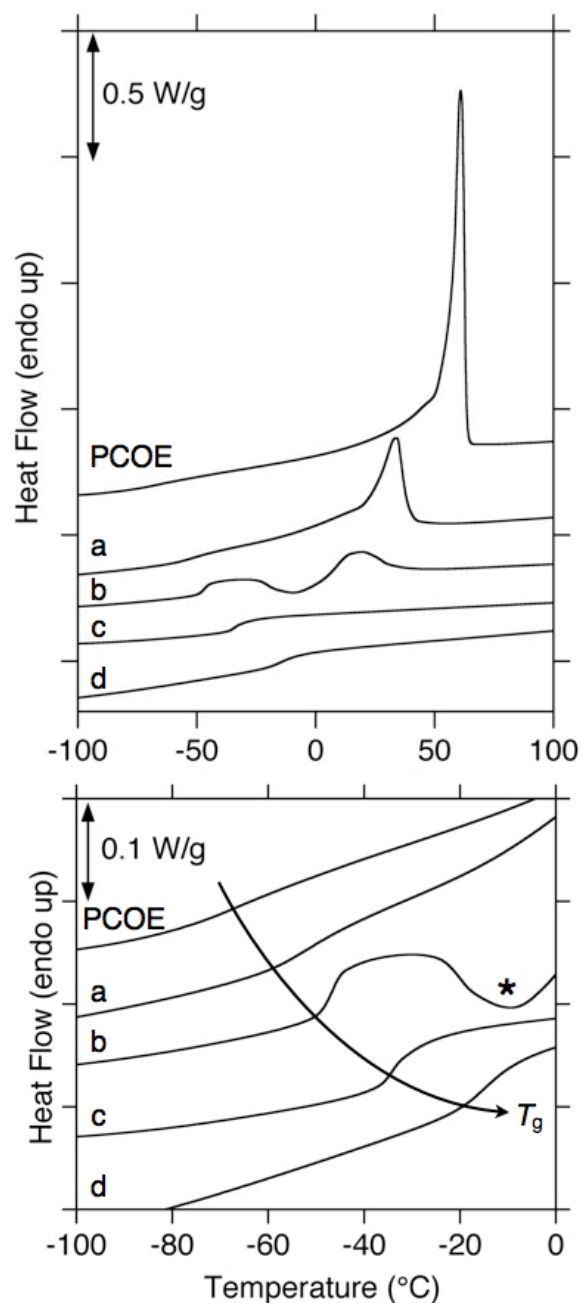
Chromatograms from SEC analysis for poly( $\text{COE}_x\text{-}s\text{-NB}_y$ ) with targeted compositions (a)  $x = 70$ ,  $y = 30$ ; (b)  $x = 50$ ,  $y = 50$ ; (c)  $x = 40$ ,  $y = 60$ .

### 2.3.2 Thermal Properties of poly(COE-*s*-NB) Statistical Copolymers

Thermal behavior of the poly(COE<sub>*x*</sub>-*s*-NB<sub>*y*</sub>) copolymers were analyzed by DSC in the temperature range  $-120\text{ }^{\circ}\text{C}$  to  $+120\text{ }^{\circ}\text{C}$  at a heating rate of  $10\text{ }^{\circ}\text{C min}^{-1}$  (Figure 2.11). The melting endotherm associated with PCOE homopolymer has a maximum in heat flow occurring at  $+61\text{ }^{\circ}\text{C}$  with a melting enthalpy corresponding to approximately 30% crystallinity ( $X$ ) according to  $X = (\Delta H_m/\Delta H_m^0) \cdot 100$ .<sup>‡</sup> Sample poly(COE<sub>70</sub>-*s*-NB<sub>30</sub>) shows diminished melting enthalpy corresponding to  $X = 9\%$ , a depressed  $T_m$  equal to  $34.4\text{ }^{\circ}\text{C}$ , and a single  $T_g$  intermediate between the two PNB and PCOE homopolymers at  $-52\text{ }^{\circ}\text{C}$ . Further decreasing the PCOE composition in sample poly(COE<sub>50</sub>-*s*-NB<sub>50</sub>) causes a single, correspondingly higher  $T_g = -46\text{ }^{\circ}\text{C}$ , and a melting endotherm with  $T_m = 25\text{ }^{\circ}\text{C}$  upon heating after cold crystallization is observed (\* in Figure 2.11). Subsequent cooling at a rate of  $10\text{ }^{\circ}\text{C min}^{-1}$  did not cause crystallization. Sample poly(COE<sub>40</sub>-*s*-NB<sub>60</sub>) contrasted with the absence of any crystallization under the conditions of DSC analysis, and contained a  $T_g$  of  $-34\text{ }^{\circ}\text{C}$ . Likewise, sample poly(COE<sub>30</sub>-*s*-NB<sub>70</sub>) was completely amorphous with a correspondingly higher  $T_g = -15\text{ }^{\circ}\text{C}$ . Table 2.4 contains a summary of the thermal transition associated with the hydroxy-telechelic statistical copolymers.

---

<sup>‡</sup>  $\Delta H_m^0$  for PCOE (polyoctenamer) is the theoretical enthalpy for a perfectly crystalline sample, equal to  $216\text{ J g}^{-1}$  according to ref. [46] Schneider, W. A.; Müller, M. F. *J. Mol. Catal.* **1988**, 46, 395–403.

**Figure 2.11**

Thermograms from DSC analysis for hydroxy-telechelic PCOE homopolymer and poly(COE<sub>x</sub>-*s*-NB<sub>y</sub>) statistical copolymers with (a)  $x = 70$ ,  $y = 30$ ; (b)  $x = 50$ ,  $y = 50$ ; (c)  $x = 40$ ,  $y = 60$ ; (d)  $x = 30$ ,  $y = 70$ . Temperature ranges are from  $-100$  to  $+100$  °C (*top*) and  $-100$  to  $0$  °C (*bottom*) to accentuate the glass transitions by magnifying the heat flow axis. \* indicates cold crystallization.



**Table 2.4**Thermal characteristics of hydroxyl-telechelic PCOE and poly(COE<sub>x</sub>-s-NB<sub>y</sub>)

Sample ID	$T_g$ (°C) <sup>a</sup>	$T_m$ (°C) <sup>b</sup>	$\Delta H_m$ (J g <sup>-1</sup> ) <sup>c</sup>	$X$ (%) <sup>d</sup>
PCOE	-70	60.7	65.5	30.3
poly(COE <sub>70</sub> -s-NB <sub>30</sub> )	-51.9	34.4	20.3	9.4
poly(COE <sub>50</sub> -s-NB <sub>50</sub> )	-46.3	25.0		
poly(COE <sub>40</sub> -s-NB <sub>60</sub> )	-34.1			
poly(COE <sub>30</sub> -s-NB <sub>70</sub> )	-15.3			

<sup>a</sup>  $T_g$  taken as the midpoint of the inflection points. <sup>b</sup>  $T_m$  taken as the temperature at which the maximum in heat flow of melting endotherm occurs. <sup>c</sup> integration of melting endotherm. <sup>d</sup> calculated by  $\Delta H_m/\Delta H_m^0 \cdot 100$

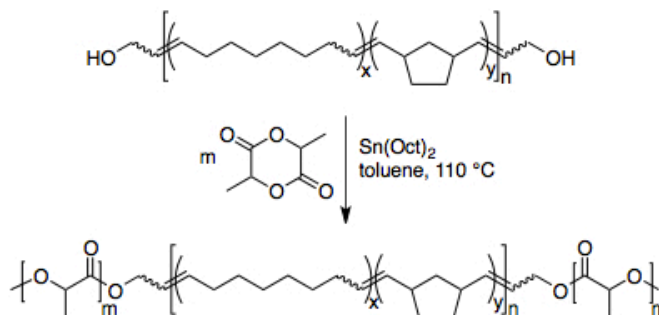
Including NB monomer in the polymerization mixture causes a drastic decline in the degree of crystallinity with increasing NB concentration. A depression of  $T_m$  and of crystallinity would be expected in block copolymers containing a semi-crystalline block, as observed by several thorough studies using DSC. A block structure hypothetically derived from a copolymerization in which one component polymerizes faster than another, and absent of chain-transfer reactions cannot be unambiguously dismissed based upon the melting/crystallization data alone. However, the strong dependence of  $T_g$  on composition and the appearance of a single  $T_g$  for all samples in the observed composition range strongly suggest a statistical distribution of repeat units. This method allows specific tailoring of the  $T_g$  and complete suppression of crystallization over a wide temperature range owing to the large disparity between  $T_g$  of the corresponding homopolymers.

### 2.3.3 Synthesis of L-CN-L Triblock Copolymers

Seeking to suppress crystallization and access an amorphous midblock with a low  $T_g$ , the sample poly(COE<sub>30-s</sub>-NB<sub>70</sub>) was initially chosen to use as macroinitiator for subsequent ROTEP of D,L-lactide in forming L-CN-L triblock copolymers. An identical protocol was used for the chain extension initiated from the hydroxyl termini, with the exception of a different catalyst. The previous Al(Et)<sub>3</sub> catalyst was substituted for stannous octanoate [tin(II) 2-ethylhexanoate; Sn(Oct)<sub>2</sub>] based on convenience (shorter polymerization time; less susceptibility to oxidative degradation – Al(Et)<sub>3</sub> is pyrophoric). The polymerization protocol is illustrated in Scheme 2.3.

#### Scheme 2.3

Chain extension from hydroxyl telechelic poly(COE<sub>30-s</sub>-NB<sub>70</sub>) by ROTEP of D,L-lactide to form L-CN-L triblock copolymers.



Polymerization of D,L-lactide was conducted by dissolving the macroinitiator poly(COE<sub>30-s</sub>-NB<sub>70</sub>) in toluene with the catalyst Sn(Oct)<sub>2</sub> and adding the desired amount of cyclic ester monomer. The mixture was heated at 110 °C for 4 h to effect ROTEP, followed by precipitation in cold (–60 °C) methanol. The polymer was isolated, dried, and characterized for molecular attributes by <sup>1</sup>H NMR spectroscopy and SEC.

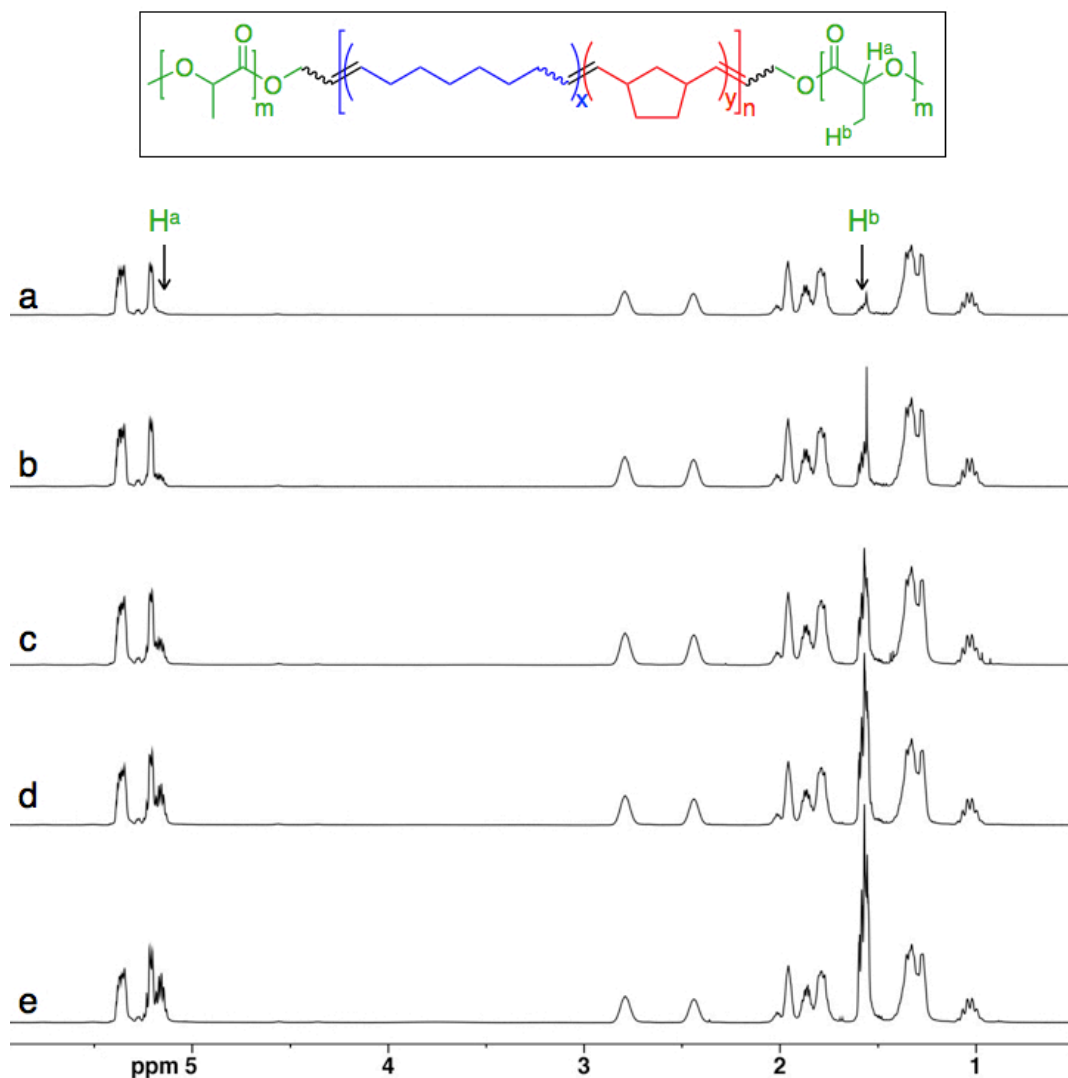
Seven samples were initially prepared with different targeted compositions corresponding to 89, 76 45, 35, 25, 15, and 5 wt % PLA. Table 2.5 contains the molecular characteristics determined by  $^1\text{H}$  NMR spectroscopy.

**Table 2.5**

Molecular characteristics of L-CN-L triblock copolymers derived from poly(COE<sub>30</sub>-s-NB<sub>70</sub>) hydroxyl telechelic macroinitiator.

Sample ID	$M_{n,\text{total}}^a$ (kg mol <sup>-1</sup> )	$M_{n,\text{PLA}}^b$ (kg mol <sup>-1</sup> )	$w_{\text{PLA}}^c$	$w_{\text{COE}}^c$	$w_{\text{NB}}^c$
poly(COE <sub>30</sub> -s-NB <sub>70</sub> )	22.2			0.32	0.68
L-CN-L [0.6-22-0.6]	23.5	1.28	0.05	0.31	0.64
L-CN-L [2.0-22-2.0]	26.2	4.05	0.15	0.28	0.57
L-CN-L [3.5-22-3.5]	29.1	6.86	0.24	0.24	0.53
L-CN-L [5.8-22-5.8]	33.8	11.6	0.34	0.21	0.44
L-CN-L [8.4-22-8.4]	39.0	16.8	0.43	0.18	0.38
L-CN-L [35-22-35]	92.7	70.5	0.76	0.08	0.16
L-CN-L [93-22-93]	207	185	0.89	0.03	0.07

<sup>a</sup> determined from  $^1\text{H}$  NMR spectroscopy by integration of the proton signals attributed to the respective repeat units and assuming constant molecular weight of the macromolecular poly(COE<sub>30</sub>-s-NB<sub>70</sub>) initiator ( $N = 226$ ). <sup>b</sup> calculated from  $M_{n,\text{total}} - M_{n,\text{CN}}$ . <sup>c</sup> determined from  $^1\text{H}$  NMR spectroscopy.

**Figure 2.12**

Stacked  $^1\text{H}$  NMR spectra for five L-CN-L triblock copolymers derived from a single precursor poly(COE<sub>30</sub>-s-NB70) with compositions of (in wt % PLA) (a) 5, (b) 15, (c) 24, (d) 34, and (e) 43.

The  $^1\text{H}$  NMR spectra clearly evince an increased PLA content in the triblock copolymer with increasing D,L-lactide feedstock concentration. Two characteristic signals from backbone of PLA, namely the methine  $[-\text{OCH}(\text{CH}_3)\text{C}(\text{O})-]$  at 5.2 ppm and the methyl signals  $[-\text{OCH}(\text{CH}_3)\text{C}(\text{O})-]$  at 1.6 ppm exhibit monotonic intensity increase relative to the signals from the midblock poly(COE<sub>30</sub>-s-NB70). Conditions

under which ROTEP is performed do not affect the midblock composition or configuration; the signal ratios remain constant among all the samples.

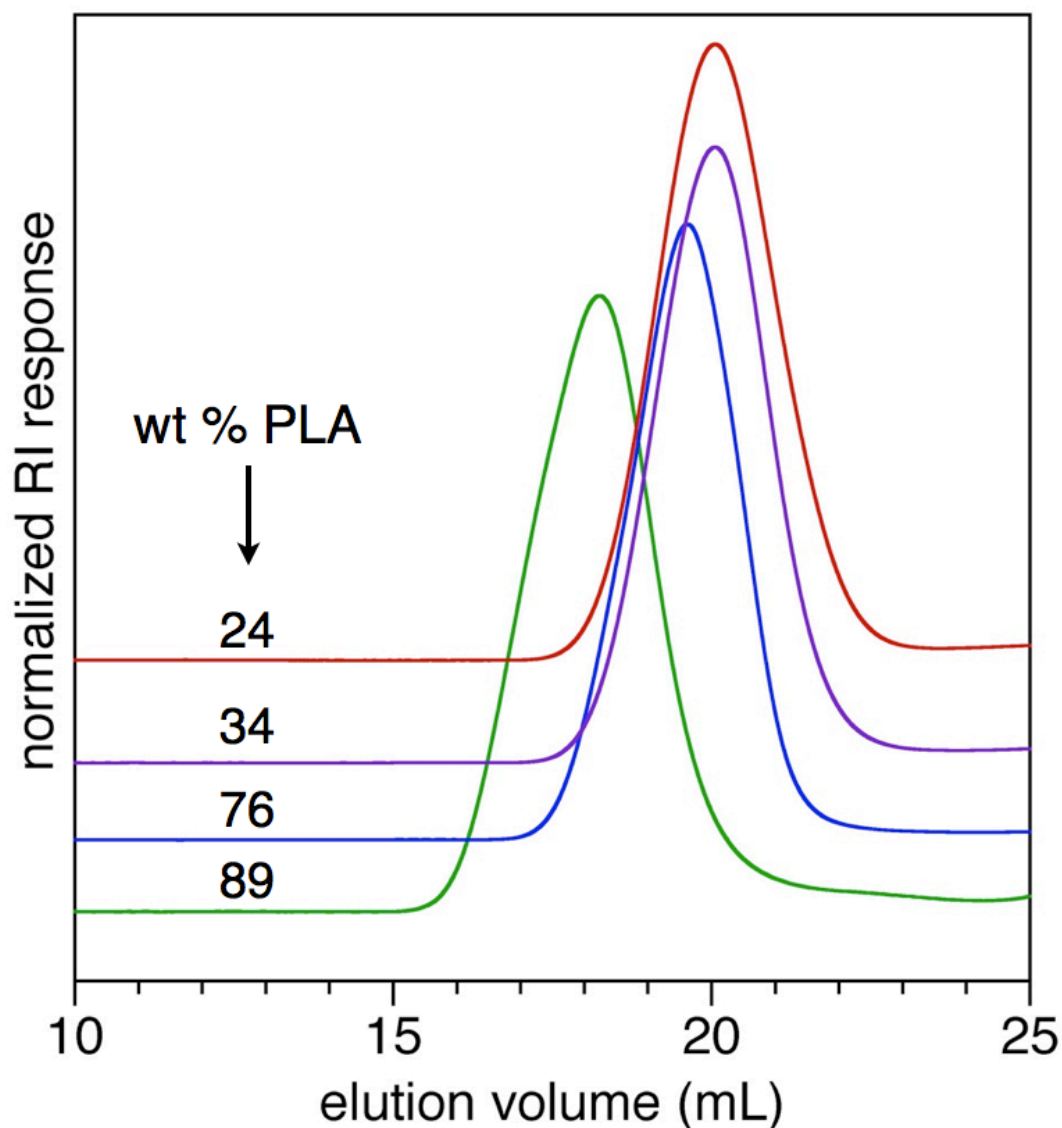


**Figure 2.13**

Chromatograms for L-CN-L triblock copolymers from the poly(COE<sub>30</sub>-s-NB<sub>70</sub>) precursor. Chromatograms are for triblock copolymers with compositions (in wt % PLA) equal to 24 (red), 34 (violet), 76 (blue), and 89 (green).

### 2.3.4 Thermal Properties of L-CN-L Triblock Copolymers

Thermal properties of the L-CN-L triblock copolymers were assessed by DSC (Figure 2.14). Absence of melting and crystallization endotherms or exotherms, respectively, signifies the lack of crystallinity under the applied conditions. Two glass transition temperatures are clearly observed for several samples, most markedly apparent in samples with high PLA content. Two distinct  $T_g$ s is consistent with microphase separation caused by the incompatibility between two components that are constrained to small domains, as is such in block copolymers tethered by a covalent bond.

The  $T_g$  remains constant for the midblock, while the  $T_g$  for the glassy PLA end-blocks shows a gradual increase before plateau is reached at approximately sample L-CN-L [8.4-22-8.4] ( $T_g = 51$  °C). This behavior is consistent with the observed increase in  $T_g$  with increasing molecular weight of PLA (and other species) homopolymer, with a threshold molecular weight in the range of  $10 \text{ kg mol}^{-1}$  being required before  $T_g$  no longer shows response to further size changes.

The samples were cast from solution or melt pressed into thick films between 0.5 and 5 mm thick after adding BHT as an antioxidant (~0.5 wt %). The resulting films were completely transparent, which suggests both the absence of crystallinity and the occurrence of microphase separation, with domains smaller than the wavelength of the visible spectrum. The glass transition temperatures of the two components fall conveniently on either side of ambient temperature, and these would serve as potential thermoplastic elastomers (at low  $w_{\text{PLA}}$ ) or tougheners (at high  $w_{\text{PLA}}$ ), perhaps with properties enhanced over the previously discussed LCL system.

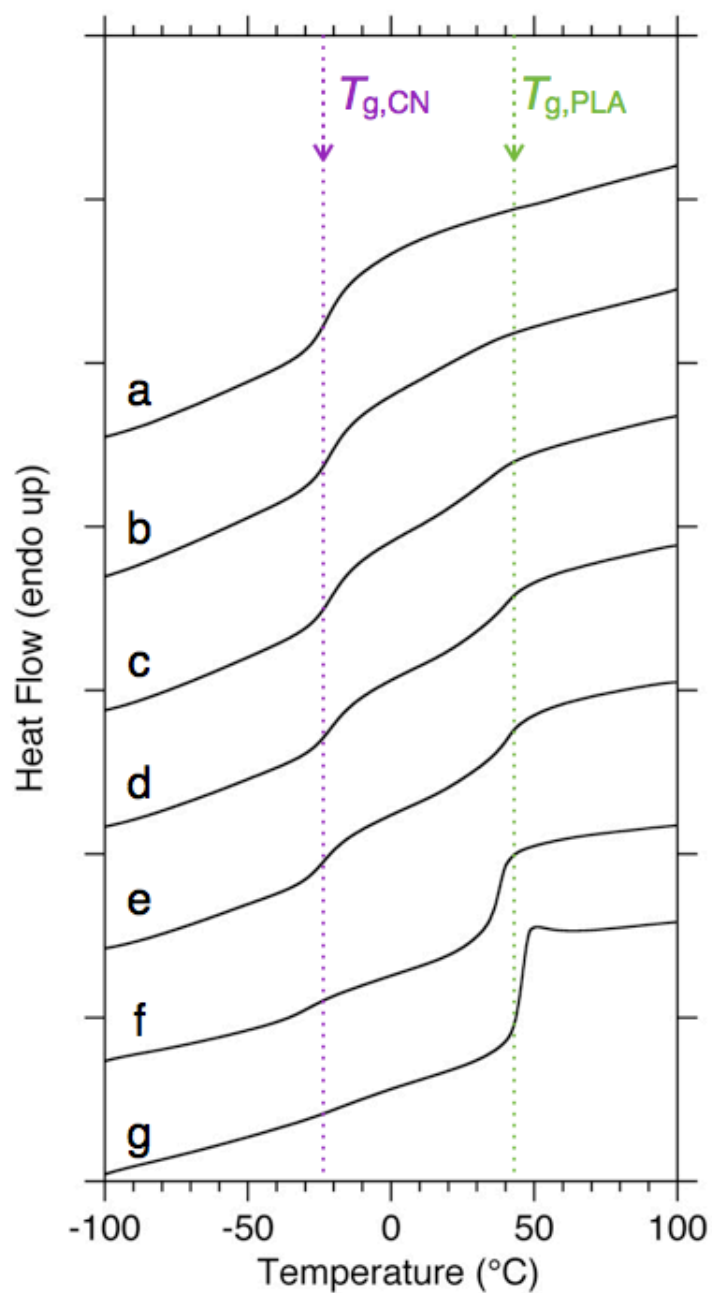


**Figure 2.14**

Thermograms from DSC analysis for L-CN-L triblock copolymers with wt % PLA compositions equal to (a) 5, (b) 15, (c) 24, (d) 34, (e) 43, (f) 76 and (g) 89.

Two distinct  $T_g$ s can be seen in each thermogram corresponding to the rubbery midblock ( $T_{g,CN}$ ) and glass end-block ( $T_{g,PLA}$ ).

### 2.3.5 Morphological Characteristics of L-CN-L Triblock Copolymers

Presumably, the triblock copolymers for which the synthetic details were described will phase separate, owing to the anticipated strong degree of incompatibility between PLA and the hydrocarbon midblock. Evidence for microphase separation will further support the block copolymer architecture proposed based on the molecular characterization methods.

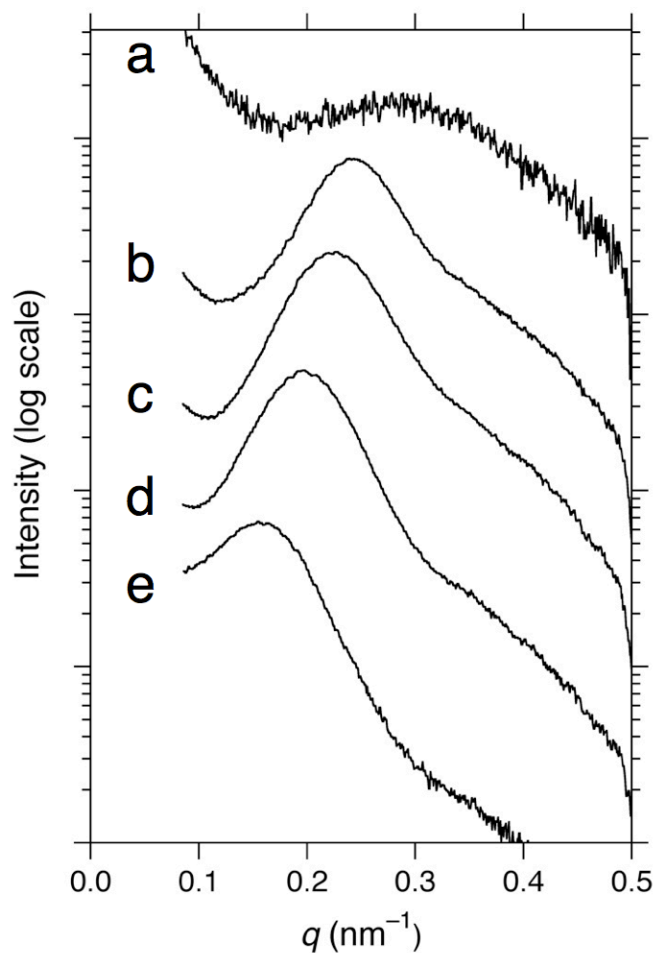


**Figure 2.15**

One-dimensional SAXS profiles from measurements at 120 °C on L-CN-L samples having compositions (in wt % PLA) of (a) 5, (b) 15, (c) 24, (d) 34 and (e) 45.



Analysis of several samples by SAXS provides evidence for microphase separation under certain circumstances (Figure 2.15). With the exception of L-CN-L (0.6-22-0.6) (Figure 2.15a), the samples all exhibit a primary scattering peak with high intensity and a clear dependence of position on molecular weight. The position monotonically decreases with increasing molar mass, corresponding to increased domain size. The absence of higher order reflections precludes the unambiguous assignment of any well-ordered morphologies. The sample with the largest asymmetry in composition L-CN-L (0.6-22-0.6) has a very low intensity, broad reflection, suggesting a homogeneous disordered phase under the measurement conditions (120 °C). Disorder, especially at elevated temperature, is consistent with theoretical predictions of phase diagrams for linear triblock copolymers having highly asymmetric compositions.

Nonetheless, the rudimentary phase behavior suggested by the preliminary SAXS measurements suggests that triblock copolymers were indeed formed, and composition can be used to modulate the size of domains within nanoscopic dimensions.

---

## 2.4 Multiblock Copolymers from Linear Triblock Copolymers

Multiblock copolymers represent an important extension from the class of simple AB-type diblock copolymers or ABA-type triblock copolymers discussed thus far. Multiblocks with two components have some number of repeating sequences of AB-type blocks within each polymer chain, and are often represented by  $(AB)_n$ . Sophisticated synthetic techniques have allowed spawning of a great architectural variety compared with the simple scenario represented by  $(AB)_n$ ; consecutive blocks of either A or B can contain drastically different average numbers of repeating units, for example. Also, increased complexity inherently results from addition of a third or fourth component, such as with ABAC tetrablock terpolymers, ABCD tetrablock quarterpolymers, or ABCDE pentablock quinterpolymers.<sup>68,69</sup>

Multiblock copolymers are nearly always prepared by one of two methods: sequential chain-growth polymerization of the respective components, or coupling of macromonomers by a step-growth mechanism (Figure 2.16).

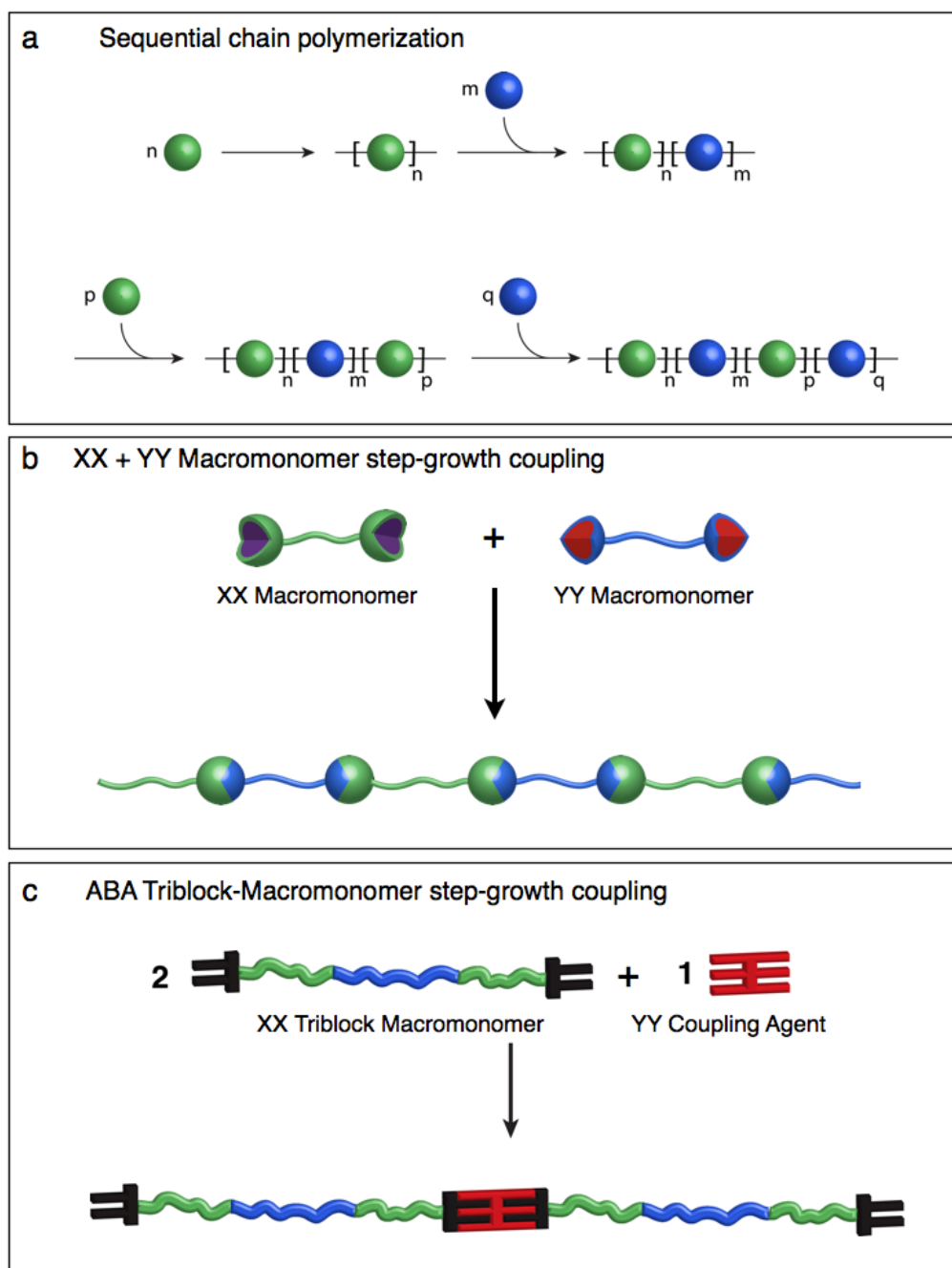


Figure 2.16

Illustrations of different routes to multiblock copolymers by (a) sequential chain growth polymerization (b) step-growth chain coupling between two different telechelic macromonomers (XX + YY) and (c) step-growth chain coupling between telechelic ABA-type triblock copolymer (XX) and a small molecule YY coupling agent.

Sequential polymerization of different monomers by a chain growth method (Figure 2.16a) requires that each monomer be polymerizable by the same mechanism. This strategy is therefore quite useful when applied to anionic polymerization, in which multiblock copolymers are easily prepared having narrow molecular weight distributions and well-defined number of blocks. Pentablock ABABA copolymers containing styrene and butadiene can be prepared by anionic polymerization, and the hydrogenated derivatives give access to a large subset of multiblock copolymers with a range of thermal and crystallization properties.<sup>63,70–73</sup> Tensile properties were found to be largely dependent on the relative amounts and arrangement of glassy, rubber, and semi-crystalline components, as well as the block architecture (i.e., pentablock vs. triblock). Recently, more complex hexablock (ABABAC-type) and undecablock (ABABACCABABA-type) terpolymers were synthesized using a sequential anionic polymerization method.<sup>74–76</sup> These copolymers exhibited enhanced mechanical properties compared with ABC triblock terpolymer counterparts and were shown to have intricately organized microphase separation behavior.

Interest in PLA block copolymers has spurred a great deal of effort toward devising methods for multiblock synthesis containing the aliphatic polyester. Exploring the architectures upon which the mechanical properties hinge is of fundamental importance, and has been applied to the biocompatible, biorenewable PLA in efforts to optimize performance in biomedical devices and thermoplastic elastomers.

The coupling of multiple telechelic homopolymers (Figure 2.16b) bearing complimentary chain termini is not typical. By this method, achieving high molecular weight materials proves difficult because of the difficulty in stoichiometric matching of end-groups between two species that inherently have a distribution of molecular weights. However, several attempts have been relatively successful. Symmetric hydroxyl-telechelic PLA was coupled with a carboxyl-telechelic poly(aniline) pentamer using dicyclohexylcarbodiimide (DCC) to mediate esterification between the chain termini.<sup>77</sup> Likewise, poly(ethylene oxide) (PEO) was modified to have carboxylic acid termini by reaction of the hydroxyl-analog

with succinic anhydride. Subsequent transesterification with PLA gave multiblocks with inherently broad distribution of block lengths.<sup>78</sup> Finally, telechelic poly( $\epsilon$ -caprolactone) (PCL) was adorned with highly reactive isocyanate groups; step-growth polymerization with  $\alpha$ -hydroxyl,  $\omega$ -carboxyl heterotelechelic PLA provided multiblocks with carbamide (i.e., urethane) junctions.<sup>79</sup>

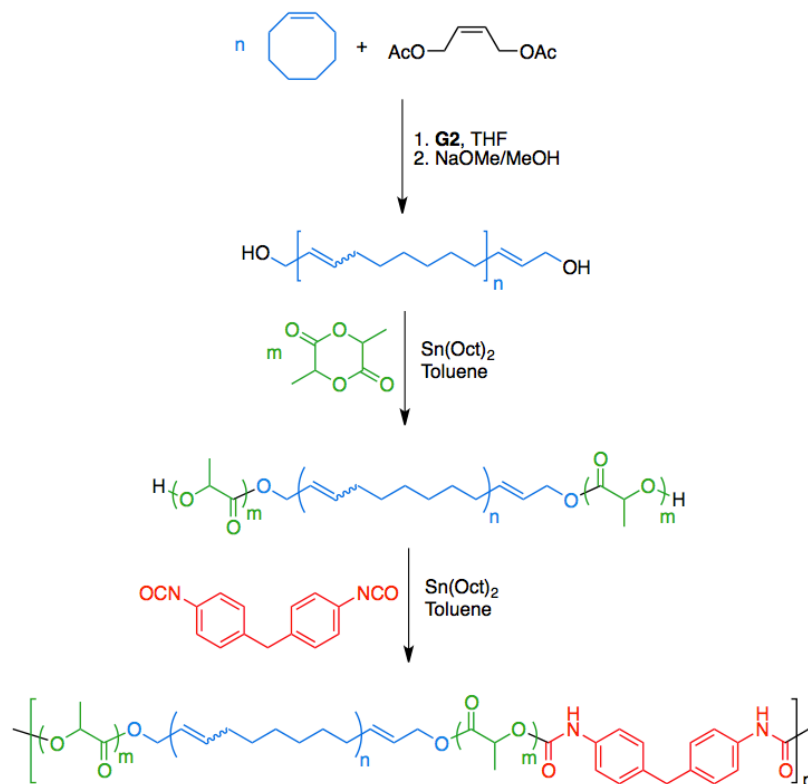
Covalently linking telechelic block copolymers (usually BAB symmetric triblocks) with a small molecule symmetric coupling agent (Figure 2.16c) is the most popular choice for preparing multiblock PLA copolymers. This method has several advantages: (1) one has access to a wide variety of comonomers to combine with PLA through mechanistic transformations; (2) high molecular weights are readily accessible because a stoichiometric balance is more easily achieved when using a discrete small molecule, in contrast to using two polydisperse coupling components. Symmetric hydroxyl telechelic PCL-PLA block copolymers have been coupled with commercially available diisocyanates, leading to urethane linkages.<sup>80–83</sup> Similarly, triblock copolymers having PLA end-groups and either poly(isobutylene) (PIB)<sup>84,85</sup> or poly(dimethylsiloxane) (PDMS)<sup>86</sup> rubbery midblocks were transformed into high molecular weight multiblocks through diisocyanate coupling.

#### 2.4.1 Synthesis of Multiblock (LCL)<sub>n</sub> Copolymers

Chain extension is demonstrated using triblock copolymers prepared by the tandem ROP strategy disclosed in the preceding sections. The triblock copolymers have poly(*cis*-cyclooctene) (PCOE) midblocks prepared by ROMP-CT method. Glassy, amorphous PLA endblocks were grown from PCOE macroinitiators. Finally, 4,4'-methylene diphenyl diisocyanate (MDI) was introduced along with an esterification/carbamidification catalyst, Sn(Oct)<sub>2</sub> to generate multiblock copolymers (Scheme 2.4).

Scheme 2.4

Synthesis of multiblock (LCL)<sub>n</sub> copolymers by tandem ring-opening polymerizations followed by diisocyanate coupling.



The synthetic protocol involving the tandem ROP is identical to that described previously except for the substitution of the aluminum pre-catalyst  $\text{Al}(\text{Et})_3$  for the tin pre-catalyst  $\text{Sn}(\text{Oct})_2$ . Two triblock copolymers were prepared in this manner. The samples were designed to be of comparable overall molar mass, but have drastically different compositions. The first sample was synthesized to contain a large majority of PLA, with which the ultimate toughness could be compared with alternate samples possessing a majority of the biorenewable component and various molecular architectures.<sup>87–90</sup> Starting from a hydroxyl-telechelic PCOE sample with degree of polymerization ( $N_c$ ) of 42 ( $M_n = 4.7 \text{ kg mol}^{-1}$ ), subsequent ROTEP of D,L-lactide was performed, finally providing a triblock copolymer LCL [27-5-27] (Table 2.6). Analysis by  $^1\text{H}$  NMR spectroscopy indicated a composition of 92 wt % PLA, commensurate with the targeted composition. The second sample

was designed to target a lamellar morphology, and as such has a composition commensurate with the linear triblock copolymers described in the preceding sections. Approximately symmetric composition (by volume) was achieved after ROTEP of D,L-lactide from a hydroxyl telechelic PCOE sample with  $N_c = 290$ , yielding a triblock LCL [23-32-23] with 60 wt % PLA (Table 2.6). The symmetric volume fraction, and hence a lamellar morphology was targeted to compare the triblock copolymers and the derivative multiblocks with previous examples prepared by alternative means. For example, pentablock copolymers adopting a lamellar morphology showed considerably improved toughness compared with a triblock with comparable composition.<sup>70,71</sup>

**Table 2.6**

Molecular characteristics of hydroxyl telechelic PCOE samples and the corresponding triblock copolymers

Sample	$M_{n,\text{total}}^a$ (kg mol <sup>-1</sup> )	$N_{n,\text{PLA}}^b$	$w_{\text{PLA}}^c$	$f_{\text{PLA}}^d$	PDI <sup>e</sup>
PCOE-42	4.71				
LCL [27-5-27]	58.6	313	0.92	0.89	1.10
PCOE-290	31.9				
LCL [23-32-23]	78.8	326	0.60	0.52	1.25

<sup>a</sup> determined from <sup>1</sup>H NMR spectroscopy by comparing the relative integration of repeat unit signals to end-group proton signals, using the repeat unit molar masses of  $m_{\text{COE}} = 110$  g mol<sup>-1</sup> and  $m_{\text{PLA}} = 144$  g mol<sup>-1</sup>. <sup>b</sup> determined from <sup>1</sup>H NMR spectroscopy by assuming a constant molar mass of the PCOE precursor, and integrating the methine signals from the PLA repeating units. <sup>c</sup> calculated from <sup>1</sup>H NMR spectroscopy. <sup>d</sup> calculated based on the weight fractions and assuming the respective densities at ambient temperature:  $\rho_{\text{PLA}} = 1.25$  g mL<sup>-1</sup>;  $\rho_{\text{PCOE}} = 0.90$  g mL<sup>-1</sup>. <sup>e</sup> measured by SEC-MALS compared to polystyrene standards.

Chain extension was performed on each of the two parent triblock copolymers using MDI as a coupling agent. Reaction of hydroxyl groups with isocyanates is well-studied, and high conversions are often observed in the presence of a transesterification catalyst. For this purpose, Sn(Oct)<sub>2</sub> was included during chain

extension. Two reactions were performed for each triblock, in which the ratio of triblock to MDI was modulated (Table 2.7). Samples are identified as  $z$ -MB [X-Y-X], where  $z$  refers to the first ( $z = a$ ) or second ( $z = b$ ) reaction, for which [MDI]:[OH] = 1 or [MDI]:[OH] = 2, respectively. X and Y refer to the molar mass (in kg mol<sup>-1</sup>) of the parent triblock copolymer. Parent triblock copolymers were dissolved in toluene with MDI and Sn(Oct)<sub>2</sub> under an inert atmosphere, following heating at 80 °C with rapid stirring for up to 20 h. After the prescribed reaction time, the polymer was isolated by precipitating the solution into a 10-fold by volume excess of hexanes.

Table 2.7

Molecular characteristics of multiblock copolymers from chain extension of triblock copolymers.

Sample	$M_n$ (LS) <sup>a</sup> (kg mol <sup>-1</sup> )	$M_w$ (LS) <sup>a</sup> (kg mol <sup>-1</sup> )	PDI	$w_{\text{PLA}}^b$	$f_{\text{PLA}}^b$
LCL [27-5-27]: $M_n$ (NMR) = 58.6 kg mol <sup>-1</sup> ; $M_n$ (LS) = 80.3 kg mol <sup>-1</sup>					
$a$ -MB [27-5-27]	145	186	1.28	0.93	0.90
$b$ -MB [27-5-27]				0.93	0.91
LCL [23-32-23]: $M_n$ (NMR) = 78.8 kg mol <sup>-1</sup> ; $M_n$ (LS) = 80.3 kg mol <sup>-1</sup>					
$a$ -MB [23-32-23]	110	147	1.34	0.60	0.53
$b$ -MB [23-32-23]				0.60	0.52

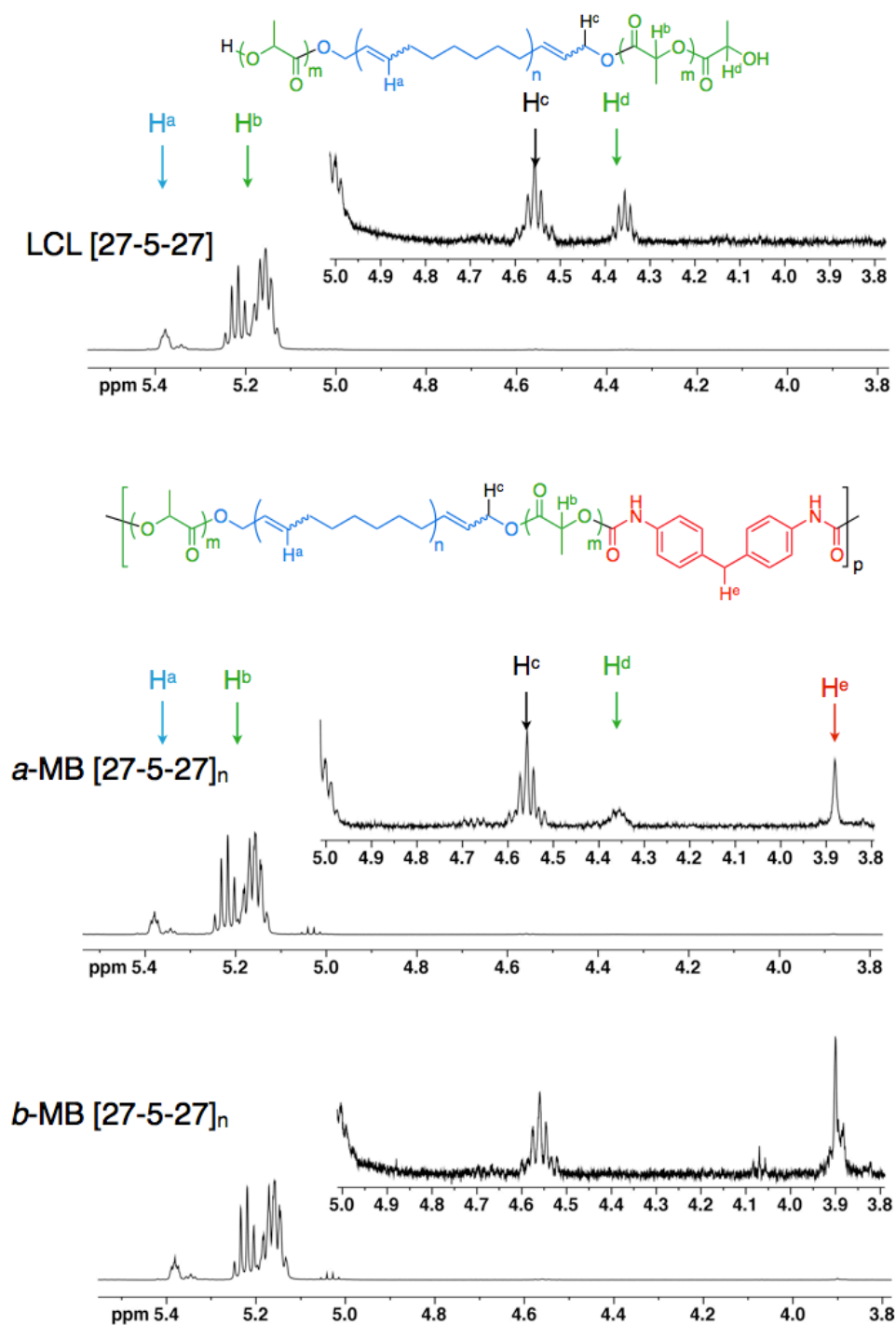
<sup>a</sup> Determined from multi-angle light-scattering detector connected with a liquid chromatograph operating with THF eluent at 30 °C, assuming the  $dn/dc$  is known for the two components ( $dn/dc_{\text{PLA}} = 0.042$  from ref. <sup>91</sup>;  $dn/dc = 0.110$  from ref. <sup>67</sup> and a linear relationship between composition and  $dn/dc$ ; ref. <sup>92</sup> <sup>b</sup> Determined from integration of signals in <sup>1</sup>H NMR spectra.

Reactions were initially monitored by <sup>1</sup>H NMR spectroscopy, with which the consumption of end-group hydroxyls is indicated by disappearance of the characteristic methine signals associated with the terminal lactic acid unit at  $\delta = 4.35$  ppm (Figure 2.17). Indeed, two hallmark signals are observed in the triblock copolymers at  $\delta = 4.56$  and 4.35 ppm that correspond to the methylene protons at the junction of PCOE-PLA [ $-\text{CH}=\text{CHCH}_2\text{O}-\text{C}(\text{O})\text{CH}(\text{CH}_3)-$ ] and the methine end-group of PLA [ $-\text{C}(\text{O})\text{CH}(\text{CH}_3)\text{OH}$ ], respectively, and integrate in the expected 2:1

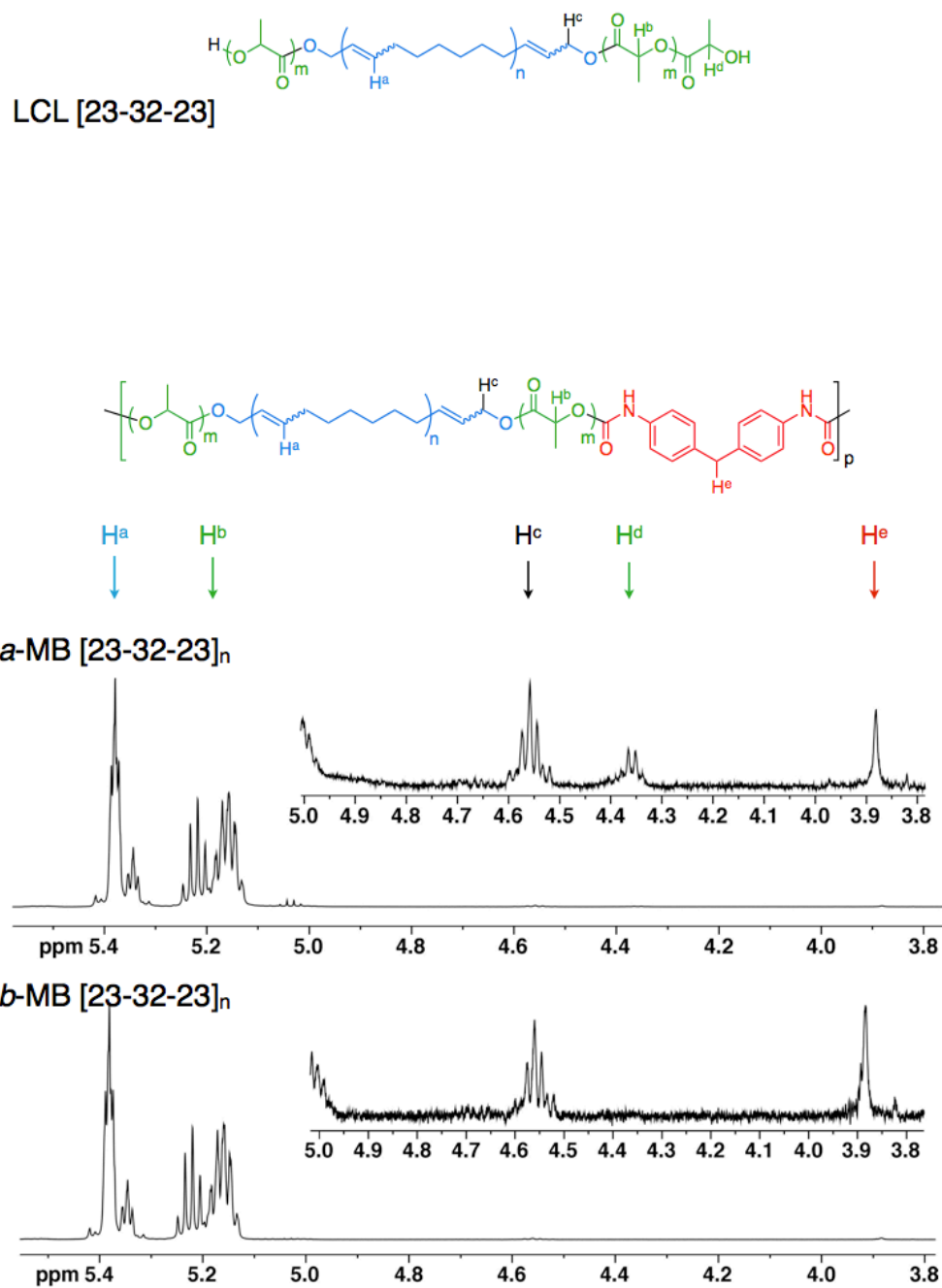


ratio within the experimental uncertainty. The spectrum for sample *a*-MB [27-5-27] clearly shows the retained intensity of the junction protons at 4.56 ppm, while the signal at 4.35 ppm is diminished substantially. This indicates that conversion after 20 h at 80 °C is not nearly complete. Although the molar mass of this multiblock copolymer is expected to be considerably larger than the parent triblock, higher molar mass should be obtainable. Indeed, when the initial concentration of MDI is doubled for sample *b*-MB-[27-5-27], the methine signal at 4.35 ppm is no longer observed, while the intensity of the junction proton signals remains constant. This suggests that substantially higher coupling conversions are achieved, and should result in larger molar mass. The signals for the methylene protons at the center of the MDI are observed at 3.9 ppm. This reference signal can be compared with the junction protons, and suggests that the MDI participates in the coupling reaction. The multiblock samples from the parent triblock LCL [23-32-23] indicate similar trends. Diminished intensity of the signal at 4.35 for sample *a*-MB-[23-32-23] suggests conversion of the end-groups from hydroxyls to carbamates has proceeded, though not nearly quantitatively. Higher molar masses are expected after adding more MDI led to complete disappearance of the methine signals at 4.35 ppm in sample *b*-MB-[23-32-23].

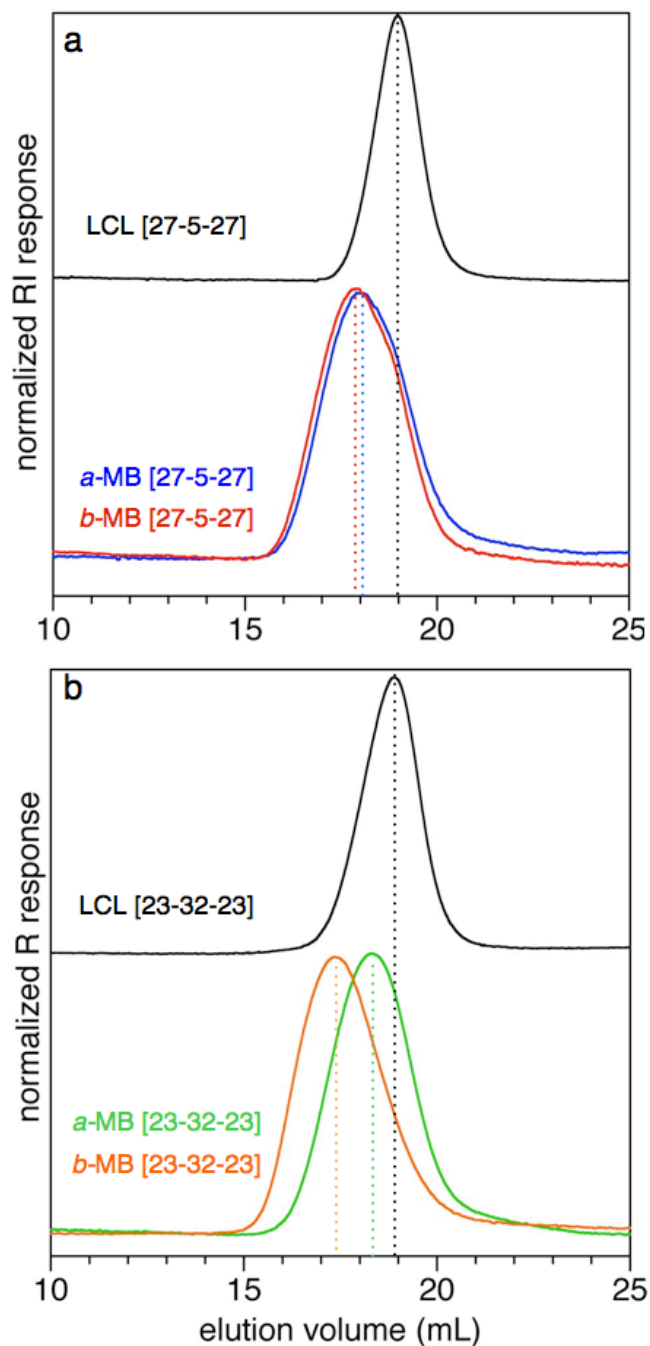
Analysis of the copolymers by SEC provides crucial evidence for chain extension by the coupling method used. The disappearance of characteristic signals from PLA end-groups in <sup>1</sup>H NMR spectroscopy indeed suggests reaction that consumes these end-groups. However, the reappearance of these signals is not observed. Chromatograms from the precursor triblocks compared with isolated polymer after isocyanate chain extension indicates a substantial increase in molecular weight in each of the four reactions described here (Figure 2.19).

**Figure 2.17**

Spectra from  $^1\text{H}$  NMR spectroscopic analysis for LCL [27-5-27] triblock copolymer (*top*), and multiblock copolymers *a*-MB [27-5-27] (*middle*) and *b*-MB [27-5-27] (*bottom*).

**Figure 2.18**

Spectra from  $^1\text{H}$  NMR spectroscopic analysis for LCL [23-32-23] triblock copolymer (*top*), and multiblock copolymers  $a\text{-MB [23-32-23]}_n$  (*middle*) and  $b\text{-MB [23-32-23]}_n$  (*bottom*).

**Figure 2.19**

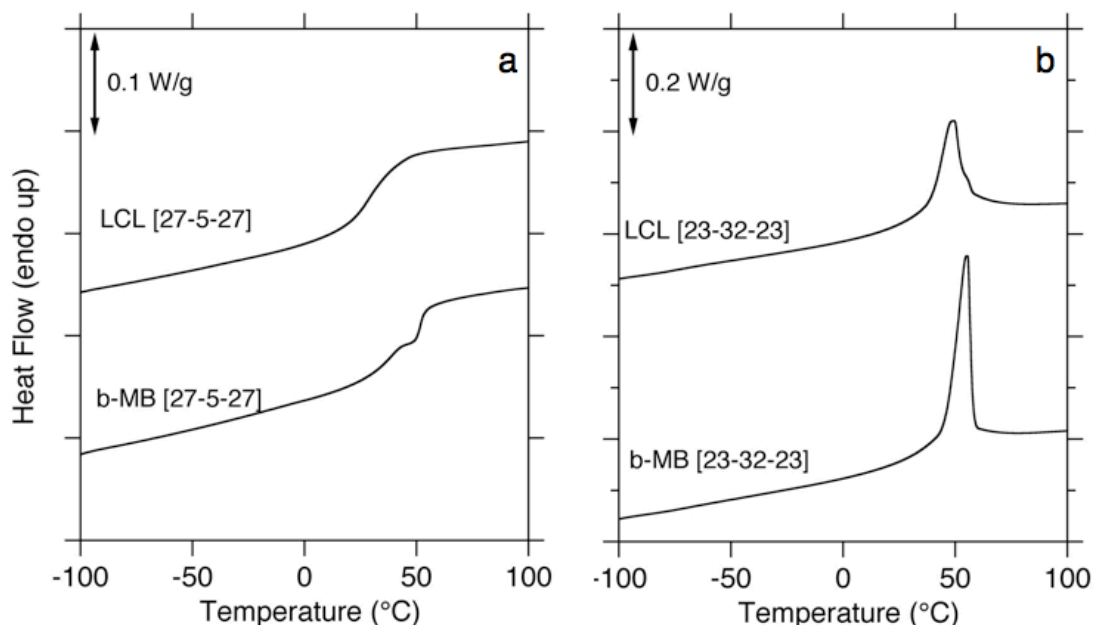
Chromatograms from SEC analysis on (a) LCL [27-5-27] triblock copolymer (*black*), and multiblock copolymers *a*-MB-[27-5-27] (*blue*) and *b*-MB-[27-5-27] (*red*) and (b) LCL [23-32-23] triblock copolymer (*black*), and multiblock copolymers *a*-MB [23-32-23] (*green*) and *b*-MB [23-32-23] (*orange*).

The chromatograms are furnished with dashed lines (correspondingly colored) extending from the maximum in the RI response for each sample to the x-axis (elution volume). Positions of interception on the x-axis provide a rough approximation of the relative average sizes of the samples, and a point of reference between different chromatograms. Evaluating the chromatograms for multiblocks derived from the triblock LCL [27-5-27] indicates a substantial increase in size for both reactions using different quantities of MDI coupling agent compared with the parent material. Incorporating a larger relative quantity of MDI led to modestly larger size, as indicated by the slightly earlier elution of sample *b*-MB-[27-5-27]<sub>n</sub> compared with *a*-MB-[27-5-27]<sub>n</sub> (Figure 2.18a *red* vs. *blue*). Chain extension gave similar results for the multiblock copolymers derived from the triblock copolymer LCL [23-32-23], for which considerable coupling is indicated by the early elution of both samples *a*-MB-[23-32-23] and *b*-MB-[27-5-27] (Figure 2.18b). Additionally, substantially larger molar masses were obtained by incorporating a larger proportion of MDI coupling agent. The inclusive SEC results provide ample evidence for extensive chain extension occurring by using MDI as coupling agent. Increased molecular weight agrees with the <sup>1</sup>H NMR spectroscopy, whereby the PLA chain ends are consumed as urethane linkages are formed, causing drastic increases in chain length in a step-wise manner.

#### 2.4.2 Thermal Properties of Multiblock Copolymers

Analysis of thermal properties offers insight with respect to the dependence of melting and glass transitions on chain architecture. DSC thermograms for the parent triblock copolymers and the corresponding multiblock copolymers reveal inconsequential influence of chain extension on the thermal transitions (Figure 2.20). These results suggest that the chain extension reaction conditions have little effect on thermal properties, and therefore a reasonable comparison of tensile properties can be made between the different chain architectures. Any difference can be reliably attributed to the contrasting block connectivity. The block copolymer and associated multiblocks having highly asymmetric composition show

a strong transition at  $\sim 45$  °C associated with  $T_{g,PLA}$ . The melting endotherm attributed to crystalline regions of PCOE has a low value and overlaps significantly with the glass transition of PLA, consistent with the highly asymmetric composition. It is not possible to reliably measure the degree of crystallinity from the overlapping melting endotherm. The nearly symmetric triblock LCL [23-32-23] and the corresponding multiblock copolymers also have similar chromatograms (Figure 2.20b). Each sample exhibits a sharp melting endotherm centered at  $50$  °C  $\pm 5$  °C, with similar enthalpies as measured from integration of the endotherms. These results signify that the multiblocks and parent triblock copolymers behave similarly with respect to the thermal characteristics.

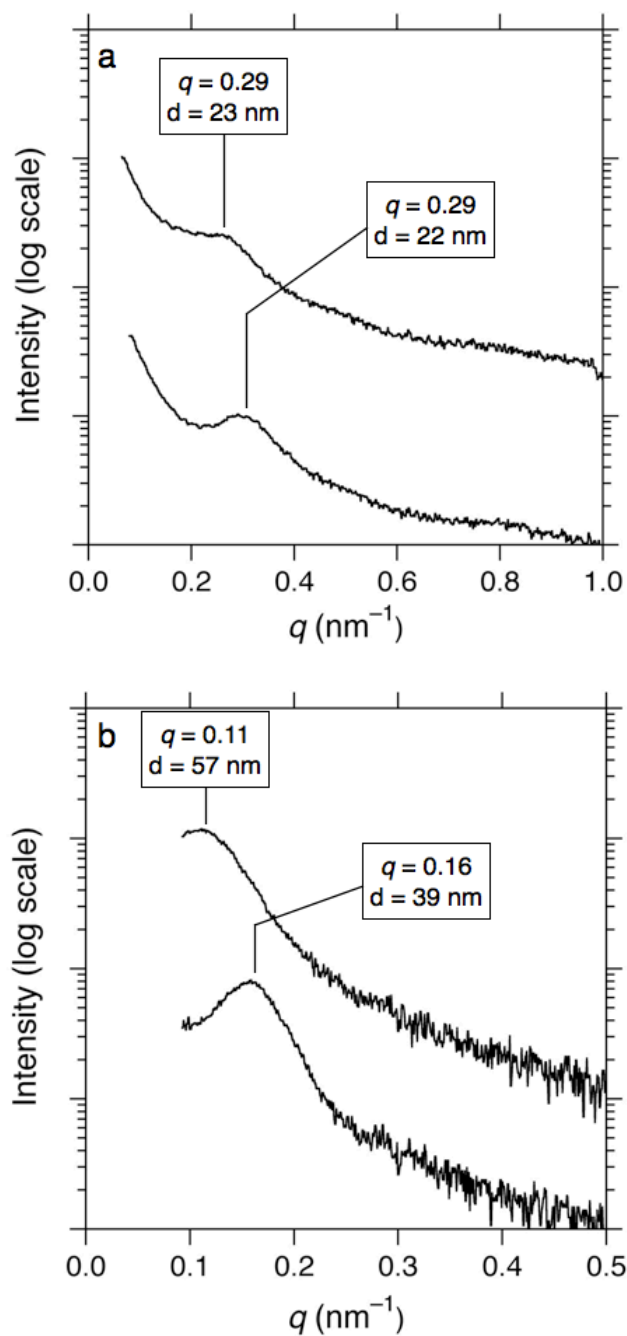


**Figure 2.20**

Thermograms from DSC analysis on linear triblock copolymers and multiblock copolymer corresponding to samples (a) LCL [27-5-27] (*top*) and b-MB [27-5-27] (*bottom*) and (b) LCL [23-32-23] (*top*) and b-MB [23-32-23] (*bottom*).

### 2.4.3 Morphological Characteristics of Multiblock Copolymers

The morphologies adopted by the parent triblock copolymers and corresponding multiblock copolymers remains an important indicator for the differences in mechanical properties. Microphase separation and domain sizes in the block copolymers with different architectures was investigated by SAXS (Figure 2.20). The parent triblock copolymer with the highly asymmetric composition exhibited one-dimensional SAXS profile consistent with a microphase separated structure lacking any long range order (Figure 2.20a, *top*). Although an ordered morphology cannot be unambiguously ascertained due to lack of higher order reflections, the primary scattering peak centered at  $q = 0.29 \text{ nm}^{-1}$  indicates a domain size  $d = 21.7 \text{ nm}$ . The corresponding multiblock copolymer (Figure 2.20a, *bottom*) exhibits a profile similar in shape with a smaller domain spacing of  $d = 23.0 \text{ nm}$ . The substantially larger molecular weight of the nearly symmetric sample LCL [23-32-23] would suggest a larger domain spacing. Indeed, the SAXS profile suggests microphase separation lacking long-range order with a single scattering peak centered at  $q = 0.11 \text{ nm}^{-1}$ , translating to a domain size  $d = 57 \text{ nm}$ . Multiblock copolymer *b*-MB [23-32-23] correspondingly has a profile with similar shape and analogously has a substantially smaller domain spacing  $d = 39 \text{ nm}$ .

**Figure 2.21**

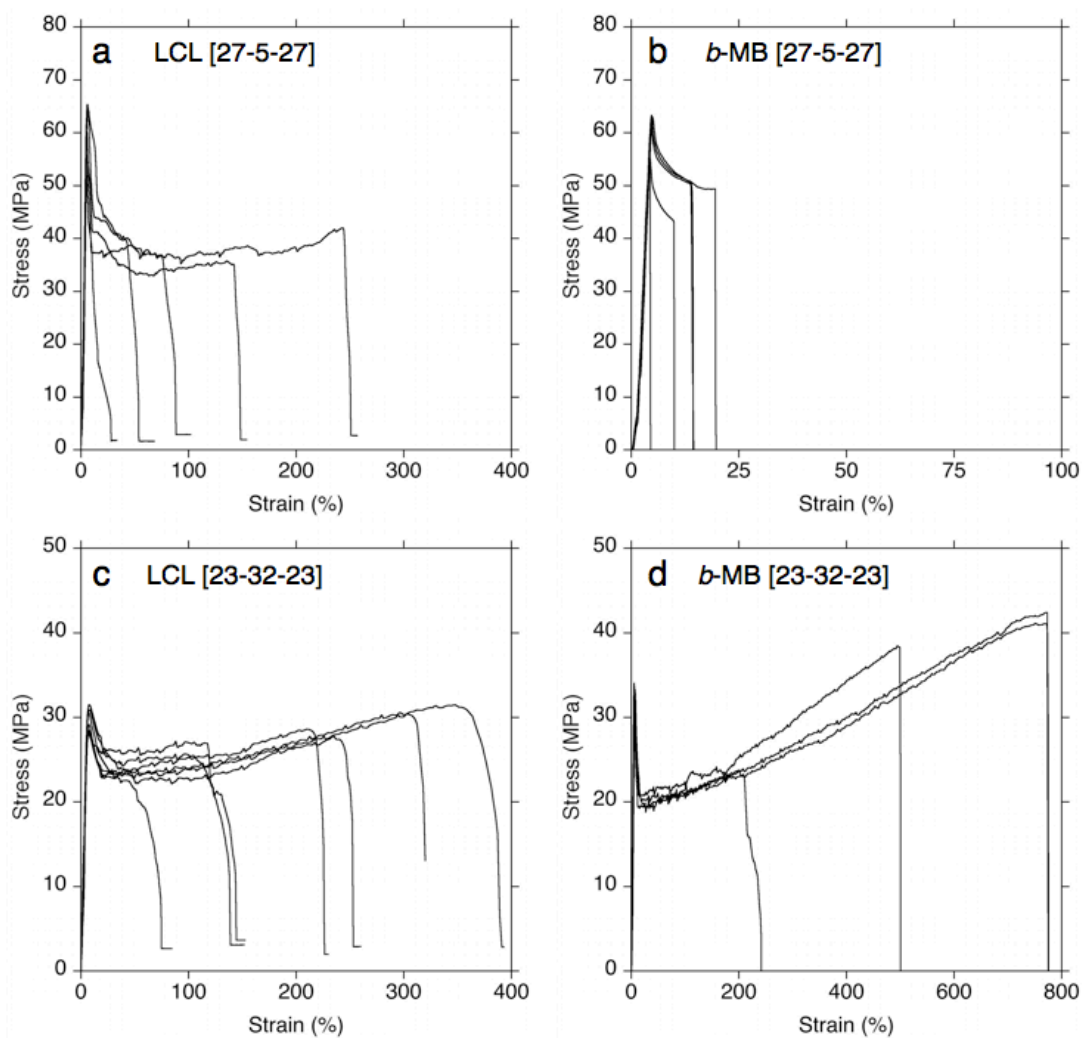
One-dimensional SAXS profiles for linear triblock copolymers and multiblock copolymers corresponding to samples (a) LCL [27-5-27] (*top*) and *b*-MB [27-5-27] (*bottom*) and (b) LCL [23-32-23] (*top*) and *b*-MB [23-32-23] (*bottom*).



#### 2.4.4 Tensile Properties of Multiblock Copolymers

The mechanical properties were preliminarily investigated by tensile testing. Dog-bone samples were prepared in the same manner as those described previously for linear LCL triblock copolymers. The triblock copolymer LCL [27-5-27] showed mechanical characteristics consistent with the triblock copolymers of similar molecular characteristics from section 2.2. The average elongation at break ( $\epsilon$ ) of approximately 120%, indicating modest ductility despite the relatively high glass content. The ultimate tensile strength at break ( $\sigma$ ) indicate relatively high strength, only slightly less than that of pristine PLA homopolymer (see Table 2.8). The corresponding multiblock copolymer *b*-MB [27-5-27] performed unexpectedly poorly compared to its parent triblock copolymer (Figure 2.22b). The multiblock behaved as a characteristically brittle material, with  $\epsilon$  averaged at 15%.

The triblock copolymer LCL [23-32-23] with nearly symmetric composition had tensile properties consistent with a sample comparatively having more soft component and less hard, glassy component. The samples elongated substantially more before fracturing and likewise had lower tensile strength. Collectively, this corresponds to a slightly larger tensile toughness compared with the LCL [27-5-27] triblock copolymer. The corresponding multiblock copolymer *b*-[23-32-23] exhibited enhanced tensile properties compared with the parent triblock. Considerably higher elongations were realized prior to fracture, and the ultimate tensile strength was also higher.

**Figure 2.22**

Tensile testing results for triblock copolymers and corresponding multiblock copolymers for samples (a) (a) LCL [27-5-27] (b) *b*-MB [27-5-27] (c) LCL [23-32-23] and (d) *b*-MB [23-32-23].

## 2.5 Conclusions

Herein, a straightforward synthesis of linear triblock copolymers was demonstrated by combining ROMP of COD with ROP of D,L-lactide. The PCOD midblock was prepared utilizing a chain transfer agent in the ROMP of COD with a commercial Ru catalyst ultimately yielding hydroxy terminated PCOD. The hydroxy functionality was employed to initiate ROP of D,L-lactide to give triblock copolymers with molecular characteristics dictated by the feedstock composition. Microphase separation was evidenced by well-defined peaks in the one-dimensional SAXS profiles. By tethering a soft midblock component with characteristically brittle PLA, tough and strong materials were realized. Tensile measurements showed impressive elongation at break for several samples with only small volume fractions of PCOD while maintaining a relatively high tensile modulus attributed to high PLA content.

The methodology introduced for combining tandem ring-opening polymerizations was expanded to include a statistical copolymer as the midblock. Copolymerization by ROMP-CT was illustrated to be effective in modulating the glass-transition and crystallization behavior through the comonomer feedstock concentrations. Telechelic polymers were successfully formed, despite the different monomer structures, and the macromolecular initiators were used to effect ROTEP of D,L-lactide, ultimately providing thermoplastic block copolymers having glassy end-blocks and low  $T_g$ , rubbery midblock.

Finally, a chain extension protocol was demonstrated using triblock poly(D,L-lactide-*b*-cyclooctene-*b*-D,L-lactide) derivatives. Diisocyanate MDI was successfully demonstrated to induce chain coupling when catalyzed by Sn(Oct)<sub>2</sub>, ultimately providing high molecular weight multiblocks with urethane linkages. The series of copolymers derived from the tandem ROP protocol introduced here should be investigated for the consequences of molecular architecture and crystallinity on the mechanical properties. The combined set of block copolymers will provide a strong basis for successfully directing future efforts toward optimizing and enhancing the behavior of partially renewable PLA materials.

## 2.6 Experimental Details

### 2.6.1 Materials

1,5-cyclooctadiene and *cis*-cyclooctene were purchased from Aldrich (99%) and were distilled under reduced pressure over CaH<sub>2</sub> prior to use. Grubbs 2<sup>nd</sup> generation catalyst was a gift from Materia and was used as received. D,L-lactide (99.5%) purchased from Purac was recrystallized twice from toluene and stored under N<sub>2</sub> atmosphere. Triethyl aluminum (AlEt<sub>3</sub>) was purchased as a 1.0 M solution in heptane from Aldrich. Sn(Oct)<sub>2</sub> was purchased from Sigma-Aldrich and was distilled under high vacuum with a Kugel-rohr apparatus before being stored under an inert atmosphere. The chain transfer agent *cis*-2-butene-1,4-diol diacetate (> 95%) obtained from TCI America was vacuum distilled. Chloroform from Mallinckrodt was thoroughly degassed prior to use with a N<sub>2</sub> purge. Toluene from Mallinckrodt was passed over an alumina column prior to use. Methanol was also purchased from Mallinckrodt and was used as received. Sodium methoxide and hydrochloric acid were from Aldrich and were used as received.

### 2.6.2 Synthetic Details

The synthesis of hydroxy telechelic poly(cyclooctadiene) was adapted from a literature procedure.<sup>30,39</sup> The precursor HT-PCOD used for all triblock copolymers in section 2.2 was prepared as described. 150 mL of CHCl<sub>3</sub> was added to a flame-dried 500 mL round-bottom single-neck flask and was thoroughly purged with N<sub>2</sub> gas. 0.42 mL (0.46 g; 2.6 mmol) of the CTA was added using a gas-tight syringe. 22 mg (26 μmol) Grubbs 2<sup>nd</sup> generation catalyst was added as a solution in 1.0 mL CHCl<sub>3</sub> using a gas-tight syringe. The mixture was immersed in a oil-bath at 40 °C with rapid stirring. 50.0 mL (43 g; 398 mmol) COD was added dropwise using a glass syringe over 1 h. The polymerization mixture was rapidly stirred for 8 h at 40 °C. The reaction was simultaneously quenched with and precipitated into 1 L of MeOH containing 15 mL of 1 M HCl<sub>(aq)</sub>. The polymer was isolated by filtration and dried further under reduced pressure for 24 h. <sup>1</sup>H NMR (CDCl<sub>3</sub>): δ 5.40–5.45 (m,

(*E*)-CH=CHCH<sub>2</sub>-, backbone), 5.35–5.40 (m, (*Z*)-CH=CHCH<sub>2</sub>-, backbone), 4.62 (d, (*E*)-CH=CHCH<sub>2</sub>OAc) 4.51 (d, (*Z*)-CH=CHCH<sub>2</sub>OAc); 2.06–2.11 (m, (*Z*)-CH=CHCH<sub>2</sub>- backbone), 2.01–2.06 (m, (*E*)-CH=CHCH<sub>2</sub>- backbone).

The entire yield (39.6 g; 92 %) was dissolved in 500 mL THF at 0 °C. 25 mL of a 0.7 M solution of NaOMe in MeOH (0.94 g; 17.5 mmol NaOMe) was added dropwise over 1 h. The mixture was allowed to stir at 0 °C for 5 h, at which point the polymer was precipitated into 2 L cold MeOH containing 15 mL 1 M HCl<sub>(aq)</sub>. The polymer was isolated by filtration and vacuum dried at RT for 24 h yielding 37.9 g (88.1 %). <sup>1</sup>H NMR (CDCl<sub>3</sub>): δ 5.40–5.45 (m, (*E*)-CH=CHCH<sub>2</sub>- backbone), 5.35–5.40 (m, (*Z*)-CH=CHCH<sub>2</sub>-, backbone), 4.18 (t, (*Z*)-CH=CHCH<sub>2</sub>OH) 4.11 (t, (*E*)-CH=CHCH<sub>2</sub>OH); 2.06–2.11 (m, (*Z*)-CH=CHCH<sub>2</sub>- backbone), 2.01–2.06 (m, (*E*)-CH=CHCH<sub>2</sub>- backbone).

The synthesis of the entry in Table 2.1 labeled LCL (8.6-16-8.6) is described here. Variable compositions were achieved by manipulating the relative amounts of D,L-lactide, Al(Et)<sub>3</sub> and toluene added to the reaction mixture. 2.0 g of the precursor HO-C-OH (20.5 kg mol<sup>-1</sup>; 9.75 × 10<sup>-2</sup> mmol OH) was placed in a 48 mL pressure vessel with a Teflon screw-cap and a Teflon-coated stir-bar. The flask was placed in a glove-box with a nitrogen atmosphere where 17 mL toluene and 97 μL of a 1 M solution of Al(Et)<sub>3</sub> in heptane were added via syringe. The molar ratio of –OH to Al was kept constant at 3:1. This reaction was stirred for 6 h at RT to functionalize the aluminum catalyst creating the aluminum alkoxide species used to initiate ring-opening polymerization of the cyclic ester. 2.50 g (17.3 mmol) D,L-lactide was placed in the vessel before sealing and removing from the glove-box. The vessel was then immersed into an oil-bath at 90 °C. The polymerization solution was allowed to react for 8 h before quenching with 2 mL of 1 M HCl<sub>(aq)</sub>. The final solution was precipitated into 150 mL of MeOH with rapid stirring and the polymer was isolated by filtration. After drying at RT for 24 h at reduced pressure (ca. 20 mtorr), the yield was 79 %. <sup>1</sup>H NMR (CDCl<sub>3</sub>): δ 5.40–5.45 (m, (*E*)-CH=CHCH<sub>2</sub>- backbone), 5.35–5.40 (m, (*Z*)-CH=CHCH<sub>2</sub>-), 5.13–5.27 (m, –C(O)CH(CH<sub>3</sub>)O- backbone) 4.62–4.70 (m, (*Z*)-CH=CHCH<sub>2</sub>-OC(O)C(CH<sub>3</sub>-) 4.52–4.62 (m, (*E*)-CH=CHCH<sub>2</sub>-OC(O)C(CH<sub>3</sub>-); 4.33–4.42 (m, C(O)CH(CH<sub>3</sub>)OH) 2.06–

2.11 (m, (*Z*)-CH=CHCH<sub>2</sub>- backbone), 2.01–2.06 (m, (*E*)-CH=CHCH<sub>2</sub>- backbone), 1.52–1.61 (m, -C(O)CH(CH<sub>3</sub>)O- backbone).

## 2.7 References

- [1] Bielawski, C. W.; Grubbs, R. H. *Angew. Chem., Int. Ed.* **2000**, *39*, 2903–2906.
- [2] Bielawski, C. W.; Grubbs, R. H. *Prog. Polym. Sci.* **2007**, *32*, 1–29.
- [3] Trnka, T. M.; Grubbs, R. H. *Acc. Chem. Res.* **2001**, *34*, 18–29.
- [4] Goethals, E. J., *Telechelic Polymers: Synthesis and Applications*. CRC Press: Boca Raton, Fla., 1989; p 402.
- [5] Bielawski, C. W.; Louie, J.; Grubbs, R. H. *J. Am. Chem. Soc.* **2000**, *122*, 12872–12873.
- [6] Burtscher, D.; Saf, R.; Slugovc, C. *J. Polym. Sci., Part A: Polym. Chem.* **2006**, *44*, 6136–6145.
- [7] Katayama, H.; Urushima, H.; Ozawa, F. *J. Organomet. Chem.* **2000**, *606*, 16–25.
- [8] Chen, B.; Metera, K.; Sleiman, H. F. *Macromolecules* **2005**, *38*, 1084–1090.
- [9] Li, M. H.; Keller, P.; Albouy, P. A. *Macromolecules* **2003**, *36*, 2284–2292.
- [10] Matson, J. B.; Grubbs, R. H. *Macromolecules* **2008**, *41*, 5626–5631.
- [11] Bielawski, C. W.; Hillmyer, M. A., In *Handbook of Metathesis*, Grubbs, R. H., Ed. Wiley-VCH: Weinham, Germany, 2003; Vol. 3, pp 255–282.
- [12] Bielawski, C. W.; Morita, T.; Grubbs, R. H. *Macromolecules* **2000**, *33*, 678–680.

- 
- [13] Coca, S.; Paik, H.-j.; Matyjaszewski, K. *Macromolecules* **1997**, *30*, 6513–6516.
- [14] Katayama, H.; Fukuse, Y.; Nobuto, Y.; Akamatsu, K.; Ozawa, F. *Macromolecules* **2003**, *36*, 7020–7026.
- [15] Katayama, H.; Yonezawa, F.; Nagao, M.; Ozawa, F. *Macromolecules* **2002**, *35*, 1133–1136.
- [16] Mahanthappa, M. K.; Bates, F. S.; Hillmyer, M. A. *Macromolecules* **2005**, *38*, 7890–7894.
- [17] Myers, S. B.; Register, R. A. *Macromolecules* **2008**, *41*, 5283–5288.
- [18] Drumright, R. E.; Gruber, P. R.; Henton, D. E. *Adv. Mater.* **2000**, *12*, 1841–1846.
- [19] Gruber, P.; O'Brien, M. *Biopolymers* **2002**, *4*, 235–250.
- [20] Vink, E. T. H.; Rabago, R.; Glassner, D. A.; Springs, B.; O'Connor, R. P.; Kolstad, J.; Gruber, P. R. *Macromol. Biosci.* **2004**, *4*, 551–564.
- [21] Auras, R.; Harte, B.; Selke, S. *Macromol. Biosci.* **2004**, *4*, 835–864.
- [22] Anderson, K. S.; Schreck, K. M.; Hillmyer, M. A. *Polym. Rev.* **2008**, *48*, 85–108.
- [23] Anderson, K. S.; Hillmyer, M. A. *Polymer* **2004**, *45*, 8809–8823.
- [24] Anderson, K. S.; Lim, S. H.; Hillmyer, M. A. *J. Appl. Polym. Sci.* **2003**, *89*, 3757–3768.
- [25] Schreck, K. M.; Hillmyer, M. A. *J. Biotechnol.* **2007**, *132*, 287–295.
- [26] Wang, Y.; Hillmyer, M. A. *J. Polym. Sci., Part A: Polym. Chem.* **2001**, *39*, 2755–2766.

- 
- [27] Garlotta, D. *J. Polym. Environ.* **2002**, *9*, 63–84.
- [28] Williams, C. K.; Hillmyer, M. A. *Polym. Rev.* **2008**, *48*, 1–10.
- [29] Gross, R. A.; Kalra, B. *Science* **2002**, *297*, 803–807.
- [30] Bielawski, C. W.; Scherman, O. A.; Grubbs, R. H. *Polymer* **2001**, *42*, 4939–4945.
- [31] Chung, T. C.; Chasmawala, M. *Macromolecules* **1992**, *25*, 5137–5144.
- [32] Fraser, C.; Hillmyer, M. A.; Gutierrez, E.; Grubbs, R. H. *Macromolecules* **1995**, *28*, 7256–7261.
- [33] Hilf, S.; Berger–Nicoletti, E.; Grubbs, R. H.; Kilbinger, A. F. M. *Angew. Chem., Int. Ed.* **2006**, *45*, 8045–8048.
- [34] Hilf, S.; Grubbs, R. H.; Kilbinger, A. F. M. *Macromolecules* **2008**, *41*, 6006–6011.
- [35] Hillmyer, M. A.; Grubbs, R. H. *Macromolecules* **1993**, *26*, 872–874.
- [36] Hillmyer, M. A.; Grubbs, R. H. *Macromolecules* **1995**, *28*, 8662–8667.
- [37] Morita, T.; Maughon, B. R.; Grubbs, R. H. *Polymer Preprints (American Chemical Society, Division of Polymer Chemistry)* **1998**, *39*, 226–227.
- [38] Bielawski, C. W.; Benitez, D.; Morita, T.; Grubbs, R. H. *Macromolecules* **2001**, *34*, 8610–8618.
- [39] Hillmyer, M. A.; Nguyen, S. T.; Grubbs, R. H. *Macromolecules* **1997**, *30*, 718–721.
- [40] Ji, S.; Hoye, T. R.; Macosko, C. W. *Macromolecules* **2004**, *37*, 5485–5489.
- [41] Dubois, P.; Jerome, R.; Teyssie, P. *Makromol. Chem.–M. Symp.* **1991**, *42/43*, 103–116.



- 
- [42] Jacobs, C.; Dubois, P.; Jerome, R.; Teyssie, P. *Macromolecules* **1991**, *24*, 3027–3034.
- [43] Penczek, S.; Duda, A. *Macromol. Symp.* **1996**, *107*, 1–15.
- [44] Witzke, D. R.; Kolstad, J. J.; Narayan, R. *Macromolecules* **1997**, *30*, 7075–7085.
- [45] Fetters, L. J.; Lohse, D. J.; Richter, D.; Witten, T. A.; Zirkel, A. *Macromolecules* **1994**, *27*, 4639–4647.
- [46] Schneider, W. A.; Müller, M. F. *J. Mol. Catal.* **1988**, *46*, 395–403.
- [47] Müller, A. J.; Arnal, M. L. *Prog. Polym. Sci.* **2005**, *30*, 559–603.
- [48] Müller, A. J.; Balsamo, V.; Arnal, M. L. *Adv. Polym. Sci.* **2005**, *190*, 1–63.
- [49] Abetz, V.; Simon, P. F. W. *Adv. Polym. Sci.* **2005**, *189*, 125–212.
- [50] Bates, F. S.; Fredrickson, G. H. *Annu. Rev. Phys. Chem.* **1990**, *41*, 525–557.
- [51] Bates, F. S.; Fredrickson, G. H. *Phys. Today* **1999**, *52*, 32–38.
- [52] Hamley, I. W., *The Physics of Block Copolymers*. Oxford University Press, USA: 1998; p 432.
- [53] Leibler, L. *Macromolecules* **1980**, *13*, 1602–1617.
- [54] Matsen, M. W.; Bates, F. S. *Macromolecules* **1996**, *29*, 1091–1098.
- [55] Matsen, M. W.; Thompson, R. B. *J. Chem. Phys.* **1999**, *111*, 7139–7146.
- [56] Matsen, M. W.; Bates, F. S. *J. Chem. Phys.* **1997**, *106*, 2436–2448.
- [57] Helfand, E.; Tagami, Y. *J. Chem. Phys.* **1972**, *56*, 3592–3601.
- [58] Helfand, E.; Wasserman, Z. R. *Macromolecules* **1976**, *9*, 879–888.

- 
- [59] Matsen, M. W. *Phys. Rev. Lett.* **2007**, *99*, 148304/148301–148304/148304.
- [60] Drzal, P. L.; Barnes, J. D.; Kofinas, P. *Polymer* **2001**, *42*, 5633–5642.
- [61] Zalusky, A. S.; Olayo–Valles, R.; Wolf, J. H.; Hillmyer, M. A. *J. Am. Chem. Soc.* **2002**, *124*, 12761–12773.
- [62] Mori, Y.; Lim, L. S.; Bates, F. S. *Macromolecules* **2003**, *36*, 9879–9888.
- [63] Phatak, A.; Lim, L. S.; Reaves, C. K.; Bates, F. S. *Macromolecules* **2006**, *39*, 6221–6228.
- [64] Perego, G.; Cella, G. D.; Bastioli, C. *J. Appl. Polym. Sci.* **1996**, *59*, 37–43.
- [65] Semba, T.; Kitagawa, K.; Ishiaku, U. S.; Hamada, H. *J. Appl. Polym. Sci.* **2006**, *101*, 1816–1825.
- [66] Bigg, D. M. *Adv. Polym. Tech.* **2005**, *24*, 69–82.
- [67] Pitet, L. M.; Chamberlain, B. M.; Hauser, A. W.; Hillmyer, M. A. *Macromolecules* **2010**, *43*, 8018–8025.
- [68] Hadjichristidis, N.; Pitsikalis, M.; Iatrou, H. *Adv. Polym. Sci.* **2005**, *189*, 1–124.
- [69] Ekizoglou, N.; Hadjichristidis, N. *J. Polym. Sci., Part A: Polym. Chem.* **2002**, *40*, 2166–2170.
- [70] Hermel, T. J.; Hahn, S. F.; Chaffin, K. A.; Gerberich, W. W.; Bates, F. S. *Macromolecules* **2003**, *36*, 2190–2193.
- [71] Hermel, T. J.; Wu, L.; Hahn, S. F.; Lodge, T. P.; Bates, F. S. *Macromolecules* **2002**, *35*, 4685–4689.
- [72] Mahanthappa, M. K.; Hillmyer, M. A.; Bates, F. S. *Macromolecules* **2008**, *41*, 1341–1351.

- [73] Mahanthappa, M. K.; Lim, L. S.; Hillmyer, M. A.; Bates, F. S. *Macromolecules* **2007**, *40*, 1585–1593.
- [74] Fleury, G.; Bates, F. S. *Macromolecules* **2009**, *42*, 3598–3610.
- [75] Fleury, G.; Bates, F. S. *Macromolecules* **2009**, *42*, 1691–1694.
- [76] Fleury, G.; Bates, F. S. *Soft Matter* **2010**, *6*, 2751–2759.
- [77] Huang, L. H.; Zhuang, X. L.; Hu, J.; Lang, L.; Zhang, P. B.; Wang, Y. S.; Chen, X. S.; Wei, Y.; Jing, X. B. *Biomacromolecules* **2008**, *9*, 850–858.
- [78] Mai, S. M.; Abbot, A.; Norton, D.; McKean, R.; Ryan, A. J. *Macromol. Chem. Phys.* **2009**, *210*, 840–851.
- [79] Teng, C. Q.; Kai, Y.; Ping, J.; Yu, M. H. *J. Polym. Sci., Part A: Polym. Chem.* **2004**, *42*, 5045–5053.
- [80] Cohn, D.; Hotovely–Salomon, A. *Polymer* **2005**, *46*, 2068–2075.
- [81] Cohn, D.; Salomon, A. F. *Biomater.* **2005**, *26*, 2297–2305.
- [82] Wang, W.; Ping, P.; Yu, H.; Chen, X.; Jing, X. *J. Polym. Sci., Part A: Polym. Chem.* **2006**, *44*, 5505–5512.
- [83] Yu, T.; Ren, J.; Gu, S.; Yang, M. *Polym. Adv. Technol.* **2010**, *21*, 183–188.
- [84] Ojha, U.; Kulkarni, P.; Cozzens, D.; Faust, R. *J. Polym. Sci., Part A: Polym. Chem.* **2010**, *48*, 3767–3774.
- [85] Ojha, U.; Kulkarni, P.; Singh, J.; Faust, R. *J. Polym. Sci., Part A: Polym. Chem.* **2009**, *47*, 3490–3505.
- [86] Ho, C. H.; Wang, C. H.; Lin, C. I.; Lee, Y. D. *Eur. Polym. J.* **2009**, *45*, 2455–2466.

- 
- [87] Gramlich, W. M.; Robertson, M. L.; Hillmyer, M. A. *Macromolecules* **2010**, *43*, 2313–2321.
- [88] Jing, F.; Hillmyer, M. A. *J. Am. Chem. Soc.* **2008**, *130*, 13826–13827.
- [89] Robertson, M. L.; Chang, K.; Gramlich, W. M.; Hillmyer, M. A. *Macromolecules* **2010**, *43*, 1807–1814.
- [90] Theryo, G.; Jing, F.; Pitet, L. M.; Hillmyer, M. A. *Macromolecules* **2010**, *43*, 7394–7397.
- [91] Dorgan, J. R.; Janzen, J.; Knauss, D. M.; Hait, S. B.; Limoges, B. R.; Hutchinson, M. H. *J. Polym. Sci., Part B: Polym. Phys.* **2005**, *43*, 3100–3111.
- [92] Medrano, R.; Laguna, M. T. R.; Saiz, E.; Tarazona, M. P. *Phys. Chem. Chem. Phys.* **2003**, *5*, 151–157.

## Chapter 3

# Complex Molecular Architectures in Block Copolymers from Tandem Ring-opening Polymerizations\*

This chapter describes the synthesis and characterization of block copolymers with symmetrically branched architectures consisting of poly(*cis*-cyclooctene) mid-segments flanked by varying numbers of poly(D,L-lactide) end-segments. The various polymers are prepared in a controlled manner with detailed molecular, morphological and thermal characteristics presented. This represents a valuable extension of the introduction to tandem ring-opening polymerization, granting access to an array of physical and morphological properties.

---

\* Reproduced in part with permission from Pitet, L. M.; Chamberlain, B. M.; Hauser, A. W.; Hillmyer, M. A. *Macromolecules* **2010**, *43*, 8018–8025. Copyright 2010 American Chemical Society.

## 3.1 Introduction

The interest in the biorenewable plastic polylactide (PLA) extends across many fields from disposable packaging, to biomedical devices, to fabrics, owing largely to increasing concern for the environmental impact of a plastics industry that was founded and has maintained reliance on non-sustainable feedstocks. Adapting the mechanical and thermal properties of a single polymer requires intricate tailoring of the structure.<sup>1</sup> As such, structure-property relationships in amorphous PLA, semicrystalline PLA, PLA blends, and PLA statistical and block copolymers<sup>2</sup> have been explored. In this report, we investigate the role of molecular architecture on microphase separation for symmetric block copolymers with glassy PLA end blocks and a rubbery, semi-crystalline polyolefin midblock.

Block copolymers are fascinating hybrid macromolecules comprising long chains of different components tethered covalently at one or more junctions. Microphase separation caused by incompatibility between the constituents is typically observed, whereby the domain sizes are confined to nanoscopic dimensions. Block polymers have proven quite useful for many applications due to the array of nanostructures they can adopt.<sup>3-5</sup> Adding more blocks (e.g., as in ABC triblock terpolymers) or altering the connectivity (ABAB... multiblock copolymers) naturally increases the architectural complexity and provides a way to fine-tune the properties and self-assembled structures.<sup>6</sup> As such, synthetic pathways toward branched block copolymers have garnered attention based on their unique contributions to the mechanical and morphological properties of a material compared with the linear counterparts.<sup>6-19</sup> Although several examples describe the synthesis of branched PLA block copolymers, the bulk self-assembly has not been explored in detail.<sup>20,21</sup>

Precise control over chemical composition and chain architecture in block polymers has been widely achieved due to the ready accessibility of various controlled polymerization techniques. Combining mechanistically incompatible monomers into these hybrid macromolecules remains an attractive approach to the development of new materials with a broad array of physical properties.<sup>22</sup> The

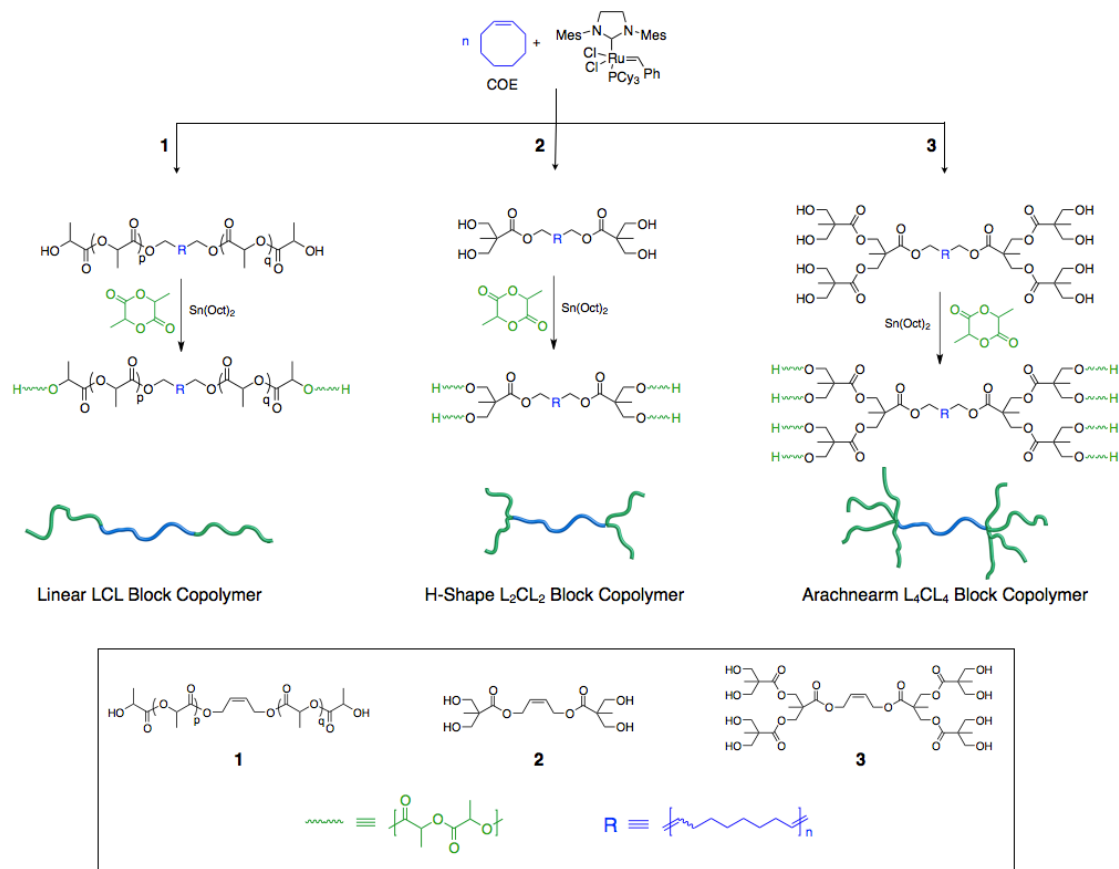
preparation of block copolymers containing mechanistically incompatible monomers is no longer a curiosity; the emergence of controlled free radical polymerizations and the development of tolerant and selective catalysts for various ring-opening polymerizations have provided access to a range of fascinating hybrid materials.<sup>23–26</sup> As a pertinent example, combining ring-opening metathesis polymerization (ROMP) with other polymerization mechanisms can be achieved by polymerizing a cyclic olefin in the presence of an acyclic olefin that acts as a chain transfer agent (CTA) and bears one or more functional groups capable of initiating the growth of another polymer.<sup>27–34</sup>

Symmetrical linear–branched hybrid block copolymers with the general architecture  $B_xAB_x$  have been synthesized from mechanistically incompatible monomers. For example, Sill and Emrick described BAB dendritic–linear hybrids by using a symmetric monounsaturated macromolecular CTA containing poly(phenyl ether) dendritic moieties in the ROMP of *cis*-cyclooctene (COE).<sup>35</sup> This general method can be extended by using end-groups capable of initiating polymerization of another monomer, as demonstrated with linear PDMS prepared anionically and modified to incorporate two hydroxyl end-groups per chain end that could be subsequently used to initiate ring-opening transesterification polymerization (ROTEP) of  $\epsilon$ -caprolactone.<sup>36</sup> Similarly, Pan and coworkers polymerized styrene using atom-transfer radical polymerization (ATRP) initiated from a symmetric difunctional species followed by post-polymerization functionalization to afford a tetrahydroxy PS macroinitiator for ring-opening polymerization of D,L-lactide (LA) resulting in  $B_2AB_2$  block polymers.<sup>37</sup> More recently, Xie and coworkers described an approach to  $AB_2$  mikto-arm block copolymers combining living ROMP with ATRP.<sup>38</sup> Poly(7-oxanorborn-5-ene) produced using the first generation Grubbs catalyst was end-functionalized with a dibromo moiety by terminating with a symmetric CTA. Branched amphiphilic block copolymers were achieved by subsequent polymerization of 2-(dimethylamino)ethyl methacrylate. As a final example, Hedrick and coworkers prepared linear polyethylene oxide (PEO) having either one or two primary amines per chain end and demonstrated the ability of each amine to initiate two PLA

chains using an organocatalyst, thus forming H-shaped and eight-arm block polymers, respectively.<sup>20</sup> This is the only example of well-defined  $B_4AB_4$  block copolymers we have found in the literature. Given the center segment in such materials is symmetrically flanked by two sets of 4 arms, they are referred to as arachne(spider)arm block copolymers in this work.

Recent studies investigated the preparation of linear BAB triblocks by combining hydroxyl initiated ROTEP of **LA** from the termini of telechelic poly(1,5-cyclooctadiene) (PCOD) prepared using ROMP (see Chapter 2).<sup>39</sup> However, the methodology employed an acetoxy protected CTA, which necessitated a somewhat tedious post-ROMP deprotection step.<sup>40</sup> This chapter describes the synthesis of three new symmetrical hydroxyl bearing CTAs with functionalities of 2, 4, and 8 through modification of commercially available *cis*-2-butene-1,4-diol (**C2B**). These CTAs undergo secondary metathesis during ROMP of *cis*-cyclooctene (**COE**) and end-group fidelity was confirmed by the successful subsequent polymerization of D,L-lactide from the poly(*cis*-cyclooctene) (PCOE) macroinitiator. Using ROMP with the multifunctional CTAs allows for direct preparation of the branched block copolymers having the  $B_xAB_x$  architectures as illustrated in Figure 3.1.



**Figure 3.1**

Schematic representation of the block copolymer synthesis with different architectures prepared in this work containing poly(*cis*-cyclooctene) [blue] and poly(D,L-lactide) [green] components.

Collectively, this chapter describes new methods for (1) the utilization of hydroxyl-bearing CTAs for ROMP that do not require post-polymerization deprotection; (2) the straightforward and direct synthesis of a set of architecturally diverse block polymers; (3) the marriage of two versatile ring-opening polymerizations that promise ready access to numerous hybrid materials; and (4) the control over secondary structure by manipulating molecular architecture in PLA-based block copolymers.

## 3.2 Results and Discussion

This section describes the synthetic procedures that were adopted to produce three new, hydroxyl-bearing CTAs with different functionality. A description of the synthesis of telechelic PCOE using the new CTAs and the subsequent polymerization of D,L-lactide from the macroinitiators follows. A large set of polymers were prepared that cover a range of compositions and molecular weights. The crystallization and bulk phase behavior for two-component symmetric triblock copolymers is evaluated.

### 3.2.1 Synthesis of Chain Transfer Agents

Hydroxyl-telechelic polymers can be routinely synthesized via ROMP of cyclic olefins in the presence of a suitably functionalized CTA.<sup>39–43</sup> Hydroxyl functionality has been achieved both directly and indirectly using **C2B**<sup>42</sup> and protected analogs of *cis* substituted CTAs,<sup>29,40,42–44</sup> respectively, which practically yield polymers with number average functionality ( $F_n$ ) = 2.<sup>†</sup> However, particular difficulty is encountered during the direct ROMP of cyclic olefins with **C2B**; low yields and poorly controlled molecular weights have been observed presumably from catalyst deactivation.

There are currently no reports<sup>‡</sup> describing the synthesis of linear polymers by ROMP with multiple hydroxyl groups per chain end. As such, three new CTAs were synthesized that ultimately lead to hydroxyl-telechelic polymers with well-controlled molecular weights and variable numbers of hydroxyl groups per chain end when polymerized with the cyclic olefin **COE** catalyzed by the 2<sup>nd</sup> generation Grubbs (**G2**) catalyst. Symmetric CTAs with two, four, or eight hydroxyl groups per molecule were synthesized starting from commercially available **C2B** according to Scheme 3.1.

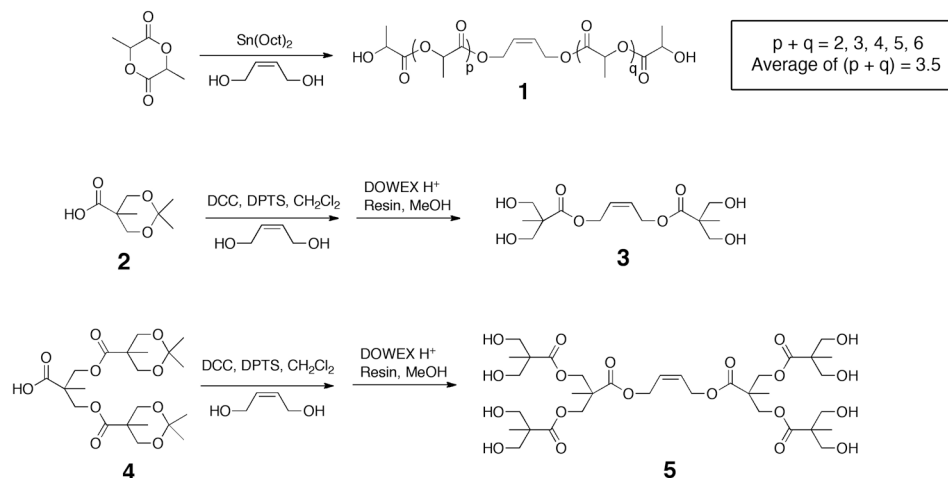
---

<sup>†</sup> Polymerization of 1,5-cyclooctadiene can yield functionality  $F_n < 2$  due to the presence of adventitious CTA vinylcyclohexene in the monomer feedstock.[45] Ji, S.; Hoyer, T. R.; Macosko, C. W. *Macromolecules* **2004**, *37*, 5485-5489.

<sup>‡</sup> This statement applies to reports outside of the literature attributed to the author of this dissertation.

## Scheme 3.1

Synthesis of difunctional (1), tetrafunctional (3), and octafunctional (5) CTAs via modification of *cis*-2-butene-1,4-diol.



Compound **1** was prepared because a CTA was desired that would lead directly to hydroxyl-telechelic ROMP products in a controlled manner, in one polymerization step, and without post-polymerization modification as was necessary using 1,4-diacetoxy-*cis*-2-butene as a CTA.<sup>39,40,42,46</sup> For practical purposes, a difunctional CTA was also sought that could be readily prepared from commercially available sources.

Compound **1** was prepared by reacting **C2B** with 2.5 equivalents of **LA** catalyzed by tin(II) 2-ethylhexanoate [ $\text{Sn}(\text{Oct})_2$ ]. The resulting product is actually a mixture of oligomers due to simultaneous ring-opening of **LA** by both **C2B** and the secondary hydroxyl that results from ring-opened **LA**. The average molecular weight of the CTA **1** mixture was estimated from  $^1\text{H}$  NMR spectroscopy and supported by elemental analysis and mass-spectrometry (see Experimental Section 3.5). The reaction conditions also facilitate transesterification to some extent according to the mass-spectrum obtained from electrospray ionization; hence, the mixture consists of **C2B** with different oligomeric lactic acid units [ $-\text{C}(\text{O})\text{C}(\text{CH}_3)\text{O}-$  =  $\text{C}_3$ ]; the average chemical make-up is reflected in Scheme 3.1, where the average of  $(p + q) \approx 3.5$ . This value is slightly larger than that expected for quantitative

initiation and conversion of lactide ring-opening  $[(p + q)_{\text{theo}} \approx 3]$ , which would be consistent with incomplete incorporation of the **C2B**. (See Experimental Details section 3.5 for further description). The critical characteristic for utility during ROMP relies on the retention of the alkene in the *cis* configuration. A high retention rate is suggested by  $^1\text{H}$  and  $^{13}\text{C}$  NMR and IR spectroscopy (see figures and discussion in Experimental Details section 3.5). The most convincing evidence for *cis* configuration comes from the accuracy with which molecular weight can be targeted based on the estimated CTA molecular weight and the ratio  $[\text{COE}]:[\text{CTA}]$ ; the *trans* version of the CTA is expected to have lower reactivity with **G2** catalyst.

The esterification of **2**<sup>47</sup> with **C2B** using dicyclohexylcarbodiimide (**DCC**) followed by deprotection of the cyclic acetal gives **3** in high yield. The first generation dendritic product formed by coupling **2** with the benzyl-ester protected derivative of bisMPA is a common building block in the preparation of hyperbranched polyesters; combining this methodology with the ROTEP of **LA** and  $\epsilon$ -caprolactone resulted in degradable hyperbranched polyesters with interesting properties.<sup>21,47–54</sup> Removal of the benzyl group by hydrogenolysis gives the acetal protected first generation dendrimer of bisMPA **4** in nearly quantitative yield. Analogous esterification of **4** with **C2B** and subsequent acid-catalyzed deprotection of the cyclic acetal yields CTA **5**. Experimental details are provided in section 3.5 along with characterization of the CTAs by  $^1\text{H}$  and  $^{13}\text{C}$  NMR spectroscopy, 2D-COSY NMR and IR spectroscopy, mass spectrometry and elemental analysis.

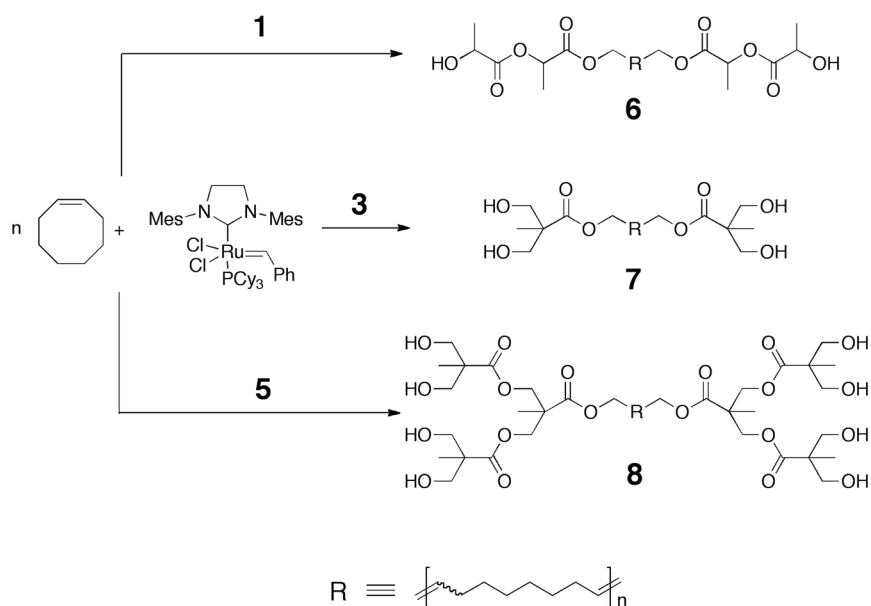
### 3.2.2 ROMP of COE with CTAs **1**, **3**, and **5**

Each of the new CTAs was used in the ROMP of **COE** to produce hydroxyl-telechelic PCOE with variable functionality as illustrated in Scheme 3.2. Polymerization in the presence of **1** provides PCOE **6** with a target  $F_n = 2$ . Likewise, CTA **3** and **COE** gives a targeted  $F_n = 4$  in the resulting telechelic PCOE homopolymer **7**, and finally polymerization of **COE** in the presence of CTA **5** provides PCOE **8** with a target  $F_n = 8$ . A catalytic quantity of **G2** ( $[\text{COE}]:[\text{Ru}] \approx 20,000$ ) facilitates simultaneous ring-opening and cross-metathesis, and the

molecular mass of the PCOE homopolymer is controlled by the molar ratio [COE]:[CTA].<sup>§</sup>

### Scheme 3.2

Polymerization of COE in the presence of CTAs **1**, **3**, and **5** to yield multiply functional hydroxy-telechelic PCOE.



Hydroxyl telechelic PCOE polymers with various targeted degree of polymerization were prepared ( $M_{n,calc}$ ) and analyzed by  $^1\text{H}$  NMR spectroscopy and SEC with a multi-angle laser light-scattering detector (MALLS). Experimentally determined molecular characteristics for the homopolymers are provided in Table 3.1; the homopolymers are identified as  $(\text{HO})_x\text{---C---}(\text{OH})_x$ , where  $x$  is the number of hydroxyl groups per chain end. For each end-functionalized homopolymer, the relative intensity of the end-group and monomer signals in the  $^1\text{H}$  NMR spectra were consistent with nearly quantitative incorporation of the CTAs. This also suggests excellent tolerance of **G2** to the hydroxyl functional groups present in the CTAs **1**,

<sup>§</sup> Such a low level of catalyst (i.e.,  $[\text{Ru}] \ll [\text{CTA}]$ ) has little bearing on the number average degree of polymerization or average functionality.

**3**, and **5** during ROMP. Apparently, the proximity of the hydroxyl group to the reactive site in **C2B** (allylic position) causes difficulty in controlling the molecular weight, presumably due to deactivation of the catalyst. The CTAs presented in this work place the hydroxyl group adequately far from the olefin in order to sustain activity and prevent deactivation. This conclusion is in line with observations made by the R. H. Grubbs research group (personal communication with R. H. Grubbs).

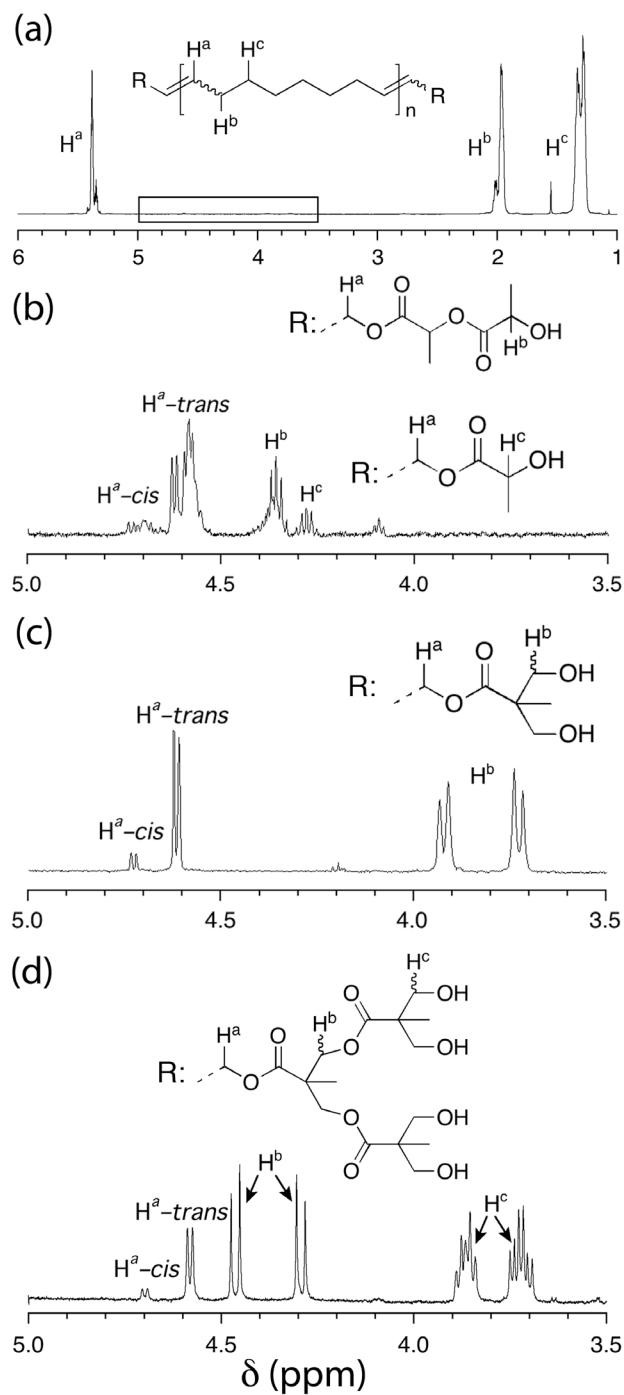
**Table 3.1**

Molecular Characteristics of PCOE homopolymers

Sample ID	$M_n^a$ (calc) kg mol <sup>-1</sup>	$M_n^b$ (NMR) kg mol <sup>-1</sup>	$M_n^c$ (LS) kg mol <sup>-1</sup>	PDI <sup>d</sup> (SEC)	$dn/dc^e$ (LS) mL/g
HO-C-OH 2k	2.3				
HO-C-OH 11k	11.5	11.4	12.9	1.8	0.111
HO-C-OH 22k	22.5	22.5	24.2	1.7	0.113
HO-C-OH 44k	44.5	49.9	47.1	1.8	0.113
HO <sub>2</sub> -C-OH <sub>2</sub> 11k	11.3	11.8	17.5	1.78	0.111
HO <sub>2</sub> -C-OH <sub>2</sub> 22k	22.3	22.8	25.5	1.71	0.112
HO <sub>2</sub> -C-OH <sub>2</sub> 44k	44.3	49.5	48.4	1.82	0.109
HO <sub>4</sub> -C-OH <sub>4</sub> 25k	25.0	27.7	30.5	1.88	0.109
HO <sub>4</sub> -C-OH <sub>4</sub> 45k	44.8	48.8	52.5		0.106

<sup>a</sup> Calculated from the initial ratio of monomer to chain transfer agent; the molar mass of the monomer and chain transfer agent are included. <sup>b</sup> Calculated from the relative intensities of signals in the <sup>1</sup>H NMR spectra corresponding to the endgroup and monomer assuming no non-functional end groups. <sup>c</sup> Measured using a light scattering detector on an SEC with THF eluant at 30 °C. <sup>d</sup> Measured using and RI detector on an SEC with CHCl<sub>3</sub> eluant at 35 °C. <sup>e</sup> Calculated from the THF SEC analysis assuming 100 % mass recovery.

Figure 3.2a shows the  $^1\text{H}$  NMR spectrum for the HO–C–OH (Table 3.1) sample of PCOE derived from CTA **1** with targeted  $M_n = 22 \text{ kg mol}^{-1}$ . For each sample of PCOE, regardless of which CTA was used, the repeat unit signals appear in identical positions and nearly identical ratios of *cis* to *trans* (~1:8) configurations were observed. Figure 3.2b, c, and d show magnified portions of the  $^1\text{H}$  NMR spectra for PCOE derived from CTAs **1**, **3**, and **5**, respectively. The  $^1\text{H}$  NMR signals associated with the allylic methylene protons adjacent to the ester on the end-groups of the different PCOE samples invariably appear at 4.6 and 4.7 ppm for the *trans* and *cis* configurations, respectively. The relative intensity of the *trans* and *cis* signals associated with the methylene protons on the end groups is consistent between samples and is also consistent with the ratio in the repeating units. These observations are consistent with a strong preference for metathesis to result in the *trans* configuration during ROMP of COE and subsequent cross-metathesis with PCOE chains.

**Figure 3.2**

$^1\text{H}$  NMR spectra for a representative homopolymer (a) showing the repeat unit signals and magnified portions showing the respective end-group signals for polymers prepared from CTAs (b) **1** [difunctional], (c) **3** [tetrafunctional], and (d) **5** [octafunctional].

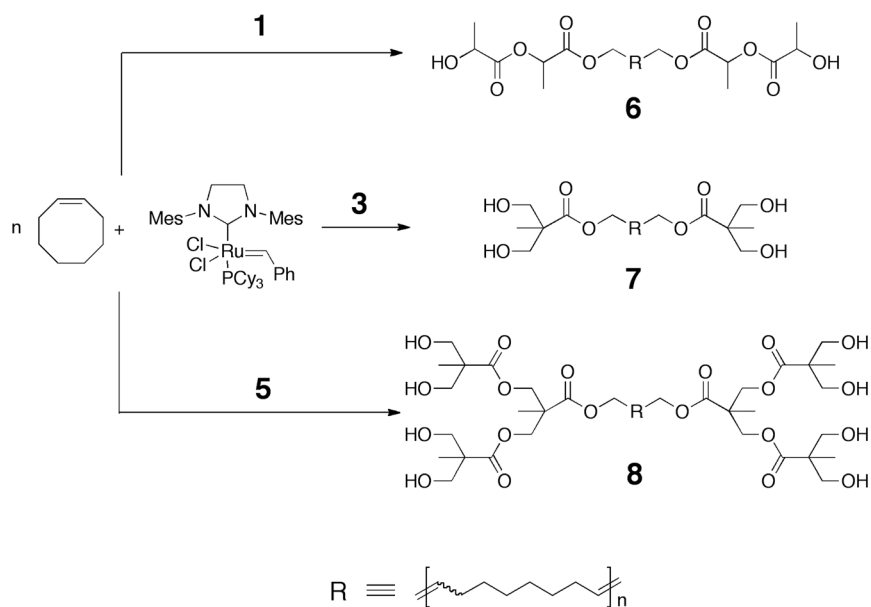


## 3.2.3 Synthesis of PCOE–PLA block copolymers

The three new CTAs described above lead to hydroxyl-telechelic polymers with well-controlled molecular weights and variable number of hydroxyl-groups per chain end; molecular weight can be modulated by changing the concentration of the CTA relative to monomer in the polymerization feed (see Table 3.1). The hydroxyl-telechelic PCOE samples shown in Table 3.1 were used to prepare symmetric  $B_xAB_x$ -type linear, H-shaped, and arachnearm block copolymers by initiating the ring-opening polymerization of D,L-lactide from the PCOE macroinitiators **6**, **7**, and **8**, respectively (Scheme 3.3). The catalyst  $\text{Sn}(\text{Oct})_2$  was chosen, relying on the well-established molecular weight control, commercial availability, and low loading ratios necessary during LA polymerization.

## Scheme 3.3

Synthesis of block copolymers from PCOE macroinitiators **6**, **7**, and **8** to prepare linear (**9**), H-shaped (**10**) and arachnearm (**11**) architectures.



Several separate block polymers with different compositions were prepared from each hydroxyl-telechelic PCOE macroinitiator. Block polymers with PLA weight fractions ( $w_L$ ) in the range 0.15–0.85 were prepared. The molecular characteristics of these samples were evaluated by  $^1\text{H}$  NMR spectroscopy and SEC with a multi-angle laser light scattering (MALLS) detector and are summarized in Table 3.2. The samples are labeled as  $L_x\text{CL}_x$  [ $\#_x\text{--}\#\text{--}\#_x$ ] where the subscript “x” specifies the number of PLA arms emanating from the branching junction between blocks (number is omitted when  $x = 1$ ) and the # is the average molecular weight of the respective block in  $\text{kg mol}^{-1}$  assuming each hydroxyl group initiated the polymerization of **LA**. The molar mass of the block copolymers were determined using the weight fractions calculated from  $^1\text{H}$  NMR spectroscopy combined with the molar mass of the hydroxy telechelic PCOE precursor determined also from  $^1\text{H}$  NMR spectroscopy (Table 3.1).

Table 3.2

Molecular characteristics of PCOE–PLA block copolymers

Sample	$M_{n,NMR}^a$ (kg mol <sup>-1</sup> )	$M_{n,MALLS}^b$ (kg mol <sup>-1</sup> )	PDI <sup>c</sup> (SEC)	$w_L^d$	$f_L^e$
<b>HO–C–OH 22k: <math>M_n</math> (NMR) = 22.5 kg mol<sup>-1</sup>; PDI = 1.70</b>					
<b>9a:</b> LCL [1.5–22–1.5]	25.0		1.67	0.12	0.09
<b>9b:</b> LCL [4–22–4]	30.1	29.5	1.54	0.27	0.21
<b>9c:</b> LCL [6–22–6]	34.8		1.45	0.37	0.30
<b>9d:</b> LCL [10–22–10]	41.1	40.8	1.39	0.46	0.39
<b>9e:</b> LCL [17–22–17]	55.1		1.34	0.60	0.52
<b>9f:</b> LCL [21–22–21]	64.1	64.0	1.31	0.66	0.58
<b>9g:</b> LCL [37–22–37]	95.1		1.36	0.77	0.71
<b>9h:</b> LCL [62–22–62]	146	124	1.32	0.85	0.80
<b>HO<sub>2</sub>–C–OH<sub>2</sub> 23k: <math>M_n</math> (NMR) = 22.8 kg mol<sup>-1</sup>; PDI = 1.71</b>					
<b>10a:</b> L <sub>2</sub> CL <sub>2</sub> [0.7 <sub>2</sub> –23–0.7 <sub>2</sub> ]	25.4		–	0.13	0.10
<b>10b:</b> L <sub>2</sub> CL <sub>2</sub> [2 <sub>2</sub> –23–2 <sub>2</sub> ]	29.5	33.5	1.56	0.25	0.20
<b>10c:</b> L <sub>2</sub> CL <sub>2</sub> [3 <sub>2</sub> –23–3 <sub>2</sub> ]	34.6		1.48	0.36	0.29
<b>10d:</b> L <sub>2</sub> CL <sub>2</sub> [5 <sub>2</sub> –23–5 <sub>2</sub> ]	40.8	45.2	1.39	0.46	0.38
<b>10e:</b> L <sub>2</sub> CL <sub>2</sub> [8 <sub>2</sub> –23–8 <sub>2</sub> ]	52.9		1.30	0.58	0.51
<b>10f:</b> L <sub>2</sub> CL <sub>2</sub> [10 <sub>2</sub> –23–10 <sub>2</sub> ]	64.5	64.2	1.27	0.66	0.58
<b>10g:</b> L <sub>2</sub> CL <sub>2</sub> [17 <sub>2</sub> –23–17 <sub>2</sub> ]	91.7		1.19	0.76	0.70
<b>10h:</b> L <sub>2</sub> CL <sub>2</sub> [30 <sub>2</sub> –23–30 <sub>2</sub> ]	144	129	1.14	0.85	0.80
<b>HO<sub>4</sub>–C–OH<sub>4</sub> 27k: <math>M_n</math> (NMR) = 27.7 kg mol<sup>-1</sup>; PDI = 1.88</b>					
<b>11a:</b> L <sub>4</sub> CL <sub>4</sub> [0.5 <sub>4</sub> –27–0.5 <sub>4</sub> ]	31.3		1.68	0.12	0.09
<b>11b:</b> L <sub>4</sub> CL <sub>4</sub> [1 <sub>4</sub> –27–1 <sub>4</sub> ]	34.3	32.9	1.62	0.19	0.15
<b>11c:</b> L <sub>4</sub> CL <sub>4</sub> [2 <sub>4</sub> –27–2 <sub>4</sub> ]	43.3		1.58	0.36	0.29
<b>11d:</b> L <sub>4</sub> CL <sub>4</sub> [3 <sub>4</sub> –27–3 <sub>4</sub> ]	49.6	44.6	1.50	0.44	0.37
<b>11e:</b> L <sub>4</sub> CL <sub>4</sub> [5 <sub>4</sub> –27–5 <sub>4</sub> ]	66.5		1.38	0.58	0.50
<b>11f:</b> L <sub>4</sub> CL <sub>4</sub> [6 <sub>4</sub> –27–6 <sub>4</sub> ]	78.0	72.3	1.33	0.65	0.57
<b>11g:</b> L <sub>4</sub> CL <sub>4</sub> [11 <sub>4</sub> –27–11 <sub>4</sub> ]	122		1.20	0.77	0.71
<b>11h:</b> L <sub>4</sub> CL <sub>4</sub> [19 <sub>4</sub> –27–19 <sub>4</sub> ]	183	164	1.15	0.85	0.80

<sup>a</sup> Determined by <sup>1</sup>H NMR spectroscopy from integration of the respective repeating unit signals and comparison with the molecular weight of the PCOE precursor. <sup>b</sup> Determined from light-scattering detector assuming known  $dn/dc$  values for the two components ( $dn/dc_{PLA} = 0.042 \text{ mL g}^{-1}$  from ref. <sup>55</sup>;  $dn/dc = 0.110 \text{ mL g}^{-1}$  from ref. <sup>56</sup>) according to eq 3.1.<sup>57</sup> <sup>c</sup> Compared with polystyrene standards. <sup>d</sup> Determined from integration of repeating unit signals in <sup>1</sup>H NMR spectroscopy. <sup>e</sup> Calculated from  $w_L$  using the reported densities of the homopolymers at ambient temperature:  $r_L = 1.25 \text{ g mL}^{-1}$  (ref. <sup>58</sup>);  $r_C = 0.89 \text{ g mL}^{-1}$  (ref. <sup>59</sup>).

The monomodality of the block polymer products observed in the SEC chromatograms in all cases suggests the absence of adventitious initiation (Figure 3.3). The chromatograms show a monotonic decrease in elution volume upon increasing  $w_L$  consistent with increasing molecular weight. Also, the PDIs relative to polystyrene standards decrease with increasing  $w_L$  (see Table 3.2). The PCOE homopolymers exhibit PDIs approaching the most probable distribution consistent with extensive chain transfer (see Table 3.1). Contrarily, Sn(Oct)<sub>2</sub>-catalyzed **LA** polymerization can provide PLA segments with relatively low PDI. The monotonic decrease in PDI upon increasing  $w_L$  suggests that the PLA blocks are significantly less polydisperse than the macroinitiator.<sup>60</sup> Indeed, several samples of PLA synthesized under identical conditions using **C2B** as an initiator resulted in PDI values of 1.1. Three samples were prepared (**C2B** initiator, Sn(Oct)<sub>2</sub> catalyst) with degrees of polymerization ( $[\text{LA}]/[\text{C2B}]$ ) equal to 50, 100 and 200 having PDIs measured in chloroform at 35 °C of 1.13, 1.14, and 1.10, respectively.

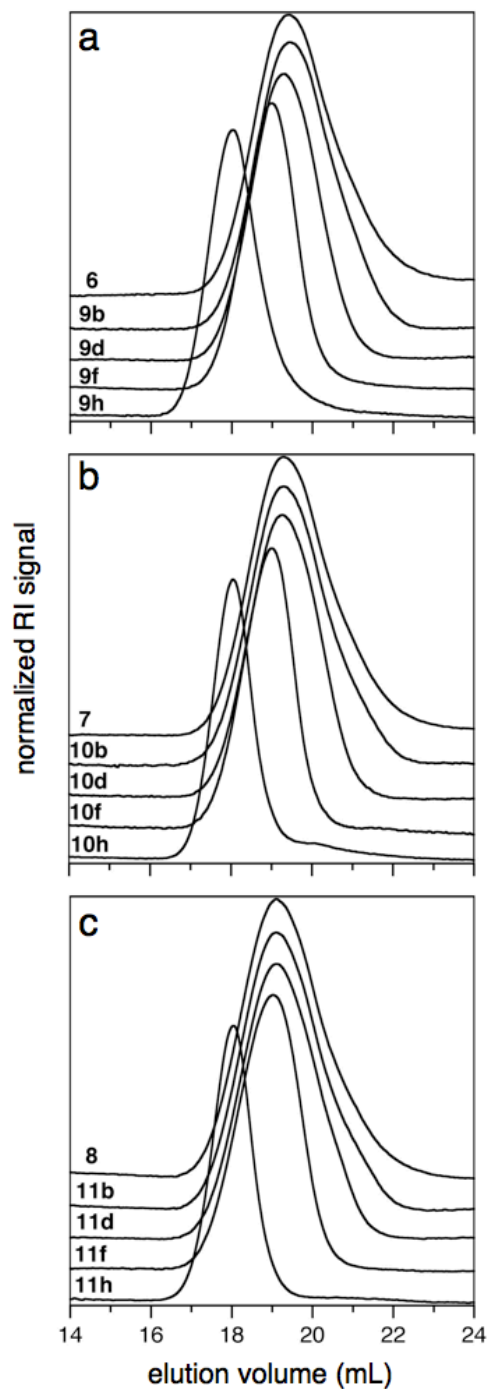


**Figure 3.3**

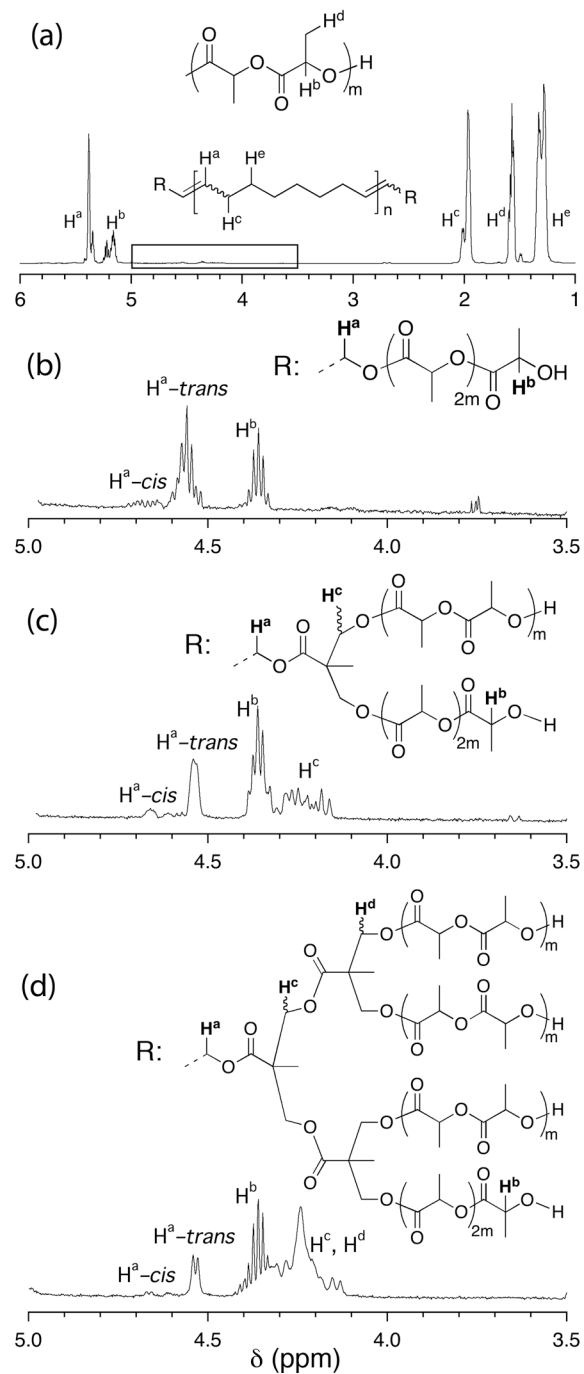
SEC chromatograms for the PCOE homopolymers and block copolymer derivatives having (a) linear [6, 9b, 9d, 9f, 9h] (b) H-shaped [7, 10b, 10d, 10f, 10h], and (c) arachnearm [8, 11b, 11d, 11f, 11h] architectures.

Chromatograms in each subset of Figure 3.3 correspond to PCOE homopolymer (**6**, **7**, **8**) and block copolymers with PLA weight fractions  $w_L$  of approximately 0.25 (**9b**, **10b**, **11b**), 0.45 (**9d**, **10d**, **11d**), 0.65 (**9f**, **10f**, **11f**), and 0.85 (**9h**, **10h**, **11h**) [see Table 3.2]. The retention time on the SEC columns correlates directly with hydrodynamic volume. As such, the subtle disparity between the relative shifts in elution volume in the SEC chromatograms accentuates the difference in hydrodynamic volume of block polymers with different architectures. The magnitude of elution volume change with increasing molecular weight becomes progressively less pronounced as the number of PLA arms increases (i.e., linear, H-shaped, and arachnearm), consistent with smaller hydrodynamic volume for branched samples compared with linear polymers of equal molecular mass.<sup>61–64</sup> The absolute molecular weights were measured using SEC with a MALLS detector. The  $dn/dc$  required for accurate molecular weight analysis was calculated for a set of PCOE homopolymers assuming 100% mass elution ( $dn/dc_{PCOE} = 0.11 \text{ mL g}^{-1}$  in THF at 30 °C). The  $dn/dc$  for PLA in THF was determined by Dorgan and coworkers ( $dn/dc_{PLA} = 0.042$  in THF at 30 °C).<sup>55</sup> The composition dependence of the  $dn/dc$  in the copolymers was calculated using eq 3.1.<sup>57</sup> The values of  $dn/dc$  tabulated in Table 3.2 were used to extract the molar masses from the MALLS detector on the SEC. The molar mass of the block polymers determined from SEC-MALLS agrees fairly well with the values calculated from end-group analysis of the telechelic PCOE precursors combined with the composition using <sup>1</sup>H NMR spectroscopy.

$$dn/dc_{AB} = \sum w_i (dn/dc)_i \quad (3.1)$$

The SEC data are consistent with the absence of adventitious initiator and the increase in molecular weight with increased **LA** concentration. However, we cannot unambiguously ascertain the initiating efficacy from SEC. The intended branched molecular architectures are only achievable with quantitative initiating efficiency. This concern is of particular relevance for the bis-MPA based dendritic–linear hybrid macroinitiators, for which the hydroxyl groups are relatively sterically hindered and therefore potentially inaccessible.

Dendritic polyesters based on bis-MPA have been shown to effectively initiate polymerization of D,L-lactide,  $\epsilon$ -caprolactone and other lactone derivatives when catalyzed by  $\text{Sn}(\text{Oct})_2$ , despite the high functional group density.<sup>21,50–54,65–69</sup> Initiating efficacy was monitored by  $^1\text{H}$  NMR spectroscopy for the branched polymers synthesized in this study. Figure 3.4a shows the full spectrum for the H-shaped copolymer sample **10d**. Again, the repeat unit signals for both components (PCOE and PLA) invariably appear at the same positions regardless of architecture or molar mass. The signals associated with the methylene units adjacent to the hydroxyl groups in the precursors (Figure 3.2b–d) were monitored and compared with the corresponding signals in the copolymers as highlighted in Figure 3.4b, 3.4c, and 3.4d for the copolymers **9d**, **10d**, and **11d** with  $w_L \approx 0.45$  having linear, H-shaped, and arachnearm architectures, respectively. The clear disappearance of the signal at 4.28 ppm was observed in comparing the linear block polymer (Figure 3.4b) to the precursor (Figure 3.2b); this further corroborates the signal being associated with the few PCOE chains having a single lactic acid unit (for discussion of this point, see the Experimental Details in section 3.5). The remaining signal at 4.35 ppm is attributed to the methine unit of PLA chain ends, whereas the signals at 4.55 and 4.68 ppm are assigned to the methylene protons situated at the junction between PCOE and PLA having *trans* and *cis* configurations, respectively. The ratio observed between the PLA endgroup and the junction protons is consistently 1 : 2, as expected. The methylene proton signals at 4.55 and 4.68 ppm appear as multiplets presumably because of the mixed stereochemistry at the PLA unit adjacent to the junction point. Similar signals were observed for analogous block polymers prepared by a different route.<sup>39</sup>

**Figure 3.4**

Representative  $^1\text{H}$  NMR spectrum for (a)  $\text{L}_x\text{CL}_x$  block copolymer and insets showing the end-group signals for block copolymers with (b) linear, (c) H-shaped and (d) arachnearm architectures.



The  $^1\text{H}$  NMR spectrum for H-shaped block copolymer **9d** in Figure 3.4c distinctly illustrates the disappearance of the methylene signal previously adjacent to the hydroxyl groups, which suggests complete initiation from each of the available hydroxyl groups. The signal reemerges downfield as a multiplet centered at 4.22 ppm, consistent with more shielding from the ester. The PLA end-group methine signal once again emerges at 4.34 ppm with an intensity ratio to the allylic methylene protons of 1 to 1. A similar trend was observed for the arachnearm block polymers; the signals associated with the hydroxyl-adjacent methylene protons at 3.72 and 3.86 ppm in Figure 3.2d disappear upon **LA** polymerization and appear as a complex multiplet between 4.1–4.4 ppm in Figure 3.4d. These signals associated with the newly formed ester overlap significantly with the PLA endgroup, as well as the methylene protons embedded in the branched structure ( $\text{H}^b$  in Figure 3.4d). The integration ratio between the composite signals from 4.1–4.4 ppm and the allylic methylene protons at 4.55 and 4.68 ppm is consistently 8 : 1 as expected from a system in which all the hydroxyls initiated **LA** polymerization *and* the branched polyester structure remains in tact, suggesting imperceptible transesterification of this sterically-hindered unit. This set of data provides compelling evidence that is consistent with the polymer samples embodying the branched architectures depicted in Figure 3.1.

### 3.2.4 Phase Behavior of Branched Block Copolymers

#### 3.2.4.1 Potential Consequences on Phase Behavior

The influence of branching on the interfacial curvature between the phase-separated domains has been explored theoretically (Figure 3.5a).<sup>70–72</sup> Experimental studies have been conducted describing the synthesis of relatively narrow molar mass distribution block copolymers prepared by anionic, cationic, controlled radical, and/or ring-opening polymerizations with simple graft (i.e.,  $\text{AB}_2$ )<sup>73–78</sup> and H-shaped (i.e.,  $\text{B}_2\text{AB}_2$ )<sup>36,37,79–84</sup> architectures. The general consequence of branching manifests itself as increased interfacial curvature away from the component with

the greater number of chains converging at the molecular junctions (i.e., the green PLA component in Figure 3.1 illustrations) compared with a completely linear chain structure. This has been illustrated on a phase-map showing the dependence of phase-boundary position on composition and arm-asymmetry combined with conformational asymmetry.<sup>85</sup> Conformational asymmetry alone has been shown to govern the position of the phase boundaries with respect to volume fraction to a moderate extent.<sup>86–90</sup> The asymmetry parameter as defined for branched block copolymers ( $\epsilon$ ) is given by eq 3.2 and reflects the disparity in branching content as well as conformational asymmetry.

$$\epsilon = \left( \frac{n_B}{n_A} \right) \left( \frac{\beta_A}{\beta_B} \right) \quad (3.1)$$

where  $n_i$  is the number of arms of component  $i$  emanating from each junction and  $\beta_i^2 = R_g^2/V = a^2/(6v_i)$ , [ $a$  = statistical segment length;  $v_i$  = standard segmental volume] and essentially reflects the relative flexibility of a particular component.<sup>91</sup> A more flexible chain inherently has smaller root mean squared radius of gyration, which would consequently give a smaller value of  $\beta$ . There is a greater entropic penalty to stretch a more flexible chain and this in turn causes curvature away from the more flexible component in self-assembled block copolymers. Therefore, both increased flexibility and increased functionality of one component (B) at a junction both cause a monotonic shift in the phase boundary of the theoretical phase diagram toward higher volume fraction of the other component (A).<sup>72,85,88,89,92,93</sup> For example, the boundaries between the lamellar (LAM) and gyroid (GYR) phases are predicted to occur at approximately  $f_A = 0.30$  and  $0.70$  for a linear block copolymer. Instead, a  $B_2A$  branched block copolymer would be expected to undergo the same phase transitions at approximately  $f_A = 0.50$  and  $0.85$ .

A conformationally symmetric block copolymer with the architecture  $B_2A$  has a value of  $\epsilon = 2.0$ . The constituting block copolymer (i.e., the most simple repeating derivative of a block copolymer) for a triblock copolymer ABA is AB, and the two

are expected to behave similarly with respect to the bulk self-assembly. This can be observed in the theoretical phase diagram for a triblock copolymer of ABA-type, for which the difference in phase boundary positions with respect to composition compared to an AB diblock copolymer is moderate (Figure 3.5b).<sup>94</sup> The constituting block copolymer for the H-shaped architecture  $B_2AB_2$  is accordingly represented by a simple graft copolymer with  $AB_2$  architecture.<sup>17</sup> Constituting block copolymers are expected to behave similarly; in other words, constituting block copolymers will typically adopt identical morphologies at a given composition and molecular weight.

The interfacial curvature, and thus the morphology adopted in a simple two-component system stems from the balance attained while simultaneously minimizing the interfacial tension and the stretching energy. A strongly segregated system, as the one dealt with in this report, has a strong tendency to minimize the interfacial area per chain; individual chains stretch relatively far from the covalent junction and thereby sharpen the A/B interface.<sup>95</sup> Copolymers having asymmetric junction functionality (i.e.,  $AB_2$  stars) contain disparate contributions to the interfacial tension among the different components, which can be accounted for in the treatment of the free energy. Intuitively, the component having two arms emanating from a covalent junction should contribute a two-fold greater energetic stretching penalty. A compositionally symmetric system can compensate for the stretching penalty by spontaneously adjusting the interfacial curvature inward toward the A domain, thereby accommodating the larger volume necessary for the two B-type chains to relax equally to the single A-type chain.<sup>96</sup>

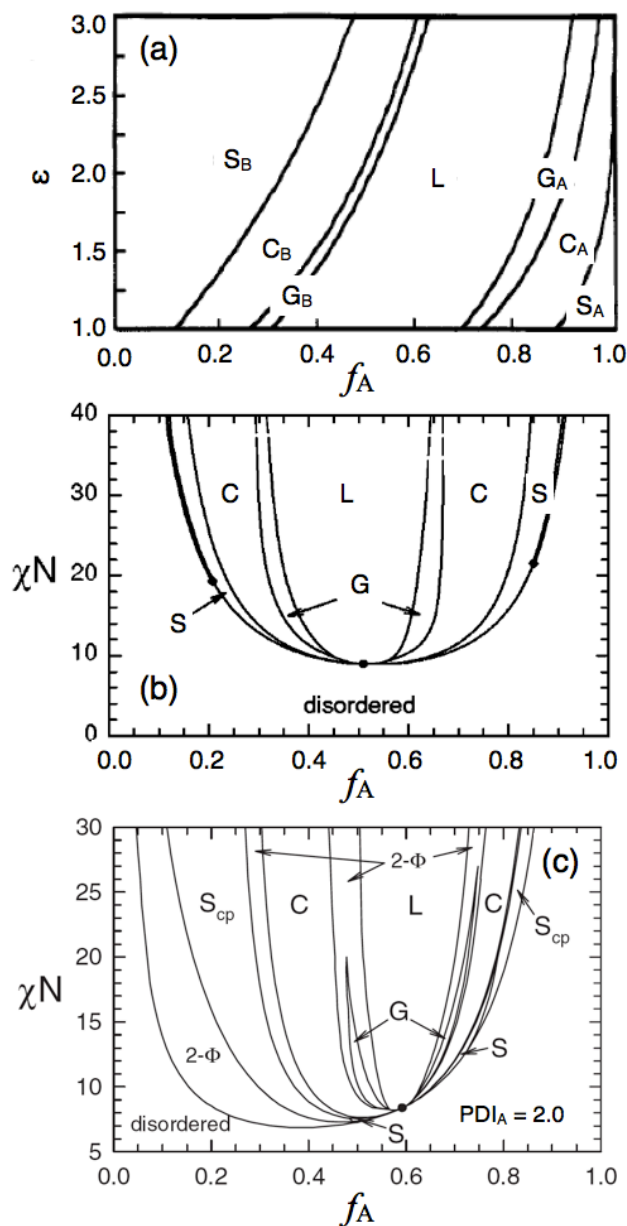


**Figure 3.5**

Theoretical phase diagrams constructed from mean-field theory for (a) monodisperse  $AB_x$  block copolymers, (b) conformationally symmetric, monodisperse, symmetric ABA triblock copolymers, and (c) conformationally symmetric AB diblock copolymers with  $PDI_A = 2.0$  and  $PDI_B = 1.0$  (Notably, relatively large windows of biphasic morphologies are predicted ( $2-\Phi$ ), as a result of macrophase separation). The x-axis in each plot corresponds to the volume fraction of the B-component ( $f_B$ ). Reproduced from references (a) <sup>72</sup>, (b) <sup>94</sup>, and (c) <sup>97</sup>

Disparity between the polydispersity of the block copolymer components may also significantly influence the phase behavior. The chain-transfer agents exploited for making the telechelic PCOE macroinitiators by ROMP effectively lead to broad polydispersity, whereby the most probable distribution is approached ( $PDI \rightarrow 2$ ). The contrasting chain-growth polymerization of lactide provides end-blocks with correspondingly narrow molecular weight distributions ( $PDI \approx 1.1\text{--}1.3$ ).

Simple AB diblock copolymers having blocks with different molar mass distributions have been theoretically<sup>85,87,98–104</sup> and experimentally<sup>105–108</sup> investigated. Ruzette and coworkers disclosed the morphological ramifications of polydisperse end-blocks in symmetric BAB-type triblock copolymers.<sup>108</sup> The high polydispersity ( $PDI \sim 1.5$ ) in the endblock comprised of poly(methyl methacrylate) (PMMA) caused an apparent shift in phase boundaries toward lower volume fraction of the midblock poly(butyl acrylate) (PBA) compared with monodisperse systems. For example, lamellar morphologies were suggested by TEM micrographs in samples where PMMA comprised the majority ( $f_{\text{PMMA}} = 0.58$ ), and a poorly organized cylindrical phase was observed with  $f_{\text{PMMA}} = 0.50$  (PMMA cylinders). The shift in morphological boundaries and spontaneous curvature toward PMMA at nearly symmetric composition was attributed to the disparity in molecular weight distributions, considering the nearly symmetric conformational characteristics (conformational asymmetry = 1.17). Notably, the polymers investigated were all relatively high molecular weight ( $M_n$  range 80–100 kg mol<sup>-1</sup>). Recently, symmetric linear BAB-type triblock copolymers with a polydisperse midblock were evaluated for morphological features by transmission electron microscopy (TEM) and small-angle x-ray scattering (SAXS).<sup>109</sup> A theoretical phase diagram has not yet been published for a triblock copolymer with disparity in the polydispersity of the component blocks. Adjusting the polydispersity in the end-block of ABC triblock terpolymers induced transitions between different ordered morphologies.<sup>110,111</sup> Increasing PDI effectively reduces the stretching energy penalty for a polymer chain. In essence, this translates to the spontaneous curvature of the A-B interface inward toward the more highly polydisperse block, corresponding to the PCOE midblock in our B<sub>x</sub>AB<sub>x</sub> system. The predicted feature of shifting the phase

boundary on the theoretical phase diagrams toward higher volume fraction of A (PCOE) moves in the same direction as that caused by asymmetry in junction functionality ( $x > 1$ ). The combined PDI disparity and branched architectures are predicted to exacerbate the phase-boundary shift and may lead to certain morphologies being adopted at compositions unprecedented in previous experimental reports.

Lastly, the bulk morphologies of block copolymers containing at least one semicrystalline component have strong path dependence and closely tied relationship to the relative values of glass transition temperature of the amorphous components and the crystallization temperature of the semicrystalline component. The block copolymers in this particular study contain PLA, which is amorphous under all observed thermal conditions with a glass transition temperature ( $T_{g,L}$ ) near  $45\text{ }^{\circ}\text{C} \pm 5\text{ }^{\circ}\text{C}$  and poly(cyclooctene) (PCOE), a semi-crystalline polymer with an equilibrium melting temperature ( $T_{m,c}$ ) of approximately  $55\text{ }^{\circ}\text{C} \pm 5\text{ }^{\circ}\text{C}$  and crystallization temperature ( $T_{c,c}$ ) of approximately  $35\text{ }^{\circ}\text{C}$ .

### 3.2.4.2 Statistical Characteristics of Block Copolymers

The statistical parameters for the system investigated in this report were taken from previous determinations. The standard reference volume ( $v_i$ ), with which segment lengths are calculated throughout the remaining text, was taken based on a four-carbon repeating unit, with the temperature dependence considered according to eq 3.3.

$$v_i = 1.084 \times 10^{-22} \cdot e^{6.85 \times 10^{-4}(T-296)} \quad (3.3)$$

Importantly, the temperature dependence of the reference volume only effects the value slightly over the experimentally relevant temperature range:  $v_i(25\text{ }^{\circ}\text{C}) = 108\text{ \AA}^3$  and  $v_i(140\text{ }^{\circ}\text{C}) = 112\text{ \AA}^3$ . The statistical segment lengths ( $a_i$ ) for the two components were acquired by different methods. For PLA, the root-mean square

(RMS) end-to-end distance ( $\langle h^2 \rangle_0$ ) was determined from neutron scattering. The ratio  $\langle h^2 \rangle_0/M$  was calculated to be  $0.699 \text{ \AA mol g}^{-1}$  at  $30 \text{ }^\circ\text{C}$  and  $0.554 \text{ \AA mol g}^{-1}$  at  $200 \text{ }^\circ\text{C}$ .<sup>112</sup> Statistical segment length for PLA ( $a_L$ ) is calculated from this measurement according to eq 3.4.

$$\frac{\langle h^2 \rangle_0}{M} = \frac{Na^2}{M} = \frac{a^2}{m_o} \quad (3.4)$$

where  $N$  is the number average repeating units of volume  $v_i$ , and correspondingly  $m_o$  is the molecular weight of the component contained within the reference volume. The value of  $m_o$  for PLA is  $81.4 \text{ g mol}^{-1}$  at  $25 \text{ }^\circ\text{C}$  and is  $77.6 \text{ g mol}^{-1}$  at  $200 \text{ }^\circ\text{C}$  as calculated using the polymer density determined by Witzke and coworkers.<sup>58</sup> This leads to a value of  $a_L$  equal to  $7.6 \text{ \AA}$  at  $25 \text{ }^\circ\text{C}$  and  $6.5 \text{ \AA}$  at  $200 \text{ }^\circ\text{C}$ .

The RMS end-to-end distance has not been directly measured for PCOE. However, the value can be estimated by taking an intermediate value between the measured values for polyethylene (PE) and 1,4-polybutadiene (PBD). The measured values of  $\langle h^2 \rangle_0/M$  for PE at  $25 \text{ }^\circ\text{C}$  and  $140 \text{ }^\circ\text{C}$  were  $1.42$  and  $1.25 \text{ \AA mol g}^{-1}$ , respectively. According to eq 3.4, this provides values of statistical segment length  $a_E$  equal to  $8.9$  and  $8.4 \text{ \AA}$  at temperatures of  $25$  and  $140 \text{ }^\circ\text{C}$ , respectively, using the repeating unit molecular weight within a volume  $v_i$  of  $56 \text{ g mol}^{-1}$  ( $\rho_{25 \text{ }^\circ\text{C}} = 0.85 \text{ g mL}^{-1}$ ;  $\rho_{140 \text{ }^\circ\text{C}} = 0.79 \text{ g mL}^{-1}$ ).<sup>113,114</sup> Likewise, the statistical segment lengths for PBD at  $25 \text{ }^\circ\text{C}$  and  $140 \text{ }^\circ\text{C}$  were calculated to be  $7.3 \text{ \AA}$  and  $7.2 \text{ \AA}$ , respectively ( $\rho_{25 \text{ }^\circ\text{C}} = 0.89 \text{ g mL}^{-1}$ ;  $\rho_{140 \text{ }^\circ\text{C}} = 0.83 \text{ g mL}^{-1}$ ).<sup>114</sup> Using this information, it was estimated that the statistical segment length for PCOE ( $a_C$ ) is approximately  $7.8\text{--}8.0 \text{ \AA}$ . Considering this information facilitates the assumption that conformational asymmetry of the system containing PLA and PCOE blocks contributes minimally to the asymmetry in the phase diagram compared with the disparity in functionality at the branching junctions, according to the calculated values of  $\beta$  (eq 3.5) and substituting into eq 3.2. Inspection of the conformational asymmetry in a similar system comprised of linear diblock copolymers containing PLA and the hydrocarbon poly(ethylene-*alt*-propylene) lends credence to this assumption. The

calculated conformational asymmetry parameter (1.06)<sup>112</sup> and the experimental phase diagram are consistent with minimal shift in the boundaries separating the ordered morphologies; the phase diagram is nearly perfectly symmetric across  $f_{\text{PLA}} = 0.50$  isopleth.<sup>112,115</sup>

$$\beta_i^2 = \frac{R_g^2}{V_{\text{tot}}} = \frac{Na^2}{6V} = \frac{a_i^2}{6v_i} = \frac{a^2 \rho N_A}{6m_o} = \frac{\langle h^2 \rangle_0}{M} \cdot \rho N_A \quad (3.5)$$

### 3.2.4.3 Morphological Characterization

Bulk self-assembly is presented for a select number of block copolymers described in Table 3.2, whereas crystallization analysis by differential scanning calorimetry (DSC) was performed on all the block copolymers.<sup>\*\*</sup>,<sup>56</sup> The morphological characteristics of certain block copolymers were evaluated by small-angle x-ray scattering (SAXS) and transmission electron microscopy (TEM). The molecular characteristics of several block copolymers with linear and H-shaped molecular architectures are provided in Table 3.3 to refresh the reader and identify the morphologies.

---

<sup>\*\*</sup> All block copolymers were evaluated with the exception of the H-shaped block copolymer having composition with approximately 15 wt % PLA.



**Table 3.3**

Molecular characteristics of several block copolymers prepared for morphological analysis.

Sample ID	$M_{n,\text{total}}^a$ kg mol <sup>-1</sup>	$M_{n,\text{PLA}}^a$ kg mol <sup>-1</sup>	$f_L^c$	PDI <sup>d</sup>	$d^*$ nm	morphology
L <sub>2</sub> CL <sub>2</sub> [2 <sub>2</sub> -23-2 <sub>2</sub> ]	29.5	7.0	0.19	1.57	32.2	lamellar
LCL [10-22-10]	41.1	18.6	0.38	1.37	35.7	lamellar
L <sub>2</sub> CL <sub>2</sub> [5 <sub>2</sub> -23-5 <sub>2</sub> ]	40.8	18.0	0.37	1.38	35.5	cylinders
LCL [21-22-21]	64.1	41.6	0.57	1.27	38.5	lamellar
L <sub>2</sub> CL <sub>2</sub> [10 <sub>2</sub> -23-10 <sub>2</sub> ]	64.5	41.6	0.57	1.23	30.2	cylinders

<sup>a</sup> Calculated from the  $M_n$  (from NMR) of the precursor PCOE being held constant, combined with the relative intensities of the respective repeat unit signals obtained from <sup>1</sup>H NMR spectroscopy. <sup>b</sup> Reported as the total molecular weight of PLA obtained from <sup>1</sup>H NMR spectroscopy; the molar mass per PLA block can be obtained by dividing by 2 for the linear copolymers or dividing by 4 for the H-shaped copolymers. <sup>c</sup> Calculated based on the weight fractions and the densities of the respective components at ambient temperature:  $\rho_L = 1.25 \text{ g mL}^{-1}$  (ref.<sup>58</sup>) and  $\rho_C = 0.89 \text{ g mL}^{-1}$  (ref.<sup>59</sup>)

One sample provides particularly compelling evidence to demonstrate certain consequences of branched architecture on morphology for the PLA–PCOE block copolymers under study. The triblock copolymer (L<sub>2</sub>CL<sub>2</sub> [2<sub>2</sub>–23–2<sub>2</sub>]; Table 3.3) with H-shaped architecture has a composition with a weight fraction of PLA ( $w_L$ )  $\approx$  0.25, which corresponds to a volume fraction of PLA ( $f_L$ )  $\approx$  0.19 at ambient temperature. Analysis of the copolymer morphology reveals microphase separation with TEM and SAXS both providing patterns consistent with a lamellar morphology. Micrographs from TEM analysis were collected at different magnifications (Figure 3.6a, b) in different areas, and are each consistent with alternating layers of light and dark components from the contrast obtained after preferential staining of PCOE with OsO<sub>4</sub> vapor. The interfaces appear on average to be relatively flat, although the lamellae are isotropically oriented within each given area. The average lamellar spacing for the microphase separated material is approximately 23 nm indicated by the measurement perpendicular to the lamellar interfaces as illustrated in Figure 3.6a. The average ratio of thickness between the light PLA

and dark PCOE layers is approximately 1:4, consistent with the estimated volume ( $f_L = 0.19$ ).

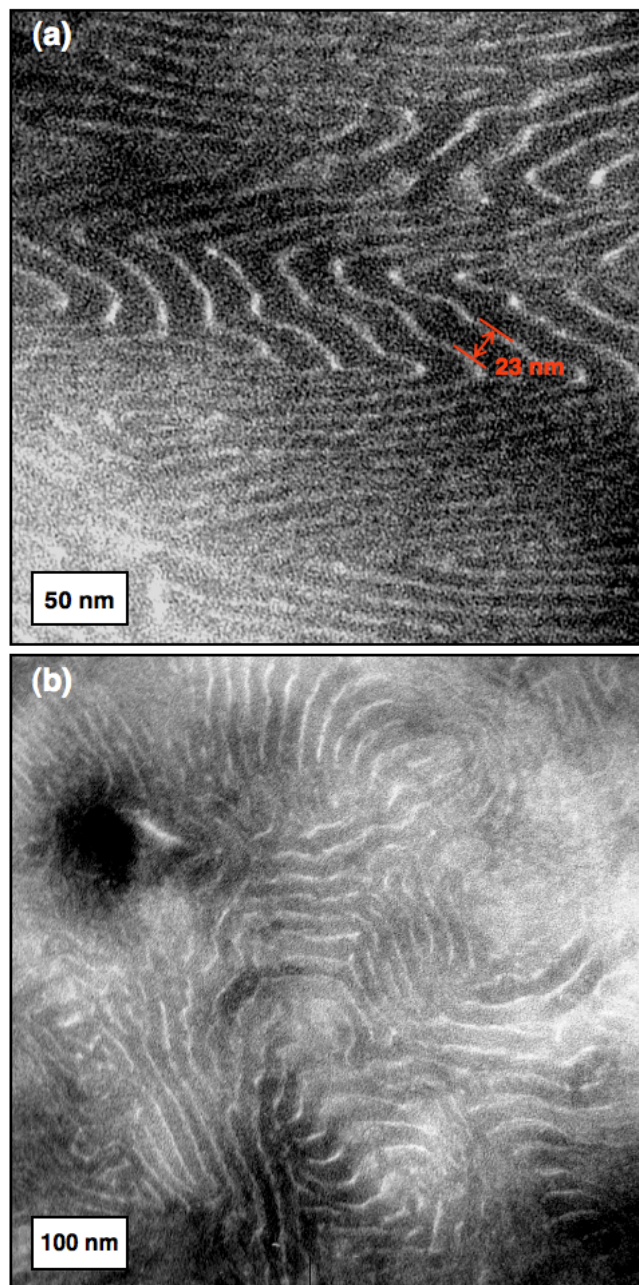
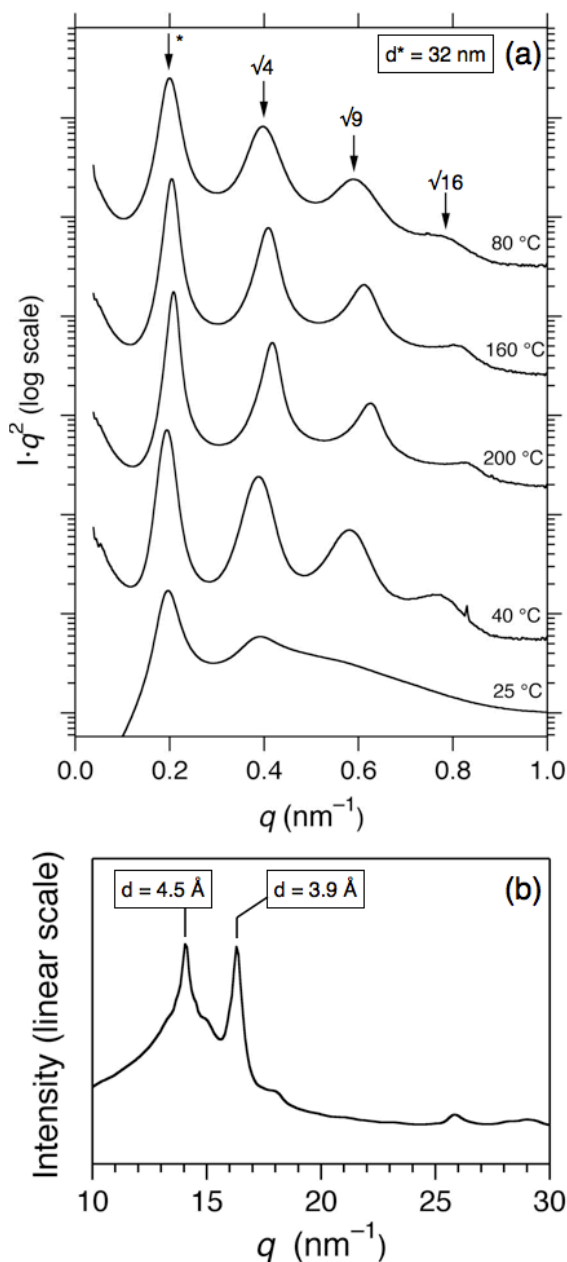


**Figure 3.6**

TEM micrographs for sample  $L_2CL_2$  [2<sub>2</sub>-23-2<sub>2</sub>] collected at magnifications of (a)  $\times 50,000$  and (b)  $\times 25,000$ . PCOE is stained dark with  $OsO_4$  vapor in the TEM micrographs.

One-dimensional SAXS profiles were collected at various consecutively increasing temperatures during heating in the melt above the crystallization temperature of PCOE ( $T_{c,c}$ ) ( $T = 80, 160, 200$  °C  $> T_{c,c}$ ) after annealing for approximately 5 minutes at each temperature. Subsequent measurements were then collected upon cooling and annealing at 40 °C ( $T > T_{c,c}$ ) and finally at 25 °C ( $T < T_{c,c}$ ). The profiles collected at  $T > T_{c,c}$  are each consistent with a lamellar morphology as indicated by several high order scattering reflections with strong intensity and maxima occurring nearly perfectly at integral multiples of the primary scattering vector  $q^*$ . Evident in the profiles provided are multiples that occur at  $2q^*$ ,  $3q^*$  and  $4q^*$ . Measurement at 25 °C (bottom profile in Figure 3.7a) shows minimal difference in the intensity and breadth of the primary scattering peak, suggesting that the morphology is preserved upon crystallization. The higher order reflections are much less pronounced at ambient temperature than at  $T > T_{c,c}$  and appear to be inundated by a broad reflection. This broad reflection suggests that crystallization has occurred, which is consistent with the crystallization temperature observed in DSC analysis ( $T_{c,c} \approx 35$  °C). The coalescence of the scattering reflections attributed to crystalline domains and the lamellar microphase separation suggest that crystallization is confined within the domains established in the melt. This crystal confinement is expected on the basis of the relative thermal transitions of the amorphous PLA which first vitrified and thereby anchored the PCOE chain ends and constrained crystallization within the prescribed microdomains. Indeed, the WAXS profile collected at 25 °C shows two reflections that are characteristic of a triclinic structure having lattice dimensions of 4.5 and 3.9 Å associated with PCOE (Figure 3.7b).<sup>116,117</sup> The domain spacing for the copolymer calculated from the position of the primary scattering peak in the SAXS profiles is  $32 \text{ nm} \pm 1 \text{ nm}$ , which is substantially larger than the lamellar periodicity observed from TEM. We hesitate to speculate upon the origin of this discrepancy. Nonetheless, the composition at which the lamellar morphology was accessed with this polymer lies well outside the window associated with the phase having flat interfacial surfaces predicted for either symmetric, monodisperse BAB triblock copolymers<sup>94</sup> or polydisperse AB diblock copolymer ( $PDI_A = 2.0$ ;  $PDI_B = 1.0$ )

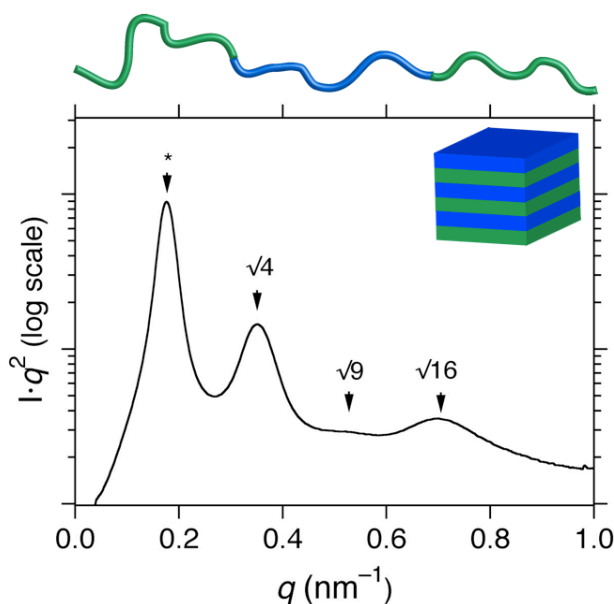
(see Figure 3.5c).<sup>97,98</sup> On the basis of theoretical predictions for the individual parameters that are combined for the system under consideration, only the asymmetry in architecture accounts for the lamellar phase predominating at such high compositional asymmetry.<sup>72</sup> Comparatively, lamellar morphologies were previously observed for linear-dendritic block copolymers having highly asymmetric compositions that lie outside of the predicted lamellar phase window experimentally and theoretically established for completely linear block copolymer counterparts. Several related branched-*block*-linear copolymers have behaved similarly. Block copolymers with a linear polystyrene block and a 6<sup>th</sup> generation poly(benzyl ether) dendritic block adopted a lamellar morphology with  $w_{\text{PS}} = 0.69$ .<sup>118</sup> Similarly, linear polystyrene combined with 5<sup>th</sup> generation poly(propylene imine) copolymers adopted a lamellar morphology as indicated by SAXS at yet higher  $w_{\text{PS}} = 0.75$ .<sup>119</sup>



**Figure 3.7**

X-ray scattering profiles for H-shaped block copolymer  $L_2CL_2$  [2<sub>2</sub>-2<sub>3</sub>-2<sub>2</sub>]: (a) one-dimensional SAXS profiles collected at various temperatures in the melt ( $T = 80, 160, 200, 40 \text{ }^\circ\text{C} > T_{c,c}$ ) and crystalline ( $T < T_{m,c}$ ) states as well as (b) one-dimensional WAXS profile collected at ambient temperature. The top SAXS profile (80 °C) has arrows indicating the position of the primary scattering peak ( $q^*$ ) and corresponding predictions for higher order peak positions associated with Bragg reflections for a lamellar morphology ( $q^*/4, q^*/9, q^*/16$ ).

The linear block copolymer LCL [10–22–10] with  $w_L = 0.46$  and  $f_L = 0.38$  was analyzed for its morphological feature by SAXS, revealing a profile consistent with a lamellar morphology (Figure 3.8).

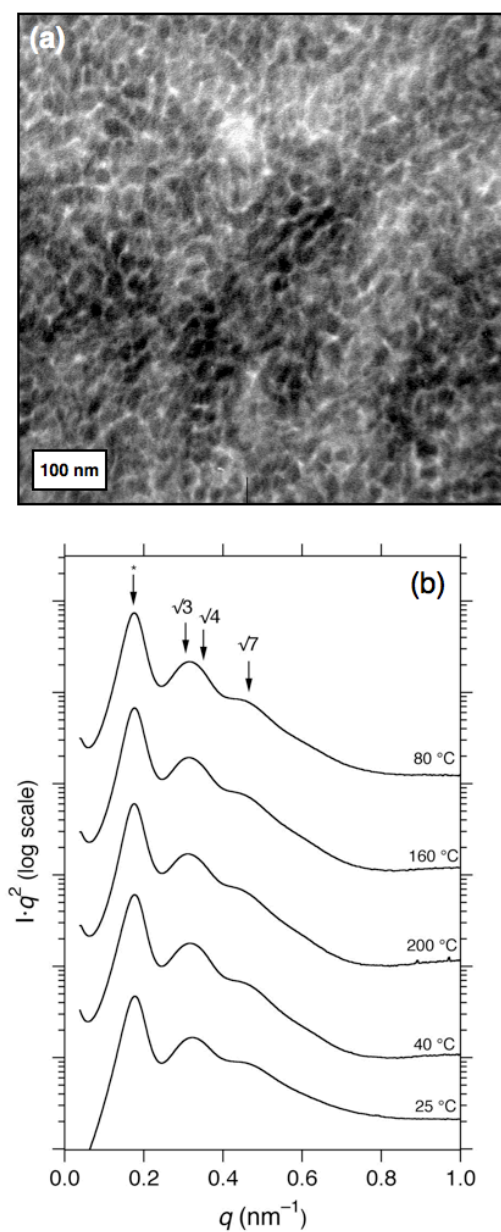


**Figure 3.8**

One-dimensional SAXS profile at 25 °C for the linear block copolymer LCL [10–22–10] having  $w_L = 0.46$  and  $f_L = 0.38$  at ambient temperature as calculated using densities of the respective homopolymers. Arrows indicate the predicted positions of Bragg reflections based on the structure factor for a lamellar morphology related to the position of the primary scattering peak at  $q^* = 0.177 \text{ nm}^{-1}$ .

Compared to the H-shaped molecular architecture, the lamellar morphology was accessed at a higher volume fraction of PLA with a completely linear architecture. The value  $f_L = 0.38$  falls within the lamellar window predicted theoretically for an AB diblock copolymer with disparate PDIs (see Figure 3.5c). The sample has a primary scattering peak at  $q^* = 0.175 \text{ nm}^{-1}$  corresponding to a periodicity of 35.8 nm.

Direct comparison between two corresponding copolymers (i.e., copolymers with different architectures and nearly identical molar mass and composition) required the preparation of the branched block copolymer  $L_2CL_2$  [5<sub>2</sub>–23–5<sub>2</sub>]. The morphology observed by TEM and SAXS revealed fascinating features (Figure 3.9).

**Figure 3.9**

$L_2CL_2$  [5<sub>2</sub>-23-5<sub>2</sub>] block copolymer: (a) TEM micrograph showing the darkly stained (with OsO<sub>4</sub>) PCOE domains on the convex side of the domain interfaces and (b) one-dimensional SAXS profiles at various temperatures with arrows indicating the predicted positions of Bragg reflections associated with a hexagonally packed cylindrical lattice.

Analysis of sample L<sub>2</sub>CL<sub>2</sub> [5<sub>2</sub>-23-5<sub>2</sub>] by TEM showed a highly disorganized array of microdomains with a clear tendency for the dark PCOE domains to reside on the concave side of highly curved interfaces. The image is not unlike the morphologies identified by Mahanthappa and coworkers for similarly polydisperse symmetric triblock copolymers of poly(styrene-*b*-butadiene-*b*-styrene).<sup>109</sup> Analogously, the midblock polybutadiene had polydispersities approaching the most probable distribution with contrastingly more narrowly dispersed polystyrene endblocks. The authors described several triblock copolymers with nearly symmetric compositions and observed molecular weight independent adoption of the disordered, bicontinuous morphology. The sample L<sub>2</sub>CL<sub>2</sub> [5<sub>2</sub>-23-5<sub>2</sub>] has substantially higher compositional asymmetry, with PCOE constituting the majority. Nevertheless, the minority PLA appears to reside predominantly on the convex side of the curved interfaces, suggesting that it constitutes the matrix domain. However, a disorganized structure with both components forming continuous paths cannot be ruled out. This observation contrasts with the predicted morphology based solely on the architectural complexity, for which a lamellar phase is expected at this composition ( $f_L = 0.38$ ). This may be related to the purported influence of disparity of polydispersity indices, essentially exasperating the shift of the phase window boundaries.

Unambiguous assignment of an ordered morphology is also difficult based on SAXS analysis of the sample L<sub>2</sub>CL<sub>2</sub> [5<sub>2</sub>-23-5<sub>2</sub>] (Figure 3.9b). The polymer is clearly microphase separated at elevated temperatures (80, 160, 200 °C > T<sub>m,c</sub>) and retains the identical morphology after cooling below T<sub>c,c</sub>. The sharp primary scattering peak occurs at  $q^* = 0.177 \text{ nm}^{-1}$  at 80 °C, corresponding to  $d = 35.8 \text{ nm}$ . This is nearly identical to the principal domain spacing for the completely linear analog LCL [10-22-10]. However, the shapes and positions of higher order reflections for the H-shaped block copolymer are unique compared with its linear analog. Most notably, the appearance of a broad reflection centered near  $q^*\sqrt{7} = 0.47 \text{ nm}^{-1}$  is suggestive of a cylindrical morphology. Additionally, the wide breadth of the secondary scattering reflection covers the region in which two other characteristic signals for hexagonally packed cylinders would be anticipated, namely  $q^*\sqrt{3}$  and



$q^*\sqrt{4}$  (see arrows in Figure 3.9). Collectively, these features suggest a hexagonal symmetry, though lacking long-range organization and perhaps mixed with a disordered microphase separated structure as observed by TEM. For the benefit of comparison, we calculated the average cylinder radius ( $r_c$ ) assuming a well-ordered hexagonal array and the interplanar domain spacing obtained by SAXS with  $f_c = 0.63$  at 25 °C, which gave a value  $r_c = 17.1$  nm according to eq 3.6. On the basis of the TEM micrograph in Figure 3.9a, the average radius of the two dimensional disk-like domains ranges from 10–15 nm. This is relatively consistent with the value obtained by SAXS assuming a cylindrical morphology. Perhaps the effects of PDI disparity and branched architecture are additive and thereby amplify the shift in the PCOE cylinder phase window beyond the  $f = 0.5$  isopleth, and causing an inverse cylindrical-type phase to exist in a small window, in which the minority phase occupies the continuous matrix.

$$r_c = \left( \frac{2d^2 f_c}{\sqrt{3}\pi} \right)^{\frac{1}{2}} \quad (3.6)$$

Brief analysis of two additional samples sharing identical composition and molar mass but differing in molecular architecture helps to emphasize the influence on morphological behavior. Two samples were prepared with virtually identically sized midblocks targeting a composition with majority PLA. Namely, samples LCL [21–22–21] with a linear structure and L<sub>2</sub>CL<sub>2</sub> [10<sub>2</sub>–23–10<sub>2</sub>] with an H-shaped architecture both have  $w_L = 0.66$ , which corresponds to  $f_L = 0.57$  at 25 °C. Profiles from SAXS of the linear block copolymer at various temperatures from 25–200 °C all suggest a lamellar morphology based on the positions of the scattering reflections appearing at integral multiples of the principal peak at  $q^* = 0.163$  nm<sup>-1</sup> (Figure 3.10a). The corresponding principal d-spacing of 38.5 nm is larger than the lamellar periodicity for the linear LCL [10–22–10] ( $d = 36$  nm) owing to the difference in chain length. Crystallization is presumably confined within the lamellar microdomains established in the melt as evinced by the similitude of profiles at temperatures both greater and less than  $T_{c,c}$ . The lamellar morphology

in the linear triblock falls within a composition range predicted for compositionally symmetric monodisperse triblock copolymers and polydisperse diblock copolymers. Despite the absence of theoretical treatment of polydisperse triblock copolymers, it is anticipated that nearly symmetric composition would be predicted to adopt a morphology with approximately flat interfaces.

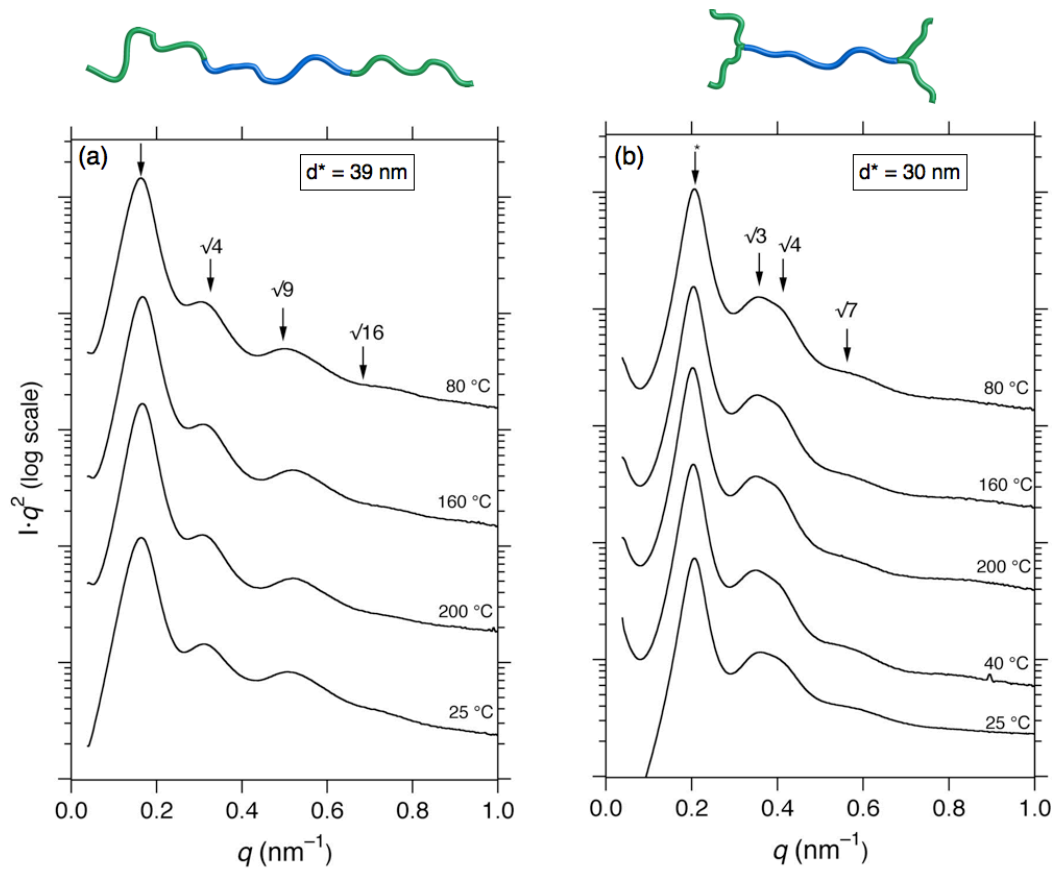


**Figure 3.10**

One dimensional SAXS profiles at various temperatures for (a) linear triblock copolymer LCL [21–22–21] with  $w_L = 0.66$  and  $f_L = 0.57$  (at 25 °C) exhibiting higher order reflections consistent with a lamellar morphology and (b) H-shaped block copolymer  $L_2CL_2$  [10<sub>2</sub>–23–10<sub>2</sub>] with  $w_L = 0.66$  and  $f_L = 0.57$  (at 25 °C) exhibiting higher order reflections consistent with a cylindrical morphology. Morphology assignments are based on the correlation of reflection positions with the predicted positions of Bragg reflections consistent with the lattice parameters.

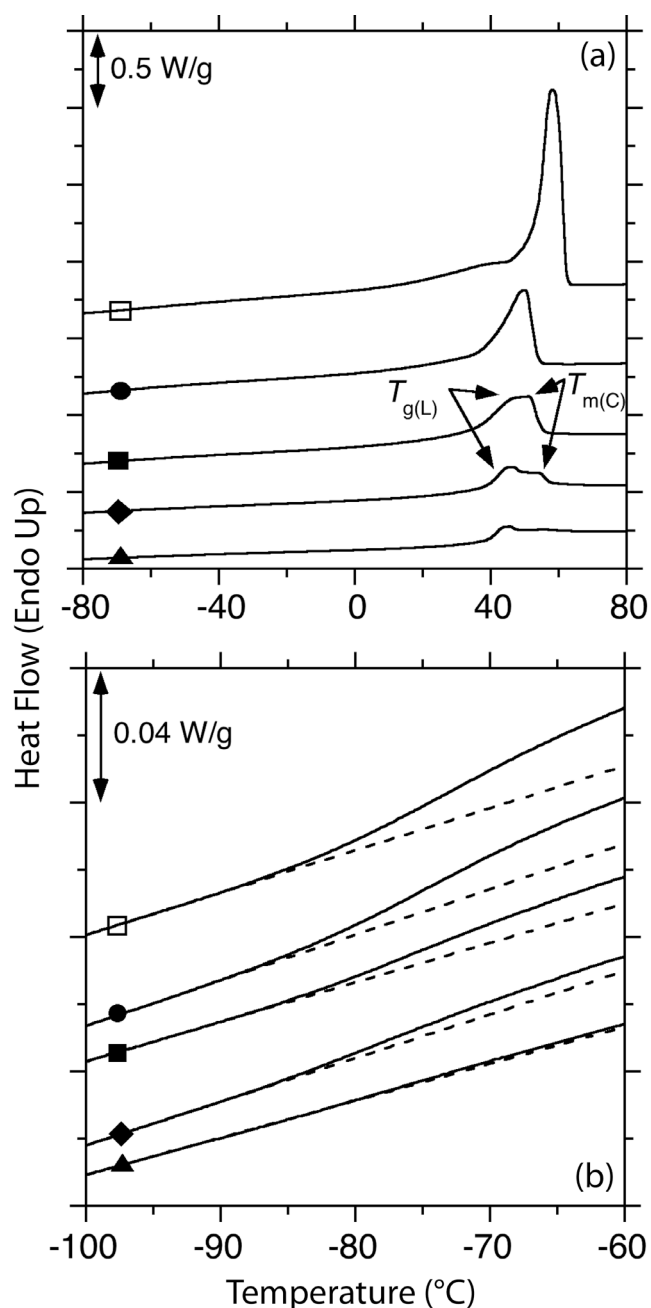
The H-shaped block copolymer L<sub>2</sub>CL<sub>2</sub> [10<sub>2</sub>–23–10<sub>2</sub>] contrastingly exhibits scattering profiles that are consistent with a hexagonal array of cylinders (Figure 3.10b). There appear clearly demarcated, albeit relatively broad, reflections occurring at multiples of  $\sqrt{3}$ ,  $\sqrt{4}$ , and  $\sqrt{7}$  to the principal scattering peak at  $q^* = 0.208 \text{ nm}^{-1}$  at 80 °C. The profiles have essentially indistinguishable features at all other temperatures with slightly varied positions in accordance with the domain-spacing temperature dependence. Cylinder radius  $r_c$  was approximated to be 12.0 nm based on the value  $f_c = 0.43$  at 25 °C and the corresponding principal domain spacing  $d^* = 30.2 \text{ nm}$ . This is consistent with the expected cylinder size compared with the sample L<sub>2</sub>CL<sub>2</sub> [5<sub>2</sub>–23–5<sub>2</sub>] with the calculated  $r_c = 17.1 \text{ nm}$ . Despite the midblock size being identical, the sample with a larger overall molar mass will have smaller cylinder radius based on the difference in packing density assuming that the same component occupies the cylinder volume; in this case that component is PCOE.

Comparing the domain spacing obtained from SAXS between the two samples in Figure 3.10 (copolymers L<sub>2</sub>CL<sub>2</sub> [10<sub>2</sub>–23–10<sub>2</sub>] and LCL [21–22–21]) suggests that two different morphologies are adopted. Mean-field approximations predict that a sample exhibiting hexagonally packed cylinders will have a substantially smaller principal domain spacing than a sample with identical molecular weight that adopts a lamellar morphology.<sup>120</sup> A summary of the morphological features in the selected block copolymers described above is provided in Table 3.3.

### 3.2.4 Thermal Properties of PCOE–PLA Block Copolymers

PCOE homopolymer is a semicrystalline material at ambient temperatures under most conditions with a melting temperature ( $T_{m,c}$ ) near 55 °C.<sup>59</sup> Polymerization of racemic LA results in amorphous PLA with a glass transition temperature ( $T_{g,L}$ ) near 50 °C. Figure 3.11 shows the differential scanning calorimetry (DSC) thermograms for the PCOE homopolymer precursor and several representative linear block copolymers with various compositions upon heating from –120 °C to 120 °C. Only a select portion of the thermograms is displayed in

Figure 3.11 to accentuate the sections in which the relevant thermal transitions occur. The heating portion represents the second heat after the thermal history of the samples was standardized by first heating to 160 °C followed by cooling to -120 °C at 10 °C min<sup>-1</sup> and second heating again to +120 °C at 10 °C min<sup>-1</sup>. The melting transition for the PCOE homopolymer occurs at  $\approx 55$  °C and the melting enthalpy corresponds to a degree of crystallinity,  $X_c = 31\%$  as calculated from  $X_c = \Delta H_m / \Delta H_m^0$  ( $\Delta H_m^0 = 216$  J/g).<sup>59</sup> The glass transition temperature of the HO-C-OH PCOE ( $T_{g,C}$ ) homopolymer occurs at -75 °C as evident from the top profile in the magnified portion of the thermograms (Figure 3.11b). The glass transition temperature of the PLA ( $T_{g,L}$ ) in the block polymers occurs between 35 °C and 40 °C and appears to overlap with the  $T_{m,C}$  during heating at 10 °C min<sup>-1</sup>. The relative invariability and well-separated  $T_g$  of each component suggests microphase separation throughout the chosen composition range, consistent with the discussion in the previous section regarding TEM and SAXS.<sup>39</sup> The relative magnitude of the glass transition for the two components is consistent with the compositional changes determined from SEC and <sup>1</sup>H NMR spectroscopy summarized previously. Figure 3.11b accentuates the variation in  $T_{g,C}$  magnitude with dashed lines added to fit the linear baseline signal at temperatures below  $T_{g,C}$ . The vertical distance between the dashed extrapolation of the baseline signal and the experimental data at temperatures greater than  $T_{g,C}$  provides an estimate of the relative magnitude of the transition and is consistent with the composition.

**Figure 3.11**

DSC thermograms representing the second heat of the HO-C-OH PCOE homopolymer precursor (□) and linear LCL triblock polymers with PLA weight fractions ( $w_L$ ) of 0.25 [9b] (●), 0.45 [9d] (■), 0.65 [9f] (◆), and 0.85 [9h] (▲). Part (a): thermograms from -80 to 80 °C; part (b): magnified portion of thermograms highlighting  $T_{g,c}$ .

Crystallization phenomena for several block copolymers were investigated using DSC. On the basis of previously reported crystallization behavior for block copolymers with at least one semicrystalline component, several important inferences can be made with respect to the melt-phase morphologies, as reviewed previously.<sup>121,122</sup>

Previous discussion of segregation strength associated with the block copolymers revealed that the system nearly always occupies the strong segregation regime within the relevant temperature range ( $T < 200$  °C). Combining strong segregation with the relationship between the relevant transition temperatures ( $T_{g,L} > T_{c,C}$ ) suggests that crystallization occurs within the confined domains of the microphase separated structures established in the melt.<sup>121,122</sup> That is, annealing at elevated temperatures ( $T \gg T_{m,C}$ ) followed by cooling at a moderate rate ( $\sim 10\text{--}50$  °C min<sup>-1</sup>) should result first in PLA vitrification followed by crystallization of PCOE within the confines that are templated by the glassy PLA.

Sizes of domains rich in either of the two components in a microphase separated system are typically on the order of 5–50 nm. As an example, diameters of spheres in this range correspond to a volume range of 65–65,500 nm<sup>3</sup>. Considering an average degree of polymerization for PCOE being  $N_c = 200$  and taking a density of 0.85 g cm<sup>-3</sup>, that volume range correlates with an average number of chains per sphere ranging from 1.5–1500. Previous micrographs demonstrated the domain sizes for the polymers in question lie somewhere intermediate between these values, and therefore several hundred chains are likely contained within a sphere of PCOE.

The mechanisms by which polymers may undergo crystallization occur in two manners. Polymer chains can spontaneously aggregate and align with one another to form an ordered crystallite, thereby serving as a nucleation site from which further crystallization can propagate. This method is termed *homogeneous* nucleation. In contrast, polymer crystallization may occur from *heterogeneous* nucleation sites from impurities (e.g., catalyst residue, dust). The former case is energetically unfavorable, and requires substantial supercooling for crystal nucleation and growth. The latter case is the most energetically favorable, and is

nearly always the mechanism by which bulk polymers crystallize, since the alternative would require unattainably pristine samples without a single impurity.<sup>123</sup> However, block copolymers offer a distinct scenario in which homogeneous nucleation may predominate, or alternatively in which multiple crystallization events can take place independently from heterogeneities with different nucleating energy barriers. For example, if the spherical domains described above contain only a few hundred polymeric chains, the probability of an isolated domain having no heterogeneities becomes statistically significant. Naturally, a considerable portion of the isolated domains may be absent of impurities, and thereby nucleate and crystallize by the homogeneous mechanism. The relative position of crystallization exotherms provide substantive support to this claim;  $T_c$  should occur at lower temperature compared with bulk crystallization as a result of the necessary supercooling for homogeneous nucleation.<sup>124</sup> Multiple crystallization exotherms are sometimes observed at separate temperatures as multiple crystallization mechanisms may be at play. For example, a large distribution of sizes in isolated crystallizable domains would statistically provide good opportunities for simultaneous homogeneous and heterogeneous nucleation, with the larger domains having correspondingly higher probabilities of containing impurities. Similarly, small domain sizes (e.g., 5–50 nm) with narrow distribution of size may have several different types of heterogeneities with considerably different energetic barriers to critically nucleate crystallization. However, complete crystallization in one isolated domain is prevented from propagating through a barrier such as a glassy matrix. Likewise, if the semicrystalline component of a block copolymer occupies a continuous matrix phase, then crystallization nucleated by even a relatively small number heterogeneities will rapidly propagate throughout the entire material, and a single exotherm is expected in the DSC cooling thermogram. The phenomenon of multiple crystallization mechanisms occurring simultaneously and independently is termed fractionated crystallization,<sup>125,126</sup> and regularly occurs in block copolymers with semicrystalline components due to the distinctly small domains accessible as a result of microphase separation.

Thermograms from DSC analysis of block copolymers containing PLA end-blocks and PCOE midblocks with different architectures and a range of compositions with approximate volume fractions of PCOE  $f_c = 0.2$ – $1.0$  reveal distinctly different behaviors (Figure 3.12).

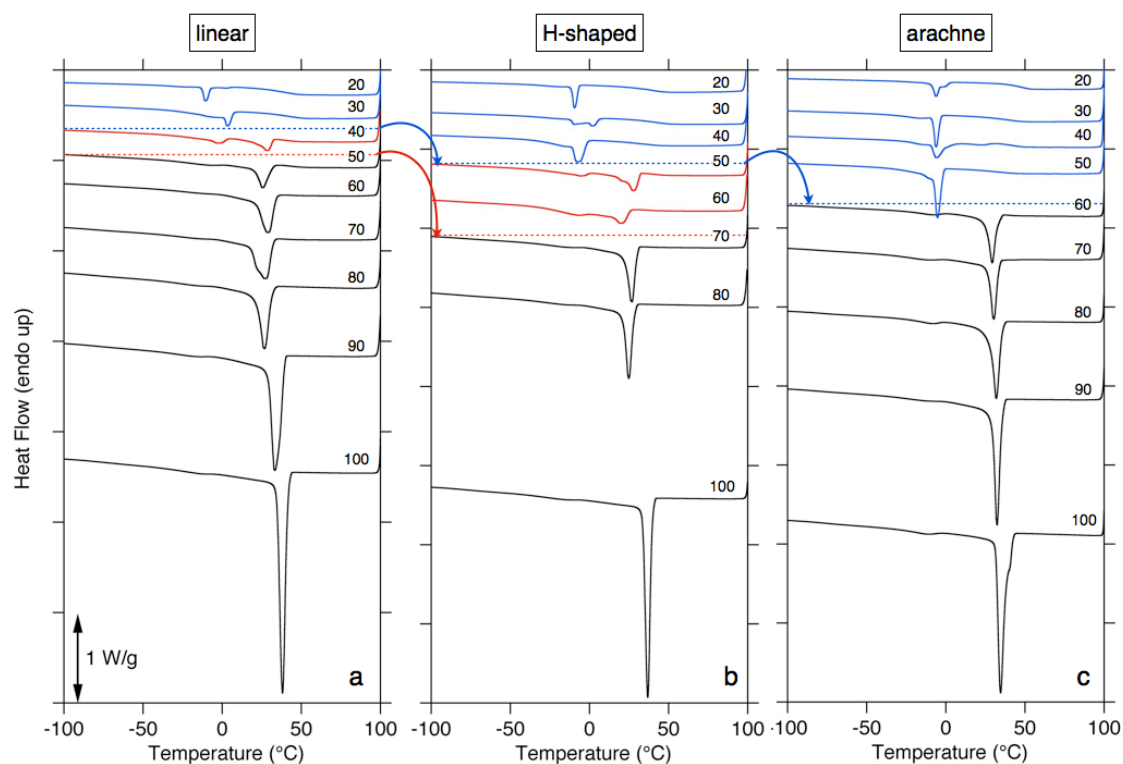


**Figure 3.12**

DSC cooling thermograms (rate =  $10\text{ °C min}^{-1}$ ) for block copolymers with a range of compositions with volume fractions of PCOE ( $f_c$ ) from 0.2–1.0 (given in percentages above the corresponding thermograms) with (a) linear, (b) H-shaped,<sup>††</sup> and (c) arachne-arm molecular architectures. Colors correspond to different regimes of crystallization behavior: only heterogeneous nucleation (black), mixed heterogeneous and homogeneous nucleation (red), and only homogeneous nucleation (blue).

<sup>††</sup> There is no sample with H-shaped architecture and 90 vol. % PCOE



The nucleation and crystallization behavior apparently depends on both composition and molecular architecture, which are intimately tied to the melt microphase separated morphologies. The thermograms indicate distinctly different nucleation phenomena occurring by the drastically different positions of crystallization exotherms with respect to supercooling temperature. The minimum in the exotherm occurs nearly identically at  $36.5\text{ }^{\circ}\text{C} \pm 2\text{ }^{\circ}\text{C}$  for the three PCOE homopolymers with different end-functionality number (i.e.  $\text{HO}_x\text{-PCOE-OH}_x$  with  $x = 1, 2, 4$ ). The crystallization and melting temperatures and enthalpies of crystallization associated with the different PCOE homopolymers shown in Figure 3.12a–c are all consistent with previous reports that evaluated thermal properties by DSC (Table 3.4).<sup>59,117</sup> The  $T_m$  and  $T_c$  both are depressed when PLA end-blocks accompany the PCOE in the triblock copolymers, in accordance with the slight decrease in crystallite size that would be expected when tethering a semicrystalline chain at either end with an incompatible component. SAXS and TEM analysis suggest that the highly incompatible pair causes microphase separation, even at highly asymmetric composition. The relative position of  $T_{c,C}$  and  $T_{g,L}$  also suggests that crystallization occurs after vitrification during cooling, thus anchoring both ends of the PCOE chains during crystallization, and thereby retarding the chain diffusion that occurs during the chain packing associated with crystallization. These topological constraints manifest themselves as depressed  $T_m$  and  $T_c$  by several degrees. Nonetheless, a single crystallization exotherm appears for the linear copolymers having  $f_C$  from 1.0–0.5 with  $T_{c,C}$  ranging from 28–38  $^{\circ}\text{C}$ , a breadth of 10  $^{\circ}\text{C}$ . Two distinct exotherms are observed with minima at 26  $^{\circ}\text{C}$  and –3  $^{\circ}\text{C}$  for the linear sample with  $f_C = 0.4$ . The sample with  $f_C$  equal to 0.3 exhibits a single sharp exotherm centered at 3  $^{\circ}\text{C}$  with a weak shoulder trailing toward lower temperature. Such a low  $T_{c,C}$ , being approximately 35  $^{\circ}\text{C}$  lower than the PCOE homopolymer, suggests an alternate nucleation mechanism as opposed to a mere artifact of anchored chain ends during crystallization. Similarly, the sample with  $f_C$  equal to 0.2 shows a single exotherm positioned at –11  $^{\circ}\text{C}$ , again suggesting an alternate nucleation mechanism. The  $T_{c,C}$  of this particular sample falls nearly 50

°C lower than the  $T_{c,c}$  for the bulk PCOE material. The combined thermal results implicate a transition in the bulk morphology adopted in the melt. Specifically, a transition apparently occurs from the sample with  $f_c = 0.5$ , in which the PCOE occupies a continuous domain, to the sample with  $f_c = 0.4$ , in which a notable portion of the PCOE occupies isolated domains that are absent of heterogeneities. The isolated domains undergo nucleation at greater supercooling. This transition is consistent with the predicted position on the theoretical phase diagram from a lamellar to a cylindrical morphology, with the minority PCOE occupying isolated cylindrical domains. In actuality, the molecular characteristics prohibit the adoption of a well ordered cylindrical morphology. Instead, the disordered morphological features suggested by the SAXS analysis cause a distribution of domain shapes and sizes, consistent with the mixed nucleation behavior attributed to the thermogram. Larger asymmetry results in increased curvature of the domain interfaces and therefore larger portions of the PCOE phase occupy isolated, sphere-like domains, accounting for the complete transition to homogeneous nucleation suggested by the thermograms for samples  $f_c = 0.3$  and  $0.2$ .

Identical transitions in nucleation behavior are observed for the H-shaped block copolymers, however the compositional boundaries at which the transitions occur are shifted to higher volume fractions of PCOE. Complete heterogeneous nucleation and a corresponding single crystallization exotherm centered at  $T_{c,c} = 27\text{--}37$  °C are observed for samples with  $f_c$  ranging from 1.0 to 0.7, whereas mixed crystallization exotherms occur for samples with  $f_c$  equal to 0.6 and 0.5. Single crystallization exotherms with significantly depressed  $T_{c,c}$  associated with homogeneous nucleation occur at  $-6$ ,  $-11$  and  $-8$  °C in samples with  $f_c$  equal to 0.4, 0.3, and 0.2, respectively. Notably, the sample with  $f_c$  equal to 0.3 exhibits a multimodal crystallization exotherm with minima occurring at  $2$  °C and  $-11$  °C, suggesting multiple nucleation mechanisms at work. However, neither mechanism appears to be consistent with heterogeneously nucleated crystal growth associated with bulk PCOE.

Table 3.4

Thermal characteristics of L<sub>x</sub>CL<sub>x</sub> block copolymers.

Sample	$T_{m,C}^a$ (°C)	$T_{c,C}^a$ (°C)	$T_{g,C}^b$ (°C)	$\Delta H_c^c$ (J g <sup>-1</sup> )	$X_C^d$ (%)
<b>HO-C-OH 22k: <math>T_m = 58</math> °C; <math>T_c = 38</math> °C; <math>T_{g,C} = -66</math> °C ; <math>X_C = 31</math>%</b>					
<b>9a:</b> LCL [1.5-22-1.5]	58	34	-69	62	33
<b>9b:</b> LCL [4-22-4]	49	27	-71	40	25
<b>9c:</b> LCL [6-22-6]	49	28	-71	32	24
<b>9d:</b> LCL [10-22-10]	50	29	-71	29	25
<b>9e:</b> LCL [17-22-17]	47	26/-9	-72	19	22
<b>9f:</b> LCL [21-22-21]	46	29/-3	-76	13	17
<b>9g:</b> LCL [37-22-37]	47	3/-10	-73	13	25
<b>9h:</b> LCL [62-22-62]	50	-11	-86	5	16
<b>HO<sub>2</sub>-C-OH<sub>2</sub> 23k: <math>T_m = 56</math> °C; <math>T_c = 37</math> °C; <math>T_{g,C} = -66</math> °C ; <math>X_C = 31</math>%</b>					
<b>10a:</b> L <sub>2</sub> CL <sub>2</sub> [0.7 <sub>2</sub> -23-0.7 <sub>2</sub> ]					
<b>10b:</b> L <sub>2</sub> CL <sub>2</sub> [2 <sub>2</sub> -23-2 <sub>2</sub> ]	49	26	-70	43	26
<b>10c:</b> L <sub>2</sub> CL <sub>2</sub> [3 <sub>2</sub> -23-3 <sub>2</sub> ]	48	27/-5	-72	34	25
<b>10d:</b> L <sub>2</sub> CL <sub>2</sub> [5 <sub>2</sub> -23-5 <sub>2</sub> ]	47	21/-7	-74	28	24
<b>10e:</b> L <sub>2</sub> CL <sub>2</sub> [8 <sub>2</sub> -23-8 <sub>2</sub> ]	44	28/-2	-72	18	20
<b>10f:</b> L <sub>2</sub> CL <sub>2</sub> [10 <sub>2</sub> -23-10 <sub>2</sub> ]	47	-6	-74	18	24
<b>10g:</b> L <sub>2</sub> CL <sub>2</sub> [17 <sub>2</sub> -23-17 <sub>2</sub> ]	44	2/-11	-74	9	17
<b>10h:</b> L <sub>2</sub> CL <sub>2</sub> [30 <sub>2</sub> -23-30 <sub>2</sub> ]	48	-8		8	25
<b>HO<sub>4</sub>-C-OH<sub>4</sub> 23k: <math>T_m = 58</math> °C; <math>T_c = 35</math> °C; <math>T_{g,C} = -72</math> °C ; <math>X_C = 31</math>%</b>					
<b>11a:</b> L <sub>4</sub> CL <sub>4</sub> [0.5 <sub>4</sub> -27-0.5 <sub>4</sub> ]	56	33	-70	52	27
<b>11b:</b> L <sub>4</sub> CL <sub>4</sub> [1 <sub>4</sub> -27-1 <sub>4</sub> ]	58	32	-76	47	27
<b>11c:</b> L <sub>4</sub> CL <sub>4</sub> [2 <sub>4</sub> -27-2 <sub>4</sub> ]	52	30	-71	35	25
<b>11d:</b> L <sub>4</sub> CL <sub>4</sub> [3 <sub>4</sub> -27-3 <sub>4</sub> ]	52	30/-8	-78	28	23
<b>11e:</b> L <sub>4</sub> CL <sub>4</sub> [5 <sub>4</sub> -27-5 <sub>4</sub> ]	51	-5	-75	23	26
<b>11f:</b> L <sub>4</sub> CL <sub>4</sub> [6 <sub>4</sub> -27-6 <sub>4</sub> ]	52	-6	-78	15	19
<b>11g:</b> L <sub>4</sub> CL <sub>4</sub> [11 <sub>4</sub> -27-11 <sub>4</sub> ]	50	-6	-75	7	15
<b>11h:</b> L <sub>4</sub> CL <sub>4</sub> [19 <sub>4</sub> -27-19 <sub>4</sub> ]	55	-6	-76	7	20

<sup>a</sup> Taken as the position of the maximum (or minimum) in the relevant endotherm (or exotherm). <sup>b</sup> Taken as the inflection point of the thermogram at the transition. <sup>c</sup> Obtained from the integration of the crystallization exotherm, normalized to the sample mass. <sup>d</sup> Calculated from  $X_C = \Delta H_c / (\Delta H_c^0 \cdot w_C)$  where the perfectly crystalline crystallization enthalpy  $\Delta H_c^0 = 216$  J g<sup>-1</sup> taken from ref. <sup>59</sup>

The boundary representing the transition to complete homogeneous nucleation occurs at a lower value of  $f_C$  for the arachne-arm block copolymers than for the H-shaped copolymers (Figure 3.12c). The sample set with arachnearm architecture that was explored did not have any samples that unambiguously exhibited coexisting nucleation mechanisms. That is, the sample with  $f_C = 0.6$  shows a predominant crystallization exotherm occurring at  $T_{c,C} = 30$  °C, whereas the sample with  $f_C = 0.5$  has a predominant exotherm with  $T_{c,C} = -6$  °C, representing a large difference of 36 °C. Comparatively, the transition to predominantly homogeneous nucleation, which has larger supercooling necessary for crystallization, occurs between values of  $f_C = 0.5$  and 0.6 for the arachnearm architecture, between  $f_C = 0.4$  and 0.5 for the H-shaped architecture, and between  $f_C = 0.3$  and 0.4 for the linear block copolymers. These results are consistent with the phase boundary shifts predicted by Milner for asymmetrically branched block copolymers. The system accommodates the increasing energetic requirements for relaxing the PLA chains as the junction functionality increases by adjusting the curvature of the domain interfaces such that PLA occupies the convex side. The highly asymmetric arachnearm architecture, for example, transitions to a spherical morphology at higher volume fractions than the less branched counterparts, which manifests itself as a transition to a homogeneous nucleation mechanism. This behavior is consistent with the DSC data associated with large supercoolings that result from the large proportion of small, isolated domains containing the semicrystalline PCOE.

### 3.4 Conclusions

Well-defined block polymers having various architectures were prepared by combining ROMP of *cis*-cyclooctene and ROTEP of D,L-lactide. ROMP was first performed separately with three newly developed acyclic monounsaturated CTAs bearing either two, four, or eight hydroxyl groups with the functionality governing the ultimate molecular architecture of the block polymer. Subsequent

polymerization of D,L-lactide resulted in linear, H-shaped and arachnearm shaped block polymer, respectively, with the soft semicrystalline PCOE tethered on either end by glassy PLA segments. This has particular relevance in developing nanostructured materials based on the ease with which the molecular weights are controlled, the vast array of monomers that could potentially be incorporated using these two mechanisms, and the potential for meticulous control over molecular architecture. The ability to independently manipulate these variables allows specific tailoring of morphological and mechanical characteristics.

The bulk phase behavior has been described for several block copolymers with BAB linear architecture and B<sub>2</sub>AB<sub>2</sub> H-shaped architectures at various compositions. Direct imaging of several samples revealed contrasting morphologies adopted by the block copolymers, with the curvature of the domain interfaces showing a strong dependence on both composition and molecular architecture. Specifically, a lamellar morphology was observed at highly asymmetric compositions ( $f_L = 0.19$ ) for an H-shaped block copolymer. Likewise, two corresponding copolymers with linear and H-shaped architectures exhibited SAXS profiles characteristic of lamellar and cylindrical morphologies, respectively, with  $f_L = 0.57$ . Lastly, the crystallization behavior for a broad range of compositions was evaluated for linear, H-shaped, and arachnearm architectures, showing a strong dependence of nucleation mechanism on extent of branching. The crystallization behavior corroborates the observed phase behavior monitored by SAXS and TEM.

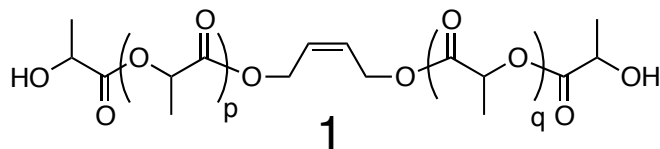
Collectively, it has been demonstrated that architectural complexity can be utilized in PLA block copolymers to access morphologies that are inaccessible with conventional linear block copolymers. Importantly, the complexity was bestowed by using straightforward polymerization techniques; identical conditions were used to prepare the different architectures using conventional techniques with commercially available starting materials. Using this protocol, the mechanical and thermal properties of PLA block copolymers can be fine-tuned to the specific demands by various applications spanning a versatile array of industries.

## 3.5 Experimental Details

### 3.5.1 Materials

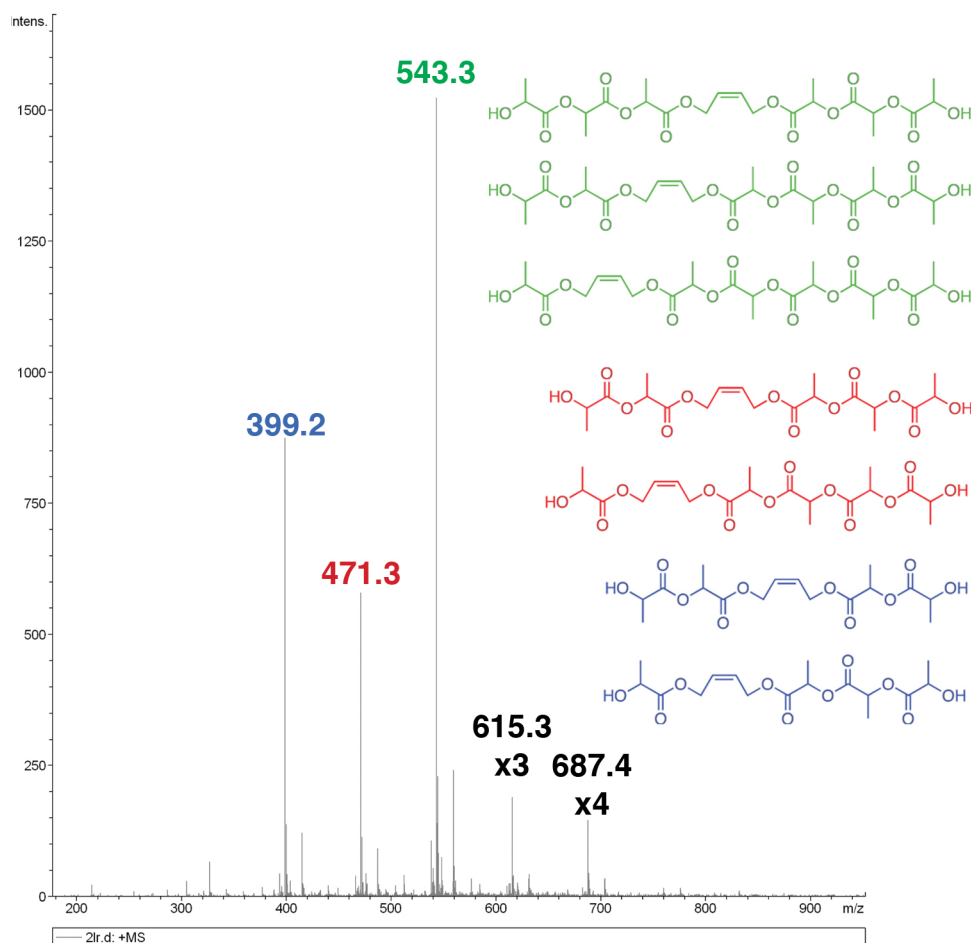
Tetrahydrofuran and toluene (Mallinkrodt) were passed through an activated alumina column under nitrogen to remove protic impurities. All other reagent grade solvents were used without further purification. *cis*-cyclooctene (COE), (IMesH<sub>2</sub>)-(Cy<sub>3</sub>P)RuCl<sub>2</sub>(CHPh) (Grubbs second generation catalyst, G2), tin(II) ethylhexanoate (Sn(Oct)<sub>2</sub>), 2,2'-bis(hydroxymethyl)propionic acid (bisMPA), dicyclohexylcarbodiimide (DCC), para-toluenesulfonic acid monohydrate (pTSA), DOWEX® 50W-100X cation exchange resin, and 4-(dimethylamino)pyridine (DMAP) were all purchased from Aldrich. 2,2-dimethoxypropane was purchased from Fluka. COE was distilled over CaH<sub>2</sub> prior to use. All other chemicals were used as received.

### 3.5.2 Synthetic details



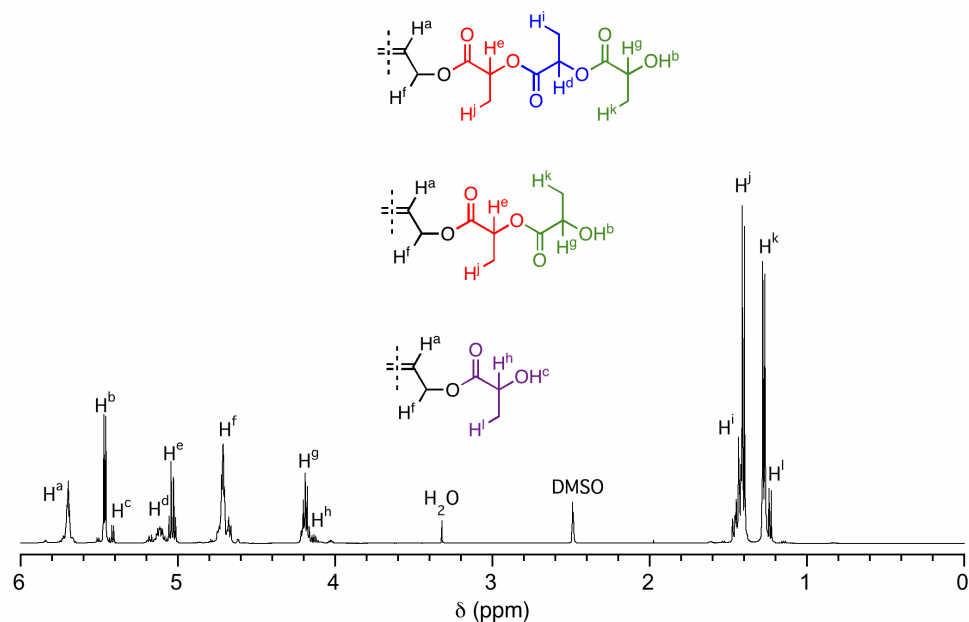
**Synthesis of 1.** First, 0.50 g (5.7 mmol) of *cis*-2-butene-1,4-diol was thoroughly degassed by three consecutive freeze-pump-thaw cycles. D,L-lactide (1.64 g; 11.4 mmol) was added under an inert atmosphere in a glove-box. The flask was sealed and removed from the glove-box before submerging in an oil bath at 130 °C for 4 h. The crude reaction mixture was purified by column chromatography using a 1:1 ratio of hexanes:ethyl acetate. Yield = 1.43 g (67%) <sup>1</sup>H NMR (DMSO-*d*<sub>6</sub>): *d* (ppm) = 5.71 (t, 2H, <sup>3</sup>J<sub>H-H</sub> = 4.0 Hz, =C(H)CH<sub>2</sub>O-), 5.48 (d, <sup>3</sup>J<sub>H-H</sub> = 6.0 Hz, -C(O)CH(CH<sub>3</sub>)OC(O)CH(CH<sub>3</sub>)OH), 5.42 (d, <sup>3</sup>J<sub>H-H</sub> = 6.0 Hz, =C(H)CH<sub>2</sub>OC(O)CH(CH<sub>3</sub>)OH), 5.13 (m, -C(O)CH(CH<sub>3</sub>)OC(O)CH(CH<sub>3</sub>)OH), 5.05 (q, <sup>3</sup>J<sub>H-H</sub> = 6.0 Hz, =C(H)CH<sub>2</sub>OC(O)CH(CH<sub>3</sub>)O-), 4.72 (dd, 4H, <sup>3</sup>J<sub>H-H</sub> = 4.0 Hz, <sup>2</sup>J<sub>H-H</sub> =

4.5 Hz, =CHCH<sub>2</sub>O-), 4.20 (m, <sup>3</sup>J<sub>H-H</sub> = 7.0 Hz, -C(O)CH(CH<sub>3</sub>)OC(O)CH(CH<sub>3</sub>)OH), 4.15 (m, <sup>3</sup>J<sub>H-H</sub> = 7.0 Hz, =C(H)CH<sub>2</sub>OC(O)CH(CH<sub>3</sub>)OH), 1.46 (m, -C(O)CH(CH<sub>3</sub>)OC(O)CH(CH<sub>3</sub>)OH), 1.41 (d, <sup>3</sup>J<sub>H-H</sub> = 7.0 Hz, =C(H)CH<sub>2</sub>OC(O)CH(CH<sub>3</sub>)O-), 1.29 (d, <sup>3</sup>J<sub>H-H</sub> = 7.0 Hz, -C(O)CH(CH<sub>3</sub>)OC(O)CH(CH<sub>3</sub>)OH), 1.24 (d, <sup>3</sup>J<sub>H-H</sub> = 7.0 Hz, =C(H)CH<sub>2</sub>OC(O)CH(CH<sub>3</sub>)OH). <sup>13</sup>C NMR (125 MHz, DMSO-*d*<sub>6</sub>, 22 °C): δ (ppm) = 174.5 (-C(O)CH(CH<sub>3</sub>)OH), 170.0 (=C(H)CH<sub>2</sub>OC(O)CH(CH<sub>3</sub>)O-), 127.8 (=C(H)CH<sub>2</sub>O-), 68.2 (=C(H)CH<sub>2</sub>OC(O)CH(CH<sub>3</sub>)O-), 66.0 (-C(O)CH(CH<sub>3</sub>)OH), 60.9 (=C(H)CH<sub>2</sub>O-), 21.1 (-C(O)CH(CH<sub>3</sub>)OH), 17.1(=C(H)CH<sub>2</sub>OC(O)CH(CH<sub>3</sub>)O-). Anal. Calcd. for C<sub>14</sub>H<sub>24</sub>O<sub>8</sub>: C, 51.04; H, 6.44; O, 43.10. Found: C, 49.87; H, 6.48; O, 44.01.

**Figure 3.13**

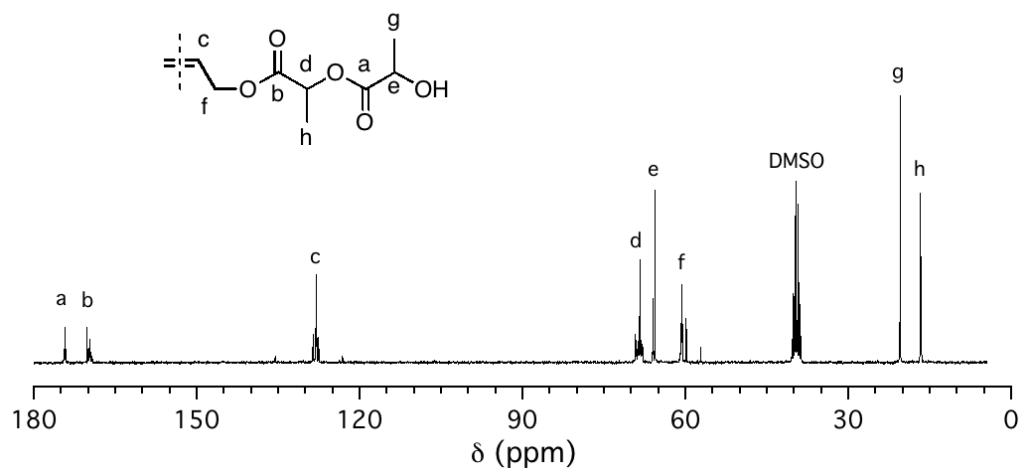
Electro-spray ionization mass spectrum for the CTA 1 showing structures for a representative sampling of the possible mixture components. The average molecular mass of the mixture was initially estimated from the relative intensity of the peaks in the mass spectrum, and supported with  $^1\text{H}$  NMR spectroscopy and elemental analysis. There are a total of fourteen different possible chemical structures from the combination of molecular weights indicated by the mass spectrum. The  $^1\text{H}$  NMR spectrum is consistent with the presence of a small quantity of CTA having a single  $\text{C}_3$  unit on at least one side, which supports the transesterification suggested by the mass spectrum. However, there does not appear to be a measurable quantity of CTA with single lactic acid units on *both* sides of the double bond based on the absence of a molecular ion peak with  $m/z = 255$  (with the  $\text{Na}^+$  ion). This along with the relatively low intensity of the  $^1\text{H}$  NMR signals associated with the single  $\text{C}_3$  unit suggests that transesterification is limited.





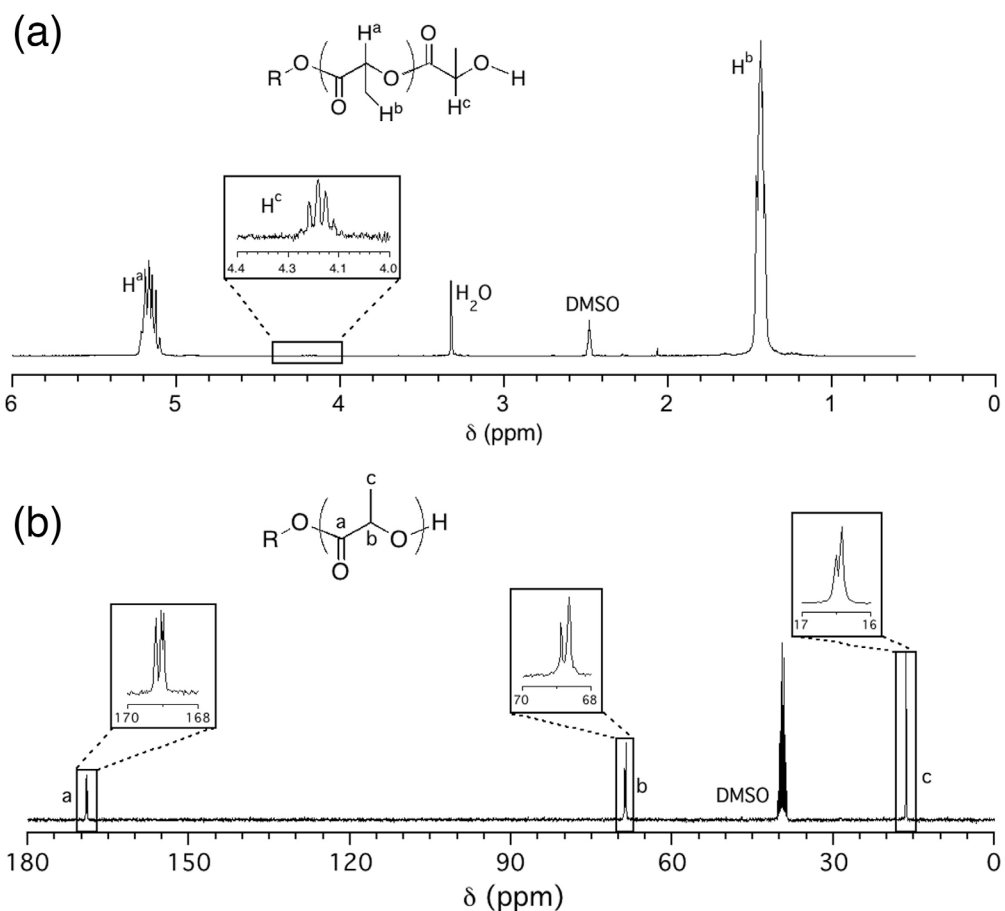
**Figure 3.14**

$^1\text{H}$  NMR spectrum of the CTA 1 in  $\text{DMSO-}d_6$  at  $25\text{ }^\circ\text{C}$  showing the signal attributed to the different oligomeric species in the mixture, which are colored to distinguish between the different electronic environments. This gives rise to the complex set of peaks observed.

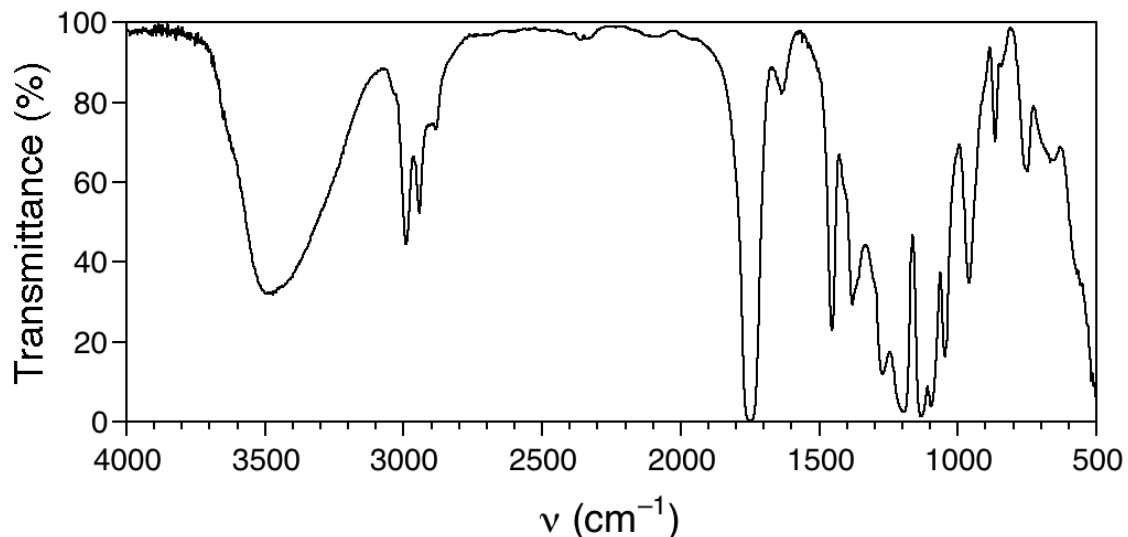


**Figure 3.15**

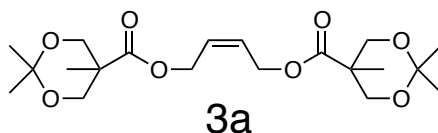
$^{13}\text{C}$  NMR spectrum of the CTA 1 in  $\text{DMSO-}d_6$  at  $25\text{ }^\circ\text{C}$  showing the signal attributed to the different oligomeric species in the mixture.

**Figure 3.16**

(a)  $^1\text{H}$  NMR spectrum of poly(D,L-lactide) initiated from benzyl alcohol with a number average degree of polymerization of approximately 100. (b)  $^{13}\text{C}$  NMR spectrum of polylactide.

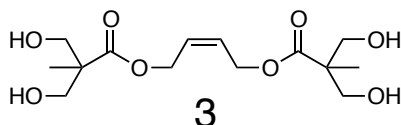
**Figure 3.17**

Infrared spectrum for CTA **1** prepared as a KBr Pellet.

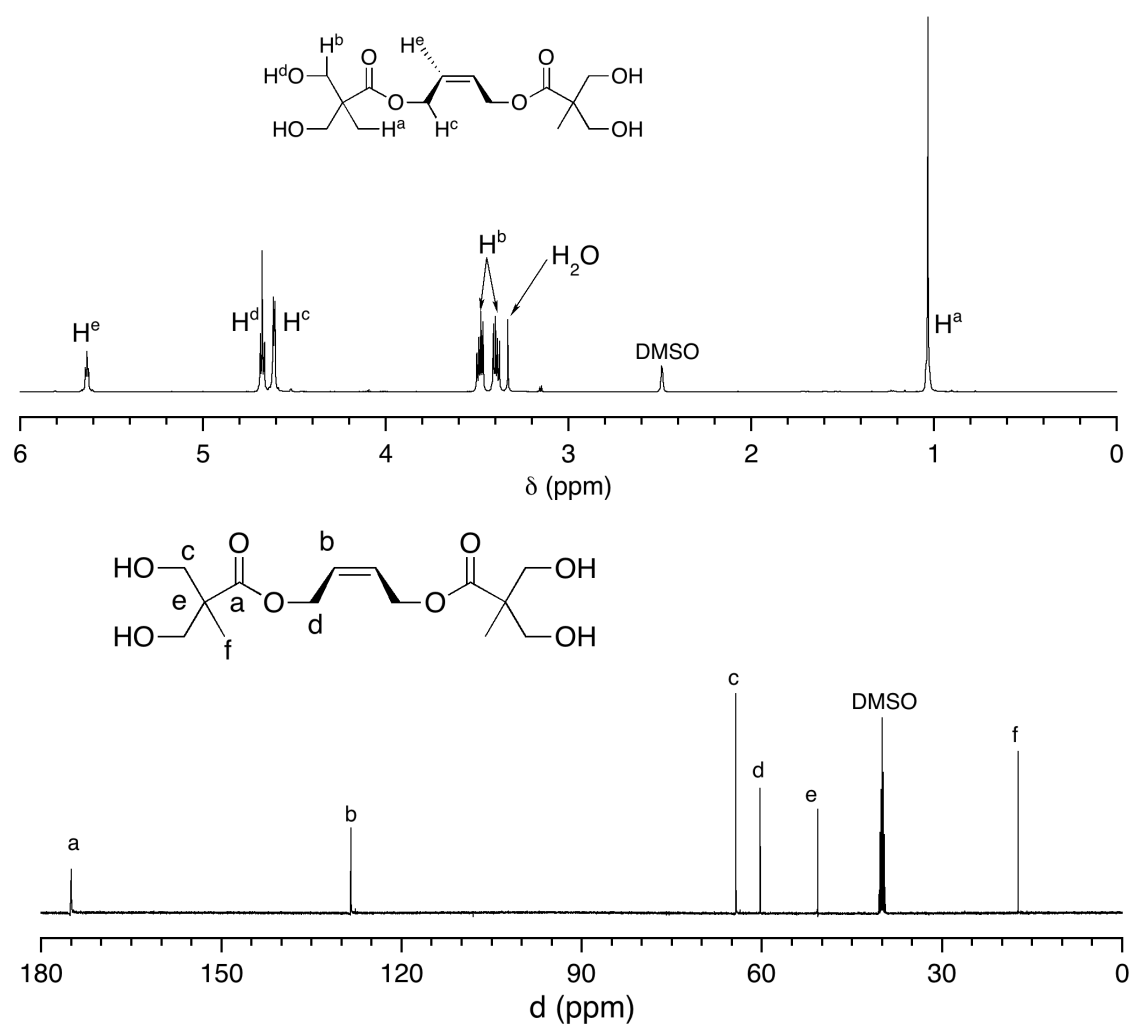


**Synthesis of 3a.** The preparation of 4-(dimethylamino)pyridinium 4-toluenesulfonate (DPTS) used as co-catalyst during DCC driven esterification has been previously reported.<sup>127</sup> The synthesis of the acetonide protected bis-MPA (**2**) has also been reported previously.<sup>47</sup> Under a nitrogen atmosphere, 150 mL of CH<sub>2</sub>Cl<sub>2</sub> was added to a 500 mL 2-neck round-bottom flask containing a Teflon® coated stir-bar. A condenser was connected to one neck while the other was sealed with a rubber septum. Under a positive flow of nitrogen, **2** (19.2 g; 0.11 mol) was added along with *cis*-2-butene-1,4-diol (4.32 mL; 4.7 g; 53 mmol) and DPTS (6.4 g; 22 mmol). After allowing all the components to dissolve at RT, DCC (26.5 g; 128 mmol) dissolved in 50 mL of CH<sub>2</sub>Cl<sub>2</sub>. The mixture was stirred vigorously for 24 h at RT, after which the solid 1,3-dicyclohexylurea (DCU) was removed by filtration. The remaining filtrate was washed with 100 mL H<sub>2</sub>O and dried over MgSO<sub>4</sub>. The CH<sub>2</sub>Cl<sub>2</sub> was removed leaving a crude mixture of the desired acetal protected CTA

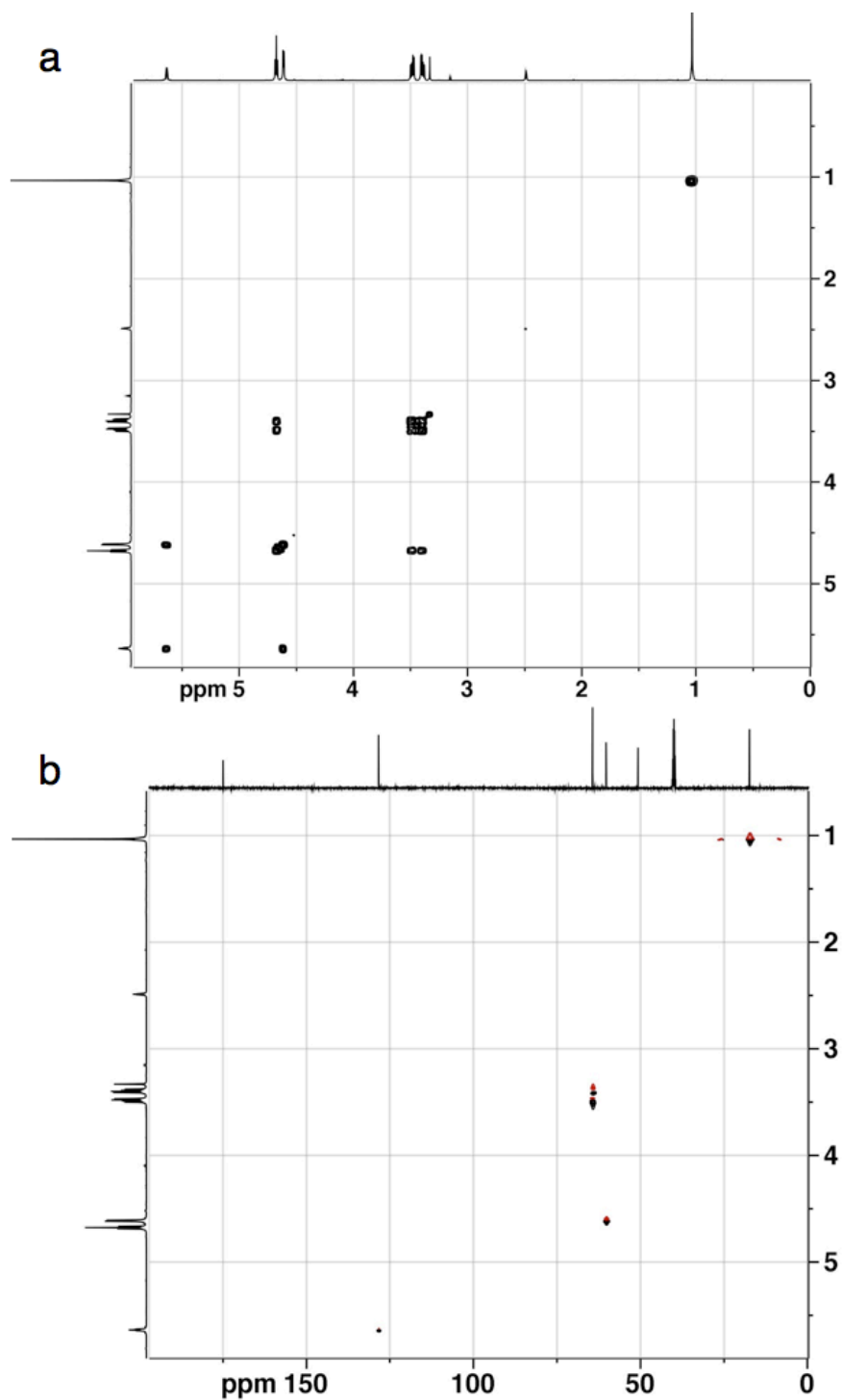
**3a** and DCU. The two components were separated by column chromatography using silica gel and a mixture of ethyl acetate and hexanes (1:3 v:v) as the eluent. After removing the solvent, a pure white crystalline acetal protected CTA was obtained. Yield = 15.2 g (72%).  $^1\text{H NMR}$  (500 MHz,  $\text{DMSO-}d_6$ , 22 °C):  $\delta$  (ppm) = 5.71 (t, 2H,  $^3J_{\text{H-H}} = 4.0$  Hz,  $=\text{C}(\text{H})\text{CH}_2\text{O-}$ ), 4.72 (d, 4H,  $^3J_{\text{H-H}} = 4.7$  Hz,  $=\text{CHCH}_2\text{O-}$ ), 3.62/4.03 (d, 8H,  $^2J_{\text{H-H}} = 11.7$  Hz,  $-\text{C}(\text{O})\text{C}(\text{CH}_3)(\text{CH}_2\text{O-})_2$ ), 1.35 (s, *axial*, 3H,  $>\text{C}(\text{CH}_3)_2$ ), 1.25 (s, *eq*, 3H,  $>\text{C}(\text{CH}_3)_2$ ), 1.06 (s, 6H,  $-\text{C}(\text{O})\text{C}(\text{CH}_3)$ ).



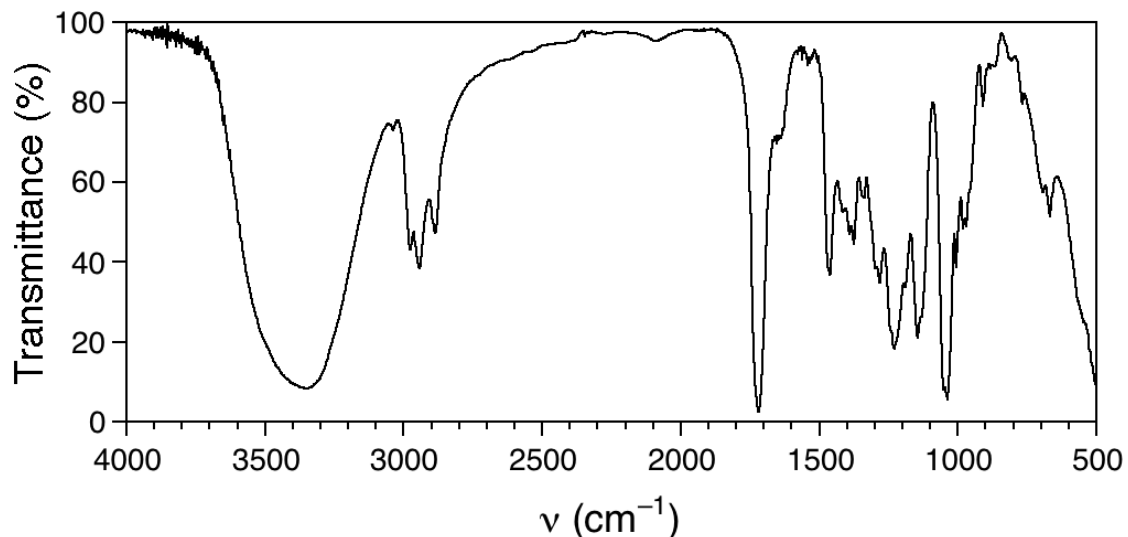
**Synthesis of 3.** The acetonide protected CTA (3.0 g; 7.5 mmol) was dissolved in 20 mL MeOH and stirred vigorously after adding 1 tsp of DOWEX 50W-100X cation exchange resin. The mixture was stirred at RT for 6 h, after which the resin was removed by filtration and the solvent removed under vacuum to give a white crystalline material, **3**. Yield = 2.1 g (88%).  $^1\text{H NMR}$  ( $\text{DMSO-}d_6$ ):  $\delta$  (ppm) = 5.65 (t, 2H,  $^3J_{\text{H-H}} = 4.0$  Hz,  $=\text{C}(\text{H})\text{CH}_2\text{O-}$ ), 4.68 (t, 4H,  $^3J_{\text{H-H}} = 5.5$  Hz,  $-\text{CH}_2\text{OH}$ ), 4.62 (d, 4H,  $^3J_{\text{H-H}} = 4.4$  Hz,  $=\text{CHCH}_2\text{O-}$ ), 3.50/3.40 (dd, 8H,  $^2J_{\text{H-H}} = 10.4$  Hz,  $^3J_{\text{H-H}} = 5.5$  Hz,  $-\text{C}(\text{O})\text{C}(\text{CH}_3)(\text{CH}_2\text{OH})_2$ ), 1.05 (s, 6H,  $-\text{C}(\text{O})\text{C}(\text{CH}_3)(\text{CH}_2\text{OH})_2$ ).  $^{13}\text{C NMR}$  (125 MHz,  $\text{DMSO-}d_6$ , 22 °C):  $\delta$  (ppm) = 175.0 ( $-\text{C}(\text{O})\text{C}(\text{CH}_3)(\text{CH}_2\text{OH})_2$ ), 128.2 ( $=\text{CHCH}_2\text{O-}$ ), 64.7 ( $-\text{C}(\text{O})\text{C}(\text{CH}_3)(\text{CH}_2\text{OH})_2$ ), 60.2 ( $=\text{CHCH}_2\text{O-}$ ), 51.0 ( $-\text{C}(\text{O})\text{C}(\text{CH}_3)(\text{CH}_2\text{OH})_2$ ), 17.2 ( $-\text{C}(\text{O})\text{C}(\text{CH}_3)(\text{CH}_2\text{OH})_2$ ). Anal. Calcd. for  $\text{C}_{14}\text{H}_{24}\text{O}_8$ : C, 42.49; H, 7.55; O, 39.96. Found: C, 42.58; H, 7.57; O, 40.05.

**Figure 3.18**

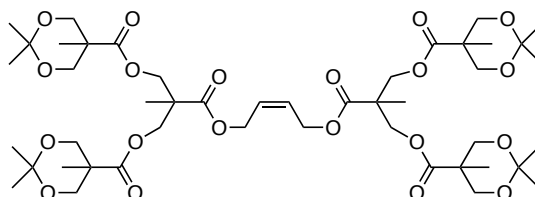
(*top*)  $^1\text{H}$  NMR spectrum and (*bottom*)  $^{13}\text{C}$  NMR spectrum of CTA 3 with 4-hydroxyl groups in  $\text{DMSO}-d_6$  at  $25^\circ\text{C}$ .

**Figure 3.19**

(a) <sup>1</sup>H-<sup>1</sup>H COSY NMR spectrum and (b) <sup>1</sup>H-<sup>13</sup>C HMQC NMR spectrum for CTA 3 in DMSO-*d*<sub>6</sub> at 25 °C.

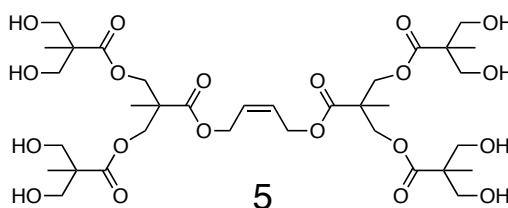
**Figure 3.20**

IR spectrum of CTA **3** prepared as a KBr pellet.

**5a**

**Synthesis of 5a.** The detailed synthesis of the acetonide protected first generation dendrimer of bisMPA (G1-bisMPA) has been previously reported.<sup>Error! Bookmark not defined.</sup> 10.0 g of G1-bisMPA (22.4 mmol) was placed into a 250 mL round bottom two-neck Schlenk flask with 1.26 g DPTS (4.28 mmol) and a Teflon coated stir bar. The flask was sealed with a rubber septum, evacuated and back-filled with argon. 25 mL of dry CH<sub>2</sub>Cl<sub>2</sub> was added via syringe to dissolve the solids with stirring. Using a syringe, 0.94 g (10.67 mmol) *cis*-2-butene-1,4-diol was added, followed by slow addition (~10 min) of 5.51 g (26.7 mmol) of DCC dissolved in 12 mL CH<sub>2</sub>Cl<sub>2</sub> via syringe with rapid stirring. White solid almost immediately dropped out of solution, after which the reaction was stirred at room temperature for an

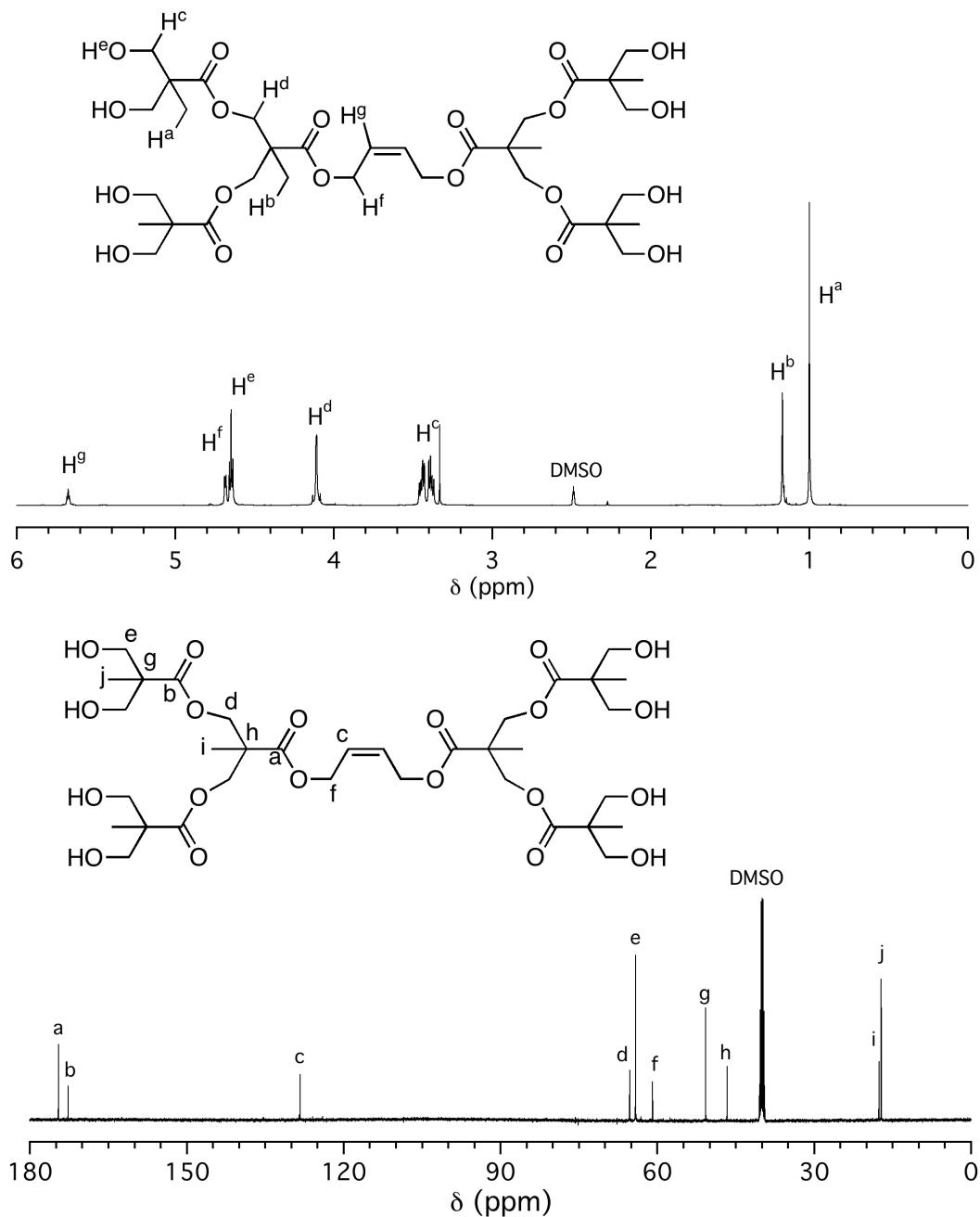
additional 15 h. The by-product dicyclohexyl urea (DCU) was filtered off and the filtrate was washed with saturated  $\text{NaHCO}_3$  (100 mL) followed by saturated  $\text{NaCl}$  (100 mL) and deionized water (100 mL). The filtrate was then dried over  $\text{MgSO}_4$  and evaporated to give the crude acetonide protected precursor to the octahydroxyl CTA **5a** as a colorless viscous oil. Yield = 8.77 g (87%).  $^1\text{H}$  NMR ( $\text{DMSO-}d_6$ ):  $\delta$  (ppm) = 5.69 (t, 2H,  $^3J_{\text{H-H}} = 4.2$  Hz,  $=\text{C}(\text{H})\text{CH}_2\text{O}-$ ), 4.70 (d, 4H,  $^3J_{\text{H-H}} = 4.6$  Hz,  $=\text{CHCH}_2\text{O}-$ ), 4.22 (s, 8H,  $=\text{CHCH}_2\text{OC}(\text{O})\text{CCH}_3(\text{CH}_2\text{O}-)_2\dots$ ), 3.98/3.60 (dd, 16H,  $^2J_{\text{H-H}} = 11.7$  Hz,  $-\text{C}(\text{O})\text{C}(\text{CH}_3)(\text{CH}_2\text{O}-)_2$ ), 1.35 (s, *axial*, 12H,  $>\text{C}(\text{CH}_3)_2$ ), 1.21 (s, *eq*, 12H,  $>\text{C}(\text{CH}_3)_2$ ), 1.21 (s, 6H,  $-\text{C}(\text{O})\text{C}(\text{CH}_3)(\text{CH}_2\text{O}-)_2$ ), 1.01 (s, 12H  $-\text{C}(\text{O})\text{C}(\text{CH}_3)(\text{CH}_2\text{O})_2>\text{C}(\text{CH}_3)_2$ ).



**Synthesis of 5.** 5.0 g (5.29 mmol) of the acetonide protected CTA was dissolved in 50 mL of dry methanol and 1 tsp of DOWEX 50W-100X cation exchange resin was added at room temperature with rapid stirring. The solution was stirred for 6 h, the resin was filtered, and the MeOH was removed under vacuum. The crude product was a colorless viscous oil, and was purified by column chromatography with EtOAc initially, and the product was collected by adding 20% MeOH to the column. The solvent was removed under vacuum to yield a white crystalline solid **5**. Yield = 2.78 g (67%).  $^1\text{H}$  NMR ( $\text{DMSO-}d_6$ ):  $\delta$  (ppm) = 5.69 (t, 2H,  $^3J_{\text{H-H}} = 4.0$  Hz,  $=\text{C}(\text{H})\text{CH}_2\text{O}-$ ), 4.69 (d, 4H,  $^3J_{\text{H-H}} = 5.0$  Hz,  $=\text{CHCH}_2\text{O}-$ ), 4.66 (t, 8H,  $^3J_{\text{H-H}} = 5.5$  Hz,  $-\text{CH}_2\text{OH}$ ), 4.10/4.14 (d, 8H,  $^2J_{\text{H-H}} = 10.9$  Hz,  $=\text{CHCH}_2\text{OC}(\text{O})\text{CCH}_3(\text{CH}_2\text{O}-)_2\dots$ ), 3.46/3.39 (dd, 16H,  $^2J_{\text{H-H}} = 10.4$  Hz,  $^3J_{\text{H-H}} = 5.5$  Hz,  $-\text{C}(\text{O})\text{C}(\text{CH}_3)(\text{CH}_2\text{OH})_2$ ), 1.17 (s, 6H,  $=\text{CHCH}_2\text{OCCH}_3(\text{CH}_2\text{O}-)_2\dots$ ), 1.03 (s, 12H,  $-\text{C}(\text{O})\text{C}(\text{CH}_3)(\text{CH}_2\text{OH})_2$ ).  $^{13}\text{C}$  NMR (125 MHz,  $\text{DMSO-}d_6$ , 22 °C):  $d$  (ppm) = 174.5 ( $=\text{CHCH}_2\text{OC}(\text{O})\text{CCH}_3(\text{CH}_2\text{O}-)_2$ ), 172.5 ( $-\text{C}(\text{O})\text{C}(\text{CH}_3)(\text{CH}_2\text{OH})_2$ ), 128.2 ( $=\text{CHCH}_2\text{O}-$ ), 65.3 ( $=\text{CHCH}_2\text{OC}(\text{O})\text{CCH}_3(\text{CH}_2\text{O}-)_2$ ), 64.2 ( $-\text{C}(\text{O})\text{C}(\text{CH}_3)(\text{CH}_2\text{OH})_2$ ), 61.3 ( $=\text{CHCH}_2\text{O}-$ ), 50.9 ( $-\text{C}(\text{O})\text{C}(\text{CH}_3)(\text{CH}_2\text{OH})_2$ ), 46.5 ( $=\text{CHCH}_2\text{OC}(\text{O})\text{CCH}_3(\text{CH}_2\text{O}-)_2$ ), 17.9

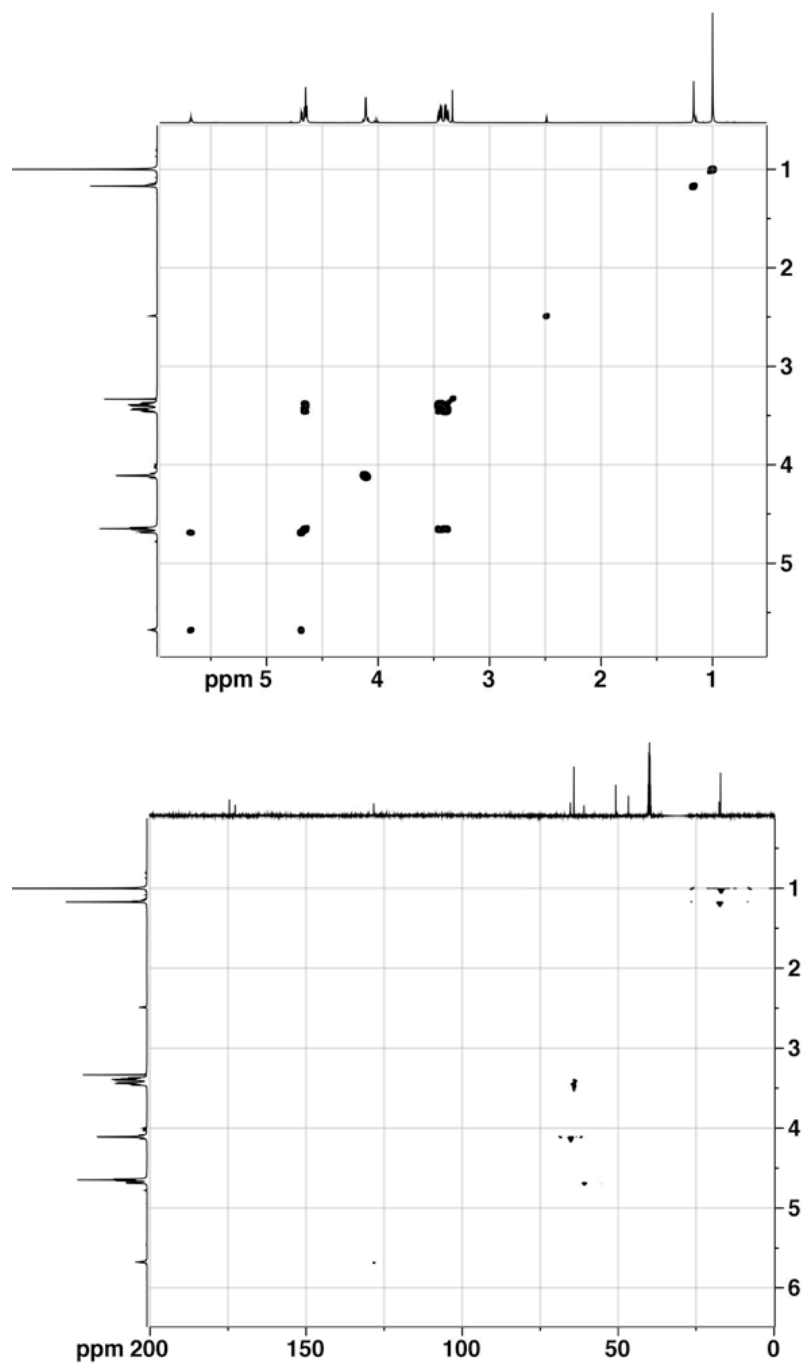


(=CHCH<sub>2</sub>OC(O)CCH<sub>3</sub>(CH<sub>2</sub>O-)<sub>2</sub>), 17.6 (-C(O)C(CH<sub>3</sub>)(CH<sub>2</sub>OH)<sub>2</sub>). Anal. Calcd. for C<sub>34</sub>H<sub>56</sub>O<sub>20</sub>: C, 52.03; H, 7.19; O, 40.77. Found: C, 51.7; H, 7.19; O, 40.50.



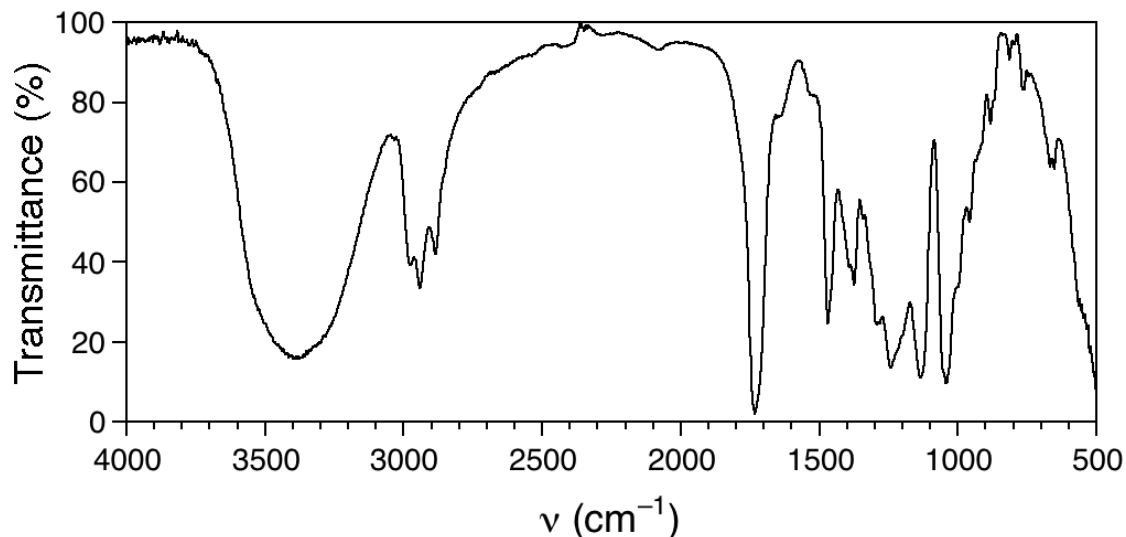
**Figure 3.21**

(top) <sup>1</sup>H NMR spectrum and (bottom) <sup>13</sup>C NMR spectrum of CTA 5 measured in DMSO-*d*<sub>6</sub> at 25 °C.



**Figure 3.22**

(a)  $^1\text{H}$ - $^1\text{H}$  COSY NMR spectrum and (b)  $^1\text{H}$ - $^{13}\text{C}$  HMQC NMR spectrum for CTA 5 in  $\text{DMSO-}d_6$  at 25 °C.

**Figure 3.23**

IR spectrum of CTA **5** prepared as a KBr pellet.

**Representative Synthesis of Telechelic Polycyclooctene.** The synthesis of the PCOE with different CTAs was identical aside from substituting the appropriate CTA. The telechelic dihydroxy PCOE analog was prepared using CTA **1**, while the tetrahydroxy PCOE was prepared using CTA **3**, and octahydroxy PCOE analog was prepared using CTA **5**. Yields and conversion were all comparable. Here, the preparation of sample HO<sub>2</sub>-C-OH<sub>2</sub> is described in detail. A single-neck 250 mL oven dried round-bottom flask with a Teflon-coated stir-bar was charged with 100 mL THF, followed by vigorous nitrogen sparging for 20 min. CTA **3** (0.493 g; 1.54 mmol) was dissolved in 10 mL THF and added via syringe to the reaction flask followed immediately by the addition of 4.0 mL (3.4 g; 31 mmol) of COE also via syringe. With vigorous stirring at 25 °C, Grubbs 2<sup>nd</sup> generation catalyst (11 mg; 13 μmol) was added as a solution in 1 mL THF via syringe. The mixture was stirred continuously during the slow injection of an additional 36 mL (31.0 g; 281 mmol) COE using a syringe pump over 1 h. This example polymerization had parameters [CTA]/[G2] = 118 and [M]/[CTA] = 202. The polymerization mixture was stirred for an additional 3 h at RT and then

precipitated into a ten-fold excess by volume of cold MeOH containing 15 mL of 1 M HCl to quench the catalyst. The polymer was isolated and dried under vacuum at RT to yield 32.7 g (95 %). SEC analysis (CHCl<sub>3</sub>, 30 °C) resulted in  $M_w/M_n = 1.77$  relative to monodisperse polystyrene standards.

**Characterization of HO-C-OH.** <sup>1</sup>H NMR, CDCl<sub>3</sub>:  $\delta = 5.39$  (m, *trans*, =C(H)CH<sub>2</sub>CH<sub>2</sub>- backbone), 5.36 (m, *cis*, =C(H)CH<sub>2</sub>CH<sub>2</sub>- backbone), 4.65–4.73 (m, =CHCH<sub>2</sub>O- *cis* endgroup), 4.55–4.62 (m, =CHCH<sub>2</sub>O- *trans* endgroup), 4.33–4.40 (m, -C(O)CH(CH<sub>3</sub>)OC(O)CH(CH<sub>3</sub>)OH endgroup), 4.27 (m, =CHCH<sub>2</sub>OC(O)CH(CH<sub>3</sub>)OH endgroup), 2.03 (m, *cis*, =CHCH<sub>2</sub>CH<sub>2</sub> backbone), 1.97 (m, *trans*, =CHCH<sub>2</sub>CH<sub>2</sub> backbone), 1.31 (m, =CHCH<sub>2</sub>CH<sub>2</sub> backbone).

**Characterization of HO<sub>2</sub>-C-OH<sub>2</sub>.** <sup>1</sup>H NMR, CDCl<sub>3</sub>:  $\delta = 5.39$  (m, *trans*, =C(H)CH<sub>2</sub>CH<sub>2</sub>- backbone), 5.36 (m, *cis*, =C(H)CH<sub>2</sub>CH<sub>2</sub>- backbone), 4.73 (d, <sup>3</sup>J<sub>H-H</sub> = 5.9 Hz, =CHCH<sub>2</sub>O- *cis* endgroup), 4.62 (d, <sup>3</sup>J<sub>H-H</sub> = 5.9 Hz, =CHCH<sub>2</sub>O- *trans* endgroup), 3.92/3.73 (d, <sup>2</sup>J<sub>H-H</sub> = 11.3 Hz, C(O)C(CH<sub>3</sub>)(CH<sub>2</sub>OH)<sub>2</sub> endgroup), 2.03 (m, *cis*, =CHCH<sub>2</sub>CH<sub>2</sub> backbone), 1.97 (m, *trans*, =CHCH<sub>2</sub>CH<sub>2</sub> backbone), 1.31 (m, =CHCH<sub>2</sub>CH<sub>2</sub> backbone).

**Characterization of HO<sub>4</sub>-C-OH<sub>4</sub>.** <sup>1</sup>H NMR, CDCl<sub>3</sub>:  $\delta = 5.39$  (m, *trans*, =C(H)CH<sub>2</sub>CH<sub>2</sub>- backbone), 5.36 (m, *cis*, =C(H)CH<sub>2</sub>CH<sub>2</sub>- backbone), 4.70 (d, <sup>3</sup>J<sub>H-H</sub> = 6.4 Hz, =CHCH<sub>2</sub>O- *cis* endgroup), 4.58 (d, <sup>3</sup>J<sub>H-H</sub> = 6.4 Hz, =CHCH<sub>2</sub>O- *trans* endgroup), 4.46/4.29 (d, <sup>2</sup>J<sub>H-H</sub> = 11.1 Hz, C(O)C(CH<sub>3</sub>)(CH<sub>2</sub>O-)<sub>2</sub> endgroup), 4.46/4.29 (td, <sup>3</sup>J<sub>H-H</sub> = 6.0 Hz, <sup>2</sup>J<sub>H-H</sub> = 11.1 Hz, C(O)C(CH<sub>3</sub>)(CH<sub>2</sub>O-)<sub>2</sub> endgroup) 2.03 (m, *cis*, =CHCH<sub>2</sub>CH<sub>2</sub> backbone), 1.97 (m, *trans*, =CHCH<sub>2</sub>CH<sub>2</sub> backbone), 1.31 (m, =CHCH<sub>2</sub>CH<sub>2</sub> backbone).

**Representative Synthesis of L<sub>x</sub>CL<sub>x</sub> Triblock Copolymer.** The addition of PLA to the hydroxy telechelic PCOE samples, regardless of functionality, was identical aside from changing the monomer molar feed composition. Here we describe the synthesis of L<sub>2</sub>CL<sub>2</sub> [10<sub>2</sub>-22-10<sub>2</sub>]. A 48 mL capacity pressure vessel sealed with a #15 size Teflon screw-cap and Viton o-ring was used for the polymerization. Tetrafunctional PCOE HO<sub>2</sub>-C-OH<sub>2</sub> (1.00 g; 0.23 mmol -OH) was placed in the oven-dried glass vessel containing a Teflon-coated ¼ in. stir-bar in an MBraun

glove-box under nitrogen atmosphere. After dissolution of the polymer in toluene (12 mL), 76  $\mu\text{L}$  of  $\text{Sn}(\text{Oct})_2$  (1.0 M solution in toluene) was added via gas-tight syringe at ambient temperature. D,L-lactide (1.25 g; 8.7 mmol) was placed in the vessel under nitrogen atmosphere and the flask was sealed before removing from the glove box and immersing in an oil bath at 120  $^\circ\text{C}$  for 2 h. After the prescribed reaction time, the mixture was opened to air and immediately precipitated into a ten-fold excess by volume of cold MeOH ( $-70$   $^\circ\text{C}$ ) before filtering and drying under reduced pressure to yield 1.8 g (94%) of triblock copolymer. SEC ( $\text{CHCl}_3$ , 35  $^\circ\text{C}$ ) analysis gave  $M_w/M_n = 1.23$  relative to monodisperse polystyrene standards.

**Characteristics of Linear LCL:**  $^1\text{H}$  NMR ( $\text{CDCl}_3$ ; 25  $^\circ\text{C}$ ):  $\delta$  (ppm) = 5.38 (m, *trans*,  $=\text{CHCH}_2\text{CH}_2-$  backbone), 5.35 (m, *cis*,  $=\text{CHCH}_2\text{CH}_2-$  backbone), 4.68 (b, *cis*,  $=\text{CHCH}_2\text{OC}(\text{O})\text{C}(\text{CH}_3)\text{O}-$ , block junction), 4.56 (b, *trans*,  $=\text{CHCH}_2\text{OC}(\text{O})\text{C}(\text{CH}_3)\text{O}-$ , block junction), 4.36 (m,  $-\text{C}(\text{O})\text{CH}(\text{CH}_3)\text{OH}$ , endgroup), 2.03 (m, *cis*,  $=\text{CHCH}_2\text{CH}_2$  backbone), 1.97 (m, *trans*,  $=\text{CHCH}_2\text{CH}_2$  backbone), 1.60 (m,  $-\text{C}(\text{O})\text{CH}(\text{CH}_3)\text{O}-$ , backbone), 1.31 (m,  $=\text{CHCH}_2\text{CH}_2$  backbone).

**Characterization of H-Shaped  $\text{L}_2\text{CL}_2$ :**  $^1\text{H}$  NMR ( $\text{CDCl}_3$ ; 25  $^\circ\text{C}$ ):  $\delta$  (ppm) = 5.39 (m, *trans*,  $=\text{CHCH}_2\text{CH}_2-$  backbone), 5.36 (m, *cis*,  $=\text{CHCH}_2\text{CH}_2-$  backbone), 4.68 (b, *cis*,  $=\text{CHCH}_2\text{OC}(\text{O})-$ , block junction), 4.56 (b, *trans*,  $=\text{CHCH}_2\text{OC}(\text{O})-$ , block junction), 4.36 (m,  $-\text{C}(\text{O})\text{CH}(\text{CH}_3)\text{OH}$ , endgroup), 4.38–4.16 (m,  $-\text{C}(\text{O})\text{C}(\text{CH}_3)[\text{CH}_2\text{O}-\text{C}(\text{O})\text{CH}(\text{CH}_3)\text{O}-]_2$ , block junction), 2.03 (m, *cis*,  $=\text{CHCH}_2\text{CH}_2$  backbone), 1.97 (m, *trans*,  $=\text{CHCH}_2\text{CH}_2$  backbone), 1.60 (m,  $-\text{C}(\text{O})\text{CH}(\text{CH}_3)\text{O}-$ , backbone), 1.31 (m,  $=\text{CHCH}_2\text{CH}_2$  backbone).

**Characteristics of arachnearm  $\text{L}_4\text{CL}_4$ :**  $^1\text{H}$  NMR ( $\text{CDCl}_3$ ; 25  $^\circ\text{C}$ ):  $\delta$  (ppm) = 5.39 (m, *trans*,  $=\text{CHCH}_2\text{CH}_2-$  backbone), 5.36 (m, *cis*,  $=\text{CHCH}_2\text{CH}_2-$  backbone), 4.68 (b, *cis*,  $=\text{CHCH}_2\text{OC}(\text{O})-$ , block junction), 4.56 (b, *trans*,  $=\text{CHCH}_2\text{OC}(\text{O})-$ , block junction), 4.36 (m,  $-\text{C}(\text{O})\text{CH}(\text{CH}_3)\text{OH}$ , endgroup), 4.38–4.16 (m,  $-\text{C}(\text{O})\text{C}(\text{CH}_3)\langle\text{CH}_2\text{OC}(\text{O})\text{CCH}_3[\text{CH}_2\text{OC}(\text{O})\text{CH}(\text{CH}_3)\text{O}-]_2\rangle_2$ , block junction), 2.03 (m, *cis*,  $=\text{CHCH}_2\text{CH}_2$  backbone), 1.97 (m, *trans*,  $=\text{CHCH}_2\text{CH}_2$  backbone), 1.60 (m,  $-\text{C}(\text{O})\text{CH}(\text{CH}_3)\text{O}-$ , backbone), 1.31 (m,  $=\text{CHCH}_2\text{CH}_2$  backbone).

### 3.6 References

- [1] Becker, J. M.; Pounder, R. J.; Dove, A. P. *Macromol. Rapid Commun.* **2010**, *31*, 1923–1937.
- [2] Dove, A. P. *Chem. Commun.* **2008**, 6446–6470.
- [3] Abetz, V.; Simon, P. F. W. *Adv. Polym. Sci.* **2005**, *189*, 125–212.
- [4] Bates, F. S.; Fredrickson, G. H. *Annu. Rev. Phys. Chem.* **1990**, *41*, 525–557.
- [5] Leibler, L. *Prog. Polym. Sci.* **2005**, *30*, 898–914.
- [6] Hadjichristidis, N.; Pitsikalis, M.; Iatrou, H. *Adv. Polym. Sci.* **2005**, *189*, 1–124.
- [7] Hadjichristidis, N.; Iatrou, H.; Pitsikalis, M.; Mays, J. *Prog. Polym. Sci.* **2006**, *31*, 1068–1132.
- [8] Hadjichristidis, N.; Pitsikalis, M.; Pispas, S.; Iatrou, H. *Chem. Rev.* **2001**, *101*, 3747–3792.
- [9] Hirao, A.; Murano, K.; Oie, T.; Uematsu, M.; Goseki, R.; Matsuo, Y. *Polymer Chemistry* **2011**.
- [10] Pitsikalis, M.; Pispas, S.; Mays, J. W.; Hadjichristidis, N. *Adv. Polym. Sci.* **1998**, *135*, 1–137.
- [11] Wurm, F.; Frey, H. *Prog. Polym. Sci.* **2011**, *36*, 1–52.
- [12] Hadjichristidis, N.; Poulos, Y.; Avgeropoulos, A. *Macromol. Symp.* **1998**, *132*, 207–220.
- [13] Lee, C.; Gido, S. P.; Poulos, Y.; Hadjichristidis, N.; Tan, N. B.; Trevino, S. F.; Mays, J. W. *Polymer* **1998**, *39*, 4631–4638.

- [14] Beyer, F. L.; Gido, S. P.; Uhrig, D.; Mays, J. W.; Tan, N. B.; Trevino, S. F. *J. Polym. Sci., Part B: Polym. Phys.* **1999**, *37*, 3392–3400.
- [15] Buzza, D. M. A.; Fzea, A. H.; Allgaier, J. B.; Young, R. N.; Hawkins, R. J.; Hamley, I. W.; McLeish, T. C. B.; Lodge, T. P. *Macromolecules* **2000**, *33*, 8399–8414.
- [16] Gido, S. P.; Lee, C.; Pochan, D. J.; Pispas, S.; Mays, J. W.; Hadjichristidis, N. *Macromolecules* **1996**, *29*, 7022–7028.
- [17] Lee, C.; Gido, S. P.; Poulos, Y.; Hadjichristidis, N.; Tan, N. B.; Trevino, S. F.; Mays, J. W. *J. Chem. Phys.* **1997**, *107*, 6460–6469.
- [18] Weidisch, R.; Gido, S. P.; Uhrig, D.; Iatrou, H.; Mays, J.; Hadjichristidis, N. *Macromolecules* **2001**, *34*, 6333–6337.
- [19] Yang, L.; Gido, S. P.; Mays, J. W.; Pispas, S.; Hadjichristidis, N. *Macromolecules* **2001**, *34*, 4235–4243.
- [20] Coulembier, O.; Kiesewetter, M. K.; Mason, A.; Dubois, P.; Hedrick, J. L.; Waymouth, R. M. *Angew. Chem., Int. Ed.* **2007**, *46*, 4719–4721.
- [21] Trollsås, M.; Kelly, M. A.; Claesson, H.; Siemens, R.; Hedrick, J. L. *Macromolecules* **1999**, *32*, 4917–4924.
- [22] Yagci, Y.; Tasdelen, M. A. *Prog. Polym. Sci.* **2006**, *31*, 1133–1170.
- [23] Bielawski, C. W.; Grubbs, R. H. *Prog. Polym. Sci.* **2007**, *32*, 1–29.
- [24] Dechy-Cabaret, O.; Martin-Vaca, B.; Bourissou, D. *Chem. Rev.* **2004**, *104*, 6147–6176.
- [25] Kamber, N. E.; Jeong, W.; Waymouth, R. M.; Pratt, R. C.; Lohmeijer, B. G.; Hedrick, J. L. *Chem. Rev.* **2007**, *107*, 5813–5840.
- [26] Matyjaszewski, K.; Xia, J. *Chem. Rev.* **2001**, *101*, 2921–2990.

- [27] Bielawski, C. W.; Louie, J.; Grubbs, R. H. *J. Am. Chem. Soc.* **2000**, *122*, 12872–12873.
- [28] Bielawski, C. W.; Morita, T.; Grubbs, R. H. *Macromolecules* **2000**, *33*, 678–680.
- [29] Katayama, H.; Fukuse, Y.; Nobuto, Y.; Akamatsu, K.; Ozawa, F. *Macromolecules* **2003**, *36*, 7020–7026.
- [30] Katayama, H.; Yonezawa, F.; Nagao, M.; Ozawa, F. *Macromolecules* **2002**, *35*, 1133–1136.
- [31] Mahanthappa, M. K.; Bates, F. S.; Hillmyer, M. A. *Macromolecules* **2005**, *38*, 7890–7894.
- [32] Matson, J. B.; Grubbs, R. H. *Macromolecules* **2008**, *41*, 5626–5631.
- [33] Maughon, B. R.; Morita, T.; Bielawski, C. W.; Grubbs, R. H. *Macromolecules* **2000**, *33*, 1929–1935.
- [34] Myers, S. B.; Register, R. A. *Macromolecules* **2008**, *41*, 5283–5288.
- [35] Sill, K.; Emrick, T. *J. Polym. Sci., Part A: Polym. Chem.* **2005**, *43*, 5429–5439.
- [36] Ekin, A.; Webster, D. C. *Macromolecules* **2006**, *39*, 8659–8668.
- [37] Han, D.-H.; Pan, C.-Y. *J. Polym. Sci., Part A: Polym. Chem.* **2006**, *44*, 2794–2801.
- [38] Liu, J. W.; Li, J. X.; Xie, M. R.; Ding, L.; Yang, D.; Zhang, L. Y. *Polymer* **2009**, *50*, 5228–5235.
- [39] Pitet, L. M.; Hillmyer, M. A. *Macromolecules* **2009**, *42*, 3674–3680.



- 
- [40] Hillmyer, M. A.; Nguyen, S. T.; Grubbs, R. H. *Macromolecules* **1997**, *30*, 718–721.
- [41] Bielawski, C. W.; Benitez, D.; Morita, T.; Grubbs, R. H. *Macromolecules* **2001**, *34*, 8610–8618.
- [42] Bielawski, C. W.; Scherman, O. A.; Grubbs, R. H. *Polymer* **2001**, *42*, 4939–4945.
- [43] Hillmyer, M. A.; Grubbs, R. H. *Macromolecules* **1993**, *26*, 872–874.
- [44] Hillmyer, M. A.; Grubbs, R. H. *Macromolecules* **1995**, *28*, 8662–8667.
- [45] Ji, S.; Hoye, T. R.; Macosko, C. W. *Macromolecules* **2004**, *37*, 5485–5489.
- [46] Scherman, O. A.; Kim, H. M.; Grubbs, R. H. *Macromolecules* **2002**, *35*, 5366–5371.
- [47] Ihre, H.; Hult, A.; Frechet, J. M. J.; Gitsov, I. *Macromolecules* **1998**, *31*, 4061–4068.
- [48] Atthoff, B.; Trollsås, M.; Claesson, H.; Hedrick, J. L. *Macromol. Chem. Phys.* **1999**, *200*, 1333–1339.
- [49] Jérôme, R.; Mecerreyes, D.; Tian, D.; Dubois, P.; Hawker, C. J.; Trollsås, M.; Hedrick, J. L. *Macromol. Symp.* **1998**, *132*, 385–403.
- [50] Trollsås, M.; Atthoff, B.; Claesson, H.; Hedrick, J. L. *J. Polym. Sci., Part A: Polym. Chem.* **2004**, *42*, 1174–1188.
- [51] Trollsås, M.; Claesson, H.; Atthoff, B.; Hedrick, J. L. *Angew. Chem., Int. Ed.* **1998**, *37*, 3132–3136.
- [52] Trollsås, M.; Hawker, C. J.; Remenar, J. F.; Hedrick, J. L.; Johansson, M.; Ihre, H.; Hult, A. *J. Polym. Sci., Part A: Polym. Chem.* **1998**, *36*, 2793–2798.

- [53] Trollsås, M.; Hedrick, J. L. *Macromolecules* **1998**, *31*, 4390–4395.
- [54] Trollsås, M.; Hedrick, J. L.; Mecerreyes, D.; Dubois, P.; Jérôme, R.; Ihre, H.; Hult, A. *Macromolecules* **1998**, *31*, 2756–2763.
- [55] Dorgan, J. R.; Janzen, J.; Knauss, D. M.; Hait, S. B.; Limoges, B. R.; Hutchinson, M. H. *J. Polym. Sci., Part B: Polym. Phys.* **2005**, *43*, 3100–3111.
- [56] Pitet, L. M.; Chamberlain, B. M.; Hauser, A. W.; Hillmyer, M. A. *Macromolecules* **2010**, *43*, 8018–8025.
- [57] Medrano, R.; Laguna, M. T. R.; Saiz, E.; Tarazona, M. P. *Phys. Chem. Chem. Phys.* **2003**, *5*, 151–157.
- [58] Witzke, D. R.; Kolstad, J. J.; Narayan, R. *Macromolecules* **1997**, *30*, 7075–7085.
- [59] Schneider, W. A.; Müller, M. F. *J. Mol. Catal.* **1988**, *46*, 395–403.
- [60] Hamley, I. W. *Developments in Block Copolymer Science and Technology* **2004**, 1–29.
- [61] Hadjichristidis, N.; Roovers, J. E. L. *J. Polym. Sci., Part B: Polym. Phys.* **1974**, *12*, 2521–2533.
- [62] Jeong, M.; Mackay, M. E.; Vestberg, R.; Hawker, C. J. *Macromolecules* **2001**, *34*, 4927–4936.
- [63] Mourey, T. H.; Turner, S. R.; Rubinstein, M.; Frechet, J. M. J.; Hawker, C. J.; Wooley, K. L. *Macromolecules* **1992**, *25*, 2401–2406.
- [64] Roovers, J.; Toporowski, P. M. *J. Polym. Sci., Part B: Polym. Phys.* **1980**, *18*, 1907–1917.
- [65] Trollsås, M.; Claesson, H.; Atthoff, B.; Hedrick, J. L.; Pople, J. A.; Gast, A. P. *Macromol. Symp.* **2000**, *153*, 87–108.

- [66] Trollsås, M.; Hedrick, J.; Mecerreyes, D.; Jérôme, R.; Dubois, P. *J. Polym. Sci., Part A: Polym. Chem.* **1998**, *36*, 3187–3192.
- [67] Trollsås, M.; Hedrick, J. L. *J. Am. Chem. Soc.* **1998**, *120*, 4644–4651.
- [68] Trollsås, M.; Hedrick, J. L.; Mecerreyes, D.; Dubois, P.; Jérôme, R.; Ihre, H.; Hult, A. *Macromolecules* **1997**, *30*, 8508–8511.
- [69] Trollsås, M.; Hedrick, J. L.; Mecerreyes, D.; Dubois, P.; Jérôme, R.; Ihre, H.; Hult, A. *Macromolecules* **1998**, *31*, 2756–2763.
- [70] Huang, C.–I.; Yang, L.–F. *Macromolecules* **2010**, *43*, 9117–9125.
- [71] Lynd, N. A.; Oyerokun, F. T.; O’Donoghue, D. L.; Handlin, D. L.; Fredrickson, G. H. *Macromolecules* **2010**, *43*, 3479–3486.
- [72] Milner, S. T. *Macromolecules* **1994**, *27*, 2333–2335.
- [73] Floudas, G.; Hadjichristidis, N.; Iatrou, H.; Pakula, T. *Macromolecules* **1996**, *29*, 3139–3146.
- [74] Floudas, G.; Hadjichristidis, N.; Iatrou, H.; Pakula, T.; Fischer, E. W. *Macromolecules* **1994**, *27*, 7735–7746.
- [75] Hadjichristidis, N.; Iatrou, H.; Behal, S. K.; Chludzinski, J. J.; Disko, M. M.; Garner, R. T.; Liang, K. S.; Lohse, D. J.; Milner, S. T. *Macromolecules* **1993**, *26*, 5812–5815.
- [76] Pochan, D. J.; Gido, S. P.; Pispas, S.; Mays, J. W. *Macromolecules* **1996**, *29*, 5099–5105.
- [77] Pochan, D. J.; Gido, S. P.; Pispas, S.; Mays, J. W.; Ryan, A. J.; Fairclough, J. P. A.; Hamley, I. W.; Terrill, N. J. *Macromolecules* **1996**, *29*, 5091–5098.
- [78] Whittaker, M. R.; Urbani, C. N.; Monteiro, M. J. *J. Am. Chem. Soc.* **2006**, *128*, 11360–11361.

- [79] Cong, Y.; Li, B.; Han, Y.; Li, Y.; Pan, C. *Macromolecules* **2005**, *38*, 9836–9846.
- [80] Floudas, G.; Hadjichristidis, N.; Iatrou, H.; Avgeropoulos, A.; Pakula, T. *Macromolecules* **1998**, *31*, 6943–6950.
- [81] Higashihara, T.; Faust, R.; Inoue, K.; Hirao, A. *Macromolecules* **2008**, *41*, 5616–5625.
- [82] Li, Y.-G.; Shi, P.-J.; Pan, C.-Y. *Macromolecules* **2004**, *37*, 5190–5195.
- [83] Liu, J.; Pan, C.-Y. *Polymer* **2005**, *46*, 11133–11141.
- [84] Wei, Y. H.; Li, B. Y.; Han, Y. C.; Pan, C. Y. *Soft Matter* **2008**, *4*, 2507–2512.
- [85] Milner, S. T. *J. Polym. Sci., Part B: Polym. Phys.* **1994**, *32*, 2743–2755.
- [86] Bates, F. S.; Schulz, M. F.; Khandpur, A. K.; Foerster, S.; Rosedale, J. H. *Faraday Discuss.* **1994**, *98*, 7–18.
- [87] Helfand, E.; Wasserman, Z. R. *Developments in Block Copolymers* **1982**, *1*, 99–125.
- [88] Lai, C.; Russel, W. B.; Register, R. A.; Marchand, G. R.; Adamson, D. H. *Macromolecules* **2000**, *33*, 3461–3466.
- [89] Matsen, M. W.; Bates, F. S. *J. Polym. Sci., Part B: Polym. Phys.* **1997**, *35*, 945–952.
- [90] Vavasour, J. D.; Whitmore, M. D. *Macromolecules* **1993**, *26*, 7070–7075.
- [91] Weimann, P. A.; Jones, T. D.; Hillmyer, M. A.; Bates, F. S.; Londono, J. D.; Melnichenko, Y.; Wignall, G. D.; Almdal, K. *Macromolecules* **1997**, *30*, 3650–3657.

- [92] Almdal, K.; Hillmyer, M. A.; Bates, F. S. *Macromolecules* **2002**, *35*, 7685–7691.
- [93] Matsen, M. W.; Schick, M. *Macromolecules* **1994**, *27*, 4014–4015.
- [94] Matsen, M. W.; Thompson, R. B. *J. Chem. Phys.* **1999**, *111*, 7139–7146.
- [95] Helfand, E.; Wasserman, Z. R. *Macromolecules* **1976**, *9*, 879–888.
- [96] Matsen, M. W.; Bates, F. S. *Macromolecules* **1996**, *29*, 7641–7644.
- [97] Matsen, M. W. *Phys. Rev. Lett.* **2007**, *99*, 148304/148301–148304/148304.
- [98] Matsen, M. W. *Eur. Phys. J. E Soft Matter* **2006**, *21*, 199–207.
- [99] Beardsley, T. M.; Matsen, M. W. *Eur. Phys. J. E* **2008**, *27*, 323–333.
- [100] Milner, S. T.; Witten, T. A.; Cates, M. E. *Macromolecules* **1988**, *21*, 2610–2619.
- [101] Milner, S. T.; Witten, T. A.; Cates, M. E. *Macromolecules* **1989**, *22*, 853–861.
- [102] Shi, A.-C.; Noolandi, J. *Macromolecules* **1994**, *27*, 2936–2944.
- [103] Fredrickson, G. H.; Helfand, E. *J. Chem. Phys.* **1987**, *87*, 697–705.
- [104] Sides, S. W.; Fredrickson, G. H. *J. Chem. Phys.* **2004**, *121*, 4974–4986.
- [105] Bendejacq, D.; Ponsinet, V.; Joanicot, M.; Loo, Y. L.; Register, R. A. *Macromolecules* **2002**, *35*, 6645–6649.
- [106] Lynd, N. A.; Hillmyer, M. A. *Macromolecules* **2005**, *38*, 8803–8810.
- [107] Lynd, N. A.; Hillmyer, M. A. *Macromolecules* **2007**, *40*, 8050–8055.
- [108] Ruzette, A.-V.; Tence-Girault, S.; Leibler, L.; Chauvin, F.; Bertin, D.; Guerret, O.; Gerard, P. *Macromolecules* **2006**, *39*, 5804–5814.

- [109] Widin, J. M.; Schmitt, A. K.; Im, K.; Schmitt, A. L.; Mahanthappa, M. K. *Macromolecules* **2010**, *43*, 7913–7915.
- [110] Meuler, A. J.; Ellison, C. J.; Hillmyer, M. A.; Bates, F. S. *Macromolecules* **2008**, *41*, 6272–6275.
- [111] Meuler, A. J.; Ellison, C. J.; Qin, J.; Evans, C. M.; Hillmyer, M. A.; Bates, F. S. *J. Chem. Phys.* **2009**, *130*, 234903/234901–234903/234917.
- [112] Anderson, K. S.; Hillmyer, M. A. *Macromolecules* **2004**, *37*, 1857–1862.
- [113] Fetters, L. J.; Lohse, D. J.; Graessley, W. W. *J. Polym. Sci., Part B: Polym. Phys.* **1999**, *37*, 1023–1033.
- [114] Fetters, L. J.; Lohse, D. J.; Richter, D.; Witten, T. A.; Zirkel, A. *Macromolecules* **1994**, *27*, 4639–4647.
- [115] Schmidt, S. C.; Hillmyer, M. A. *J. Polym. Sci., Part B: Polym. Phys.* **2002**, *40*, 2364–2376.
- [116] Bassi, I. W.; Fagherazzi, G. *Eur. Polym. J.* **1968**, *4*, 123–132.
- [117] Liu, C.; Chun, S. B.; Mather, P. T.; Zheng, L.; Haley, E. H.; Coughlin, E. B. *Macromolecules* **2002**, *35*, 9868–9874.
- [118] Mackay, M. E.; Hong, Y.; Jeong, M.; Tande, B. M.; Wagner, N. J.; Hong, S.; Gido, S. P.; Vestberg, R.; Hawker, C. J. *Macromolecules* **2002**, *35*, 8391–8399.
- [119] Román, C.; Fischer, H. R.; Meijer, E. W. *Macromolecules* **1999**, *32*, 5525–5531.
- [120] Matsen, M. W.; Bates, F. S. *J. Chem. Phys.* **1997**, *106*, 2436–2448.
- [121] Hamley, I. W. *Adv. Polym. Sci.* **1999**, *148*, 114–137.

- [122] Muller, A. J.; Balsamo, V.; Arnal, M. L. *Adv. Polym. Sci.* **2005**, *190*, 1–63.
- [123] Barham, P. J.; Jarvis, D. A.; Keller, A. *Journal of Polymer Science: Polymer Physics Edition* **1982**, *20*, 1733–1748.
- [124] Santana, O. O.; Mueller, A. J. *Polym. Bull.* **1994**, *32*, 471–477.
- [125] Frensch, H.; Harnischfeger, P.; Jungnickel, B. J. *ACS Symp. Ser.* **1989**, *395*, 101–125.
- [126] Frensch, H.; Jungnickel, B. J. *Colloid. Polym. Sci.* **1989**, *267*, 16–27.
- [127] Moore, J. S.; Stupp, S. I. *Macromolecules* **1990**, *23*, 65–70.

## Chapter 4

# Nanoporous Linear Polyethylene Templated from Triblock Copolymers\*

This chapter describes the preparation of nanoporous materials comprising completely linear polyethylene (LPE). The porous polymers were prepared by removing one component from several templating block copolymers exhibiting microphase separation. The sacrificial component, poly(D,L-lactide), was hydrolyzed to lactic acid under mildly basic conditions to leave a LPE scaffold with nanoscopic void dimensions owing to the microphase separation in the parent triblock copolymers. The LPE scaffold contains a tortuous void path interpenetrating the matrix phase, resulting from the parent triblock copolymers adopting disorganized structures. It is shown that essentially identical phase behavior was exhibited by block copolymers over a wide range of compositions and molar masses, allowing a facile method for tailoring pore size. The nanoporous LPE behaved prototypically with respect to resistance to corrosive chemical environments and thermal stability.

---

\* Reproduced in part with permission from Pitet, L. M.; Amendt, M. A.; Hillmyer, M. A. *J. Am. Chem. Soc.* **2010**, *132*, 8230–8231. Copyright 2010 American Chemical Society.



## 4.1 Introduction

### 4.1.1 Nanoporous Materials from Block Copolymer Templates

Porous materials and membranes serve as crucial media in countless size-selective separation mechanisms from filtering of large grounds during coffee brewing to lipid bilayers that regulate protein migration and salt concentrations in cell membranes. Considering these two examples alone, it is immediately obvious that pore-size is a critical factor influencing the effectiveness of a membrane in its intended function. The development of porous materials with pore dimensions in the size-regime between 5–50 nm is becoming of ever-increasing importance. For example, viruses have dimensions commensurate with this regime, and as such, millions of people rely on these so-called nanoporous membranes for access to clean drinking water that is devoid of potentially life-threatening disease carriers. The self-assembly of block copolymers into well-ordered arrays having dimensions that lie exactly in this desired regime provides an opportunity with tremendous potential for templating nanoporous materials by selective removal of one component. Collectively, nanoporous polymers have been designed and fabricated with various intended applications in mind, ranging from virus removal during water filtration,<sup>1–7</sup> to drug-delivery carriers, to nanolithographic masks,<sup>8,9</sup> to battery separators,<sup>10–12</sup> to glucose sensors.<sup>13</sup>

Two reviews written within the span of the last decade cover nanoporous plastics derived from block copolymers, and the breadth of strategies attests to the potential of the protocol for addressing technical challenges across several fields.<sup>14,15</sup> The abundance of examples in the subsequent years following those reviews also indicates a great deal of enthusiasm for the technique, and demonstrate the tremendous progress made on improving the strategies used to control the material properties.

The general strategy may be summarized in three principal consecutive steps; each main step may, of course, have additional complexities and much research has been devoted to simplifying the procedures. Nonetheless, it starts with the

synthetic preparation of a block copolymer having a composition that will induce self-assembly into a desired morphology having domain sizes in the range that is proportional to individual polymer chain dimensions (*i.e.*, 5–20 nm). The first step provides the opportunity to strategically choose the components for the specific chemical and thermal properties that they embody, taking into consideration the ease with which one component will ultimately be removable. The second step explicitly involves self-assembly, and inherently entails strategies that have been developed to manipulate the particular geometric arrangement of microdomains and, as is often the case, direct the orientation of said domains. The third and final step involves selective removal of one component to leave voids in the space that it originally occupied, rendering the material porous while ideally retaining the morphological contours adopted by the pristine block copolymer that served as a template. These three steps are dutifully illustrated by an example of poly(styrene-*b*-lactide) (PS-PLA) starting polymer adopting a morphology of aligned PLA cylinders packed hexagonally in a PS matrix, followed by PLA removal to provide nanoporous polystyrene (Figure 4.1).<sup>16,17</sup> Each of these steps will be briefly reviewed, with an emphasis placed on the advances that have been made recently.

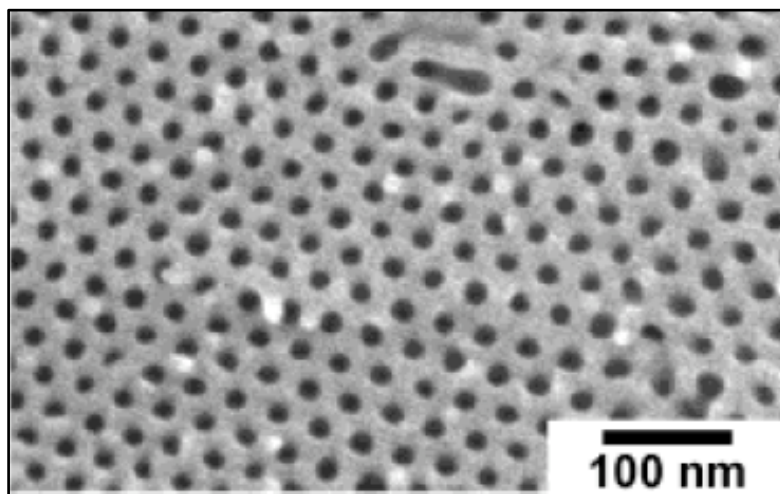


**Figure 4.1**

Scanning electron micrograph of nanoporous polystyrene templated from a diblock copolymer of poly(styrene-*b*-lactide) that adopted hexagonally packed cylindrical morphology, after selective PLA removal.<sup>17</sup> Reproduced with permission from reference 17. Copyright 2002 American Chemical Society.

Many different polymeric materials have been incorporated as the matrix component (*i.e.*, the non-sacrificial component) in block copolymers intended as templating agents. The matrix component must be mechanically robust at room temperature to prevent pore collapse, and it must remain solid and robust at any temperature for which the desired application intends to be used. Polystyrene, with a glass transition temperature ( $T_g$ ) near 100 °C and ready incorporation into well-defined block copolymers via anionic polymerization, has been chosen in certain instances by attachment to polylactide (PLA)<sup>16,17</sup> or poly(methyl methacrylate) (PMMA).<sup>18</sup> The templates were rendered nanoporous by basic hydrolysis of the polyester or by *uv* irradiation to chemically cleave the PMMA chains, respectively. This strategy was expanded upon with triblock copolymers of poly(styrene-*b*-dimethylacrylamide-*b*-lactide)<sup>19,20</sup> and poly(styrene-*b*-isoprene-*b*-lactide)<sup>21,22</sup> that formed core-shell cylindrical morphologies. Basic hydrolysis to selectively remove the PLA left nanoporous PS having functionalized pore-walls, with which further chemical transformations provided access to hydrophilic pores. Hedrick et al. described copolymers with poly(imide) matrices characterized by very high  $T_g$  (> 400 °C).<sup>23</sup> The minority component was subsequently removed by thermal degradation. Uehara and coworkers described preparation of nanoporous polyethylene (PE) derived from a hydrogenated 1,4-polybutadiene-*b*-polystyrene block copolymer, which itself adopted a crystallization-induced bicontinuous disordered morphology, after which removal of the PS phase was achieved by chemical degradation with fuming nitric acid.<sup>13,24</sup> The astounding mechanical properties of crosslinked dicyclopentadiene (DCPD) led Hillmyer and coworkers to devise a polymerization induced phase separation strategy with poly(norbornyl styrene)-poly(lactide) block copolymers that formed a bicontinuous morphology upon crosslinking between the norbornyl side groups and DCPD. PLA removal gave mechanically robust membranes with nanoscopic pore dimensions.<sup>6,25,26</sup>

Block copolymers have been shown experimentally to regularly adopt one of four conventional morphologies: alternating lamellae, hexagonally packed cylinders, bicontinuous double gyroid, and spheres packed on a body-centered cubic lattice. The different conventional morphologies can be accessed by judicious choice

of composition, provided the different components are reasonably incompatible and have adequate chain lengths to cause phase separation.<sup>27</sup> Two of these morphologies are particularly suitable for precursors to nanoporous materials, namely the cylindrical and gyroid phases. The gyroid phase is particularly attractive; the thermodynamically stable bicontinuous phase allows for monoliths and thin films to be prepared without any post-processing to ensure the sacrificial block permeates throughout the material. Poly(styrene-*b*-isoprene) diblock copolymers were shown to adopt the gyroid morphology at a particular composition and were subsequently subjected to ozonolysis to degrade the PI block, leaving a nanoporous PS scaffold with a tortuous void-channel having an average diameter of approximately 25 nm.<sup>28</sup> Advancements of this strategy have also been achieved through incorporation of an additional block in ABC type triblock terpolymers that adopted a core-shell gyroid morphology. Loos and coworkers described using supramolecular interaction between a small molecule pentadecylphenol (PDP) and the poly(4-vinylpyridine) core block, which was attached to a polystyrene core and poly(*tert*-butoxystyrene) matrix. Facile removal of the PDP by washing caused collapse of the P4VP chains with retention of the morphology, leaving a nanoporous matrix with a continuous void space having 12 nm diameter.<sup>29</sup> Nanoporous PS was also generated from a gyroid forming block copolymer with PLA, which was removed by basic hydrolysis.<sup>30</sup> The drawback of the gyroid morphology is that it occurs in a very small composition window, and is therefore not the most accessible of the conventional mesophases.<sup>27</sup> Hexagonally packed cylinders, on the other hand, can be accessed over a substantially wider range of compositions. As such, block copolymers adopting this morphology have been more widely studied as precursors to mesoporous materials. However, cylinders come with the challenge of creating cylindrical domains that penetrate the bulk of the material and are aligned in the plane of flow. Long-range order and alignment of cylinders perpendicularly to the surface can, under certain circumstances, be achieved with thin films, although examples have also arisen that describe monolithic nanoporous polymers. Several sophisticated techniques have been developed to induce alignment of cylinders, including reciprocating shear<sup>31–35</sup> melt-flow with a

channel die<sup>16,17,19,20,36–39</sup>, applying an electric field,<sup>40–46</sup> and solvent annealing/evaporation.<sup>47–53</sup> The latter two are only applicable with thin films (< 100  $\mu\text{m}$ ), whereas the first two are only appropriate for bulk samples. Although well-oriented cylinders covering large surface areas are attainable using these methods, they constitute additional processing in order to form channels that extend through the material. Bicontinuous phases are therefore desirable to avoid extensive processing requirements, but the ordered gyroid phase is rather difficult to access synthetically. A bicontinuous, disordered phase was observed in the polymerization induced phase separation system described previously using DCPD and a doubly reactive poly(norbornyl styrene) block connected to PLA (Figure 4.2).

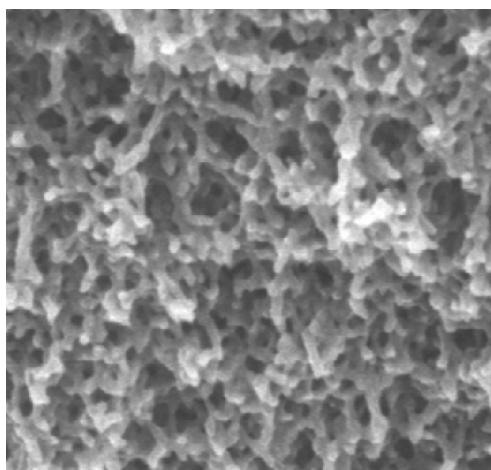


**Figure 4.2**

SEM micrograph of nanoporous membrane derived from a disordered bicontinuous multiphase thermoset from crosslinking of poly[(norbornyl styrene-*s*-styrene)-*b*-lactide] with DCPD, followed by PLA removal.<sup>26</sup> Reproduced with permission from reference 26. Copyright 2007 American Chemical Society.

Bicontinuous disordered morphologies were also reported upon cooling a poly(ethylene-*b*-styrene) copolymer from the melt through the crystallization temperature of the PE block. The crystallization induced rearrangement of the melt-state morphology into a disordered state, the exact nature of which could be modulated by the crystallization/cooling rate. Upon subsequent chemical degradation of the PS with fuming nitric acid, a nanoporous PE sample with tortuous nanoscopic channels was realized (Figure 4.3).<sup>13,24</sup>

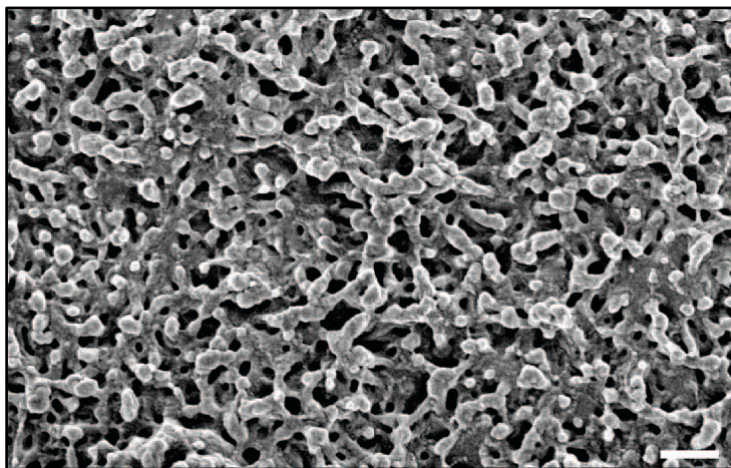


**Figure 4.3**

Nanoporous PE (from anionic polymerization and hydrogenation of 1,4-polybutadiene) derived from fuming nitric acid etch of a PE-PS diblock copolymer to selectively degrade the PS. Scale bar = 200 nm.<sup>13</sup> Reproduced with permission from reference 13. Copyright 2009 American Chemical Society.

An additional innovative route to mesoporosity involves first allowing self-assembly into an ordered structure followed by selective swelling of one component (the minority) with solvent to dilate the associated domain, which is on occasion accompanied by morphological transition. Fast removal of the solvent has been shown to cause collapse of the chains occupying the swelled domains, and thereby create porosity. This approach was effectively demonstrated with poly(styrene-*b*-4-vinylpyridine) (PS-P4VP) using ethanol to selectively swell the P4VP.<sup>53,54</sup> This ingenious approach avoids selective removal of either block in the copolymer and in one case led to a bicontinuous phase that had a relatively narrow pore-size distribution according to nitrogen sorption analysis (from the desorption isotherm) (Figure 4.4).<sup>54</sup>

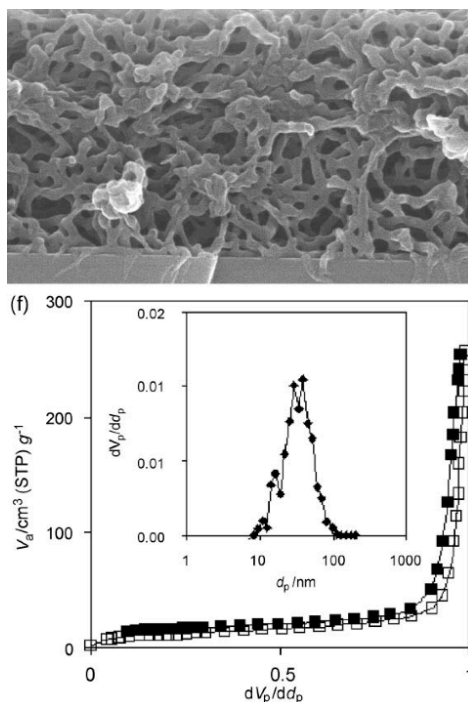


**Figure 4.4**

SEM micrograph (*top*) of a nanoporous block copolymer derived from selective swelling of a poly(styrene-*b*-4-vinylpyridine) and the corresponding adsorption and desorption isotherms with BJH pore size distribution (*bottom*).<sup>54</sup> Reproduced with permission from reference 54. Copyright 2010 John Wiley & Sons.

The aforementioned examples predominantly described block copolymer templates having linear molecular architectures. As such, the accessible domain sizes are correlated with the bulk chain dimensions, which are typically in the range of 2–20 nm. Certain commercial targets require larger pore sizes, which necessitated innovative modifications to molecular design to render block copolymers capable of addressing such needs. Bottlebrush block copolymers were prepared having a backbone with segments containing either polystyrene arms or PLA arms. The very large molecular dimensions of the brush copolymers provided self-assembled materials having domains that were larger than is accessible with conventional linear copolymers. Nonetheless, ordered morphologies, like hexagonally packed cylinders, provided convenient templates from which the PLA was easily hydrolyzed to leave a pores with diameters in excess of 50 nm.<sup>55</sup>

Similarly, large-pore ( $> 50$  nm diameter) materials exhibiting disordered morphologies with cocontinuous domains are accessible using bicontinuous microemulsions as templates.<sup>56,57</sup> The microemulsion can be attained with mixtures of two homopolymers and the corresponding block copolymer within a specific composition window, and is at thermodynamic equilibrium. Such attributes are attractive because of the ease with which the sacrificial component is removed (*e.g.*, selective solvent washing, as opposed to degradative chemical transformations) and the stability of a bicontinuous phase that avoids tedious cylinder alignment. In this way, polyethylene–poly(ethylene-*alt*-propylene) (PE–PEP) microemulsions were prepared from hydrogenation of 1,4-polybutadiene–polyisoprene from anionic polymerization, followed by washing the amorphous PEP with toluene to leave a porous PE scaffold.<sup>58</sup> Lodge and coworkers also described the crosslinking of poly(isoprene) with sulfur monochloride in a microemulsion with polystyrene comprising the second component. Crosslinking allowed immobilization of the PI phase, after which the PS was easily washed away to provide a porous structure having average pore diameters greater than 50 nm as suggested by nitrogen adsorption analysis (Figure 4.5b).<sup>59</sup>

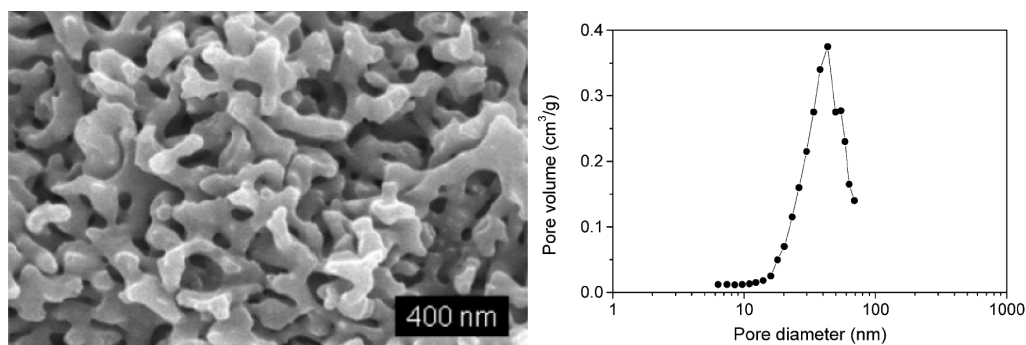


**Figure 4.5**

(*left*) SEM micrograph of nanoporous crosslinked poly(isoprene) after washing of the polystyrene homopolymer and (*right*) Barret-Joyner-Halenda pore-size distribution from nitrogen desorption isotherm.<sup>59</sup> Reproduced with permission from reference 59. Copyright 2006 American Chemical Society.



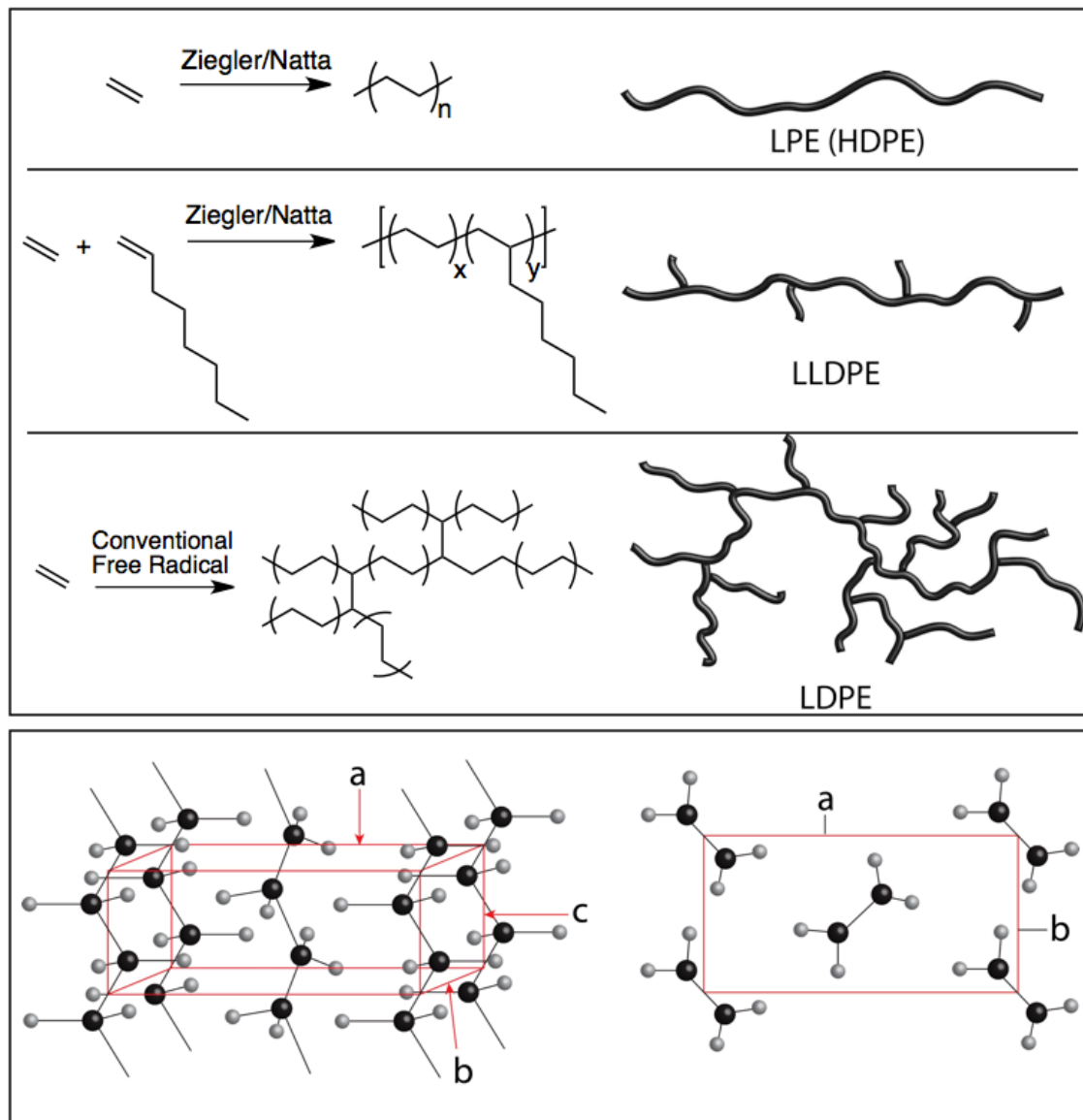
These examples highlight several of the potential pathways towards selective removal of one component in block copolymer templates. Collectively, several prominent strategies employed include ozonolysis of unsaturated polyolefins,<sup>28,60</sup> reactive ion etching,<sup>53</sup> hydrolytic degradation of polyesters,<sup>12,16,17,19–22,25,26,38,39</sup> *uv* irradiation of polyacrylates,<sup>18,52,53</sup> thermal degradation,<sup>23,61</sup> and chemical degradation.<sup>13,24</sup>

The aforementioned examples provide a broad overview of various techniques used to access nanoporous materials derived from block copolymers. The strengths and weaknesses associated with these different routes were evaluated prior to designing the system described in the subsequent report. Certain attributes were desired: (1) a matrix component that exhibits outstanding thermal and chemical stability in various, potentially corrosive environments at elevated temperatures (~50–100 °C); (2) a synthetic protocol that is versatile and flexible enough to easily modify for further chemical enhancement (*e.g.*, adding additional components that exhibit hydrophilicity or have "attachment" sites for catalyst binding). This requires that the synthesis be tolerant to exotic functional groups; (3) the processing conditions should be technically simple and ideally grant access to a bicontinuous phase. The materials will ideally be suitable for production of monoliths or films with retention of the bicontinuity despite the demands for various macroscopic proportions; (4) finally, the synthesis should allow combination of the initial matrix-forming block with subsequent ring-opening polymerization of the cyclic ester D,L-lactide to prepare block copolymers. This will allow the sacrificial polyester block to be removed under relatively mild conditions with environmentally benign byproducts being formed (*e.g.*, weakly basic aqueous solution, hydrolysis to lactic acid).

### 4.1.2 Linear Polyethylene Block Copolymers by ROMP

Polyethylene, and specifically the completely linear analog, arguably constitutes the most economically and mechanically important polymeric material yet discovered. Completely linear polyethylene (LPE; also referred to as high density polyethylene, HDPE) has properties that make it useful in a countless number of products. Its strength, durability, thermal stability, chemical inertness and ductility make it ideal for a wide range of applications, from hip replacements, to underground pipes, to automobile engine components. We store our laundry detergents, toiletries, and laboratory solvents in LPE bottles; our waste is stored in LPE trash containers. In short, the global impact of LPE cannot be understated. The extensive use of LPE has far reaching consequences both in positive and negative senses. A comprehensive review of LPE and its uses, properties, and impacts might easily consume an entire lifetime. Hence, the introductory remarks in this section will remain minimal and focus specifically on several examples of block copolymers containing polyethylene as a component, with particular emphasis on those prepared using metathesis polymerizations. In addition to LPE from hydrogenated metathesis polymers, some examples of hydrogenated 1,4-polybutadiene are included to emphasize the consequences and advantages of the contrasting structural characteristics.

Polyethylene comprises long chains of covalently linked methylene repeating units ( $-\text{CH}_2-$ ) and can be prepared with various architectures, the nature of which have profound influence on the thermal, mechanical and optical properties. Three major classes of polyethylene include LPE (or HDPE), linear low-density polyethylene (LLDPE) and low-density polyethylene (LPDE) (Figure 4.6).

**Figure 4.6**

(*top box*) Schematic illustration of different polyethylene classes and the conventional preparation methods. (*bottom box*) Schematic representation of crystalline polyethylene packing in a orthorhombic unit cell with 3-dimensional perspective shown on left and top view of **ab** plane shown on right.

Polyethylene prepared by conventional polymerization of ethylene using Ziegler-Natta titanium complexes leads to a linear chain essentially absent of branching. In contrast, short chain branches can be introduced to disrupt formation of large crystallites by copolymerizing ethylene monomer with  $\alpha$ -olefins (*e.g.*, 1-octene) using similar titanium complexes (Ziegler-Natta). Polyethylene exhibiting low levels of crystallinity is produced during conventional free-radical polymerization of ethylene, during which long chain branches are formed along with high polydispersity indices (PDIs). Typically long strands of methylene repeat units can pack together in a regular fashion and form crystalline regions; typically, the level of crystallinity is inversely proportional to the degree of branching. Polyethylene crystallites pack in an orthorhombic space group with regularly repeating dimensions  $a = 7.40 \text{ \AA}$ ,  $b = 4.93 \text{ \AA}$ , and  $c = 2.53 \text{ \AA}$  (Figure 4.6).<sup>62–65</sup>

Polyethylene can also be synthesized by hydrogenating certain unsaturated hydrocarbon polymers. One advantage of this method derives from the controlled manner in which unsaturated polyolefins are readily produced using either anionic or metathesis polymerization. Until relatively recently, living polymerization of ethylene monomer was not practical,<sup>66</sup> while samples exhibiting narrow polydispersity indices have been accessible using anionic polymerization for more than half a century.<sup>67–69</sup> Additionally, metathesis polymerization offers unprecedented access to polyethylene with functional groups of various identities (*e.g.*, hydroxyl, acid, ester, ether, cyano) at positions strictly controlled through synthetic conditions. The three conventional mechanisms by which PE is prepared from unsaturated polyolefins are anionic polymerization of 1,3-butadiene, acyclic  $\alpha,\omega$ -diene metathesis–chain transfer (ADMET) polymerization, and ring-opening metathesis polymerization (ROMP) of cyclic olefins. Each unsaturated polymer produced by these mechanisms can be hydrogenated by various techniques including chemical hydrogenation<sup>70</sup> or using  $\text{H}_{2(g)}$  with a catalyst<sup>71</sup> (Figure 4.7).

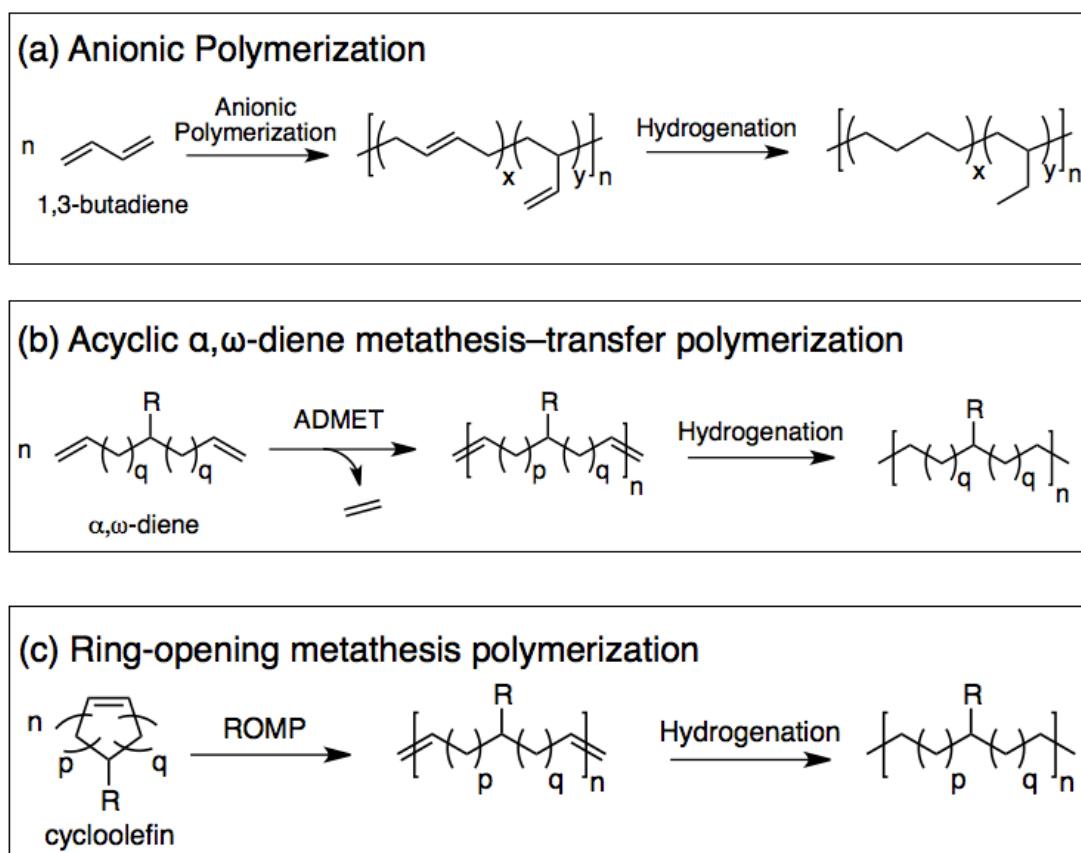


**Figure 4.7**

Polyethylene synthesis from (a) anionic polymerization of 1,3-butadiene followed by hydrogenation, (b) ADMET polymerization of an  $\alpha,\omega$ -diene followed by hydrogenation, and (c) ROMP of a cyclic olefin followed by hydrogenation.

Anionic polymerization of 1,3-butadiene provides polybutadiene (PBD) with controlled chain lengths, narrow PDI, and controlled microstructure (*i.e.*, 1,4 vs. 1,2 addition, thereby controlling the ratio of  $x:y$ ), ultimately providing access to polymeric materials exhibiting a spectrum of thermal and rheological properties. Hydrogenation thus allows access to PEs having a statistically controlled number of ethyl branches per chain and polymerization conditions provide a handle with which judicious tuning of crystallinity is possible.<sup>72</sup> However, the lower limit of 1,2-addition during polymerization of 1,3-butadiene is approximately 7 mol % (*i.e.*,  $x:y = 13.4$ ; 18 ethyl branches/1000 backbone carbons)<sup>73–75</sup> This has substantial influence on the chain-folding capabilities in the hydrogenated derivatives, as

discussed subsequently, and represents a ceiling for the accessible crystallinity and melting temperature that ultimately determine mechanical properties.

ADMET polymerization proceeds by a metathetical *step-growth* polymerization mechanism (see Chapter 1) from  $\alpha,\omega$ -diene monomers and therefore requires the removal of a condensate, which is usually ethylene. Discrete monomers having well defined molecular characteristics provide completely linear polymeric structures devoid of branching. Therefore, access to LPE is straightforward when  $\mathbf{R} = \mathbf{H}$  in Figure 4.7b after hydrogenation of the unsaturated polymer; the prototypical monomer demonstrating the efficacy of the approach is 1,9-decadiene ( $\mathbf{R} = \mathbf{H}$ ;  $\mathbf{p} + \mathbf{q} = 5$ ).<sup>76</sup> The strength of this approach derives mainly from the ability to precisely control the position of alkyl or heteroatom substituents on linear polyethylene backbones. Examples of substituents placed on PE backbones is versatile and include methyl,<sup>77–83</sup> ethyl,<sup>80,82,84</sup> geminal dimethyl,<sup>82,85,86</sup> butyl,<sup>87</sup> hexyl,<sup>81,88,89</sup> phenyl,<sup>90</sup> hydroxy,<sup>91</sup> chloro,<sup>90,92</sup> carboxylic acid,<sup>90,93,94</sup> carboxylic esters,<sup>90,94</sup> acetoxy,<sup>94,95</sup> polyether,<sup>80,96–99</sup> and phosphonic and sulfonic acids,<sup>100,101</sup> among others.<sup>102–104</sup> The effect of precisely placed alkyl branches on thermal properties and crystallinity has been extensively investigated using polymers prepared by ADMET and the extent of branching can be tuned by copolymerization with an unsubstituted monomer such as 1,9-decadiene. Substantial challenges encountered with ADMET include (1) precise placement of functional end-groups in making telechelic polymers as precursors to block copolymers,<sup>86</sup> for example, and (2) obtaining high molecular weight materials; scrupulously pure monomers and very high conversions are necessary for a successful *step-growth* polymerization.<sup>105,106</sup>

ROMP has been exploited for polyethylene preparation as well. This approach offers facile access to high molecular weight materials at low conversion due to the chain propagation mechanism (see Chapter 1). The ability to precisely place functional groups with wide ranging chemical identities remains of unequivocal importance, and ultimately allows transformation to alternate mechanisms for block/graft copolymer synthesis utilizing a monomer pool of near limitless complexity and sophistication.

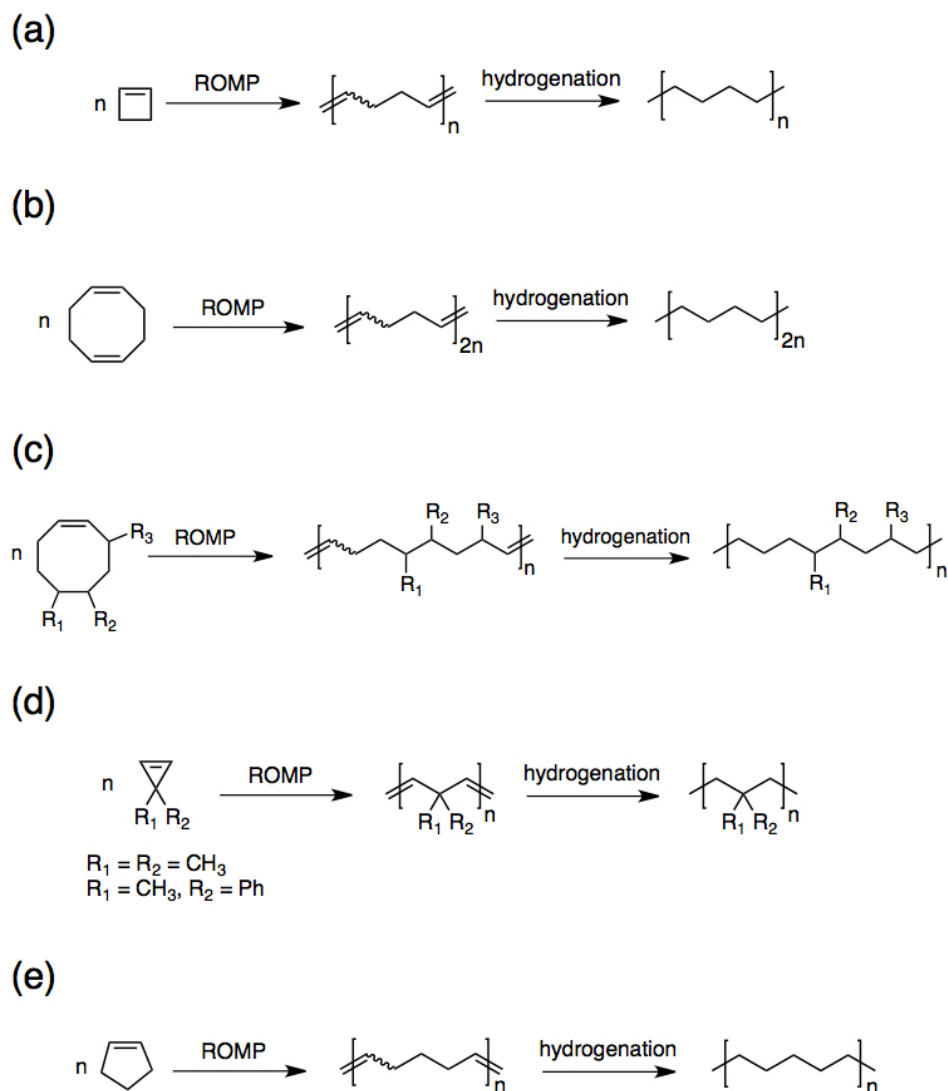


Figure 4.8

Synthetic approaches to form linear polyethylene and substituted derivatives by ROMP and subsequent hydrogenation to give saturated polymers: (a) cyclobutene, (b) 1,5-cyclooctadiene, (c) *cis*-cyclooctene and substituted derivatives, (d) substituted cyclopropene derivatives, and (e) cyclopentene.

The first report by Grubbs and co-workers of hydrogenating polymers prepared by ROMP described a completely linear, perfectly 1,4-polybutadiene analog. The living ROMP of cyclobutene was achieved using a tungsten-based metathesis catalyst, followed by chemical hydrogenation with *p*-tosyl hydrazide (Figure

4.8a).<sup>107</sup> Shortly thereafter, the hydrogenation of hydroxy-telechelic poly(1,5-cyclooctadiene) was reported to give the analogous perfectly linear telechelic polyethylene (Figure 4.8b).<sup>108</sup> Additionally, the ROMP of 5-acetoxycyclooct-1-ene was described as giving linear unsaturated polymers with acetoxy groups spaced 7, 8, and 9 carbons apart due to the asymmetric monomer structure and regio-random polymerization (Figure 4.8c;  $R_1 = H$ ,  $R_2 = OAc$ ).<sup>109</sup> Regardless of the specific substituent location, hydrogenation with *p*-tosyl hydrazide provided LPE substituted with pendant polar substituents analogous to important commercial ethylene-vinyl acetate copolymers (EVAC). The structures of polyethylenes from ROMP of substituted cyclooctenes can be further tailored by copolymerization with unsubstituted cyclooctene (COE). The extensive chain transfer (CT) observed with some more recently developed ruthenium centered metathesis catalysts has been exploited to prepare LPE having essentially randomly distributed substituents. With this comes the ability to fine-tune crystallinity, phase-transition temperatures and ultimately mechanical behavior. Analogs of poly(vinyl chloride)-LPE copolymers were synthesized by ROM copolymerization of 5-chlorocyclooctene or 5,6-dichlorocyclooctene with COE followed by chemical hydrogenation (Figure 4.8c;  $R_1 = H$ ,  $R_2 = Cl$ ;  $R_1 = R_2 = Cl$ ).<sup>110,111</sup> The ROM copolymerization of 5-hexylcyclooct-1-ene (Figure 4.8c;  $R_1 = H$ ;  $R_2 = n$ -hexyl) with COE with subsequent heterogeneously catalyzed hydrogenation was demonstrated as a potential alternative route to LLDPE samples traditionally prepared by copolymerization of 1-octene with ethylene.<sup>112</sup> Further demonstrating the efficacy of Ru-based catalysts in preparing well-defined LPE having functional pendant substituents, Wagener and coworkers described the ROM copolymerization of COE with cyclooctene derivatives having hydroxyl [ $R_1 = R_3 = H$ ;  $R_2 = OH$ ], acetoxy [ $R_1 = R_3 = H$ ;  $R_2 = OAc$ ], carboxylic acid [ $R_1 = R_3 = H$ ;  $R_2 = COOH$ ], methyl carboxylate [ $R_1 = R_3 = H$ ;  $R_2 = COOCH_3$ ], and tert-butyl carboxylate [ $R_1 = R_3 = H$ ;  $R_2 = COOC(CH_3)_3$ ] substituents in the 5-position (Figure 4.8c).<sup>94</sup> Recently, regio-regular LPE with aryl and alkyl side-chain substituents were prepared from ROMP of 3-substituted cyclooctenes ( $R_1 = R_2 = H$ ;  $R_3 = CH_3, C_2H_5, C_6H_{13}, C_6H_5$ ) followed by chemical hydrogenation with *p*-tosyl hydrazide.<sup>113</sup>

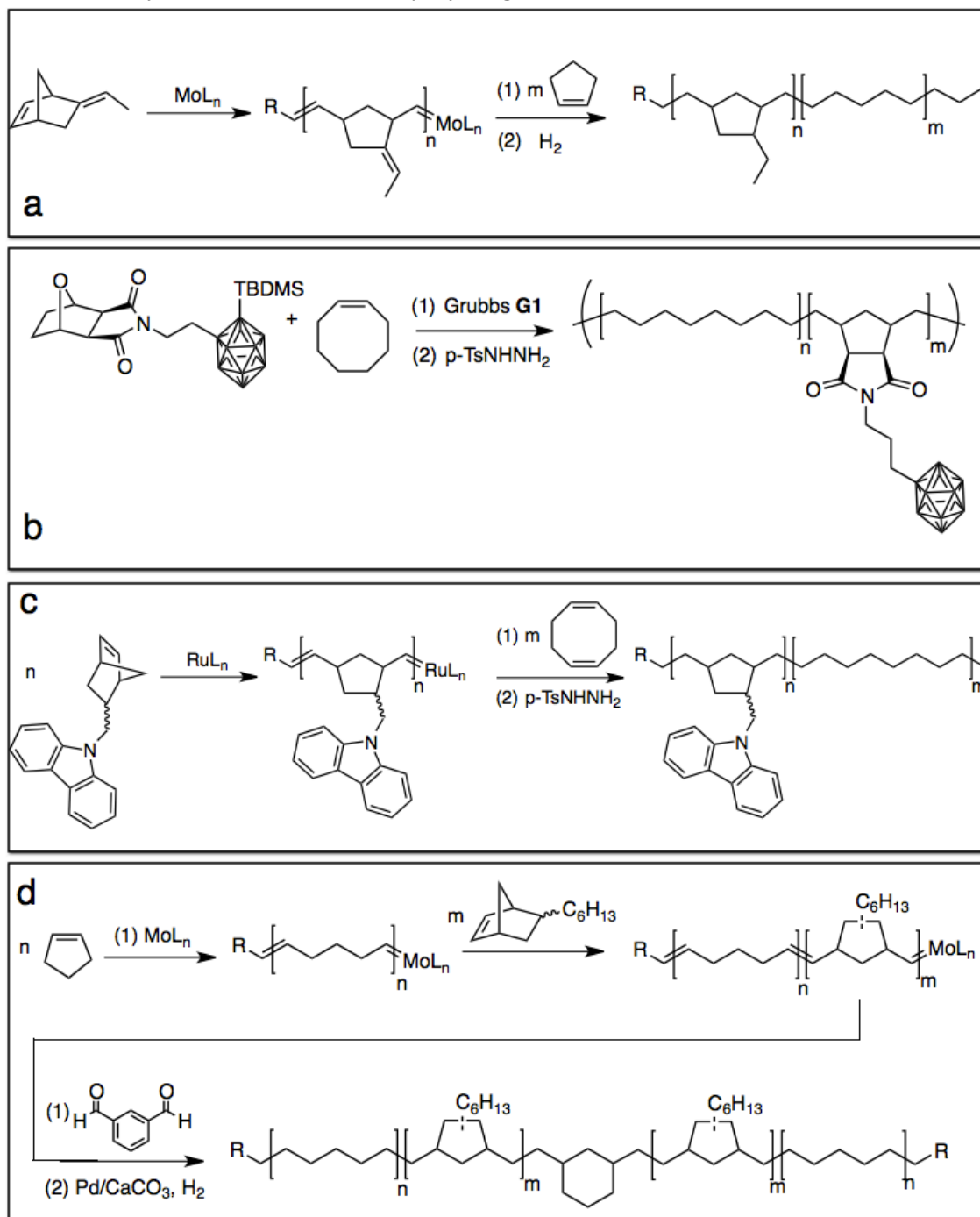


Other cyclic olefins and substituted derivatives have been polymerized and hydrogenated to form linear polyethylene and substituted analogs. Notably, 3,3-dimethylcyclopropene and 3-methyl-3-phenylcyclopropene were polymerized and the resulting polymers hydrogenated to give saturated rubbers (Figure 4.8d).<sup>114</sup> Likewise, the living polymerization and subsequent hydrogenation of cyclopentene (Figure 4.8e) gives LPE with narrow PDIs<sup>115</sup> and allows for straightforward chain extension with other monomers to form block copolymers (Scheme 4.1a).<sup>116,117</sup>

Several additional block copolymers and statistical copolymers with linear polyethylene have been prepared by exploiting the living nature of ROMP or by hydrogenating hybrid materials prepared from mechanistic transformations (see Chapter 1). For example, statistical copolymers were prepared by simultaneous copolymerization of cyclopentene and norbornene with **G1** catalyst followed by hydrogenation (Scheme 4.1b).<sup>118</sup> The influence of microstructure and monomer distribution on thermal properties was explored in these LPE hybrid materials. After similar statistical copolymerization between *cis*-cyclooctene and a silyl protected oxonorbornene imide carborane (SONIC), the hydrogenated derivatives were investigated as potential radiation shielding materials with mechanical integrity provided by the LPE component (Scheme 4.1c).<sup>119</sup> The living nature of certain monomer polymerizations has been used to produce block copolymers by sequential polymerizations. A bulky carbazole-substituted norbornene polymerized with a ruthenium catalyst followed by ROMP of 1,5-cyclooctadiene (COD) provided block copolymers; subsequent hydrogenation gave the LPE analog (Scheme 4.1d).<sup>120</sup> Thermoplastic elastomers were prepared by sequential polymerization of cyclopentene and hexyl-substituted norbornene followed by a coupling reaction and hydrogenation (Scheme 4.1e).<sup>121,122</sup>

## Scheme 4.1

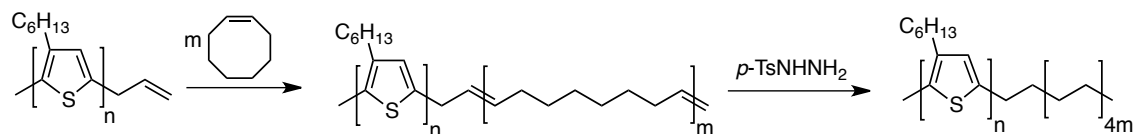
Synthesis of block and statistical copolymers with LPE as a component from ROMP of different cyclic olefins followed by hydrogenation.



Block copolymers containing LPE and the conductive poly(3-hexyl thiophene) were prepared by a macromolecular chain-transfer agent (CTA) with ROMP protocol (Scheme 4.2).<sup>123</sup> The CTA showed near quantitative incorporation during ROMP, and the resulting crystalline-crystalline block copolymers exhibited interesting morphological behavior. This represents an alternative strategy to block copolymers to those previously discussed; mechanistically incompatible monomers were combined to form block copolymers.

### Scheme 4.2

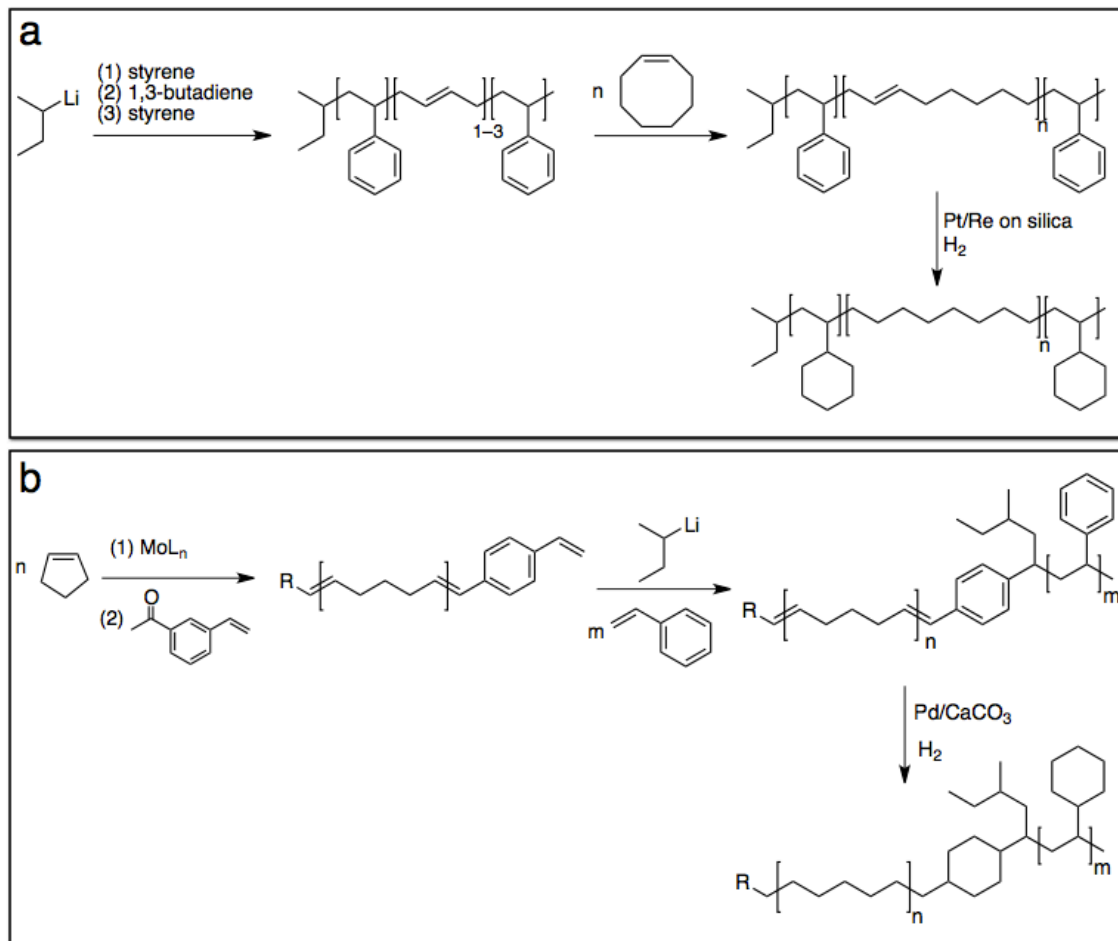
Synthesis of poly(3-hexylthiophene)-LPE block copolymers by a macromolecular CTA protocol during ROMP of COE followed by chemical hydrogenation.



Several authors have demonstrated another mechanistic transformation through the successful combination of anionic polymerization and ROMP. Bates and coworkers first polymerized styrene with small amounts of 1,3-butadiene, strategically placing several double bonds within the backbone.<sup>124</sup> The polystyrene was utilized as a macromolecular CTA during ROMP of COE (Scheme 4.3a) to provide linear triblock copolymers. The exhaustive hydrogenation with a silica supported Pt/Re heterogeneous catalyst gave TPEs with semicrystalline LPE midblocks and high  $T_g$  endblocks. Representing the opposite order of polymerization, Register and coworkers designed poly(cyclopentene) with a single styrenic end groups through termination of a ROMP (Scheme 4.3b).<sup>125</sup> Subsequent anionic polymerization of styrene was initiated from the macromolecules, ultimately providing diblock copolymers. Hydrogenation gave the corresponding LPE block copolymer hybrid materials.

Scheme 4.3

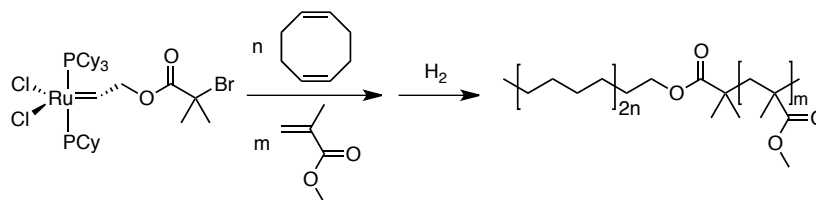
Synthesis of block copolymers with LPE from mechanistic transformation between ROMP and anionic polymerization.



One final example involves the simultaneous polymerization of methyl methacrylate by ATRP and COD by ROMP with a specially designed multifunctional ruthenium catalyst (Scheme 4.4).<sup>126</sup> Residual ruthenium was used to catalyze the subsequent hydrogenation to give LPE block copolymers. The catalyst effectively allowed three mechanistically distinct reactions. These examples give inspiration to combine other mechanistically incompatible monomers to prepare alternative LPE hybrid materials. The remainder of the chapter is dedicated to describing the combination of ring-opening transesterification polymerization (ROTEP) and ROMP to form functional materials as precursors to nanoporous materials.

Scheme 4.4

PMMA–LPE block copolymer synthesis from simultaneous ROMP and ATRP followed by hydrogenation.



### 4.1.3 Design of Nanoporous Linear Polyethylene

Triblock copolymers containing LPE and PLA were prepared with the intention of making porous materials with nanoscopic channels. Using self-assembled microstructures as templates, the LPE was intended to comprise the interconnected matrix after removal of the sacrificial PLA. The desired outcome would be to design a system with which the pore size, pore-size distribution, and porosity can be directly manipulated via synthetic finesse while optimizing the resistance to chemical corrosion and mechanical durability of the matrix material. These challenges were addressed by two different means. Block copolymers with different molecular characteristics were prepared; namely, molecular weight and composition were tailored using a tandem ring-opening polymerization strategy and the consequences on self-assembly and ultimately on pore-structure were investigated. Connecting molecular weight with resulting mechanical durability was also paramount in establishing the potential utility of the synthetic protocol for preparing commercially relevant porous membranes and monoliths.

Introducing branching into block copolymers has substantial effect on the particular morphology adopted in the bulk. The effect on the morphology occasionally manifests itself as differences in the interfacial curvature at the phase boundaries between microphase separated domains. For a simple two-component system, the consequences of both asymmetry ( $\epsilon$ ) and increased junction functionality ( $F_j$ ) on adoption of ordered morphology has been theoretically evaluated by Milner (Figure 4.9).<sup>127</sup> Additionally, the influence of  $F_j$  on domain

spacing in block copolymers has been evaluated by self-consistent mean-field theory, which predicts that star-shaped block copolymers (e.g.  $A_2B_2$ ) may have increased domain spacing at equivalent molar mass and composition to the linear counterparts.<sup>128</sup> The predicted increase in lamellar domain spacing was substantiated experimentally with  $A_xB_x$  starblock copolymers comprised of polystyrene and polyisoprene with  $x = 2, 4,$  and  $16$ .<sup>129</sup> This feature may potentially be exploited in tailoring pore size for block copolymer templates that adopt morphologies other than ordered lamellae. The difference in domain spacing, however, is modest, and may not be reflected in the pore size of said materials.

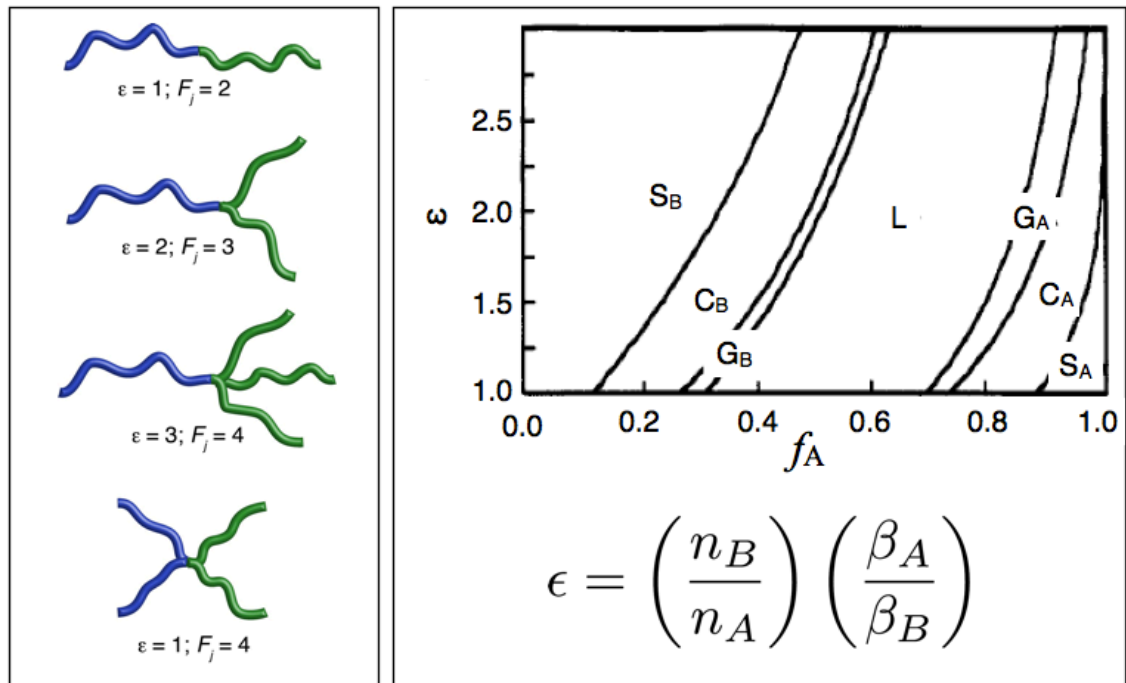
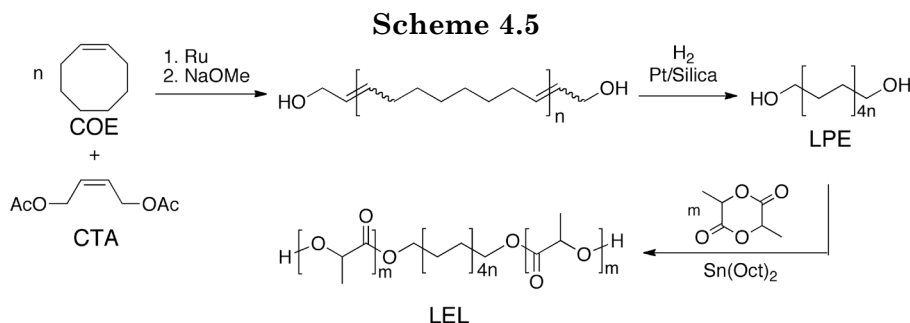


**Figure 4.9**

Illustration of different block copolymer junction functionality ( $F_j$ ) and asymmetry parameter ( $\epsilon$ ) and the theoretical phase diagram for the influence of branching on ordered morphology.

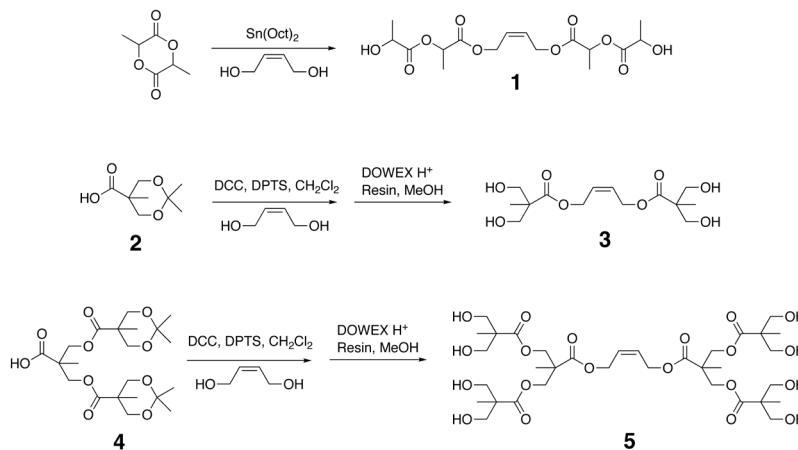
The current work was designed to simultaneously explore the possibility of tailoring pore-size and/or mechanical integrity of nanoporous materials derived from block copolymer precursors by using branched molecular architectures. A system designed and introduced in Chapter 3 showed that branching is easily accessible using a tandem ring-opening polymerization (ROP) strategy, leading to polymers with polyolefin midblocks and PLA end blocks.<sup>130</sup> The tandem ring-opening polymerization strategy begins with the ring-opening metathesis polymerization (ROMP) of the commercially available cycloolefin *cis*-cyclooctene (COE) in the presence of a chain transfer agent (CTA). This provides telechelic poly(cyclooctene) (PCOE) with the molar mass controlled through the initial concentration ratio between monomer and the CTA (*i.e.*,  $[\text{COE}]_0:[\text{CTA}]_0$ ). The CTA that was initially investigated was *cis*-1,4-diacetoxy-2-butene (DAB). Deprotection by hydrolysis after ROMP provides hydroxy-telechelic PCOE with which subsequent ring-opening transesterification polymerization (ROTEP) has been demonstrated to form symmetric BAB triblock copolymers with well-controlled compositions.<sup>130,131</sup> The catalytic heterogeneous hydrogenation of the hydroxy-telechelic PCOE prior to ROTEP provides convenient route to perfectly linear polyethylene (LPE) with well-preserved hydroxyl functionality. Proceeding with ROTEP of the cyclic ester D,L-lactide (LA) gives the linear LEL triblock copolymers (Scheme 4.5) from which nanoporous LPE is derived in a straightforward manner.



An extension of this tandem polymerization strategy was reported recently.<sup>130</sup> The extension uses alternate CTAs with different numbers of hydroxyl groups. The CTAs still contain the crucial monounsaturations with the *cis* conformation and are each symmetric about the double bond. These CTAs were nearly quantitatively incorporated into PCOE when included during ROMP catalyzed by **G2**. CTAs **1**, **3**, and **5** were synthesized according to Scheme 4.6 and contain two, four, and eight hydroxyl groups per molecule, respectively. Hence, it was shown that indistinguishable BAB-type triblock copolymer could be accessed using CTA **1** or by using **DAB** followed by deprotection (Scheme 4.5).

### Scheme 4.6

Synthesis of hydroxyl CTAs **1**, **3**, and **5** with various functionality ( $F_n$ ).



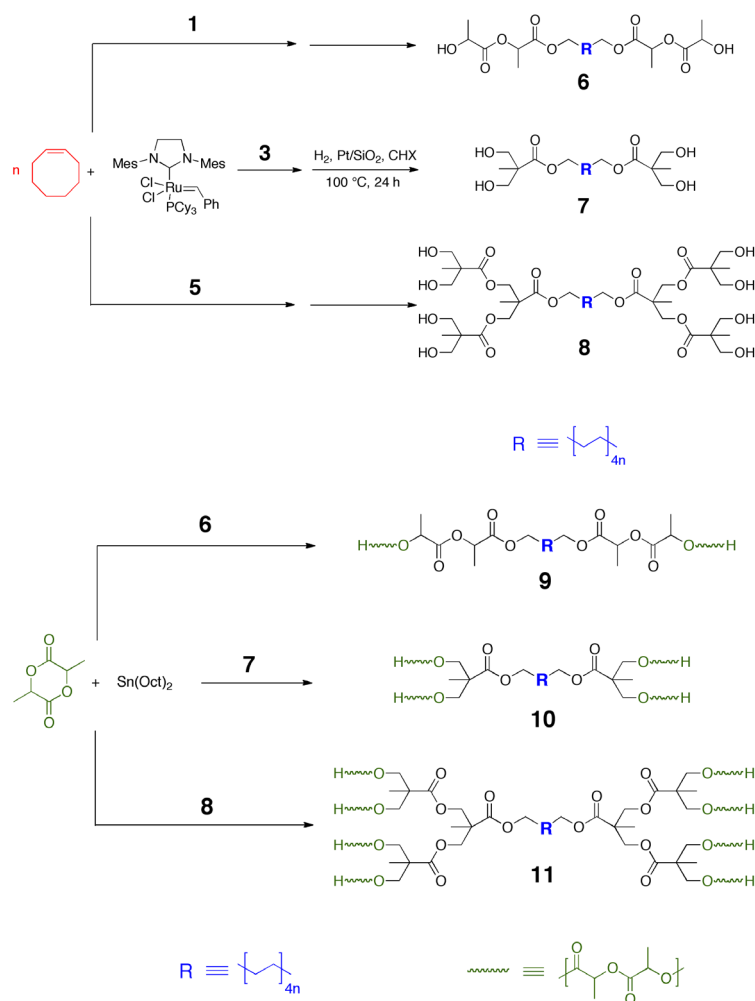
These CTAs were used to prepare telechelic LPE with molar masses approaching by using the ROMP–hydrogenation protocol outlined in the original report (Scheme 4.7).<sup>12</sup> The telechelic LPE samples derived from CTAs **1**, **3**, and **5** give rise to hydroxyl functional polymer chains **6**, **7**, and **8**, respectively, with average functionality ( $F_n$ ) equal to two, four and eight. Block copolymers were then prepared by using the LPE adorned with hydroxyl groups at the termini as macroinitiators during ROTEP of D,L-lactide. The molar mass of the PCOE precursors can easily be tuned by changing the ratio  $[\text{COE}]_0: [\text{CTA}]_0$  and several



samples have been prepared with different molar masses. The final composition of the block copolymers is easily tuned by adjusting the feedstock concentration during subsequent LA polymerization (*i.e.*, [PCOE]:[LA]). The polymerization of LA catalyzed by stannous octoate [Sn(Oct)<sub>2</sub>] is well documented and the conversion of monomer to polymer is used to control the composition.

### Scheme 4.7

(*top*) Synthesis of telechelic LPE macroinitiators from CTAs 1, 3, and 5 and (*bottom*) synthesis of symmetric block copolymers after ROTEP of D,L-lactide.



Each of the block copolymers was then subjected to two different processing protocols. The first used high temperature (160–180 °C) melt pressing with a hydraulic press to form a monolith of plastic. The second protocol began with the polymers in solution at high temperature (150–160 °C) in a high boiling solvent (b.p. > 200 °C). The polymers were then cast onto a hot surface (~160 °C) and the solvent allowed to evaporate slowly (~30 min) leaving a free-standing plastic film. The two types of samples (monolith vs. film) were then subjected to degradative conditions for selective polyester hydrolysis to remove the PLA block. The resulting porous (or non-porous as the case may be) structures are characterized by electron microscopy and nitrogen adsorption to evaluate the pore topology and porosity.

## 4.2 Results

### 4.2.1 Synthesis and Molecular Characterization

Initially, a number of PCOE homopolymer precursors were prepared with various degrees of polymerization using the conventional CTA for difunctional hydroxy-telechelic ( $F_n \approx 2$ ) polymers (Scheme 4.5, Table 4.1; 4k, 11k, 17k, 29k).<sup>131–133</sup> These are ultimately used to demonstrate (1) the versatility of the polymerization strategy for preparing well-defined polymeric materials with controlled degrees of polymerization and (2) tailoring porosity with molar mass in nanoporous materials derived from polyethylene–polylactide block copolymers. Furthermore, three samples with relatively high molar mass were prepared using CTAs **1**, **3** and **5**, respectively  $\{[\text{COE}]_0:[\text{CTA}]_0 = N_{\text{target}} = 400; M_{\text{n(theo)}} = 44.3\text{--}44.7 \text{ kg mol}^{-1}\}$  (Scheme 4.7, Table 4.1). These were designed to either confirm or invalidate the hypothesis that the degree of branching will have noticeable influence on the pore sizes in the nanoporous materials derived from block copolymers with comparable compositions.

Table 4.1

Molecular characteristics of PCOE telechelic homopolymers.

Sample ID <sup>a</sup>	[COE] <sub>o</sub> : [CTA] <sub>o</sub>	unsaturated <sup>b</sup>		saturated <sup>c</sup>	
		$N_C$ <sup>d</sup>	$M_{n,C}$ <sup>e</sup> (kg mol <sup>-1</sup> )	$N_E$ <sup>f</sup>	$M_{n,E}$ <sup>e</sup> (kg mol <sup>-1</sup> )
HO-Y-OH (4k)	30	39	4.29	39	4.37
HO-Y-OH (11k)	100 <sup>h</sup>	90	9.72	96	10.7
HO-Y-OH (17k)	150	152	16.7	157	17.6
HO-Y-OH (29k)	250	249	27.4	260	29.1
HO-Y-OH (50k)	450	448	49.2	448 <sup>g</sup>	50.2
HO <sub>2</sub> -Y-OH <sub>2</sub> (52k)	450	468	51.5	468 <sup>g</sup>	52.4
HO <sub>4</sub> -Y-OH <sub>4</sub> (50k)	450	451	49.6	451 <sup>g</sup>	50.5

<sup>a</sup> Sample ID displayed as HO<sub>x</sub>-Y-OH<sub>x</sub> (#k): x = chain end functionality (*e.g.*, x = 2 implies  $F_n = 4$ ) with value omitted when x = 1 (*i.e.*,  $F_n = 2$ ); Y = either PCOE (C, unsaturated) or LPE (E, saturated); # = approximate value of the number average molar mass for the saturated derivative in kg mol<sup>-1</sup>. <sup>b</sup> refers to the PCOE from ROMP of cyclooctene in the presence of the respective chain transfer agent. <sup>c</sup> refers to the hydrogenated PCOE samples to form LPE. <sup>d</sup> degree of polymerization of the PCOE as determined from end group analysis by <sup>1</sup>H NMR spectroscopy. <sup>e</sup> Calculated from the degree of polymerization and the 8-carbon repeat unit structure ( $M_{n,C} = N_C \times 110$  g/mol;  $M_{n,E} = N_E \times 112$  g/mol). <sup>f</sup> degree of polymerization of the LPE block as determined from end-group analysis by <sup>1</sup>H NMR spectroscopy measured in toluene-d<sub>8</sub> at 100 °C and using an 8-carbon repeat unit structure analogous to the PCOE precursor. <sup>g</sup> End group signals did not provide integration values with a reasonable uncertainty; degree of polymerization taken as identical to the PCOE precursor. <sup>h</sup> prepared with 1,5-cyclooctadiene monomer

The hydroxy-telechelic PCOE samples prepared in the conventional manner (Scheme 4.5) made use of the protected CTA *cis*-1,4-diacetoxy-2-butene, whereby the resulting acetoxy-telechelic PCOE is hydrolyzed in a post-polymerization deprotection. The deprotection was monitored by <sup>1</sup>H NMR spectroscopy and the molar mass was determined by comparing the relative integration of end group signals to repeat unit signals (Figure 4.10).

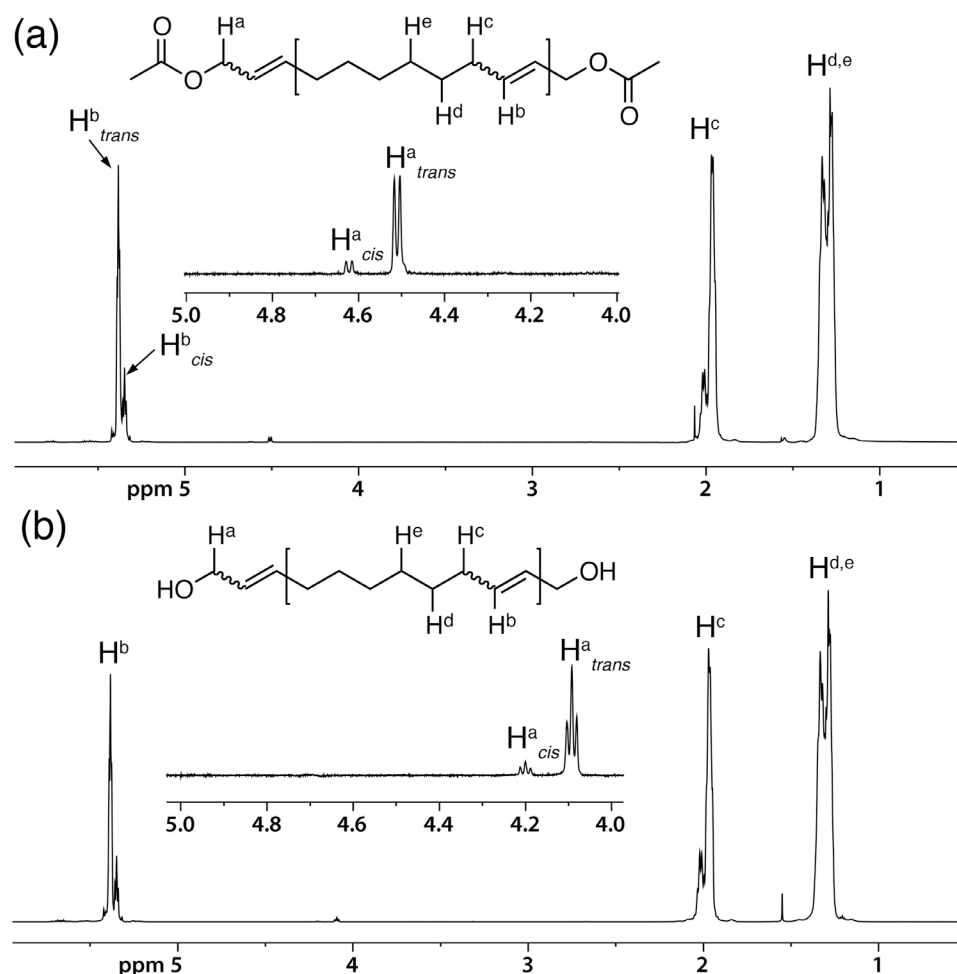


**Figure 4.10**

$^1\text{H}$  NMR spectra for (a) acetoxy-telechelic PCOE from conventional CTA *cis*-1,4-diacetoxy-2-butene employed during COE polymerization with  $[\text{COE}]:[\text{CTA}]_0 = 150$  and (b) hydroxy-telechelic PCOE from hydrolysis of acetoxy groups to give HO-C-OH (17k). Insets show portions of spectra from 4.0–5.0 ppm magnified  $\times 20$ .

The shift in the *cis* and *trans* end group signals ( $\text{H}^{\text{a}}$ ) from 4.62 and 4.51 ppm, respectively, in the acetoxy terminal PCOE to 4.20 and 4.10 ppm indicates complete hydrolysis in the transformation to hydroxy-telechelic PCOE. Likewise, the splitting patterns of the methylene end group protons  $\text{H}^{\text{a}}$  from doublet in the acetoxy terminal polymer ( $^3J_{\text{trans}} = 6.5$  Hz;  $^3J_{\text{cis}} = 7.3$  Hz) doublet of doublet in the hydroxy terminal polymer ( $^3J_{\text{trans}} = 5.72$  Hz;  $^3J_{\text{cis}} = 6.4$  Hz) suggest coupling with the hydroxyl proton and the vinylic protons. The structures of acetoxy and hydroxy terminal PCOE with  $N_{\text{C}} = 30$  were analyzed by  $^{13}\text{C}$  and  $^1\text{H}$ - $^1\text{H}$  correlated NMR

spectroscopy, and the results are consistent with complete hydrolysis. Each sample of hydroxy-telechelic PCOE having  $F_n = 2$  in Table 4.1 gave nearly identical molar mass ( $\pm 5\%$ ) after hydrolysis by end group analysis and by SEC-MALS analysis (see Chapter 3).

The hydrogenation of PCOE samples was carried out by heterogeneous catalysis using a silica supported Pt catalyst (5 wt % Pt) in cyclohexane at 100–110 °C and 500–700 psi  $H_{2(g)}$  over a period of 24 h to give telechelic completely linear polyethylene (LPE). The saturation of double bonds is conveniently monitored by various techniques. Both the degree of saturation and the molar mass of the saturated derivatives having  $F_n = 2$  can be determined by the conventional end group analysis using  $^1H$  NMR spectroscopy (Figure 4.11a and 4.11c). Further corroboration of hydrogenation extent is provided by  $^{13}C$  NMR spectroscopy and differential scanning calorimetry (DSC) (Figure 4.11b and 4.11d; see also next section on thermal characteristics).

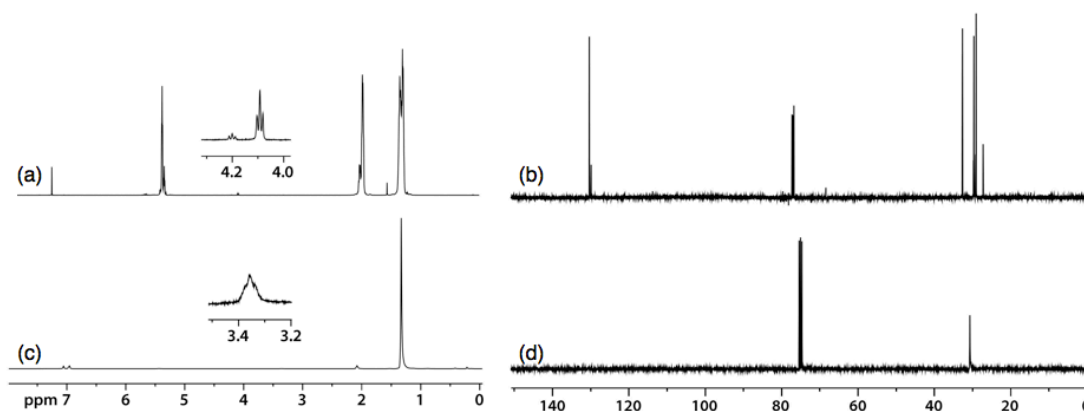


**Figure 4.11**

PCOE sample HO-C-OH (17k) (a)  $^1H$  NMR spectrum with inset showing end-group methylene proton signals and (b)  $^{13}C$  NMR spectrum in  $CDCl_3$  at 25 °C; LPE sample HO-E-OH (10k) (c)  $^1H$  NMR spectrum in  $toluene-d_8$  at 100 °C with inset showing end-group methylene proton signals and (d)  $^{13}C$  NMR spectrum in  $TCE-d_2$  at 100 °C.

Regarding hydrogenation of hydroxy telechelic PCOEs having  $F_n = 4$  and  $F_n = 8$ , the stability of the hydroxy-ester end group is crucial to achieving block copolymers with the purported branched architectures. The bisMPA end group

fidelity was verified by  $^1\text{H}$  NMR spectroscopy on a sample of hydrogenated PCOE having  $F_n = 4$ . The multifunctional end-groups based on bis-methylolpropionic acid linkages remained intact during the Pt-catalyzed heterogeneous saturation reaction performed at temperatures in excess of  $100\text{ }^\circ\text{C}$  (Figure 4.12). For example, a sample of PCOE with a targeted degree of polymerization ( $N_C$ ) equal to 100 was prepared by ROMP and subsequently hydrogenated with a silica supported Pt catalyst (Dow Chemical Company). The relatively low molar mass allowed for adequately high concentration of end-groups so that the protons' signals were reliably observed with adequate resolution in the  $^1\text{H}$  NMR spectra both before and after saturation (Figure 4.12).

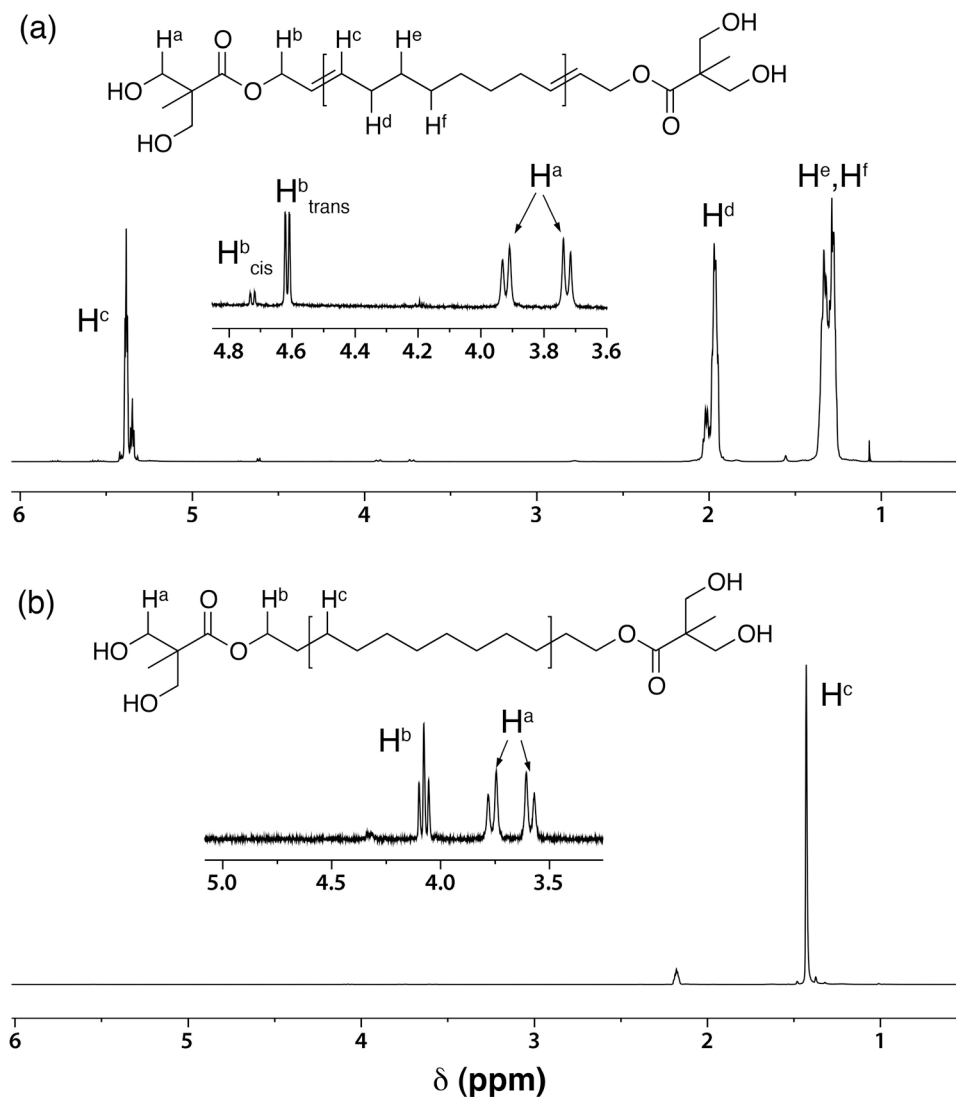


**Figure 4.12**

$^1\text{H}$  NMR spectra: (a) ( $\text{CDCl}_3$ ,  $25^\circ\text{C}$ ) H-shaped PCOE sample with targeted  $N_c = 100$  with the end group methylene protons  $\text{H}^b$  with both *cis* and *trans* conformation and the geminal methylene protons  $\text{H}^a$  and (b) ( $\text{toluene-}d_8$ ,  $100^\circ\text{C}$ ) H-shaped LPE sample from hydrogenated PCOE showing the persistent geminal protons  $\text{H}^a$  and methylene protons  $\text{H}^b$ .

The H-shaped PCOE precursor is shown to accentuate the end group protons and the characteristic chemical shifts, splitting patterns, and coupling constants associated with the *bis*-hydroxy(methylol) propionyl (*bis*MPA) end groups. The geminal protons  $\text{H}^a$  in the H-shaped PCOE appear at 3.73 and 3.92 ppm with measured coupling constants  $^2J_{\text{gem}} = 11.4$  and 11.1 Hz, respectively, consistent with

the relatively large coupling constant values typically observed with geminal splitting. The allylic methylene protons H<sup>b</sup> in the PCOE appear as two signals with distinctive chemical shifts at 4.62 and 4.73 ppm respectively assigned to the *Z* and *E* stereochemical configurations about the terminal double bond. Both types of protons with *Z* and *E* stereochemical configurations show doublet multiplicity having calculated coupling constants  ${}^3J_{bc} = 6.8$  and 6.5 Hz, respectively. Upon quantitative hydrogenation, a single narrow signal is seen for the repeating methylene units in the perfectly linear chain (1.34 ppm). Additionally, the geminal protons (H<sup>a</sup> in Figure 4.12b) remain intact, appearing at 3.50 and 3.67 ppm with coupling constants  ${}^2J_{gem} = 11.0$  and 11.3 Hz, respectively. The chemical shifts of the protons are clearly different before and after hydrogenation resulting partly from the different chemical environment and different solvent (CDCl<sub>3</sub> vs. toluene-*d*<sub>8</sub>) and temperature (25 °C vs. 100 °C). The methylene protons adjacent to the ester-oxygen (H<sup>b</sup> in Figure 4.12b) now appear as a signal at 3.99 ppm with triplet multiplicity ( ${}^3J_{bc} = 6.7$  Hz) resulting from the saturation of the terminal olefin. The molar masses of the hydroxy telechelic PCOE samples are straightforward to measure by end group analysis using <sup>1</sup>H NMR analysis.<sup>130,131</sup> Molar masses of the PCOE precursors to the saturated LPE samples in Table 4.1 were also measured by SEC-MALS and the values agree reasonably well with those measured by end group analysis (see Chapter 3). The lower molar mass hydroxy-telechelic LPE samples were also be evaluated by <sup>1</sup>H NMR in toluene-*d*<sub>8</sub> at 100 °C (due to insolubility at low temperature). The molar mass for samples HO-E-OH (4k), (11k), (17k), and (28k) were all amenable to end-group analysis, and the molar masses agreed within 10% of the values associated with the corresponding precursors.

After thorough molecular characterization of the lower molar mass H-shaped LPE in order to confirm the persistence of the unique structural moieties (*i.e.*, bisMPA end group), higher molar mass ( $N_C \sim 450$ ) linear, H-shaped and arachne-arm PCOE precursors were also hydrogenated. Furthermore, block copolymers were prepared from each of three precursors having targeted  $N_C = 450$ . A comprehensive set of block copolymers was prepared with various molar masses, architectures and compositions starting from several LPE precursors (Table 4.2).



Table 4.2

Molecular characteristics of linear and branched L<sub>x</sub>EL<sub>x</sub> block copolymers.

Sample ID	$M_{n, \text{total}}$ (kg mol <sup>-1</sup> )	$M_{n, \text{PLA}}$ (kg mol <sup>-1</sup> )	$w_L$	$f_L$
<i>HO-LPE-OH (11k): <math>M_n = 10.8</math> kg mol<sup>-1</sup></i>				
LEL [10-11-10]	30.4	19.6	0.645	0.58
<i>HO-LPE-OH (17k): <math>M_n = 16.7</math> kg mol<sup>-1</sup></i>				
LEL [15-17-15]	47.2	30.5	0.65	0.58
<i>HO-LPE-OH (28k): <math>M_n = 28.8</math> kg mol<sup>-1</sup></i>				
LEL [8-28-8]	44.2	16.2	0.37	0.31
LEL [14-28-14]	55.7	27.7	0.50	0.43
LEL [25-28-25]	77.6	49.6	0.64	0.57
LEL [37-28-37]	102	73.8	0.73	0.67
LEL [46-28-46]	120	92.0	0.77	0.71
LEL [59-28-59]	146	118	0.81	0.76
<i>HO-LPE-OH (50k): <math>M_n = 50.1</math> kg mol<sup>-1</sup></i>				
LEL [36-50-36]	116	64	0.59	0.52
LEL [65-50-65]	181	130.5	0.72	0.66
LEL [75-50-75]	200	150	0.75	0.69
<i>HO<sub>2</sub>-LPE-OH<sub>2</sub> (52k): <math>M_n = 52.4</math> kg mol<sup>-1</sup></i>				
L <sub>2</sub> EL <sub>2</sub> [13 <sub>2</sub> -52-13 <sub>2</sub> ]	104	51.8	0.50	0.43
L <sub>2</sub> EL <sub>2</sub> [24 <sub>2</sub> -52-24 <sub>2</sub> ]	149	97.3	0.65	0.59
L <sub>2</sub> EL <sub>2</sub> [38 <sub>2</sub> -52-38 <sub>2</sub> ]	205	153	0.75	0.69
<i>HO<sub>4</sub>-LPE-OH<sub>4</sub> (50k): <math>M_n = 50.5</math> kg mol<sup>-1</sup></i>				
L <sub>4</sub> EL <sub>4</sub> [8 <sub>4</sub> -50-8 <sub>4</sub> ]	111	61.1	0.55	0.48
L <sub>4</sub> EL <sub>4</sub> [11 <sub>4</sub> -50-11 <sub>4</sub> ]	139	89.2	0.64	0.58
L <sub>4</sub> EL <sub>4</sub> [19 <sub>4</sub> -50-19 <sub>4</sub> ]	202	152	0.75	0.70

<sup>a</sup> Sample ID refers to the architecture and average molar mass of the respective blocks. L<sub>x</sub>EL<sub>x</sub> refers to linear, H-shaped and arachne arm architectures when x = 1, 2, and 4, respectively. [#<sub>x</sub>-#-#<sub>x</sub>] refers to the respective molar masses in kg mol<sup>-1</sup>. <sup>b</sup> Total molar mass was calculated based on the assumption that the PCOE molar mass measured by end group analysis by <sup>1</sup>H NMR spectroscopy was maintained after hydrogenation. The total molar mass was calculated from composition as measured by <sup>1</sup>H NMR spectroscopy ( $M_{n, \text{total}} = M_{n, \text{LPE}} \div w_{\text{LPE}}$ ). <sup>c</sup> Calculated from composition as measured by <sup>1</sup>H NMR spectroscopy, with the value being the sum of molar mass of all PLA arms per molecule. <sup>d</sup> Calculated from the relative integration of the repeating unit signals measured by <sup>1</sup>H NMR spectroscopy. <sup>e</sup> Calculated from the composition determined by <sup>1</sup>H NMR spectroscopy and the densities of the repeating units at 25 °C:  $\rho_{\text{PLA}} = 1.25$  g mL<sup>-1</sup> (ref. <sup>134</sup>) and  $\rho_{\text{LPE}} = 0.95$  g mL<sup>-1</sup> (ref. <sup>62</sup>)

The compositions of the block copolymers were ascertained by  $^1\text{H}$  NMR spectroscopy by comparing the integration of signals associated with the respective repeating units. The methine signal from the PLA repeating units  $[-\text{C}(\text{O})\text{CH}(\text{CH}_3)\text{O}-]$  is observed at 5.1 ppm in toluene- $d_6$  at 100 °C. The methyl signals from the PLA and signals from the methylene repeating units of LPE overlap substantially, appearing between 1.3–1.5 ppm (Figure 4.13).

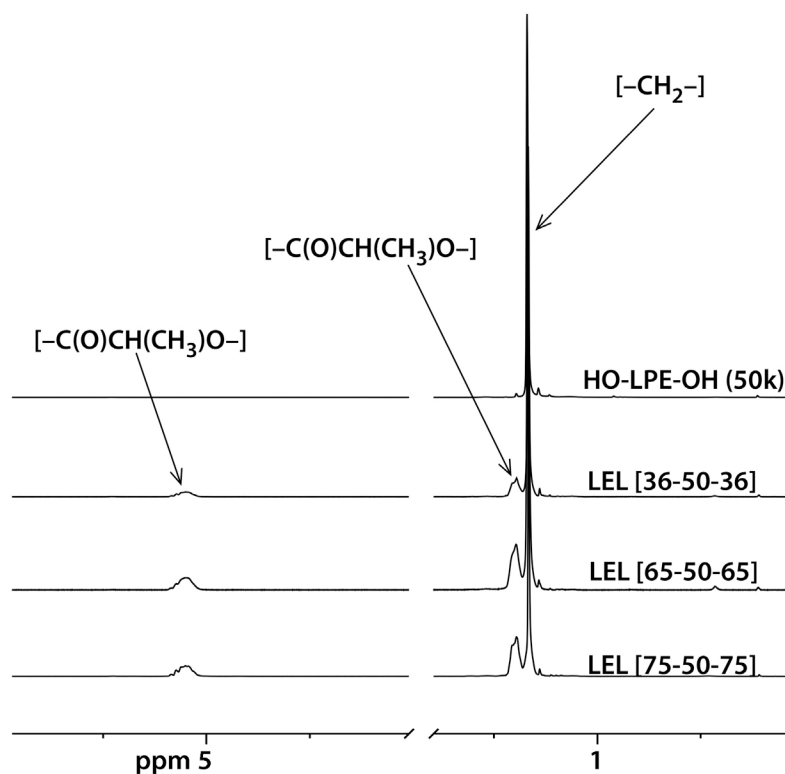


**Figure 4.13**

$^1\text{H}$  NMR spectra for (top) difunctional homopolymer LPE with molar mass of approximately  $50 \text{ kg mol}^{-1}$  and three linear block copolymers with increasing PLA fractions going down (see Table 4.2).

#### 4.2.2 Thermal Analysis Polymers

The DSC thermographs for the block copolymers having LPE midsegments with molar mass of  $\approx 50 \text{ kg mol}^{-1}$  and different molecular architectures have several similarities (Figure 4.14a–c). The hydroxy telechelic PCOE with  $F_n = 2$  and

calculated molar mass equal to  $51.6 \text{ kg mol}^{-1}$  ( $N_c = 468$ ) from  $^1\text{H}$  NMR spectroscopy has a DSC thermogram showing a relatively sharp PCOE melting transition ( $T_{m,c}$ ) near  $54 \text{ }^\circ\text{C}$  (Figure 4.14a).

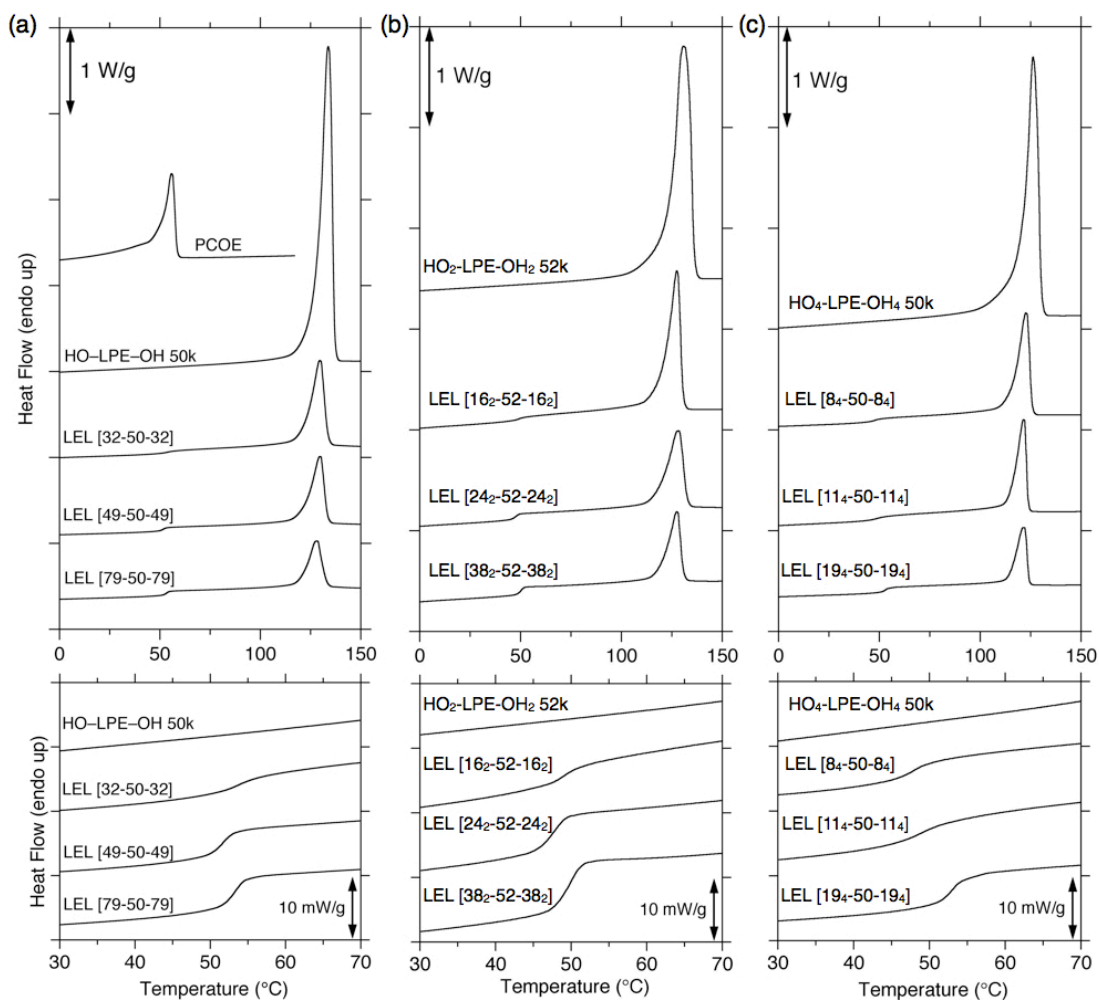


**Figure 4.14**

DSC thermograms from the second heating cycle for: (a) hydroxy telechelic ( $F_n \approx 2$ ) PCOE with  $M_n \approx 50 \text{ kg mol}^{-1}$ , saturated LPE and three LEL block copolymers; (b) H-shape ( $F_n \approx 4$ ) LPE precursor with  $M_n \approx 52 \text{ kg mol}^{-1}$  and three  $L_2EL_2$  block copolymers; (c) arachne ( $F_n \approx 8$ ) LPE precursor with  $M_n \approx 50 \text{ kg mol}^{-1}$  and three  $L_4EL_4$  block copolymers. The top set of thermograms show the temperature range from 0–150  $^\circ\text{C}$ , while the bottom set of thermograms are the identical data sets magnified ( $\approx 100\times$ ) with a temperature range from 30–70  $^\circ\text{C}$  accentuating the  $T_g$  of poly(D,L-lactide).

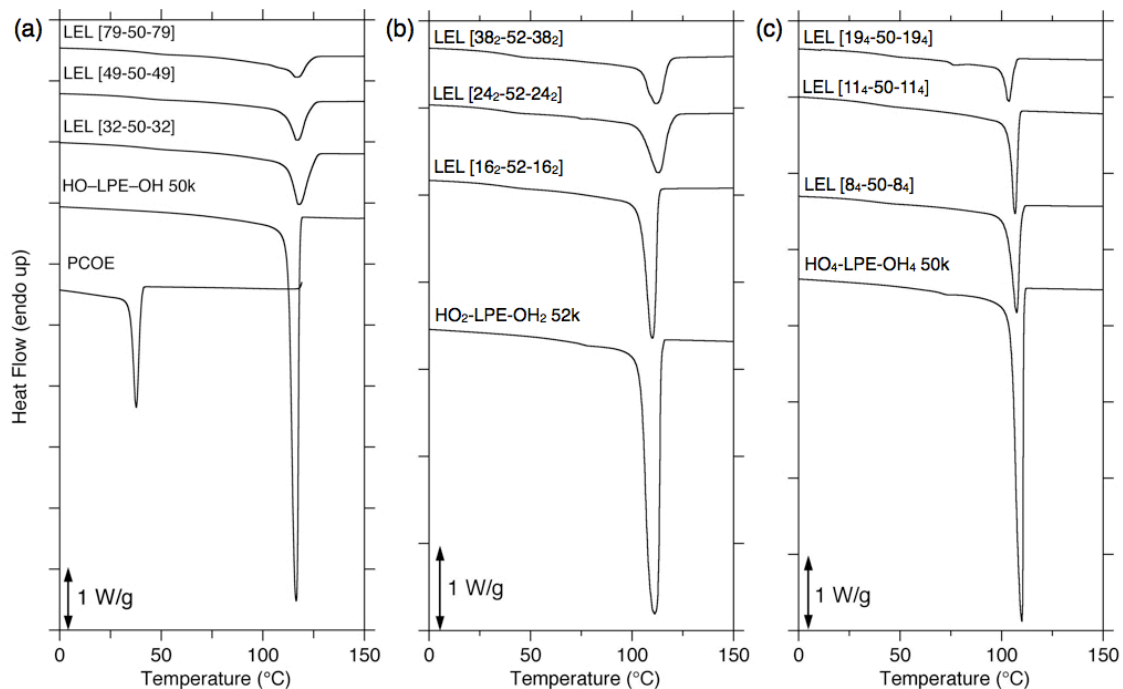


**Figure 4.15**

DSC thermograms for the cooling cycle for: (a) hydroxy telechelic ( $F_n \approx 2$ ) PCOE with molar mass  $\approx 50 \text{ kg mol}^{-1}$ , saturated LPE and three LEL block copolymers; (b) H-shape ( $F_n \approx 4$ ) LPE precursor with molar mass  $\approx 52 \text{ kg mol}^{-1}$  and three  $L_2EL_2$  block copolymers; (c) arachne ( $F_n \approx 8$ ) LPE precursor with molar mass  $\approx 50 \text{ kg mol}^{-1}$  and three  $L_4EL_4$  block copolymers.

Exhaustive hydrogenation of the PCOE homopolymer samples gave completely linear methylene repeating units (*i.e.*, LPE) that exhibit a corresponding increase in melting temperature ( $T_{m,E}$ ) and crystallization temperature ( $T_{c,E}$ ), which occur at approximately  $130 \text{ }^\circ\text{C} \pm 4 \text{ }^\circ\text{C}$  and  $113 \text{ }^\circ\text{C} \pm 3 \text{ }^\circ\text{C}$ , respectively. These values are in line with those observed for commercial high density polyethylene and suggest the absence of side chain imperfections in the linear samples prepared from PCOE saturation. The thermal transitions occur at nearly the same temperatures regardless of the molecular weight or end-group identity, which suggests that the multiple hydroxyl end groups for the H-shape and arachne-arm precursors have essentially no influence on the ability of chains to align during cooling at the prescribed rate ( $10 \text{ }^\circ\text{C min}^{-1}$ ). The melting enthalpies calculated from integration of

the melting endotherms are all consistent with a large degree of crystallization as calculated from comparison with a perfectly crystalline polyethylene sample. (Polymer Handbook). The degree of crystallinity ( $X_E$  as percent) was approximately  $55 \pm 10$  % during the second heating cycle after homogenizing the thermal history by annealing above  $T_{m,E}$  for 5 minutes and subsequently cooling to  $-120$  °C.

The block copolymers all behaved similarly among each other, whereby the  $T_{m,E}$  of the LPE midsegments occurred at a temperature slightly depressed compared with the homopolymer LPE precursors. Likewise,  $T_{c,E}$  was slightly decreased for the block copolymers. The glass transition temperature of PLA ( $T_{g,L}$ ) was observed at  $50$  °C  $\pm$   $3$  °C in all the samples. Portions of the 2<sup>nd</sup> heating cycle having magnified heat flow for the copolymers with different architectures and  $M_n \approx 50$  kg mol<sup>-1</sup> clearly illustrates the  $T_g$  and shows the monotonic increase in magnitude with increasing PLA content (Figure 4.14). A correspondingly diminishing melting enthalpy is also evident with increasing PLA content. Crystalline content in the LPE domains was calculated according to  $X_E = \Delta H_m / (\Delta H_m \cdot w_E) \cdot 100$  and is nearly constant across the entire composition range. Values associated with the thermal transitions and crystal characteristics are displayed in Table 4.3 for the comprehensive set of LPE homopolymers and corresponding block copolymers.

**Table 4.3**Thermal Characteristics of L<sub>x</sub>EL<sub>x</sub> linear and branched block copolymers.

Sample ID	$w_L$	$T_{g,L}$ (°C)	$T_{c,E}$ (°C)	$T_{m,E}$ (°C)	$\Delta H_m$ (J g <sup>-1</sup> )	$X_E$ (%)
<i>HO-LPE-OH (11k): <math>M_n = 10.8 \text{ kg mol}^{-1}</math>; <math>T_m = 130.0 \text{ °C}</math>; <math>T_c = 117.0 \text{ °C}</math>; <math>X_E = 80\%</math></i>						
LEL [10-11-10]	0.65	48.9	100.4	127.0	71	72
<i>HO-LPE-OH (17k): <math>M_n = 16.7 \text{ kg mol}^{-1}</math>; <math>T_m = 129.8 \text{ °C}</math>; <math>T_c = 116.2 \text{ °C}</math>; <math>X_E = 71\%</math></i>						
LEL [15-17-15]	0.65	52.9	103.2	123.8	44	45
<i>HO-LPE-OH (28k): <math>M_n = 28.8 \text{ kg mol}^{-1}</math>; <math>T_m = 130.3 \text{ °C}</math>; <math>T_c = 113.5 \text{ °C}</math>; <math>X_E = 67\%</math></i>						
LEL [8-28-8]	0.37	49.9	110.5	127.1	87	50
LEL [14-28-14]	0.50	49.9	109.0	125.9	68	49
LEL [25-28-25]	0.64	51.2	106.5	124.0	47	47
LEL [37-28-37]	0.73	49.0	104.5	123.2	34	45
LEL [46-28-46]	0.77	52.7	101.9	121.7	27	42
LEL [59-28-59]	0.81	53.4	88.8	122.0	20	37
<i>HO-LPE-OH (50k): <math>M_n = 50.5 \text{ kg mol}^{-1}</math>; <math>T_m = 128.5 \text{ °C}</math>; <math>T_c = 111.4 \text{ °C}</math>; <math>X_E = 53\%</math></i>						
LEL [36-50-36]	0.59	53.9	118.0	129.5	48	42
LEL [65-50-65]	0.72	51.8	117.7	129.8	39	50
LEL [75-50-75]	0.75	53.2	116.7	128.1	27	38
<i>HO<sub>2</sub>-LPE-OH<sub>2</sub> (52k): <math>M_n = 51.6 \text{ kg mol}^{-1}</math>; <math>T_m = 130.8 \text{ °C}</math>; <math>T_c = 111.2 \text{ °C}</math>; <math>X_E = 54\%</math></i>						
L <sub>2</sub> EL <sub>2</sub> [13 <sub>2</sub> -52-13 <sub>2</sub> ]	0.50	47.6	112.5	128.1	61	44
L <sub>2</sub> EL <sub>2</sub> [24 <sub>2</sub> -52-24 <sub>2</sub> ]	0.65	50.6	112.8	127.6	43	45
L <sub>2</sub> EL <sub>2</sub> [38 <sub>2</sub> -52-38 <sub>2</sub> ]	0.75	49.2	109.9	127.4	32	45
<i>HO<sub>4</sub>-LPE-OH<sub>4</sub> (50k): <math>M_n = 50.1 \text{ kg mol}^{-1}</math>; <math>T_m = 126.2 \text{ °C}</math>; <math>T_c = 109.9 \text{ °C}</math>; <math>X_E = 48\%</math></i>						
L <sub>4</sub> EL <sub>4</sub> [8 <sub>4</sub> -50-8 <sub>4</sub> ]	0.55	48.0	107.4	122.6	45	36
L <sub>4</sub> EL <sub>4</sub> [11 <sub>4</sub> -50-11 <sub>4</sub> ]	0.64	48.9	106.7	121.5	33	33
L <sub>4</sub> EL <sub>4</sub> [19 <sub>4</sub> -50-19 <sub>4</sub> ]	0.75	53.0	104.2	121.5	22	32

<sup>a</sup> Taken as the midpoint between the two inflection points measured on the second heating cycle at a rate of 10 °C min<sup>-1</sup>. <sup>b</sup> Reported as the temperature at the minimum in the heat capacity change during the exothermic crystallization. <sup>c</sup> reported as the temperature at the maximum in the heat capacity change during the endothermic melting. <sup>d</sup> calculated using the integration of the melting endotherm ( $\Delta H_m$ , J/g) and the literature value for a perfectly crystalline linear polyethylene crystallite ( $\Delta H_m^0 = 277 \text{ J/g}$ ) in the equation  $X_E = \Delta H_m / (\Delta H_m^0 \cdot w_E)^{-1}$ .<sup>135</sup>

These results point to several important factors that are related to the mesoscopic structures developed above  $T_{m,E}$  and below  $T_{c,E}$ , respectively. Firstly, the relatively high degree of crystallinity suggests that crystal development is not substantially impeded in the block copolymers compared with the LPE homopolymer precursors. This could mean that either (1) the polymers are not microphase separated above  $T_{m,E}$  and microdomain formation therefore has limited influence on the ability of the LPE segments to nucleate and grow; (2) the polymers are microphase separated above  $T_{m,E}$ , but the two components are only weakly segregated and crystal break-out occurs due to the highly mobile PLA chains ( $T_{c,E} \gg T_g$ ) during crystallization and spherulite development disrupts the melt-microphase separated structure or (3) the polymers are microphase separated above  $T_{m,E}$ , and the two components are segregated strongly enough to confine crystallization within the melt-phase microdomains, which are large enough to accommodate several crystalline lamellae. These scenarios are addressed with additional structural analysis by complementary methods.

### 4.2.3 Preparation of Nanoporous LPE

The block copolymers described in section 4.2.1 were each processed in two different ways. In one case, the polymers were melt-pressed into discs at 160 °C for approximately 5 minutes under 1000 psi in a hydraulic press. The discs had a diameter of 1.2 cm and a thickness of 2 mm (Figure 4.16a). The approximate volume of each disc was 0.23 cm<sup>3</sup>. The discs were translucent, with opacity depending on the composition; discs from block copolymers with higher LPE content naturally scatter more light from the crystalline-amorphous phase separation. The discs were rendered nanoporous by selectively removing the PLA with a slightly basic solution of NaOH in aqueous methanol (40 vol % MeOH; 0.5 M NaOH<sub>aq</sub>). The discs were submerged in the solution in a closed container which was subsequently heated at 50–60 °C for several days (2–3 days). The discs were removed from the solution after cooling to ambient temperature and dried at 40 °C under vacuum for up to one day. The thickness of the discs required the etching

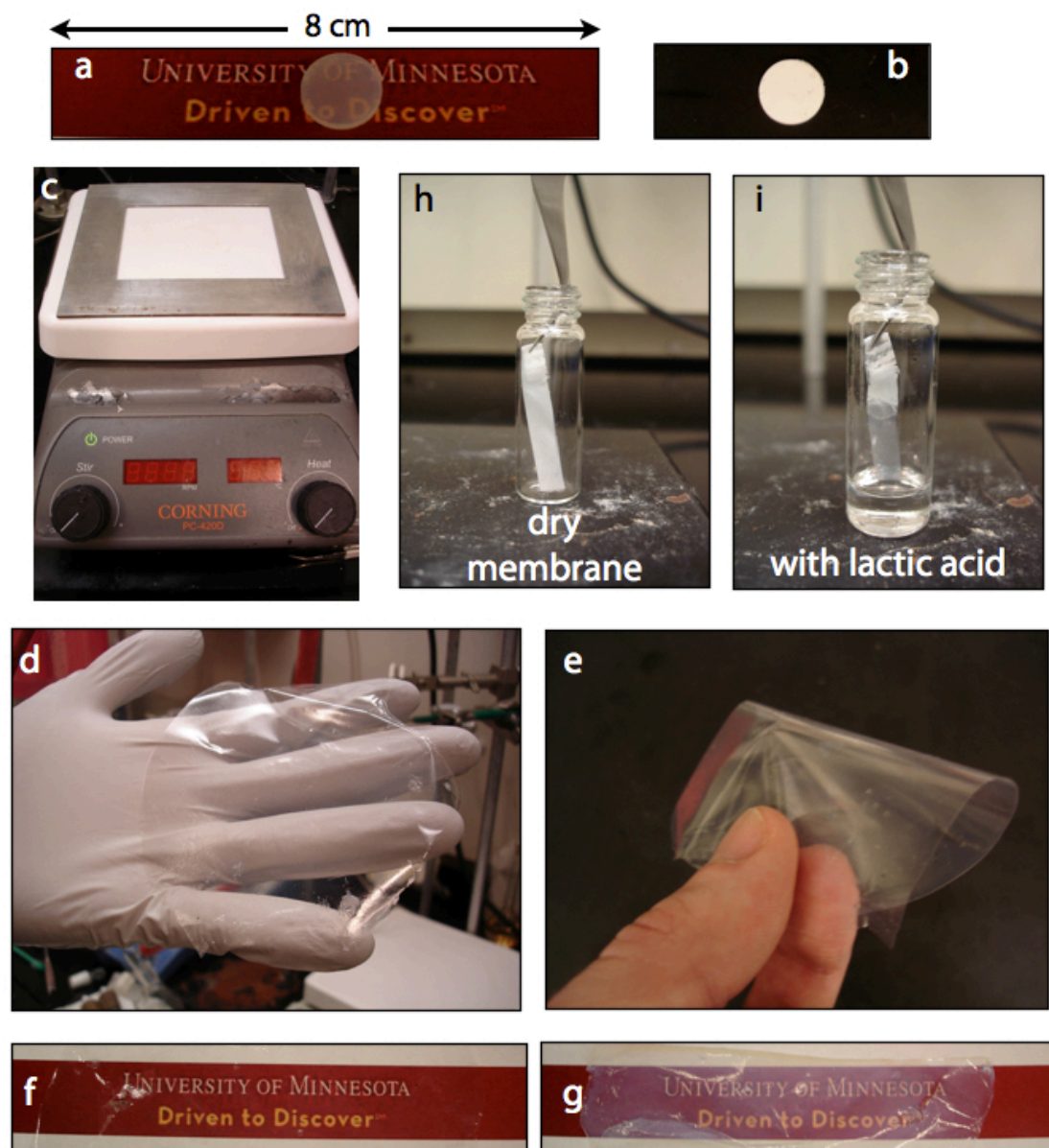
procedure at this temperature to be conducted for at least 2 days; less time was insufficient for complete PLA removal. In contrast, the thinner films could be effectively etched at ambient temperature in several hours. The porous discs were white and completely opaque after drying (Figure 4.16b).

Films of various thicknesses ranging from  $\sim 10$ – $500 \mu\text{m}$  were also prepared by a solvent casting method. Generally, the films were dissolved in 1,2,4-trichlorobenzene at concentrations ranging from  $\sim 30$ – $60 \text{ mg mL}^{-1}$ . The concentration was chosen based on the estimated viscosity of the solution during casting; the cast solution was required to spread across a relatively broad area to fill a mold that was used. Higher molecular weight LEL triblock copolymers were prepared with concentrations lower than the low molecular weight counterparts. A mold with dimensions of  $8 \text{ cm} \times 10 \text{ cm} \times 2 \text{ mm}$ . Dissolution of the powdered triblock copolymer samples required heating at temperatures in excess of  $140 \text{ }^\circ\text{C}$ . Mixtures were heated at  $150$ – $160 \text{ }^\circ\text{C}$  until the solution was clear and colorless, after which the solution was poured onto a ceramic surface heated to  $\sim 160 \text{ }^\circ\text{C}$ . The solution spread out to fill the aluminum mold that was secured to the ceramic heating surface. The surface temperature was maintained at  $150$ – $160 \text{ }^\circ\text{C}$  until the solvent had completely evaporated ( $\sim 25$ – $30 \text{ min}$ ), at which point the heating was ceased and the ceramic surface allowed to cool to ambient temperature slowly ( $\sim 30 \text{ min}$ ). The mold was removed and the resulting block copolymer film was gently peeled from the ceramic surface, yielding a transparent sheet with dimensions proximate to the mold and thickness dependent on the original solution concentration (Figure 4.16d and 4.16f). The block copolymer films were generally strong and flexible enough to handle with ease and bend or roll into a desired shape (Figure 4.16e). The films were also easily cut with a razor or scissors to prepare block copolymer films with various dimensions. The films were etched in the identical solution as previously described. However, the time required for complete PLA removal were significantly decreased compared with the discs because of the thinness. PLA was easily removed within 1 day at  $25 \text{ }^\circ\text{C}$ . The films were washed with a slightly acidic aqueous solution and with pure MeOH and subsequently dried at ambient temperature under vacuum after PLA removal. The



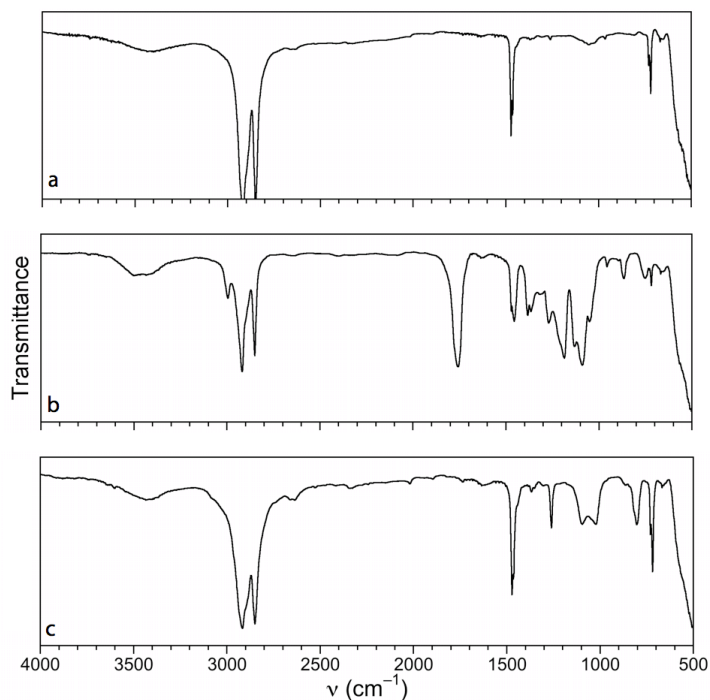
---

resulting nanoporous LPE films were translucent, with the opacity depending largely on the thickness. For example, a film with 10–20  $\mu\text{m}$  thickness appeared to be nearly transparent with a slight blue/white tinge (Figure 4.16g), while a film of 100  $\mu\text{m}$  thickness was almost completely opaque in its dry state (Figure 4.16h). The increased opacity presumably arises from the increased refractive index mismatch between air and LPE compared with PLA and LPE. Expectedly, the film becomes nearly transparent again after partial submergence into L-lactic acid, upon which the liquid is absorbed into the void volume comprising nanoscopic channels through capillary action (Figure 4.16i).

**Figure 4.16**

Digital photographs of different  $L_xEL_x$  block copolymers and the corresponding nanoporous LPE in different states: (a) LEL [46-28-46] block copolymer disc and (b) its nanoporous derivative; (c) experimental setup for solvent casting  $L_xEL_x$  block copolymers; (d), (e), and (f) films of  $L_2EL_2$  [24<sub>2</sub>-52-24<sub>2</sub>] block copolymer after solvent casting and (g) the nanoporous derivative; (h) dry section of nanoporous film derived from  $L_2EL_2$  [13<sub>2</sub>-52-13<sub>2</sub>] and (i) film partially submerged in L-lactic acid, which has been absorbed by capillary action into the nanochannels.

The presence of PLA was monitored by infrared (IR) spectroscopy. Complete PLA removal was confirmed by the absence of the characteristically strong carbonyl stretch associated with the polyester backbone. Powdered samples of the LPE precursors (prepared in a KBr matrix in pellet form) show a structure with relatively few infrared responses due to the uniform hydrocarbon  $-\text{CH}_2-$  backbone structure (Figure 4.17a). A number of additional signals are observed in samples of block copolymers, illustrated with a spectrum from LEL [15–17–15] (Figure 4.17b). Most markedly, the strong adsorption from the carbonyl of the polyester ( $1750\text{ cm}^{-1}$ ) is clearly demarcated from the other signals. After removal of the PLA by hydrolysis and washing, the archetypal carbonyl signal has disappeared from the example using a disc of melt-pressed LEL [15–17–15] for the porous template (Figure 4.17c). Remnants of the signal would suggest that the structure had not been continuous in the PLA or that the removal strategy was ineffective.

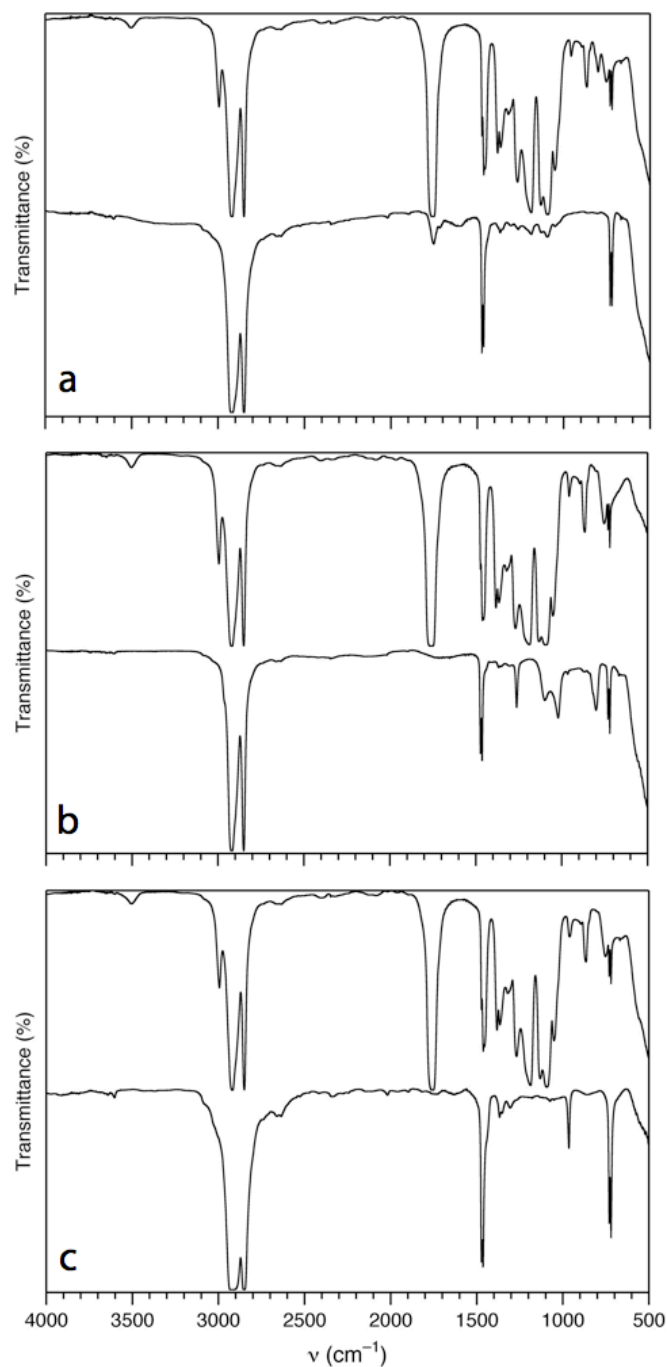


**Figure 4.17**

Infrared spectra for (a) hydroxy telechelic LPE sample HO-E-OH 17k (Table 4.2) prior to D,L-lactide polymerization, (b) LEL [15–17–15] triblock copolymer and (c) nanoporous LPE after removing PLA from the triblock precursor LEL [15–17–15]. All spectra were measured after preparing KBr pellets with the powdered polymer samples incorporated.

---

The etching protocol used to remove PLA was effective for all the samples in the composition range represented by the sample set in Table 4.2, regardless of molar mass, molecular architecture or sample geometry (*i.e.*, disc *vs.* film), with one notable exception. The block copolymer sample LEL [8-28-8] was not amenable to PLA degradation, which suggested that the PLA phase was not continuous. As such, all additional samples were prepared with higher PLA concentrations in order to coerce interpenetration of both components. As examples, IR spectra obtained for two samples having either linear or arachne-arm architecture and nearly identical compositions and molecular weights both before and after the removal of PLA show similar results (Figure 4.18). Likewise, comparison of a disc with a film provides evidence for the efficacy of the etching protocol and the consistency with which the continuous mesoscale PLA phase is formed, regardless of the geometry or sample processing strategy (*i.e.*, solvent casting *vs.* bulk melt pressing).

**Figure 4.18**

Infrared spectra of block copolymer templates before (*top*) and after (*bottom*) the etching of PLA from samples (a) bulk melt-pressed disc of linear LEL [36–50–36], (b) solvent-cast film of H-shaped L<sub>2</sub>EL<sub>2</sub> [24<sub>2</sub>–52–24<sub>2</sub>], and (c) bulk melt-pressed disc of arachnearm L<sub>4</sub>EL<sub>4</sub> [8<sub>4</sub>–50–8<sub>4</sub>].

#### 4.2.4 X-ray Scattering from Block Copolymers

Small and wide-angle x-ray scattering was performed on a hydroxy-telechelic LPE sample HO-E-OH 11k (Figure 4.19). The one-dimensional WAXS profile contains two strong reflections that are characteristic of the 110 and 200 planes of the orthorhombic crystal unit cells associated with polyethylene. The positions of the two reflections at  $q = 15.4$  and  $17.1 \text{ nm}^{-1}$  correspond with the unit cell dimensions of  $4.07 \text{ \AA}$  and  $3.68 \text{ \AA}$ , respectively. The SAXS profile has two broad signals with intensity maxima occurring at approximately  $q = 0.28$  and  $0.57 \text{ nm}^{-1}$ . These reflections at ambient temperature can be attributed to the Bragg reflections from alternating crystalline and amorphous layers, with an approximate lamellar periodicity  $d = 22 \text{ nm}$  ( $d = 2\pi/q^*$ ).

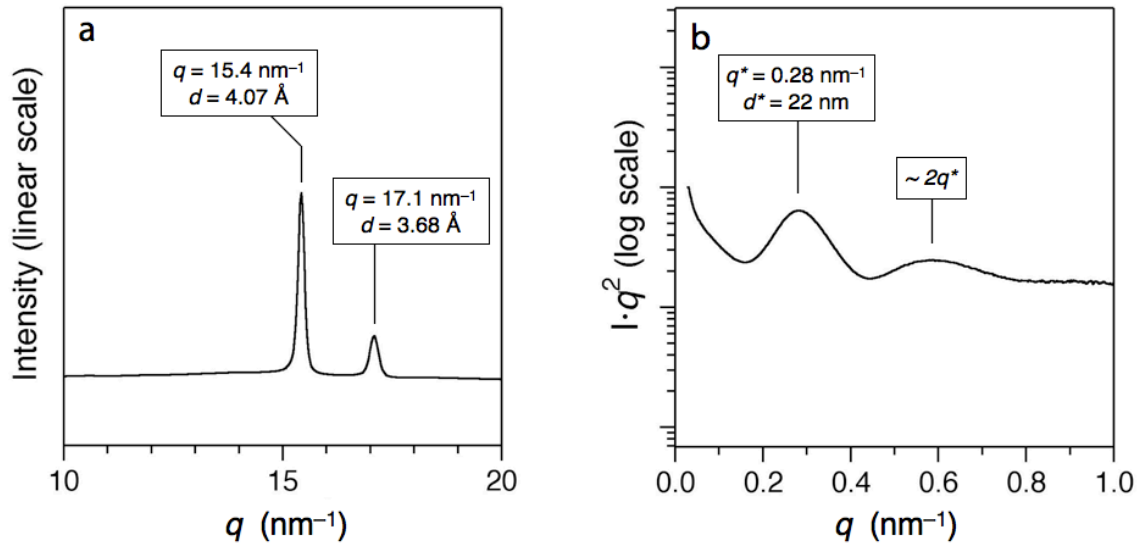


**Figure 4.19**

One-dimensional x-ray scattering profiles from (a) wide angle detector and (b) small angle detector for HO-E-OH (11k) linear polyethylene sample.

Upon forming block copolymers, the LPE midblock component crystallizes despite being covalently tethered at either end by the glassy PLA. The overall degree of crystallinity decreases proportionally to the composition, as suggested by

complementary DSC and WAXS results, regardless of the molecular architecture. This phenomenon is exemplified by comparing the normalized intensity in WAXS profiles for HO-E-OH (11k) with two H-shaped block copolymers L<sub>2</sub>EL<sub>2</sub> [24<sub>2</sub>-52-24<sub>2</sub>] and L<sub>2</sub>EL<sub>2</sub> [38<sub>2</sub>-52-38<sub>2</sub>] having  $w_L = 0.65$  and  $0.75$ , respectively (Figure 4.20).

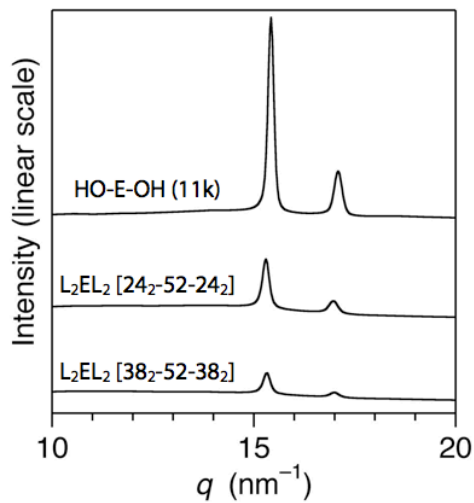


**Figure 4.20**

One-dimensional WAXS profiles for hydroxyl-telechelic LPE sample HO-E-OH (11k) and two H-shaped block copolymers L<sub>2</sub>EL<sub>2</sub> [24<sub>2</sub>-52-24<sub>2</sub>] ( $w_L = 0.65$ ) and L<sub>2</sub>EL<sub>2</sub> [38<sub>2</sub>-52-38<sub>2</sub>] ( $w_L = 0.75$ ).

In addition to establishing the presence of crystalline LPE portions in the block copolymers, establishing the microphase separation behavior and the evolution of morphology is desirable, especially in descending below the crystallization temperature of the LPE ( $T_{c,E}$ ). The DSC cooling curves presented in Figure 4.15 are demonstrative of a large difference between  $T_{c,E}$  and the PLA glass transition temperature ( $T_{g,L}$ ), whereby the latter occurs at  $\sim 60$  °C lower. The molten state of PLA, during which appreciable chain diffusion is expected to occur, may allow the rearrangement of melt microphase morphology during evolution of crystal formation in the LPE block. Taking into consideration the relative values of the thermal transitions during cooling, the extent of melt-phase morphology disruption that can be expected depends largely on the segregation strength of the system.

PLA combined with any polyolefin in a block copolymer is expected to have a large Flory-Huggins interaction parameter ( $\chi$ ).<sup>136</sup> Combining this prediction with the relatively large molar masses for many of the block copolymers prepared for this study leads to the conviction that the PLA–LPE block copolymers are highly segregated at all temperatures within the accessible range.<sup>†</sup> Indeed, the order–disorder transition temperature ( $T_{ODT}$ ) was not accessible for any of the polymers prepared in this study. Crystallization is predicted to occur within the confines of the melt-segregated microdomains upon cooling, despite the predictably high mobility of the PLA endblocks preceding vitrification.<sup>137</sup>

Small-angle x-ray scattering (SAXS) was used to examine the melt-phase morphology and the confinement of crystallization. The linear block copolymers with various compositions that were prepared from the single hydroxy-telechelic precursor HO-E-OH (28k) all appear to behave similarly with respect to morphological contours above  $T_{m,E}$ , as evinced by one-dimensional SAXS profiles (Figure 4.21a). Several features of the system contribute to the prohibitively slow ordering kinetics, including a relatively broad PLA, highly entangled LPE phase, and high segregation strength.

---

<sup>†</sup> The PLA is expected to degrade at temperatures well above 200 °C, providing the upper limit for the experiments investigating melt morphology.



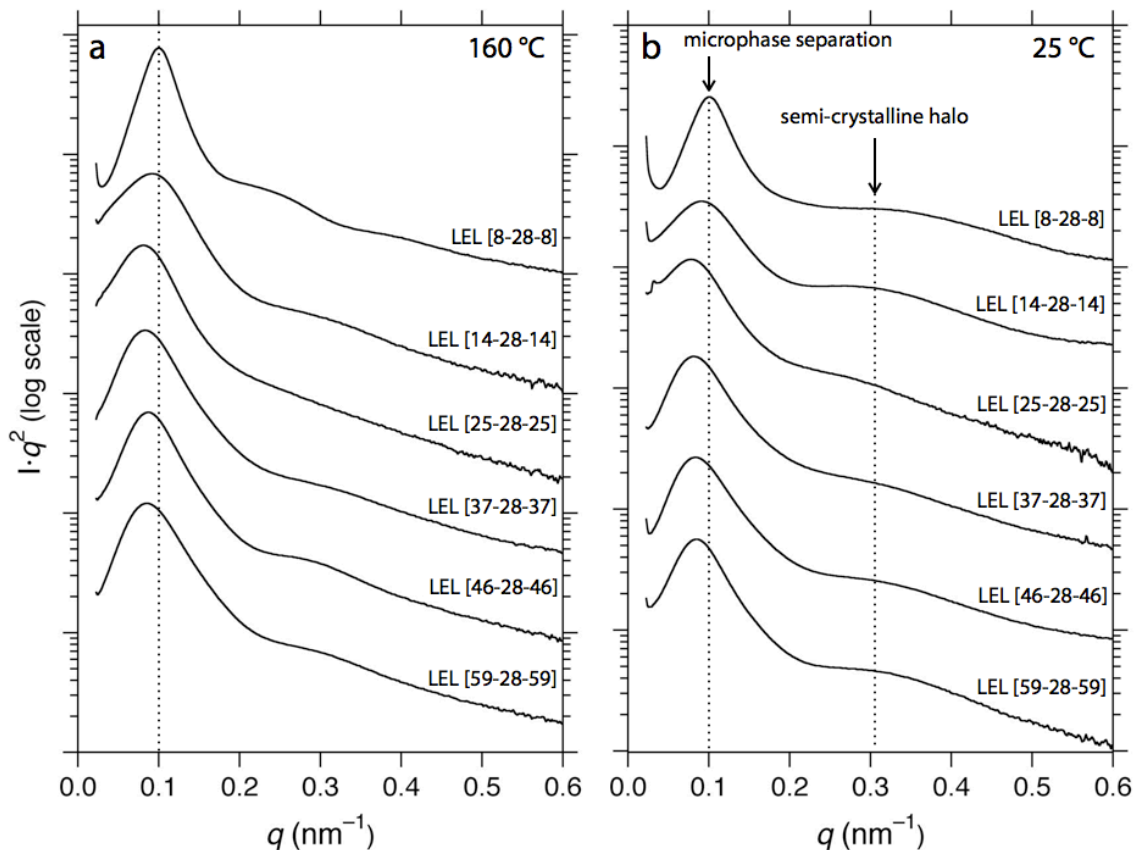


**Figure 4.21**

One-dimensional SAXS profiles for linear block copolymers prepared from the hydroxy-telechelic LPE sample HO-E-OH (28k) with various compositions at (a) 160 °C in the melt and (b) at 25 °C after cooling below the crystallization of LPE and vitrification of PLA. Profiles have been vertically shifted. Dashed lines have been added to guide the eye.

The profiles all share similar shape and the general lack of well-defined higher order reflections, suggesting that the block copolymers fail to adopt a morphology denoted by an organized lattice. With the exception of LEL [8-28-8], all the profiles have a single, relatively broad principal reflection with maxima in intensity occurring near  $q^* = 0.086 \text{ nm}^{-1} \pm 0.005$ . The precise values for each sample do not correlate with molecular weight or composition, and are scattered about the median value given above (Table 4.4). Correspondingly, the domain periodicity has an approximate length scale  $d = 73 \text{ nm}$ . Similarly shaped scattering profiles and the failure to adopt organized microdomains are potentially the result of

prohibitively slow ordering kinetics, even at a relatively high temperature ( $> T_{m,E}$ ), owing to the highly entangled polyethylene domain (entanglement molecular weight,  $M_e \approx 1 \text{ kg mol}^{-1}$ )<sup>138</sup> combined with the purportedly high segregation between PLA and LPE.<sup>136</sup> Considerable disparity between the polydispersity in the two components in a symmetric triblock copolymer has been partially credited for stabilizing a bicontinuous, disorganized morphology.<sup>139</sup> This morphology persisted over a large range of molar masses for copolymers with nearly symmetric composition comprised of poly(styrene-*b*-butadiene-*b*-styrene) (SBS), where the midblock had  $PDI \approx 1.9$ . Furthermore, the scattering profiles for the samples in Figure 4.21 have strikingly similar contour to those observed for bicontinuous microemulsions (B $\mu$ E)<sup>56,57,140,141</sup> Comprehensive scattering results for all the block copolymers within the molar mass range displayed from Table 4.2 suggest that each polymer adopts a similar structure, leaving no question about the absence of organization. This contrasts with PLE-PE block copolymers, in which the PE phase was prepared by hydrogenation of 1,4-polybutadiene synthesized by anionic polymerization. The previously investigated copolymers formed ordered morphologies. Notably, the copolymers have drastically different PDIs in addition to the slightly different backbone microstructure. Nonetheless, the profile contours suggest that the samples may have all adopted bicontinuous phases, offering an opportune template for nanoporous materials after the selective sacrifice of one component. Indeed, bicontinuous microemulsions have been used as templates for porous materials.<sup>58,59</sup> The PLA-LPE block copolymers exhibit a similar structure according to the SAXS profiles over a very large composition window ( $w_L = 0.5\text{--}0.8$ , excluding sample LEL [8-28-8] because of the notable discrepancy in profile contour compared with the other samples). Notably, the profile for the sample LEL [8-28-8] stands out as having a principal scattering reflection with considerably narrower breadth. This interesting trait corresponds coincidentally with the fact that this sample alone failed to form a morphology with a continuous PLA phase, and was therefore ineffective as a precursor to porous material. At this stage, we hesitate to postulate a reason for this or speculate about the connection between the scattering profile and the lack of PLA continuity.

Samples were cooled at a rate on the order of  $50\text{ }^{\circ}\text{C min}^{-1}$  after collecting scattering data at  $160\text{ }^{\circ}\text{C}$ . Profiles collected at  $25\text{ }^{\circ}\text{C}$  have nearly identical features as those collected in the melt (Figure 4.21b). At ambient temperature, both LPE crystallization and PLA vitrification have occurred, in that order, suggesting that the melt morphology was retained through both thermal transitions and LPE crystallization was confined within the microdomains. A vertical dashed line in Figures 4.21a and 4.21b are located at  $q = 0.1\text{ nm}^{-1}$  to guide the eye toward realization that both the shape and position of the principal scattering peaks are nearly identical before and after crystallization. Nearly all the profiles at  $25\text{ }^{\circ}\text{C}$  contain a broad, diffuse reflection with intensity maxima near  $q = 0.3\text{ nm}^{-1}$ , which may correspond to the "semi-crystalline halo" from the lamellar periodicity attributed to the semi-crystalline/amorphous LPE portions (Figure 4.19). The domain sizes from the principal scattering profile attributed to microphase separation are large enough that the LPE domain could accommodate at least one crystallite with a lamellar periodicity near  $20\text{ nm}$ , as suggested by the position of the diffuse reflection. The perfect retention of morphology despite  $T_{c,E} \gg T_{g,L}$  may be attributed to the strong segregation strength.<sup>137</sup> A relatively high PDI disparity has also been shown to increase the  $T_{ODT}$  compared with block copolymers with narrow molar mass distributions.<sup>139</sup> The effective segregation strength may therefore be larger than originally anticipated in the PLA–LPE system, thereby exacerbating the degree of crystallization confinement.

Expanding the protocol to different molecular weight midblock components should provide access to templates with various domain sizes, and nanoporous materials with correspondingly different pore-sizes. The straightforward method for preparing different molecular weights in the tandem ROP synthesis may translate to an equally convenient method for tailoring pore-size for applications with a range of requirements. Mahanthappa and coworkers prepared triblock copolymer with nearly symmetric compositions, but with a wide range of molecular weights ( $12\text{--}36\text{ kg mol}^{-1}$ ).<sup>139</sup> However, the samples each exhibited a scattering profile that indicated nearly equal domain spacing, regardless of molecular weight. Nonetheless, PLA–LPE block copolymers with larger molecular weights were

prepared and had scattering profiles with correspondingly larger  $d$ -values (smaller  $q$ ) but contours consistent with a disorganized structure (Figure 4.22).

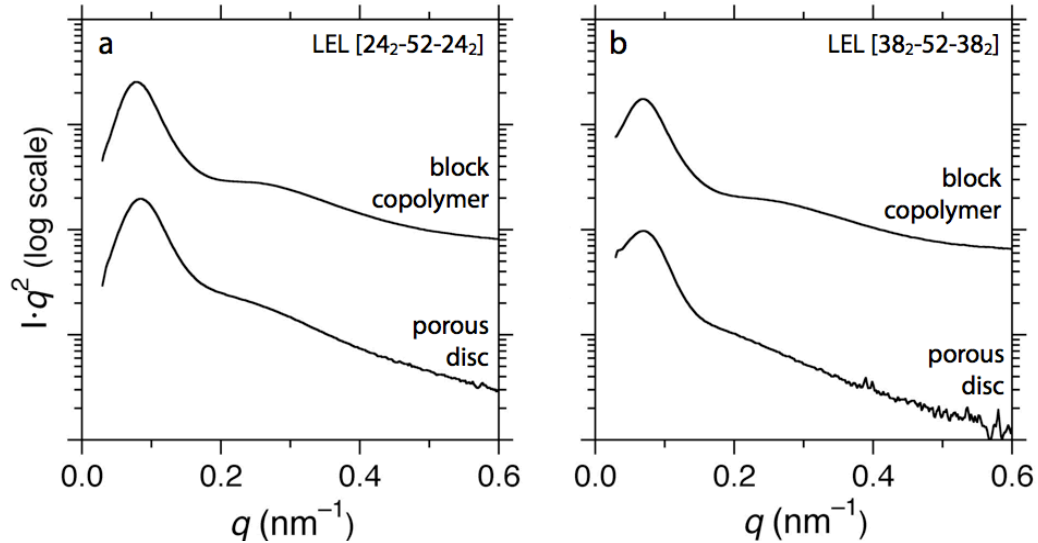


**Figure 4.22**

One-dimensional SAXS profiles for H-shaped block copolymers (a) L<sub>2</sub>EL<sub>2</sub> [24<sub>2</sub>-52-24<sub>2</sub>] with  $w_L = 0.65$  and (b) L<sub>2</sub>EL<sub>2</sub> [38<sub>2</sub>-52-38<sub>2</sub>] with  $w_L = 0.75$ . The *top* profile in each plot is the block copolymer template at 25 °C and the *bottom* profile is the porous derivative with all PLA having been removed.

Scattering profiles from block copolymers with H-shaped molecular architecture have essentially identical shapes to those with linear architectures, suggesting that the same morphology can be accessed with the branched analogs. Two block copolymer L<sub>2</sub>EL<sub>2</sub> [24<sub>2</sub>-52-24<sub>2</sub>] with  $w_L = 0.65$  and (b) L<sub>2</sub>EL<sub>2</sub> [38<sub>2</sub>-52-38<sub>2</sub>] with  $w_L = 0.75$  had intensity maxima at ambient temperature occurring at 0.081 and 0.069 nm<sup>-1</sup> corresponding to  $d = 78$  and 90 nm, respectively. Essentially indistinguishable profiles were observed after basic hydrolysis to remove the PLA component (*bottom* profiles in Figure 4.22a and 4.22b), demonstrating that the mild etching conditions had minimal effect on the bulk morphology. The nanoporous discs were therefore predicted to consist of a disorganized scaffold of LPE with intertwined void space.

Likewise, discs of melt-pressed linear block copolymers with smaller midblock molar masses were prepared and the PLA was removed. These block copolymers, with commensurate compositions, have profiles again consistent with disorganized mesoscale morphologies (Figure 4.23). The maxima in intensity are positioned at  $q = 0.159$  and  $0.147 \text{ nm}^{-1}$  for the porous structures derived from block copolymer samples LEL [10-11-10] and LEL [15-17-15], respectively, giving values of  $d = 39$  and  $42 \text{ nm}$ .

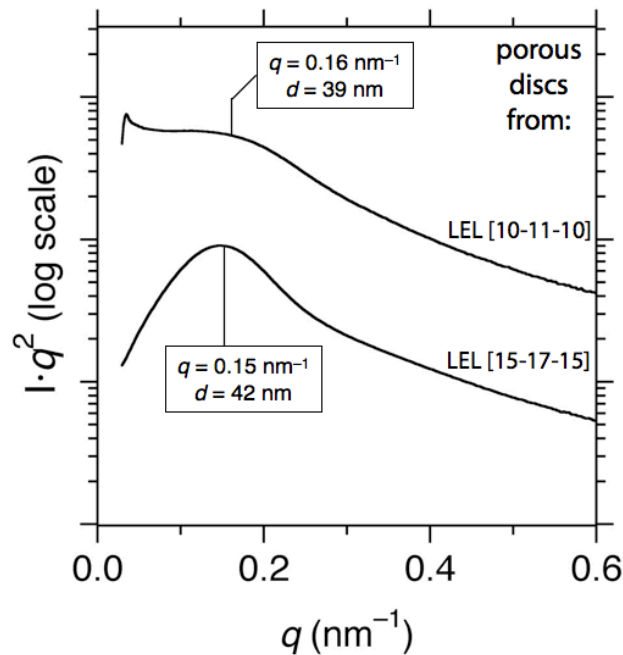


**Figure 4.23**

One-dimensional SAXS profiles for nanoporous LPE derived from linear block copolymers LEL [10-11-10] (*top*) and LEL [15-17-15] (*bottom*).

Collectively, the x-ray scattering suggests that (1) the domain size can be tailored by judicious selection of molecular weight and composition and (2) the tortuous morphology is bicontinuous in the melt-pressed block copolymer discs as indicated by the ability to completely remove the PLA component and the retention of contours in the SAXS profiles. Further evidence for the microphase structures

and the consistency of morphology across a range of molecular weights, molecular architectures, and compositions can be garnered from microscopic analysis of the porous samples.

#### 4.2.5 Imaging of Nanoporous Materials by SEM

The films and bulk discs were evaluated for porosity by several methods, including scanning electron microscopy (SEM). The bulk discs were fractured at ambient temperature and the interior was imaged after coating with  $\sim 3$  nm of Pt using a sputter coater. The specimens from Table 4.2 all appeared porous with a disordered continuous scaffold of polymer, which is presumed to be the remaining LPE. Both  $^1\text{H}$  NMR and IR spectroscopies suggest that pristine LPE remains after etching PLA. A typical image of the interior of a bulk nanoporous LPE derived from LEL [15-17-15] provides an illustration of the pore structure (Figure 4.24). However, the average pore diameter is difficult to estimate based on SEM alone owing to the highly tortuous nature of the phases and the fracturing technique. The fractures likely run at random orientations to the pore topology, giving the impression that a relatively large pore-size distribution exists. This shortcoming in the microscopy of such irregular, disorganized phase-structures will be addressed in a subsequent section with an alternative technique of nitrogen adsorption. Despite the difficulty assessing the exact pore size and distribution, a rough estimate of pore diameter may be garnered along with additionally relevant information regarding the uniformity of the claimed bicontinuous structure throughout the material and the dependence of phase behavior on surface properties, molar mass, composition, and molecular architecture of the precursor.

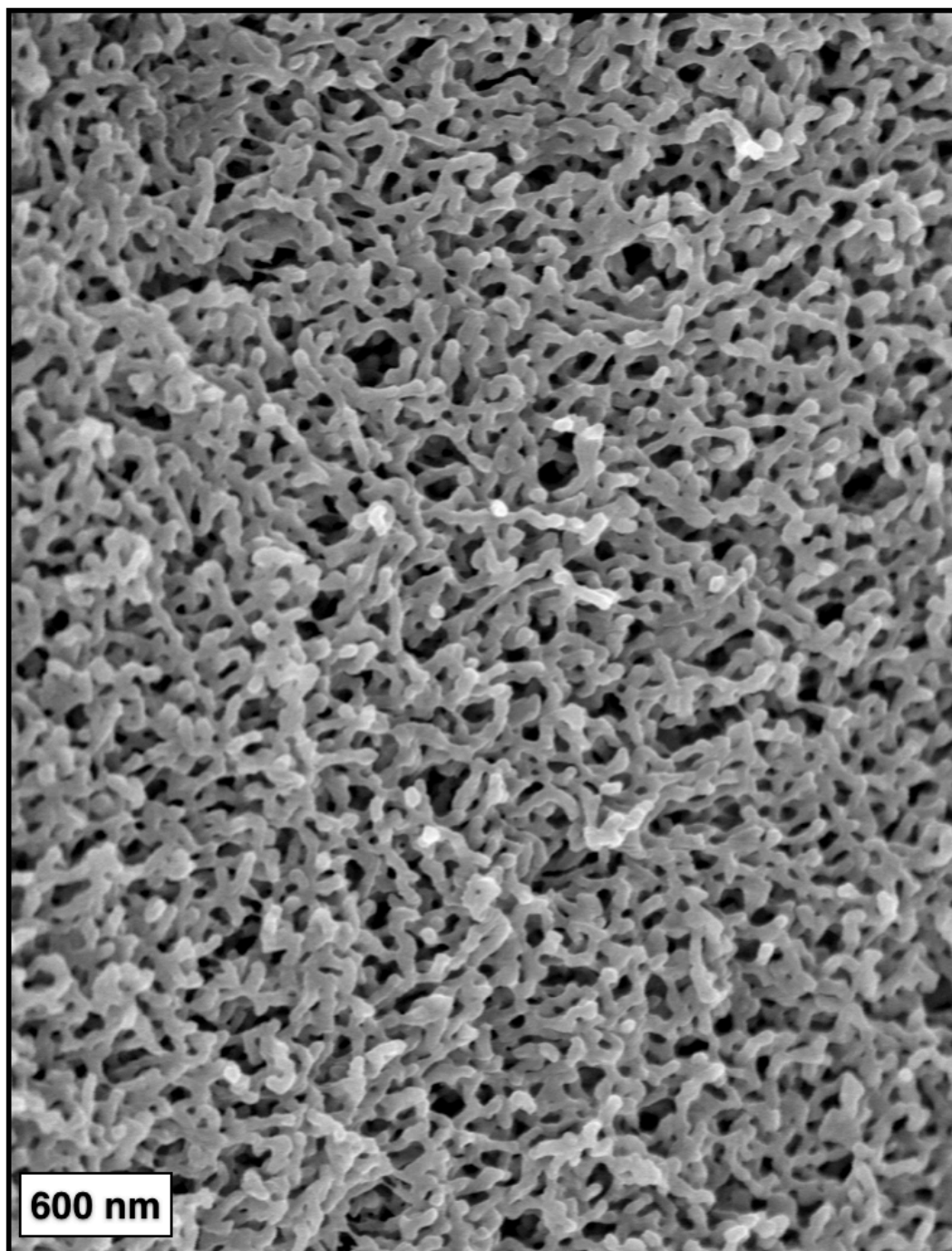


**Figure 4.24**

Micrograph from SEM for a fractured disc of nanoporous LPE sample derived from linear block copolymer LEL [15-17-15]. Coated with  $\sim 3$  nm Pt.

Samples with a linear molecular architecture and composition commensurate with LEL [15-17-15] but with different molecular weight adopted similar bicontinuous structures during bulk melt pressing as suggested by the nanoporous derivatives observed by SEM. Nanoporous samples derived from LEL [10-11-10], LEL [25-28-25] and LEL [60-50-65] each apparently possess a tortuous void space surrounded by an LPE scaffold on the interior of fracture discs (Figure 4.25).

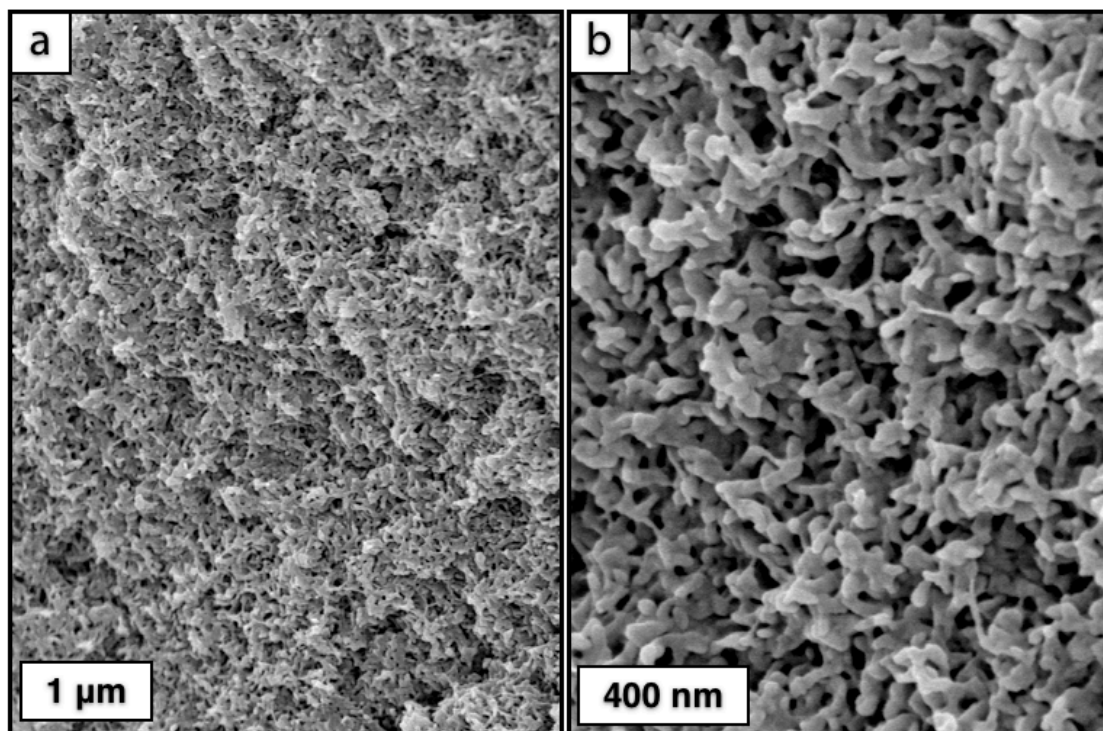


**Figure 4.25**

Micrographs at different magnifications of nanoporous LPE derived from LEL [10-11-10]. Sample was prepared by fracturing a disc at ambient temperature and coating with Pt ( $\sim 3$  nm).

Certain samples prepared by the solvent casting method adopted similar structures lacking any notable level of organization. Scaffold structures similar to those observed in bulk samples resulted after removing PLA from films of block copolymers prepared by solvent casting above  $T_{m,E}$ . The block copolymer samples were cast in air onto a ceramic surface with relatively uniform heating. The film



sides originating at the ceramic interface and the air interface were observed microscopically after degradation of the PLA to create porous films. Some samples had "top" (*i.e.*, air) and "bottom" (*i.e.*, ceramic) surface structures that were indistinguishable. Others had noticeably different structures between the two interfaces, and still others appeared to be non-porous on either side. These features showed a marked dependence on the composition, which stands in stark contrast to the bulk disc samples prepared from melt-pressing. The qualitative mechanical integrity of the films was also strongly dependent on the composition of the block copolymer derivative.

Nanoporous films could not be prepared from either the block copolymer LEL [10-11-10] or LEL [15-17-15]. It is postulated that the resulting LPE scaffolds were not of adequately high molecular weight to instill the strength and flexibility necessary to sustain the interconnecting web defining the nanoporous structure at an overall thickness less than 100  $\mu\text{m}$ .

Additionally, none of the samples derived from block copolymers with compositions corresponding to  $w_L > 0.7$  possessed adequate mechanical integrity to undergo PLA removal and retain the macroscopic structure; the films fell apart during isolation. However, samples originating from block copolymers with  $w_L < 0.7$  were mechanically robust after PLA removal, and the films were easily recovered using forceps. The films were free standing and easily manipulated after drying and could foreseeably be employed as flexible lithium-ion battery separators, for example. Examples of the film morphologies are provided with SEM micrographs (Figures 4.26–4.31).

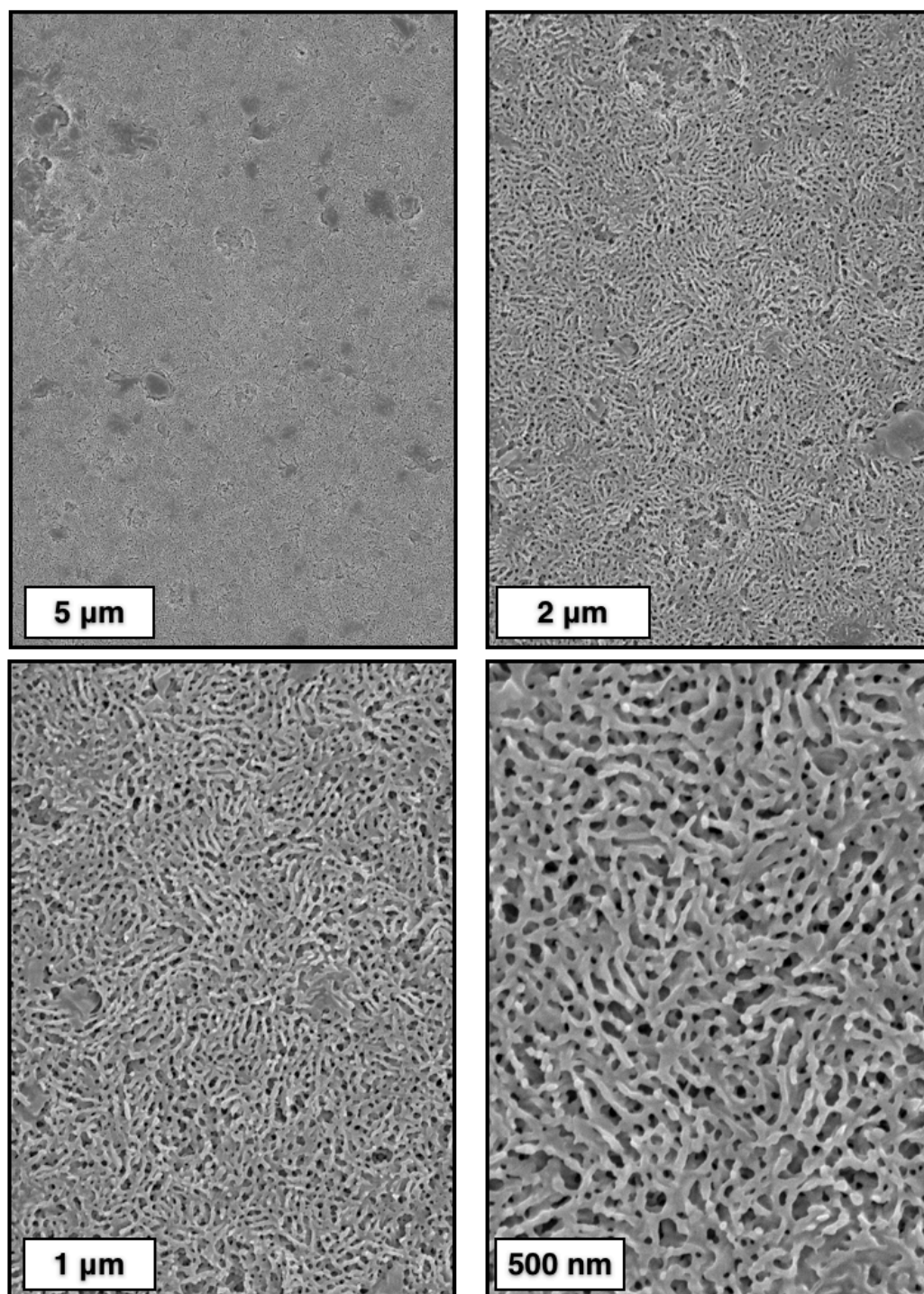


**Figure 4.26**

SEM micrographs at various magnifications for nanoporous samples derived from LEL [36-50-36] after solvent casting and PLA removal. Images were taken from the ceramic–film interface after coating with  $\sim 3$  nm Pt.

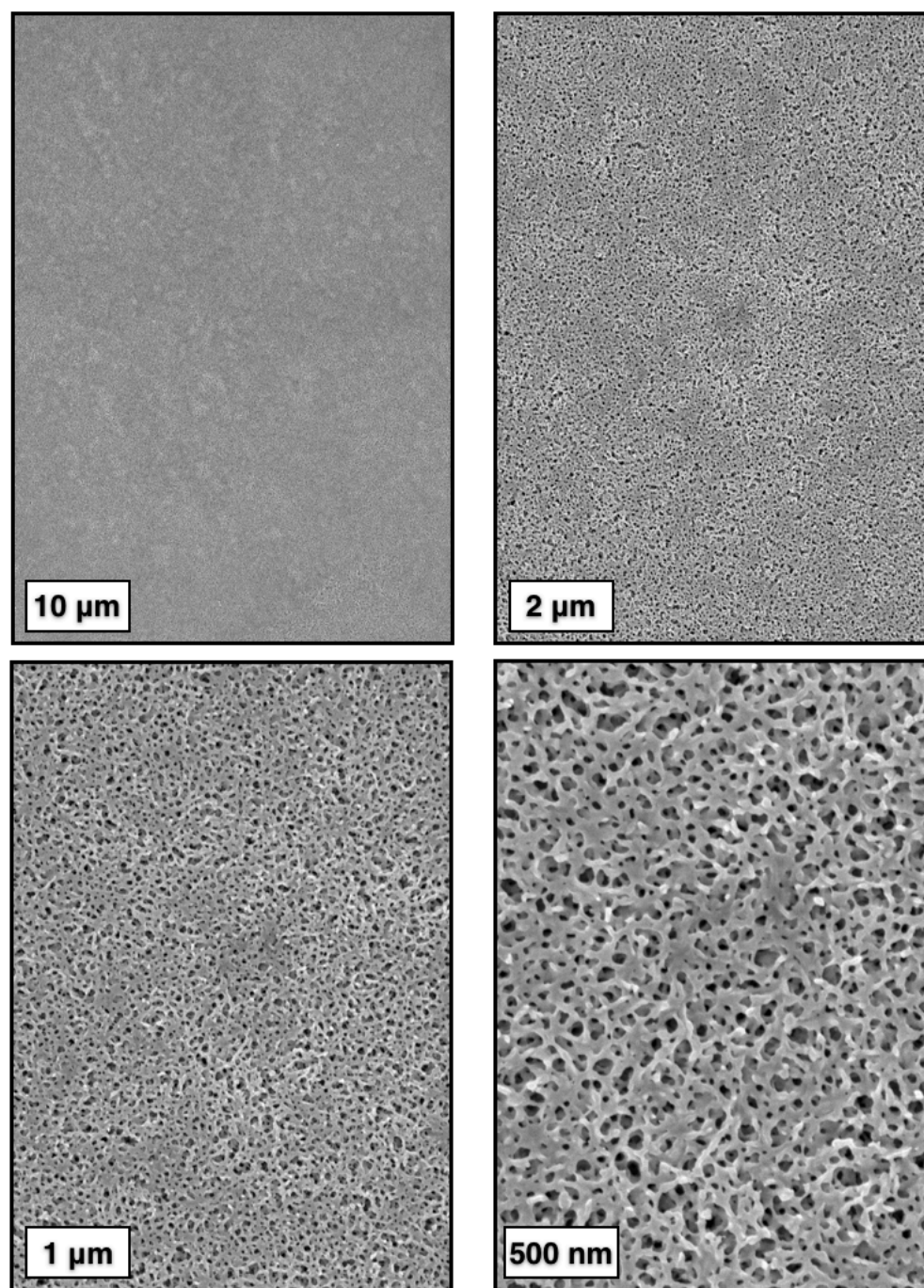


**Figure 4.27**

SEM micrographs at various magnifications for nanoporous samples derived from LEL [36-50-36] after solvent casting and PLA removal. Images were taken from the air–film interface after coating with ~3 nm Pt.

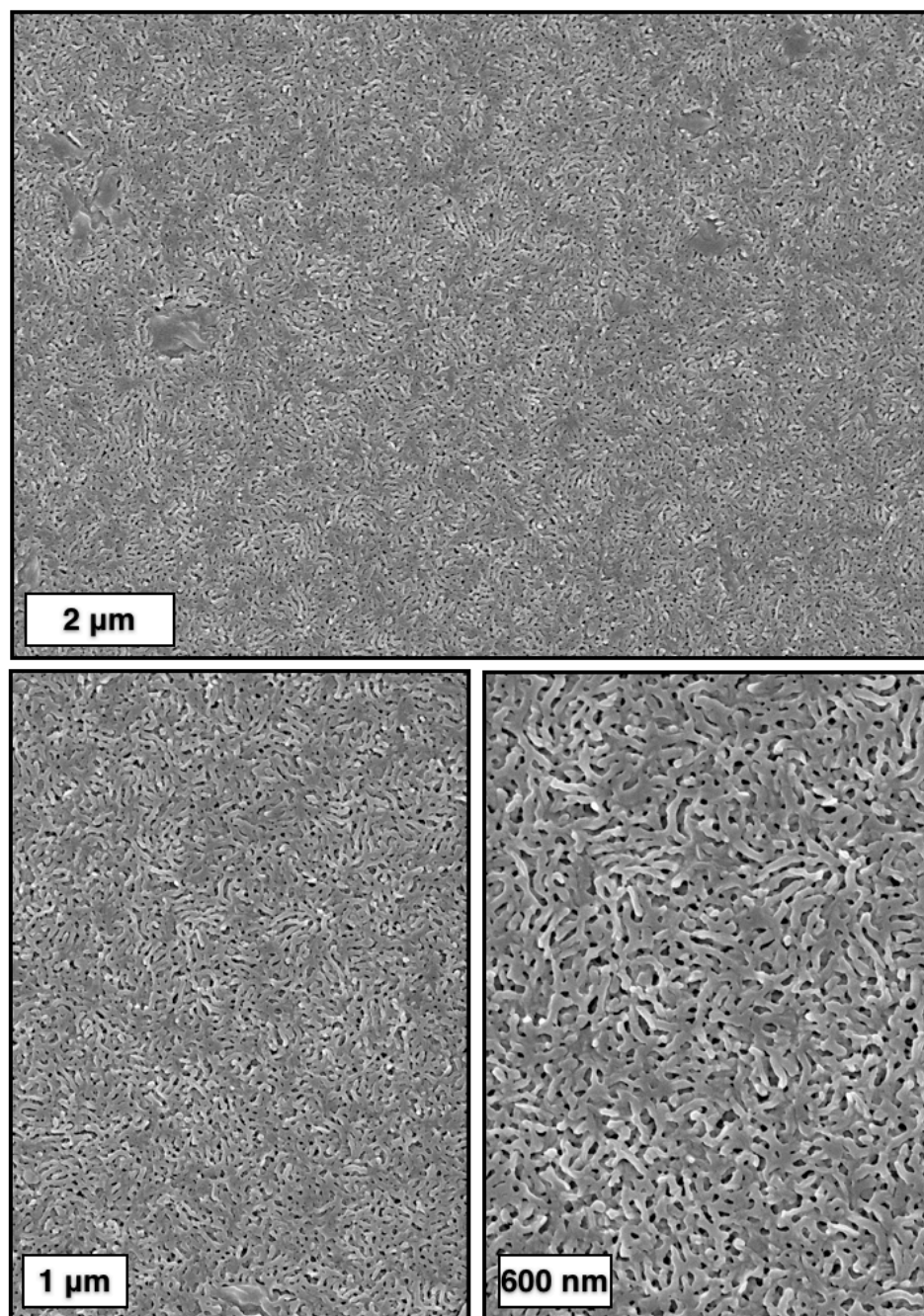


**Figure 4.28**

SEM micrographs at various magnifications for nanoporous samples derived from LEL [65-50-65] after solvent casting and PLA removal. Images were taken from the ceramic–film interface after coating with ~3 nm Pt.

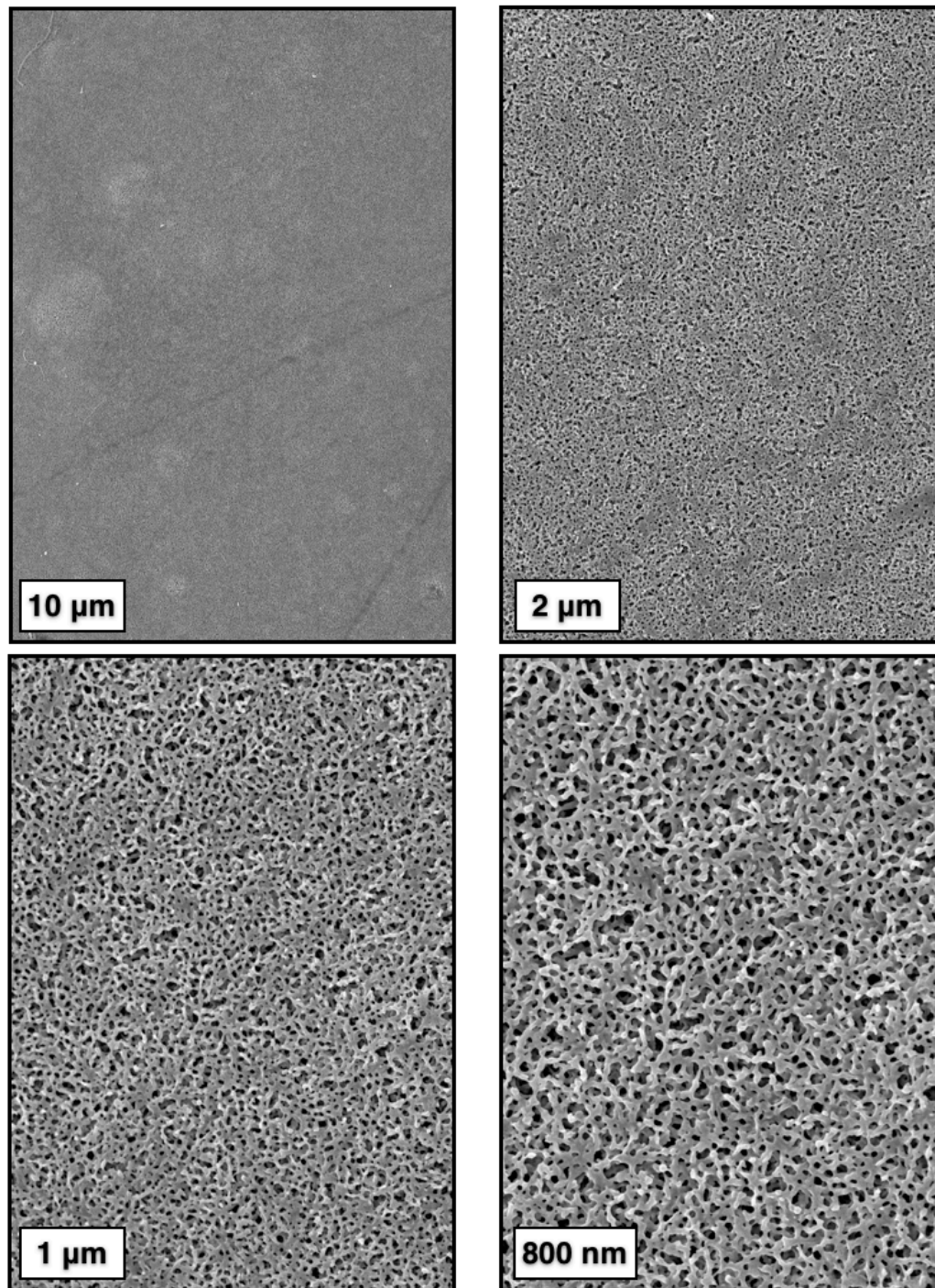


**Figure 4.29**

SEM micrographs at various magnifications for nanoporous samples derived from LEL [65-50-65] after solvent casting and PLA removal. Images were taken from the air–film interface after coating with ~3 nm Pt.

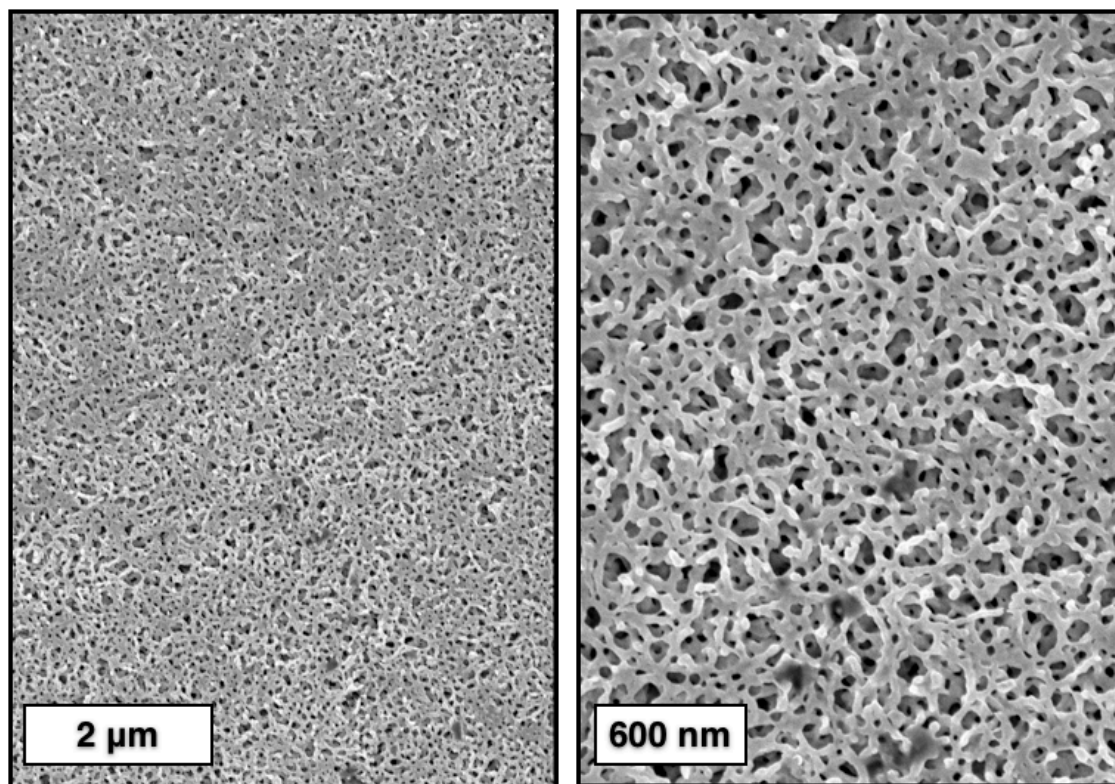


**Figure 4.30**

SEM micrographs at various magnifications for nanoporous samples derived from L<sub>2</sub>EL<sub>2</sub> [24<sub>2</sub>-50-24<sub>2</sub>] after solvent casting and PLA removal. Images were taken from the ceramic–film interface after coating with ~3 nm Pt.

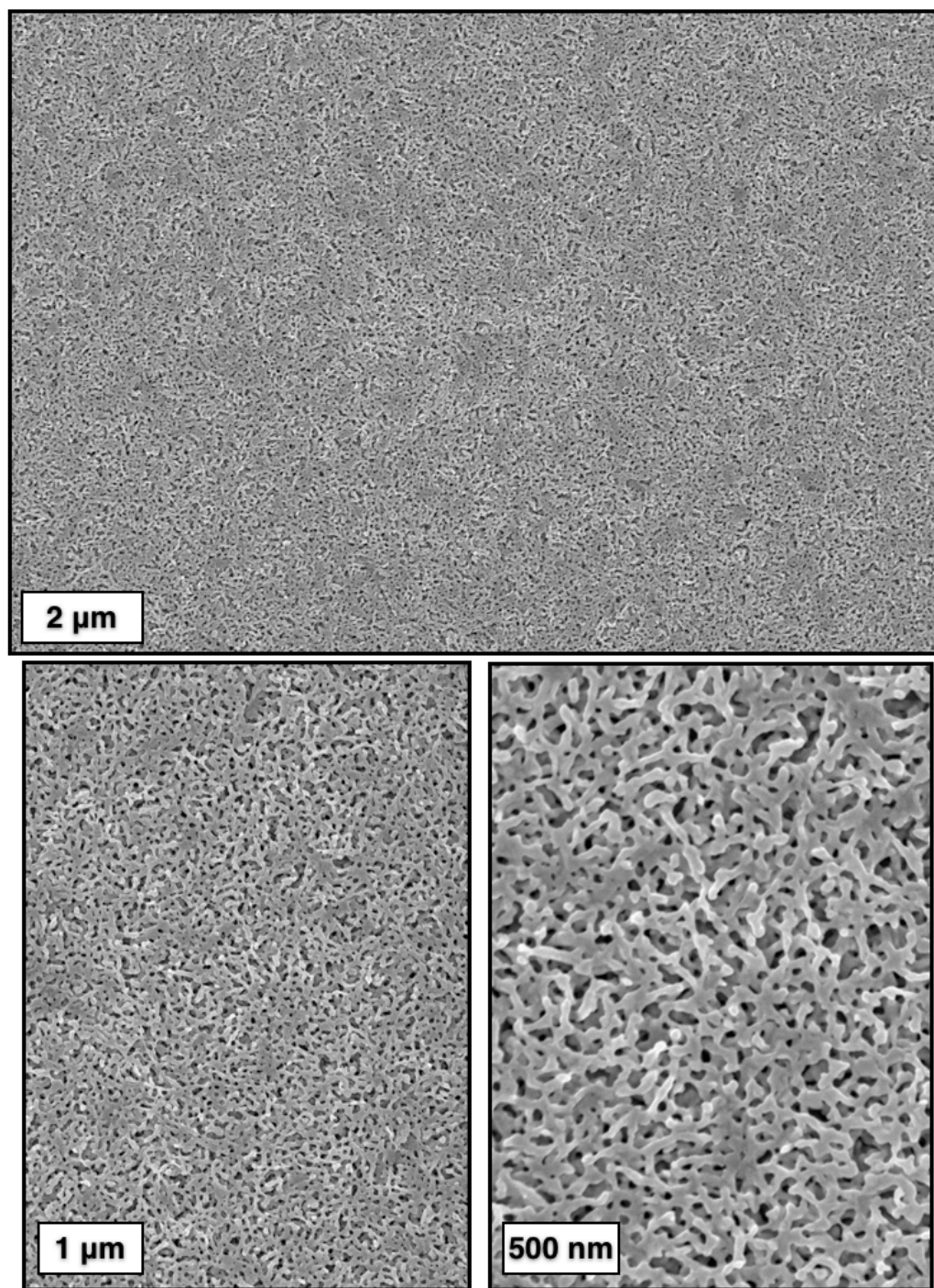


**Figure 4.31**

SEM micrographs at various magnifications for nanoporous samples derived from L<sub>2</sub>EL<sub>2</sub> [24<sub>2</sub>-50-24<sub>2</sub>] after solvent casting and PLA removal. Images were taken from the air–film interface after coating with ~3 nm Pt.

The pore structures in each of the SEM images in Figures 4.26–4.31 appear to be relatively independent of composition, molar mass, or molecular architecture of the precursor triblock copolymers. On the basis of the above examples, the ideal composition for obtaining a uniformly porous structure at both interfaces during solvent casting appears to be  $w_L \approx 0.65$ . The apparent pore size distribution from SEM is believed to be artificially large based on the fracturing technique. The smaller tubular shaped pores appear to generally be in the approximate range of 30–60 nm in diameter for the film-based membranes. The samples derived from smaller molar mass precursors appear to have on average smaller pore sizes. These results are consistent with the SAXS profiles previously discussed, for which the position of the principal scattering peak depended markedly on molar mass. Also, the length scale of the  $d$ -spacing obtained from SAXS corresponds well with the SEM results.

#### 4.2.6 Nitrogen Sorption

Nitrogen adsorption experiments were conducted on the nanoporous derivatives prepared from bulk melt-pressed discs for each sample in Table 4.2. The film from solvent casting one sample (L<sub>2</sub>EL<sub>2</sub> [24<sub>2</sub>-52-24<sub>2</sub>]) was analyzed to serve as a comparison. Starting with the two smallest molecular weight samples derived from LEL [10-11-10] and LEL [15-17-15] allows one to obtain the general features associated with the nanoporous materials produced by this method (Figure 4.32).



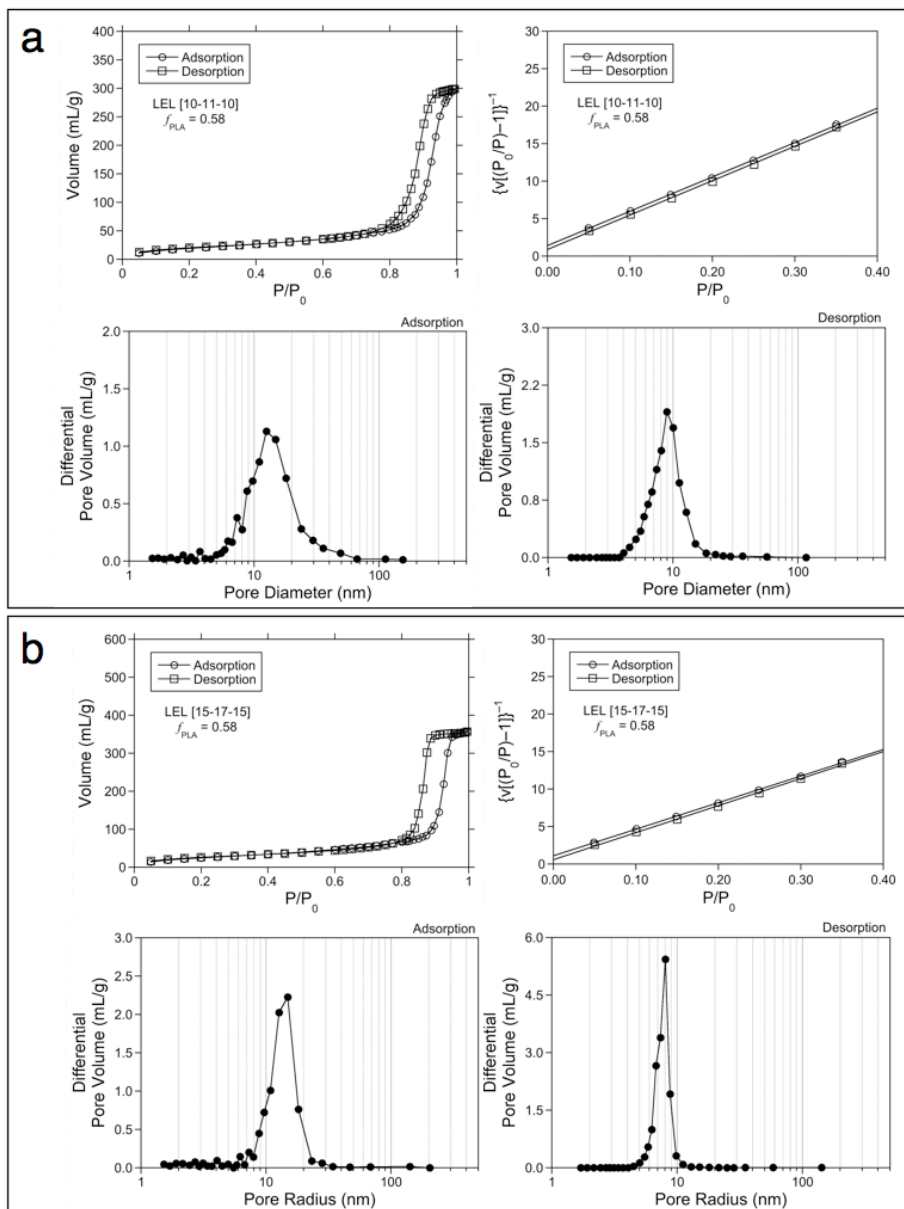


**Figure 4.32**

Results from nitrogen sorption experiments for nanoporous discs derived from (a) LEL [10-11-10] and (b) LEL [15-17-15], including adsorption and desorption isotherms, BET analysis (for surface area calculation) and BJH pore-size distribution from adsorption and desorption isotherms.

The nitrogen sorption results for these two samples show both the adsorption and desorption isotherms with volume of the gas sorbed with respect to the relative partial pressure ( $P/P_0$ ) (*top left* in Figure 4.32a and 4.32b). The behavior for both

samples is consistent with a type IV isotherm, showing clear hysteresis and correspondingly suggesting that the discs have a structure with pore sizes in the mesoscale range.<sup>142</sup> The hysteresis is further evinced by the difference in the position of the maxima with respect to pore radius, as illustrated with pore-size distribution plots calculated by the Barret-Joyner-Halenda (BJH) method (*bottom left and right* in Figure 4.32a and 4.32b).<sup>143</sup> Distributions are shown for both adsorption and desorption isotherms for these two samples to illustrate the relatively good agreement between the two. For all other samples, only the distribution for desorption isotherms is shown, as that arguably gives a more accurate indication of the size and breadth. Surface area is obtained from Brunauer–Emmet–Teller (BET) analysis (see Appendix A) associated with the plots taken from data points of relative pressure  $P/P_0 < 0.35$  (*top right* in Figure 4.32a and 4.32b).<sup>144</sup> Values associated with all the graphical descriptions are provided in tabular form (Table 4.5).

Nanoporous samples derived from LEL [10-11-10] and LEL [15-17-15] have pore-radius maxima in the pore-size distribution plots from desorption isotherms occurring at 8.1 nm and 9.0 nm, respectively. Both samples have relatively narrow breadth in the distribution, despite the pore radii being inversely proportional to molecular weight. The results suggest that an approximate pore radius range of less than 10 nm can reproducibly be accessed with block copolymer precursors having  $w_L = 0.65$  and PLA block lengths in the range of 10–15 kg mol<sup>-1</sup>.

Immediate affirmation that substantially larger molecular weight leads to larger pore-size was obtained by nitrogen sorption analysis of the series with linear architecture and midblock LPE molar mass of approximately 50 kg mol<sup>-1</sup> (Figure 4.33). Furthermore, the relationship between pore-size and composition with constant midblock molar mass was investigated with the three block copolymers LEL [36-50-36], LEL [65-50-65] and LEL [75-50-75], exhibiting a range of  $w_L = 0.59$ – $0.75$ . Each of the three samples exhibited type IV sorption isotherms, consistent with the purported mesoporosity. The peaks in the pore-size distribution correspond to pore radii of 12.9 nm, 12.8 nm, and 15.1 nm, respectively, which suggests a modest dependence of pore-size on composition. Also, all these samples

---

exhibited substantially larger pore-size than the smaller molar mass counterparts with commensurate composition. The total adsorbed volume (the maximum in the isotherm) also increases monotonically with increasing  $f_L$ , consistent with a direct relationship between porosity and original PLA content.<sup>‡</sup> Surface area also dramatically increased with increasing  $f_L$  (Table 4.5) according to BET analysis. Having direct control over porosity could ultimately lead to tailoring of flow rates across membranes derived from these materials, while maintaining a nanoscopic pore-radius.

---

<sup>‡</sup> All sample sizes were essentially equal during sorption measurements (50–60 mg).

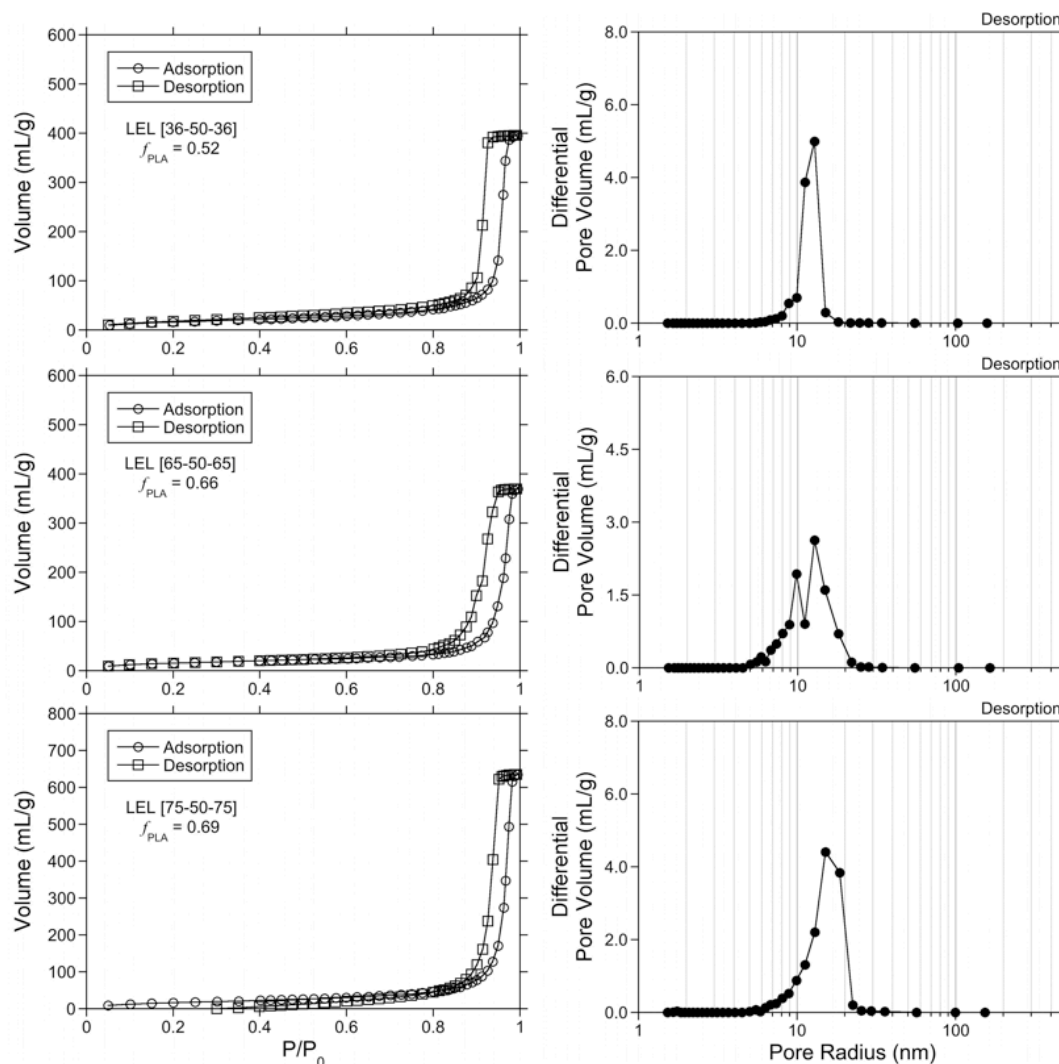


**Figure 4.33**

Nitrogen sorption results for porous discs derived from (*top*) LEL [36-50-36], (*middle*) LEL [65-50-65], and (*bottom*) LEL [75-50-75] including (*left column*) adsorption and desorption isotherms and (*right column*) pore-size distribution from BJH analysis on desorption isotherm.

The next obvious step is to explore the connection between pore size and the molecular architecture of the derivative block copolymers. Nitrogen sorption data for the nanoporous samples derived from H-shaped block copolymers  $L_2EL_2$  [13<sub>2</sub>-52-13<sub>2</sub>],  $L_2EL_2$  [24<sub>2</sub>-52-24<sub>2</sub>], and  $L_2EL_2$  [38<sub>2</sub>-52-38<sub>2</sub>] (Figure 4.34). These samples fall within a composition range comparable to that of the previously discussed linear block copolymers and show similar characteristics. Namely, the pore radii are approximately 11.3 nm, 15.1 nm, and 24.3 nm, respectively, which further

corroborates the suspected pore-size dependence on composition. However, a clear demarcation was not realized for the different architecture. Nonetheless, a direct correlation between the original PLA content and total adsorbed gas volume and BET surface area was observed.

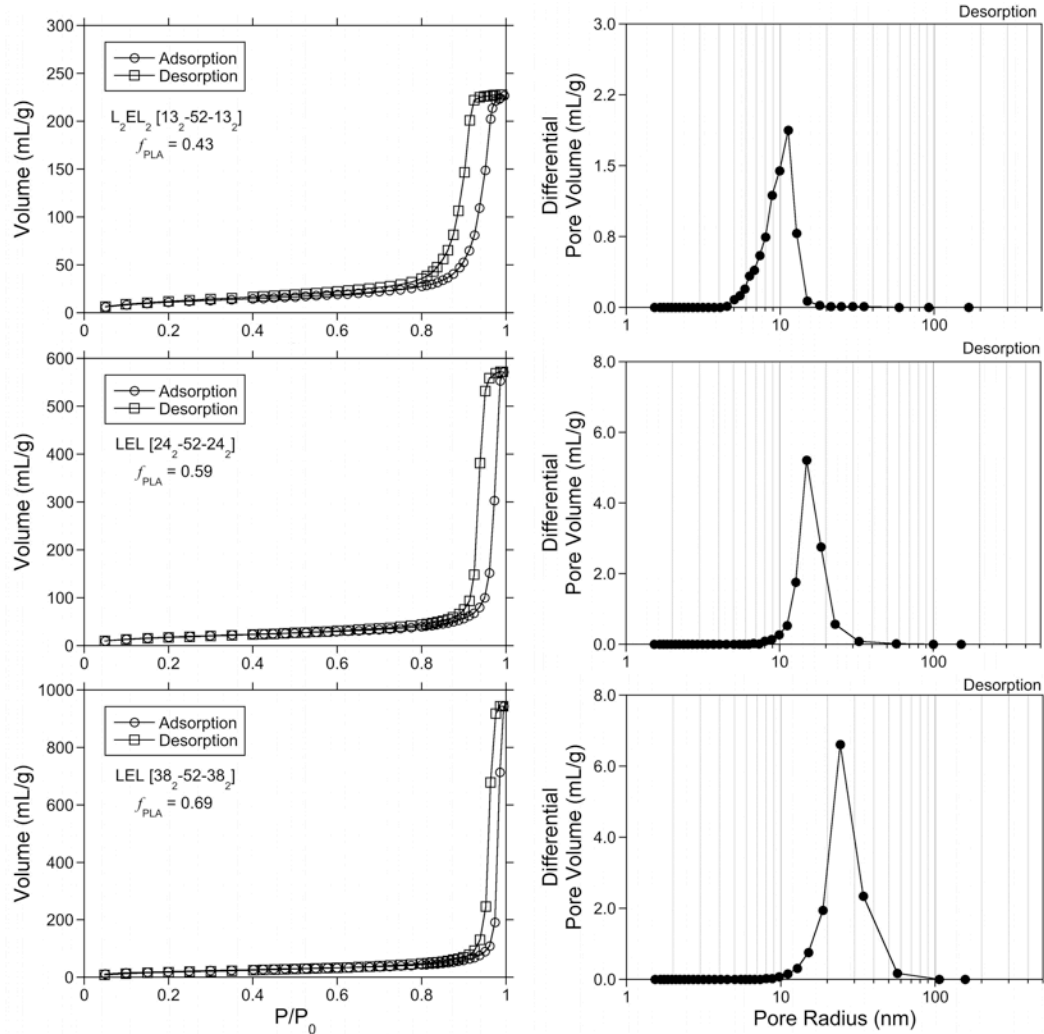


**Figure 4.34**

Nitrogen sorption results for porous discs derived from (*top*) L<sub>2</sub>EL<sub>2</sub> [13<sub>2</sub>-52-13<sub>2</sub>], (*middle*) L<sub>2</sub>EL<sub>2</sub> [24<sub>2</sub>-52-24<sub>2</sub>], and (*bottom*) L<sub>2</sub>EL<sub>2</sub> [38<sub>2</sub>-52-38<sub>2</sub>] including (*left column*) adsorption and desorption isotherms and (*right column*) pore-size distribution from BJH analysis on desorption isotherm.

---

Nitrogen sorption of the nanoporous samples derived from the arachne-arm block copolymers of commensurate molar mass and composition helps support the conclusions drawn from the previous comparisons (Figure 4.35). Specifically, porous samples from block copolymers L<sub>4</sub>EL<sub>4</sub> [8<sub>4</sub>-50-8<sub>4</sub>], L<sub>4</sub>EL<sub>4</sub> [11<sub>4</sub>-50-11<sub>4</sub>], and L<sub>4</sub>EL<sub>4</sub> [19<sub>4</sub>-50-19<sub>4</sub>] all showed type IV isotherm behavior consistent with nanochannels permeating throughout the material and had corresponding pore radii equal to 6.3 nm, 14.8 nm, and 15.0 nm, respectively. These samples attest to the conviction that pore-size can be tuned by changing the molar mass and composition of the derivative block copolymers, but that molecular architecture is unsubstantial. Nanoporous discs were accessed across a wide range of compositions regardless of the original molecular architecture and free standing membranes with robust mechanical characteristics resulted.

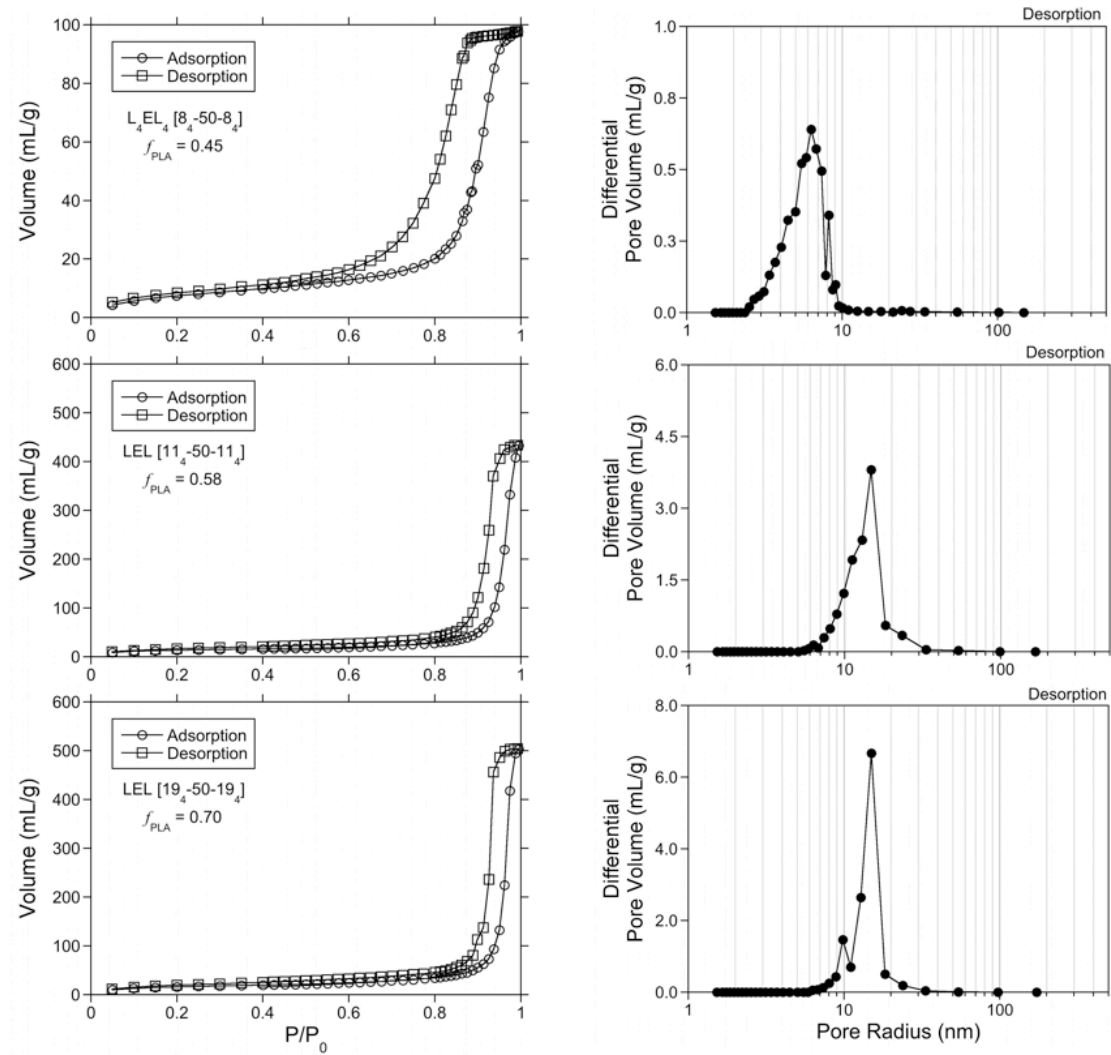


**Figure 4.35**

Nitrogen sorption results for porous discs derived from (*top*)  $L_4EL_4 [8_4-50-8_4]$ , (*middle*)  $L_4EL_4 [11_4-50-11_4]$ , and (*bottom*)  $L_4EL_4 [19_4-50-19_4]$  including (*left column*) adsorption and desorption isotherms and (*right column*) pore-size distribution from BJH analysis on desorption isotherm.

**Table 4.4**

Porous characteristics of membranes derived from  $L_xEL_x$  linear and branched block copolymers determined from nitrogen sorption experiments.

Sample ID	$f_L$	$w_L$	Surface Area ( $m^2 g^{-1}$ )			Pore Radius (nm)	
			BET	BJH(a)	BJH(d)	BJH(a)	BJH(d)
<i>HO-LPE-OH (11k): <math>M_n = 10.8 kg mol^{-1}</math></i>							
LEL [10-11-10]	0.58	0.65	74	80	114	12.6	9.0
<i>HO-LPE-OH (17k): <math>M_n = 16.7 kg mol^{-1}</math></i>							
LEL [15-17-15]	0.58	0.65	95	100	157	12.7	8.1
<i>HO-LPE-OH (28k): <math>M_n = 28.8 kg mol^{-1}</math></i>							
LEL [8-28-8]	0.30	0.37	N/A	N/A	N/A	N/A	N/A
LEL [14-28-14]	0.43	0.50	8	10	30	15.2	7.3
LEL [25-28-25]	0.57	0.64	65	52	100	19.7	15.1
LEL [37-28-37]	0.67	0.73	75	72	127	33.9	10.1
LEL [46-28-46]	0.71	0.77	75	71	117	33.9	15.1
LEL [59-28-59]	0.76	0.81	82	78	121	33.4	18.5
<i>HO-LPE-OH (52k): <math>M_n = 50.1 kg mol^{-1}</math></i>							
LEL [36-50-36]	0.52	0.59	65	64	109	23.0	12.9
LEL [65-50-65]	0.66	0.72	57	53	107	17.8	12.8
LEL [72-50-72]	0.70	0.75	–	83	148	28.5	15.1
<i>HO<sub>2</sub>-LPE-OH<sub>2</sub> (52k): <math>M_n = 52.4 kg mol^{-1}</math></i>							
L <sub>2</sub> EL <sub>2</sub> [13 <sub>2</sub> -52-13 <sub>2</sub> ]	0.43	0.50	44	45	79	14.9	11.3
L <sub>2</sub> EL <sub>2</sub> [24 <sub>2</sub> -52-24 <sub>2</sub> ]	0.59	0.65	67	57	120	30.6	15.1
L <sub>2</sub> EL <sub>2</sub> [38 <sub>2</sub> -52-38 <sub>2</sub> ]	0.69	0.75	73	60	124	53.2	24.3
<i>HO<sub>4</sub>-LPE-OH<sub>4</sub> (50k): <math>M_n = 50.5 kg mol^{-1}</math></i>							
L <sub>4</sub> EL <sub>4</sub> [8 <sub>4</sub> -50-8 <sub>4</sub> ]	0.48	0.55	29	30	61	7.8	6.3
L <sub>4</sub> EL <sub>4</sub> [11 <sub>4</sub> -50-11 <sub>4</sub> ]	0.58	0.64	51	57	113	18.2	14.8
L <sub>4</sub> EL <sub>4</sub> [19 <sub>4</sub> -50-19 <sub>4</sub> ]	0.70	0.75	62	62	123	23.3	15.0

The BET results are consistent with the length scales visualized with SEM, and those values obtained from SAXS of the triblock precursors as well as the porous membranes. As with the SAXS results, the domain size obtained from BET measurements depends on molar mass and composition.



### 4.2.7 Performance Characteristics of Nanoporous LPE Membranes.

The LPE membranes described here, with high porosity, could potentially be envisioned as replacements for conventional polyolefin lithium-ion battery separators. A shutdown mechanism is one crucial attribute in battery separators, whereby pore collapse can be induced by thermal runaway. This safety feature could potentially prevent fires sometimes observed in such batteries. The membranes must maintain general mechanical durability even after pore collapse in order to prevent direct anode-cathode contact. The thermal shutdown was investigated in this system by heating a sample at 150 °C for 2 minutes; the pore structure was observed by SEM before and after the thermal treatment (Figure 4.36).

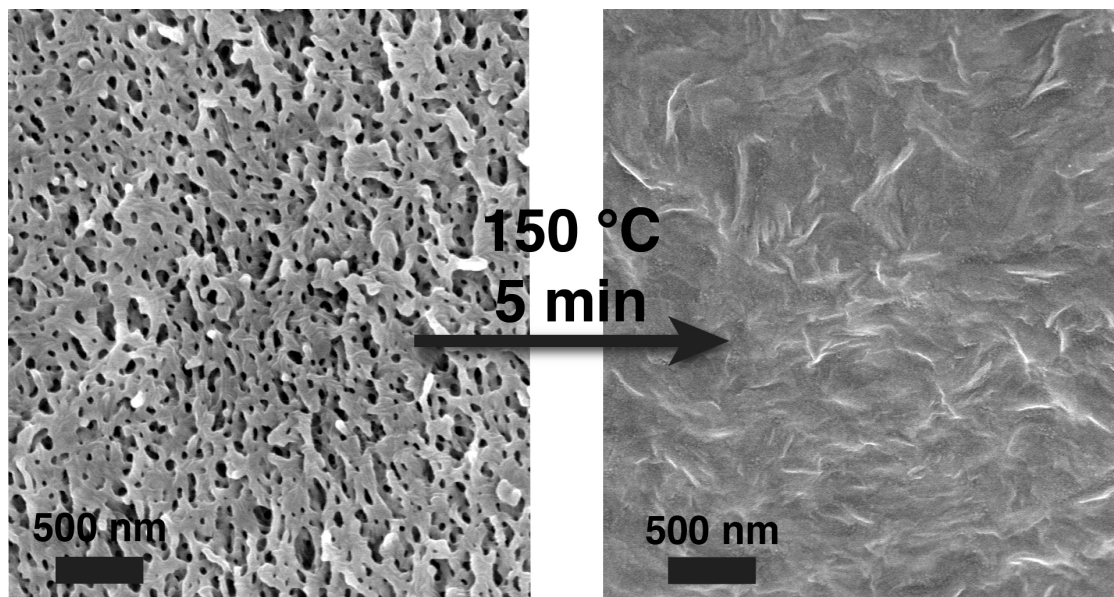


**Figure 4.36**

Thermally induced pore collapse of porous membrane derived from LEL [14–28–14] after heating at 150 °C for 5 min. Samples coated with ~2 nm Pt before imaging.

Battery separators may encounter relatively harsh chemical environments. As such, the membrane performance and pore-structure preservation in several harsh environments was investigated. Porous samples derived from LEL [37-28-37] were soaked in either concentrated sulfuric or nitric acid and were imaged by SEM (Figure 4.37). The pore structures did not appear to be detrimentally effected.

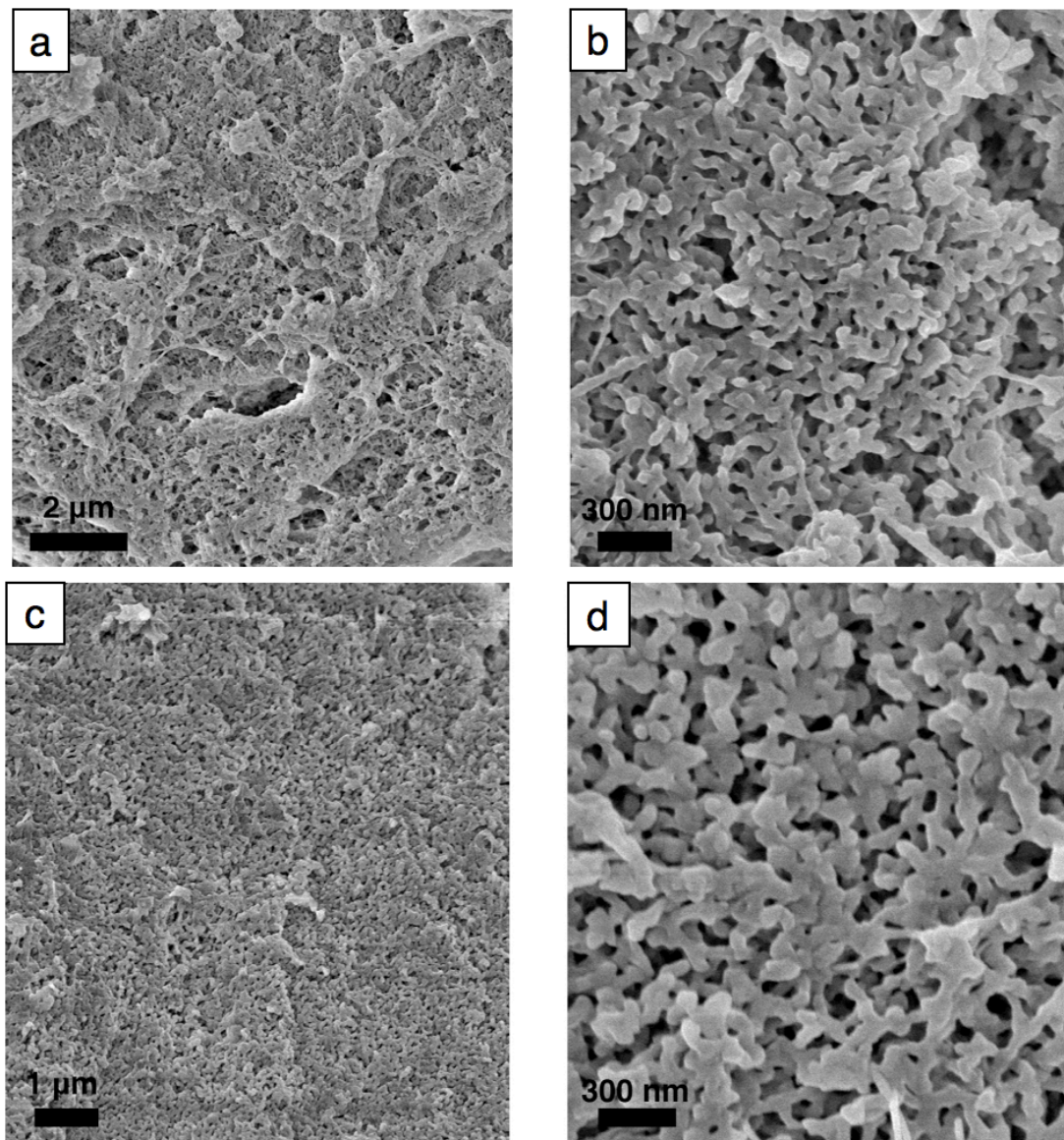


**Figure 4.37**

SEM images of porous membranes derived from LEL [37-28-37] after soaking for 24 h at 25 °C in (a,b) concentrated nitric acid and (c,d) concentrated sulfuric acid.

---

The durability and flexibility of the porous membranes was qualitatively confirmed by handling the membranes. They were not fragile, and could be manipulated into various shapes. The tensile testing of block copolymer precursors and the porous derivatives suggests that the mechanical integrity is indeed noteworthy, making the LPE membranes amenable to several mechanically demanding applications. Figure 4.37a shows the tensile properties of the block copolymer LEL [14-28-14] (solid line) and its porous derivative. It is obvious that a great deal of strength was lost in rendering the material porous. However, the porous materials still exhibits tensile strength of approximately 10 MPa and elongation to 50 % before catastrophic failure. Figure 37b shows tensile results from uniaxial extension of block copolymer LEL [37-28-37] and its porous derivative. Again the loss in mechanical strength is expected when removing upwards of 50 wt % from the template.

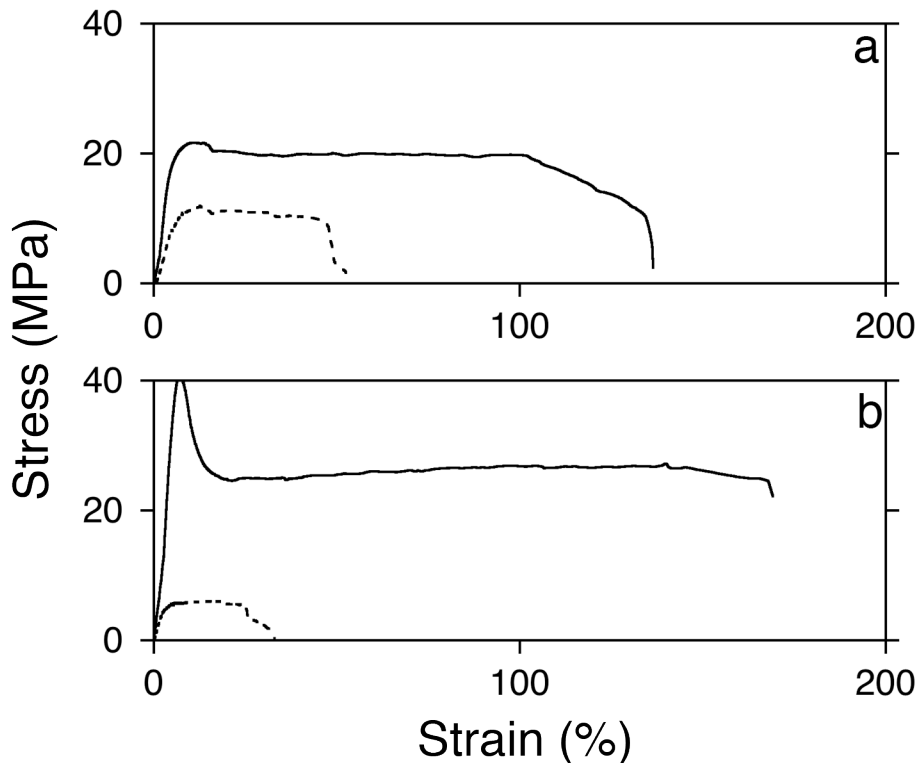


**Figure 4.38**

Tensile testing of block copolymers (—) and membranes (- - -) from (a) LEL [14-28-14] and (b) LEL [37-28-37].

### 4.3 Conclusions

The porous materials described in this chapter offer several advantages over many previously reported examples. First, the linear structure of the polyethylene offers the corrosion resistance and toughness that are lacking from brittle and oxidatively susceptible components like polystyrene and poly(methyl methacrylate). Second, the disorganized bicontinuous morphology adopted by the block copolymer templates avoids the tedious post-processing alignment necessary for certain well-organized microphases, such as hexagonally packed cylinders, which are traditionally used as precursors to nanoporous materials. Bicontinuous microemulsions represent another convenient template for nanoporous materials, embodying the disorganized bicontinuous structure. However, very small domain sizes ( $\sim 5\text{--}50$  nm) are inaccessible with B $\mu$ E templates. The PLA-LPE block

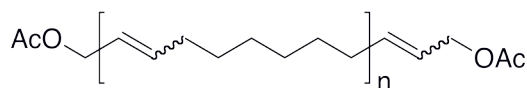
copolymers comparatively combine PDI disparity with a highly entangled, semicrystalline midblock to provide access to a bicontinuous phase over an impressive range of composition and molecular weight.

The nanoporous LPE samples derived from block copolymer have many features that make them attractive for several potentially viable commercial applications. The membranes are resistant to strong acids and bases, owing to the chemical nature of the hydrocarbon LPE scaffold. This feature lends itself to be suitable in highly corrosive environments like lithium-ion batteries. The high surface area and stability of the LPE membranes in nearly every solvent at ambient temperatures could lend itself to applications in high surface area catalyst supports. Methods of incorporating catalysts or reactive functionality into the pores would be required for such an endeavor, and is suggested as a potentially lucrative pathway. Furthermore, nanoporous LPE membranes are currently being explored as templates for zeolite growth. The structures are retained in the demanding conditions required for zeolite synthesis (*e.g.*, prolonged steaming at 100 °C) After growing a microporous material within the void-space of a nanoporous membrane, the LPE could be sacrificed through thermal decomposition by calcining. This would ultimately leave a hierarchically porous zeolite material, with the larger mesopores templated from the LPE membrane. Nanoporous LPE membranes might also be viable ultrafiltration membranes for water purification, which would require thinner membranes than those described previously.

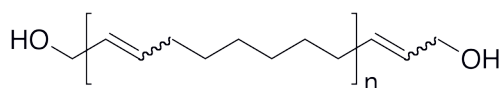
With further development, the membranes could foreseeably be realized in one or more of these applications. Reliably accessing this pore structure in large area membranes is one processing challenge that requires further attention. Considerable headway has been achieved on this front, but safer production steps are desirable. Avoiding toxic solvents like 1,2,4-trichlorobenzene is necessary. Additionally, avoiding the hot-solution filtering process employed after the heterogeneous metal-catalyzed (Platinum or Palladium) hydrogenation would be a beneficial safety enhancement. Exploring alternative catalysts remains one viable enhancement, such as the hydrocarbon-soluble (*e.g.*, cyclohexane, toluene) Rh-based Wilkinson's catalyst.

## 4.4 Experimental Details

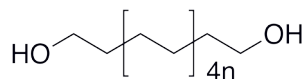
**Materials.** All bulk solvents were purchased from Mallinkrodt and used as received unless otherwise specified. Tetralin was purchased from TCI Chemicals and was vacuum distilled prior to use. The second generation Grubbs catalyst was purchased from Aldrich and used as received. Both *cis*-cyclooctene from Acros (95%) and *cis*-1,4-diacetoxy-2-butene from TCI Chemical (95%) were distilled over CaH<sub>2</sub> prior to polymerizations. Tetrahydrofuran (THF) and toluene were passed through alumina columns and thoroughly degassed. Purac provided the D,L-lactide (99%), which was recrystallized twice from toluene prior to being stored in a glove box under N<sub>2</sub> atmosphere. Sn(Oct)<sub>2</sub> from Aldrich was distilled using a Kugelrohr apparatus and stored under N<sub>2</sub>. The catalyst used in hydrogenation reactions was a silica-supported Pt catalyst supplied from Dow Chemical Company.



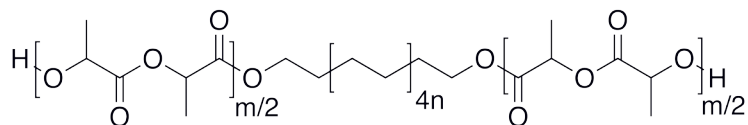
**Synthesis of HO-LPE-OH macroinitiator.** The procedure for preparing hydroxy-telechelic polyolefins by ring-opening metathesis polymerization has been described previously.<sup>131,132</sup> Briefly, 0.25 g (0.23 mL; 1.45 mmol) of the chain transfer agent (CTA) *cis*-1,4-diacetoxy-2-butene was transferred to an air-free flask through a rubber septum along with 180 mL of THF. This mixture was rapidly stirred and the temperature was maintained at 35 °C. Using a syringe pump, 40 g (47 mL; 363 mmol) of *cis*-cyclooctene were added to the mixture over 1.5 h. Shortly ( $\approx$  5 min) after starting the gradual monomer addition, 15 mg (18  $\mu$ mol) of Grubbs 2<sup>nd</sup> Generation catalyst was added as a solution in 1 mL THF. After 6 h, the reaction contents were slowly poured into 2 L of cold MeOH made slightly acidic with 20 mL of 1M HCl (aq). The precipitated polymer was isolated and dried under reduced pressure at 40 °C for 2 days.



The entire yield was dissolved into 200 mL of THF and stirred at 0 °C for 6 h after adding 10 mL of a 0.7 M solution of NaOMe in MeOH (7 mmol NaOMe). The polymer solution was again precipitated into 2 L of slightly acidic MeOH, isolated, and dried for 2 days, yielding 37.5 g (94 %). <sup>1</sup>H NMR (CDCl<sub>3</sub>, 25 °C): δ (ppm) = 5.40 (m, (*E*)-CH=CHCH<sub>2</sub>CH<sub>2</sub>-, backbone), 5.35 (m, (*Z*)-CH=CHCH<sub>2</sub>CH<sub>2</sub>-, backbone), 4.20 (t, (*Z*)-CH=CHCH<sub>2</sub>OH), 4.10 (t, (*E*)-CH=CHCH<sub>2</sub>OH), 2.05 (*Z*)-CH=CHCH<sub>2</sub>CH<sub>2</sub>-backbone), 1.95 (m, (*E*)-CH=CHCH<sub>2</sub>CH<sub>2</sub> backbone), 1.30 (m, (*Z*)-CH=CHCH<sub>2</sub>CH<sub>2</sub>-backbone).



The hydroxy-telechelic PCOE (HO-PCOE-OH) (10.0 g; 45.4 mmol double bonds) was dissolved in 150 mL cyclohexane and the solution was purged with bubbling argon for 20 minutes. A silica supported Pt/Re catalyst (1.0 g of 10 %) was placed in the high-pressure reactor, which was sealed, evacuated of air, and refilled with Ar. The polymer solution was added to the reactor at which point hydrogen was introduced (500 psig) and the temperature increased to 90 °C. The reaction mixture was stirred for 24 hours, after which the solvent was removed and replaced with 150 mL toluene. The catalyst was removed by filtering the solution at 110 °C and the solvent was again evaporated to afford 8.2 g of HO-LPE-OH (82 % yield). <sup>1</sup>H NMR (toluene-*d*<sub>8</sub>, 100 °C): δ (ppm) = 3.37 (t, -CH<sub>2</sub>OH), 1.35 (s, -CH<sub>2</sub>-, backbone).



The synthesis of one triblock is described, which is representative of all samples where the D,L-lactide feedstock was adjusted accordingly to target the desired polymer compositions. The concentration of LA was kept constant at 1 M. HO-

LPE-OH (2.0 g; 0.14 mmol OH) was placed with a stir-bar in a pressure vessel fitted with a Teflon screw-cap and Viton o-ring seal. This was transferred to a glove box, wherein D,L-lactide (2.5 g; 17 mmol), toluene (17 mL) and Sn(Oct)<sub>2</sub> (7 mg; 17 μmol) were added before sealing and removing from the box. The flask was immersed in an oil-bath at 110 °C for 6 h followed by precipitation into a ten-fold excess by volume of MeOH. The isolated polymer was dried at 60 °C for 24 h to yield 4.2 g (93%). <sup>1</sup>H NMR (toluene-*d*<sub>8</sub>, 100 °C): δ (ppm) = 5.10 (bm, –C(O)CH(CH<sub>3</sub>)O– backbone), 4.05–4.25 (m, –C(O)CH(CH<sub>3</sub>)OH), 3.70–4.00 (m, –CH=CHCH<sub>2</sub>OC(O)CH(CH<sub>3</sub>)O–) 1.40–1.45 (–C(O)CH(CH<sub>3</sub>)O– backbone), 1.30–1.40 (–CH<sub>2</sub>–, backbone).

**Preparation of films.** The mold that was used had inner dimensions of 8 cm × 10 cm × 0.2 cm. These dimensions are amenable to casting films from solutions up to 16 mL in theory and 12 mL in practice. Films prepared by this method have a distribution of thickness across a given film based on unevenly distributed heating, unbalanced surface and/or substantial air-flow during casting (done in a fume-hood). Dissolving 0.4 g of a block copolymer having a midblock LPE molar mass approximately 50 kg mol<sup>-1</sup> in 8 mL of 1,2,4-trichlorobenzene gave a solution that had viscosity such that the solution spreads across the entire area but has enough surface tension to minimize leakage between the aluminum mold and the ceramic hotplate surface. The solutions were prepared in 20 mL glass vials with rapid stirring. The glass vials were submerged in an oil-bath at 160 °C and stirred for approximately 10 minutes. The clear, colorless solutions were then poured onto the ceramic surface of the hotplate which was maintained at 155 °C (according to the digital temperature readout on the hotplate). The solvent was allowed to completely evaporate, which required approximately 30 minutes. The aluminum mold was removed and the excess solvent was wiped from the surfaces. The hotplate was then turned off and allowed to cool to room temperature before peeling the film off. The films cannot be peeled off above approximately 40 °C.



## 4.5 References

- [1] Phillip, W. A.; Rzaev, J.; Hillmyer, M. A.; Cussler, E. L. *J. Membr. Sci.* **2006**, *286*, 144–152.
- [2] Bernards, D. A.; Desai, T. A. *Soft Matter* **2010**, *6*, 1621–1631.
- [3] Yang, S. Y.; Park, J.; Yoon, J.; Ree, M.; Jang, S. K.; Kim, J. K. *Adv. Funct. Mater.* **2008**, *18*, 1371–1377.
- [4] Jackson, E. A.; Hillmyer, M. A. *ACS Nano* **2010**, *4*, 3548–3553.
- [5] Nunes, S. P.; Sougrat, R.; Hooghan, B.; Anjum, D. H.; Behzad, A. R.; Zhao, L.; Pradeep, N.; Pinnau, I.; Vainio, U.; Peinemann, K. V. *Macromolecules* **2010**, *43*, 8079–8085.
- [6] Phillip, W. A.; Amendt, M.; O'Neill, B.; Chen, L.; Hillmyer, M. A.; Cussler, E. L. *Acs Applied Materials & Interfaces* **2009**, *1*, 472–480.
- [7] Phillip, W. A.; O'Neill, B.; Rodwogin, M.; Hillmyer, M. A.; Cussler, E. L. *Acs Applied Materials & Interfaces* **2010**, *2*, 847–853.
- [8] Jung, Y. S.; Ross, C. A. *Small* **2009**, *5*, 1654–1659.
- [9] Park, M.; Harrison, C.; Chaikin, P. M.; Register, R. A.; Adamson, D. H. *Science* **1997**, *276*, 1401–1404.
- [10] Arora, P.; Zhang, Z. *Chem. Rev.* **2004**, *104*, 4419–4462.
- [11] Zhang, S. S. *J. Power Sources* **2007**, *164*, 351–364.
- [12] Pitet, L. M.; Amendt, M. A.; Hillmyer, M. A. *J. Am. Chem. Soc.* **2010**, *132*, 8230–+.
- [13] Uehara, H.; Kakiage, M.; Sekiya, M.; Sakuma, D.; Yamonobe, T.; Takano, N.; Barraud, A.; Meurville, E.; Ryser, P. *ACS Nano* **2009**, *3*, 924–932.

- [14] Olson, D. A.; Chen, L.; Hillmyer, M. A. *Chem. Mater.* **2008**, *20*, 869–890.
- [15] Hillmyer, M. A. *Adv. Polym. Sci.* **2005**, *190*, 137–181.
- [16] Zalusky, A. S.; Olayo–Valles, R.; Taylor, C. J.; Hillmyer, M. A. *J. Am. Chem. Soc.* **2001**, *123*, 1519–1520.
- [17] Zalusky, A. S.; Olayo–Valles, R.; Wolf, J. H.; Hillmyer, M. A. *J. Am. Chem. Soc.* **2002**, *124*, 12761–12773.
- [18] Thurn–Albrecht, T.; Steiner, R.; DeRouchey, J.; Stafford, C. M.; Huang, E.; Bal, M.; Tuominen, M.; Hawker, C. J.; Russell, T. P. *Adv. Mater.* **2000**, *12*, 787–790.
- [19] Rzayev, J.; Hillmyer, M. A. *J. Am. Chem. Soc.* **2005**, *127*, 13373–13379.
- [20] Rzayev, J.; Hillmyer, M. A. *Macromolecules* **2005**, *38*, 3–5.
- [21] Bailey, T. S.; Rzayev, J.; Hillmyer, M. A. *Macromolecules* **2006**, *39*, 8772–8781.
- [22] Guo, S.; Rzayev, J.; Bailey, T. S.; Zalusky, A. S.; Olayo–Valles, R.; Hillmyer, M. A. *Chem. Mater.* **2006**, *18*, 1719–1721.
- [23] Hedrick, J. L.; Carter, K. R.; Labadie, J. W.; Miller, R. D.; Volksen, W.; Hawker, C. J.; Yoon, D. Y.; Russell, T. P.; McGrath, J. E.; Briber, R. M. *Adv. Polym. Sci.* **1999**, *141*, 1–43.
- [24] Uehara, H.; Yoshida, T.; Kakiage, M.; Yamanobe, T.; Komoto, T.; Nomura, K.; Nakajima, K.; Matsuda, M. *Macromolecules* **2006**, *39*, 3971–3974.
- [25] Amendt, M. A.; Chen, L.; Hillmyer, M. A. *Macromolecules* **2010**, *43*, 3924–3934.
- [26] Chen, L.; Phillip, W. A.; Cussler, E. L.; Hillmyer, M. A. *J. Am. Chem. Soc.* **2007**, *129*, 13786–13787.

- [27] Cochran, E. W.; Garcia–Cervera, C. J.; Fredrickson, G. H. *Macromolecules* **2006**, *39*, 2449–2451.
- [28] Hashimoto, T.; Tsutsumi, K.; Funaki, Y. *Langmuir* **1997**, *13*, 6869–6872.
- [29] du Sart, G. G.; Vukovic, I.; Vukovic, Z.; Polushkin, E.; Hiekkataipale, P.; Ruokolainen, J.; Loos, K.; ten Brinke, G. *Macromol. Rapid Commun.* **2011**, *32*, 366–370.
- [30] Hsueh, H. Y.; Chen, H. Y.; She, M. S.; Chen, C. K.; Ho, R. M.; Gwo, S.; Hasegawa, H.; Thomas, E. L. *Nano Lett.* **2010**, *10*, 4994–5000.
- [31] Chen, Z.–R.; Kornfield, J. A.; Smith, S. D.; Grothaus, J. T.; Satkowski, M. *Science* **1997**, *277*, 1248–1253.
- [32] Chen, Z. R.; Issaian, A. M.; Kornfield, J. A.; Smith, S. D.; Grothaus, J. T.; Satkowski, M. M. *Macromolecules* **1997**, *30*, 7096–7114.
- [33] Chen, Z. R.; Kornfield, J. A. *Polymer* **1998**, *39*, 4679–4699.
- [34] Vigild, M. E.; Chu, C.; Sugiyama, M.; Chaffin, K. A.; Bates, F. S. *Macromolecules* **2001**, *34*, 951–964.
- [35] Vedrine, J.; Hong, Y.–R.; Marencic, A. P.; Register, R. A.; Adamson, D. H.; Chaikin, P. M. *Appl. Phys. Lett.* **2007**, *91*, 143110/143111–143110/143113.
- [36] Drzal, P. L.; Barnes, J. D.; Kofinas, P. *Polymer* **2001**, *42*, 5633–5642.
- [37] Drzal, P. L.; Halasa, A. F.; Kofinas, P. *Polymer* **2000**, *41*, 4671–4677.
- [38] Chen, L.; Hillmyer, M. A. *Macromolecules* **2009**, *42*, 4237–4243.
- [39] Wolf, J. H.; Hillmyer, M. A. *Langmuir* **2003**, *19*, 6553–6560.
- [40] Matsen, M. W. *Phys. Rev. Lett.* **2005**, *95*, 258302/258301–258302/258304.
- [41] Matsen, M. W. *Macromolecules* **2006**, *39*, 5512–5520.

- [42] Crossland, E. J. W.; Ludwigs, S.; Hillmyer, M. A.; Steiner, U. *Soft Matter* **2007**, *3*, 94–98.
- [43] Crossland, E. J. W.; Ludwigs, S.; Hillmyer, M. A.; Steiner, U. *Soft Matter* **2010**, *6*, 670–676.
- [44] Amundson, K.; Helfand, E.; Davis, D. D.; Quan, X.; Patel, S. S.; Smith, S. D. *Macromolecules* **1991**, *24*, 6546–6548.
- [45] Amundson, K.; Helfand, E.; Quan, X.; Smith, S. D. *Macromolecules* **1993**, *26*, 2698–2703.
- [46] Boeker, A.; Elbs, H.; Haensel, H.; Knoll, A.; Ludwigs, S.; Zettl, H.; Zvelindovsky, A. V.; Sevink, G. J. A.; Urban, V.; Abetz, V.; Mueller, A. H. E.; Krausch, G. *Macromolecules* **2003**, *36*, 8078–8087.
- [47] Bang, J.; Kim, S. H.; Drockenmuller, E.; Misner, M. J.; Russell, T. P.; Hawker, C. J. *J. Am. Chem. Soc.* **2006**, *128*, 7622–7629.
- [48] Kim, S. H.; Misner, M. J.; Russell, T. P. *Adv. Mater.* **2004**, *16*, 2119–2123.
- [49] Kim, S. H.; Misner, M. J.; Xu, T.; Kimura, M.; Russell, T. P. *Adv. Mater.* **2004**, *16*, 226–231.
- [50] Vayer, M.; Hillmyer, M. A.; Dirany, M.; Thevenin, G.; Erre, R.; Sinturel, C. *Thin Solid Films* **2010**, *518*, 3710–3715.
- [51] Phillip, W. A.; Hillmyer, M. A.; Cussler, E. L. *Macromolecules* **2010**, *43*, 7763–7770.
- [52] Lee, D. H.; Park, S.; Gu, W. Y.; Russell, T. P. *ACS Nano* **2011**, *5*, 1207–1214.
- [53] Park, S.; Wang, J. Y.; Kim, B.; Xu, J.; Russell, T. P. *ACS Nano* **2008**, *2*, 766–772.

- [54] Wang, Y.; He, C. C.; Xing, W. H.; Li, F. B.; Tong, L.; Chen, Z. Q.; Liao, X. Z.; Steinhart, M. *Adv. Mater.* **2010**, *22*, 2068–+.
- [55] Bolton, J.; Bailey, T. S.; Rzayev, J. *Nano Lett.* **2011**, *11*, 998–1001.
- [56] Bates, F. S.; Maurer, W. W.; Lipic, P. M.; Hillmyer, M. A.; Almdal, K.; Mortensen, K.; Fredrickson, G. H.; Lodge, T. P. *Phys. Rev. Lett.* **1997**, *79*, 849–852.
- [57] Hillmyer, M. A.; Maurer, W. W.; Lodge, T. P.; Bates, F. S.; Almdal, K. *J. Phys. Chem. B* **1999**, *103*, 4814–4824.
- [58] Jones, B. H.; Lodge, T. P. *J. Am. Chem. Soc.* **2009**, *131*, 1676–1677.
- [59] Zhou, N.; Bates, F. S.; Lodge, T. P. *Nano Lett.* **2006**, *6*, 2354–2357.
- [60] Mansky, P.; Harrison, C. K.; Chaikin, P. M.; Register, R. A.; Yao, N. *Appl. Phys. Lett.* **1996**, *68*, 2586–2588.
- [61] Oh, S.; Lee, J.-K.; Theato, P.; Char, K. *Chem. Mater.* **2008**, *20*, 6974–6984.
- [62] Aggarwal, S. L.; Sweeting, O. J. *Chem. Rev.* **1957**, *57*, 665–742.
- [63] Mandelkern, L.; Peacock, A. J. *Polym. Bull.* **1986**, *16*, 529–536.
- [64] Alamo, R. G.; Mandelkern, L. *Macromolecules* **1989**, *22*, 1273–1277.
- [65] Mandelkern, L.; Alamo, R. G.; Kennedy, M. A. *Macromolecules* **1990**, *23*, 4721–4723.
- [66] Domski, G. J.; Rose, J. M.; Coates, G. W.; Bolig, A. D.; Brookhart, M. *Prog. Polym. Sci.* **2007**, *32*, 30–92.
- [67] Szwarc, M. *Nature (London, United Kingdom)* **1956**, *178*, 1168–1169.
- [68] Szwarc, M.; Levy, M.; Milkovich, R. *J. Am. Chem. Soc.* **1956**, *78*, 2656–2657.

- [69] Hadjichristidis, N.; Iatrou, H.; Pitsikalis, M.; Mays, J. *Prog. Polym. Sci.* **2006**, *31*, 1068–1132.
- [70] Hahn, S. F. *J. Polym. Sci., Part A: Polym. Chem.* **1992**, *30*, 397–408.
- [71] Hucul, D. A.; Hahn, S. F. *Adv. Mater.* **2000**, *12*, 1855–1858.
- [72] Falk, J. C.; Schlott, R. J. *Macromolecules* **1971**, *4*, 152–154.
- [73] Ryan, A. J.; Hamley, I. W.; Bras, W.; Bates, F. S. *Macromolecules* **1995**, *28*, 3860–3868.
- [74] Rangarajan, P.; Register, R. A.; Fetters, L. J. *Macromolecules* **1993**, *26*, 4640–4645.
- [75] Morton, M.; Fetters, L. J. *Rubber Chem. Technol.* **1975**, *48*, 359–409.
- [76] O'Gara, J. E.; Wagener, K. B. *Makromol. Chem., Rapid Commun.* **1993**, *14*, 657–662.
- [77] Wagener, K. B.; Valenti, D.; Hahn, S. F. *Macromolecules* **1997**, *30*, 6688–6690.
- [78] Smith, J. A.; Brzezinska, K. R.; Valenti, D. J.; Wagener, K. B. *Macromolecules* **2000**, *33*, 3781–3794.
- [79] Sworen, J. C.; Smith, J. A.; Wagener, K. B.; Baugh, L. S.; Rucker, S. P. *J. Am. Chem. Soc.* **2003**, *125*, 2228–2240.
- [80] Berda, E. B.; Baughman, T. W.; Wagener, K. B. *J. Polym. Sci., Part A: Polym. Chem.* **2006**, *44*, 4981–4989.
- [81] Rojas, G.; Inci, B.; Wei, Y. Y.; Wagener, K. B. *J. Am. Chem. Soc.* **2009**, *131*, 17376–17386.

- [82] Qiu, W.; Sworen, J.; Pyda, M.; Nowak–Pyda, E.; Habenschuss, A.; Wagener, K. B.; Wunderlich, B. *Macromolecules* **2006**, *39*, 204–217.
- [83] Baughman, T. W.; Sworen, J. C.; Wagener, K. B. *Macromolecules* **2006**, *39*, 5028–5036.
- [84] Sworen, J. C.; Smith, J. A.; Berg, J. M.; Wagener, K. B. *J. Am. Chem. Soc.* **2004**, *126*, 11238–11246.
- [85] Schwendeman, J. E.; Wagener, K. B. *Macromol. Chem. Phys.* **2005**, *206*, 1461–1471.
- [86] Schwendeman, J. E.; Wagener, K. B. *Macromol. Chem. Phys.* **2009**, *210*, 1818–1833.
- [87] Zuluaga, F.; Inci, B.; Nozue, Y.; Hosoda, S.; Wagener, K. B. *Macromolecules* **2009**, *42*, 4953–4955.
- [88] Sworen, J. C.; Wagener, K. B. *Macromolecules* **2007**, *40*, 4414–4423.
- [89] Rojas, G.; Wagener, K. B. *Macromolecules* **2009**, *42*, 1934–1947.
- [90] Watson, M. D.; Wagener, K. B. *Macromolecules* **2000**, *33*, 8963–8970.
- [91] Valenti, D. J.; Wagener, K. B. *Macromolecules* **1998**, *31*, 2764–2773.
- [92] Alamo, R. G.; Jeon, K.; Smith, R. L.; Boz, E.; Wagener, K. B.; Bockstaller, M. R. *Macromolecules* **2008**, *41*, 7141–7151.
- [93] Baughman, T. W.; Chan, C. D.; Winey, K. I.; Wagener, K. B. *Macromolecules* **2007**, *40*, 6564–6571.
- [94] Lehman, S. E., Jr.; Wagener, K. B.; Baugh, L. S.; Rucker, S. P.; Schulz, D. N.; Varma–Nair, M.; Berluce, E. *Macromolecules* **2007**, *40*, 2643–2656.
- [95] Watson, M. D.; Wagener, K. B. *Macromolecules* **2000**, *33*, 5411–5417.

- [96] Baughman, T. W.; van der Aa, E.; Wagener, K. B. *Macromolecules* **2006**, *39*, 7015–7021.
- [97] Berda, E. B.; Lande, R. E.; Wagener, K. B. *Macromolecules* **2007**, *40*, 8547–8552.
- [98] Berda, E. B.; Wagener, K. B. *Macromol. Chem. Phys.* **2008**, *209*, 1601–1611.
- [99] Berda, E. B.; Wagener, K. B. *Macromolecules* **2008**, *41*, 5116–5122.
- [100] Opper, K. L.; Fassbender, B.; Brunklaus, G.; Spiess, H. W.; Wagener, K. B. *Macromolecules* **2009**, *42*, 4407–4409.
- [101] Opper, K. L.; Wagener, K. B. *Macromol. Rapid. Commun.* **2009**, *30*, 915–919.
- [102] Boz, E.; Nemeth, A. J.; Wagener, K. B.; Jeon, K.; Smith, R.; Nazirov, F.; Bockstaller, M. R.; Alamo, R. G. *Macromolecules* **2008**, *41*, 1647–1653.
- [103] Aitken, B. S.; Lee, M.; Hunley, M. T.; Gibson, H. W.; Wagener, K. B. *Macromolecules* **2010**, *43*, 1699–1701.
- [104] Leonard, J. K.; Turek, D.; Sloan, K. B.; Wagener, K. B. *Macromol. Chem. Phys.* **2010**, *211*, 154–165.
- [105] Odian, G., *Principles of Polymerization*. 4th ed.; Wiley: Chichester, New York, 2004; p 812.
- [106] Hiemenz, P. C.; Lodge, T. P., *Polymer Chemistry*. 2nd ed.; CRC Press: Boca Raton, 2007.
- [107] Wu, Z.; Grubbs, R. H. *Macromolecules* **1994**, *27*, 6700–6703.
- [108] Fraser, C.; Hillmyer, M. A.; Gutierrez, E.; Grubbs, R. H. *Macromolecules* **1995**, *28*, 7256–7261.



- [109] Hillmyer, M. A.; Laredo, W. R.; Grubbs, R. H. *Macromolecules* **1995**, *28*, 6311–6316.
- [110] Stephens, C. H.; Yang, H.; Islam, M.; Chum, S. P.; Rowan, S. J.; Hiltner, A.; Baer, E. *J. Polym. Sci., Part B: Polym. Phys.* **2003**, *41*, 2062–2070.
- [111] Yang, H.; Islam, M.; Budde, C.; Rowan, S. J. *J. Polym. Sci., Part A: Polym. Chem.* **2003**, *41*, 2107–2116.
- [112] Kobayashi, S.; Macosko, C. W.; Hillmyer, M. A. *Aust. J. Chem.* **2010**, *63*, 1201–1209.
- [113] Kobayashi, S.; Pitet, L. M.; Hillmyer, M. A. *J. Am. Chem. Soc.* **2011**, *133*, 5794–5797.
- [114] Binder, W. H.; Kurzhals, S.; Pulamagatta, B.; Decker, U.; Manohar Pawar, G.; Wang, D.; Kühnel, C.; Buchmeiser, M. R. *Macromolecules* **2008**, *41*, 8405–8412.
- [115] Dounis, P.; Feast, W. J. *Polymer* **1996**, *37*, 2547–2554.
- [116] Trzaska, S. T.; Lee, L.-B. W.; Register, R. A. *Macromolecules* **2000**, *33*, 9215–9221.
- [117] Myers, S. B.; Register, R. A. *Polymer* **2008**, *49*, 877–882.
- [118] Naga, N.; Kikuchi, G.; Toyota, A. *Polymer* **2006**, *47*, 6081–6090.
- [119] Simon, Y. C.; Coughlin, E. B. *J. Polym. Sci., Part A: Polym. Chem.* **2010**, *48*, 2557–2563.
- [120] Liaw, D. J.; Wu, P. L. *J. Mol. Catal. A-Chem.* **2000**, *160*, 35–43.
- [121] Myers, S. B.; Register, R. A. *Macromolecules* **2008**, *41*, 6773–6779.
- [122] Myers, S. B.; Register, R. A. *Macromolecules* **2009**, *42*, 6665–6670.

- [123] Radano, C. P.; Scherman, O. A.; Stingelin–Stutzmann, N.; Mueller, C.; Breiby, D. W.; Smith, P.; Janssen, R. A. J.; Meijer, E. W. *J. Am. Chem. Soc.* **2005**, *127*, 12502–12503.
- [124] Switek, K. A.; Chang, K.; Bates, F. S.; Hillmyer, M. A. *J. Polym. Sci., Part A: Polym. Chem.* **2006**, *45*, 361–373.
- [125] Myers, S. B.; Register, R. A. *Macromolecules* **2008**, *41*, 5283–5288.
- [126] Bielawski, C. W.; Louie, J.; Grubbs, R. H. *J. Am. Chem. Soc.* **2000**, *122*, 12872–12873.
- [127] Milner, S. T. *Macromolecules* **1994**, *27*, 2333–2335.
- [128] Matsen, M. W.; Gardiner, J. M. *J. Chem. Phys.* **2000**, *113*, 1673–1676.
- [129] Zhu, Y.; Gido, S. P.; Moshakou, M.; Iatrou, H.; Hadjichristidis, N.; Park, S.; Chang, T. *Macromolecules* **2003**, *36*, 5719–5724.
- [130] Pitet, L. M.; Chamberlain, B. M.; Hauser, A. W.; Hillmyer, M. A. *Macromolecules* **2010**, *43*, 8018–8025.
- [131] Pitet, L. M.; Hillmyer, M. A. *Macromolecules* **2009**, *42*, 3674–3680.
- [132] Bielawski, C. W.; Scherman, O. A.; Grubbs, R. H. *Polymer* **2001**, *42*, 4939–4945.
- [133] Hillmyer, M. A.; Nguyen, S. T.; Grubbs, R. H. *Macromolecules* **1997**, *30*, 718–721.
- [134] Witzke, D. R.; Kolstad, J. J.; Narayan, R. *Macromolecules* **1997**, *30*, 7075–7085.
- [135] Wunderlich, B.; Dole, M. *Journal of Polymer Science* **1957**, *24*, 201–213.
- [136] Schmidt, S. C.; Hillmyer, M. A. *Macromolecules* **1999**, *32*, 4794–4801.

- 
- [137] Castillo, R. V.; Muller, A. J.; Lin, M.-C.; Chen, H.-L.; Jeng, U. S.; Hillmyer, M. A. *Macromolecules* **2008**, *41*, 6154–6164.
- [138] Fetters, L. J.; Lohse, D. J.; Richter, D.; Witten, T. A.; Zirkel, A. *Macromolecules* **1994**, *27*, 4639–4647.
- [139] Widin, J. M.; Schmitt, A. K.; Im, K.; Schmitt, A. L.; Mahanthappa, M. K. *Macromolecules* **2010**, *43*, 7913–7915.
- [140] Ellison, C. J.; Meuler, A. J.; Qin, J.; Evans, C. M.; Wolf, L. M.; Bates, F. S. *J. Phys. Chem. B* **2009**, *113*, 3726–3737.
- [141] Teubner, M.; Strey, R. *J. Chem. Phys.* **1987**, *87*, 3195.
- [142] Brunauer, S.; Deming, L. S.; Deming, W. E.; Teller, E. *J. Am. Chem. Soc.* **1940**, *62*, 1723–1732.
- [143] Barrett, E. P.; Joyner, L. G.; Halenda, P. P. *J. Am. Chem. Soc.* **1951**, *73*, 373–380.
- [144] Brunauer, S.; Emmett, P. H.; Teller, E. *J. Am. Chem. Soc.* **1938**, *60*, 309–319.

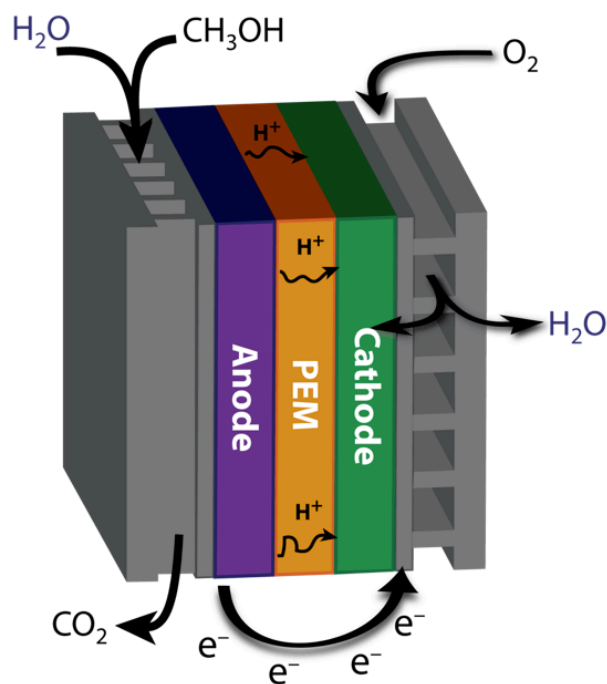
## Chapter 5

### Linear Polyethylene Copolymers from Sequential ROMP

Block copolymers with AB diblock architecture were prepared by sequential ring-opening metathesis polymerization of two cyclic olefins catalyzed by the 3-bromopyridine ligated Grubbs catalyst. The relatively slow polymerization of 3-phenylcyclooct-1-ene was conducted followed by the fast polymerization of unsubstituted *cis*-cyclooctene. In contrast, simultaneous polymerization of the two monomers provides copolymers with essentially statistical monomer distribution owing to extensive chain transfer. The architectural variance between the materials from simultaneous and sequential polymerizations is reflected by the thermal and molecular characteristics. The resulting poly(3-phenylcyclooctene-*block*-cyclooctene) diblock copolymers were subjected to hydrogenation to selectively saturate the backbone alkenes, leaving the pendent aryl substituents for further functionalization. The aryl side chains were sulfonated to various extents, after which the stress-strain behavior was evaluated to reveal tough materials owing to the high molecular weight, highly entangled linear polyethylene component. These materials are promising models for anion exchange membranes in which the ion exchange capacity can be tailored with the phenyl composition and sulfonation reaction and the saturated backbone offers flexibility, strength, and resistance to chemical corrosion.

## 5.1 Introduction

Polymer electrolyte membranes (PEM) play crucial roles in typical proton exchange fuel cells and other emerging technologies that are focused on improving efficiency and durability of power sources.<sup>1-5</sup> The PEM separates the anode and cathode of the cell and facilitates transport of protons generated by oxidation of the fuel (e.g., methanol) at the anode to the cathode, at which point reduction of oxygen occurs.<sup>6</sup> The electrons generated during MeOH oxidation can be used to power portable electronic devices (Figure 5.1). The extraordinary opportunity offered by MeOH fuel cells derives from the potential for enhanced efficiency and high energy density, and the renewability of the fuel source, contrasting conventional fossil fuel alternatives.<sup>7,8</sup>

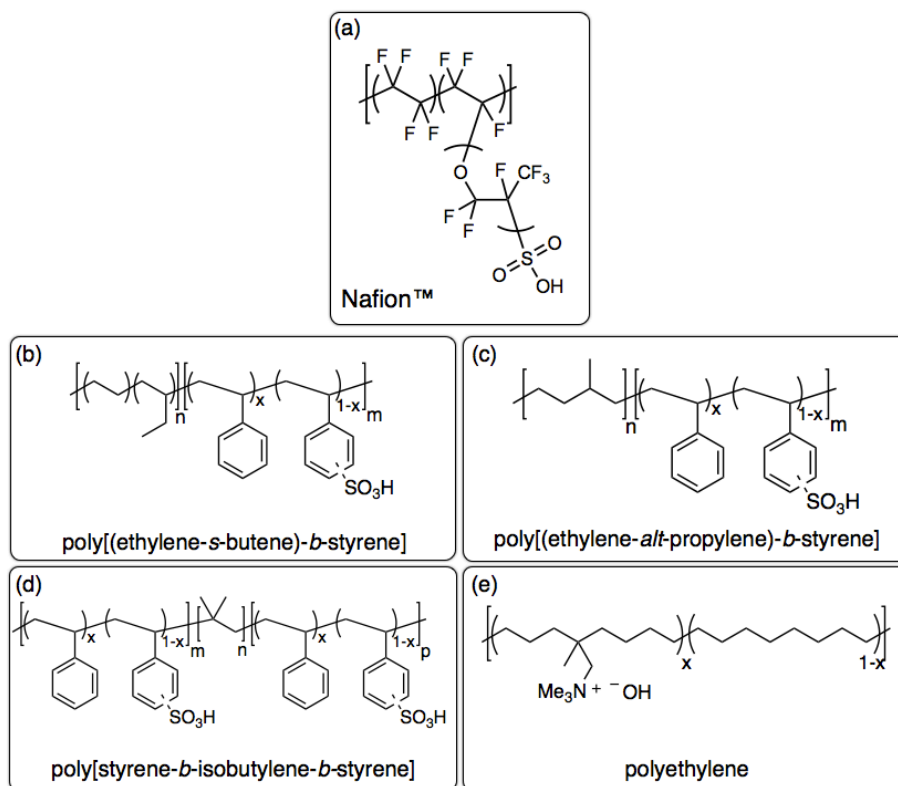


**Figure 5.1**

Illustration of methanol fuel cell membrane.

PEMs are conventionally composed of a hydrophilic component and a hydrophilic component, the latter of which forms channels through which ions can travel. Transport behavior has been observed to depend on the size and arrangement of the channels. The exact relationship between morphologies of the hybrid PEMs and conductivity has only recently been systematically explored.<sup>9–12</sup> Nonetheless, PEM requires an interpenetrating component that can accommodate ion transport; Nafion, which is the current industry standard, fulfills that demand. Nafion consists of a perfluorinated polyolefin backbone having pendant sulfonate groups (Figure 5.2a).<sup>11</sup> The sulfonate density can be modulated to tailor the ion-exchange capacity (IEC). Nafion suffers, however, from high cost and high methanol crossover, which causes short circuits.<sup>13</sup>

Block copolymers have emerged as promising candidates for fuel-cell membranes and, more generically, proton-exchange membranes.<sup>14</sup> The reasons for the strong potential are two-fold: (1) availability of many monomers and controlled polymerization techniques, which are readily combined in tandem (see Chapter 1), grants access to nearly limitless tuneability of chemical properties and (2) the unique self-assembly of block copolymer into nanoscale secondary structures grants impressive chemical (and ionic) transport phenomena. Block copolymers containing a hydrophobic polyolefin block and sulfonated styrenyl block have shown particular promise because of the ease with which they are accessible with conventional polymerization techniques.<sup>15</sup> The sulfonated polystyrene offers a straightforward way to tailor the IEC and are less prone to methanol crossover than Nafion.<sup>16</sup>

**Figure 5.2**

Chemical structures of Nafion and block copolymers with polyolefin blocks and sulfonated styrene blocks from references (b) 17, (c) 12, (d) 18, and (e) 19.

Several promising examples of PEMs having polyolefin blocks or sulfonated polystyrenyl blocks or both have recently emerged. One such example employed poly[(ethylene-*s*-butene)-*b*-styrene]<sup>\*</sup>, with the first block derived from hydrogenated 1,4-polybutadiene and the second block being sulfonated in a post-polymerization reaction to promote conductivity (Figure 5.2a).<sup>17</sup> Another example described a similar structure of poly[(ethylene-*alt*-propylene)-*b*-styrene] from hydrogenation of polyisoprene prepared by anionic polymerization; sulfonation of the polystyrene block rendered the materials conductive (Figure 5.2c).<sup>12</sup> Yet another example used a symmetric triblock architecture and poly(isobutylene) as the aliphatic hydrocarbon component (Figure 5.2d).<sup>18</sup> An example pertinent to the

\* The naming scheme of copolymers uses "*s*" to imply statistical copolymer, "*alt*" to imply perfectly alternating copolymer, and "*b*" to imply block copolymer.

work described here involves the ring-opening metathesis copolymerization of an ionic trimethylammonium substituted cyclooctene and unsubstituted *cis*-cyclooctene, followed by hydrogenation to give a linear polyethylene with statistical distribution of ionic groups (Figure 5.2e).<sup>19</sup> These polymers were mechanically robust and had adequate conductivity despite the essentially random distribution of hydrophilic pendent groups.

This chapter describes a novel synthetic approach to block copolymers that contain both a component having tunable ionic character and linear polyethylene (LPE). The LPE serves to enhance the strength, durability, and flexibility in the polymer, and offers robust resistance to chemical corrosion in a potentially caustic environment. Additionally, the thermal properties of LPE, owing to its semi-crystalline nature and relatively high melting temperature ( $T_{m,E}$ ), offer an attractive vantage point from the perspective of fuel cells that require high temperatures.<sup>20</sup> The second block contains a hydrocarbon backbone having aryl substituents; the phenyl rings may be rendered ionic by sulfonation in a controlled manner.<sup>21</sup>

Ring-opening metathesis polymerization is an indispensable tool for making complex, multicomponent block copolymers with great precision. The living nature of polymerization using the highly active Ru-centered Grubbs catalyst derivatives allows multiple monomers to be sequentially polymerized to form discrete, chemically distinct blocks.<sup>22</sup> Based on the isodesmic nature of the ROMP reactions, the resulting double bonds in the backbone are also prone to metathesize. It follows that extensive chain transfer accompanies certain conditions, and randomization of the sequence distribution in a copolymer may occur. The extent to which the repeating unit sequences are redistributed depends largely on the steric environment around the double bond after ring-opening; less sterically encumbered backbones will undergo more secondary metathesis. Therefore, living polymerizations and block copolymers are most typically formed using bulk monomers like substituted norbornenes (Scheme 5.1).

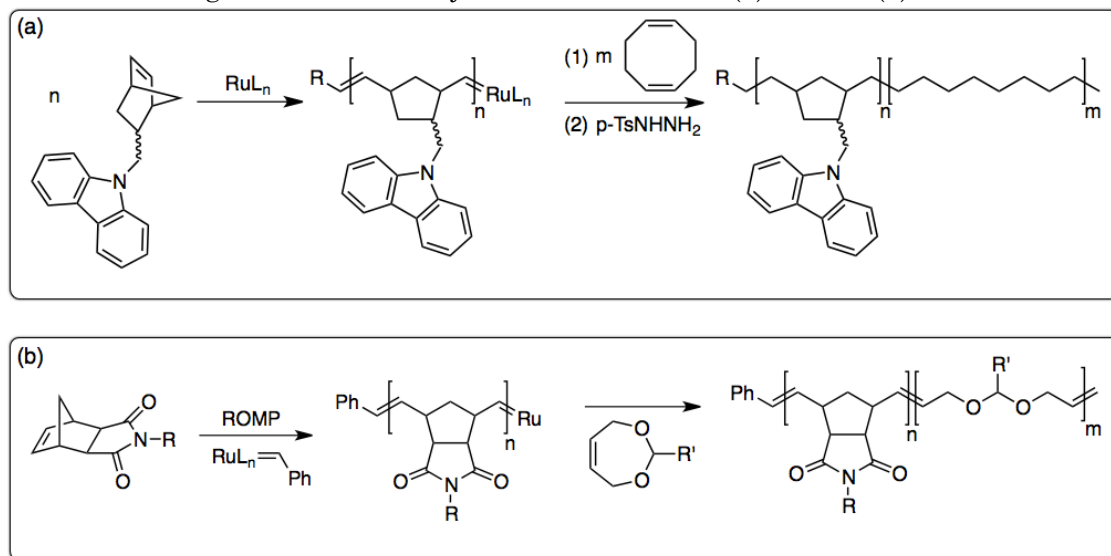
One strategy that has been employed to form block copolymers involves one bulky monomer (hindered cross-metathesis) and one less encumbered monomer



(extensive cross-metathesis). The carefully chosen sequence of polymerization must be in that particular order, such that the second monomer polymerizes very quickly and undergoes cross-metathesis during polymerization with a preference for itself as opposed to the first bulky monomer.<sup>23</sup> For example, cyclooctene and cyclooctadiene are both consumed very quickly but undergo substantial cross metathesis during polymerization using conventional ruthenium catalysts, and therefore give polymers with relatively broad molecular weight distribution.<sup>24,25</sup> Several attempts to prepare blocky copolymers with these unhindered cyclic olefins have been successful, including the consecutive polymerization of a substituted norbornene derivative followed by 1,5-cyclooctadiene (Scheme 5.1a)<sup>26</sup> or sequential polymerization of *exo*-N-arylnorbornene-2,3-dicarboximides followed by dioxepine (Scheme 5.1b).<sup>27–29</sup>

**Scheme 5.1**

Synthesis of blocky copolymers by consecutive ROMP of different cyclic olefin derivatives using ruthenium catalysts from references (a) 26 and (b) 27–29.



## 5.2 Results and Discussion

The synthesis of block copolymers from sequential polymerization of two monomers by ROMP is described in this chapter. Using the 3-bromopyridine ligated derivative of the ruthenium-centered Grubbs catalyst (**G3**),<sup>30</sup> 3-phenylcyclooct-1-ene (3PC) is polymerized. After nearly complete monomer consumption, the second monomer *cis*-cyclooctene (COE) is added and nearly instantaneously consumed. The reaction is quenched with ethyl vinyl ether, and the polymer isolated by precipitation. The unsaturated diblock copolymer poly(3-phenylcyclooct-1-ene-*block*-cyclooctene) (poly(3PC-*b*-COE)) can be exposed to hydrogen in conjunction with a silica supported Platinum catalyst or by chemical hydrogenation with *p*-tosyl hydrazide to form a diblock copolymer containing a phenylsubstituted polyethylene hybrid block and a completely linear polyethylene block (*h*-poly(3PC-*b*-COE)). The aryl groups can be sulfonated to varying extents through nucleophilic aromatic substitution using the strong electrophile acetylsulfate. This provides ionic character, and the self-assembly of the block copolymers may contain ionic channels through which ion transport would potentially render the polymers proton exchange membranes. The sulfonation reaction is briefly explored in this chapter. The ultimate emphasis is placed on synthesis and the implications of the linear polyethylene block for strongly enhancing the toughness and chemical inertness in membranes that encounter inherently corrosive environments.

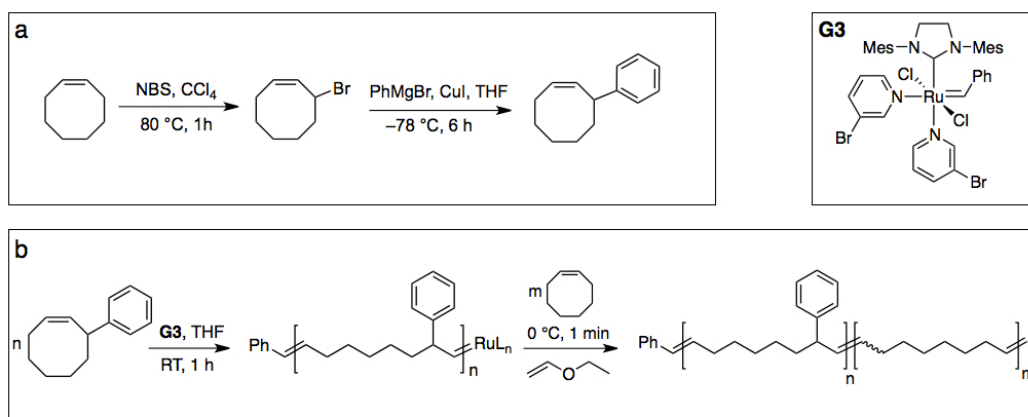
### 5.2.1 Synthesis and Molecular Characterization

To start, the 3-phenylcyclooct-1-ene (3PC) monomer was prepared by initially brominating *cis*-cyclooctene (COE) in the allyl position followed by CuI catalyzed Grignard substitution using phenyl magnesium bromide (Scheme 5.2a; see Experimental section for detailed explanation).<sup>31</sup> Unsaturated block copolymers are formed by sequential polymerization of two different monocyclic cyclooctenes; the first step involves ROMP of 3PC followed by polymerization of unsubstituted COE catalyzed by an N-heterocyclic carbene-coordinated ruthenium benzylidene

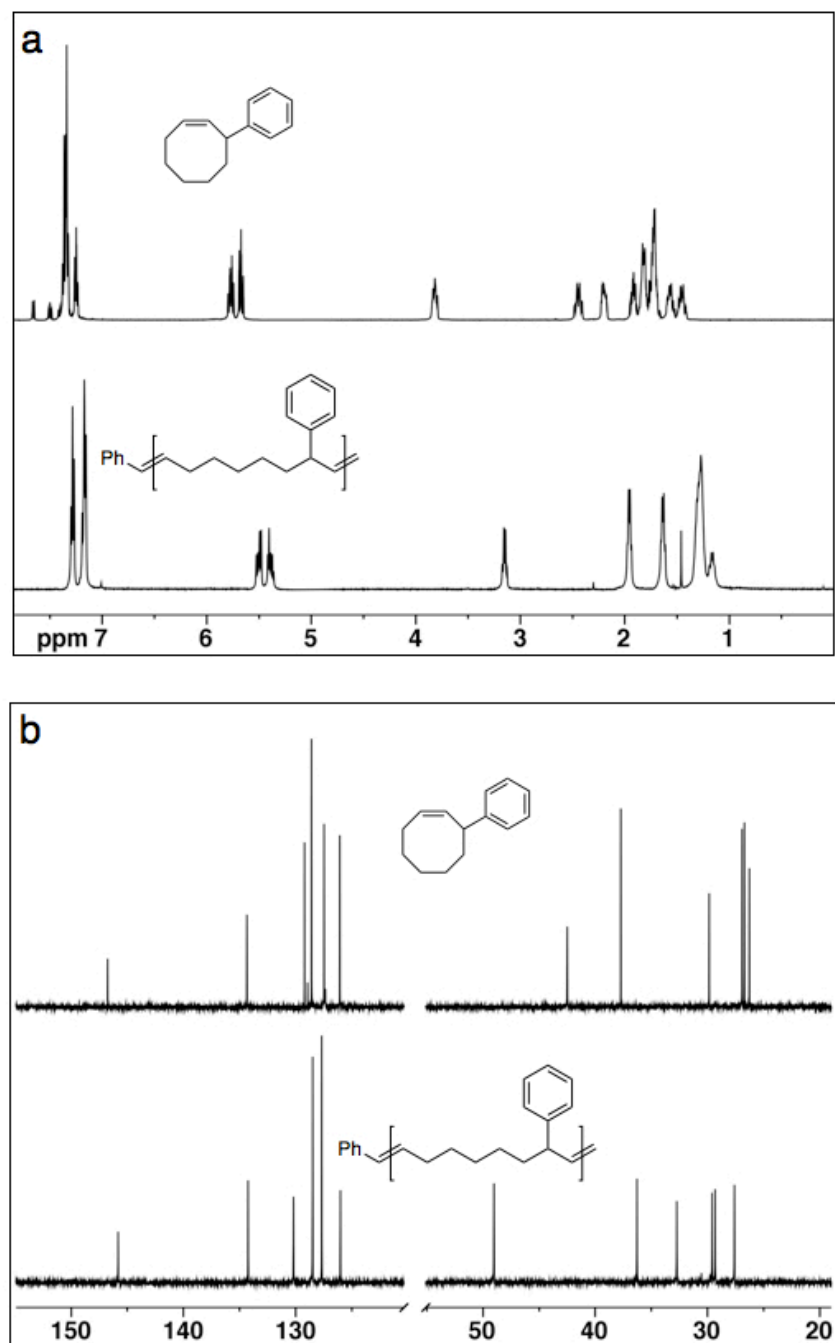
complex  $[(\text{H}_2\text{IMes})(3\text{-Br-py})_2(\text{Cl})_2\text{Ru}=\text{CHPh}]$  (**G3**) (Scheme 5.2b). The catalyst **G3** shows unprecedented initiation and propagation rates during metathesis, and as such is conducive to living polymerizations of certain strained and sterically obstructive cyclic olefins.<sup>30,32</sup>

### Scheme 5.2

Synthesis of (a) 3PC monomer starting from COE and (b) sequential polymerization of 3PC and COE monomers to form poly(3PC-*b*-COE) diblock copolymers.



The 3PC monomer was polymerized in THF at ambient temperature after initiation with **G3**. An aliquot was removed to analyze by <sup>1</sup>H and <sup>13</sup>C nuclear magnetic resonance (NMR) spectroscopy after precipitation in cold MeOH (Figure 5.3).

**Figure 5.3**

Measurement of (a)  $^1\text{H}$  NMR and (b)  $^{13}\text{C}$  NMR spectra for the monomer 3PC (*top*) and the resulting homopolymer poly(3PC) (*bottom*) from polymerization with **G3**.

Polymerization of 3PC catalyzed by **G3** appears to proceed in a regio- and stereo-specific manner.<sup>33</sup> This unprecedented observation during ROMP of substituted cyclooctene monomers having a disubstituted double bond manifests itself in the NMR spectra, IR spectra, and H–H correlated spectroscopy (COSY) (see experimental details). Briefly, the one-dimensional <sup>1</sup>H NMR spectrum of the polymer shows only two signals with 1:1 integration in the olefinic region corresponding to the alkenyl protons adjacent to the phenyl-substituted carbon and the unsubstituted carbon. The <sup>13</sup>C NMR spectrum of the monomer shows twelve discrete signals associated with the twelve distinct carbons (4 aromatic signals, 8 cyclooctene signals) in the asymmetric monomer. The polymer from ROMP with **G3** also contains merely 12 discrete signals. This alone suggests a highly regular polymerization with stereo- and regio-specificity during each metathesis reaction. There are two possible scenarios that would provide this regularity. The polymer either exhibits pure *cis* (*i.e.*, *Z*) or pure *trans* (*i.e.*, *E*) configuration, as suggested by the sole two olefinic signals at 146 and 134 ppm. With respect to regiospecificity, the two possible scenarios include perfectly head-to-tail (HT) or perfectly alternating head-to-head and tail-to-tail isomers (HH-*alt*-TT). Accurately elucidating the resulting microstructure requires further investigation by H–H COSY and IR spectroscopy. The H–H COSY spectra of the starting 3PC monomer and poly(3PC) are provided in Figure 5.4a and 5.4b, respectively.

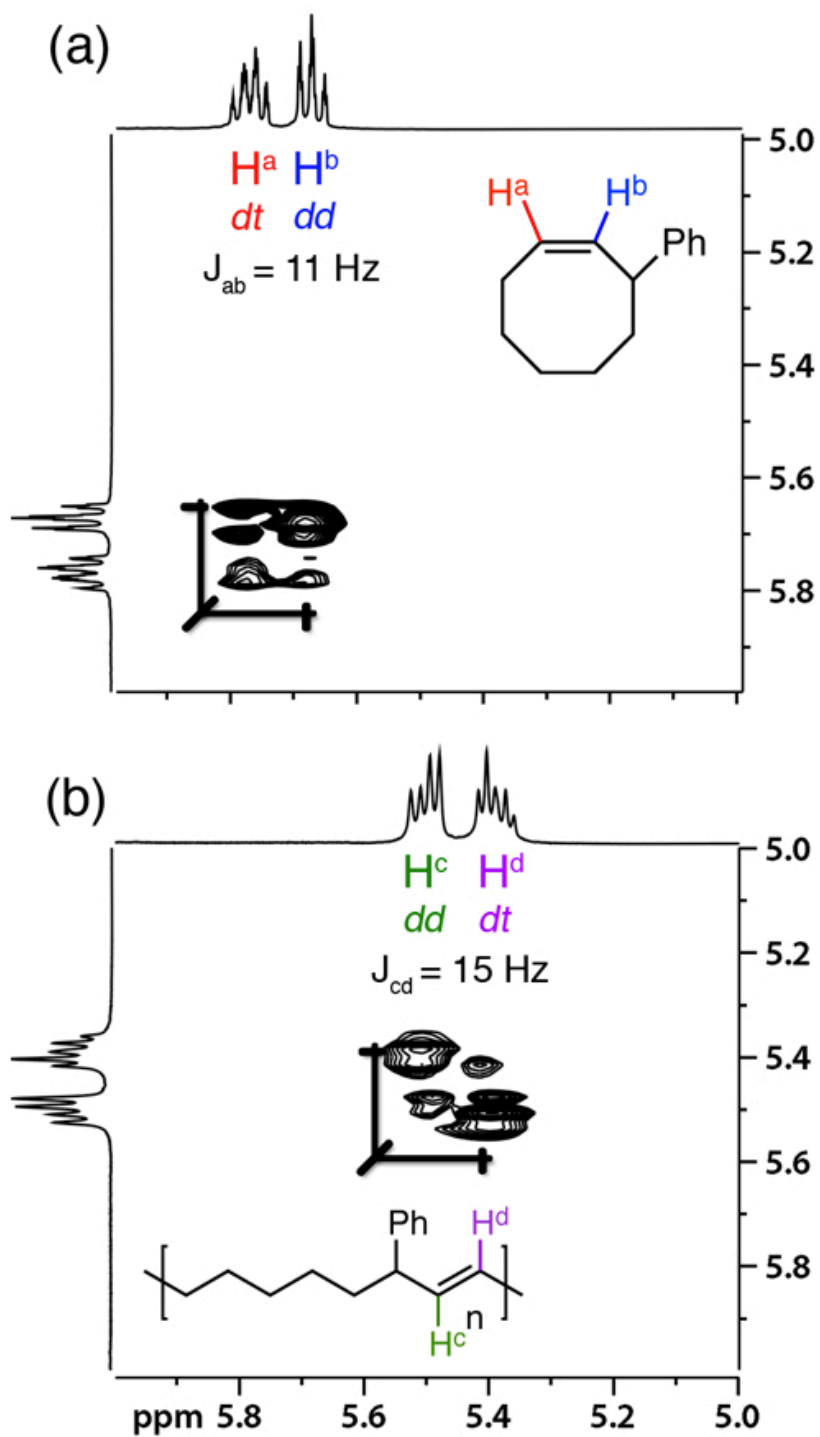


Figure 5.4.

H-H COSY spectra showing the olefinic region for (a) 3PC monomer and (b) poly(3PC) homopolymer.<sup>33</sup>

The monomer 3PC gives two olefinic signals, inherent to the asymmetric structure. The proton H<sup>b</sup> shows doublet of doublet of doublet of doublet (dddd) multiplicity with the largest coupling constant  $J_{ab} = 10.4$  Hz consistent with the *Z* configuration about the double bond as observed in the commercially available *cis*-cyclooctene starting material for the substituted monomer synthesis. This configuration is consistent with the product retaining the configuration of the starting unsubstituted COE. The olefin signals for the polymer, H<sup>c</sup> and H<sup>d</sup>, show doublet of doublet (dd) and doublet of triplet (dt) multiplicity at chemical shifts of 5.50 and 5.39 ppm, respectively. The olefinic coupling constant of these signals is  $J_{cd} = 15.2$  Hz, which is consistent with *E* configuration about the double bond. This configuration purportedly agrees with the preferred orientation of catalyst residue relative to monomer during ring-opening metathesis, which was ultimately illuminated by the stoichiometric metathesis reaction between **G2** and 3PC. The H–H COSY spectrum for poly3PC provides conclusive evidence for the scenario in which perfect HT regiospecificity predominates. The proton signals H<sup>c</sup> and H<sup>d</sup> are strongly coupled, which strongly suggests adjacency; the two signals that would hypothetically result from HH-*alt*-TT would not be correlated due to the relatively large spatial separation.

The polymerization of 3PC progresses relatively slowly at RT using the highly reactive **G3** catalyst relative to the unsubstituted COE analog. Polymerization was initially monitored by <sup>1</sup>H NMR spectroscopy in THF-*d*<sub>8</sub> at RT (Figure 5.5). Conversion was tracked by integration of the methine protons on the monomer and polymer at 5.72 and 3.20 ppm, respectively. Conversion *p* is calculated by comparing the integrals (concentrations) of polymer [P]<sub>t</sub> and monomer [M]<sub>t</sub> over time (eq 5.1). According to the rate equations for chain growth polymerization in which instantaneous initiation occurs in the absence of chain termination or transfer reactions (eq 5.2), a linear relationship between  $\ln [M]_0/[M]_t$  and time indicates a living polymerization.<sup>34</sup>

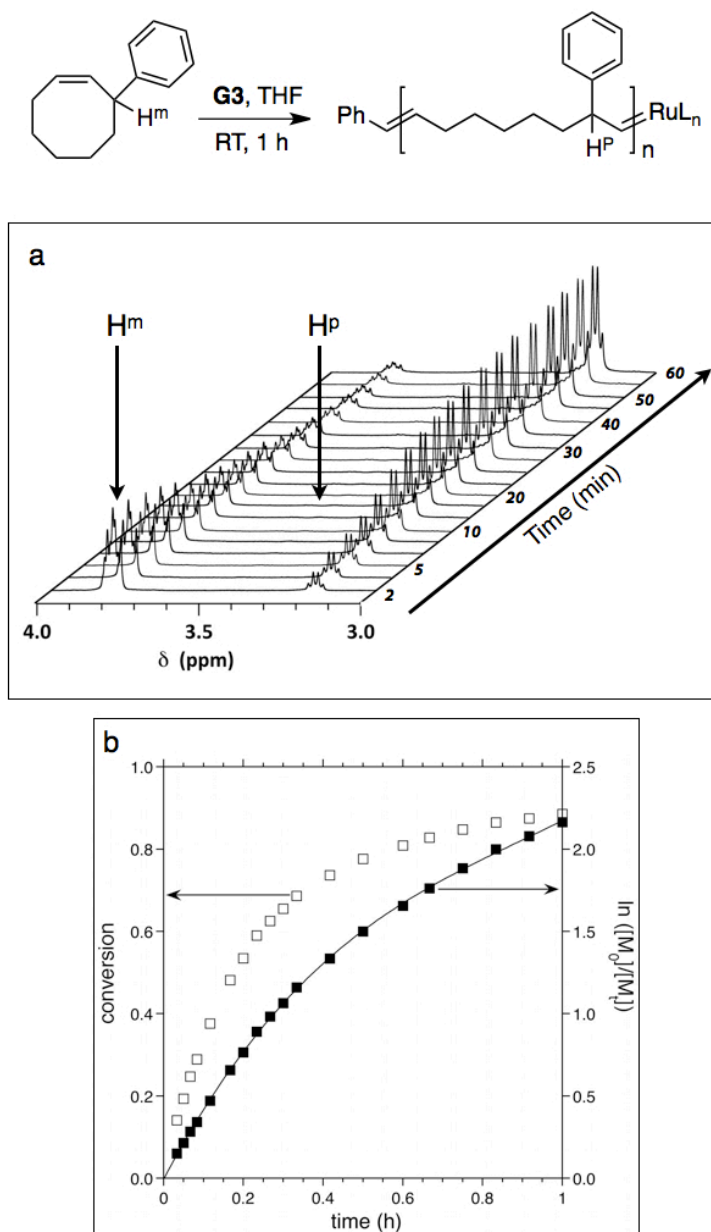
---

$$p = \frac{[P]_t}{[P]_t + [M]_t} = \frac{[P]_t}{[M]_0} = \frac{[M]_0 - [M]_t}{[M]_0} = 1 - \frac{[M]_t}{[M]_0} \quad (5.1)$$

$$R_p = -\frac{d[M]}{dt} = k_p[M][I]_0 \quad (5.2)$$

$$\ln \frac{[M]_0}{[M]_t} = k_p[I]_0 t \quad (5.3)$$



**Figure 5.5.**

ROM polymerization kinetics of 3PC monomer conversion to poly3PC at ambient temperature in THF-d<sub>8</sub>. (a) <sup>1</sup>H NMR spectrum tracking monomer consumption by methine protons on monomer (H<sup>M</sup>) and on polymer (H<sup>P</sup>). (b) Kinetic plot showing conversion and  $\ln([M_0]/[M_t])$  vs. time.

Figure 5.5a clearly exhibits the consumption of monomer as polymerization proceeds. Figure 5.5b shows monomer conversion on the left axis with respect to time (h), indicating that approximately 90% of monomer is consumed after 1 h. The conversion apparently begins to plateau at this time, and would presumably take significantly longer to reach near-quantitative consumption. The right axis shows  $\ln [M]_0/[M]_t$  vs time according to eq 5.3, with which the "livingness" of the polymerization is gauged. The data in Figure 5.5b is clearly not linear over the entire time scale. This suggests that either some of the catalyst/initiator is being deactivated or that chain transfer is occurring to some extent, or a combination of both. The slowing of monomer consumption becomes more pronounced after approximately 50% conversion. However, the deviation from linearity in Figure 5.5b is not extremely large, and not necessarily prohibitive to subsequent monomer addition in order to synthesize block copolymers. It is postulated that chain transfer via cross-metathesis influences the non-linearity in the plot to a greater extent than catalyst/initiator death. The purported ability to undergo chain transfer was explored by conducting a homopolymerization of 3PC in the presence of an acyclic chain transfer agent (CTA) 1,4-diacetoxy-2-butene (DAB). The incorporation of the acyclic CTA into the polymer chain is easily monitored by  $^1\text{H}$  NMR spectroscopy, in which the methylene end-group protons are adequately separated in chemical shift from the repeat unit signals and also chemically distinct from the starting materials.

The  $^1\text{H}$  NMR spectrum for the product from ROMP of 3PC in the presence of DAB is consistent with substantial chain transfer occurring. Allyl signals associated with chain-end groups with acetoxy identity are observed and consistent with signals from model compounds and previously reported acetoxy-telechelic polycycloolefins.

Intramolecular cross metathesis during polymerization manifests itself in the distribution of chain end functionalization; a small proportion of chains will be non-functional, having benzylidene chain termini from the initiator residue, while the same proportion of chains will contain active Ru chain termini. Upon subsequent monomer addition, this scenario will result in a mixture of homopolymer poly3PC,

diblock copolymer, and symmetric triblock copolymer assuming the absence of chain transfer in the second polymerization step. Based on the minimal deviation from linearity in the data provided in Figure 5.5b, it is postulated that the molar majority of species will be diblock copolymers.

The relatively spacious environment about the reactive olefinic bonds in cyclooctenes provides ample room for cross-metathesis in the polymeric backbone. Therefore extensive chain transfer typically occurs during polymerization with certain Ru-centered Grubbs catalysts, reflected in the molecular weight distribution.

Chain extension was performed to synthesize copolymers with a blocky structure from the pseudo-living polymerization solution containing poly3PC (Scheme 5.2b). After one hour of 3PC homopolymerization, the solution was cooled to  $\sim 5$  °C using an ice bath and the an amount of unsubstituted COE was added to the polymerization solution under an argon atmosphere. The amount of COE added was such to target a copolymer composition of 75 wt % PCOE/ 25 wt % poly3PC. The polymerization solution almost immediately (within 5 seconds) became extremely viscous to the point of being nearly solid. This behavior indicates very fast polymerization of COE using **G3** compared with the polymerization rate of 3PC. It is hypothesized that the extent of chain transfer among the poly(3PC) block within the time-frame of COE polymerization is minimal enough that the polymer structure contains predominantly segmented architecture associated with pristine diblock copolymers. Of course, extensive chain transfer within the PCOE block as COE polymerization proceeds is established for the Grubbs ruthenium-benzylidene catalyst systems having N-heterocyclic carbene ligands and presumably occurs in this chain extension process, leading to a broadened molecular weight distribution. Nevertheless, the architecture should be blocky, and the number average molecular weight should be proportional to the initial **G3** concentration.

Initially, two samples were prepared by the method described. **G3** was used as the initiator system, ultimately dictating the degree of polymerization ( $N_i$ ), assuming complete initiation, by eq 5.4.

$$N_{3PhCOE} = \frac{[3PhCOE]}{[G3]} \cdot x \quad (5.4)$$

$$N_{COE} = \frac{[COE]}{[G3]} \cdot x \quad (5.5)$$

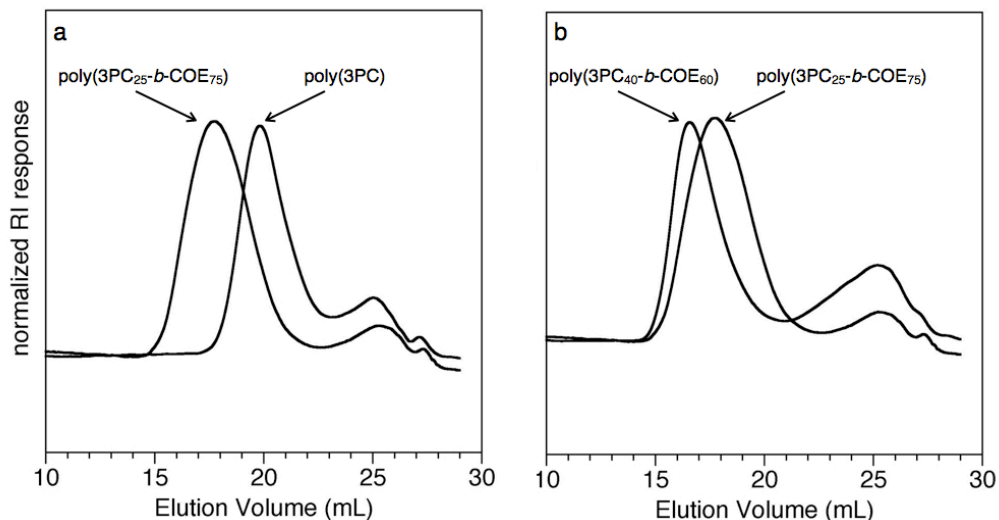
where  $N_{3PC}$  is the degree of polymerization of the first segment and  $x$  is the fractional conversion of monomer to polymer. The degree of polymerization of the second block is similarly calculated by substituting the concentration of COE (eq 5.5). The targeted degree of polymerization of the first block for the first sample was 170, while the targeted degree of polymerization of the second block was 780. These targets assume quantitative monomer consumption. This combination translates to a total degree of polymerization equal to 950 and targeted number average molar mass of 118 kg/mol. The sample had a targeted composition of 73 wt % PCOE (82 mol %). The second sample was produced with a larger targeted degree of polymerization and a higher fraction of poly(3PC). The targeted degree of polymerization for the poly(3PC) block was 950 and was 1600 for the PCOE block, giving a targeted composition of 50 wt % PCOE (63 mol %). These parameters are summarized in Table 5.1 along with the experimentally determined values using  $^1\text{H}$  NMR spectroscopy, as described subsequently. The samples are labeled in accordance with the approximate measured compositions by  $^1\text{H}$  NMR spectroscopy; the labels are poly(3PC $_x$ -*b*-COE $_y$ ), where  $x$  and  $y$  are the wt % of the respective blocks (*i.e.*,  $x + y = 100$ ).

**Table 5.1**

Molecular and composition targets and experimental values for poly(3PC-*b*-COE) block copolymers and the precursors.

Sample	$N_{\text{target}}$	Mn, target (kg mol <sup>-1</sup> )	target		experimental	
			$w_{3\text{PC}}$	$n_{3\text{PC}}$	$w_{3\text{PC}}$	$n_{3\text{PC}}$
poly(3PC)-170	170	31.6				
poly(3PC <sub>25</sub> - <i>b</i> -COE <sub>75</sub> )	950	117	0.269	0.179	0.241	0.158
fraction 1	950	117	0.269	0.179	0.227	0.148
poly(3PC)-950	950	176.7				
poly(3PC <sub>40</sub> - <i>b</i> -COE <sub>60</sub> )	1600	352.7	0.500	0.372	0.382	0.267

Analysis of the first poly(3PC) block by SEC and the resulting copolymer after chain extension shows a clear increase in molecular weight for the predominant polymer peak (Figure 5.6a). The SEC chromatograms for the two different block copolymer samples show the relative size and molecular weight distributions (Figure 5.6b).

**Figure 5.6**

Comparison of SEC chromatograms for (a) homopolymer poly(3PC) and the block copolymer after chain extension with COE polymerization to give poly(3PC<sub>25</sub>-*b*-COE<sub>75</sub>) and (b) two block copolymers poly(3PC<sub>25</sub>-*b*-COE<sub>75</sub>) and poly(3PC<sub>40</sub>-*b*-COE<sub>60</sub>).

Homopolymerization of 3PC leads to a signal in the SEC chromatogram with a main peak centered at 20 mL elution volume and a smaller peak eluting much later centered near 25 mL, indicating a substantial low molar mass portion. It is unclear from what process this stems. Purification of the polymers is addressed in a subsequent discussion. Nevertheless, upon addition of COE, chain extension is indicated by the clear shift to lower elution volume, consistent with increased molar mass. The larger breadth of the peak attributed to the block copolymer compared with the homopolymer suggests a larger molecular weight distribution, which could result from significant chain transfer during chain extension or homopolymer contamination from non-functional poly(3PC) (see previous discussion).

The compositions of the resulting block copolymers are determined by  $^1\text{H}$  NMR spectroscopy. The signals associated with the respective repeating units are easily demarcated and integrated to calculate weight and mole fractions (Figure 5.7).

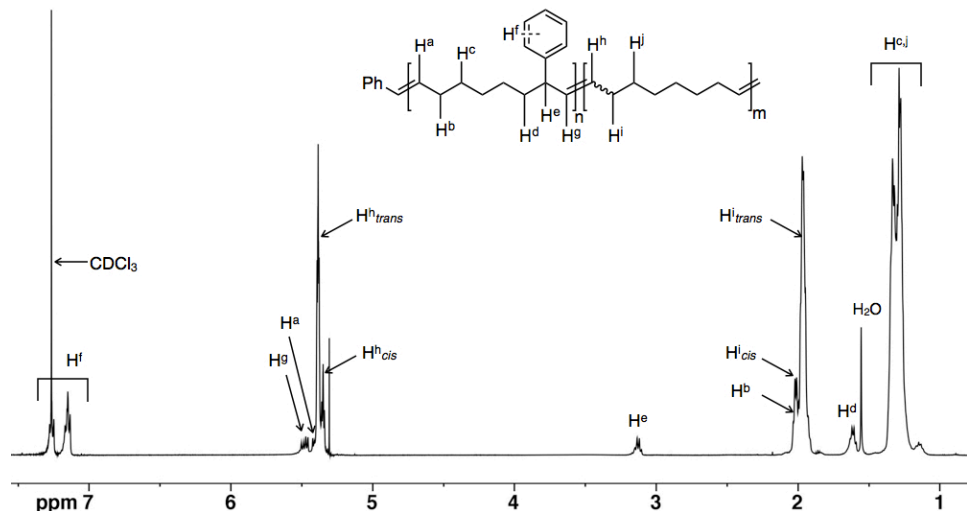


**Figure 5.7**

$^1\text{H}$  NMR spectrum for sample poly(3PC<sub>40</sub>-b-COE<sub>60</sub>) with detailed signal designations.

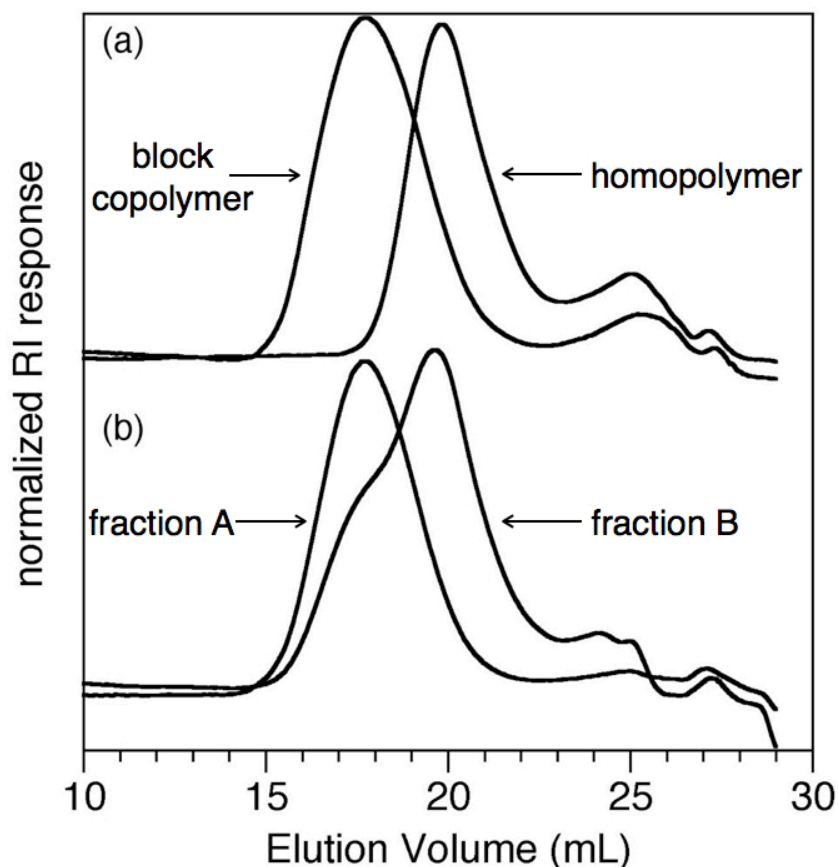
The two parent block copolymers originally synthesized by the sequential ROMP had 76 and 62 wt % PCOE, both slightly higher than originally targeted with the monomer feed compositions assuming quantitative monomer consumption (Figure



$^1\text{H}$  NMR spectroscopy provides tenable evidence for the presence of both poly(3PC) and PCOE segments after sequential polymerization, while providing an indispensable method for accurate composition measurement. However, the absence of any signals undeniably associated with protons at the block junction makes any absolute claims of a block architecture unsubstantiated from this analysis alone. The protons at the purported block juncture in this system would be chemically identical to those in the repeat units. The polymer samples may well contain mixtures of the two homopolymer species, or statistically distributed repeat units within copolymer chains. SEC analysis compels belief in the block copolymer architecture.

Evolution of molecular weight and evidence for the successful chain extension process to form block copolymers were initially gathered from size-exclusion chromatographic (SEC) analysis (Figure 5.9). Further purification was attempted in an effort to separate the low and high molecular weight fractions that appear in the original SEC chromatograms.



**Figure 5.9**

Size exclusion chromatograms for (a) homopolymer poly(3PC) and block copolymer after chain extension with COE to form poly(3PC-*b*-COE). SEC chromatograms for (b) fractionated block copolymer samples to remove low molar mass and non-functional poly(3PC) homopolymer contaminants, with fraction A being purified block copolymer, and fraction B being the second, low molar mass fraction.

The fractionation of poly(3PC<sub>25</sub>-*b*-COE<sub>75</sub>) was performed by dissolving the parent polymer in a good solvent (THF) and slowly adding a non-solvent (MeOH) until partial dissolution was observed visually. Upon a relatively small portion of MeOH addition (~ 5 % by volume), a majority of the polymer precipitated from solution. The polymer was removed by vacuum filtration and dried for analysis. A second fraction was taken by further addition of MeOH to the filtrate. The second recovery yielded only small portions of solid material (~ 5 wt % of the original mass). SEC analysis of the two fractions (Figure 5.9b) illustrates the successful purification of the high molecular weight fraction that constitutes the block

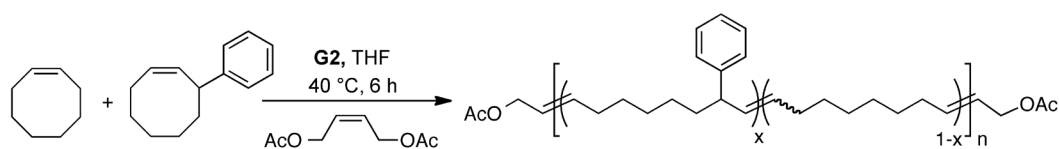
copolymer. Removal of low molar mass contaminants that previously eluted at 25 mL is nearly quantitative. Additionally, removal of homopolymer poly(3PC) contaminant appears to have been accomplished, with the second fraction containing polymeric species eluting nearly identically to the parent homopolymer. The second, low molar mass fraction also apparently contains some block copolymer, evidenced from the broad shoulder toward low elution volume. The RI signals are normalized, and thus do not represent weight fractions. The small mass recovery in the second fraction suggests that the chain extension process is effective in preparing relatively well-resolved block copolymer samples by exploiting the disparate polymerization kinetics between sterically hindered and sterically free monomers. The composition of the two fractions measured by  $^1\text{H}$  NMR spectroscopy indicate a slight dilution of the poly(3PC) in fraction A compared with the parent material (see Table 5.1). The weight fraction of PCOE in the parent was originally 0.76; fraction A contained a weight fraction of PCOE equal to 0.77. This is within the error associated with the measurement; it is possible that slight poly(3PC) dilution occurred, but the parent and first fraction essentially contain the same amount of each component.

The physical behavior of the block copolymers is important for determining the effect of composition and molecular architecture on certain properties. For example, self-assembly, thermal properties, and mechanical characteristics are all crucial parameters to control for applications in ion exchange membranes (see section 5.1, Introduction). Before exhaustive hydrogenation to prepare linear polyethylene components from the two block copolymers, two additional samples were prepared in which the simultaneous polymerization of COE and 3PC leads to statistically distributed repeat unit sequences (Scheme 5.3). The same compositions as contained in the block copolymers were targeted. A chain transfer agent was added to restrict the average chain length and further gauge the efficacy of chain transfer with the linear, trans configured poly(3PC) segments. The second generation derivative of Grubbs catalyst was used [Benzylidene[1,3-bis(2,4,6-trimethylphenyl)-2-imidazolidinylidene] dichloro (tricyclohexylphosphine) ruthenium, **G2**] because of its ready availability; the faster initiation rate touted

with the **G3** is irrelevant when the CTA is being used for chain length control. The activity of **G2** and **G3** are comparable during polymerization due to the identical propagating residue after dissociation of the tricyclohexylphosphinyl or 3-bromopyridinyl ligands, respectively.

### Scheme 5.3.

Synthesis of statistical copolymers poly(3PC-*s*-COE) from simultaneous ROMP of 3PC and COE monomers in the presence of CTA *cis*-1,4-diacetoxy-2-butene.



Adjusting the monomer feed concentration allows control of the compositions in the copolymers ( $x$  = mole fraction of 3PC); quantitative monomer consumption is assumed. Two samples were prepared by adding DAB with a given molar ratio to target  $N_{\text{total}} = ([3\text{PC}] + [\text{COE}]) / [\text{DAB}] = 500/1$ . The catalyst **G2** was added with the molar ratio  $([3\text{PC}] + [\text{COE}]) / [\text{DAB}] / [\text{G2}] = 10800/22/1$ . Table 5.2 contains the targeted and experimental molecular characteristics as measured by  $^1\text{H}$  NMR spectroscopy (Figure 5.10).

**Table 5.2**

Molecular characteristics of statistical copolymers poly(3PC-*s*-COE)

Sample	target			experimental		
	$N^a$	WPCOE	mPCOE	$N^b$	WPCOE	mPCOE
poly(3PC <sub>25</sub> - <i>s</i> -COE <sub>75</sub> )	500	0.75	0.84	484	0.76	0.84
poly(3PC <sub>40</sub> - <i>s</i> -COE <sub>60</sub> )	500	0.60	0.72	491	0.59	0.71

<sup>a</sup> Calculated assuming quantitative monomer consumption, and taking the respective repeating units associated with the monomers. <sup>b</sup> Measured by  $^1\text{H}$  NMR spectroscopy by comparing the integral ratios between the end groups and repeating units.



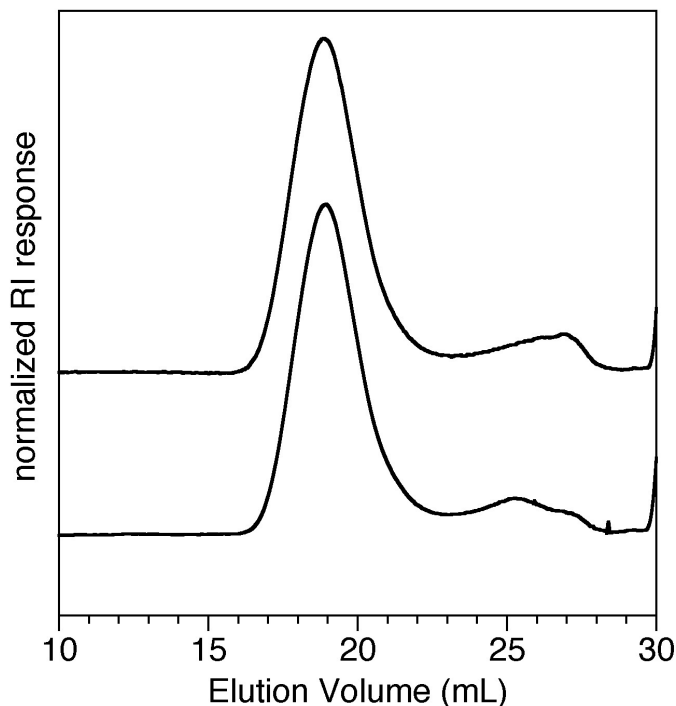


**Figure 5.11**

Comparison of SEC chromatograms for simultaneous polymerization of 3PC and COE to give statistical copolymers poly(3PC<sub>25</sub>-s-COE<sub>75</sub>) (*top*) and poly(3PC<sub>40</sub>-s-COE<sub>60</sub>) (*bottom*).

The four different copolymers were analyzed for secondary structural features before rendering them saturated. Thermal characteristics can provide both an indication of molecular architecture (*i.e.*, sequence distribution – triblock *vs.* statistical), but also give definitive information on thermal range in which the polymers may be useful. The crystallographic information also provides a wealth of information related to morphology formation (see Chapter 4). PCOE is a semicrystalline polymer under ambient conditions with a melting temperature near 50 °C.<sup>35</sup> The sequence length strongly influences the capacity to organize onto a crystalline lattice, and the purported architectures should have noticeable contrast in thermal characteristics. Differential scanning calorimetry (DSC) was used initially to investigate the thermal characteristics (Figure 5.12). The thermograms provide information on important thermal transitions like melting temperature ( $T_m$ ) and glass transition temperature ( $T_g$ ) for the copolymers and the relevant homopolymer samples.

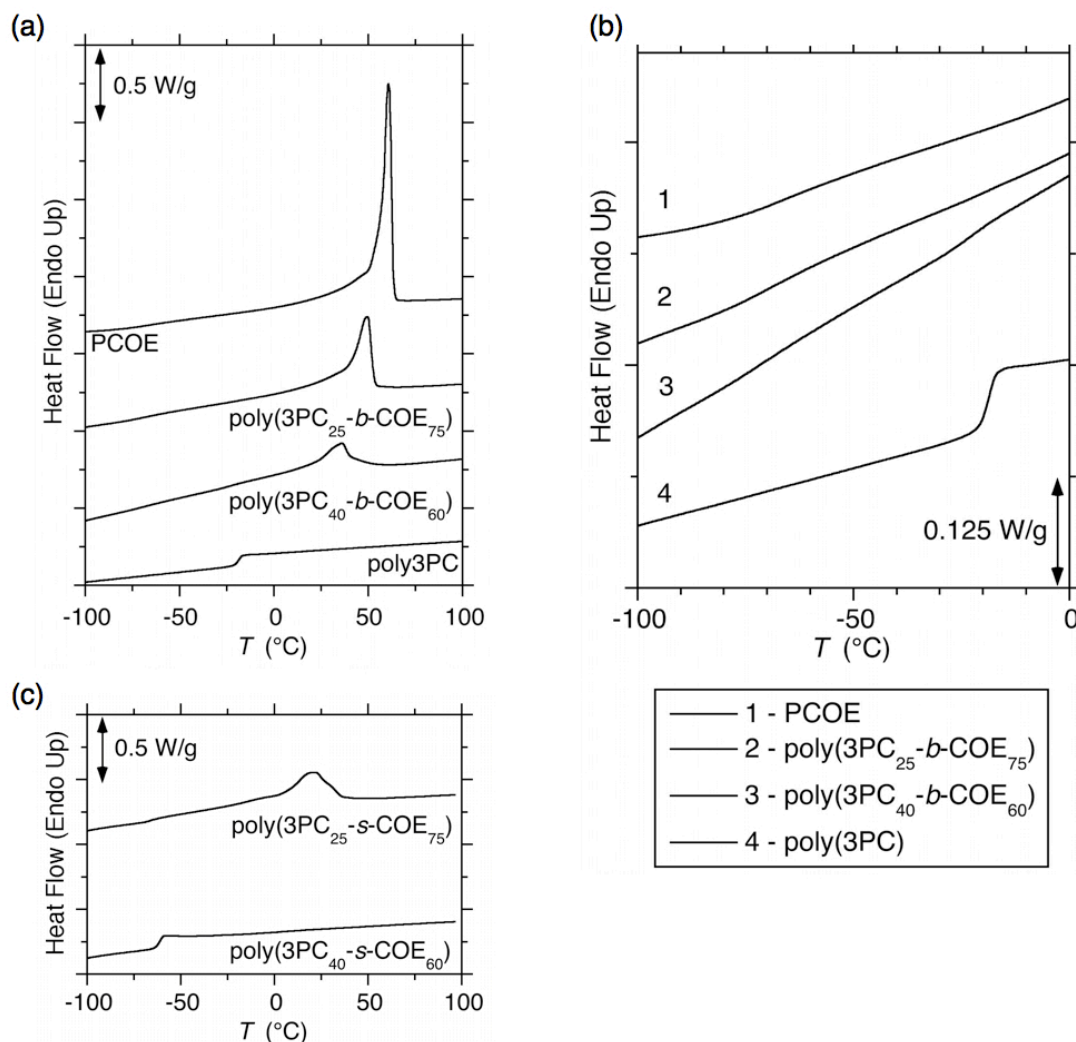


**Figure 5.12**

DSC thermograms for (a) full temperature range (–100 to 100 °C) of PCOE homopolymer, poly(3PC-*b*-COE)s and poly(3PC) homopolymer and (b) magnified heat flow for temperature range –100 to 0 °C to accentuate the  $T_g$ s and DSC thermograms for (c) full temperature range poly(3PC-*s*-COE)s.

The homopolymer PCOE ( $M_n = 50 \text{ kg mol}^{-1}$ ; PDI = 1.8) prepared by ROMP shows a melting transition with  $T_m$  at the maximum of the endothermic peak equal to 58 °C and a melting enthalpy ( $\Delta H_m$ ) of 69 J g<sup>–1</sup>, from which the extent of crystallinity is calculated to be 32 % ( $\Delta H_m^0 = 216 \text{ J g}^{-1}$ ).<sup>36</sup> A weak glass transition is observed for the PCOE homopolymer near –70 °C (Figure 5.12b). Homopolymer

poly(3PC) in contrast lacks crystallinity as a result of the bulky aryl substituents. Poly(3PC) is completely amorphous with a sticky, liquid like consistency at ambient temperature owing to the low  $T_g$  ( $-20$  °C; Figure 5.12b). The block copolymer poly(3PC<sub>25</sub>-*b*-COE<sub>75</sub>) likewise shows a strong melting endotherm with  $T_m = 51$  °C and a weak  $T_g = -69$  °C. This slightly depressed  $T_m$  compared with the PCOE is typical of block copolymers exhibiting microphase separation in the melt. Likewise, the fact that the  $T_g$  occurs very closely to the PCOE further suggests a microphase separated structure. Microphase separation is expected in samples with long segments of different, incompatible components (i.e., block copolymers), lending credence to the purported block architecture suggested by the molecular characteristics outlined previously. The crystallinity of the poly(3PC<sub>25</sub>-*b*-COE<sub>75</sub>) is calculated as 27% ( $\Delta H_m = 43.4$  J g<sup>-1</sup>;  $w_{PCOE} = 0.76$ ), commensurate with a block architecture with only slightly less crystallinity within the majority PCOE matrix compared with pristine homopolymer. Similarly, the sample poly(3PC<sub>40</sub>-*b*-COE<sub>60</sub>) shows a melting endotherm centered at 35.4 °C. This value is substantially lower than pristine PCOE; however, the crystallinity is nevertheless indicative of significantly long segments of PCOE that pack onto an ordered lattice and suggests a blocky structure. The melting endotherm had an enthalpy  $\Delta H_m$  of 16.1 J g<sup>-1</sup>, corresponding to a crystallinity within the PCOE block of 12.4%. The thermal characteristics of the block copolymers contrast starkly with those associated with the statistical copolymers (Figure 5.12c). The statistical copolymer poly(3PC<sub>25</sub>-*s*-COE<sub>75</sub>) does exhibit a small degree of crystallinity with a melting temperature  $T_m = 21.8$  °C and melting enthalpy  $\Delta H_m$  of 19.9 J g<sup>-1</sup> corresponding to a crystallinity of 12.3%. The degree of crystallinity and  $T_m$  are substantially lower than the corresponding block copolymer having essentially equal composition.

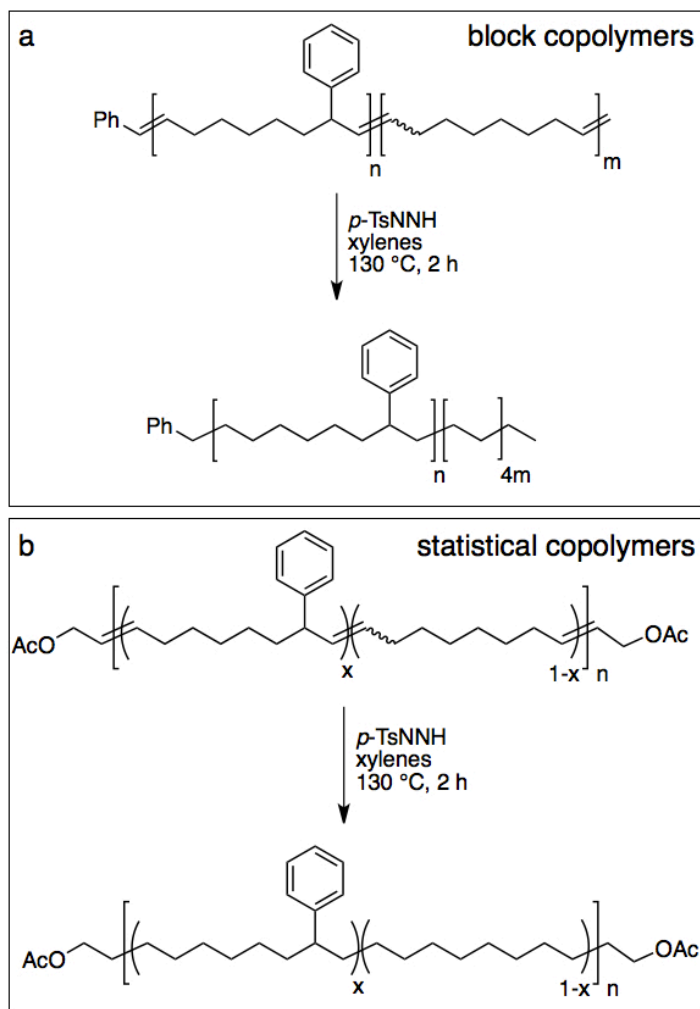
## 5.2.2 Hydrogenation of Copolymers

The four copolymers were saturated by chemical hydrogenation using *p*-tosylhydrazide (*p*-TsNHNH<sub>2</sub>) in xylenes at 130 °C (Scheme 5.4). The chemical

hydrogenation is known to saturate alkenyl bonds like those in the backbone of the copolymers, while the unsaturation in the pendant aryl substituents is retained.

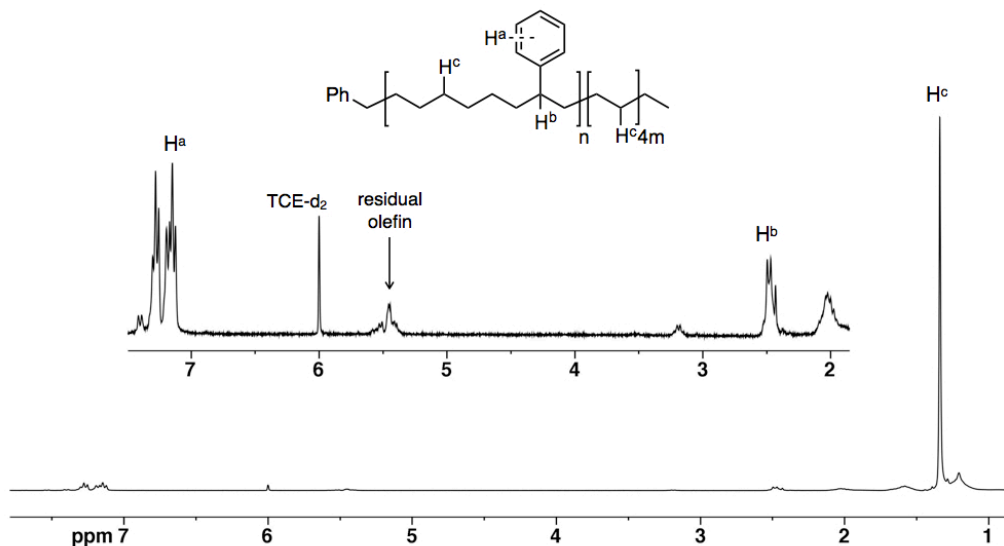
#### Scheme 5.4.

Chemical hydrogenation of unsaturated poly(3PC-*b*-COE)s and poly(3PC-*s*-COE)s to form linear polyethylene copolymers (a) *h*-poly(3PC-*b*-COE)s and (b) *h*-poly(3PC-*s*-COE)s



Saturation of the copolymers was initially monitored by  $^1\text{H}$  NMR spectroscopy. The backbone alkene bonds are selectively hydrogenated to give linear polyethylene (LPE) segments having sequential  $-\text{CH}_2-$  repeating units that have essentially equivalent chemical shifts at 1.3 ppm (Figure 5.13).



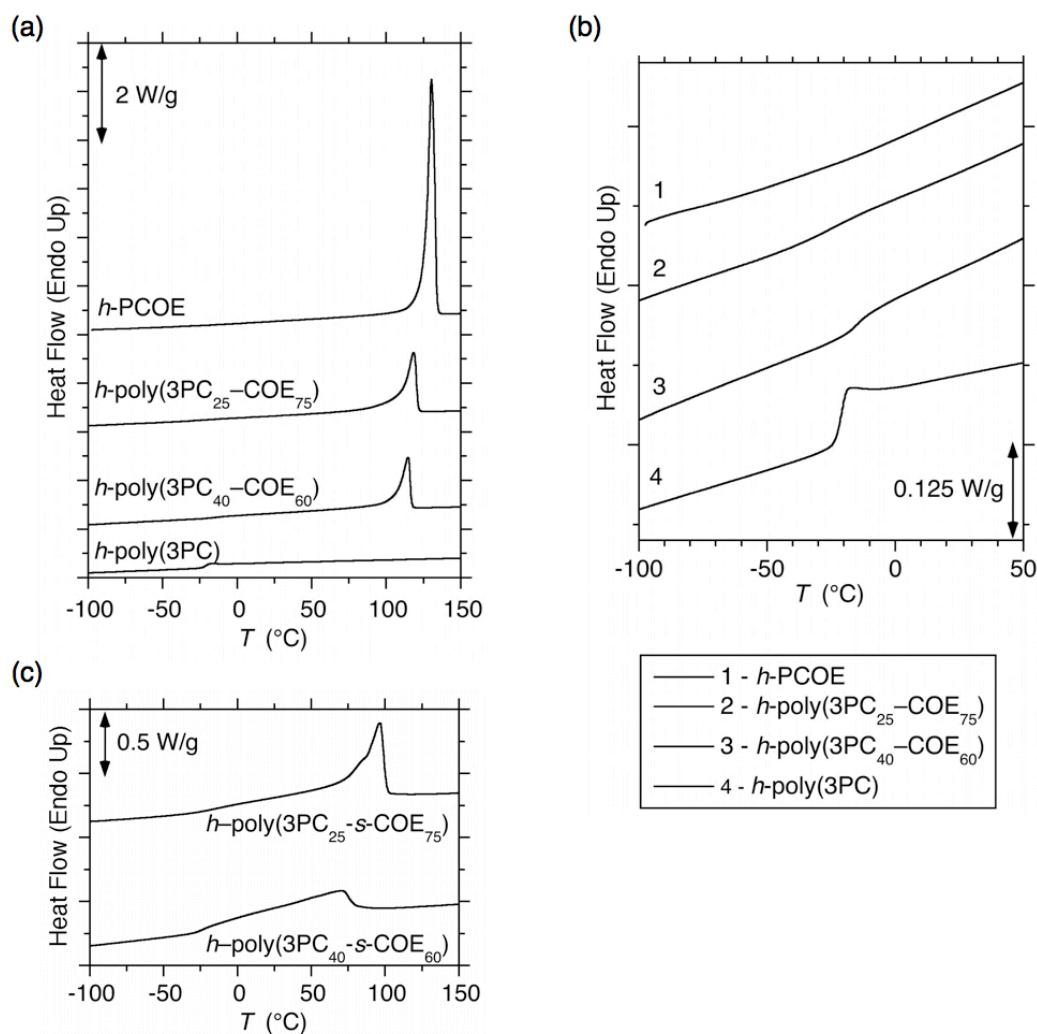
**Figure 5.13**

$^1\text{H}$  NMR spectrum for *h*-poly(3PC<sub>40</sub>-*b*-COE<sub>60</sub>) showing the saturated backbone –CH<sub>2</sub>– signals (H<sup>c</sup>; 1.3 ppm), the unsaturated aryl proton signals (H<sup>a</sup>; 7.3–7.1 ppm) and some residual unsaturated olefin protons (5.5 ppm; >95% saturation). Measured at 100 °C in 1,1,2,2-tetrachloroethane-*d*<sub>2</sub> (TCE-*d*<sub>2</sub>).

The saturation of the backbone was not quantitative as indicated by signals in the  $^1\text{H}$  NMR spectrum associated with residual olefinic signals centered at a chemical shift of 5.5 ppm. However, the degree of saturation is very high (>95%), leading to appreciably long segments of LPE (see DSC analysis below). Importantly, the aryl substituents remain unsaturated as evidenced by the aromatic proton signals at a chemical shift of 7.3–7.1 ppm. The ratio of integrated signals associated with the aryl substituents and linear methylene repeat units agree within 5% of the original composition.

## 5.2.3 Thermal Properties of Hydrogenated Polymers

The thermal properties of the hydrogenated polymers offers further insight into the architectural features – the statistical copolymers behave significantly differently than the block copolymers stemming from the different segmental run-lengths (Figure 5.14).

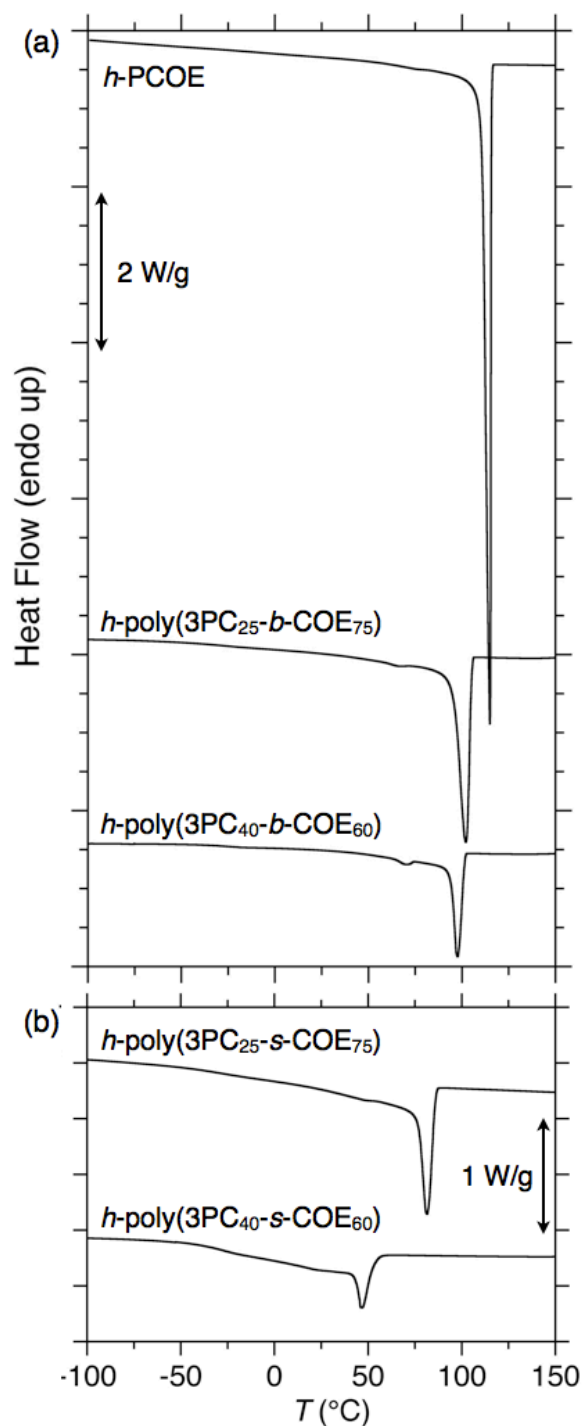


**Figure 5.14**

DSC thermograms for (a) full temperature range (–100 to 150 °C) of *h*-PCOE (*i.e.*, LPE) homopolymer, *h*-poly(3PC-*b*-COE)s and *h*-poly(3PC) homopolymer and (b) magnified heat flow for temperature range –100 to 50 °C to accentuate the T<sub>g</sub>s and DSC thermograms for (c) full temperature range *h*-poly(3PC-*s*-COE)s.

A sample of pristine PCOE was hydrogenated completely to LPE and evaluated for its thermal characteristics to provide values with which the block and statistical copolymer could be compared. Several samples of LPE (*h*-PCOE) show melting endotherms with relatively consistent  $T_m = 130\text{--}134\text{ }^\circ\text{C}$  and  $\Delta H_m = 165\text{--}200\text{ J g}^{-1}$  which corresponds to crystallinities in the vicinity of 60–72% when compared to the enthalpy of a perfectly crystalline sample ( $\Delta H_m = 277\text{ J g}^{-1}$ ).<sup>37</sup> For rational comparison, homopolymer poly(3PC) was also hydrogenated to give *h*-poly(3PC) (*h* prescript refers to "hydrogenated") using an identical protocol employing the *p*-TsNHNH<sub>2</sub> (see experimental section for evidence of saturation by <sup>1</sup>H NMR spectroscopy). Evaluation of the thermal properties associated with *h*-poly(3PC) reveals an amorphous material with a  $T_g = -21\text{ }^\circ\text{C}$ . The saturated block polymer *h*-poly(3PC<sub>25</sub>-*b*-COE<sub>75</sub>) exhibits a similar melting endotherm to pristine LPE with a slightly depressed  $T_m$  of 120.5 °C, consistent with the decrease in melting temperature associated with block copolymers in which a semi-crystalline block is tethered to an amorphous block. The melting enthalpy  $\Delta H_m = 101\text{ J g}^{-1}$  corresponds to 49% crystallinity within the LPE matrix component. Observing the temperature range between -100 and +50 °C on a magnified heat capacity scale shows that a very weak  $T_g$  can be observed near -20 °C (Figure 5.14b). Likewise, the hydrogenated derivative *h*-poly(3PC<sub>40</sub>-*b*-COE<sub>60</sub>) unambiguously exhibits a glass transition at  $T_g = -18\text{ }^\circ\text{C}$ , which is very close to the amorphous homopolymer *h*-poly(3PC). These results strongly suggest microphase separation and long segments composed predominantly of *h*-poly(3PC) repeat units segregated from an LPE matrix. The sample *h*-poly(3PC<sub>40</sub>-*b*-COE<sub>60</sub>) also exhibits a relatively large endothermic response with a peak  $T_m = +115\text{ }^\circ\text{C}$  after homogenization of the thermal history compared with all other samples. Furthermore, the melting enthalpy and  $\Delta H_m = 53\text{ J g}^{-1}$  corresponds to a crystallinity of approximately 32%.

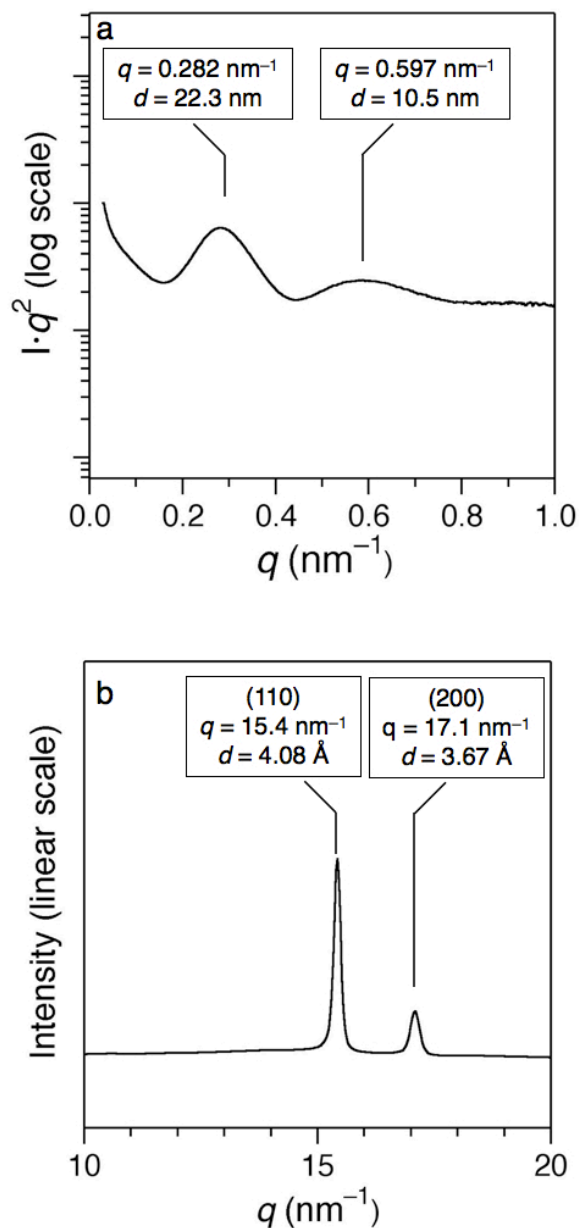
Similarly, the thermograms obtained upon cooling the blocky copolymer samples from the melt indicate substantial crystallinity with crystallization temperatures only slightly depressed compared with pristine LPE (Figure 5.15a). This behavior contrasts with that from the statistical copolymer, for which only modest crystallinity is observed, with crystallization temperatures well below 100 °C.

**Figure 5.15**

DSC cooling curves for (a) LPE homopolymer and block copolymers  $h$ -poly(3PC<sub>25</sub>- $b$ -COE<sub>75</sub>) and  $h$ -poly(3PC<sub>40</sub>- $b$ -COE<sub>60</sub>) and (b) statistical copolymer  $h$ -poly(3PC<sub>25</sub>- $s$ -COE<sub>75</sub>) and  $h$ -poly(3PC<sub>40</sub>- $s$ -COE<sub>60</sub>).

### 5.2.4 X-ray Scattering of Hydrogenated Block Copolymers

X-ray scattering is an indispensable tool for characterizing morphological and crystalline/amorphous domain size and arrangements. One dimensional scattering profiles from azimuthal integration of patterns obtained from a two-dimensional detector provide spatial relationships if coherent scattering is observed. Spot patterns from anisotropic two-dimensional scattering patterns provide information regarding bulk arrangement of segmented domains within a structure (*e.g.*, aligned cylinders or aligned lamellae). One dimensional profiles taken at both small and large scattering angles are provided for a pristine LPE sample at ambient temperature after cooling from a homogeneous melt-state at 160 °C (Figure 5.16).

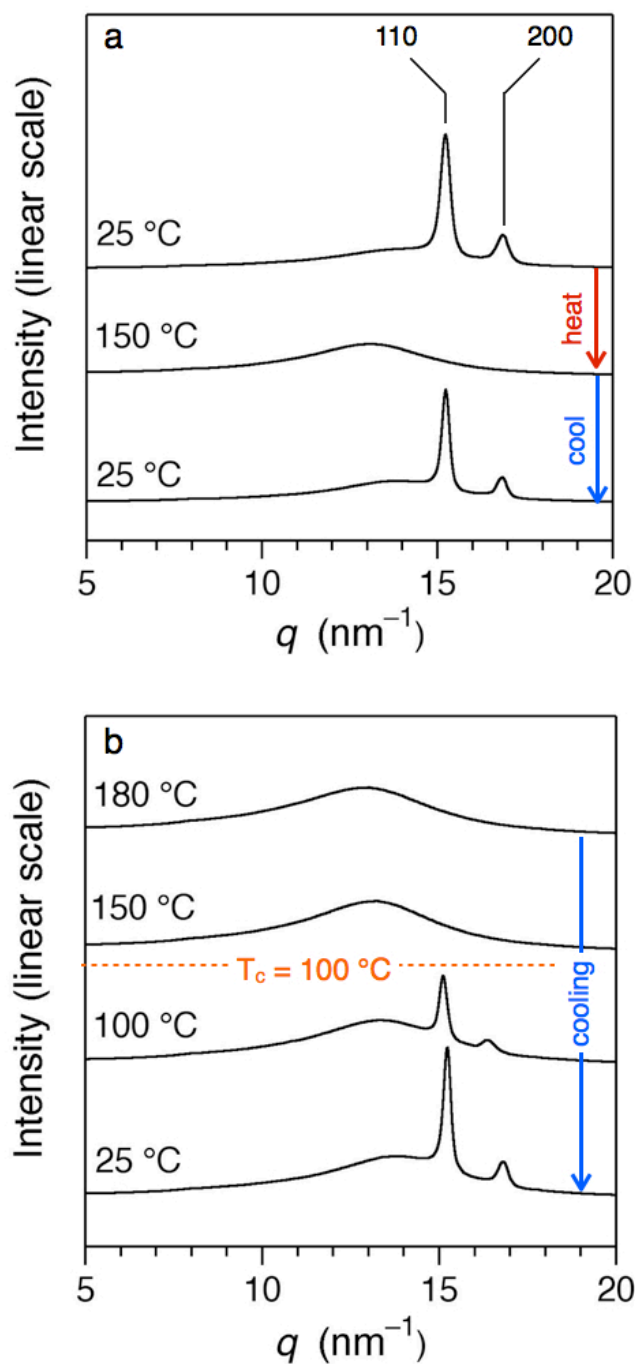
**Figure 5.16**

One-dimensional profiles from (a) SAXS and (b) WAXS of a linear polyethylene sample ( $M_n = 20 \text{ kg mol}^{-1}$ ) at ambient temperature after cooling at  $10 \text{ }^\circ\text{C min}^{-1}$  from homogeneous melt.

The small angle x-ray scattering (SAXS) plot shows the scattering intensity on a log scale as a function of the spatial scattering vector  $q = 4\pi \cdot (\sin \theta) \lambda^{-1}$ , where  $2\theta$  is the scattering angle and  $\lambda$  is the wavelength of incident radiation ( $1.3776 \text{ \AA}$ ). The LPE sample shows two broad reflections located at approximately  $q = 0.28$  and  $0.60$

$\text{nm}^{-1}$ , respectively corresponding to dimensions ( $d$ ) equal to 22 and 10 nm according to  $d = 2\pi/q$  (Figure 5.16b). These reflections presumably arise from the periodic arrangement of alternating crystalline and amorphous lamellae ( $q_2:q_1 \approx 2:1$ ), which have appreciably large electron density contrast to create scattering reflections of this magnitude.

The wide-angle x-ray scattering (WAXS) profile contains two sharp peaks corresponding to the (110) and (200) planes at  $q = 15.4$  and  $17.1 \text{ nm}^{-1}$ , respectively, associated with the orthorhombic crystal lattice conventionally adopted by LPE chains.<sup>38</sup> One-dimensional WAXS profiles for the two hydrogenated block copolymers reveal Bragg scattering reflections that are consistent with a substantial degree of crystallinity with identical orthorhombic lattice packing as seen for pristine LPE (Figure 5.17). This suggests considerable segment lengths of LPE resulting from the copolymerization–hydrogenation protocol, and the reversibility of the crystallization/melting process is illustrated with profiles after heating above  $T_m$  and subsequent cooling back to ambient temperature.

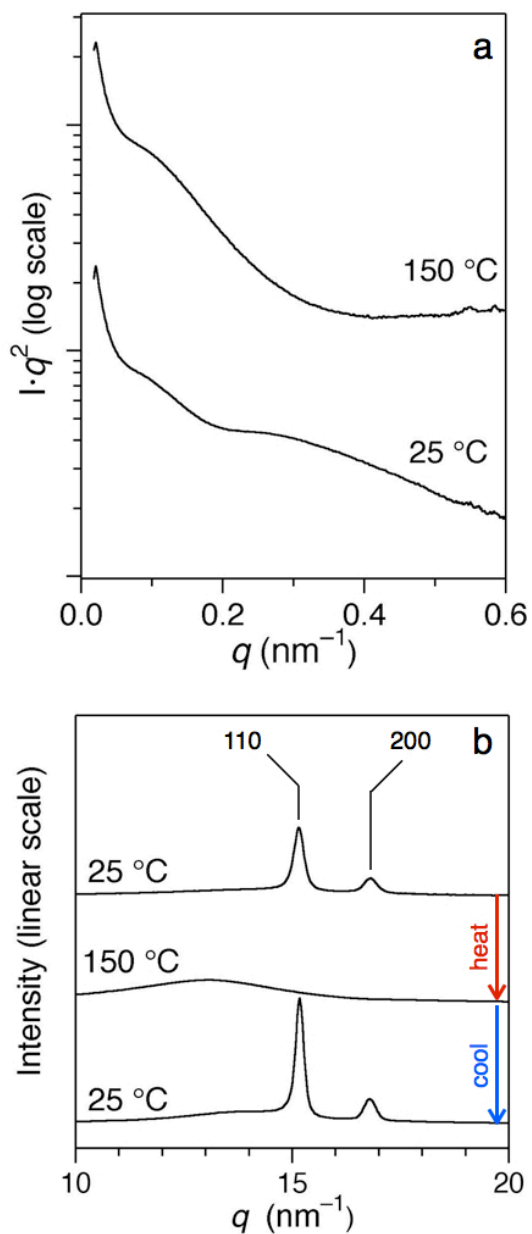
**Figure 5.17**

One-dimensional WAXS profiles for the block copolymers (a)  $h$ -poly(3PC<sub>25</sub>- $b$ -COE<sub>75</sub>) beginning at 25 °C, after heating to 150 °C ( $> T_{m,LPE}$ ), and again after cooling back to ambient temperature (rate  $> 50$  °C min<sup>-1</sup>) and (b)  $h$ -poly(3PC<sub>40</sub>- $b$ -COE<sub>60</sub>) beginning in the melt at 180 °C and consecutively cooling to 150 °C, 100 °C (5 min anneal), and 25 °C.



SAXS profiles for the block copolymer poly(3PC<sub>25</sub>-*b*-COE<sub>75</sub>) both above and below the  $T_m$  reveal a distinct yet broad reflection centered at approximately  $q = 0.1 \text{ nm}^{-1}$ , corresponding to a domain spacing  $d = 63 \text{ nm}$  (Figure 5.18a). The reflection is located in nearly identical positions above and below  $T_m$ , which suggests the preservation of a microphase separated morphology, albeit disorganized, upon crystallization of the LPE block. The crystallinity is suggested by the evolution of a very broad reflection at 25 °C that does not exist at 150 °C; the location of the broad reflection is consistent with that observed in LPE homopolymer. The sharp upturn in scattering intensity in approaching the beamstop suggests that the primary peak from microphase separation could be unresolved in this beam configuration. The large molar mass of the sample would potentially cause domain spacing considerably larger than 63 nm upon phase separation.

The WAXS profiles for this sample is consistent with the DSC results, suggesting that the crystalline portions associated with LPE are melted at 150 °C, and that the crystallization/melting phenomena are reversible (Figure 5.18b). These results corroborate the SAXS results, and the postulated relationship between crystal formation and microphase separation.

**Figure 5.18**

One-dimensional scattering profiles for the block copolymer  $h$ -poly(3PC<sub>25</sub>- $b$ -COE<sub>75</sub>) at (a) small angle and (b) wide angle beginning at 25 °C, after heating to 150 °C ( $> T_{m,LPE}$ ), and again after cooling back to ambient temperature (rate  $> 50$  °C min<sup>-1</sup>).

### 5.2.5 Sulfonation of hydrogenated poly(3PC-COE) copolymers

Sulfonation of the copolymers was conducted by reaction of the polymers with acetyl sulfate ( $\text{AcHSO}_3$ ) in 1,1,2,2-tetrachloroethane solution at 140 °C, in accordance with previously reported sulfonation of styrenyl copolymers.<sup>21,39</sup> The copolymers were dissolved at elevated temperature; lower temperatures were not adequate for solubilizing the LPE. A solution of  $\text{AcHSO}_3$  in the TCE solvent was added to the polymer solution and stirred rapidly for 30 min before precipitating into a ten-fold volume excess of MeOH. The sulfonated copolymer was isolated by filtration and dried under vacuum at 50 °C for at least 12 h. The resulting polymers were brownish in color and the darkness correlated loosely with the targeted sulfonic acid content (Figure 5.19).

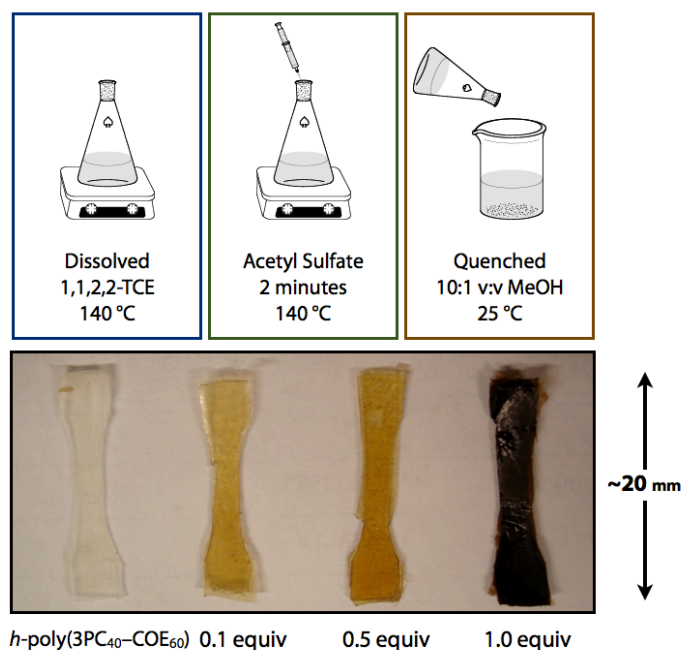


**Figure 5.19**

Schematic illustration of sulfonation procedure and photographs of block copolymer poly(3PC<sub>40</sub>-*b*-COE<sub>60</sub>) before (*far left*) and after sulfonation with increasing acetyl sulfate content increasing from left to right.

The extent of sulfonation was determined by elemental analysis (Table 5.3). Block copolymers and statistical copolymers were sulfonated in the same manner, and the theoretical targeted sulfonation was calculated by adding measured quantities of AcHSO<sub>3</sub> with respect to the measured aryl content by <sup>1</sup>H NMR spectroscopy. The targeted molar ratios of AcHSO<sub>3</sub>:aryl were 0.5 and 1.0 for each copolymer, with the exception of poly(3PC<sub>40</sub>-*b*-COE<sub>60</sub>), which was also sulfonated with the ratio of 0.1.

Theoretical targeted sulfonation extent is referred to in Table 5.3 as equivalents of AcHSO<sub>3</sub> added per aryl group calculated from the polymer composition using <sup>1</sup>H NMR spectroscopy. The IEC values are also presented as determined from eq 5.X in terms of mmol of sulfonic acid groups per gram of polymer. Theoretical values and experimental values provide a basis with which to evaluate the efficacy of the chosen sulfonation protocol.

$$IEC = \left( \frac{n_{SA}}{n_{COE} \cdot m_{COE} + n_{3PC} \cdot m_{3PC} + n_{S3PC} \cdot m_{S3PC}} \right) \quad (5.6)$$

where  $n_i$  is the number of mmol of species  $i$  per mmol of polymer and  $m_i$  is the molar mass of species  $i$ .<sup>†</sup>

---

<sup>†</sup> COE = cyclooctene repeating unit; 3PC = 3-phenylcyclooctene; S3PC = monosulfonic acid substituted 3-phenylcyclooctene repeating unit.

**Table 5.3**

Sulfonation characteristics of block and statistical copolymers

Sample	$w_{3PC}^a$	$n_{3PC}^b$	HSO <sub>3</sub> equiv <sup>c</sup>		IEC (mmol g <sup>-1</sup> ) <sup>d</sup>	
			target	measured	target	measured
<b>A: <i>h</i>-poly(3PC<sub>25</sub>-<i>b</i>-COE<sub>75</sub>)</b>						
A-1	22.7	14.8	0.5	0.09	0.57	0.11
A-2	22.7	14.8	1.0	0.17	1.10	0.20
<b>B: <i>h</i>-poly(3PC<sub>40</sub>-<i>b</i>-COE<sub>60</sub>)</b>						
B-1	38.2	26.7	0.1	0.06	0.20	0.12
B-2	38.2	26.7	0.5	0.15	0.94	0.30
B-3	38.2	26.7	1.0	0.26	1.74	0.51
<b>C: <i>h</i>-poly(3PC<sub>25</sub>-<i>s</i>-COE<sub>75</sub>)</b>						
C-1	24.3	16.0	0.5	0.04	0.61	0.05
C-2	24.3	16.0	1.0	0.04	1.17	0.06
<b>D: <i>h</i>-poly(3PC<sub>40</sub>-<i>s</i>-COE<sub>60</sub>)</b>						
D-1	40.9	29.1	0.5	0.02	1.00	0.03
D-2	40.9	29.1	1.0	0.00	1.85	0.00

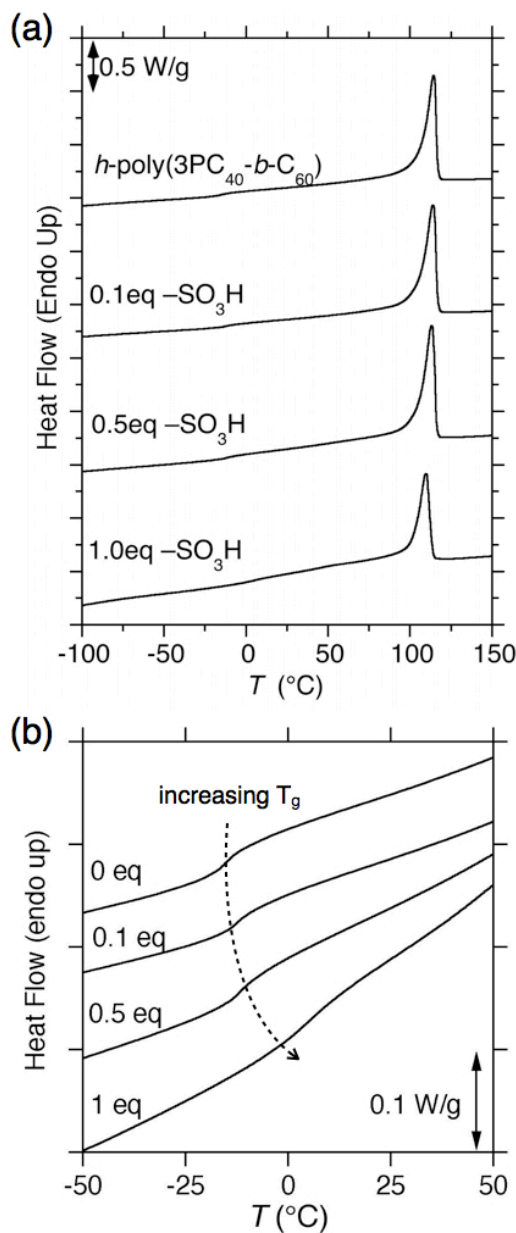
<sup>a</sup> Calculated from <sup>1</sup>H NMR spectroscopy of the unsaturated derivatives and converted assuming complete hydrogenation. <sup>b</sup> Calculated using the assumed molar mass of the saturated repeating units ( $m_{3PC} = 188 \text{ g mol}^{-1}$ ;  $m_{h-COE} = 112 \text{ g mol}^{-1}$ ). <sup>c</sup> Given as equivalents per 3PC repeating unit. <sup>d</sup> Calculated by eq 5.6, in terms of mmol of sulfonic acid per gram of polymer.

It appears that the post-polymerization sulfonation strategy employed here failed to react quantitatively in the block copolymers. There is approximately 20–30% of the targeted sulfonic acid content for the block copolymers, suggesting that longer reaction times may be required for quantitative functionalization. Furthermore, it is unclear whether sulfonation has occurred singly on each aromatic ring; some aryl groups may contain multiple sulfonic acid groups. Nonetheless, the elemental analysis is consistent with some degree of sulfonation of the block copolymers, and the extent is directly proportional to the amount of acetyl sulfate added. Structural analyses and comparison with the parent

materials were performed on the sulfonated derivatives. Surprisingly, the sulfonation procedure appears to have failed nearly altogether, for which there is currently no explanation.

### 5.2.6 Thermal Properties of sulfonated *h*-poly(3PC-COE) copolymers

There is minimal variability in the  $T_{m,E}$  or  $T_{c,E}$  with increasing sulfonate content according to thermal analysis by DSC; the effects are demonstrated for sulfonated samples derived from poly(3PC<sub>40</sub>-*b*-COE<sub>60</sub>) (Figure 5.20). The  $T_g$  associated with the poly3PC block appeared to vary slightly, increasing slightly with increasing sulfonation from approximately  $-15\text{ }^\circ\text{C}$  to  $0\text{ }^\circ\text{C}$  (Figure 5.20b).

**Figure 5.20**

DSC thermograms for pristine block copolymer  $h\text{-poly}(3\text{PC}_{40}\text{-}b\text{-COE}_{60})$  and the sulfonated derivative with targeted equivalents of 0.1, 0.5, and 1.0 corresponding to  $\text{AcHSO}_3\text{:aryl}$ . (a) full thermograms from  $-100$  to  $+150$   $^{\circ}\text{C}$  and (b) magnified thermograms from  $-50$  to  $+50$   $^{\circ}\text{C}$ , accentuating the  $T_g$ .

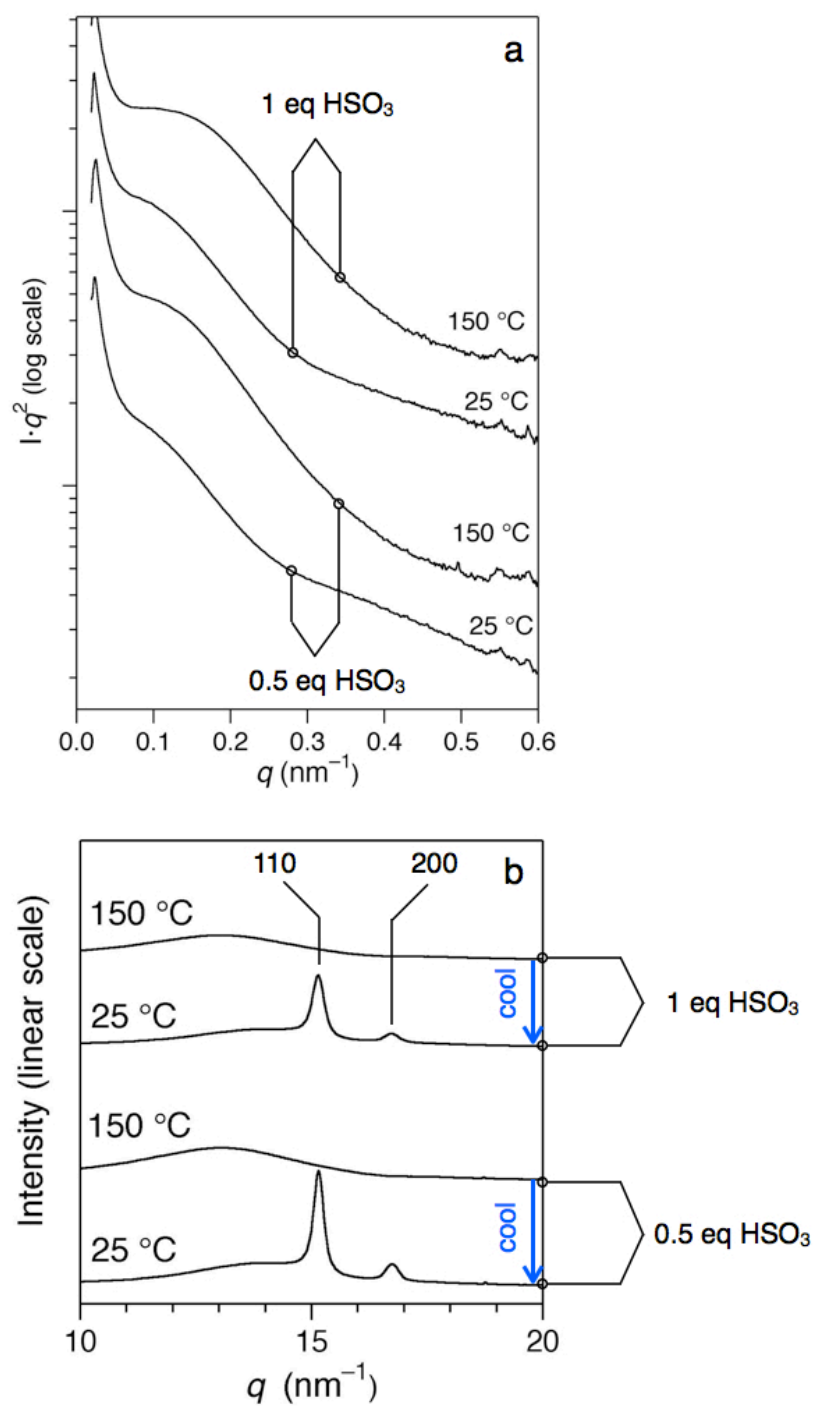
The composite thermal characteristics, showing a consistency of the position of the melting endotherm and slight shift in the  $T_g$ , suggest that the sulfonation selectively affected the aryl side groups as opposed to the linear methylene

segments associated with the LPE block. The selective aryl sulfonation was the desired outcome.

### 5.2.7 Scattering from sulfonated *h*-poly(3PC-COE) copolymers

X-ray scattering performed at both small and wide angles provides compelling corroboration with the results suggested by DSC analysis. Namely, the sulfonation appears to have selectively occurred at the pendent aryl groups. The general behavior is exemplified by one-dimensional scattering profiles for samples of sulfonated *h*-poly(3PC<sub>40</sub>-*b*-COE<sub>60</sub>) (Figure 5.21). SAXS profiles at elevated temperature (150 °C) followed by cooling to ambient temperature (25 °C) suggest that the polymers are microphase separated, albeit lacking long-range order, and the melt-phase morphology is maintained upon cooling below  $T_c$ . The broad reflection appears at nearly identical locations for two sulfonated samples with targeted AcHSO<sub>3</sub>:aryl = 0.5 and 1.0 at 150 °C, and the position of the reflection is shifted to slightly lower  $q$ -value upon cooling to 25 °C, suggesting a slight increase in domain spacing. The strong upturn in intensity as the beamstop is approached at low  $q$ -value suggests that a primary scattering peak is buried in the beam-stop, and was not accessible with this particular beamline configuration. That would imply that the broad reflections observed in Figure 5.21a are attributable to higher order reflections. This would be consistent with a microphase separated structure lacking long range order, and fits with the predicted size range expected from domains adopted in block copolymers with large molar mass ( $\sim 300 \text{ kg mol}^{-1}$ ).



**Figure 5.21**

One dimensional x-ray scattering profiles for two sulfonated derivatives of *h*-poly(3PC<sub>40</sub>-*b*-COE<sub>60</sub>) (targeted AcHSO<sub>3</sub>:aryl = 0.5 and 1.0) at (a) small angles and (b) wide angles.

WAXS profiles for the two sulfonated derivatives of *h*-poly(3PC<sub>40</sub>-*b*-COE<sub>60</sub>) in Figure 5.21b suggest that the LPE crystallizability was not compromised, consistent with selective sulfonation. The reflections associated with LPE crystals were not observed at 150 °C, but appear after cooling below  $T_{c,E}$ . The transition is reversible upon multiple heating and cooling cycles. The reversibility is demonstrated with WAXS profiles for three sulfonated derivatives of *h*-poly(3PC<sub>40</sub>-*b*-COE<sub>60</sub>).

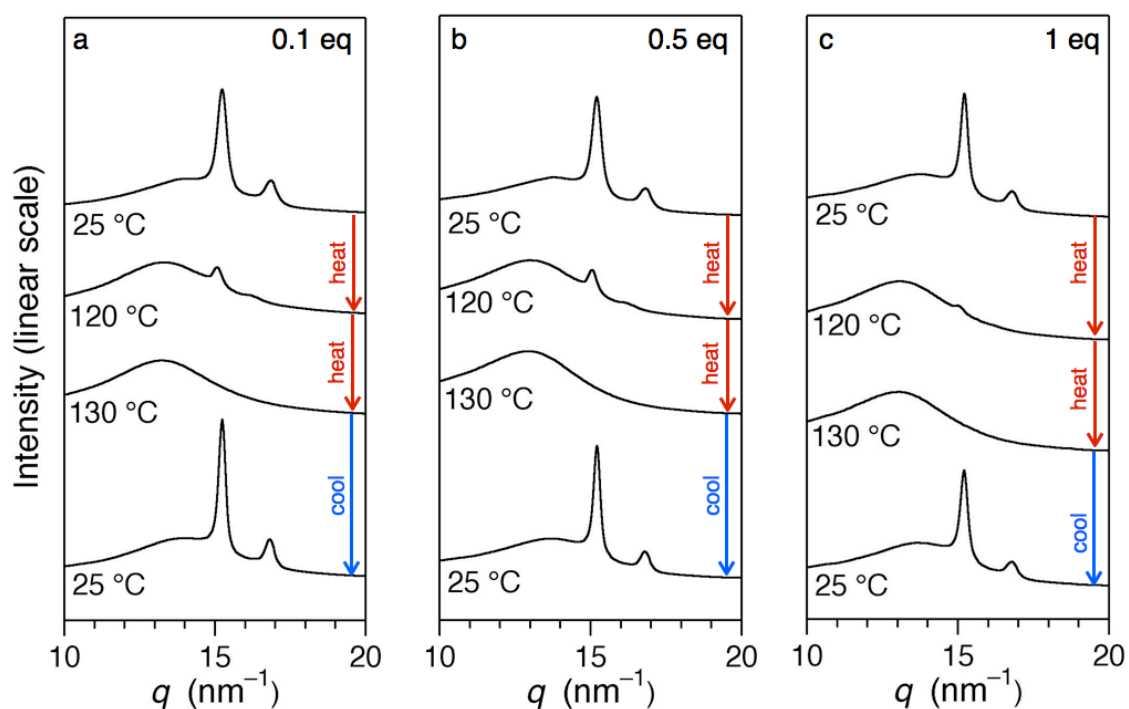


**Figure 5.22**

One-dimensional WAXS profiles for sulfonated derivatives of *h*-poly(3PC<sub>40</sub>-*b*-COE<sub>60</sub>) with targeted HSO<sub>3</sub> equivalents equal to (a) 0.1, (b) 0.5, and (c) 1.0 starting at 25 °C followed by heating to 120 °C, 130 °C and cooling back to 25 °C.

It was observed that the crystals associated with LPE segments were nearly melted at 120 °C and completely melted at 130 °C, consistent with the DSC results. Crystallization then ensued upon cooling back to ambient temperature, suggesting that the crystallization is reversible. There appears to be less crystallinity in the sample with the highest sulfonic acid content, although there is still substantial crystalline content.

### 5.2.8 Mechanical properties of copolymers

The mechanical properties of the pristine block copolymers and sulfonated derivatives were evaluated by uniaxial tensile elongation. Dogbone shaped samples were prepared by melt-pressing samples in molds at  $\sim 160$  °C. Stress–strain curves were generated, from which tensile toughness and modulus were extracted. The block copolymers were both flexible and ductile, with Young's moduli ( $E$ ) in the range of 60–80 MPa and with ultimate elongations in the range of 500–800%.

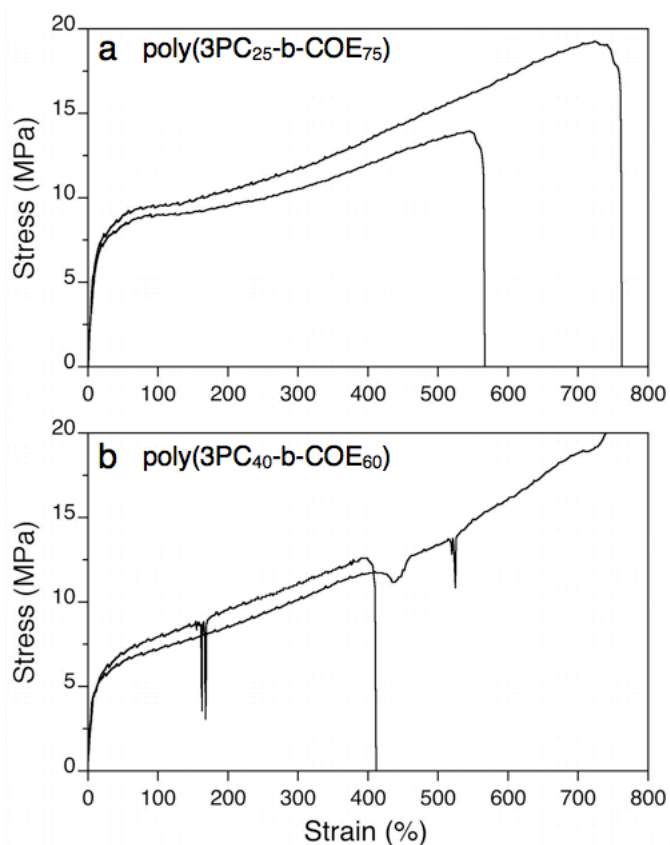


**Figure 5.23**

Stress–strain curves for block copolymers (a) poly(3PC<sub>25</sub>-*b*-COE<sub>75</sub>) and (b) poly(3PC<sub>40</sub>-*b*-COE<sub>60</sub>). Two tests were performed for each sample.

The two block copolymers have relatively high elongations and the two tests performed for each sample have consistent values for the modulus. One test for the sample in Figure 5.23b did not fracture upon reaching the limit of elongation for the instrument. Tensile testing performed on sulfonated derivatives of poly(3PC<sub>40</sub>-*b*-COE<sub>60</sub>) reveal that sulfonation had detrimental effects on the tensile strength, but influenced the modulus to a lesser extent (Figure 5.24).

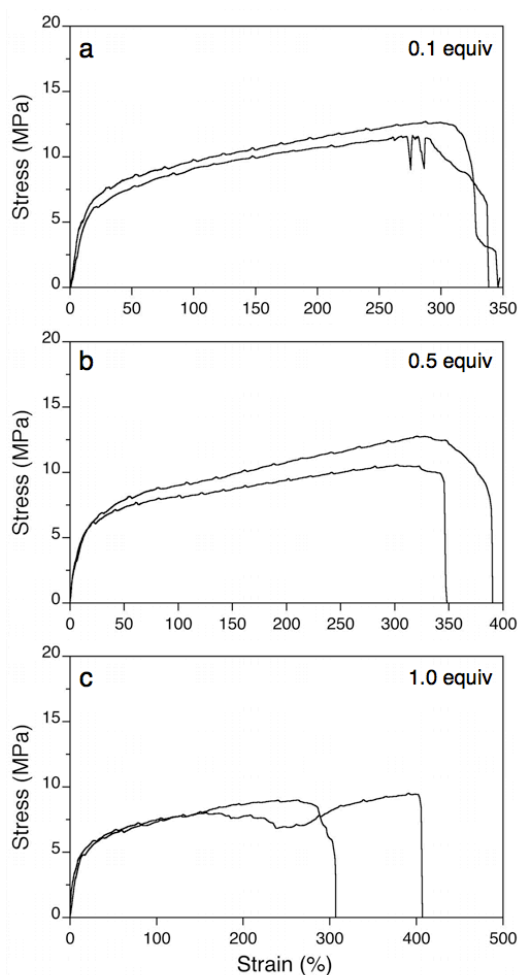


**Figure 5.24**

Stress–strain curves for sulfonated derivatives of block copolymer poly(3PC<sub>40</sub>-*b*-COE<sub>60</sub>) with targeted sulfonic acid content of (a) 0.1 equiv, (b) 0.5 equiv, and (c) 1.0 equiv. Two tests were performed for each sample.

The tensile toughness (TT) and the Young's modulus ( $E$ ) were for each sample were calculated from the stress-strain curves (Table 5.4).

**Table 5.4**  
Mechanical properties for some block copolymers and sulfonated derivatives

Sample	TT <sup>a</sup> MJ m <sup>-3</sup>	$E$ <sup>b</sup> MPa	tensile stress MPa
<b>A:</b> <i>h</i> -poly(3PC <sub>25</sub> - <i>b</i> -COE <sub>60</sub> )	81	73	16
<b>B:</b> <i>h</i> -poly(3PC <sub>40</sub> - <i>b</i> -COE <sub>60</sub> )	65	63	18
<b>B</b> -0.1 equiv	33	50	
<b>B</b> -0.5 equiv	35	68	
<b>B</b> -1.0 equiv	27	56	

<sup>a</sup> Calculated from the area under the stress–strain curve. <sup>b</sup> Calculated from the slope of the stress–strain curves at the onset of the test (elongation < 5%).

The sulfonation appears to have had minimal effect on the modulus. The TT and the ultimate tensile stress, however, were both significantly decreased after sulfonation. Nonetheless, the materials are relatively ductile and strong.

### 5.3 Conclusions and Outlook

The synthetic strategy described here entails a straightforward route to making block copolymers with segments comprising high density polyethylene and a charge carrying, sulfonated styrenyl derivative. LPE imparts its superior qualities on hybrid materials with various functionalities by designing comonomers (*e.g.*, 3-substituted cyclooctenes). The relatively slow polymerization of 3-phenylcyclooct-1-ene was conducted followed by the fast polymerization of unsubstituted *cis*-cyclooctene to give copolymers having a blocky distribution of repeating units. In contrast, simultaneous polymerization of the two monomers provided copolymers with essentially statistical monomer distribution owing to extensive chain transfer. The architectural variance between the materials from simultaneous and

sequential polymerizations was reflected by the thermal and molecular characteristics. The resulting poly(3-phenylcyclooctene-*block*-cyclooctene) diblock copolymers were subjected to hydrogenation to selectively saturate the backbone alkenes, leaving the pendent aryl substituents for further functionalization. The aryl side chains were sulfonated to various extents, after which the stress-strain behavior was evaluated to reveal tough materials owing to the high molecular weight, highly entangled linear polyethylene component. These materials are promising models for ion exchange membranes in which the ion exchange capacity can be tailored with the phenyl composition and sulfonation reaction. The saturated LPE backbone offers flexibility, strength, and resistance to chemical corrosion.

The strategy for sulfonation could be enhanced using several approaches. Sulfonation after polymerization could be conducted for longer duration or in alternative solvents in order to achieve more quantitative reaction. Competitive membranes could be realized with IEC > 1. Alternatively, sulfonated derivatives of *cis*-cyclooctene monomer could be designed and synthesized. It is reasonable to be confident in the polymerizability of such molecules on the basis of ruthenium metathesis catalyst tolerance to wide ranging functional groups, including those with ionic character.

Conductivity measurements are needed to ascertain the potential efficacy of these block copolymers as proton exchange membranes. Upon evaluating the conductivity, the molecular characteristics of the blocks can easily be modified to enhance the performance. For example, it may or may not be necessary to have a blocky structure; the statistical copolymers may have superior qualities with respect to charge transport. Furthermore, the molecular weight and composition can be tailored with the block copolymers to give access to smaller domain spacing and higher IEC values, respectively. The synthetic strategy is amenable to these changes being made without substantial difficulty.

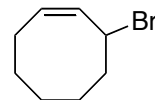
## 5.4 Experimental Details

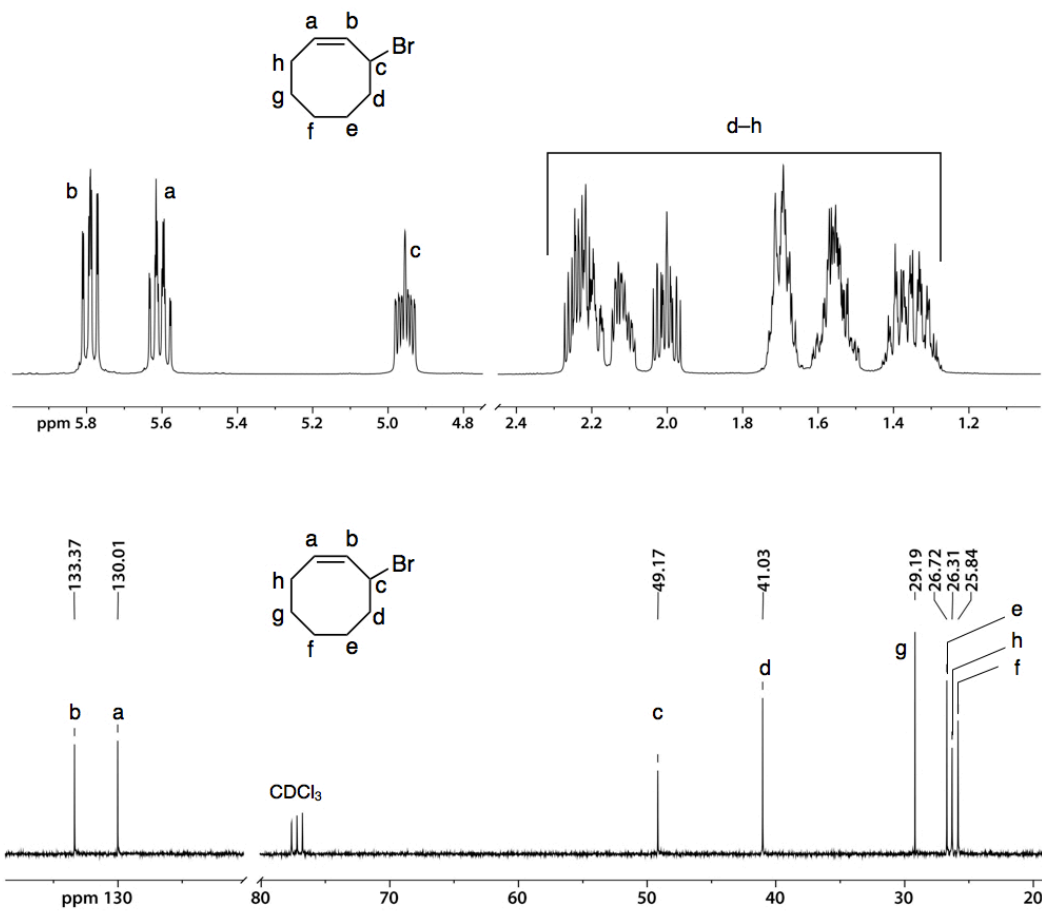
### 5.4.1 Materials

The starting material *cis*-cyclooctene was purchased from Acros Chemical and dried over CaH<sub>2</sub> before distilling at reduced pressure. N-bromosuccinimide was purchased from Sigma-Aldrich and was recrystallized from methanol. Chlorosulfonic acid, 2,2'-azobis(2-propionitrile) (AIBN), CuI, MgSO<sub>4</sub>, NaHCO<sub>3</sub>, Mg, NH<sub>4</sub>Cl, bromobenzene, and 1,2-dibromoethane were obtained from Sigma-Aldrich and used as received. The solvents CH<sub>2</sub>Cl<sub>2</sub>, CCl<sub>4</sub>, Et<sub>2</sub>O, THF were purchased from Mallinkrodt and used as received.

### 5.4.2 Synthetic Details

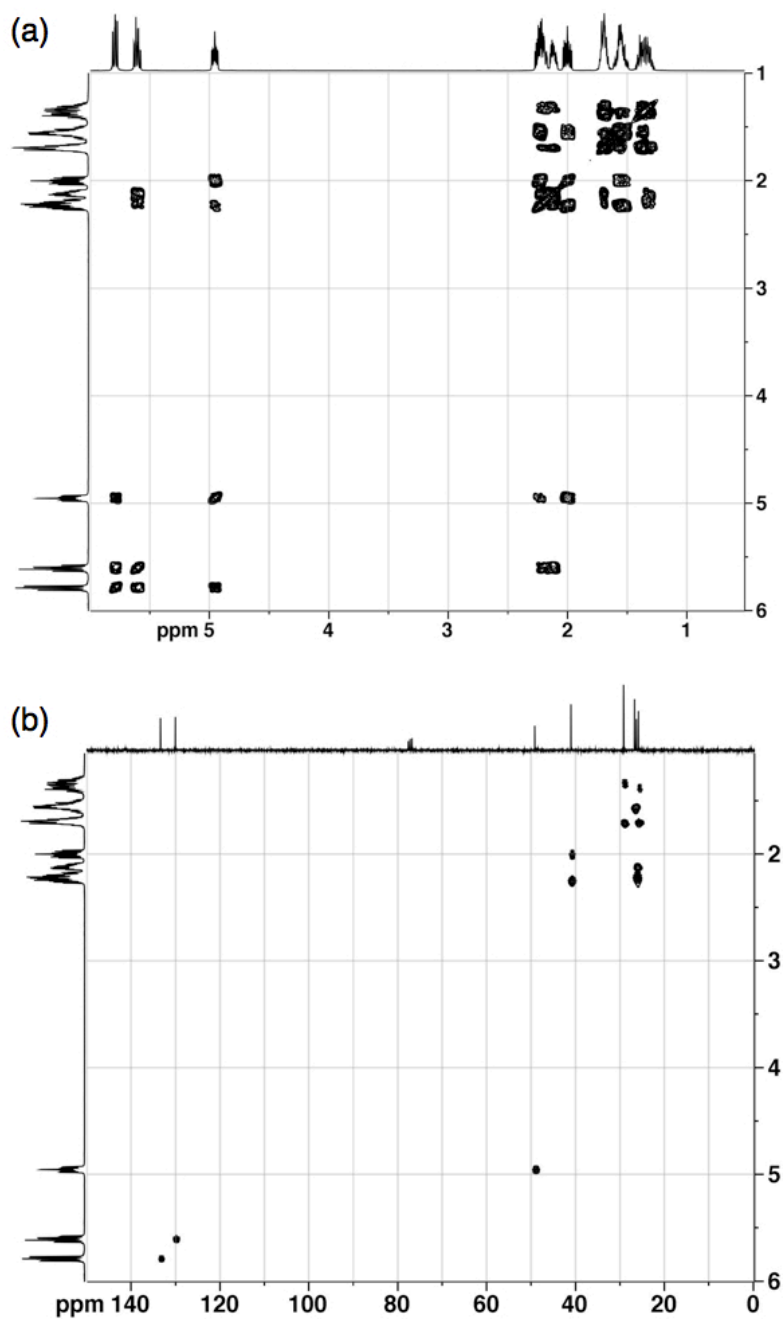
**Synthesis of 3-bromocyclooct-1-ene.** In a 500 mL two neck flask was poured 96 mL of *cis*-cyclooctene (82.6 g; 751 mmol) along with 300 mL of CCl<sub>4</sub>. In one neck was affixed a reflux condenser, while the other neck was sealed with a rubber septum. The system was thoroughly purged with argon before adding 50 mg of AIBN and heating to 80 °C. The reaction progress was monitored by watching the slightly yellow solid on the bottom of the flask (NBS) float to the top upon conversion to succinimide. After 2 h, the reaction was cooled to RT and filtered to remove the succinimide. The CCl<sub>4</sub> was diluted with 200 mL of CH<sub>2</sub>Cl<sub>2</sub> and washed with NaHCO<sub>3(aq)</sub> and water. The organic phase was dried over MgSO<sub>4</sub> and solvent removed under reduced pressure to yield a slightly yellow viscous liquid. The desired product was purified by fractional distillation to yield a clear colorless liquid (85% yield). <sup>1</sup>H NMR, CDCl<sub>3</sub>: δ (ppm) = 5.79 [ddd, 1H, *J* = 10.5, 8.6, 1.6 Hz]; 5.61 [dddd, 1H, *J* = 10.6, 9.1, 7.7, 1.4 Hz, -CH=CHCHBr-]; 4.94 [m, 1H]; 1.30–2.30 [m, 10H]. <sup>13</sup>C NMR, CDCl<sub>3</sub>: δ (ppm) = 133.39, 130.04, 49.18, 41.05, 29.20, 26.72, 26.32, 25.85.



**Figure 5.25**

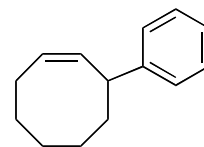
Molecular characterization of 3-bromocyclooct-1-ene by <sup>1</sup>H (*top*) and <sup>13</sup>C (*bottom*) NMR spectroscopy with detailed proton and carbon assignments.



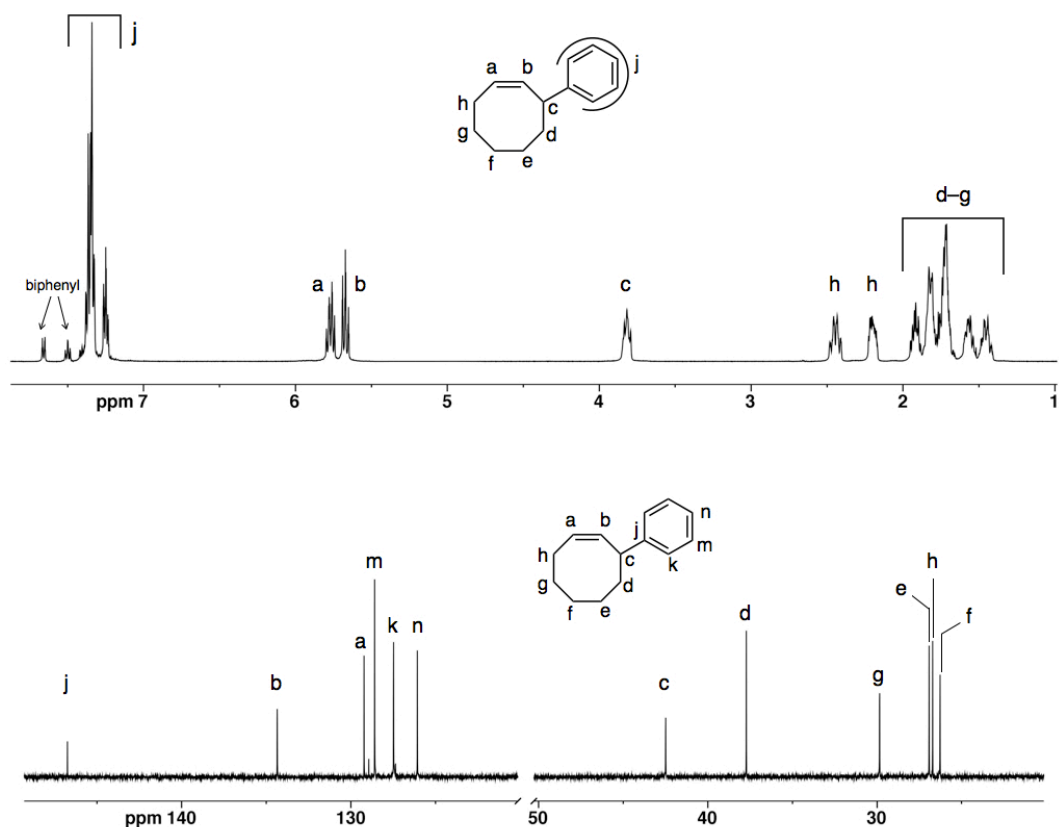
**Figure 5.26**

NMR spectra from (a) H-H COSY and (b) H-C heteronuclear multiple quantum coherence (HMQC) spectroscopy for structure determination of 3BrCOE. Measured in  $\text{CDCl}_3$  at 20 °C with 500 MHz.

**Synthesis of 3-phenylcyclooctene (LMP-4122)** A Schlenk flask containing 5.2 g of magnesium turnings (217 mmol) was flame dried under vacuum and back-filled with argon. Under an argon flow, 150 mL of dry THF was added via cannula followed by



several drops of 1,2-dibromoethane to initiate the Grignard reaction. A syringe containing 21 mL of bromobenzene (31.4 g; 200 mmol) was used for dropwise addition to the magnesium/THF mixture over 2 h while heating at 60 °C. Rapid bubbling and black coloration confirmed the Grignard (Bromomagnesiumbenzene,  $\text{BrMgC}_6\text{H}_6$ ) formation. In a separate dried flask with a reflux condensor under an argon atmosphere was placed 1.2 g of CuI (6.3 mmol) with 200 mL dry THF and 20.0 g of 3-bromocyclooctene (106 mmol). This mixture was cooled to  $-5$  °C before adding the Grignard solution dropwise via cannula over 1 h. The solution was allowed to warm to 25 °C and stirred for an additional 15 h before diluting with 300 mL of  $\text{Et}_2\text{O}$  and quenching with 500 mL saturated  $\text{NH}_4\text{Cl}_{(\text{aq})}$ . The organic phase was extracted with 500 mL water and dried over  $\text{MgSO}_4$  before removing the  $\text{Et}_2\text{O}$  under reduced pressure to yield a slightly yellow oil. The crude product was purified by fractional distillation (78% yield).  $^1\text{H}$  NMR ( $\text{CDCl}_3$ ):  $\delta$  (ppm) = 7.18–7.34 [m, 5H]; 5.71 [1H; dddd,  $J$  = 10.31, 8.80, 7.41, 1.35 Hz]; 5.59 [ddd, 1H,  $J$  = 10.41, 8.91, 1.43 Hz]; 3.76 [ddd, 1H,  $J$  = 11.89, 8.53, 3.77 Hz]; 2.39 [m, 1H]; 2.15 [m, 1H]; 1.38–1.88 [m, 8H].  $^{13}\text{C}$  NMR ( $\text{CDCl}_3$ ):  $\delta$  (ppm) = 146.62, 134.25, 129.08, 128.48, 127.35, 125.95, 42.39, 37.60, 29.73, 26.81, 26.59, 26.17.

**Figure 5.27**

Molecular characterization of 3-phenylcyclooct-1-ene by  $^1\text{H}$  (*top*) and  $^{13}\text{C}$  (*bottom*) NMR spectroscopy with detailed proton and carbon assignments.

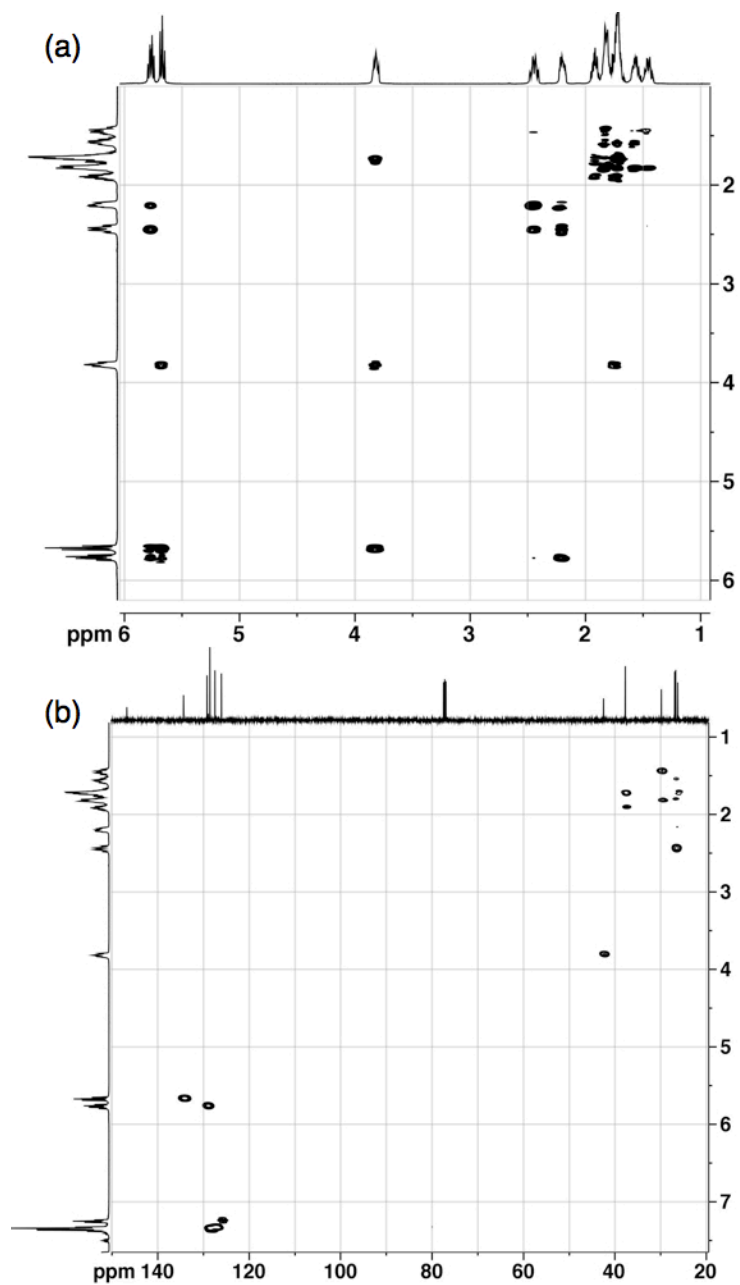
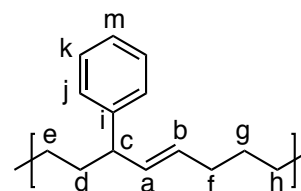


**Figure 5.28**

NMR spectra from (a) H-H COSY and (b) H-C heteronuclear multiple quantum coherence (HMQC) spectroscopy for structure determination of 3PC monomer. The aromatic region (7.0–7.5 ppm) of part (a) H-H COSY is omitted; the aromatic protons correlated only with each other, and the zoomed in spectrum accentuates the remaining correlations for accurate spectral analysis.

**Polymerization procedure for homopolymer poly3PC using CTA.** A solution of 1.0 g of 3-phenylcyclooctene (5.4 mmol) with 9  $\mu\text{L}$  of *cis*-1,4-diacetoxy-2-butene ( $\sim 9.7$  mg; 57  $\mu\text{mol}$ ;  $[\text{M}]/[\text{CTA}] \sim 100$ ) was prepared in 5 mL of  $\text{CH}_2\text{Cl}_2$ . Grubbs second



generation catalyst was added via syringe as a solution (1 mg in 0.5 mL  $\text{CH}_2\text{Cl}_2$ ) under an argon atmosphere. The polymerization was stirred at RT for 12 h and precipitated into 50 mL of MeOH at  $-78$   $^\circ\text{C}$ .  $^1\text{H}$  NMR ( $\text{CDCl}_3$ ):  $\delta$  (ppm) = 7.10–7.28 (**j**, **k**, **m**; 5H), 5.50 (**a**; 1H; dd,  $J = 15.2, 7.7$  Hz), 5.39 (**b**; 1H; dt,  $J = 14.6, 7.0$  Hz), 3.15 (**c**; 2H; dt,  $J = 7.4, 7.5$  Hz), 1.96 (**f**; 2H; dt,  $J = 7.1, 6.3$  Hz), 1.64 (**d**; 2H; dt,  $J = 7.2, 7.2$  Hz), 1.6–1.4 (**e**, **g**, **h**; 6H; m).  $^{13}\text{C}$  NMR ( $\text{CDCl}_3$ ):  $\delta$  (ppm) = 145.84 (**i**), 134.26 (**a**), 130.21 (**b**), 128.51 (**k**), 127.70 (**j**), 126.03 (**m**), 49.03 (**c**), 36.29 (**f**), 32.74 (**d**), 29.60 (**e**), 29.33 (**h**), 27.61 (**g**).

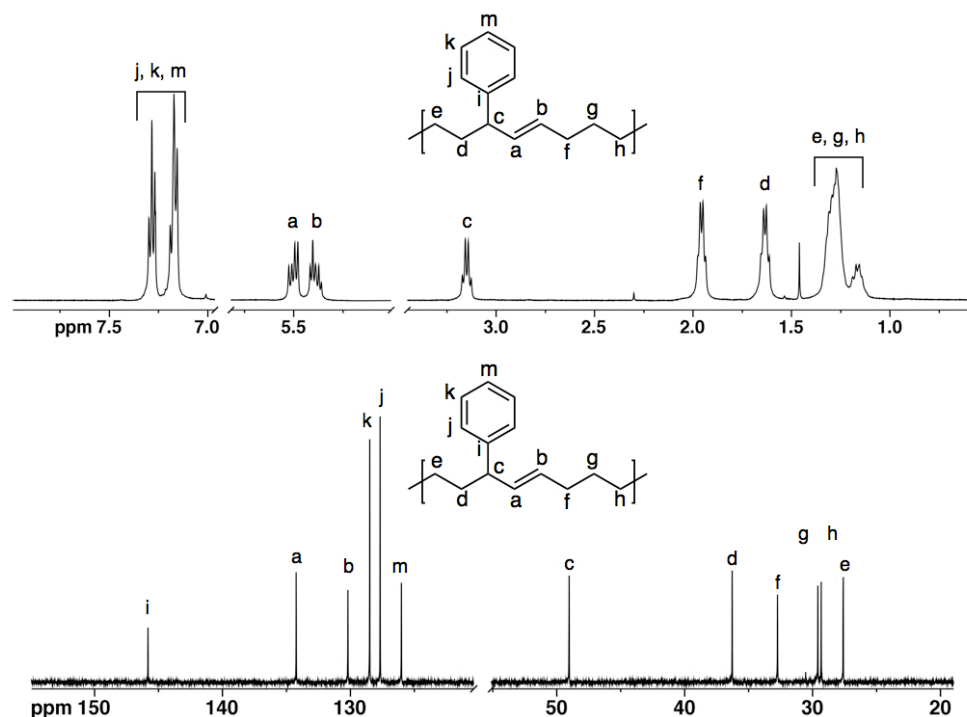
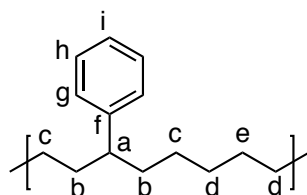


**Figure 5.29**

Molecular characteristics of homopolymer poly3PC by  $^1\text{H}$  (*top*) and  $^{13}\text{C}$  (*bottom*) NMR spectroscopy with detailed signal assignments designated.



### Hydrogenation of poly(3PC) homopolymer.

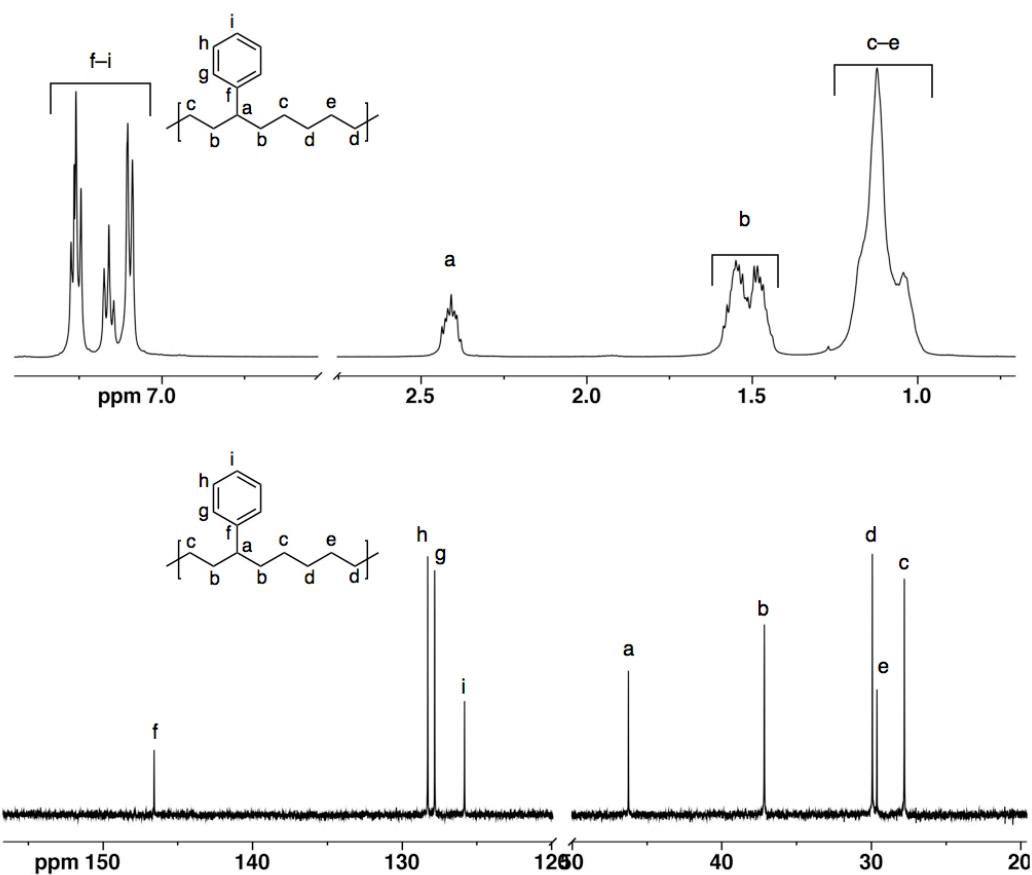
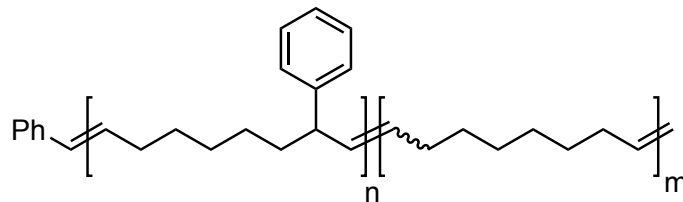


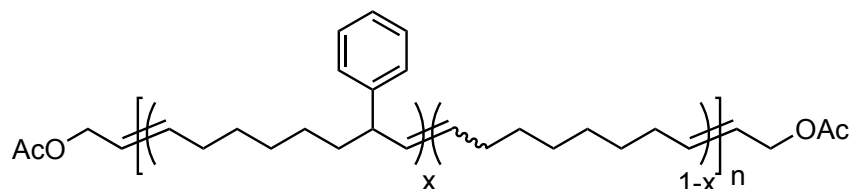
**Figure 5.30**

Molecular characterization of hydrogenated poly(3PC) (*i.e.*, *h*-poly(3PC)) by  $^1\text{H}$  (*top*) and  $^{13}\text{C}$  (*bottom*) NMR spectroscopy. Measured in  $\text{CDCl}_3$  at 20 °C with 500 MHz.



#### Polymerization procedure for poly(3PC-*b*-COE) diblock copolymers.

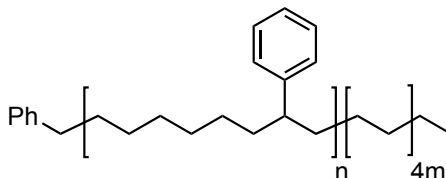
The synthesis of sample poly(3PC<sub>25</sub>-*b*-COE<sub>75</sub>) is described. The synthetic procedure for the other block copolymer is identical aside from the different ratio of monomers used. A 50 mL Schlenk flask containing a magnetic Teflon coated stir-bar was evacuated and flame-dried prior to refilling with argon. Under constant argon pressure, the flask was charged with 10.0 mL of dry THF and 1.07 g of 3PC monomer (5.75 mmol). The catalyst (30 mg of **G3**;  $3.4 \times 10^{-5}$  mol) was dissolved in 1.0 mL of dry THF before adding to the monomer solution via syringe. The solution almost immediately changed from faintly green to orange, indicating that the polymerization had initiated. The solution was stirred at room temperature for 50 min before adding 3.4 mL (2.92 g; 26.6 mmol) of COE. The solution almost immediately became solid-like, and stirring ceased. After 10 sec a few drops of ethyl vinyl ether were added to terminate the reaction. The entire yield was diluted with 150 mL of additional dry THF before precipitating into 1 L of cold ( $-40$  °C) MeOH. The polymer was isolated and dried under vacuum at  $50$  °C for at least 24 h prior to analysis.



#### Polymerization procedure for poly(3PC-*s*-C) statistical copolymers.

The polymerization protocol for statistical copolymers is similar to the block copolymers, with several important modifications. The synthesis of sample poly(3PC<sub>25</sub>-*s*-COE<sub>75</sub>) is described briefly; the other polymer was prepared identically, with the monomer ratio changed to reflect the different targeted composition. A flame-dried Schlenk flask was charged with 1.0 g of 3PC monomer

(5.37 mmol) and 3.4 g (2.9 mL; 26 mmol) of COE monomer along with 25 mL of dry THF ( $\approx 1$  M in total monomer), all under argon. The mixture was stirred rapidly before adding 10  $\mu$ L of 1,4-diacetoxy-2-butene to act as CTA. Finally, the monomer solution was heated to 40 °C before adding 2.5 mg of **G2** catalyst ( $3.3 \times 10^{-6}$  mol) as a solution in 1 mL of dry THF. The solution turned from faintly pink to orange after approximately 1 min indicating polymerization was proceeding. After 6 h at 40 °C, the solution was diluted with 25 mL additional THF and quenched with a few drops of ethyl vinyl ether. The polymer was isolated by precipitation into 500 mL of cold MeOH and dried under vacuum (3.5 g yield).



#### Hydrogenation of 3PC-C diblock and statistical copolymers.

Block copolymers and statistical copolymers were hydrogenated in the same manner. The hydrogenation of poly(3PC<sub>40-s</sub>-COE<sub>60</sub>) is described briefly. The entire yield of the copolymer (3.5 g) was dissolved at ambient temperature in 120 mL of xylenes. The solution was transferred to a pressure vessel with a side-arm affixed with a Teflon screw-seal. To the mixture was added 11.0 g of *p*-tosyl hydrazide (59 mmol) and a trace quantity ( $\sim 5$  mg) of 2,6-di-*tert*-butyl-4-methylphenol (BHT). The pressure vessel was sealed and then three consecutive freeze-pump-thaw cycles were performed on the mixture. Finally, under argon, the mixture was heated while rapidly stirring at 130 °C for 4 h before precipitating into 1 L of cold MeOH. The isolated polymer was dried for 24 h at 50 °C under vacuum (3.5 g yield).





- 
- [7] Neburchilov, V.; Martin, J.; Wang, H.; Zhang, J. *J. Power Sources* **2007**, *169*, 221-238.
- [8] Deluca, N. W.; Elabd, Y. A. *J. Polym. Sci., Part B: Polym. Phys.* **2006**, *44*, 2201-2225.
- [9] Goswami, M.; Sumpter, B. G.; Huang, T.; Messman, J. M.; Gido, S. P.; Isaacs-Sodeye, A. I.; Mays, J. W. *Soft Matter* **2010**, *6*, 6146-6154.
- [10] Yang, Y. S.; Siu, A.; Peckham, T. J.; Holdcroft, S., Structural and Morphological Features of Acid-Bearing Polymers for PEM Fuel Cells. In *Fuel Cells I*, 2008; Vol. 215, pp 55-126.
- [11] Yu, X.; Roy, A.; Dunn, S.; Badami, A. S.; Yang, J.; Good, A. S.; McGrath, J. E. *J. Polym. Sci., Part A: Polym. Chem.* **2009**, *47*, 1038-1051.
- [12] Park, M. J.; Downing, K. H.; Jackson, A.; Gomez, E. D.; Minor, A. M.; Cookson, D.; Weber, A. Z.; Balsara, N. P. *Nano Lett.* **2007**, *7*, 3547-3552.
- [13] Mauritz, K. A.; Moore, R. B. *Chem. Rev.* **2004**, *104*, 4535-4585.
- [14] Elabd, Y. A.; Hickner, M. A. *Macromolecules* **2011**, *44*, 1-11.
- [15] Carretta, N.; Tricoli, V.; Picchioni, F. *J. Membr. Sci.* **2000**, *166*, 189-197.
- [16] Heinzl, A.; Barragan, V. M. *J. Power Sources* **1999**, *84*, 70-74.
- [17] Kim, J.; Kim, B.; Jung, B. *J. Membr. Sci.* **2002**, *207*, 129-137.
- [18] Elabd, Y. A.; Napadensky, E.; Sloan, J. M.; Crawford, D. M.; Walker, C. W. *J. Membr. Sci.* **2003**, *217*, 227-242.
- [19] Kostalik, H. A.; Clark, T. J.; Robertson, N. J.; Mutolo, P. F.; Longo, J. M.; Abruna, H. D.; Coates, G. W. *Macromolecules* **2010**, *43*, 7147-7150.

- [20] Li, Q. F.; Jensen, J. O.; Savinell, R. F.; Bjerrum, N. J. *Prog. Polym. Sci.* **2009**, *34*, 449-477.
- [21] Baigl, D.; Seery, T. A. P.; Williams, C. E. *Macromolecules* **2002**, *35*, 2318-2326.
- [22] Grubbs, R. H.; Trnka, T. M. *Ruthenium in Organic Synthesis* **2004**, 153-177.
- [23] Alonso-Villanueva, J.; Rodriguez, M.; Vilas, J. L.; Laza, J. M.; Leon, L. M. *J. Macromol. Sci., Part A: Pure Appl. Chem.* **2010**, *47*, 1130-1134.
- [24] Alb, A. M.; Enohnyaket, P.; Craymer, J. F.; Eren, T.; Coughlin, E. B.; Reed, W. F. *Macromolecules* **2007**, *40*, 444-451.
- [25] Benedicto, A. D.; Claverie, J. P.; Grubbs, R. H. *Macromolecules* **1995**, *28*, 500-511.
- [26] Liaw, D. J.; Wu, P. L. *J. Mol. Catal. A-Chem.* **2000**, *160*, 35-43.
- [27] Hilf, S.; Berger-Nicoletti, E.; Grubbs, R. H.; Kilbinger, A. F. M. *Angew. Chem., Int. Ed.* **2006**, *45*, 8045-8048.
- [28] Hilf, S.; Grubbs, R. H.; Kilbinger, A. F. M. *Macromolecules* **2008**, *41*, 6006-6011.
- [29] Hilf, S.; Kilbinger, A. F. M. *Macromolecules* **2009**, *42*, 4127-4133.
- [30] Love, J. A.; Morgan, J. P.; Trnka, T. M.; Grubbs, R. H. *Angew. Chem., Int. Ed.* **2002**, *41*, 4035-4037.
- [31] Calderon, N.; Ofstead, E. A.; Judy, W. A. *J. Polym. Sci., Part A: Polym. Chem.* **1967**, *5*, 2209-2217.
- [32] Trnka, T. M.; Morgan, J. P.; Sanford, M. S.; Wilhelm, T. E.; Scholl, M.; Choi, T. L.; Ding, S.; Day, M. W.; Grubbs, R. H. *J. Am. Chem. Soc.* **2003**, *125*, 2546-2558.

- 
- [33] Kobayashi, S.; Pitet, L. M.; Hillmyer, M. A. *J. Am. Chem. Soc.* **2011**, *133*, 5794-5797.
- [34] Odian, G., *Principles of Polymerization*. 4th ed.; Wiley: Chichester, New York, 2004; p 812.
- [35] Calderon, N.; Morris, M. C. *J. Polym. Sci., Polym. Phys. Ed.* **1967**, *5*, 1283-1292.
- [36] Schneider, W. A.; Müller, M. F. *J. Mol. Catal.* **1988**, *46*, 395–403.
- [37] Wunderlich, B.; Dole, M. *Journal of Polymer Science* **1957**, *24*, 201-213.
- [38] Gaur, U.; Wunderlich, B. *J. Phys. Chem. Ref. Data* **1981**, *10*, 119-152.
- [39] Saito, T.; Moore, H. D.; Hickner, M. A. *Macromolecules* **2009**, *43*, 599-601.

## Chapter 6

### Carboxy-telechelic Polyolefins from ROMP with Maleic Acid as Chain Transfer Agent\*

Carboxy-telechelic polyolefins were prepared using a chain transfer–ring-opening metathesis polymerization strategy. Carboxylic acid end-groups were incorporated into poly(cyclooctene) utilizing maleic acid as a chain transfer agent. Efficient chain transfer and subsequent re-initiation was observed with this electron deficient chain transfer agent by employing the second-generation Grubbs catalyst. The metathesis with maleic acid led quantitatively to *trans* configuration about the terminal double bond in the polymer, corroborated by model cross-metathesis reactions between maleic acid and *cis*-4-octene that formed 2-hexenoic acid with exclusively *E* configuration. Subsequent chemical hydrogenation of the unsaturated telechelic polymers provided carboxy-telechelic linear polyethylene. The polymerization–hydrogenation protocol is a straightforward route to telechelic linear polyethylene using readily available starting materials that avoids tedious post-polymerization transformations.

---

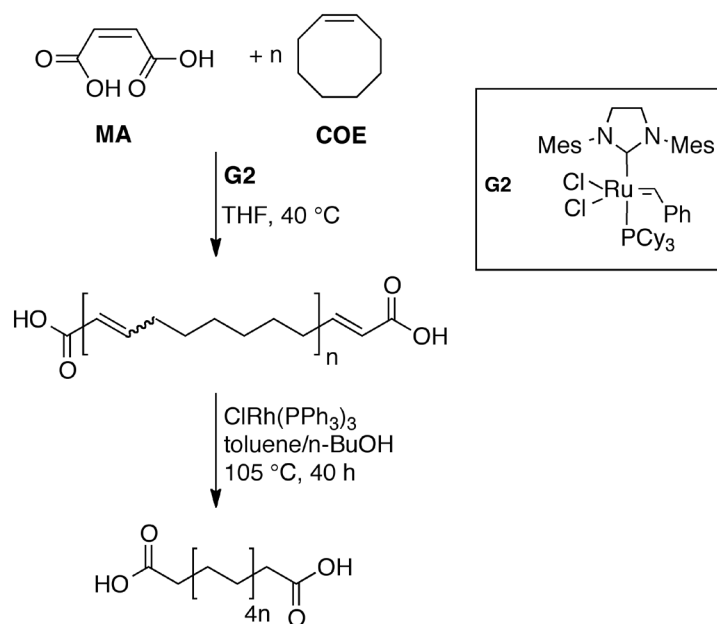
\* Reproduced in part with permission from Pitet, L. M.; Hillmyer, M. A. *Macromolecules* **2011**, *44*, 2378–2381. Copyright 2011 American Chemical Society.

## 6.1 Introduction

Functionalized polyolefins remain valuable and desirable synthetic targets.<sup>1–8</sup> More often than not, functional groups are incorporated by post-polymerization reactions.<sup>9–13</sup> Metathesis polymerizations can enable a straightforward route to functional polyolefins through a polymerization–hydrogenation strategy.<sup>14–22</sup> For example,  $\alpha,\omega$ -functional (i.e., telechelic) polyolefins are readily prepared by including a symmetric acyclic alkene during ring-opening metathesis polymerization (ROMP) of a cyclic olefin.<sup>23</sup> The simultaneous ring-opening and cross-metathesis (chain transfer, CT) between the propagating center and the chain transfer agent (CTA) results in the chain-end functionality. The efficacy of preparing chains with high functionality (i.e., average number of functional groups per chain,  $F_n \rightarrow 2$ ) rests on the transition metal-alkylidene catalyst being reactive toward the CTA, being able to reinitiate a new chain, and remaining active at low levels relative to the CTA (i.e.,  $[M]_0 > [CTA]_0 \gg [catalyst]_0$ ). The latter criterion can be fulfilled by using the highly reactive ruthenium alkylidene having N-heterocyclic carbene ligand (**G2**) developed by Grubbs.<sup>24</sup> This note describes the use of unprotected maleic acid (**MA**) as a CTA during ROMP of *cis*-cyclooctene (**COE**) to provide carboxy-telechelic PCOE with an average degree of polymerization ( $N$ ) dictated by the ratio of  $[COE]_0:[MA]_0$  (Scheme 1). The resulting ester-substituted metallo-carbene readily reacts with the cycloalkene/linear poly(alkene), in accordance with the observations by Grubbs and coworkers regarding the reactivity/stability of ester-substituted carbenes.<sup>25</sup> Subsequent hydrogenation provides linear polyethylene (LPE) with retention of the carboxy end-functionality.

Scheme 6.1

Synthesis of carboxy-telechelic poly(cyclooctene) and polyethylene by a CT-ROMP/hydrogenation approach



Cross-metathesis with vinylic compounds having electron withdrawing groups in the  $\alpha$ -position ( $\alpha$ -EWGs) such as acrylic amides,<sup>26–28</sup> acrylic acid,<sup>26,27,29,30</sup> and acrylonitrile<sup>31–34</sup> emerged in tandem with development of Ru-alkylidene precatalyst derivatives. Success of the CT-ROMP strategy relies on extensive cross-metathesis between a CTA and polymer chains. However, there are only a few examples including acyclic alkenes with  $\alpha$ -EWGs during ROMP,<sup>35,36</sup> despite the ROMP of 1-amide-cyclobutene derivatives being reported.<sup>37–39</sup> Conventional structures of symmetric CTAs for ROMP contain at least one methylene unit separating the alkene from the functional groups. For example, nitrile-telechelic poly(cyclooctadiene) (PCOD) was prepared with 1,4-dicyano-2-butene and 1,8-dicyano-4-octene as CTAs, the latter of which was reduced with  $\text{LiAlH}_4$  to provide amino-telechelic polymers.<sup>40,41</sup> Carboxy-terminal PCOD has been prepared using the CT-ROMP strategy with *cis*-1,4-bis(tert-butoxycarbonyl)-2-butene as a protected CTA and the first generation Grubbs catalyst.<sup>42</sup> Direct preparation of hydroxy-telechelic PCOD was also managed with *cis*-2-butene-1,4-diol as CTA;

however, the yields were consistently low and difficulty was encountered controlling molar mass with  $[\text{COD}]_0:[\text{CTA}]_0$ .<sup>24</sup> Additional methods have been reported for preparing carboxy terminal polynorbornenes by ROMP through termination of a living chain with a vinyl lactone<sup>43,44</sup> or cleavage of multiblocks.<sup>45</sup> Although  $\alpha$ -substituted vinyl compounds are routinely used in cross-metathesis, we could find no examples of CTAs for ROMP with the generic  $\text{FG}-\text{CH}=\text{CH}-\text{FG}$  structure [FG, functional group].<sup>35</sup>

## 6.2 Results and Discussion

Four samples were initially prepared by polymerizing **COE** in tetrahydrofuran at 40 °C with varying concentrations of **MA** (samples **1–5** in Table 6.1).

**Table 6.1.**

Degree of polymerization ( $N_n$ ) measured by SEC-MALS and NMR spectroscopy of carboxy-telechelic poly(cyclooctene)s

Sample #	CTA	$[\text{COE}]_0:[\text{CTA}]_0$	$N_n^a$ (NMR)	$N_n^b$ (SEC)	PDI <sup>c</sup>
<b>1</b>	<b>MA</b>	10	15	52	2.49 <sup>e</sup>
<b>2</b>	<b>MA</b>	50	53	71	2.30 <sup>e</sup>
<b>3</b>	<b>MA</b>	100	94	119	1.83
<b>4</b>	<b>MA</b>	200	210	236	1.77
<b>5</b>	<b>FA</b>	50	<i>d</i>	645	2.05
<b>6</b>	<b>2HA</b>	50	<i>d</i>	688	1.88

<sup>a</sup> calculated from the ratio of relative integration from repeat unit and end-group protons in the <sup>1</sup>H NMR spectrum. <sup>b</sup> determined by size-exclusion chromatography (SEC) with multi-angle light scattering (MALS) detection in THF, using  $dn/dc$  for PCOE determined previously ( $dn/dc_{\text{PCOE}} = 0.110 \text{ mL/g}$ ) (ref. <sup>46</sup>) <sup>c</sup> determined from size-exclusion chromatography in  $\text{CHCl}_3$  at 30 °C compared with polystyrene standards. <sup>d</sup> end-group signals were not observed in the <sup>1</sup>H NMR spectrum of this sample. <sup>e</sup> a small shoulder containing monomeric and/or oligomeric units was included in analysis, and thus PDI values are larger than expected for an equilibrium process with chain transfer.



The concentration of **G2** was kept approximately constant at  $[\text{COE}]_0:[\text{G2}]_0 \approx 20,000$ . Number average degrees of polymerization ( $N_n$ ) were determined by end-group analysis using  $^1\text{H}$  nuclear magnetic resonance (NMR) spectroscopy assuming exactly two end groups per polymer chain and compared to values obtained using size-exclusion chromatography (SEC) with multi-angle light scattering (MALS) detection.

The  $^1\text{H}$  NMR spectrum of a poly(cyclooctene) (PCOE) sample with  $[\text{COE}]_0:[\text{MA}]_0 = 50$  (Figure 1a) shows signals associated with the repeating units of PCOE and the olefinic protons adjacent to the carboxylic acid end-groups (Figure 6.2). The “external” olefinic proton ( $\text{H}^g$ ) appears at 5.8 ppm with doublet of triplet multiplicity (doublet,  $^3J_{gf} = 15.6$  Hz; triplet,  $^4J_{ge} = 1.6$  Hz). The “internal” terminal olefinic protons ( $\text{H}^i$ ) appear downfield at 6.1 ppm with doublet of triplet multiplicity and coupling constants (doublet,  $^3J_{fg} = 15.5$  Hz; triplet,  $^3J_{fe} = 6.0$  Hz) consistent with *E* configuration. The strong EW carboxyl groups influence the methylene protons  $\alpha$  ( $\text{H}^e$ ) to the “internal” terminal olefinic carbon, causing a slight downfield shift compared to the main repeating unit methylene signals. The value of the triplet coupling constant attributed to the olefinic protons  $\text{H}^f$  suggests coupling to the methylene protons  $\text{H}^e$  at 2.23 ppm (triplet,  $^3J_{ed} = 6.4$  Hz; doublet,  $^3J_{ef} = 6.0$  Hz; doublet  $^4J_{eg} = 1.6$  Hz), and is consistent with the assignments depicted in Figure 1a. Further structural corroboration is provided by two-dimensional  $^1\text{H}$ – $^1\text{H}$  correlated NMR spectroscopy (COSY) (Figure 6.3). The integration values of the end-group signals compared with the repeat units are in good agreement with the targeted degree of polymerization assuming quantitative monomer consumption and exactly two functional groups per polymer chain. The high polymer yield for each sample (> 90% in all cases) suggests near-quantitative monomer conversion. Molecular weight control by  $[\text{COE}]_0:[\text{MA}]_0$  is further evidenced by the relative elution volumes observed in SEC chromatograms (Figure 6.1b). The values of  $N_n$  of the polymer samples 1–4 as determined by NMR spectroscopy and SEC–MALS scale linearly with  $[\text{COE}]_0:[\text{MA}]_0$  (inset of Figure 6.1b). The discrepancy between  $N$  measured by NMR spectroscopy and SEC for sample 1 possibly arises from aggregation of the carboxylic end-groups due to their

relatively high concentration at this low molar mass. In that case, the scattering intensity of the aggregates would be artificially high. For sample **1**, the NMR results likely give a more accurate degree of polymerization.

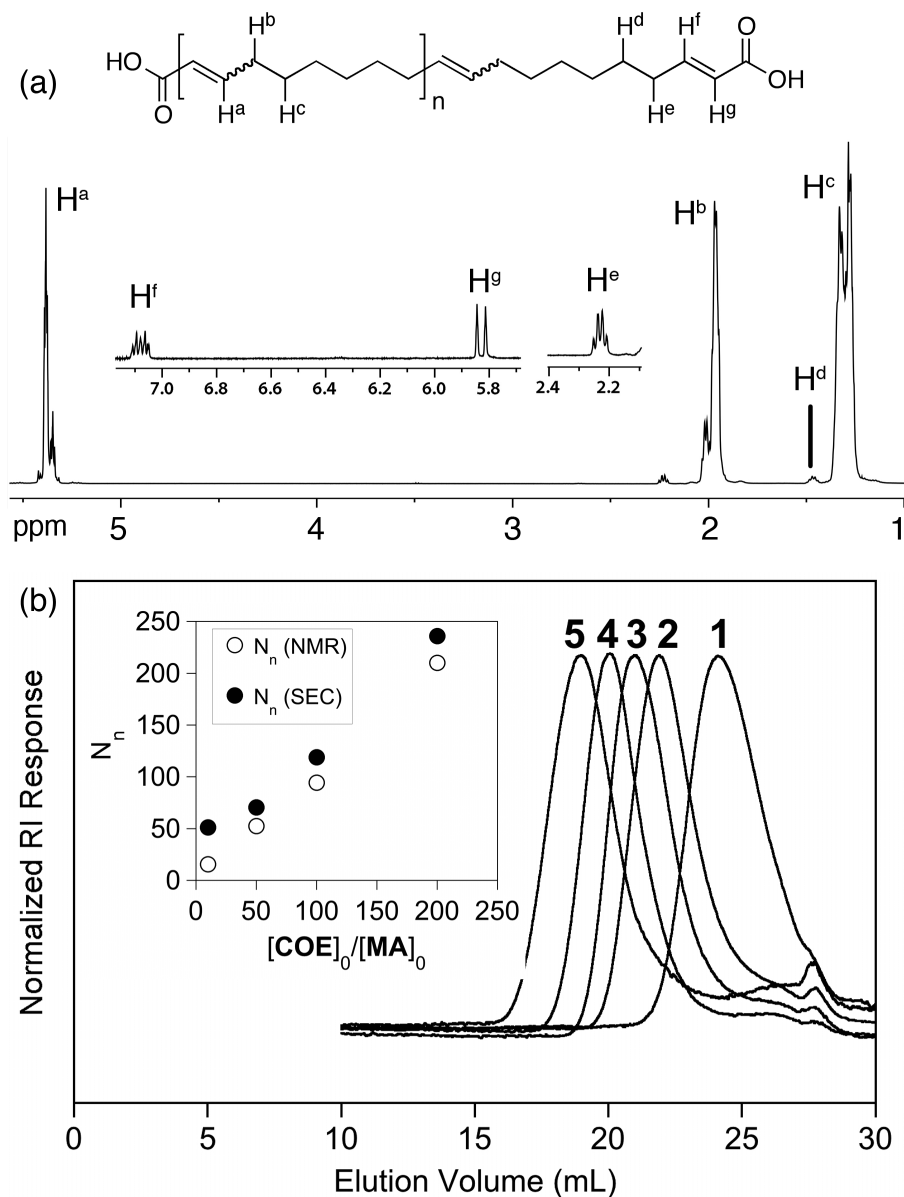


**Figure 6.1**

(a)  $^1\text{H}$  NMR ( $\text{CDCl}_3$ ) spectra for the carboxy-telechelic PCOE **2** ( $[\text{COE}]_0/[\text{MA}]_0 = 50$ ); (b) SEC chromatograms for samples **1**, **2**, **3**, **4** and **5** and relationship between  $N_n$  and  $[\text{COE}]_0/[\text{MA}]_0$  for samples **1**, **2**, **3**, and **4** (inset).



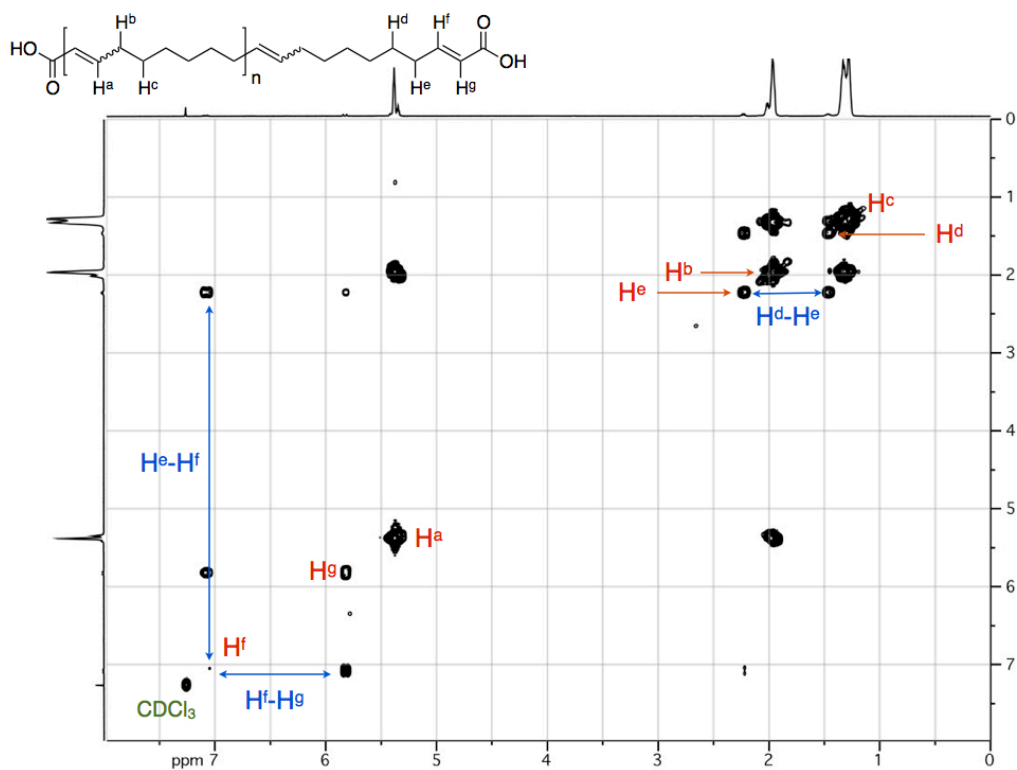


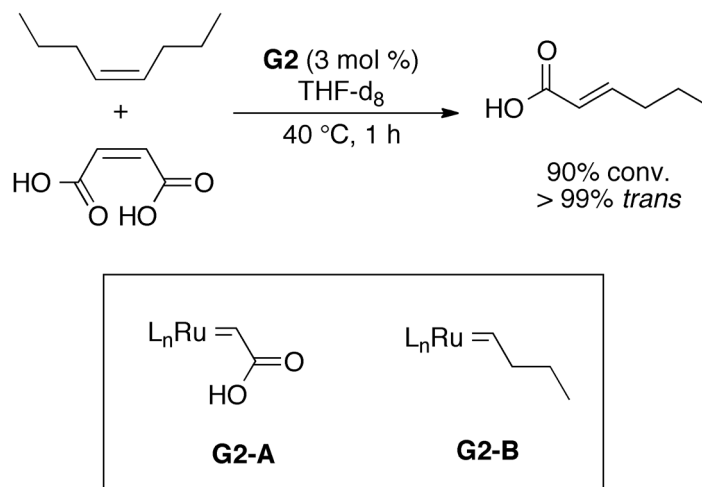
**Figure 6.3.**

$^1\text{H}$ - $^1\text{H}$  correlated spectroscopy (COSY) NMR spectrum for PCOE sample **1** from Table 1 highlighting the relevant proton correlations.

Once incorporated into the chain, the end-group is essentially non-reactive. Indeed, when **COE** was polymerized with **G2** in the presence of either fumaric acid (**FA**, i.e., *trans* isomer of maleic acid) or *trans*-2-hexenoic acid (**2HA**), carboxyl end-groups were not observed by  $^1\text{H}$  NMR spectroscopy and high molecular weight polymer was obtained (entries **5** and **6** in Table 6.1; also see Figure 6.1b). Cross-metathesis between *cis*-4-octene (**4Oct**) and **MA** provides direct evidence for the preferred stereochemical orientation of the Ru-alkylidene species during each metathetical cycle. An equimolar mixture of **MA** and **4Oct** using 3 mol % (per double bond) **G2** catalyst in  $\text{THF-d}_8$  at 40 °C formed predominantly **2HA** (Scheme 6.2).

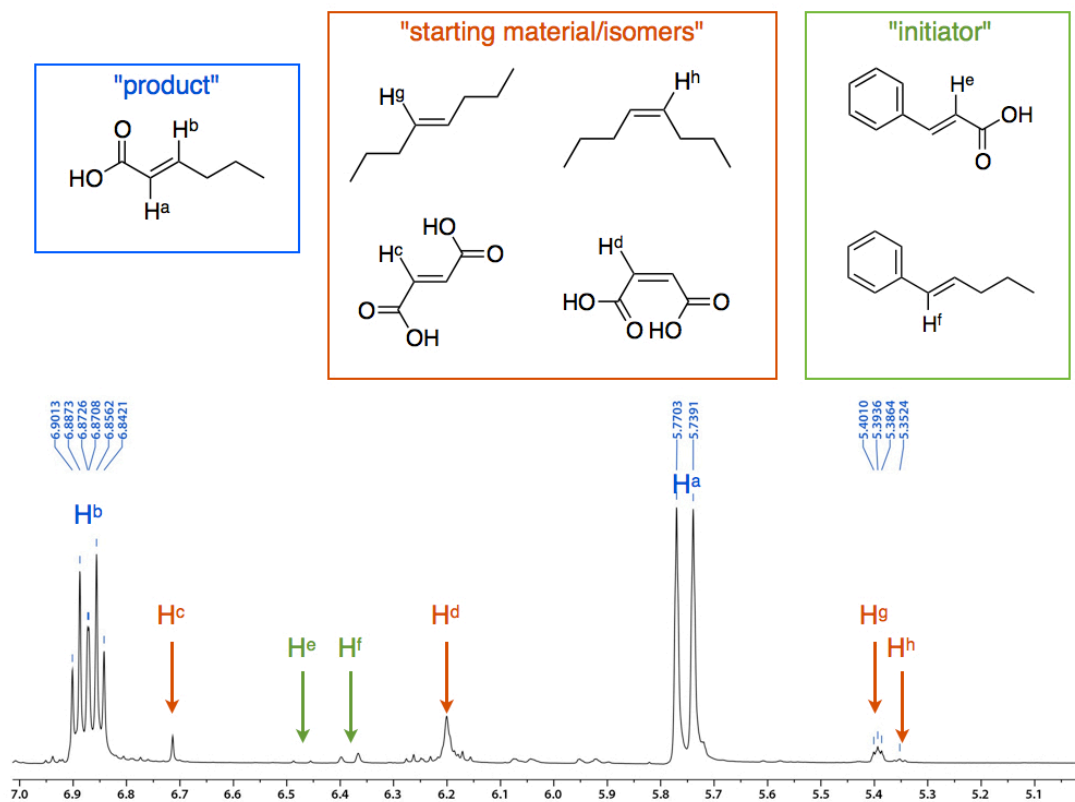
## Scheme 6.2

Cross-metathesis between **MA** and **4Oct** to synthesize *trans*-2-hexenoic acid. The two possible reactive Ru-alkylidene species are shown resulting from **MA** metathesis (**G2-A**) or **4Oct** metathesis (**G2-B**).



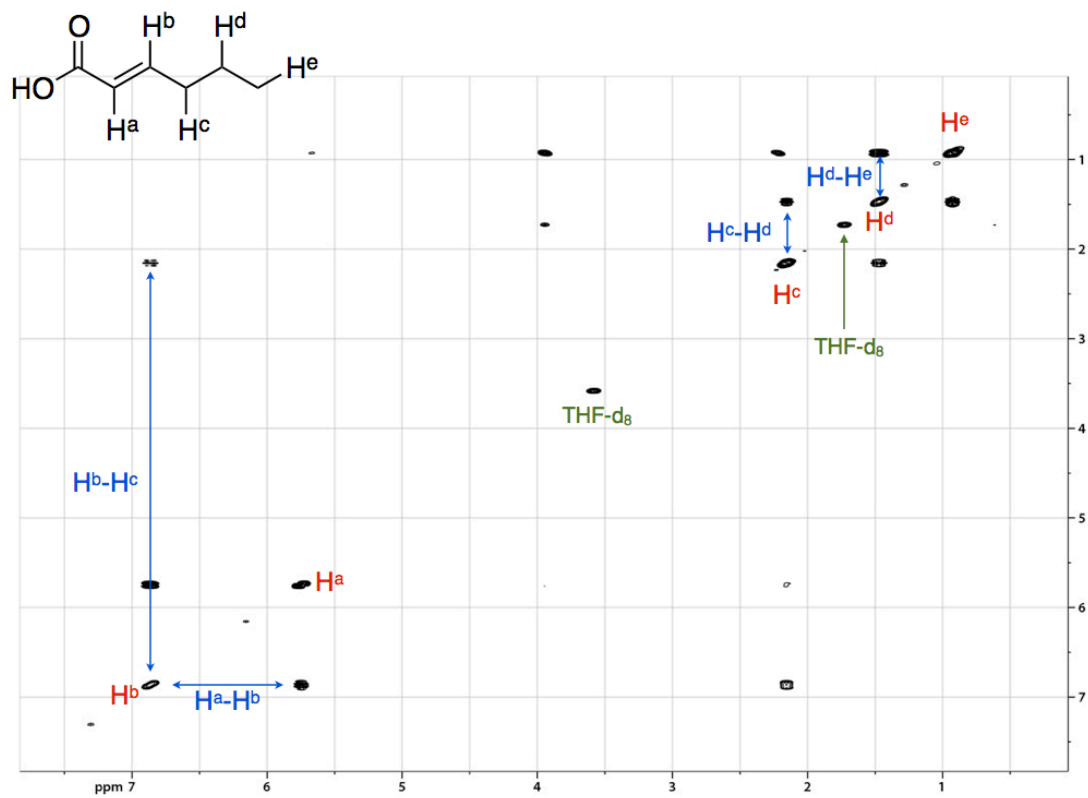
The  $^1\text{H}$  NMR spectrum of the product (Supporting Information) reveals greater than 90 % conversion to **2HA** product having essentially pure *E* configuration about the double bond (Figure 6.3). It is assumed that the *cis* isomer of the **2HA** would exhibit significant differences in chemical shift in either  $^1\text{H}$  or  $^{13}\text{C}$  NMR spectra to clearly observe and quantify if it were present. The different isomers can clearly be detected for the reactants (*cis* vs. *trans*-4-octene and maleic vs. fumaric acid). The presence of a sterically unencumbered Ru-alkylidene active species (**G2-B** in Scheme 6.2) is crucial to efficient metathesis with **MA**. The electron deficient Ru-alkylidene **G2-A** is nearly prohibited from cross-metathesizing with **MA**; reaction with **4Oct** is far more favorable. Indeed, self-cross-metathesis of maleic acid under identical conditions converted only 2.5 mol % of the double bonds to the *E* configuration. The commercial maleic acid contained 1.2 mol % *trans* double bonds. The cross metathesis reaction led to 3.7 mol % *trans* configuration in the equilibrium product. The proposed metathetical cycle (Figure 6.4) entails the preferred reaction between **G2-A** with **4Oct**. Of course, isomerization of *Z*-4Oct to *E*-4Oct may well proceed throughout the reaction and thus **G2-A** could react with either isomer. We suggest that *E*-2-hexenoic acid is the thermodynamically





**Figure 6.5.**

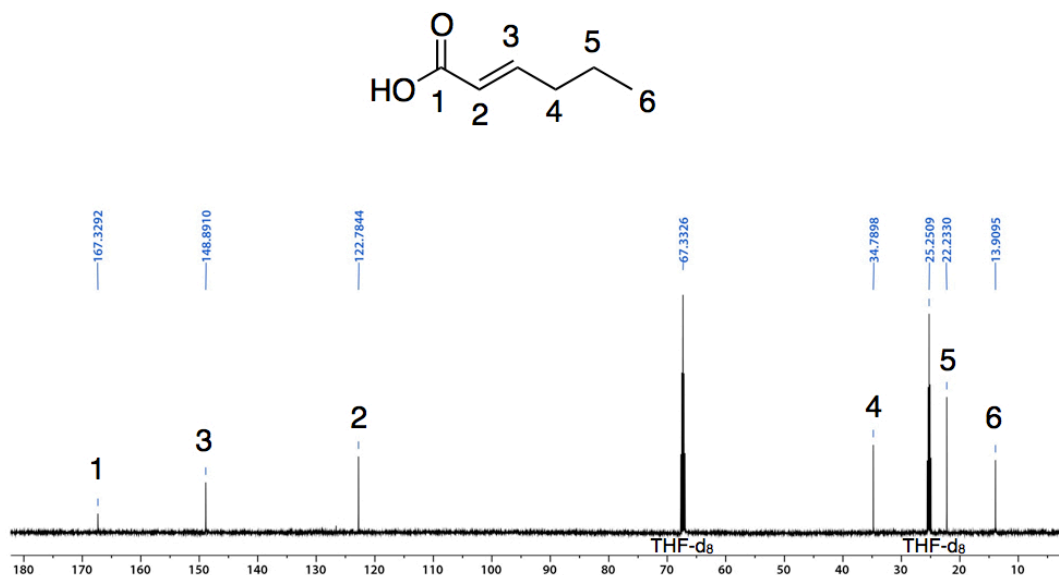
$^1\text{H}$  NMR spectrum for the olefinic region for the cross-metathesis between **MA** and **4Oct**, in THF- $d_6$  at 40 °C for 1.5 h. This spectrum highlights the signals associated with the components described in the text and illustrated (color-coded) above the spectrum here. This included starting materials, isomerized starting materials, initiator benzylidene compounds, and the product *trans-2HA* comprising the majority of formed compounds.



**Figure 6.6.**

<sup>1</sup>H-<sup>1</sup>H correlated spectroscopy (COSY) NMR spectrum for *trans*-2HA in THF-d<sub>8</sub>. The correlations support the purported structure of the major product, and agree well with the spectrum in CDCl<sub>3</sub> reported in the literature and by commercial vendors.

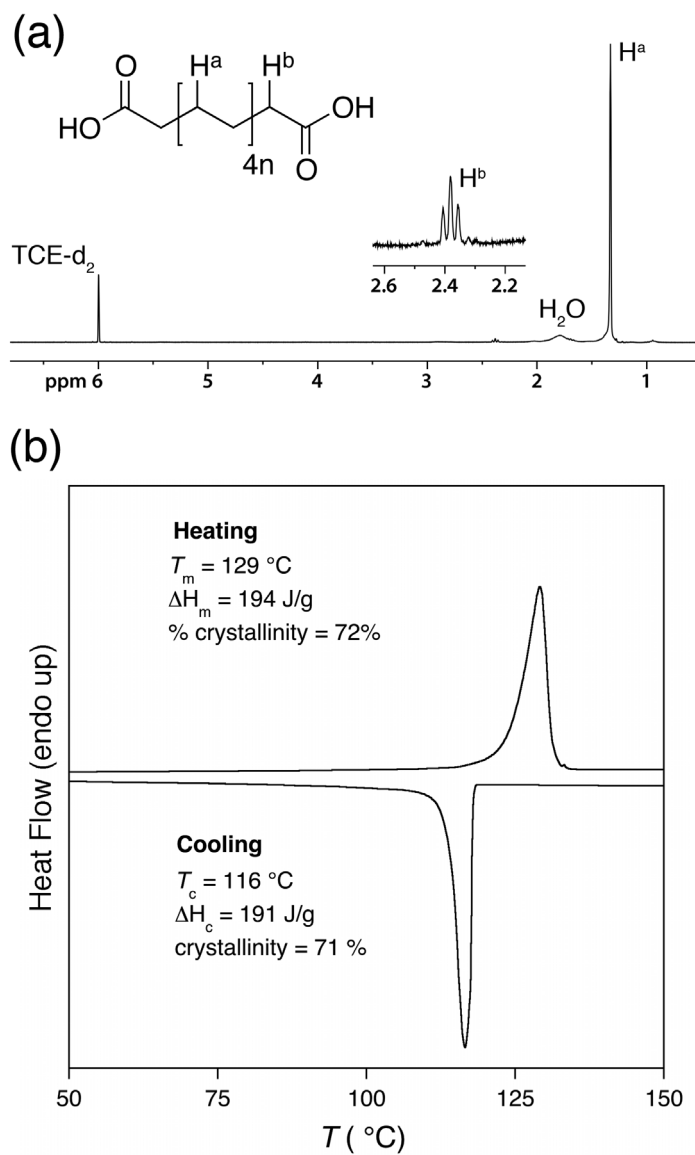


**Figure 6.7**

<sup>13</sup>C NMR spectrum of the *trans*-2HA formed from cross-metathesis between *cis*-4-octene and maleic acid in THF-*d*<sub>8</sub>.

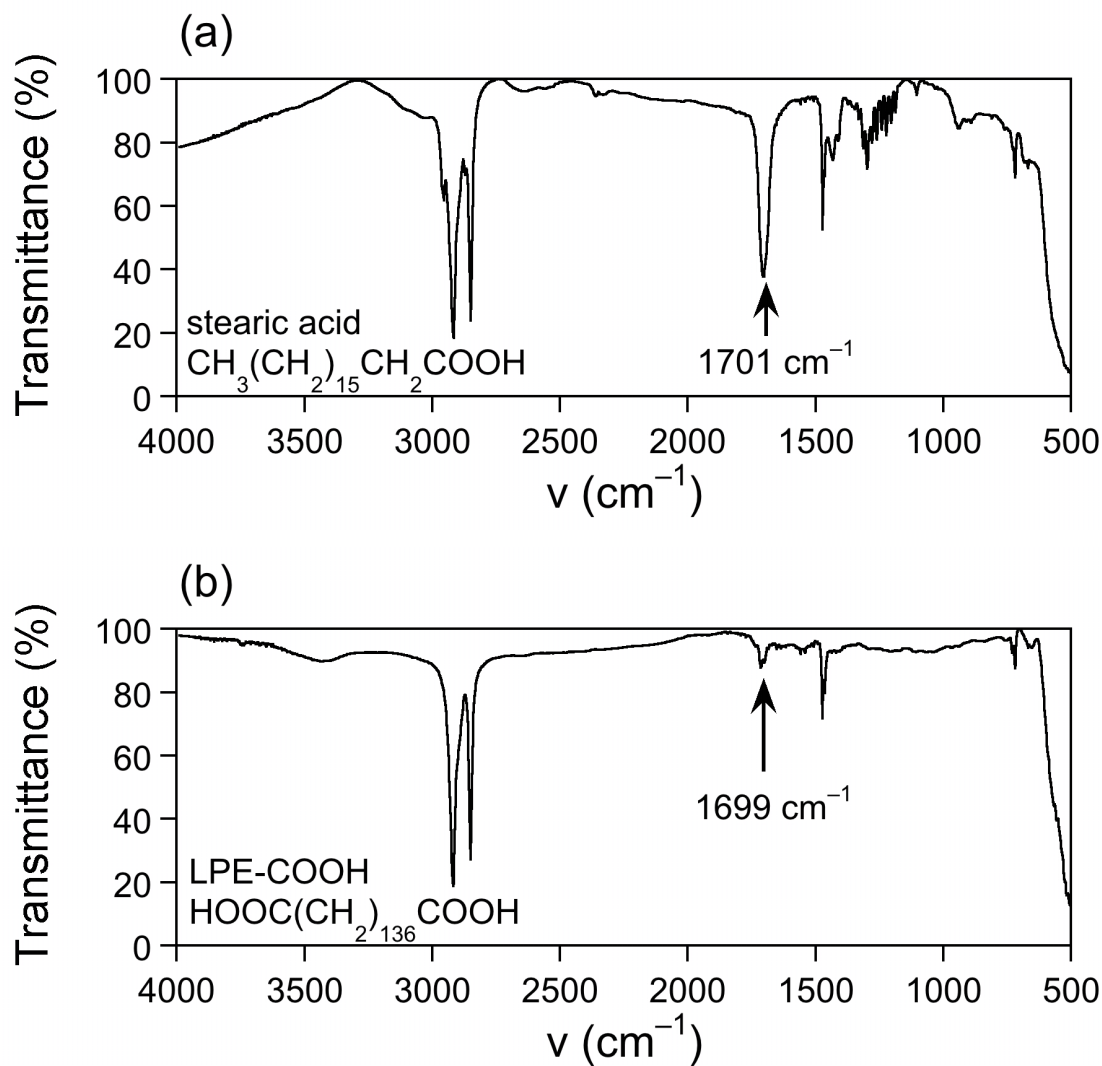
Hydrogenation of the carboxy-telechelic PCOE represents a convenient path toward LPE with reactive end functionality (see Scheme 6.1).<sup>49–53</sup> Attempts at heterogeneous hydrogenation with a silica-supported Pt catalyst provided saturated materials, although reduction of the carboxyl groups to hydroxyl functionality was not entirely preventable. This observation is consistent with reports by Wagener and coworkers in hydrogenating unsaturated polyolefins having pendant carboxyl functionality.<sup>54</sup> Alternatively, hydrogenation with Wilkinson's catalyst [tris(triphenylphosphine)rhodium(I) chloride]<sup>55</sup> provided essentially quantitative saturation of backbone double bonds without reduction of carboxyl groups. The <sup>1</sup>H NMR spectrum obtained in CDCl<sub>2</sub>CDCl<sub>2</sub> (1,1,2,2-tetrachloroethane-*d*<sub>2</sub>) at 100 °C shows the signals for the methylene protons α to the carboxyl groups (Figure 6.8a). The position of the peak is in agreement with analogous protons in the model compound stearic acid [CH<sub>3</sub>(CH<sub>2</sub>)<sub>16</sub>COOH]. The relative integration of the signals from the end-groups compared with the repeating unit provides a value for the degree of polymerization, *N*<sub>n</sub>, for the linear polyethylene (8-carbon repeating unit; *N*<sub>n</sub> = 17) that agrees reasonably well with

the unsaturated PCOE precursor ( $N_n = 15$ ). IR spectroscopy provides further evidence for the polymer retaining the carboxyl end-groups during hydrogenation, especially upon comparison with a model spectrum of stearic acid (Figure 6.9).



**Figure 6.8**

(a)  $^1\text{H}$  NMR spectrum showing the saturated backbone protons and end-group protons adjacent to the carboxyl end-groups magnified. (b) DSC thermogram for the cooling cycle and the second heating cycle and the corresponding phase change temperatures ( $T$ ), enthalpies ( $\Delta H$ ) and crystallinities.

**Figure 6.9**

Infrared spectra for (a) model linear alkane with carboxyl end-group, stearic acid, with 16 methylene units per carboxyl group and (b) linear polyethylene from hydrogenated sample 1 (from Table 6.1,  $N_n = 17$ ) having ~68 methylene units per end group.

The thermograms (heating rate = 10 °C min<sup>-1</sup>) from differential scanning calorimetry (DSC) reveal temperatures of melting ( $T_m = 129$  °C) and crystallization ( $T_c = 116$  °C) that are consistent with a completely linear saturated hydrocarbon backbone (Figure 6.8b). The melting and crystallization enthalpies indicate typical values for LPE crystallinity (ca. 70%). This carboxy-telechelic LPE offers the possibility to further functionalize the chain ends and create hybrid soft-materials that combine the physical attributes of LPE and with other materials. This straightforward approach to carboxyl functional LPE enhances the convenience with which similarly complex materials can be prepared utilizing metathesis.

## 6.3 Conclusions

The method described here represents a progressive approach to single-step end-functionalization of polyolefins with carboxylic acids. These materials have potential commercial relevance.

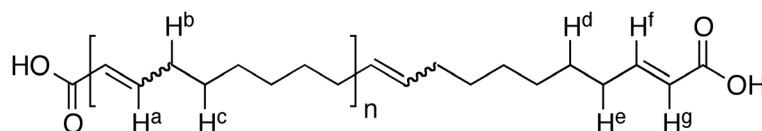
## 6.4 Experimental Details

### 6.4.1 Materials

Tetrahydrofuran (THF) and toluene (both from Avantor<sup>TM</sup>) were passed through an activated alumina column under nitrogen to remove protic impurities. All other reagent grade solvents were used without further purification. *cis*-cyclooctene (**COE**), (IMesH<sub>2</sub>)-(Cy<sub>3</sub>P)RuCl<sub>2</sub>(CHPh) (Grubbs second generation catalyst, **G2**), maleic acid (**MA**), fumaric acid (**FA**) were purchased from Sigma-Aldrich. Wilkinson's catalyst [chloro tris(triphenylphosphine)Rhodium(I)] was purchased from Strem Chemicals. The deuterated solvents CDCl<sub>3</sub>, THF-*d*<sub>8</sub> and 1,1,2,2-tetrachloroethane-*d*<sub>2</sub> were purchased from Cambridge Isotope Laboratories. **COE** was distilled over CaH<sub>2</sub> prior to use. All other chemicals were used as received.

## 6.4.2 Synthetic Details

### 6.4.2.1 Polymerization of *cis*-cyclooctene with maleic acid chain-transfer agent



The synthesis of each PCOE sample was similar. The only changes made between samples were the initial concentration of CTA. The preparation of sample 2 ( $[\text{COE}]_0/[\text{MA}]_0 = 50$ ) in Table 2 is described in detail: maleic acid (253 mg; 2.18 mmol) was placed in a two-neck 100 mL flask with a Teflon® coated magnetic stir-bar. The flask and its contents were placed under vacuum and then recharged with argon. The evacuation–fill cycle was repeated three times over 30 min. Anhydrous THF (60 mL) was transferred via cannula into the reaction flask with a constant argon purge. An oven-dried glass syringe was used to transfer COE (12 g; 109 mmol) into the flask. The flask was immersed in an oil-bath at 40 °C immediately before transferring G2 catalyst (5 mg; 5.9  $\mu\text{mol}$ ) as a solution in 1 mL of THF. The reaction completely gelled into a highly viscous polymer solution within 2 min; the stir-bar completely stopped moving. The viscosity then slowly decreased over the next 20 min, until the stir-bar was freely spinning and the solution had a viscosity comparable to vegetable oil. After 2 h, the entire solution was quenched with ~0.5 mL of ethyl vinyl ether and stirred for 5 min before precipitating into 500 mL cold MeOH (–40 °C). The polymer was isolated and dried under *vacuo* for 15 h at room temperature (94% yield). The polymer was characterized by  $^1\text{H}$  NMR,  $^{13}\text{C}$  NMR, COSY NMR spectroscopies, SEC-MALS, DSC and IR spectroscopy.

$^1\text{H}$  NMR (500 MHz;  $\text{CDCl}_3$ )  $\delta$  6.072 ( $\text{H}^f$ , dt, trans,  $^3J_{fg} = 15.52$ ,  $^3J_{fe} = 6.03$  Hz), 5.826 ( $\text{H}^g$ , dt, trans,  $^3J_{gf} = 15.58$  Hz,  $^4J_{ge} = 1.61$  Hz), 5.383 ( $\text{H}^a$ , t, trans), 5.348 ( $\text{H}^a$ , t, cis), 2.230 ( $\text{H}^e$ , tdd, trans,  $^3J_{ed} = 6.37$ ,  $^3J_{ef} = 6.05$ ,  $^4J_{eg} = 1.60$  Hz), 2.013 ( $\text{H}^b$ , q, cis), 1.964 ( $\text{H}^b$ , q, trans), 1.462 ( $\text{H}^d$ , m, trans), 1.33–1.26 ( $\text{H}^c$ , m).

$^{13}\text{C}$  NMR (125 MHz;  $\text{CDCl}_3$ ): repeat unit –  $\delta$  130.34 (trans), 129.88 (cis), 32.63, 29.77, 29.66, 29.24, 29.20, 29.11, 29.07, 26.24; end-group – 152.46 (carbonyl), 130.55 ( $\beta$ -olefin), 130.18 ( $\alpha$ -olefin), 32.54, 32.34, 29.49, 28.87, 26.85.

#### 6.4.2.2 Synthesis of *trans*-2-hexenoic acid

An NMR tube was charged with maleic acid (22 mg; 0.189 mmol) and *cis*-4-octene (21 mg; 0.186 mmol) before adding G2 (10 mg; 11.8  $\mu\text{mol}$ ) as a solution in 1.0 mL of THF- $d_8$ . The solution was shaken vigorously and immediately immersed in a bath and kept at 40  $^\circ\text{C}$  for 1.5 h before cooling and analyzing by NMR spectroscopy.

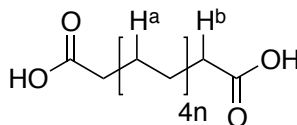
$^1\text{H}$  NMR (500 MHz; THF- $d_8$ , 20  $^\circ\text{C}$ ):  $\delta$  6.87 (dt,  $J = 15.4$ , 6.2 Hz, 1H), 5.75 (d,  $J = 15.6$  Hz, 1H), 2.16 (tdd,  $J = 6.3$ , 6.2, 1.5 Hz, 2H), 1.48 (tq,  $J = 6.4$ , 6.3 Hz, 2H), 0.93 (t,  $J = 6.4$  Hz, 3H).

$^{13}\text{C}$  NMR (125 MHz; THF- $d_8$ ):  $\delta$  166.33, 148.89, 122.78, 34.77, 22.23, 13.91

*cis*-4-octene (manufacturer)

$^1\text{H}$ -NMR (500 MHz; thf- $d_8$ ):  $\delta$  5.35 (t,  $J = 5.0$  Hz, 2H), 2.02 (q,  $J = 6.4$  Hz, 4H), 1.37 (sextet,  $J = 6.3$  Hz, 1H), 0.90 (t,  $J = 6.4$  Hz, 1H).

#### 6.4.2.3 Synthesis of carboxyl terminal LPE by hydrogenation



The precursor PCOE (1.0 g of sample 1 in Table 1;  $\sim 9$  mmol double bonds) was dissolved in a mixture of 50 mL of toluene and 20 mL of *n*-butanol, which required slight warming ( $\sim 35$   $^\circ\text{C}$ ). Wilkinson's catalyst (9 mg; 9.5  $\mu\text{mol}$ ) was placed in the

polymer solution and the entire mixture was transferred to a high-pressure reactor (Pressure Products Industries Inc.). The reactor was sealed and charged three times with 100 psi of argon to remove much of the air. The solution was then charged with 700 psi of H<sub>2</sub> and heated to 105 °C while stirring rapidly with an overhead mechanical stirrer. The reactor was recharged once when the pressure subsided to ~400 psi. The solution was stirred like this for two days before cooling to ambient temperature and disassembling the reactor. The solution was precipitated into 500 mL of MeOH, isolated by filtration and dried at 50 °C overnight. The slightly off-white polymer was analyzed by <sup>1</sup>H, <sup>13</sup>C NMR and IR spectroscopy. <sup>1</sup>H NMR (300 MHz; CDCl<sub>2</sub>CDCl<sub>2</sub> [TCE-d<sub>2</sub>]; 100 °C): δ 2.38 (H<sup>c</sup>), 1.33 (H<sup>a</sup>). <sup>13</sup>C NMR (75 MHz; TCE-d<sub>2</sub>; 100 °C): δ 30.5

## 6.5 References

- [1] Amin, S. B.; Marks, T. J. *Angew. Chem., Int. Ed.* **2008**, *47*, 2006–2025.
- [2] Boalen, N. K.; Hillmyer, M. A. *Chem. Soc. Rev.* **2005**, *34*, 267–275.
- [3] Domski, G. J.; Rose, J. M.; Coates, G. W.; Bolig, A. D.; Brookhart, M. *Prog. Polym. Sci.* **2007**, *32*, 30–92.
- [4] Kawahara, N.; Saito, J.; Matsuo, S.; Kaneko, H.; Matsugi, T.; Kashiwa, N., Polymer Hybrids Based on Polyolefins – Syntheses, Structures, and Properties. In *New Frontiers in Polymer Synthesis*, Springer–Verlag Berlin: Berlin, 2008; Vol. 217, pp 79–119.
- [5] Mkhallid, I. A. I.; Barnard, J. H.; Marder, T. B.; Murphy, J. M.; Hartwig, J. F. *Chem. Rev.* **2009**, *110*, 890–931.
- [6] Moad, G. *Prog. Polym. Sci.* **1999**, *24*, 81–142.
- [7] Passaglia, E.; Coiai, S.; Augier, S. *Prog. Polym. Sci.* **2009**, *34*, 911–947.
- [8] Zhao, Y.; Wang, L.; Xiao, A.; Yu, H. *Prog. Polym. Sci.* **2010**, *35*, 1195–1216.

- [9] Bae, C.; Hartwig, J. F.; Chung, H.; Harris, N. K.; Switek, K. A.; Hillmyer, M. A. *Angew. Chem., Int. Ed.* **2005**, *44*, 6410–6413.
- [10] Boasen, N. K.; Hillmyer, M. A. *Macromolecules* **2003**, *36*, 7027–7034.
- [11] Kondo, Y.; Garcia-Cuadrado, D.; Hartwig, J. F.; Boasen, N. K.; Wagner, N. L.; Hillmyer, M. A. *J. Am. Chem. Soc.* **2002**, *124*, 1164–1165.
- [12] Mathers, R. T.; Coates, G. W. *Chem. Commun.* **2004**, 422–423.
- [13] Shin, J.; Chang, A. Y.; Brownell, L. V.; Racoma, I. O.; Ozawa, C. H.; Chung, H. Y.; Peng, S.; Bae, C. S. *J. Polym. Sci., Part A: Polym. Chem.* **2008**, *46*, 3533–3545.
- [14] Aitken, B. S.; Lee, M.; Hunley, M. T.; Gibson, H. W.; Wagener, K. B. *Macromolecules* **2010**, *43*, 1699–1701.
- [15] Baughman, T. W.; Wagener, K. B. *Adv. Polym. Sci.* **2005**, *176*, 1–42.
- [16] Bielawski, C. W.; Grubbs, R. H. *Prog. Polym. Sci.* **2007**, *32*, 1–29.
- [17] Clark, T. J.; Robertson, N. J.; Kostalik, H. A.; Lobkovsky, E. B.; Mutolo, P. F.; Abruna, H. D.; Coates, G. W. *J. Am. Chem. Soc.* **2009**, *131*, 12888–+.
- [18] Kostalik, H. A.; Clark, T. J.; Robertson, N. J.; Mutolo, P. F.; Longo, J. M.; Abruna, H. D.; Coates, G. W. *Macromolecules* **2010**, *43*, 7147–7150.
- [19] Opper, K. L.; Fassbender, B.; Brunklaus, G.; Spiess, H. W.; Wagener, K. B. *Macromolecules* **2009**, *42*, 4407–4409.
- [20] Opper, K. L.; Markova, D.; Klapper, M.; Mullen, K.; Wagener, K. B. *Macromolecules* **2010**, *43*, 3690–3698.
- [21] Opper, K. L.; Wagener, K. B. *Macromol. Rapid. Commun.* **2009**, *30*, 915–919.



- [22] Robertson, N. J.; Kostalik, H. A.; Clark, T. J.; Mutolo, P. F.; Abruna, H. D.; Coates, G. W. *J. Am. Chem. Soc.* **2010**, *132*, 3400–3404.
- [23] Tasdelen, M. A.; Kahveci, M. U.; Yagci, Y. *Prog. Polym. Sci.* **2011**, *36*, 455–567.
- [24] Bielawski, C. W.; Scherman, O. A.; Grubbs, R. H. *Polymer* **2001**, *42*, 4939–4945.
- [25] Ulman, M.; Belderrain, T. R.; Grubbs, R. H. *Tetrahedron Lett.* **2000**, *41*, 4689–4693.
- [26] Chatterjee, A. K.; Choi, T. L.; Sanders, D. P.; Grubbs, R. H. *J. Am. Chem. Soc.* **2003**, *125*, 11360–11370.
- [27] Choi, T. L.; Chatterjee, A. K.; Grubbs, R. H. *Angew. Chem., Int. Ed.* **2001**, *40*, 1277–+.
- [28] Streuff, J.; Muñiz, K. *J. Organomet. Chem.* **2005**, *690*, 5973–5978.
- [29] Choi, T. L.; Lee, C. W.; Chatterjee, A. K.; Grubbs, R. H. *J. Am. Chem. Soc.* **2001**, *123*, 10417–10418.
- [30] Cossy, J.; Bargiggia, F.; BouzBouz, S. *Org. Lett.* **2003**, *5*, 459–462.
- [31] Bruneau, C.; Fischmeister, C.; Miao, X. W.; Malacea, R.; Dixneuf, P. H. *Eur. J. Lipid Sci. Technol.* **2010**, *112*, 3–9.
- [32] Love, J. A.; Morgan, J. P.; Trnka, T. M.; Grubbs, R. H. *Angew. Chem., Int. Ed.* **2002**, *41*, 4035–4037.
- [33] Malacea, R.; Fischmeister, C.; Bruneau, C.; Dubois, J.-L.; Couturier, J.-L.; Dixneuf, P. H. *Green Chem.* **2009**, *11*, 152–155.
- [34] Rivard, M.; Blechert, S. *Eur. J. Org. Chem.* **2003**, 2225–2228.

- 
- [35] Feast, W. J.; Harrison, D. B. *Polymer* **1991**, *32*, 558–563.
- [36] Cramail, H.; Fontanille, M.; Soum, A. *J. Mol. Catal.* **1991**, *65*, 193–203.
- [37] Lee, J. C.; Parker, K. A.; Sampson, N. S. *J. Am. Chem. Soc.* **2006**, *128*, 4578–4579.
- [38] Song, A.; Lee, J. C.; Parker, K. A.; Sampson, N. S. *J. Am. Chem. Soc.* **2010**, *132*, 10513–10520.
- [39] Song, A.; Parker, K. A.; Sampson, N. S. *J. Am. Chem. Soc.* **2009**, *131*, 3444–3445.
- [40] Ji, S.; Hoyer, T. R.; Macosko, C. W. *Macromolecules* **2004**, *37*, 5485–5489.
- [41] Ji, S. X.; Hoyer, T. R.; Macosko, C. W. *Polymer* **2008**, *49*, 5307–5313.
- [42] Morita, T.; Maughon, B. R.; Bielawski, C. W.; Grubbs, R. H. *Macromolecules* **2000**, *33*, 6621–6623.
- [43] Hilf, S.; Grubbs, R. H.; Kilbinger, A. F. M. *J. Am. Chem. Soc.* **2008**, *130*, 11040–11048.
- [44] Hilf, S.; Kilbinger, A. F. M. *Macromolecules* **2010**, *43*, 208–212.
- [45] Xie, M.; Wang, W.; Ding, L.; Liu, J.; Yang, D.; Wei, L.; Zhang, Y. *J. Polym. Sci., Part A: Polym. Chem.* **2010**, *48*, 380–388.
- [46] Pitet, L. M.; Chamberlain, B. M.; Hauser, A. W.; Hillmyer, M. A. *Macromolecules* **2010**, *43*, 8018–8025.
- [47] Hillmyer, M. A.; Nguyen, S. T.; Grubbs, R. H. *Macromolecules* **1997**, *30*, 718–721.
- [48] Pitet, L. M.; Hillmyer, M. A. *Macromolecules* **2009**, *42*, 3674–3680.
- [49] Myers, S. B.; Register, R. A. *Macromolecules* **2008**, *41*, 5283–5288.

- 
- [50] Myers, S. B.; Register, R. A. *Macromolecules* **2008**, *41*, 6773–6779.
- [51] Myers, S. B.; Register, R. A. *Macromolecules* **2009**, *42*, 6665–6670.
- [52] Myers, S. B.; Register, R. A. *Macromolecules* **2010**, *43*, 393–401.
- [53] Pitet, L. M.; Amendt, M. A.; Hillmyer, M. A. *J. Am. Chem. Soc.* **2010**, *132*, 8230–8231.
- [54] Lehman, S. E., Jr.; Wagener, K. B.; Baugh, L. S.; Rucker, S. P.; Schulz, D. N.; Varma–Nair, M.; Berluce, E. *Macromolecules* **2007**, *40*, 2643–2656.
- [55] Baughman, T. W.; Chan, C. D.; Winey, K. I.; Wagener, K. B. *Macromolecules* **2007**, *40*, 6564–6571.

## Bibliography

Abetz, V.; Simon, P. F. W. *Adv. Polym. Sci.* **2005**, *189*, 125–212.

Ackermann, L.; Furstner, A.; Weskamp, T.; Kohl, F. J.; Herrmann, W. A. *Tetrahedron Lett.* **1999**, *40*, 4787–4790.

Adlhart, C.; Chen, P. *J. Am. Chem. Soc.* **2004**, *126*, 3496–3510.

Adlhart, C.; Hinderling, C.; Baumann, H.; Chen, P. *J. Am. Chem. Soc.* **2000**, *122*, 8204–8214.

Aggarwal, S. L.; Sweeting, O. J. *Chem. Rev.* **1957**, *57*, 665–742.

Aitken, B. S.; Lee, M.; Hunley, M. T.; Gibson, H. W.; Wagener, K. B. *Macromolecules* **2010**, *43*, 1699–1701.

Alamo, R. G.; Jeon, K.; Smith, R. L.; Boz, E.; Wagener, K. B.; Bockstaller, M. R. *Macromolecules* **2008**, *41*, 7141–7151.

Alamo, R. G.; Mandelkern, L. *Macromolecules* **1989**, *22*, 1273–1277.

Alb, A. M.; Enohnyaket, P.; Craymer, J. F.; Eren, T.; Coughlin, E. B.; Reed, W. F. *Macromolecules* **2007**, *40*, 444–451.

Almdal, K.; Hillmyer, M. A.; Bates, F. S. *Macromolecules* **2002**, *35*, 7685–7691.

Alonso-Villanueva, J.; Rodriguez, M.; Vilas, J. L.; Laza, J. M.; Leon, L. M. *J. Macromol. Sci., Part A: Pure Appl. Chem.* **2010**, *47*, 1130–1134.

Ambade, A. V.; Burd, C.; Higley, M. N.; Nair, K. P.; Weck, M. *Chem. Eur. J.* **2009**, *15*, 11904–11911.

Ambade, A. V.; Yang, S. K.; Weck, M. *Angew. Chem., Int. Ed.* **2009**, *48*, 2894–2898.

Amendt, M. A.; Chen, L.; Hillmyer, M. A. *Macromolecules* **2010**, *43*, 3924–3934.

Amin, S. B.; Marks, T. J. *Angew. Chem., Int. Ed.* **2008**, *47*, 2006–2025.

- Amundson, K.; Helfand, E.; Davis, D. D.; Quan, X.; Patel, S. S.; Smith, S. D. *Macromolecules* **1991**, *24*, 6546–6548.
- Amundson, K.; Helfand, E.; Quan, X.; Smith, S. D. *Macromolecules* **1993**, *26*, 2698–2703.
- Anderson, K. S.; Hillmyer, M. A. *Polymer* **2004**, *45*, 8809–8823.
- Anderson, K. S.; Hillmyer, M. A. *Macromolecules* **2004**, *37*, 1857–1862.
- Anderson, K. S.; Lim, S. H.; Hillmyer, M. A. *J. Appl. Polym. Sci.* **2003**, *89*, 3757–3768.
- Anderson, K. S.; Schreck, K. M.; Hillmyer, M. A. *Polym. Rev.* **2008**, *48*, 85–108.
- Arora, P.; Zhang, Z. *Chem. Rev.* **2004**, *104*, 4419–4462.
- Atthoff, B.; Trollsås, M.; Claesson, H.; Hedrick, J. L. *Macromol. Chem. Phys.* **1999**, *200*, 1333–1339.
- Auras, R.; Harte, B.; Selke, S. *Macromol. Biosci.* **2004**, *4*, 835–864.
- Bae, C.; Hartwig, J. F.; Chung, H.; Harris, N. K.; Switek, K. A.; Hillmyer, M. A. *Angew. Chem., Int. Ed.* **2005**, *44*, 6410–6413.
- Bae, C.; Hartwig, J. F.; Harris, N. K. B.; Long, R. O.; Anderson, K. S.; Hillmyer, M. A. *J. Am. Chem. Soc.* **2005**, *127*, 767–776.
- Baigl, D.; Seery, T. A. P.; Williams, C. E. *Macromolecules* **2002**, *35*, 2318–2326.
- Bailey, T. S.; Rzyayev, J.; Hillmyer, M. A. *Macromolecules* **2006**, *39*, 8772–8781.
- Bang, J.; Kim, S. H.; Drockenmuller, E.; Misner, M. J.; Russell, T. P.; Hawker, C. J. *J. Am. Chem. Soc.* **2006**, *128*, 7622–7629.
- Barbotin, F.; Monteil, V.; Llauro, M.-F.; Boisson, C.; Spitz, R. *Macromolecules* **2000**, *33*, 8521–8523.
- Barham, P. J.; Jarvis, D. A.; Keller, A. *Journal of Polymer Science: Polymer Physics Edition* **1982**, *20*, 1733–1748.
- Barrett, E. P.; Joyner, L. G.; Halenda, P. P. *J. Am. Chem. Soc.* **1951**, *73*, 373–380.
- Bassi, I. W.; Fagherazzi, G. *Eur. Polym. J.* **1968**, *4*, 123–132.
- Bates, F. S. *Science (Washington, DC, United States)* **1991**, *251*, 898–905.
- Bates, F. S.; Fredrickson, G. H. *Annu. Rev. Phys. Chem.* **1990**, *41*, 525–557.

- Bates, F. S.; Fredrickson, G. H. *Phys. Today* **1999**, *52*, 32–38.
- Bates, F. S.; Maurer, W. W.; Lipic, P. M.; Hillmyer, M. A.; Almdal, K.; Mortensen, K.; Fredrickson, G. H.; Lodge, T. P. *Phys. Rev. Lett.* **1997**, *79*, 849–852.
- Bates, F. S.; Schulz, M. F.; Khandpur, A. K.; Foerster, S.; Rosedale, J. H. *Faraday Discuss.* **1994**, *98*, 7–18.
- Baughman, T. W.; Chan, C. D.; Winey, K. I.; Wagener, K. B. *Macromolecules* **2007**, *40*, 6564–6571.
- Baughman, T. W.; Sworen, J. C.; Wagener, K. B. *Macromolecules* **2006**, *39*, 5028–5036.
- Baughman, T. W.; van der Aa, E.; Wagener, K. B. *Macromolecules* **2006**, *39*, 7015–7021.
- Baughman, T. W.; Wagener, K. B. *Adv. Polym. Sci.* **2005**, *176*, 1–42.
- Bazan, G. C.; Khosravi, E.; Schrock, R. R.; Feast, W. J.; Gibson, V. C.; O'Regan, M. B.; Thomas, J. K.; Davis, W. M. *J. Am. Chem. Soc.* **1990**, *112*, 8378–8387.
- Bazan, G. C.; Oskam, J. H.; Cho, H. N.; Park, L. Y.; Schrock, R. R. *J. Am. Chem. Soc.* **1991**, *113*, 6899–6907.
- Beardsley, T. M.; Matsen, M. W. *Eur. Phys. J. E* **2008**, *27*, 323–333.
- Becker, J. M.; Pounder, R. J.; Dove, A. P. *Macromol. Rapid Commun.* **2010**, *31*, 1923–1937.
- Bendejacq, D.; Ponsinet, V.; Joanicot, M.; Loo, Y. L.; Register, R. A. *Macromolecules* **2002**, *35*, 6645–6649.
- Benedicto, A. D.; Claverie, J. P.; Grubbs, R. H. *Macromolecules* **1995**, *28*, 500–511.
- Berda, E. B.; Baughman, T. W.; Wagener, K. B. *J. Polym. Sci., Part A: Polym. Chem.* **2006**, *44*, 4981–4989.
- Berda, E. B.; Lande, R. E.; Wagener, K. B. *Macromolecules* **2007**, *40*, 8547–8552.
- Berda, E. B.; Wagener, K. B. *Macromolecules* **2008**, *41*, 5116–5122.
- Berda, E. B.; Wagener, K. B. *Macromol. Chem. Phys.* **2008**, *209*, 1601–1611.
- Bernards, D. A.; Desai, T. A. *Soft Matter* **2010**, *6*, 1621–1631.
- Beyer, F. L.; Gido, S. P.; Uhrig, D.; Mays, J. W.; Tan, N. B.; Trevino, S. F. *J. Polym. Sci., Part B: Polym. Phys.* **1999**, *37*, 3392–3400.

- Bielawski, C. W.; Benitez, D.; Morita, T.; Grubbs, R. H. *Macromolecules* **2001**, *34*, 8610–8618.
- Bielawski, C. W.; Grubbs, R. H. *Angew. Chem., Int. Ed.* **2000**, *39*, 2903–2906.
- Bielawski, C. W.; Grubbs, R. H. *Prog. Polym. Sci.* **2007**, *32*, 1–29.
- Bielawski, C. W.; Hillmyer, M. A., In *Handbook of Metathesis*, Grubbs, R. H., Ed. Wiley–VCH: Weinham, Germany, 2003; Vol. 3, pp 255–282.
- Bielawski, C. W.; Louie, J.; Grubbs, R. H. *J. Am. Chem. Soc.* **2000**, *122*, 12872–12873.
- Bielawski, C. W.; Morita, T.; Grubbs, R. H. *Macromolecules* **2000**, *33*, 678–680.
- Bielawski, C. W.; Scherman, O. A.; Grubbs, R. H. *Polymer* **2001**, *42*, 4939–4945.
- Bieniek, M.; Michrowska, A.; Usanov, D. L.; Grela, K. *Chem. Eur. J.* **2008**, *14*, 806–818.
- Bigg, D. M. *Adv. Polym. Tech.* **2005**, *24*, 69–82.
- Binder, W. H.; Kurzhals, S.; Pulamagatta, B.; Decker, U.; Manohar Pawar, G.; Wang, D.; KuÅhnel, C.; Buchmeiser, M. R. *Macromolecules* **2008**, *41*, 8405–8412.
- Blackwell, H. E.; O'Leary, D. J.; Chatterjee, A. K.; Washenfelder, R. A.; Busmann, D. A.; Grubbs, R. H. *J. Am. Chem. Soc.* **2000**, *122*, 58–71.
- Boaen, N. K.; Hillmyer, M. A. *Macromolecules* **2003**, *36*, 7027–7034.
- Boaen, N. K.; Hillmyer, M. A. *Chem. Soc. Rev.* **2005**, *34*, 267–275.
- Boeker, A.; Elbs, H.; Haensel, H.; Knoll, A.; Ludwigs, S.; Zettl, H.; Zvelindovsky, A. V.; Sevink, G. J. A.; Urban, V.; Abetz, V.; Mueller, A. H. E.; Krausch, G. *Macromolecules* **2003**, *36*, 8078–8087.
- Bolton, J.; Bailey, T. S.; Rzaev, J. *Nano Lett.* **2011**, *11*, 998–1001.
- Boz, E.; Nemeth, A. J.; Wagener, K. B.; Jeon, K.; Smith, R.; Nazirov, F.; Bockstaller, M. R.; Alamo, R. G. *Macromolecules* **2008**, *41*, 1647–1653.
- Bradshaw, C. P. C.; Howman, E. J.; Turner, L. *J. Catal.* **1967**, *7*, 269–276.
- Breslow, D. S. *Prog. Polym. Sci.* **1993**, *18*, 1141–1195.
- Brunauer, S.; Deming, L. S.; Deming, W. E.; Teller, E. *J. Am. Chem. Soc.* **1940**, *62*, 1723–1732.

- Brunauer, S.; Emmett, P. H.; Teller, E. *J. Am. Chem. Soc.* **1938**, *60*, 309–319.
- Bruneau, C.; Fischmeister, C.; Miao, X. W.; Malacea, R.; Dixneuf, P. H. *Eur. J. Lipid Sci. Technol.* **2010**, *112*, 3–9.
- Buchmeiser, M. R. *Chem. Rev.* **2000**, *100*, 1565–1604.
- Burtscher, D.; Saf, R.; Slugovc, C. *J. Polym. Sci., Part A: Polym. Chem.* **2006**, *44*, 6136–6145.
- Buzza, D. M. A.; Fzea, A. H.; Allgaier, J. B.; Young, R. N.; Hawkins, R. J.; Hamley, I. W.; McLeish, T. C. B.; Lodge, T. P. *Macromolecules* **2000**, *33*, 8399–8414.
- Calderon, N. *Acc. Chem. Res.* **1972**, *5*, 127–132.
- Calderon, N. *Journal of Macromolecular Science, Reviews in Macromolecular Chemistry* **1972**, *7*, 105–159.
- Calderon, N.; Chen, H. Y.; Scott, K. W. *Tetrahedron Lett.* **1967**, 3327–3329.
- Calderon, N.; Morris, M. C. *J. Polym. Sci., Polym. Phys. Ed.* **1967**, *5*, 1283–1292.
- Calderon, N.; Ofstead, E. A.; Judy, W. A. *J. Polym. Sci., Part A: Polym. Chem.* **1967**, *5*, 2209–2217.
- Calderon, N.; Ofstead, E. A.; Judy, W. A. *Angew. Chem.* **1976**, *88*, 433–442.
- Calderon, N.; Ofstead, E. A.; Ward, J. P.; Judy, W. A.; Scott, K. W. *J. Am. Chem. Soc.* **1968**, *90*, 4133–4140.
- Carretta, N.; Tricoli, V.; Picchioni, F. *J. Membr. Sci.* **2000**, *166*, 189–197.
- Castillo, R. V.; Muller, A. J.; Lin, M.-C.; Chen, H.-L.; Jeng, U. S.; Hillmyer, M. A. *Macromolecules* **2008**, *41*, 6154–6164.
- Chatterjee, A. K.; Choi, T. L.; Sanders, D. P.; Grubbs, R. H. *J. Am. Chem. Soc.* **2003**, *125*, 11360–11370.
- Chatterjee, A. K.; Grubbs, R. H. *Org. Lett.* **1999**, *1*, 1751–1753.
- Chatterjee, A. K.; Grubbs, R. H. *Angew. Chem., Int. Ed.* **2002**, *41*, 3171–+.
- Chatterjee, A. K.; Sanders, D. P.; Grubbs, R. H. *Org. Lett.* **2002**, *4*, 1939–1942.
- Chatterjee, A. K.; Toste, F. D.; Choi, T. L.; Grubbs, R. H. *Adv. Synth. Catal.* **2002**, *344*, 634–637.



- Chatterjee, A. K.; Toste, F. D.; Goldberg, S. D.; Grubbs, R. H. *Pure Appl. Chem.* **2003**, *75*, 421–425.
- Chauvin, Y. *Angew. Chem., Int. Ed.* **2006**, *45*, 3740–3747.
- Chen, B.; Metera, K.; Sleiman, H. F. *Macromolecules* **2005**, *38*, 1084–1090.
- Chen, L.; Hallinan, D. T.; Elabd, Y. A.; Hillmyer, M. A. *Macromolecules* **2009**, *42*, 6075–6085.
- Chen, L.; Hillmyer, M. A. *Macromolecules* **2009**, *42*, 4237–4243.
- Chen, L.; Phillip, W. A.; Cussler, E. L.; Hillmyer, M. A. *J. Am. Chem. Soc.* **2007**, *129*, 13786–13787.
- Chen, W. N.; Luo, W. J.; Wang, S. G.; Bei, J. Z. *Polym. Adv. Technol.* **2003**, *14*, 245–253.
- Chen, X. H.; McCarthy, S. P.; Gross, R. A. *Macromolecules* **1997**, *30*, 4295–4301.
- Chen, Z.-R.; Kornfield, J. A.; Smith, S. D.; Grothaus, J. T.; Satkowski, M. M. *Science* **1997**, *277*, 1248–1253.
- Chen, Z. R.; Issaian, A. M.; Kornfield, J. A.; Smith, S. D.; Grothaus, J. T.; Satkowski, M. M. *Macromolecules* **1997**, *30*, 7096–7114.
- Chen, Z. R.; Kornfield, J. A. *Polymer* **1998**, *39*, 4679–4699.
- Choi, T. L.; Chatterjee, A. K.; Grubbs, R. H. *Angew. Chem., Int. Ed.* **2001**, *40*, 1277–+.
- Choi, T. L.; Lee, C. W.; Chatterjee, A. K.; Grubbs, R. H. *J. Am. Chem. Soc.* **2001**, *123*, 10417–10418.
- Chung, T. C.; Chasmawala, M. *Macromolecules* **1992**, *25*, 5137–5144.
- Clark, T. J.; Robertson, N. J.; Kostalik, H. A.; Lobkovsky, E. B.; Mutolo, P. F.; Abruna, H. D.; Coates, G. W. *J. Am. Chem. Soc.* **2009**, *131*, 12888–+.
- Clavier, H.; Grela, K.; Kirschning, A.; Mauduit, M.; Nolan, S. P. *Angew. Chem., Int. Ed.* **2007**, *46*, 6786–6801.
- Coca, S.; Paik, H.-j.; Matyjaszewski, K. *Macromolecules* **1997**, *30*, 6513–6516.
- Cochran, E. W.; Garcia-Cervera, C. J.; Fredrickson, G. H. *Macromolecules* **2006**, *39*, 2449–2451.
- Cohn, D.; Hotovely-Salomon, A. *Polymer* **2005**, *46*, 2068–2075.

- Cohn, D.; Salomon, A. F. *Biomater.* **2005**, *26*, 2297–2305.
- Cong, Y.; Li, B.; Han, Y.; Li, Y.; Pan, C. *Macromolecules* **2005**, *38*, 9836–9846.
- Cossy, J.; Bargiggia, F.; BouzBouz, S. *Org. Lett.* **2003**, *5*, 459–462.
- Coulembier, O.; Kiesewetter, M. K.; Mason, A.; Dubois, P.; Hedrick, J. L.; Waymouth, R. M. *Angew. Chem., Int. Ed.* **2007**, *46*, 4719–4721.
- Cramail, H.; Fontanille, M.; Soum, A. *Makromol. Chem.–M. Symp.* **1991**, *42/43*, 281–292.
- Cramail, H.; Fontanille, M.; Soum, A. *J. Mol. Catal.* **1991**, *65*, 193–203.
- Crossland, E. J. W.; Ludwigs, S.; Hillmyer, M. A.; Steiner, U. *Soft Matter* **2007**, *3*, 94–98.
- Crossland, E. J. W.; Ludwigs, S.; Hillmyer, M. A.; Steiner, U. *Soft Matter* **2010**, *6*, 670–676.
- Dechy–Cabaret, O.; Martin–Vaca, B.; Bourissou, D. *Chem. Rev.* **2004**, *104*, 6147–6176.
- Deiters, A.; Martin, S. F. *Chem. Rev.* **2004**, *104*, 2199–2238.
- Deluca, N. W.; Elabd, Y. A. *J. Polym. Sci., Part B: Polym. Phys.* **2006**, *44*, 2201–2225.
- Dias, E. L.; Nguyen, S. T.; Grubbs, R. H. *J. Am. Chem. Soc.* **1997**, *119*, 3887–3897.
- Ding, L.; Xie, M.; Yang, D.; Song, C. *Macromolecules* **2010**, *43*, 10336–10342.
- Domski, G. J.; Rose, J. M.; Coates, G. W.; Bolig, A. D.; Brookhart, M. *Prog. Polym. Sci.* **2007**, *32*, 30–92.
- Dorati, R.; Genta, I.; Colonna, C.; Modena, T.; Pavanetto, F.; Perugini, P.; Conti, B. *Polym. Degrad. Stab.* **2007**, *92*, 1660–1668.
- Dorgan, J. R.; Janzen, J.; Knauss, D. M.; Hait, S. B.; Limoges, B. R.; Hutchinson, M. H. *J. Polym. Sci., Part B: Polym. Phys.* **2005**, *43*, 3100–3111.
- Dounis, P.; Feast, W. J. *Polymer* **1996**, *37*, 2547–2554.
- Dove, A. P. *Chem. Commun.* **2008**, 6446–6470.
- Drumright, R. E.; Gruber, P. R.; Henton, D. E. *Adv. Mater.* **2000**, *12*, 1841–1846.
- Drzal, P. L.; Barnes, J. D.; Kofinas, P. *Polymer* **2001**, *42*, 5633–5642.

- Drzal, P. L.; Halasa, A. F.; Kofinas, P. *Polymer* **2000**, *41*, 4671–4677.
- du Sart, G. G.; Vukovic, I.; Vukovic, Z.; Polushkin, E.; Hiekkataipale, P.; Ruokolainen, J.; Loos, K.; ten Brinke, G. *Macromol. Rapid Commun.* **2011**, *32*, 366–370.
- Dubois, P.; Jerome, R.; Teyssie, P. *Makromol. Chem.–M. Symp.* **1991**, *42/43*, 103–116.
- Ekin, A.; Webster, D. C. *Macromolecules* **2006**, *39*, 8659–8668.
- Elabd, Y. A.; Hickner, M. A. *Macromolecules* **2011**, *44*, 1–11.
- Elabd, Y. A.; Napadensky, E.; Sloan, J. M.; Crawford, D. M.; Walker, C. W. *J. Membr. Sci.* **2003**, *217*, 227–242.
- Elabd, Y. A.; Napadensky, E.; Walker, C. W.; Winey, K. I. *Macromolecules* **2005**, *39*, 399–407.
- Ellison, C. J.; Meuler, A. J.; Qin, J.; Evans, C. M.; Wolf, L. M.; Bates, F. S. *J. Phys. Chem. B* **2009**, *113*, 3726–3737.
- Falk, J. C.; Schlott, R. J. *Macromolecules* **1971**, *4*, 152–154.
- Feast, W. J.; Harrison, D. B. *Polymer* **1991**, *32*, 558–563.
- Feldman, J.; Davis, W. M.; Thomas, J. K.; Schrock, R. R. *Organometallics* **1990**, *9*, 2535–2548.
- Fetters, L. J.; Lohse, D. J.; Graessley, W. W. *J. Polym. Sci., Part B: Polym. Phys.* **1999**, *37*, 1023–1033.
- Fetters, L. J.; Lohse, D. J.; Richter, D.; Witten, T. A.; Zirkel, A. *Macromolecules* **1994**, *27*, 4639–4647.
- Fleury, G.; Bates, F. S. *Macromolecules* **2009**, *42*, 1691–1694.
- Fleury, G.; Bates, F. S. *Macromolecules* **2009**, *42*, 3598–3610.
- Fleury, G.; Bates, F. S. *Soft Matter* **2010**, *6*, 2751–2759.
- Floudas, G.; Hadjichristidis, N.; Iatrou, H.; Avgeropoulos, A.; Pakula, T. *Macromolecules* **1998**, *31*, 6943–6950.
- Floudas, G.; Hadjichristidis, N.; Iatrou, H.; Pakula, T. *Macromolecules* **1996**, *29*, 3139–3146.

- Floudas, G.; Hadjichristidis, N.; Iatrou, H.; Pakula, T.; Fischer, E. W. *Macromolecules* **1994**, *27*, 7735–7746.
- Fraser, C.; Hillmyer, M. A.; Gutierrez, E.; Grubbs, R. H. *Macromolecules* **1995**, *28*, 7256–7261.
- Fredrickson, G. H.; Helfand, E. *J. Chem. Phys.* **1987**, *87*, 697–705.
- Frensch, H.; Harnischfeger, P.; Jungnickel, B. J. *ACS Symp. Ser.* **1989**, *395*, 101–125.
- Frensch, H.; Jungnickel, B. J. *Colloid. Polym. Sci.* **1989**, *267*, 16–27.
- Frenzel, U.; Nuyken, O. *J. Polym. Sci., Part A: Polym. Chem.* **2002**, *40*, 2895–2916.
- Frenzel, U.; Weskamp, T.; Kohl, F. J.; Schattenman, W. C.; Nuyken, O.; Herrmann, W. A. *J. Organomet. Chem.* **1999**, *586*, 263–265.
- Fürstner, A. *Angew. Chem., Int. Ed.* **2000**, *39*, 3012–3043.
- Furstner, A.; Thiel, O. R.; Ackermann, L. *Org. Lett.* **2001**, *3*, 449–451.
- Garlotta, D. *J. Polym. Environ.* **2002**, *9*, 63–84.
- Gascon, C.; Lucas, F.; Carlotti, S.; Deffieux, A. *J. Appl. Polym. Sci.* **2010**, *118*, 1830–1836.
- Gaur, U.; Wunderlich, B. *J. Phys. Chem. Ref. Data* **1981**, *10*, 119–152.
- Gibson, V. C.; Okada, T. *Macromolecules* **2000**, *33*, 655–656.
- Gido, S. P.; Lee, C.; Pochan, D. J.; Pispas, S.; Mays, J. W.; Hadjichristidis, N. *Macromolecules* **1996**, *29*, 7022–7028.
- Gilliom, L. R.; Grubbs, R. H. *J. Am. Chem. Soc.* **1986**, *108*, 733–742.
- Goethals, E. J., *Telechelic Polymers: Synthesis and Applications*. CRC Press: Boca Raton, Fla., 1989; p 402.
- Goswami, M.; Sumpter, B. G.; Huang, T.; Messman, J. M.; Gido, S. P.; Isaacs-Sodeye, A. I.; Mays, J. W. *Soft Matter* **2010**, *6*, 6146–6154.
- Gramlich, W. M.; Robertson, M. L.; Hillmyer, M. A. *Macromolecules* **2010**, *43*, 2313–2321.
- Gross, R. A.; Kalra, B. *Science* **2002**, *297*, 803–807.
- Grubbs, R. H. *Angew. Chem., Int. Ed.* **2006**, *45*, 3760–3765.

- Grubbs, R. H.; Chang, S. *Tetrahedron* **1998**, *54*, 4413–4450.
- Grubbs, R. H.; Miller, S. J.; Fu, G. C. *Acc. Chem. Res.* **1995**, *28*, 446–452.
- Grubbs, R. H.; Trnka, T. M. *Ruthenium in Organic Synthesis* **2004**, 153–177.
- Grubbs, R. H.; Tumas, W. *Science (Washington, DC, United States)* **1989**, *243*, 907–915.
- Gruber, P.; O'Brien, M. *Biopolymers* **2002**, *4*, 235–250.
- Guo, S.; Rzayev, J.; Bailey, T. S.; Zalusky, A. S.; Olayo-Valles, R.; Hillmyer, M. A. *Chem. Mater.* **2006**, *18*, 1719–1721.
- Hadjichristidis, N.; Iatrou, H.; Behal, S. K.; Chludzinski, J. J.; Disko, M. M.; Garner, R. T.; Liang, K. S.; Lohse, D. J.; Milner, S. T. *Macromolecules* **1993**, *26*, 5812–5815.
- Hadjichristidis, N.; Iatrou, H.; Pitsikalis, M.; Mays, J. *Prog. Polym. Sci.* **2006**, *31*, 1068–1132.
- Hadjichristidis, N.; Pitsikalis, M.; Iatrou, H. *Adv. Polym. Sci.* **2005**, *189*, 1–124.
- Hadjichristidis, N.; Pitsikalis, M.; Pispas, S.; Iatrou, H. *Chem. Rev.* **2001**, *101*, 3747–3792.
- Hadjichristidis, N.; Poulos, Y.; Avgeropoulos, A. *Macromol. Symp.* **1998**, *132*, 207–220.
- Hadjichristidis, N.; Roovers, J. E. L. *J. Polym. Sci., Part B: Polym. Phys.* **1974**, *12*, 2521–2533.
- Hahn, S. F. *J. Polym. Sci., Part A: Polym. Chem.* **1992**, *30*, 397–408.
- Hamley, I. W., *The Physics of Block Copolymers*. Oxford University Press, USA: 1998; p 432.
- Hamley, I. W. *Adv. Polym. Sci.* **1999**, *148*, 114–137.
- Hamley, I. W. *Developments in Block Copolymer Science and Technology* **2004**, 1–29.
- Hamrock, S. J.; Yandrasits, M. A. *Polym. Rev.* **2006**, *46*, 219–244.
- Han, D.-H.; Pan, C.-Y. *J. Polym. Sci., Part A: Polym. Chem.* **2006**, *44*, 2794–2801.
- Hashimoto, T.; Tsutsumi, K.; Funaki, Y. *Langmuir* **1997**, *13*, 6869–6872.

- Hedrick, J. L.; Carter, K. R.; Labadie, J. W.; Miller, R. D.; Volksen, W.; Hawker, C. J.; Yoon, D. Y.; Russell, T. P.; McGrath, J. E.; Briber, R. M. *Adv. Polym. Sci.* **1999**, *141*, 1–43.
- Heinzel, A.; Barragan, V. M. *J. Power Sources* **1999**, *84*, 70–74.
- Helfand, E.; Tagami, Y. *J. Chem. Phys.* **1972**, *56*, 3592–3601.
- Helfand, E.; Wasserman, Z. R. *Macromolecules* **1976**, *9*, 879–888.
- Helfand, E.; Wasserman, Z. R. *Developments in Block Copolymers* **1982**, *1*, 99–125.
- Herisson, J. L.; Chauvin, Y. *Makromol. Chem.* **1971**, *141*, 161–176.
- Hermel, T. J.; Hahn, S. F.; Chaffin, K. A.; Gerberich, W. W.; Bates, F. S. *Macromolecules* **2003**, *36*, 2190–2193.
- Hermel, T. J.; Wu, L.; Hahn, S. F.; Lodge, T. P.; Bates, F. S. *Macromolecules* **2002**, *35*, 4685–4689.
- Hickner, M. A.; Ghassemi, H.; Kim, Y. S.; Einsla, B. R.; McGrath, J. E. *Chem. Rev.* **2004**, *104*, 4587–4611.
- Hickner, M. A.; Pivovar, B. S. *Fuel Cells* **2005**, *5*, 213–229.
- Hiemenz, P. C.; Lodge, T. P., *Polymer Chemistry*. 2nd ed.; CRC Press: Boca Raton, 2007.
- Higashihara, T.; Faust, R.; Inoue, K.; Hirao, A. *Macromolecules* **2008**, *41*, 5616–5625.
- Higley, M. N.; Pollino, J. M.; Hollebeak, E.; Weck, M. *Chem. Eur. J.* **2005**, *11*, 2946–2953.
- Hilf, S.; Berger–Nicoletti, E.; Grubbs, R. H.; Kilbinger, A. F. M. *Angew. Chem., Int. Ed.* **2006**, *45*, 8045–8048.
- Hilf, S.; Grubbs, R. H.; Kilbinger, A. F. M. *J. Am. Chem. Soc.* **2008**, *130*, 11040–11048.
- Hilf, S.; Grubbs, R. H.; Kilbinger, A. F. M. *Macromolecules* **2008**, *41*, 6006–6011.
- Hilf, S.; Kilbinger, A. F. M. *Macromolecules* **2009**, *42*, 1099–1106.
- Hilf, S.; Kilbinger, A. F. M. *Macromolecules* **2009**, *42*, 4127–4133.
- Hilf, S.; Kilbinger, A. F. M. *Macromolecules* **2010**, *43*, 208–212.

- Hilf, S.; Wurm, F.; Kilbinger, A. F. M. *J. Polym. Sci., Part A: Polym. Chem.* **2009**, *47*, 6932–6940.
- Hillmyer, M. A. *Adv. Polym. Sci.* **2005**, *190*, 137–181.
- Hillmyer, M. A.; Grubbs, R. H. *Macromolecules* **1993**, *26*, 872–874.
- Hillmyer, M. A.; Grubbs, R. H. *Macromolecules* **1995**, *28*, 8662–8667.
- Hillmyer, M. A.; Laredo, W. R.; Grubbs, R. H. *Macromolecules* **1995**, *28*, 6311–6316.
- Hillmyer, M. A.; Maurer, W. W.; Lodge, T. P.; Bates, F. S.; Almdal, K. *J. Phys. Chem. B* **1999**, *103*, 4814–4824.
- Hillmyer, M. A.; Nguyen, S. T.; Grubbs, R. H. *Macromolecules* **1997**, *30*, 718–721.
- Hinderling, C.; Adlhart, C.; Chen, P. *Angew. Chem., Int. Ed.* **1998**, *37*, 2685–2689.
- Hirao, A.; Murano, K.; Oie, T.; Uematsu, M.; Goseki, R.; Matsuo, Y. *Polymer Chemistry* **2011**.
- Ho, C. H.; Wang, C. H.; Lin, C. I.; Lee, Y. D. *Eur. Polym. J.* **2009**, *45*, 2455–2466.
- Howard, T. R.; Lee, J. B.; Grubbs, R. H. *J. Am. Chem. Soc.* **1980**, *102*, 6876–6878.
- Hsueh, H. Y.; Chen, H. Y.; She, M. S.; Chen, C. K.; Ho, R. M.; Gwo, S.; Hasegawa, H.; Thomas, E. L. *Nano Lett.* **2010**, *10*, 4994–5000.
- Huang, C.-I.; Yang, L.-F. *Macromolecules* **2010**, *43*, 9117–9125.
- Huang, L. H.; Zhuang, X. L.; Hu, J.; Lang, L.; Zhang, P. B.; Wang, Y. S.; Chen, X. S.; Wei, Y.; Jing, X. B. *Biomacromolecules* **2008**, *9*, 850–858.
- Hucul, D. A.; Hahn, S. F. *Adv. Mater.* **2000**, *12*, 1855–1858.
- Ihre, H.; Hult, A.; Frechet, J. M. J.; Gitsov, I. *Macromolecules* **1998**, *31*, 4061–4068.
- Jackson, E. A.; Hillmyer, M. A. *ACS Nano* **2010**, *4*, 3548–3553.
- Jacobs, C.; Dubois, P.; Jerome, R.; Teyssie, P. *Macromolecules* **1991**, *24*, 3027–3034.
- Jeong, M.; Mackay, M. E.; Vestberg, R.; Hawker, C. J. *Macromolecules* **2001**, *34*, 4927–4936.
- Jérôme, R.; Mecerreyes, D.; Tian, D.; Dubois, P.; Hawker, C. J.; Trollsås, M.; Hedrick, J. L. *Macromol. Symp.* **1998**, *132*, 385–403.

- Ji, S.; Hoyer, T. R.; Macosko, C. W. *Macromolecules* **2004**, *37*, 5485–5489.
- Ji, S. X.; Hoyer, T. R.; Macosko, C. W. *Polymer* **2008**, *49*, 5307–5313.
- Jing, F.; Hillmyer, M. A. *J. Am. Chem. Soc.* **2008**, *130*, 13826–13827.
- Jones, B. H.; Lodge, T. P. *J. Am. Chem. Soc.* **2009**, *131*, 1676–1677.
- Jung, Y. S.; Ross, C. A. *Small* **2009**, *5*, 1654–1659.
- Kamber, N. E.; Jeong, W.; Waymouth, R. M.; Pratt, R. C.; Lohmeijer, B. G. G.; Hedrick, J. L. *Chem. Rev.* **2007**, *107*, 5813–5840.
- Katayama, H.; Fukuse, Y.; Nobuto, Y.; Akamatsu, K.; Ozawa, F. *Macromolecules* **2003**, *36*, 7020–7026.
- Katayama, H.; Urushima, H.; Nishioka, T.; Wada, C.; Nagao, M.; Ozawa, F. *Angew. Chem., Int. Ed.* **2000**, *39*, 4513–+.
- Katayama, H.; Urushima, H.; Ozawa, F. *Chem. Lett.* **1999**, 369–370.
- Katayama, H.; Urushima, H.; Ozawa, F. *J. Organomet. Chem.* **2000**, *606*, 16–25.
- Katayama, H.; Yonezawa, F.; Nagao, M.; Ozawa, F. *Macromolecules* **2002**, *35*, 1133–1136.
- Katz, T. J.; McGinnis, J. *J. Am. Chem. Soc.* **1975**, *97*, 1592–1594.
- Kawahara, N.; Saito, J.; Matsuo, S.; Kaneko, H.; Matsugi, T.; Kashiwa, N., Polymer Hybrids Based on Polyolefins – Syntheses, Structures, and Properties. In *New Frontiers in Polymer Synthesis*, Springer-Verlag Berlin: Berlin, 2008; Vol. 217, pp 79–119.
- Khandpur, A. K.; Foerster, S.; Bates, F. S.; Hamley, I. W.; Ryan, A. J.; Bras, W.; Almdal, K.; Mortensen, K. *Macromolecules* **1995**, *28*, 8796–8806.
- Kim, J.; Kim, B.; Jung, B. *J. Membr. Sci.* **2002**, *207*, 129–137.
- Kim, S. H.; Misner, M. J.; Russell, T. P. *Adv. Mater.* **2004**, *16*, 2119–2123.
- Kim, S. H.; Misner, M. J.; Xu, T.; Kimura, M.; Russell, T. P. *Adv. Mater.* **2004**, *16*, 226–231.
- Ko, J. M.; Min, B. G.; Kim, D. W.; Ryu, K. S.; Kim, K. M.; Lee, Y. G.; Chang, S. H. *Electrochim. Acta* **2004**, *50*, 367–370.
- Kobayashi, S.; Macosko, C. W.; Hillmyer, M. A. *Aust. J. Chem.* **2010**, *63*, 1201–1209.



- Kobayashi, S.; Pitet, L. M.; Hillmyer, M. A. *J. Am. Chem. Soc.* **2011**, *133*, 5794–5797.
- Kondo, Y.; Garcia–Cuadrado, D.; Hartwig, J. F.; Boasen, N. K.; Wagner, N. L.; Hillmyer, M. A. *J. Am. Chem. Soc.* **2002**, *124*, 1164–1165.
- Kostalík, H. A.; Clark, T. J.; Robertson, N. J.; Mutolo, P. F.; Longo, J. M.; Abruna, H. D.; Coates, G. W. *Macromolecules* **2010**, *43*, 7147–7150.
- Kress, J.; Osborn, J. A.; Greene, R. M. E.; Ivin, K. J.; Rooney, J. J. *J. Am. Chem. Soc.* **1987**, *109*, 899–901.
- Kreuer, K. D. *J. Membr. Sci.* **2001**, *185*, 29–39.
- Kurzahls, S.; Binder, W. H. *J. Polym. Sci., Part A: Polym. Chem.* **2010**, *48*, 5522–5532.
- Lai, C.; Russel, W. B.; Register, R. A.; Marchand, G. R.; Adamson, D. H. *Macromolecules* **2000**, *33*, 3461–3466.
- Lee, C.; Gido, S. P.; Poulos, Y.; Hadjichristidis, N.; Tan, N. B.; Trevino, S. F.; Mays, J. W. *J. Chem. Phys.* **1997**, *107*, 6460–6469.
- Lee, C.; Gido, S. P.; Poulos, Y.; Hadjichristidis, N.; Tan, N. B.; Trevino, S. F.; Mays, J. W. *Polymer* **1998**, *39*, 4631–4638.
- Lee, D. H.; Park, S.; Gu, W. Y.; Russell, T. P. *ACS Nano* **2011**, *5*, 1207–1214.
- Lee, J. C.; Parker, K. A.; Sampson, N. S. *J. Am. Chem. Soc.* **2006**, *128*, 4578–4579.
- Lee, S. H.; Kim, S. H.; Han, Y. K.; Kim, Y. H. *J. Polym. Sci., Part A: Polym. Chem.* **2002**, *40*, 2545–2555.
- Lehman, S. E., Jr.; Wagener, K. B.; Baugh, L. S.; Rucker, S. P.; Schulz, D. N.; Varma–Nair, M.; Berluce, E. *Macromolecules* **2007**, *40*, 2643–2656.
- Leibler, L. *Macromolecules* **1980**, *13*, 1602–1617.
- Leibler, L. *Prog. Polym. Sci.* **2005**, *30*, 898–914.
- Leitgeb, A.; Wappel, J.; Slugovc, C. *Polymer* **2010**, *51*, 2927–2946.
- Leonard, J. K.; Turek, D.; Sloan, K. B.; Wagener, K. B. *Macromol. Chem. Phys.* **2010**, *211*, 154–165.
- Li, F.; Li, S. M.; Vert, M. *Macromol. Biosci.* **2005**, *5*, 1125–1131.
- Li, M.; Coenjarts, C. A.; Ober, C. K. *Adv. Polym. Sci.* **2005**, *190*, 183–226.

- Li, M. H.; Keller, P.; Albouy, P. A. *Macromolecules* **2003**, *36*, 2284–2292.
- Li, Q. F.; Jensen, J. O.; Savinell, R. F.; Bjerrum, N. J. *Prog. Polym. Sci.* **2009**, *34*, 449–477.
- Li, Y.-G.; Shi, P.-J.; Pan, C.-Y. *Macromolecules* **2004**, *37*, 5190–5195.
- Liaw, D. J.; Wu, P. L. *J. Mol. Catal. A-Chem.* **2000**, *160*, 35–43.
- Liu, C.; Chun, S. B.; Mather, P. T.; Zheng, L.; Haley, E. H.; Coughlin, E. B. *Macromolecules* **2002**, *35*, 9868–9874.
- Liu, J.; Pan, C.-Y. *Polymer* **2005**, *46*, 11133–11141.
- Liu, J. W.; Li, J. X.; Xie, M. R.; Ding, L.; Yang, D.; Zhang, L. Y. *Polymer* **2009**, *50*, 5228–5235.
- Love, J. A.; Morgan, J. P.; Trnka, T. M.; Grubbs, R. H. *Angew. Chem., Int. Ed.* **2002**, *41*, 4035–4037.
- Love, J. A.; Sanford, M. S.; Day, M. W.; Grubbs, R. H. *J. Am. Chem. Soc.* **2003**, *125*, 10103–10109.
- Lu, D. D.; Zhang, X. W.; Zhou, T. H.; Ren, Z. L.; Wang, S. F.; Lei, Z. Q. *Prog. Chem.* **2008**, *20*, 339–350.
- Lucas, F.; Peruch, F.; Carlotti, S.; Deffieux, A.; Leblanc, A.; Boisson, C. *Polymer* **2008**, *49*, 4935–4941.
- Lynd, N. A.; Hillmyer, M. A. *Macromolecules* **2005**, *38*, 8803–8810.
- Lynd, N. A.; Hillmyer, M. A. *Macromolecules* **2007**, *40*, 8050–8055.
- Lynd, N. A.; Oyerokun, F. T.; O'ÄDonoghue, D. L.; Handlin, D. L.; Fredrickson, G. H. *Macromolecules* **2010**, *43*, 3479–3486.
- Mackay, M. E.; Hong, Y.; Jeong, M.; Tande, B. M.; Wagner, N. J.; Hong, S.; Gido, S. P.; Vestberg, R.; Hawker, C. J. *Macromolecules* **2002**, *35*, 8391–8399.
- Madkour, A. E.; Koch, A. H. R.; Lienkamp, K.; Tew, G. N. *Macromolecules* **2010**, *43*, 4557–4561.
- Mahanthappa, M. K.; Bates, F. S.; Hillmyer, M. A. *Macromolecules* **2005**, *38*, 7890–7894.
- Mahanthappa, M. K.; Hillmyer, M. A.; Bates, F. S. *Macromolecules* **2008**, *41*, 1341–1351.

- Mahanthappa, M. K.; Lim, L. S.; Hillmyer, M. A.; Bates, F. S. *Macromolecules* **2007**, *40*, 1585–1593.
- Mai, S.-M.; Mingvanish, W.; Turner, S. C.; Chaibundit, C.; Fairclough, J. P. A.; Heatley, F.; Matsen, M. W.; Ryan, A. J.; Booth, C. *Macromolecules* **2000**, *33*, 5124–5130.
- Mai, S. M.; Abbot, A.; Norton, D.; McKean, R.; Ryan, A. J. *Macromol. Chem. Phys.* **2009**, *210*, 840–851.
- Malacea, R.; Fischmeister, C.; Bruneau, C.; Dubois, J.-L.; Couturier, J.-L.; Dixneuf, P. H. *Green Chem.* **2009**, *11*, 152–155.
- Mandelkern, L.; Alamo, R. G.; Kennedy, M. A. *Macromolecules* **1990**, *23*, 4721–4723.
- Mandelkern, L.; Peacock, A. J. *Polym. Bull.* **1986**, *16*, 529–536.
- Mangold, S. L.; Carpenter, R. T.; Kiessling, L. L. *Org. Lett.* **2008**, *10*, 2997–3000.
- Mansky, P.; Harrison, C. K.; Chaikin, P. M.; Register, R. A.; Yao, N. *Appl. Phys. Lett.* **1996**, *68*, 2586–2588.
- Marmo, J. C.; Wagener, K. B. *Macromolecules* **1993**, *26*, 2137–2138.
- Marmo, J. C.; Wagener, K. B. *Macromolecules* **1995**, *28*, 2602–2606.
- Marmo, J. C.; Wagener, k. B. *Rubber Chem. Technol.* **1997**, *70*, 519–529.
- Mathers, R. T.; Coates, G. W. *Chem. Commun.* **2004**, 422–423.
- Matsen, M. W. *J. Chem. Phys.* **2001**, *114*, 10528–10530.
- Matsen, M. W. *Phys. Rev. Lett.* **2005**, *95*, 258302/258301–258302/258304.
- Matsen, M. W. *Eur. Phys. J. E Soft Matter* **2006**, *21*, 199–207.
- Matsen, M. W. *Macromolecules* **2006**, *39*, 5512–5520.
- Matsen, M. W. *Phys. Rev. Lett.* **2007**, *99*, 148304/148301–148304/148304.
- Matsen, M. W.; Bates, F. S. *Macromolecules* **1996**, *29*, 7641–7644.
- Matsen, M. W.; Bates, F. S. *Macromolecules* **1996**, *29*, 1091–1098.
- Matsen, M. W.; Bates, F. S. *J. Chem. Phys.* **1997**, *106*, 2436–2448.
- Matsen, M. W.; Bates, F. S. *J. Polym. Sci., Part B: Polym. Phys.* **1997**, *35*, 945–952.

- Matsen, M. W.; Gardiner, J. M. *J. Chem. Phys.* **2000**, *113*, 1673–1676.
- Matsen, M. W.; Schick, M. *Macromolecules* **1994**, *27*, 4014–4015.
- Matsen, M. W.; Schick, M. *Phys. Rev. Lett.* **1994**, *72*, 2660–2663.
- Matsen, M. W.; Thompson, R. B. *J. Chem. Phys.* **1999**, *111*, 7139–7146.
- Matson, J. B.; Grubbs, R. H. *Macromolecules* **2008**, *41*, 5626–5631.
- Matson, J. B.; Grubbs, R. H. *Macromolecules* **2010**, *43*, 213–221.
- Matyjaszewski, K.; Xia, J. *Chem. Rev.* **2001**, *101*, 2921–2990.
- Maughon, B. R.; Morita, T.; Bielawski, C. W.; Grubbs, R. H. *Macromolecules* **2000**, *33*, 1929–1935.
- Mauritz, K. A.; Moore, R. B. *Chem. Rev.* **2004**, *104*, 4535–4585.
- Maynard, H. D.; Grubbs, R. H. *Macromolecules* **1999**, *32*, 6917–6924.
- McLain, S. J.; Sauer, B. B.; Firment, L. E. *Macromolecules* **1996**, *29*, 8211–8219.
- Medrano, R.; Laguna, M. T. R.; Saiz, E.; Tarazona, M. P. *Phys. Chem. Chem. Phys.* **2003**, *5*, 151–157.
- Meuler, A. J.; Ellison, C. J.; Hillmyer, M. A.; Bates, F. S. *Macromolecules* **2008**, *41*, 6272–6275.
- Meuler, A. J.; Ellison, C. J.; Qin, J.; Evans, C. M.; Hillmyer, M. A.; Bates, F. S. *J. Chem. Phys.* **2009**, *130*, 234903/234901–234903/234917.
- Milner, S. T. *Macromolecules* **1994**, *27*, 2333–2335.
- Milner, S. T. *J. Polym. Sci., Part B: Polym. Phys.* **1994**, *32*, 2743–2755.
- Milner, S. T.; Witten, T. A.; Cates, M. E. *Macromolecules* **1988**, *21*, 2610–2619.
- Milner, S. T.; Witten, T. A.; Cates, M. E. *Macromolecules* **1989**, *22*, 853–861.
- Mitchell, J. P.; Gibson, V. C.; Schrock, R. R. *Macromolecules* **1991**, *24*, 1220–1221.
- Mkhalid, I. A. I.; Barnard, J. H.; Marder, T. B.; Murphy, J. M.; Hartwig, J. F. *Chem. Rev.* **2009**, *110*, 890–931.
- Moad, G. *Prog. Polym. Sci.* **1999**, *24*, 81–142.
- Moore, J. S.; Stupp, S. I. *Macromolecules* **1990**, *23*, 65–70.

- Mori, Y.; Lim, L. S.; Bates, F. S. *Macromolecules* **2003**, *36*, 9879–9888.
- Morita, T.; Maughon, B. R.; Bielawski, C. W.; Grubbs, R. H. *Macromolecules* **2000**, *33*, 6621–6623.
- Morita, T.; Maughon, B. R.; Grubbs, R. H. *Polymer Preprints (American Chemical Society, Division of Polymer Chemistry)* **1998**, *39*, 226–227.
- Morton, M.; Fetters, L. J. *Rubber Chem. Technol.* **1975**, *48*, 359–409.
- Mourey, T. H.; Turner, S. R.; Rubinstein, M.; Frechet, J. M. J.; Hawker, C. J.; Wooley, K. L. *Macromolecules* **1992**, *25*, 2401–2406.
- Muller, A. J.; Balsamo, V.; Arnal, M. L. *Adv. Polym. Sci.* **2005**, *190*, 1–63.
- Myers, S. B.; Register, R. A. *Macromolecules* **2008**, *41*, 5283–5288.
- Myers, S. B.; Register, R. A. *Macromolecules* **2008**, *41*, 6773–6779.
- Myers, S. B.; Register, R. A. *Polymer* **2008**, *49*, 877–882.
- Myers, S. B.; Register, R. A. *Macromolecules* **2009**, *42*, 6665–6670.
- Myers, S. B.; Register, R. A. *Macromolecules* **2010**, *43*, 393–401.
- Naga, N.; Kikuchi, G.; Toyota, A. *Polymer* **2006**, *47*, 6081–6090.
- Natta, G.; Dall'Asta, G.; Mazzanti, G. *Angewandte Chemie International Edition in English* **1964**, *3*, 723–729.
- Neburchilov, V.; Martin, J.; Wang, H.; Zhang, J. *J. Power Sources* **2007**, *169*, 221–238.
- Nguyen, S. T.; Grubbs, R. H.; Ziller, J. W. *J. Am. Chem. Soc.* **1993**, *115*, 9858–9859.
- Nguyen, S. T.; Johnson, L. K.; Grubbs, R. H.; Ziller, J. W. *J. Am. Chem. Soc.* **1992**, *114*, 3974–3975.
- Nolan, S. P.; Clavier, H. *Chem. Soc. Rev.* **2010**, *39*, 3305–3316.
- Notestein, J. M.; Lee, L.-B. W.; Register, R. A. *Macromolecules* **2002**, *35*, 1985–1987.
- Novak, B. M.; Risse, W.; Grubbs, R. H. *Adv. Polym. Sci.* **1992**, *102*, 47–72.
- Nunes, S. P.; Sougrat, R.; Hooghan, B.; Anjum, D. H.; Behzad, A. R.; Zhao, L.; Pradeep, N.; Pinnau, I.; Vainio, U.; Peinemann, K. V. *Macromolecules* **2010**, *43*, 8079–8085.

- O'Gara, J. E.; Wagener, K. B. *Makromol. Chem., Rapid Commun.* **1993**, *14*, 657–662.
- Odian, G., *Principles of Polymerization*. 4th ed.; Wiley: Chichester, New York, 2004; p 812.
- Oh, S.; Lee, J.-K.; Theato, P.; Char, K. *Chem. Mater.* **2008**, *20*, 6974–6984.
- Ojha, U.; Kulkarni, P.; Cozzens, D.; Faust, R. *J. Polym. Sci., Part A: Polym. Chem.* **2010**, *48*, 3767–3774.
- Ojha, U.; Kulkarni, P.; Singh, J.; Faust, R. *J. Polym. Sci., Part A: Polym. Chem.* **2009**, *47*, 3490–3505.
- Olson, D. A.; Chen, L.; Hillmyer, M. A. *Chem. Mater.* **2008**, *20*, 869–890.
- Opper, K. L.; Fassbender, B.; Brunklaus, G.; Spiess, H. W.; Wagener, K. B. *Macromolecules* **2009**, *42*, 4407–4409.
- Opper, K. L.; Wagener, K. B. *Macromol. Rapid. Commun.* **2009**, *30*, 915–919.
- Otton, J.; Colleuille, Y.; Varagnat, J. *J. Mol. Catal.* **1980**, *8*, 313–324.
- Owen, R. M.; Gestwicki, J. E.; Young, T.; Kiessling, L. L. *Org. Lett.* **2002**, *4*, 2293–2296.
- Pariya, C.; Jayaprakash, K. N.; Sarkar, A. *Coord. Chem. Rev.* **1998**, *168*, 1–48.
- Park, L. Y.; Schrock, R. R.; Stieglitz, S. G.; Crowe, W. E. *Macromolecules* **1991**, *24*, 3489–3495.
- Park, M.; Harrison, C.; Chaikin, P. M.; Register, R. A.; Adamson, D. H. *Science* **1997**, *276*, 1401–1404.
- Park, M. J.; Balsara, N. P. *Macromolecules* **2008**, *41*, 3678–3687.
- Park, M. J.; Downing, K. H.; Jackson, A.; Gomez, E. D.; Minor, A. M.; Cookson, D.; Weber, A. Z.; Balsara, N. P. *Nano Lett.* **2007**, *7*, 3547–3552.
- Park, S.; Wang, J. Y.; Kim, B.; Xu, J.; Russell, T. P. *ACS Nano* **2008**, *2*, 766–772.
- Passaglia, E.; Coiai, S.; Augier, S. *Prog. Polym. Sci.* **2009**, *34*, 911–947.
- Penczek, S.; Duda, A. *Macromol. Symp.* **1996**, *107*, 1–15.
- Perego, G.; Cella, G. D.; Bastioli, C. *J. Appl. Polym. Sci.* **1996**, *59*, 37–43.

- Phatak, A.; Lim, L. S.; Reaves, C. K.; Bates, F. S. *Macromolecules* **2006**, *39*, 6221–6228.
- Phillip, W. A.; Amendt, M.; O'Neill, B.; Chen, L.; Hillmyer, M. A.; Cussler, E. L. *ACS Applied Materials & Interfaces* **2009**, *1*, 472–480.
- Phillip, W. A.; Hillmyer, M. A.; Cussler, E. L. *Macromolecules* **2010**, *43*, 7763–7770.
- Phillip, W. A.; O'Neill, B.; Rodwogin, M.; Hillmyer, M. A.; Cussler, E. L. *ACS Applied Materials & Interfaces* **2010**, *2*, 847–853.
- Phillip, W. A.; Rzayev, J.; Hillmyer, M. A.; Cussler, E. L. *J. Membr. Sci.* **2006**, *286*, 144–152.
- Pinazzi, C. P.; Campistron, I.; Croissandeau, M. C.; Reyx, D. *J. Mol. Catal.* **1980**, *8*, 325–328.
- Pitet, L. M.; Amendt, M. A.; Hillmyer, M. A. *J. Am. Chem. Soc.* **2010**, *132*, 8230–+.
- Pitet, L. M.; Chamberlain, B. M.; Hauser, A. W.; Hillmyer, M. A. *Macromolecules* **2010**, *43*, 8018–8025.
- Pitet, L. M.; Hillmyer, M. A. *Macromolecules* **2009**, *42*, 3674–3680.
- Pitet, L. M.; Hillmyer, M. A. *Macromolecules* **2011**, *44*, 2378–2381.
- Pitsikalis, M.; Pispas, S.; Mays, J. W.; Hadjichristidis, N. *Adv. Polym. Sci.* **1998**, *135*, 1–137.
- Pochan, D. J.; Gido, S. P.; Pispas, S.; Mays, J. W. *Macromolecules* **1996**, *29*, 5099–5105.
- Pochan, D. J.; Gido, S. P.; Pispas, S.; Mays, J. W.; Ryan, A. J.; Fairclough, J. P. A.; Hamley, I. W.; Terrill, N. J. *Macromolecules* **1996**, *29*, 5091–5098.
- Qiu, W.; Sworen, J.; Pyda, M.; Nowak–Pyda, E.; Habenschuss, A.; Wagener, K. B.; Wunderlich, B. *Macromolecules* **2006**, *39*, 204–217.
- Quirk, R. P.; Kuang, J. *Polym. Int.* **1994**, *33*, 181–186.
- Radano, C. P.; Scherman, O. A.; Stingelin–Stutzmann, N.; Mueller, C.; Breiby, D. W.; Smith, P.; Janssen, R. A. J.; Meijer, E. W. *J. Am. Chem. Soc.* **2005**, *127*, 12502–12503.
- Randall, M. L.; Snapper, M. L. *J. Mol. Catal. A: Chem.* **1998**, *133*, 29–40.
- Rangarajan, P.; Register, R. A.; Fetters, L. J. *Macromolecules* **1993**, *26*, 4640–4645.

- Reyx, D.; Hamza, M.; Campistron, I. *J. Mol. Catal.* **1987**, *42*, 289–299.
- Riegler, S.; Slugovc, C.; Trimmel, G.; Stelzer, F. *Macromol. Symp.* **2004**, *217*, 231–246.
- Ritter, T.; Hejl, A.; Wenzel, A. G.; Funk, T. W.; Grubbs, R. H. *Organometallics* **2006**, *25*, 5740–5745.
- Rivard, M.; Blechert, S. *Eur. J. Org. Chem.* **2003**, 2225–2228.
- Robertson, M. L.; Chang, K.; Gramlich, W. M.; Hillmyer, M. A. *Macromolecules* **2010**, *43*, 1807–1814.
- Rojas, G.; Inci, B.; Wei, Y. Y.; Wagener, K. B. *J. Am. Chem. Soc.* **2009**, *131*, 17376–17386.
- Rojas, G.; Wagener, K. B. *Macromolecules* **2009**, *42*, 1934–1947.
- Román, C.; Fischer, H. R.; Meijer, E. W. *Macromolecules* **1999**, *32*, 5525–5531.
- Roovers, J.; Toporowski, P. M. *J. Polym. Sci., Part B: Polym. Phys.* **1980**, *18*, 1907–1917.
- Ruzette, A.-V.; Tence-Girault, S.; Leibler, L.; Chauvin, F.; Bertin, D.; Guerret, O.; Gerard, P. *Macromolecules* **2006**, *39*, 5804–5814.
- Ryan, A. J.; Hamley, I. W.; Bras, W.; Bates, F. S. *Macromolecules* **1995**, *28*, 3860–3868.
- Rzayev, J.; Hillmyer, M. A. *J. Am. Chem. Soc.* **2005**, *127*, 13373–13379.
- Rzayev, J.; Hillmyer, M. A. *Macromolecules* **2005**, *38*, 3–5.
- Saetung, N.; Campistron, I.; Pascual, S.; Pilard, J. F.; Fontaine, L. *Macromolecules* **2011**, *44*, 784–794.
- Saito, T.; Moore, H. D.; Hickner, M. A. *Macromolecules* **2009**, *43*, 599–601.
- Sanford, M. S.; Love, J. A.; Grubbs, R. H. *J. Am. Chem. Soc.* **2001**, *123*, 6543–6554.
- Sanford, M. S.; Ulman, M.; Grubbs, R. H. *J. Am. Chem. Soc.* **2001**, *123*, 749–750.
- Santana, O. O.; Mueller, A. J. *Polym. Bull.* **1994**, *32*, 471–477.
- Scherman, O. A.; Kim, H. M.; Grubbs, R. H. *Macromolecules* **2002**, *35*, 5366–5371.
- Scherman, O. A.; Ligthart, G. B. W. L.; Ohkawa, H.; Sijbesma, R. P.; Meijer, E. W. *Proc. Natl. Acad. Sci.* **2006**, *103*, 11850–11855.



- Scherman, O. A.; Rutenberg, I. M.; Grubbs, R. H. *J. Am. Chem. Soc.* **2003**, *125*, 8515–8522.
- Scherman, O. A.; Walker, R.; Grubbs, R. H. *Macromolecules* **2005**, *38*, 9009–9014.
- Schmidt, S. C.; Hillmyer, M. A. *Macromolecules* **1999**, *32*, 4794–4801.
- Schmidt, S. C.; Hillmyer, M. A. *J. Polym. Sci., Part B: Polym. Phys.* **2002**, *40*, 2364–2376.
- Schneider, W. A.; Müller, M. F. *J. Mol. Catal.* **1988**, *46*, 395–403.
- Scholl, M.; Ding, S.; Lee, C. W.; Grubbs, R. H. *Org. Lett.* **1999**, *1*, 953–956.
- Scholl, M.; Trnka, T. M.; Morgan, J. P.; Grubbs, R. H. *Tetrahedron Lett.* **1999**, *40*, 2247–2250.
- Schreck, K. M.; Hillmyer, M. A. *J. Biotechnol.* **2007**, *132*, 287–295.
- Schrock, R. R. *Tetrahedron* **1999**, *55*, 8141–8153.
- Schrock, R. R. *Angew. Chem., Int. Ed.* **2006**, *45*, 3748–3759.
- Schrock, R. R.; DePue, R. T.; Feldman, J.; Yap, K. B.; Yang, D. C.; Davis, W. M.; Park, L.; DiMare, M.; Schofield, M.; et, a. *Organometallics* **1990**, *9*, 2262–2275.
- Schrock, R. R.; Feldman, J.; Cannizzo, L. F.; Grubbs, R. H. *Macromolecules* **1987**, *20*, 1169–1172.
- Schrock, R. R.; Hoveyda, A. H. *Angew. Chem., Int. Ed.* **2003**, *42*, 4592–4633.
- Schrock, R. R.; Murdzek, J. S.; Bazan, G. C.; Robbins, J.; DiMare, M.; O'Regan, M. *J. Am. Chem. Soc.* **1990**, *112*, 3875–3886.
- Schulz, M. F.; Khandpur, A. K.; Bates, F. S.; Almdal, K.; Mortensen, K.; Hajduk, D. A.; Gruner, S. M. *Macromolecules* **1996**, *29*, 2857–2867.
- Schuster, M.; Blechert, S. *Angew. Chem., Int. Ed.* **1997**, *36*, 2036–2056.
- Schwab, P.; France, M. B.; Ziller, J. W.; Grubbs, R. H. *Angew. Chem., Int. Ed.* **1995**, *34*, 2039–2041.
- Schwab, P.; Grubbs, R. H.; Ziller, J. W. *J. Am. Chem. Soc.* **1996**, *118*, 100–110.
- Schwendeman, J. E.; Wagener, K. B. *Macromol. Chem. Phys.* **2005**, *206*, 1461–1471.

- Schwendeman, J. E.; Wagener, K. B. *Macromol. Chem. Phys.* **2009**, *210*, 1818–1833.
- Semba, T.; Kitagawa, K.; Ishiaku, U. S.; Hamada, H. *J. Appl. Polym. Sci.* **2006**, *101*, 1816–1825.
- Shi, A.-C.; Noolandi, J. *Macromolecules* **1994**, *27*, 2936–2944.
- Shin, J.; Chang, A. Y.; Brownell, L. V.; Racoma, I. O.; Ozawa, C. H.; Chung, H. Y.; Peng, S.; Bae, C. S. *J. Polym. Sci., Part A: Polym. Chem.* **2008**, *46*, 3533–3545.
- Sides, S. W.; Fredrickson, G. H. *J. Chem. Phys.* **2004**, *121*, 4974–4986.
- Sill, K.; Emrick, T. *J. Polym. Sci., Part A: Polym. Chem.* **2005**, *43*, 5429–5439.
- Simon, Y. C.; Coughlin, E. B. *J. Polym. Sci., Part A: Polym. Chem.* **2010**, *48*, 2557–2563.
- Slugovc, C. *Macromol. Rapid Commun.* **2004**, *25*, 1283–1297.
- Smith, D.; Pentzer, E. B.; Nguyen, S. T. *Polym. Rev.* **2007**, *47*, 419–459.
- Smith, J. A.; Brzezinska, K. R.; Valenti, D. J.; Wagener, K. B. *Macromolecules* **2000**, *33*, 3781–3794.
- Smitha, B.; Sridhar, S.; Khan, A. A. *J. Membr. Sci.* **2005**, *259*, 10–26.
- Song, A.; Lee, J. C.; Parker, K. A.; Sampson, N. S. *J. Am. Chem. Soc.* **2010**, *132*, 10513–10520.
- Song, A.; Parker, K. A.; Sampson, N. S. *J. Am. Chem. Soc.* **2009**, *131*, 3444–3445.
- Stephens, C. H.; Yang, H.; Islam, M.; Chum, S. P.; Rowan, S. J.; Hiltner, A.; Baer, E. *J. Polym. Sci., Part B: Polym. Phys.* **2003**, *41*, 2062–2070.
- Streuff, J.; Muñiz, K. *J. Organomet. Chem.* **2005**, *690*, 5973–5978.
- Sutthasupa, S.; Shiotsuki, M.; Sanda, F. *Polym. J.* **2010**, *42*, 905–915.
- Switek, K. A.; Chang, K.; Bates, F. S.; Hillmyer, M. A. *J. Polym. Sci., Part A: Polym. Chem.* **2006**, *45*, 361–373.
- Sworen, J. C.; Smith, J. A.; Berg, J. M.; Wagener, K. B. *J. Am. Chem. Soc.* **2004**, *126*, 11238–11246.
- Sworen, J. C.; Smith, J. A.; Wagener, K. B.; Baugh, L. S.; Rucker, S. P. *J. Am. Chem. Soc.* **2003**, *125*, 2228–2240.

- Sworen, J. C.; Wagener, K. B. *Macromolecules* **2007**, *40*, 4414–4423.
- Szwarc, M. *Nature (London, United Kingdom)* **1956**, *178*, 1168–1169.
- Szwarc, M.; Levy, M.; Milkovich, R. *J. Am. Chem. Soc.* **1956**, *78*, 2656–2657.
- Tamura, H.; Nakayama, A. *Journal of Macromolecular Science, Pure and Applied Chemistry* **2002**, *A39*, 745–758.
- Tasdelen, M. A.; Kahveci, M. U.; Yagci, Y. *Prog. Polym. Sci.* **2011**, *36*, 455–567.
- Teng, C. Q.; Kai, Y.; Ping, J.; Yu, M. H. *J. Polym. Sci., Part A: Polym. Chem.* **2004**, *42*, 5045–5053.
- Teubner, M.; Strey, R. *J. Chem. Phys.* **1987**, *87*, 3195.
- Theryo, G.; Jing, F.; Pitet, L. M.; Hillmyer, M. A. *Macromolecules* **2010**, *43*, 7394–7397.
- Thomas, R. M.; Grubbs, R. H. *Macromolecules* **2010**, *43*, 3705–3709.
- Thuilliez, J.; Monteil, V.; Spitz, R.; Boisson, C. *Angew. Chem., Int. Ed.* **2005**, *44*, 2593–2596.
- Thurn–Albrecht, T.; Steiner, R.; DeRouchey, J.; Stafford, C. M.; Huang, E.; Bal, M.; Tuominen, M.; Hawker, C. J.; Russell, T. P. *Adv. Mater.* **2000**, *12*, 787–790.
- Trnka, T. M.; Grubbs, R. H. *Acc. Chem. Res.* **2001**, *34*, 18–29.
- Trnka, T. M.; Morgan, J. P.; Sanford, M. S.; Wilhelm, T. E.; Scholl, M.; Choi, T. L.; Ding, S.; Day, M. W.; Grubbs, R. H. *J. Am. Chem. Soc.* **2003**, *125*, 2546–2558.
- Trollsås, M.; Atthoff, B.; Claesson, H.; Hedrick, J. L. *J. Polym. Sci., Part A: Polym. Chem.* **2004**, *42*, 1174–1188.
- Trollsås, M.; Claesson, H.; Atthoff, B.; Hedrick, J. L. *Angew. Chem., Int. Ed.* **1998**, *37*, 3132–3136.
- Trollsås, M.; Claesson, H.; Atthoff, B.; Hedrick, J. L.; Pople, J. A.; Gast, A. P. *Macromol. Symp.* **2000**, *153*, 87–108.
- Trollsås, M.; Hawker, C. J.; Remenar, J. F.; Hedrick, J. L.; Johansson, M.; Ihre, H.; Hult, A. *J. Polym. Sci., Part A: Polym. Chem.* **1998**, *36*, 2793–2798.
- Trollsås, M.; Hedrick, J.; Mecerreyes, D.; Jérôme, R.; Dubois, P. *J. Polym. Sci., Part A: Polym. Chem.* **1998**, *36*, 3187–3192.
- Trollsås, M.; Hedrick, J. L. *J. Am. Chem. Soc.* **1998**, *120*, 4644–4651.

- Trollsås, M.; Hedrick, J. L. *Macromolecules* **1998**, *31*, 4390–4395.
- Trollsås, M.; Hedrick, J. L.; Mecerreyes, D.; Dubois, P.; Jérôme, R.; Ihre, H.; Hult, A. *Macromolecules* **1997**, *30*, 8508–8511.
- Trollsås, M.; Hedrick, J. L.; Mecerreyes, D.; Dubois, P.; Jérôme, R.; Ihre, H.; Hult, A. *Macromolecules* **1998**, *31*, 2756–2763.
- Trollsås, M.; Hedrick, J. L.; Mecerreyes, D.; Dubois, P.; Jérôme, R.; Ihre, H.; Hult, A. *Macromolecules* **1998**, *31*, 2756–2763.
- Trollsås, M.; Kelly, M. A.; Claesson, H.; Siemens, R.; Hedrick, J. L. *Macromolecules* **1999**, *32*, 4917–4924.
- Truett, W. L.; Johnson, D. R.; Robinson, I. M.; Montague, B. A. *J. Am. Chem. Soc.* **1960**, *82*, 2337–2340.
- Trzaska, S. T.; Lee, L.-B. W.; Register, R. A. *Macromolecules* **2000**, *33*, 9215–9221.
- Uehara, H.; Kakiage, M.; Sekiya, M.; Sakuma, D.; Yamanobe, T.; Takano, N.; Barraud, A.; Meurville, E.; Ryser, P. *ACS Nano* **2009**, *3*, 924–932.
- Uehara, H.; Yoshida, T.; Kakiage, M.; Yamanobe, T.; Komoto, T.; Nomura, K.; Nakajima, K.; Matsuda, M. *Macromolecules* **2006**, *39*, 3971–3974.
- Ulman, M.; Belderrain, T. R.; Grubbs, R. H. *Tetrahedron Lett.* **2000**, *41*, 4689–4693.
- Valenti, D. J.; Wagener, K. B. *Macromolecules* **1998**, *31*, 2764–2773.
- Vavasour, J. D.; Whitmore, M. D. *Macromolecules* **1993**, *26*, 7070–7075.
- Vayer, M.; Hillmyer, M. A.; Dirany, M.; Thevenin, G.; Erre, R.; Sinturel, C. *Thin Solid Films* **2010**, *518*, 3710–3715.
- Vedrine, J.; Hong, Y.-R.; Marencic, A. P.; Register, R. A.; Adamson, D. H.; Chaikin, P. M. *Appl. Phys. Lett.* **2007**, *91*, 143110/143111–143110/143113.
- Vigild, M. E.; Chu, C.; Sugiyama, M.; Chaffin, K. A.; Bates, F. S. *Macromolecules* **2001**, *34*, 951–964.
- Vink, E. T. H.; Rabago, R.; Glassner, D. A.; Springs, B.; O'Connor, R. P.; Kolstad, J.; Gruber, P. R. *Macromol. Biosci.* **2004**, *4*, 551–564.
- Vougioukalakis, G. C.; Grubbs, R. H. *Chem. Rev.* **2010**, *110*, 1746–1787.
- Wagener, K. B.; Valenti, D.; Hahn, S. F. *Macromolecules* **1997**, *30*, 6688–6690.

- Walker, R.; Conrad, R. M.; Grubbs, R. H. *Macromolecules* **2009**, *42*, 599–605.
- Wan, Y. Q.; Chen, W. N.; Yang, J.; Bei, J. Z.; Wang, S. G. *Biomater.* **2003**, *24*, 2195–2203.
- Wang, F.; Hickner, M.; Kim, Y. S.; Zawodzinski, T. A.; McGrath, J. E. *J. Membr. Sci.* **2002**, *197*, 231–242.
- Wang, W.; Ping, P.; Yu, H.; Chen, X.; Jing, X. *J. Polym. Sci., Part A: Polym. Chem.* **2006**, *44*, 5505–5512.
- Wang, Y.; He, C. C.; Xing, W. H.; Li, F. B.; Tong, L.; Chen, Z. Q.; Liao, X. Z.; Steinhart, M. *Adv. Mater.* **2010**, *22*, 2068–+.
- Wang, Y.; Hillmyer, M. A. *J. Polym. Sci., Part A: Polym. Chem.* **2001**, *39*, 2755–2766.
- Wang, Y. Q.; Noga, D. E.; Yoon, K.; Wojtowicz, A. M.; Lin, A. S. P.; Garcia, A. J.; Collard, D. M.; Weck, M. *Adv. Funct. Mater.* **2008**, *18*, 3638–3644.
- Watson, M. D.; Wagener, K. B. *Macromolecules* **2000**, *33*, 5411–5417.
- Watson, M. D.; Wagener, K. B. *Macromolecules* **2000**, *33*, 8963–8970.
- Weck, M.; Mohr, B.; Maughon, B. R.; Grubbs, R. H. *Macromolecules* **1997**, *30*, 6430–6437.
- Wei, Y. H.; Li, B. Y.; Han, Y. C.; Pan, C. Y. *Soft Matter* **2008**, *4*, 2507–2512.
- Weidisch, R.; Gido, S. P.; Uhrig, D.; Iatrou, H.; Mays, J.; Hadjichristidis, N. *Macromolecules* **2001**, *34*, 6333–6337.
- Weimann, P. A.; Jones, T. D.; Hillmyer, M. A.; Bates, F. S.; Londono, J. D.; Melnichenko, Y.; Wignall, G. D.; Almdal, K. *Macromolecules* **1997**, *30*, 3650–3657.
- Whittaker, M. R.; Urbani, C. N.; Monteiro, M. J. *J. Am. Chem. Soc.* **2006**, *128*, 11360–11361.
- Widin, J. M.; Schmitt, A. K.; Im, K.; Schmitt, A. L.; Mahanthappa, M. K. *Macromolecules* **2010**, *43*, 7913–7915.
- Williams, C. K.; Hillmyer, M. A. *Polym. Rev.* **2008**, *48*, 1–10.
- Witzke, D. R.; Kolstad, J. J.; Narayan, R. *Macromolecules* **1997**, *30*, 7075–7085.
- Wolf, J. H.; Hillmyer, M. A. *Langmuir* **2003**, *19*, 6553–6560.
- Wu, Z.; Grubbs, R. H. *Macromolecules* **1994**, *27*, 6700–6703.

- Wu, Z.; Nguyen, S. T.; Grubbs, R. H.; Ziller, J. W. *J. Am. Chem. Soc.* **1995**, *117*, 5503–5511.
- Wunderlich, B.; Dole, M. *Journal of Polymer Science* **1957**, *24*, 201–213.
- Wurm, F.; Frey, H. *Prog. Polym. Sci.* **2011**, *36*, 1–52.
- Xia, Y.; Verduzco, R.; Grubbs, R. H.; Kornfield, J. A. *J. Am. Chem. Soc.* **2008**, *130*, 1735–1740.
- Xie, M.; Wang, W.; Ding, L.; Liu, J.; Yang, D.; Wei, L.; Zhang, Y. *J. Polym. Sci., Part A: Polym. Chem.* **2010**, *48*, 380–388.
- Xie, M. R.; Kong, Y.; Han, H. J.; Shi, J. X.; Ding, L.; Song, C. N.; Zhang, Y. Q. *React. Funct. Polym.* **2008**, *68*, 1601–1608.
- Yagci, Y.; Tasdelen, M. A. *Prog. Polym. Sci.* **2006**, *31*, 1133–1170.
- Yang, H.; Islam, M.; Budde, C.; Rowan, S. J. *J. Polym. Sci., Part A: Polym. Chem.* **2003**, *41*, 2107–2116.
- Yang, L.; Gido, S. P.; Mays, J. W.; Pispas, S.; Hadjichristidis, N. *Macromolecules* **2001**, *34*, 4235–4243.
- Yang, S. K.; Ambade, A. V.; Weck, M. *Chem. Eur. J.* **2009**, *15*, 6605–6611.
- Yang, S. K.; Ambade, A. V.; Weck, M. *J. Am. Chem. Soc.* **2010**, *132*, 1637–1645.
- Yang, S. K.; Ambade, A. V.; Weck, M. *Chem. Soc. Rev.* **2011**, *40*, 129–137.
- Yang, S. Y.; Park, J.; Yoon, J.; Ree, M.; Jang, S. K.; Kim, J. K. *Adv. Funct. Mater.* **2008**, *18*, 1371–1377.
- Yang, Y. S.; Siu, A.; Peckham, T. J.; Holdcroft, S., Structural and Morphological Features of Acid-Bearing Polymers for PEM Fuel Cells. In *Fuel Cells I*, 2008; Vol. 215, pp 55–126.
- Yu, T.; Ren, J.; Gu, S.; Yang, M. *Polym. Adv. Technol.* **2010**, *21*, 183–188.
- Yu, X.; Roy, A.; Dunn, S.; Badami, A. S.; Yang, J.; Good, A. S.; McGrath, J. E. *J. Polym. Sci., Part A: Polym. Chem.* **2009**, *47*, 1038–1051.
- Zalusky, A. S.; Olayo-Valles, R.; Taylor, C. J.; Hillmyer, M. A. *J. Am. Chem. Soc.* **2001**, *123*, 1519–1520.
- Zalusky, A. S.; Olayo-Valles, R.; Wolf, J. H.; Hillmyer, M. A. *J. Am. Chem. Soc.* **2002**, *124*, 12761–12773.

- 
- Zaman, S.; Curnow, O. J.; Abell, A. D. *Aust. J. Chem.* **2009**, *62*, 91–100.
- Zhang, S. S. *J. Power Sources* **2007**, *164*, 351–364.
- Zhao, Y.; Wang, L.; Xiao, A.; Yu, H. *Prog. Polym. Sci.* **2010**, *35*, 1195–1216.
- Zheng, L.; Farris, R. J.; Coughlin, E. B. *J. Polym. Sci., Part A: Polym. Chem.* **2001**, *39*, 2920–2928.
- Zheng, Y.; Li, Y. G.; Pan, L.; Li, Y. S. *Polymer* **2007**, *48*, 2496–2502.
- Zhou, N.; Bates, F. S.; Lodge, T. P. *Nano Lett.* **2006**, *6*, 2354–2357.
- Zhu, Y.; Gido, S. P.; Moshakou, M.; Iatrou, H.; Hadjichristidis, N.; Park, S.; Chang, T. *Macromolecules* **2003**, *36*, 5719–5724.
- Zuluaga, F.; Inci, B.; Nozue, Y.; Hosoda, S.; Wagener, K. B. *Macromolecules* **2009**, *42*, 4953–4955.

# Appendix A

## Characterization Methods

This appendix summarizes the common techniques used for extensive characterization of all the materials described in the preceding chapters. Instrument models are included and, where appropriate, a brief discussion of data treatment is discussed.



## A.1 Nuclear Magnetic Resonance Spectroscopy

All spectra using nuclear magnetic resonance (NMR) spectroscopy were obtained in boro-silicate glass tubes with the material as a dilute solution (5–50 mg mL<sup>-1</sup>) in a deuterated solvent. The solvents and temperatures were chosen for suitability at fostering the dissolution of substrates to create homogeneous solutions.

Spectra for substrates that were fully soluble at ambient temperature (20 °C) were collected on a Varian Inova 500 instrument operating at 500 MHz for <sup>1</sup>H NMR spectra and 125 MHz for <sup>13</sup>C spectra. The signals were referenced with respect to the trace hydrogenous signals from the deuterated solvents (Table A.1). Spectra for substrates that required elevated temperature for dissolution were collected on a Varian Inova 300 instrument, for which the accessible temperature range was –100 °C to +100 °C.

**Table A.1**

Characteristics of deuterated solvents used for NMR spectroscopy.

Solvent	<sup>1</sup> H-signal (ppm)	<sup>13</sup> C-signal (ppm)	temp. (°C)
chloroform (CDCl <sub>3</sub> )	7.26	77.23	20
dimethylsulfoxide (DMSO- <i>d</i> <sub>6</sub> )	2.50	39.51	20
tetrahydrofuran (THF- <i>d</i> <sub>8</sub> )	3.58/1.73	67.57/25.37	20
toluene- <i>d</i> <sub>8</sub>	2.09	20.4	100
1,1,2,2-tetrachloroethane (TCE- <i>d</i> <sub>2</sub> )	6.00	73.78	100

## A.2 IR Spectroscopy

Infrared (IR) spectroscopy was performed on a Magna-IR 550 spectrometer from Nicolet (Thermo Scientific). The samples were prepared as KBr discs or as

pristine thin films ( $\sim 10 \mu\text{m}$ ) and measurements were made at ambient temperature.

### A.3 Elemental Analysis

Elemental analysis was performed off-site using a commercial service provider. Samples were sent to Atlantic Microlab, Inc. at:

6180 Atlantic Blvd. Suite M  
Norcross, GA 30071  
Tel. 770.242.0082  
Fax. 770.242.0236

Samples were evaluated for carbon, hydrogen, oxygen, and sulfur content.

### A.4 Differential Scanning Calorimetry

Certain thermal transitions were determined with differential scanning calorimetry (DSC). A typical experiment involves loading an aluminum pan with between 3–10 mg of sample and sealing it with an aluminum lid. The pan is placed in a sealed container on a pedestal that can be heated and cooled in a controlled manner. Another pedestal contains an empty aluminum pan. The two pans are heated or cooled simultaneously, and maintained at identical temperatures while the heat flow necessary to maintain the temperature is measured. When a sample undergoes a thermal transition, a change in the heat capacity occurs, which is accompanied by either the release or consumption of energy in the form of heat. The change in heat capacity is reflected in the heat flow, whereby either more or less energy is required to maintain equal temperatures in the two pans. A plot of heat flow provided by the heating element with respect to the empty pan versus temperature will essentially have a flat baseline accented with features that are

characteristic of different thermal transitions (e.g., melting, crystallization or glass transition). The enthalpy associated with the different thermal transitions can be measured by integrating the area under (or over) a peak (or trough).

DSC was performed with a model Q1000 from TA Instruments. A small amount of material (3–10 mg) was hermetically sealed in an aluminum pan. Typically, samples were heated initially from ambient temperature to a temperature 20 °C above the highest thermal transition (either  $T_g$  or  $T_m$ ) at a rate of 20 °C min<sup>-1</sup>. The sample was annealed at the highest temperature for 5 min, followed by cooling at 10 °C min<sup>-1</sup> to a prescribed temperature below all the thermal transitions. A second heating ramp was performed at a rate of 10 °C min<sup>-1</sup>. All heating and cooling was performed with the sample pan in a chamber under a helium purge.

Thermal transitions were analyzed using Universal Analysis software from TA Instruments. Glass transition temperatures ( $T_g$ ) were taken as the midpoint between the two inflection points. Melting temperatures ( $T_m$ ) were taken as the maximum in the melting endotherms and crystallization temperatures ( $T_c$ ) were taken as the minimum in the crystallization exotherm. Melting and crystallization enthalpies were measured by integrating the endotherm and exotherm, respectively.

## A.5 Size Exclusion Chromatography

Size exclusion chromatography (SEC) was used to evaluate the relative sizes of different polymeric species. The SEC consists of a high-pressure liquid chromatograph housing several columns in series that contain porous media with well-prescribed pore sizes. Polymer solutions injected onto the columns will diffuse into the pores, with the diffusion coefficient being dependant on the hydrodynamic radius of the particle, which is roughly correlated with the molecular weight. The hydrodynamic radius depends on the polymer-solvent interactions and the polymer architecture in addition to molar mass, and this must be accounted for during analysis of molar mass. Generally speaking, larger particles spend less time within

the pores and consequentially elute from the columns earlier than smaller particles. The presence and concentration of particles eluting from the columns can be monitored in several different ways. The work within this dissertation relies on refractive index detector and a multi-angle laser light scattering detector. Extensive theory of SEC and light scattering can be found in most polymer science textbooks.\*

SEC measurements were made using several different instruments, depending on the solubility of the substrate and the intended analysis. Analysis on certain samples was performed with a series 1100 HPLC pump from Agilent Technologies equipped with a Hewlett Packard 1047a refractive index (RI) detector. The instrument houses three columns in series of model PL-gel  $\mu$ C from Polymer Laboratories. Molecular weights and polydispersity indices (PDI) were calculated as compared to polystyrene standards (Polymer Laboratories). The samples were dissolved in HPLC-grade chloroform ( $\text{CHCl}_3$ ) at approximately  $3 \text{ mg mL}^{-1}$  and injected onto the columns

Absolute molecular weights were measured on an instrument using an HPLC pump and housing three Phenomenex Phenogel columns. The instrument was equipped with multi-angle laser light scattering (MALS) MiniDawn detector with 18 angles from Wyatt Technologies. Samples were dissolved in tetrahydrofuran (THF) at approximately  $5 \text{ mg mL}^{-1}$  before injecting onto the columns. The HPLC pump was operating at  $30 \text{ }^\circ\text{C}$  with a flow rate of  $1 \text{ mL min}^{-1}$ . Analysis was done using Astra software from Wyatt Technologies.

## A.6 Small Angle X-ray Scattering

Small angle x-ray scattering was performed at Argonne National Laboratories on the synchrotron source. The sample to detector distance was variable in order to access different spatial ranges within the materials being investigated. A typical setup involved a sample-to-detector distance of 5.65 m. The detector radius was 81

---

\* Hiemenz, P. C.; Lodge, T. P. in *Polymer Chemistry*, 2<sup>nd</sup> ed. 2007, CRC Press, Boca Raton, FL.

mm. Scattering intensity was monitored by a Mar 165 mm diameter CCD detector with a resolution of  $2048 \times 2048$ . The two-dimensional scattering patterns were azimuthally integrated to afford one-dimensional profiles presented as spatial frequency ( $q$ ) versus scattered intensity. The beamline is maintained by the Dow–Northwestern–DuPont Collaborative Access Team (DND-CAT) at Beamline 5 of Argonne National Laboratories. DND-CAT is supported by E.I. DuPont de Nemours & Co., The Dow Chemical Company and Northwestern University. Use of the APS, an Office of Science User Facility operated for the U.S. Department of Energy (DOE) Office of Science by Argonne National Laboratory, was supported by the U.S. DOE under Contract No. DE-AC02-06CH11357.

## A.7 Wide Angle X-ray Scattering

Wide-angle X-ray scattering (WAXS) was performed at Argonne National Laboratories, at Beamline 5. The WAXS was integrated with the SAXS measurements, with both spatial ranges being collected simultaneously. The WAXS detector was a Roper CCD wide-area detector.

## A.8 Scanning Electron Microscopy

Scanning electron microscopy relies on the interaction of a substrate while being bombarded with electrons. Two separate instruments were used for obtaining SEM images. One instrument was a Hitachi S900 with a cold field emission gun (FEG). The instrument was operated at 3 kV accelerating voltage. The second instrument was a Hitachi S4700 with a FEG, also operated at 3 kV accelerating voltage. The samples were prepared by first mounting on aluminum sample holders with carbon tape or colloidal graphite (in isopropanol) followed by sputter coating with platinum. A thin layer ( $\sim 2$ – $3$  nm) of Pt was deposited using a VCR high resolution indirect ion beam sputtering system.

## A.9 Transmission Electron Microscopy

Transmission electron microscopy (TEM) was performed on thin sections of polymer samples to elucidate the microphase separated structures. The thin sections were prepared by microtoming at either room temperature or cryogenic temperatures, depending on the glassy content of samples. Microtomy was performed using a Leica EM UC6 microtome equipped with a cryo stage with temperature capabilities down to  $-140\text{ }^{\circ}\text{C}$ . Thin sections were cut using a diamond knife from Microstar Technologies (3 mm blade) and transferred from the boat to a copper grid (Ted Pella, 200 mesh) using an eyelash. After transfer to the copper grids, the samples were exposed to  $\text{OsO}_4$  vapor (generated from 4 wt % aqueous solution) in order to preferentially stain the polyolefin portions of the unsaturated block copolymers. The contrast gained from selective staining allows for visualization by TEM of the microphase separation. The TEM predominantly used was a JEOL 1210 operating at 120 kV accelerating voltage. The images were captured by a bottom mounted Gatan multiscan CCD camera with  $1024\times 1024$  resolution.

## A.10 Nitrogen Sorption

Nitrogen adsorption experiments were conducted using an Autosorb iQ2 from Quantachrome Instruments. Samples were outgassed for 20 h at  $40\text{ }^{\circ}\text{C}$ . Analysis was performed at 77 K. The pressure relative to the saturation pressure is measured with respect to the volume of gas adsorbed. The pressure is gradually increased from low values of relative pressure ( $p/p_0 = 0.05$ ) up to saturation pressure ( $p/p_0 = 1$ ) and the volume of gas required to attain each pressure is measured. According to theory, initially, the entire surface of the adsorbate is covered with a unimolecular layer of the adsorbing gas. The volume of gas required for unimolecular coverage ( $v_m$ ) can be calculated from the slope and intercept of the linear portion of the isotherm data obtained in the range of relative pressures 0.05–0.35. It has been shown that the isotherms typically deviate from linearity

outside of this range. The surface area is then extracted by the BET method by multiplying  $v_m$  by the cross sectional area of the adsorbing gas and dividing by the mass of adsorbate. The surface area is extracted according to equations A.1–2.

$$\frac{1}{v \left( \frac{p}{p_0} - 1 \right)} = \frac{1}{v_m c} + \frac{c - 1}{v_m c} \cdot \frac{p}{p_0} \quad (\text{A.1})$$

where  $v$  is the total volume of gas administered during the pressure increase,  $v_m$  is the volume of gas of a monolayer, and  $c$  is the BET constant. The slope and intercept of the line provided by plotting  $1/(v(p/p_0-1))$  versus  $(p/p_0)$  provide values of  $v_m$  and  $c$ . The BET surface area ( $S_{\text{BET}}$ ) is found by eq A.2.

$$S_{\text{BET}} = \frac{v_m \cdot N \cdot s}{a \cdot V} \quad (\text{A.2})$$

where  $V$  is the molar volume of the adsorbing gas,  $s$  is the molar cross-sectional area of the adsorbing gas,  $a$  is the mass of the adsorbate, and  $N$  is Avogadro's number.

The average pore radius and pore-size distributions were calculated using the theory developed by Barret, Joyner, and Halenda. The theory is discussed in length in several references. The important points are that the pore-radii are calculated assuming a cylindrical pore-geometry. The disorganized pore topology for the LPE samples presented in Chapter 4 must be considered, and the pore-radii should not be taken as perfect representations of the actual pore-size. However, the mesoporosity is nonetheless indicated by the shapes of the isotherms (type IV).





## Appendix B

### Functional Polymers from Ring-opening Metathesis Polymerization of 3-substituted cyclooct-1-enes

This appendix describes the preliminary results from the synthesis of monomers and the polymers resulting from ring-opening metathesis polymerization (ROMP). The monomers are all based on the substitution of *cis*-cyclooctene in the 3-position. Different functional groups were placed in the 3-position of cyclooctene, and the microstructure of the resulting polymer was investigated by  $^1\text{H}$  NMR and  $^{13}\text{C}$  NMR spectroscopy.

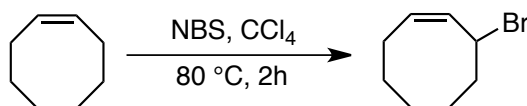
## B.1 Substituted Cyclooctenes

This section describes the synthesis and ring-opening metathesis polymerization of several *cis*-cyclooctene (COE) derivatives with functional substituents in the 3-position. The monomers were each synthesized by starting with the allyl-bromination of commercially available COE. Polymerizations were attempted with the second-generation Grubbs catalyst (**G2**); several monomers did not polymerize to an appreciable extent. The polymerizations consistently proceeded in a regio- and stereo-selective fashion to give polymer with substituents located perfectly on every eighth backbone carbon. The monomers and corresponding polymers were characterized by  $^1\text{H}$  and  $^{13}\text{C}$  NMR spectroscopy, as well as  $^1\text{H}$ - $^1\text{H}$  and  $^1\text{H}$ - $^{13}\text{C}$  correlated spectroscopy.

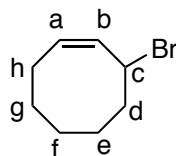
The subsequent sections give exhaustive characterization data for the different monomers. Polymer characteristics follow directly after the monomer from which they were derived.

B.1.1 3-bromo-*cis*-cyclooct-1-ene

The compound 3-bromo-*cis*-cyclooct-1-ene (3BrCOE) forms the basis for the other monomers synthesized. The brominated carbon is amenable to nucleophilic substitution to a wide range of substrates. Upon substitution, additional transformations can be performed, giving access to a wide range of substituents exhibiting various physical characteristics. 3BrCOE was not effected by **G2** or **G3** catalysts, and there is therefore no description of polymer from this substrate.

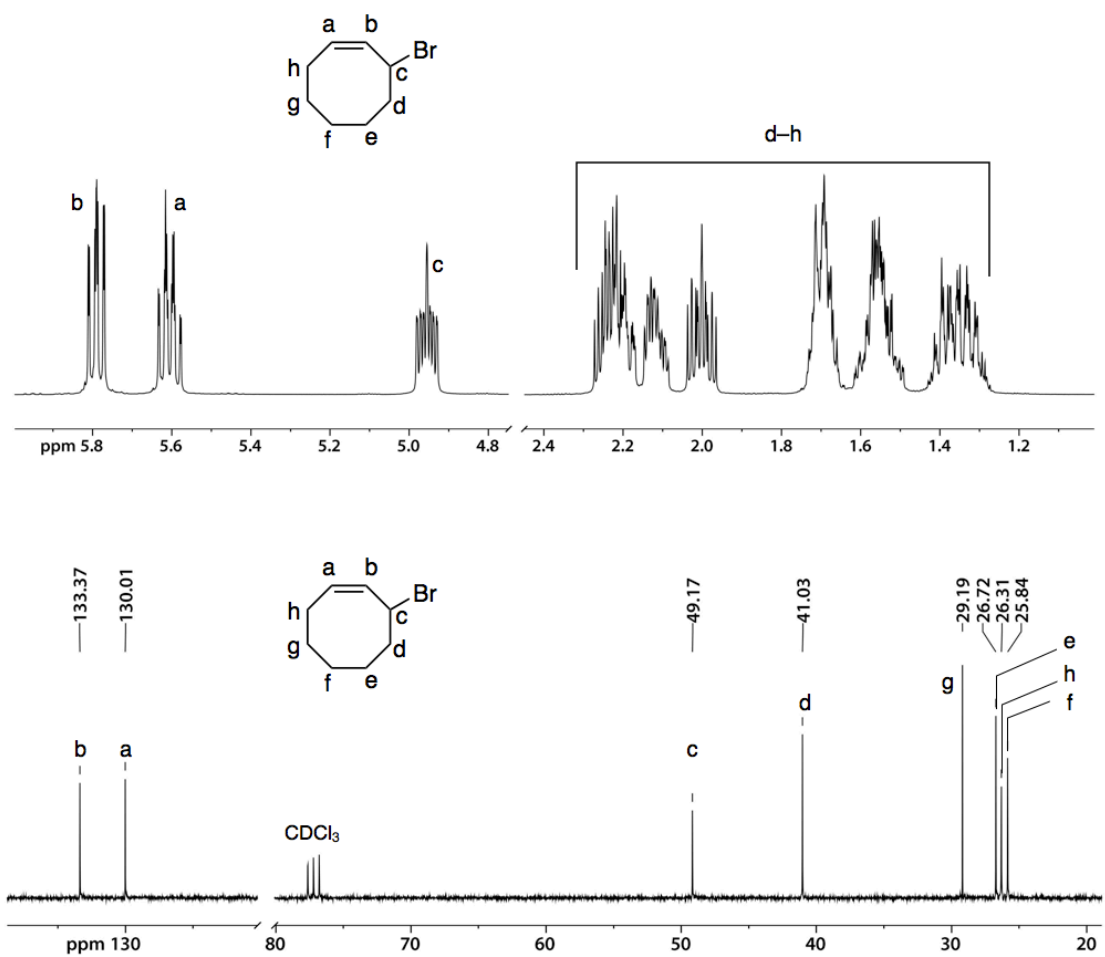


In a 500 mL two neck flask was poured 96 mL of *cis*-cyclooctene (82.6 g; 751 mmol) along with 300 mL of CCl<sub>4</sub>. In one neck was affixed a reflux condenser, while the other neck was sealed with a rubber septum. The system was thoroughly purged with argon before adding 50 mg of AIBN and heating to 80 °C. The reaction progress was monitored by watching the slightly yellow solid on the bottom of the flask (NBS) float to the top upon conversion to succinimide. After 2 h, the reaction was cooled to RT and filtered to remove the succinimide. The CCl<sub>4</sub> was diluted with 200 mL of CH<sub>2</sub>Cl<sub>2</sub> and washed with NaHCO<sub>3(aq)</sub> and water. The organic phase was dried over MgSO<sub>4</sub> and solvent removed under reduced pressure to yield a slightly yellow viscous liquid. The desired product was purified by fractional distillation to yield a clear colorless liquid.

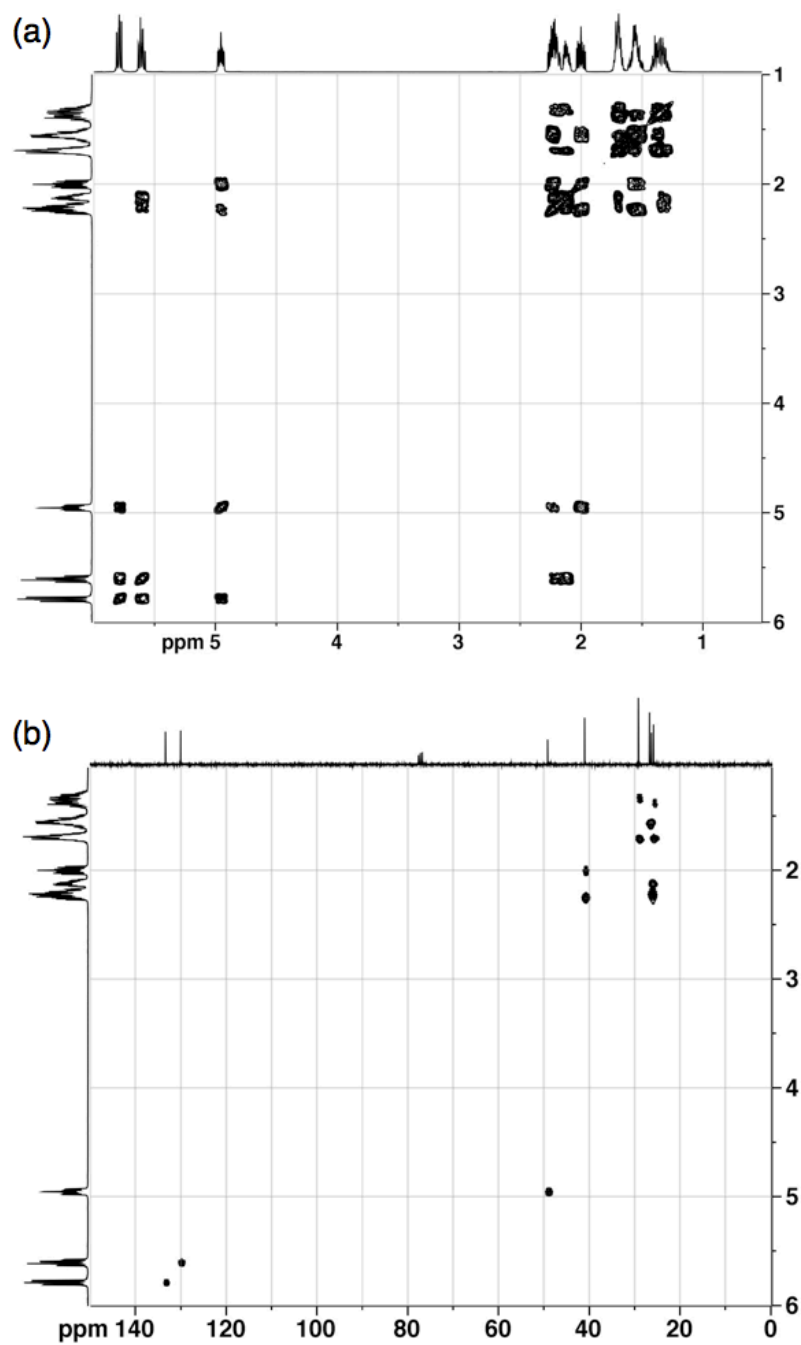


<sup>1</sup>H NMR, CDCl<sub>3</sub>: δ (ppm) = 5.79 [**b**, ddd, 1H, *J* = 10.5, 8.6, 1.6 Hz]; 5.61 [**a**, dddd, 1H, *J* = 10.6, 9.1, 7.7, 1.4 Hz,]; 4.94 [**c**, m, 1H]; 1.30–2.30 [**d–h**, m, 10H].

<sup>13</sup>C NMR, CDCl<sub>3</sub>: δ (ppm) = 133.37 [**b**]; 130.01 [**a**]; 49.17 [**c**]; 41.03 [**d**]; 29.19 [**g**]; 26.72 [**e**]; 26.32 [**h**]; 25.85 [**f**].

**Figure B.1**

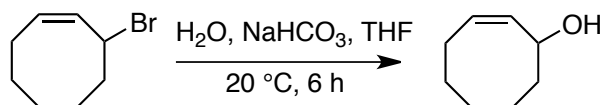
Characterization of *cis*-3-bromo-cyclooct-1-ene monomer precursor by (a)  $^1\text{H}$  NMR spectroscopy and (b)  $^{13}\text{C}$  NMR spectroscopy.

**Figure B.2**

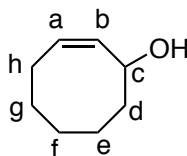
Characterization of *cis*-3-bromo-cyclooct-1-ene monomer precursor by (a)  $^1\text{H}$ - $^1\text{H}$  correlated NMR spectroscopy and (b)  $^1\text{H}$ - $^{13}\text{C}$  NMR spectroscopy.

B.1.2 3-hydroxy-*cis*-cyclooct-1-ene

The monomer 3-hydroxy-*cis*-cyclooct-1-ene (3OH-COE) was prepared by hydrolyzing 3BrCOE. This particular substrate was not amenable to ROMP with the **G2** or **G3** catalyst under the conditions explored. However, this substrate was used as a springboard toward other potential monomers.

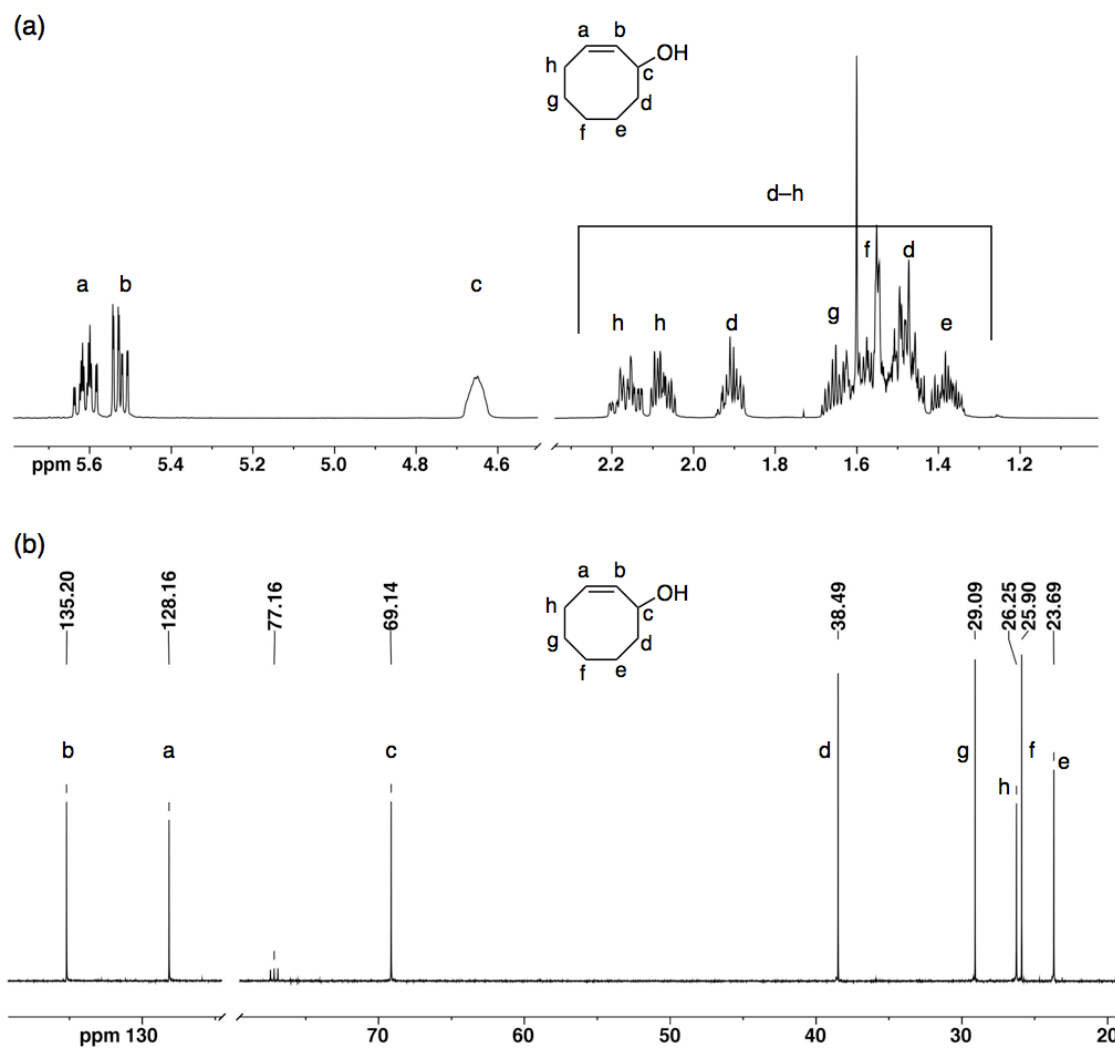


In a 100 mL round-bottom flask was placed 10.0 g 3-bromo-*cis*-cyclooct-1-ene (52.9 mmol) with 50 mL of deionized water buffered with NaHCO<sub>3</sub> and 10 mL THF. The mixture was stirred rapidly for 12 h at 25 °C. The mixture was diluted with 100 mL Et<sub>2</sub>O and extracted with 100 mL of saturated NaHCO<sub>3(aq)</sub>. The organic phase was washed with 100 mL of water and 100 mL of saturated brine. The organic phase was dried over MgSO<sub>4</sub> and solvent was removed under reduced pressure. The product was purified by fractional distillation to yield a clear, colorless liquid.

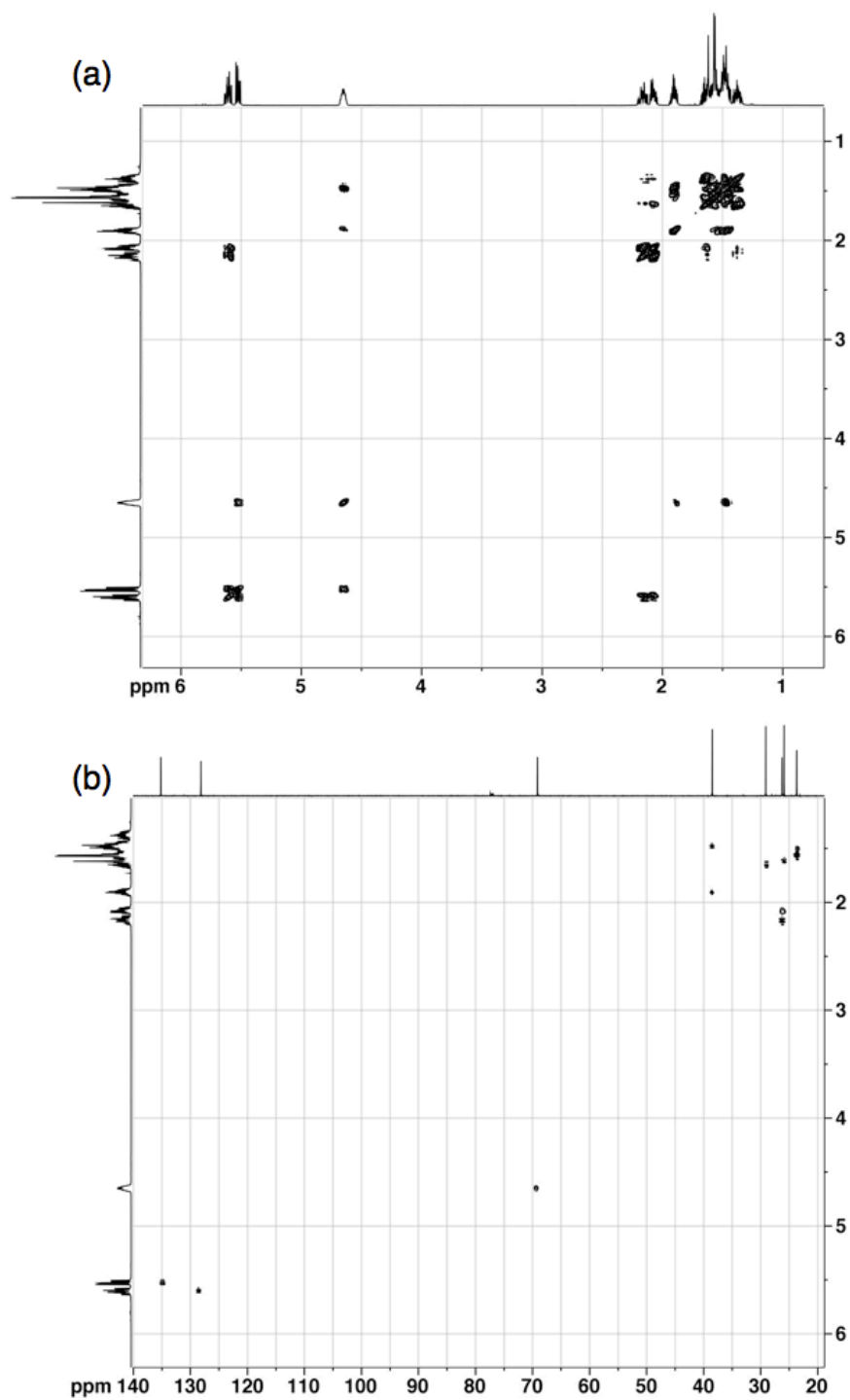


<sup>1</sup>H NMR (CDCl<sub>3</sub>): δ (ppm) = 5.61 [**a**, dddd, 1H, *J* = 10.7, 9.0, 7.3, 1.7 Hz]; 5.52 [**b**, ddd, 1H, *J* = 10.8, 6.7, 1.2 Hz]; 4.66 [**c**, bm, 1H]; 2.05–2.22 [**h**, m, 2H]; 1.91 [**d**, m, 1H]; 1.65 [**g**, m, 2H]; 1.55 [**f**, m, 2H]; 1.50 [**d**, m, 1H]; 1.40 [**e**, m, 2H].

<sup>13</sup>C NMR (CDCl<sub>3</sub>): δ (ppm) = 135.20 [**b**]; 128.17 [**a**]; 69.14 [**c**]; 38.49 [**d**]; 29.10 [**g**]; 26.25 [**h**]; 25.90 [**f**]; 23.69 [**e**].

**Figure B.3**

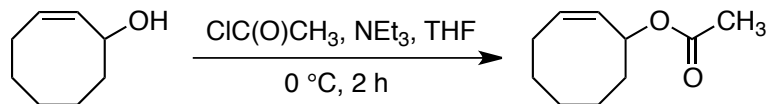
Characterization of *cis*-3-hydroxycyclooct-1-ene (3OHCOE) monomer precursor by (a)  $^1\text{H}$  NMR spectroscopy and (b)  $^{13}\text{C}$  NMR spectroscopy.

**Figure B.4**

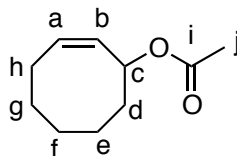
Characterization of *cis*-3-hydroxycyclooct-1-ene monomer precursor by (a)  $^1\text{H}$ - $^1\text{H}$  correlated NMR spectroscopy and (b)  $^1\text{H}$ - $^{13}\text{C}$  NMR spectroscopy.



## B.1.3 3-acetoxycyclooct-1-ene

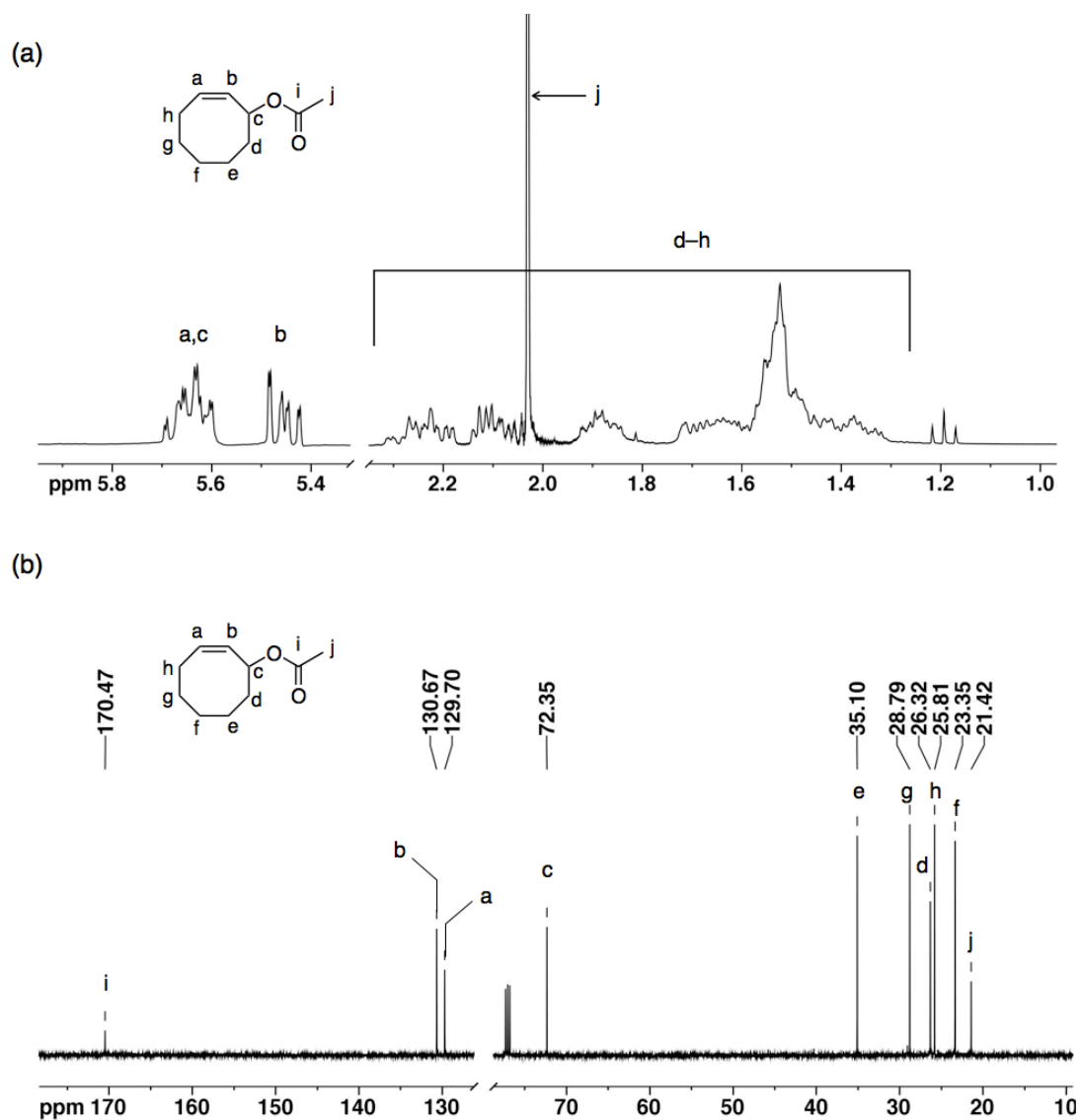


In a 10 mL round-bottom flask was placed 0.5 g of 3OH-COE (3.96 mmol), which was cooled with an ice bath. Acetyl chloride (0.5 g; 6.36 mmol; 1.6 equiv) was dropped slowly directly into the flask, which caused the solution to turn orange. The solution was diluted with 5 mL of THF, which caused the color to disappear. 0.5 mL (0.36 g; 3.56 mmol) of triethylamine was added, which caused a white precipitate to form. The solution was diluted with 5 mL of CH<sub>2</sub>Cl<sub>2</sub> and washed with dilute HCl<sub>aq</sub> and finally water. The organic layer was dried over MgSO<sub>4</sub> and concentrated to afford the product. The monomer was purified by distillation.

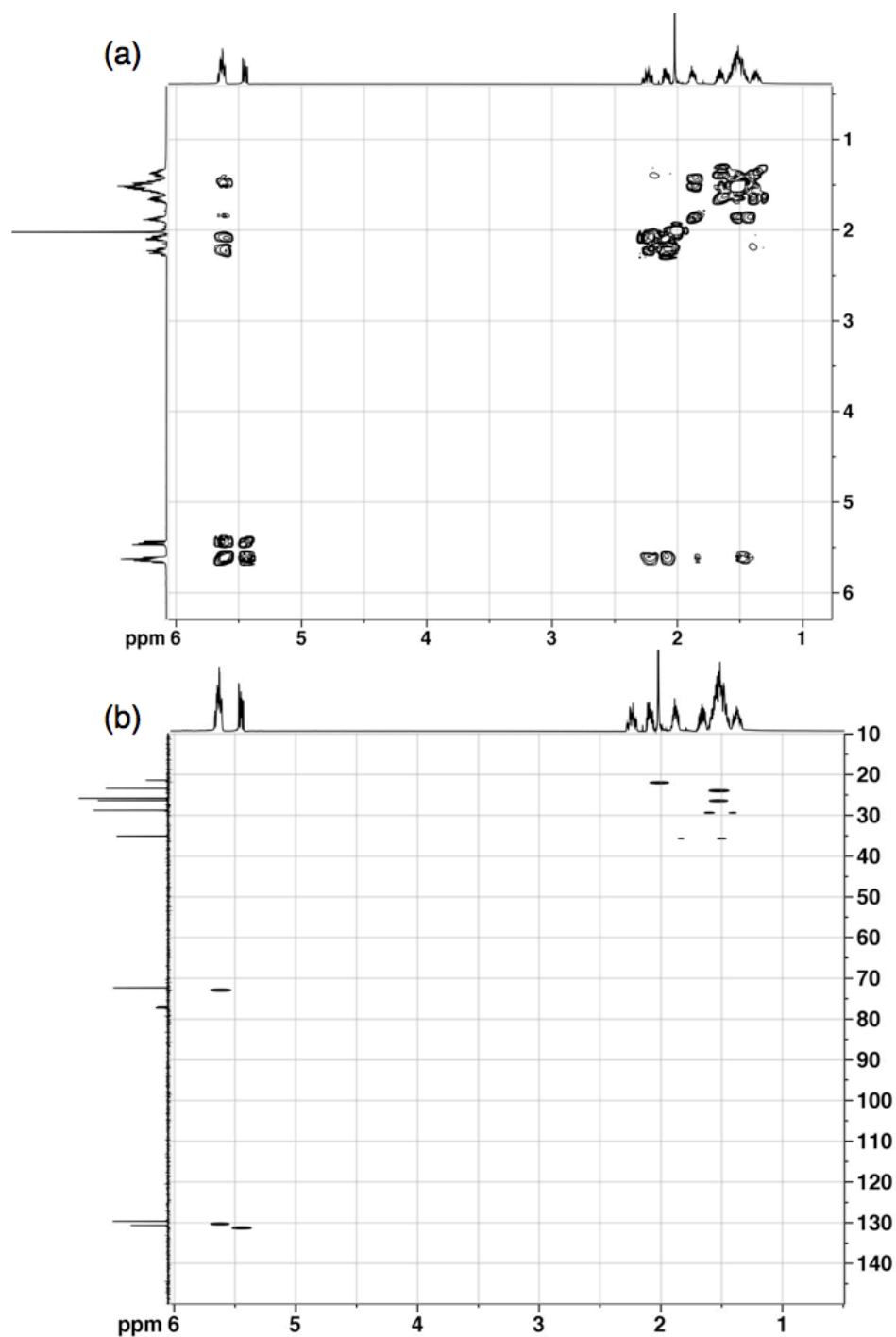


<sup>1</sup>H NMR (CDCl<sub>3</sub>): δ (ppm) = 5.64 [**a**, m, 1H], 5.62 [**c**, m, 1H]; 5.45 [**b** ddd, 1H, *J* = 10.8, 7.1, 1.3 Hz]; 2.02 [**j**, s, 3H]; 1.3–2.3 [**d–h**, m, 10H].

<sup>13</sup>C NMR (CDCl<sub>3</sub>): δ (ppm) = 170.5 [**i**]; 130.7 [**b**]; 129.7 [**a**]; 72.3 [**c**]; 35.1 [**e**]; 28.8 [**g**]; 26.3 [**d**]; 25.8 [**h**]; 23.3 [**f**]; 21.42 [**j**].

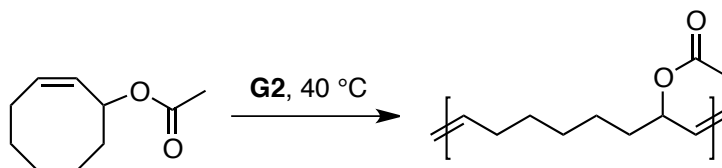
**Figure B.5**

Characterization of *cis*-3-acetoxycyclooct-1-ene (3OAcCOE) monomer by (a)  $^1\text{H}$  NMR spectroscopy and (b)  $^{13}\text{C}$  NMR spectroscopy.

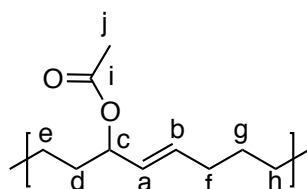
**Figure B.6**

Characterization of *cis*-3-acetoxycyclooct-1-ene (3OAcCOE) monomer by (a)  $^1\text{H}$ - $^1\text{H}$  correlated NMR spectroscopy and (b)  $^1\text{H}$ - $^{13}\text{C}$  NMR spectroscopy.

## Polymerization of 3-acetoxycyclooct-1-ene

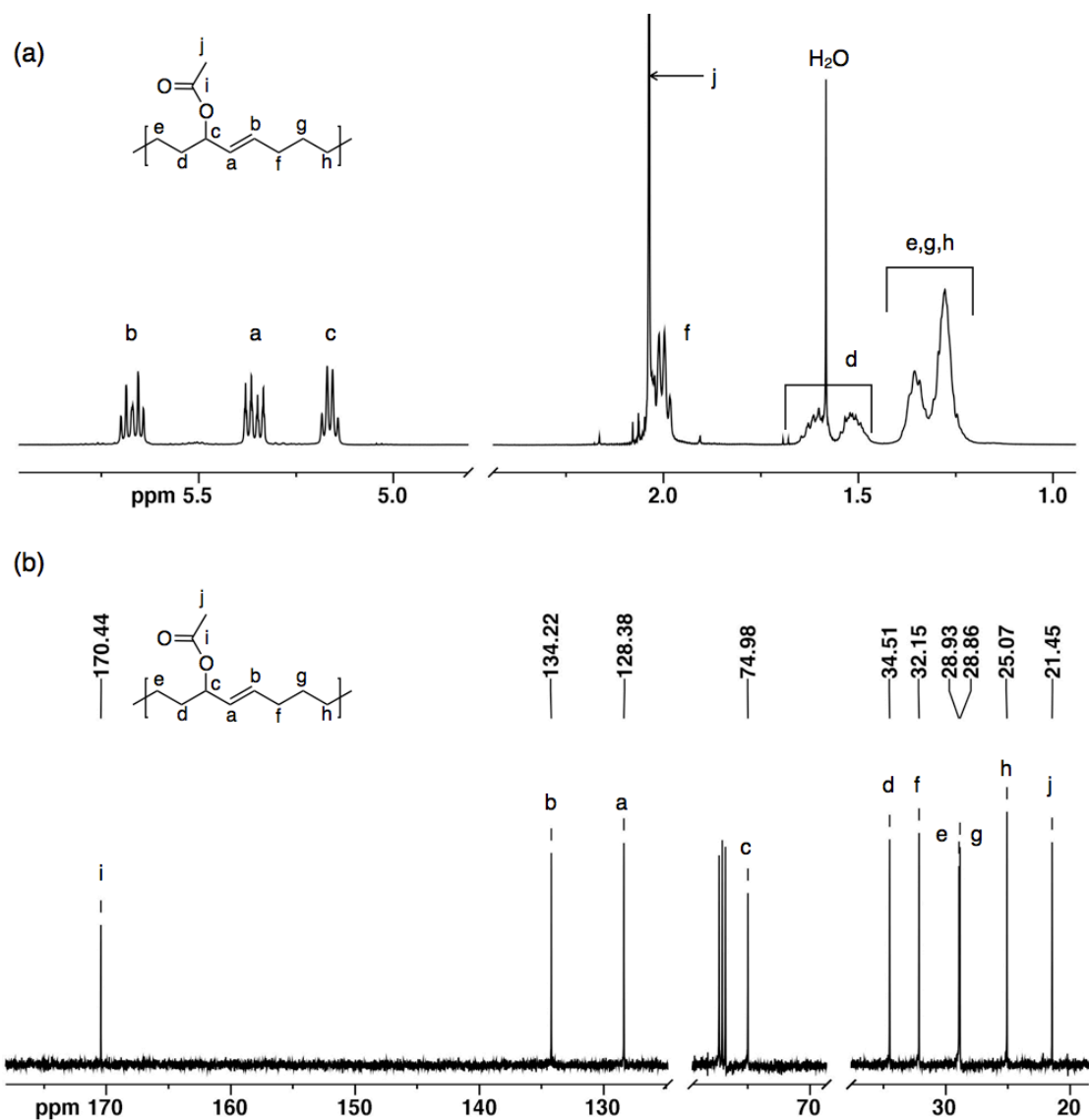


The monomer 3OAcCOE (0.50 g; 2.97 mmol) was dissolved in THF at 40 °C before adding **G2** (1.5 mg;  $1.7 \times 10^{-6}$ ) as a solution in THF. The color of the solution almost immediately turned from faintly pink to orange, suggesting initiation. The polymerization was performed for 15 h before precipitating into cold MeOH.



$^1\text{H}$  NMR ( $\text{CDCl}_3$ ):  $\delta$  (ppm) = 5.67 [**b**, ddd, 1H,  $J$  = 15.4, 6.9, 6.5 Hz]; 5.36 [**a**, ddt, 1H,  $J$  = 15.4, 7.4, 1.4 Hz]; 5.16 [**c**, dt, 1H,  $J$  = 7.3, 6.3 Hz]; 2.04 [**j**, s, 3H]; 2.01 [**f**, dt, 2H]; 1.60, 1.52 [**d**, m, 2H]; 1.36 [**g**, m, 2H]; 1.28 [**e**, **h**, m, 4H].

$^{13}\text{C}$  NMR ( $\text{CDCl}_3$ ):  $\delta$  (ppm) = 170.44 [**i**]; 134.22 [**b**]; 128.38 [**a**]; 74.98 [**c**]; 34.51 [**d**]; 32.15 [**f**]; 28.93 [**e**]; 28.86 [**g**]; 25.07 [**h**]; 21.45 [**j**].

**Figure B.7**

Characterization of poly(3OAcCOE) by (a) <sup>1</sup>H NMR spectroscopy and (b) <sup>13</sup>C NMR spectroscopy.

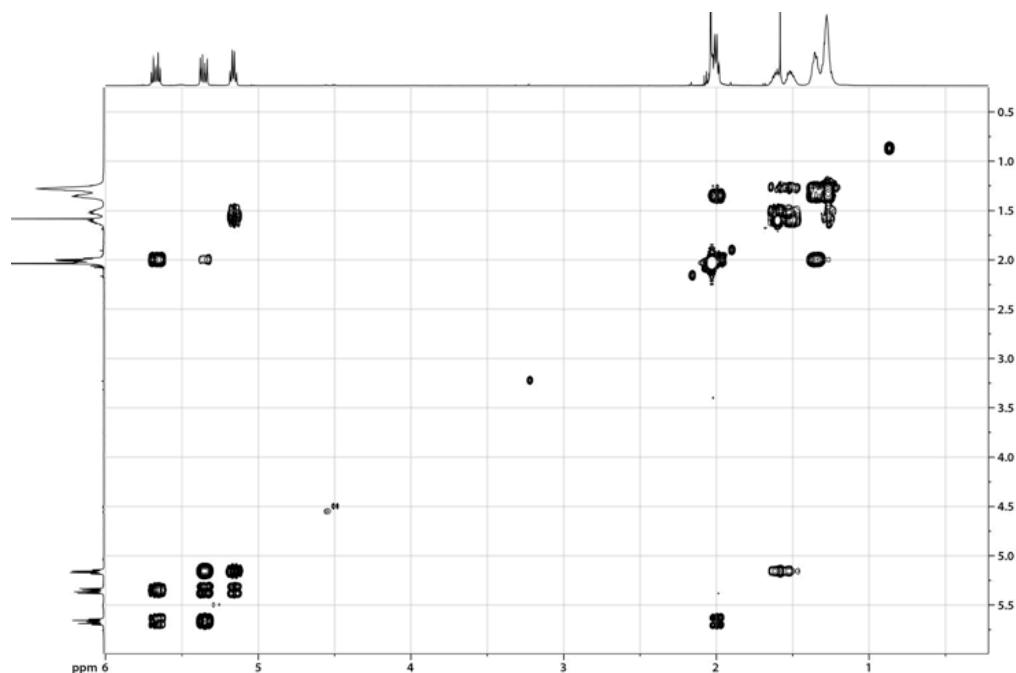
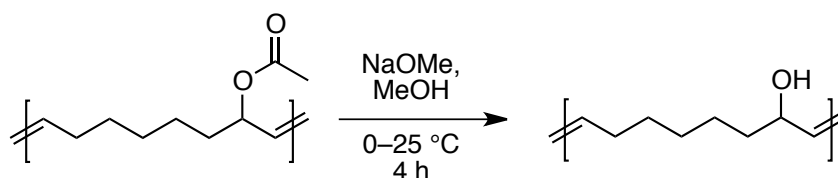


**Figure B.8**

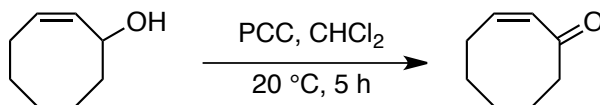
Characterization of poly(3OAcCOE) by  $^1\text{H}$ - $^1\text{H}$  correlated NMR spectroscopy.

#### hydrolysis of poly(3OAcCOE)

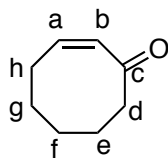


0.40 g of the poly(3OAcCOE) was dissolved in 10 mL of dry THF. A solution of 0.257 g of NaOMe (4.76 mmol; 2 equiv) in 0.5 mL MeOH was slowly added to the polymer solution dropwise. Solid white precipitate appears as the reaction proceeds; hydroxy PCOE is apparently insoluble in THF under these conditions. After stirring for 4 h, the polymer solution was diluted with  $\text{Et}_2\text{O}$  and washed with water. The ether was removed under vacuum to yield the hydroxy polymer. The polymer is insoluble in  $\text{CH}_2\text{Cl}_2$ , THF, and  $\text{Et}_2\text{O}$  at ambient temperature, but readily soluble in MeOH.

## B.1.4 3-oxocyclooct-1-ene

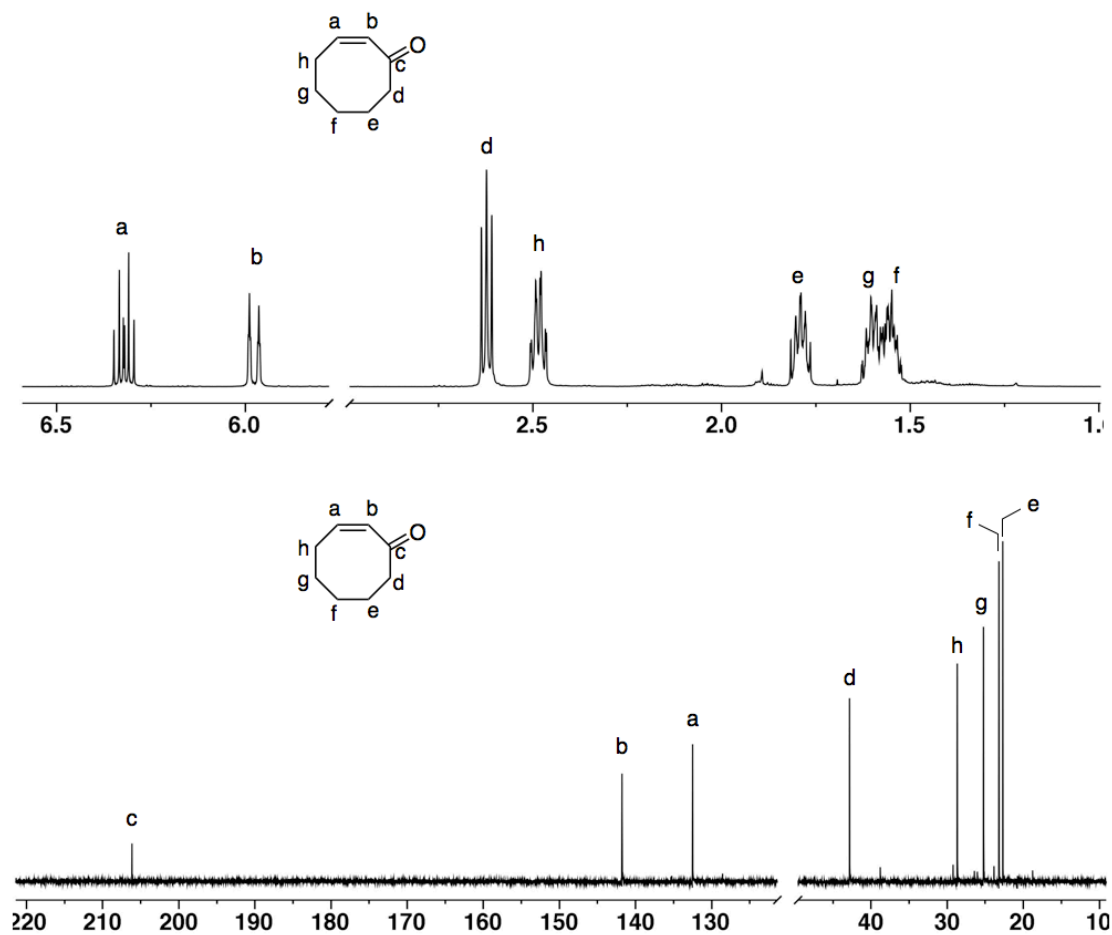


To a mixture of 5.2 g of pyridinium chlorochromate (24.1 mmol) in 40 mL of dry CH<sub>2</sub>Cl<sub>2</sub> was added 2.0 g of cyclooct-2-enol (15.8 mmol) in 30 mL of CH<sub>2</sub>Cl<sub>2</sub> under an argon atmosphere. The solid material dissolved within 30 s and the solution turned dark brown. The solution was stirred at 25 °C for an additional 4 h before diluting with 50 mL of Et<sub>2</sub>O. The solid chromium salts were filtered and the Et<sub>2</sub>O was removed in *vacuo* to yield a yellow oil. The oil was passed over a silica column (80/20 hexanes/ethyl acetate) to give a clear colorless liquid.



<sup>1</sup>H NMR (CDCl<sub>3</sub>): δ (ppm) = 6.32 [**a**, dt, 1H, *J* = 12.46, 7.08 Hz,]; 5.97 [**b**, t, 1H, *J* = 12.46 Hz,]; 2.62 [**d**, t, 2H, *J* = 6.86 Hz,]; 2.49 [**h**, m, 2H]; 1.80 [**e**, m, 2H]; 1.62 [**g**, m, 2H]; 1.55 [**f**, m, 2H].

<sup>13</sup>C NMR (CDCl<sub>3</sub>): δ (ppm) = 206.2 [**c**]; 141.8 [**b**]; 132.5 [**a**]; 42.8 [**d**]; 28.7 [**h**]; 25.2 [**g**]; 23.2 [**f**]; 22.7 [**e**].

**Figure B.10**

Characterization of *cis*-3-oxo-cyclooct-1-ene monomer precursor by (a)  $^1\text{H}$  NMR spectroscopy and (b)  $^{13}\text{C}$  NMR spectroscopy.



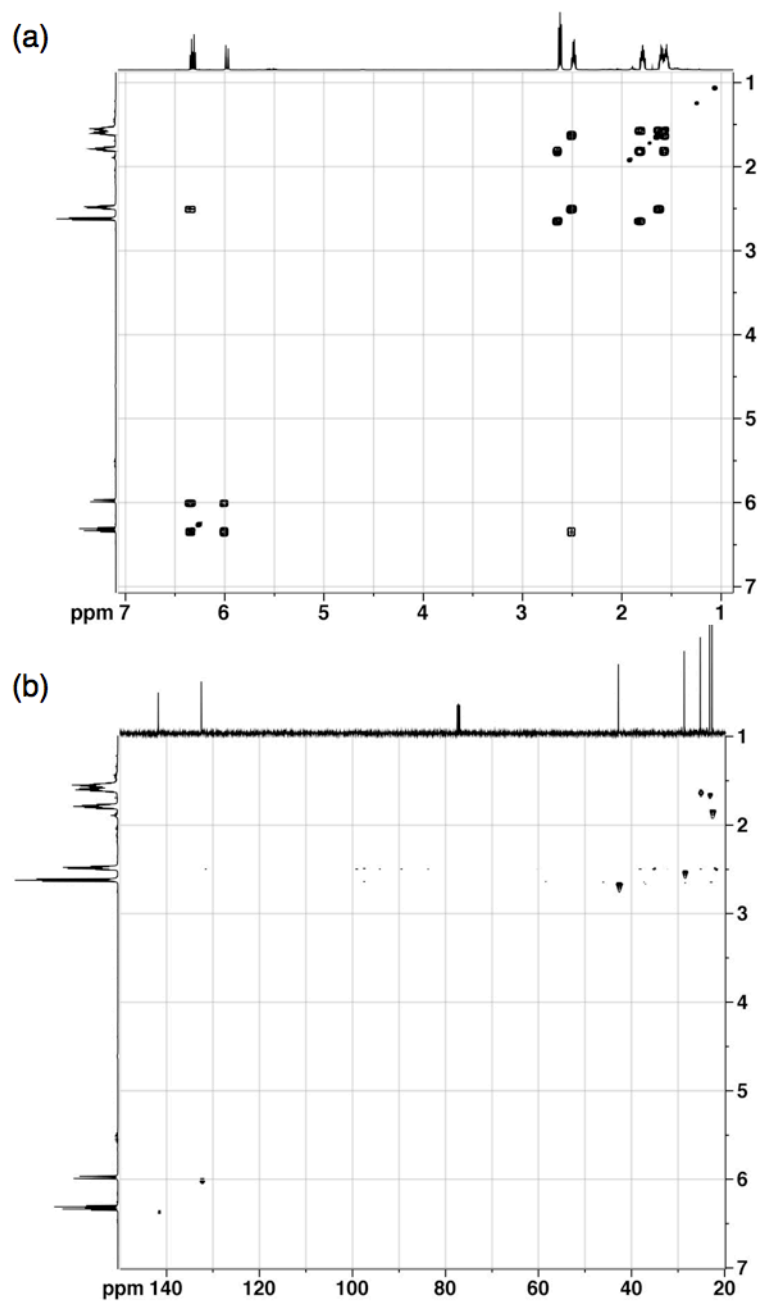
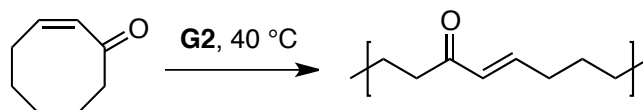


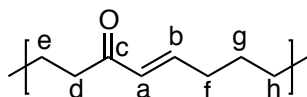
**Figure B.11**

Characterization of *cis*-3-oxocyclooct-1-ene (3oxoCOE) monomer by (a)  $^1\text{H}$ - $^1\text{H}$  correlated NMR spectroscopy and (b)  $^1\text{H}$ - $^{13}\text{C}$  NMR spectroscopy.

## Polymerization of cyclooct-2-enone

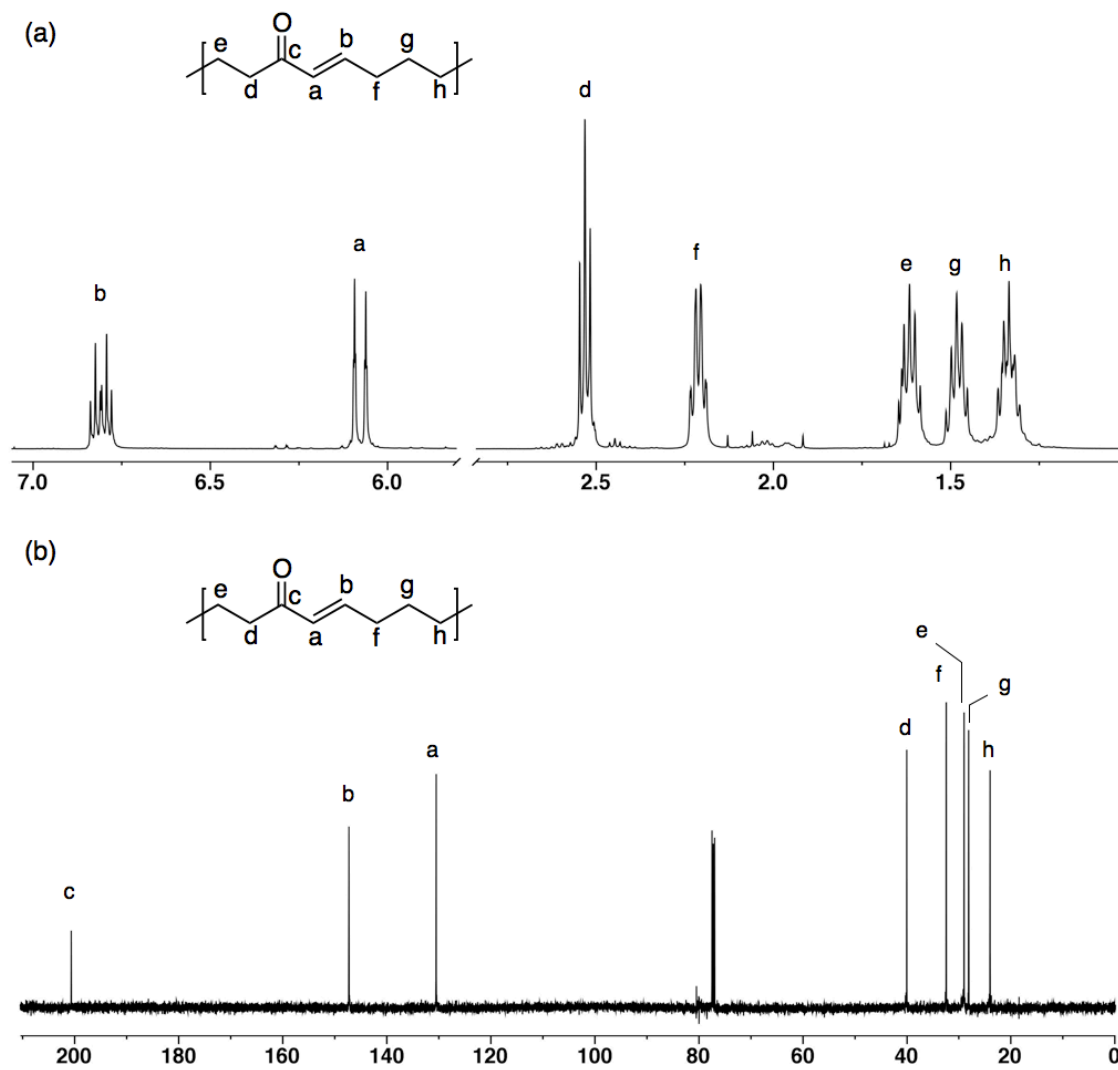


A solution of 200 mg of monomer (1.6 mmol) in 1.5 mL of dry  $\text{CH}_2\text{Cl}_2$  was stirred under an argon atmosphere while 2  $\mu\text{L}$  of *cis*-1,4-diacetoxy-2-butene ( $\sim 12 \mu\text{mol}$ ;  $[\text{M}]/[\text{CTA}] = 138$ ) was added via syringe. Finally, 0.5 mg of grubbs 2<sup>nd</sup> generation catalyst ( $\sim 0.59 \mu\text{mol}$ ;  $[\text{M}]/[\text{G2}] = 2700$ ). The polymerization mixture was stirred at RT for 10 h and precipitated into 10 mL of slightly acidic MeOH at 25 °C. The solvent was decanted and polymer dried under vacuum at RT for 6 h.



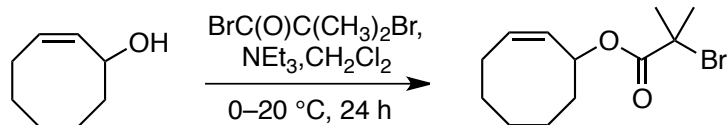
$^1\text{H}$  NMR ( $\text{CDCl}_3$ ):  $\delta$  (ppm) = 6.81 [**b**, dt, 1H,  $J = 15.83, 6.92$  Hz,]; 6.08 [**a**, dt, 1H,  $J = 15.84, 1.40$  Hz,]; 2.53 [**d**, t, 2H,  $J = 7.37$  Hz,]; 2.21 [**f**, m, 2H]; 1.62 [**e**, m, 2H]; 1.48 [**g**, m, 2H]; 1.34 [**h**, m, 2H].

$^{13}\text{C}$  NMR ( $\text{CDCl}_3$ ):  $\delta$  (ppm) = 200.7 [**c**]; 147.3 [**b**]; 130.5 [**a**]; 40.0 [**d**]; 32.4 [**h**]; 29.0 [**g**]; 28.1 [**f**]; 24.0 [**e**].

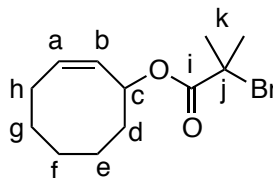
**Figure B.12**

Characterization of poly(3oxoCOE) by (a)  $^1\text{H}$  NMR spectroscopy and (b)  $^{13}\text{C}$  NMR spectroscopy.

## B.1.5 3-(2-bromo-2-methyl propionate)cyclooct-1-ene

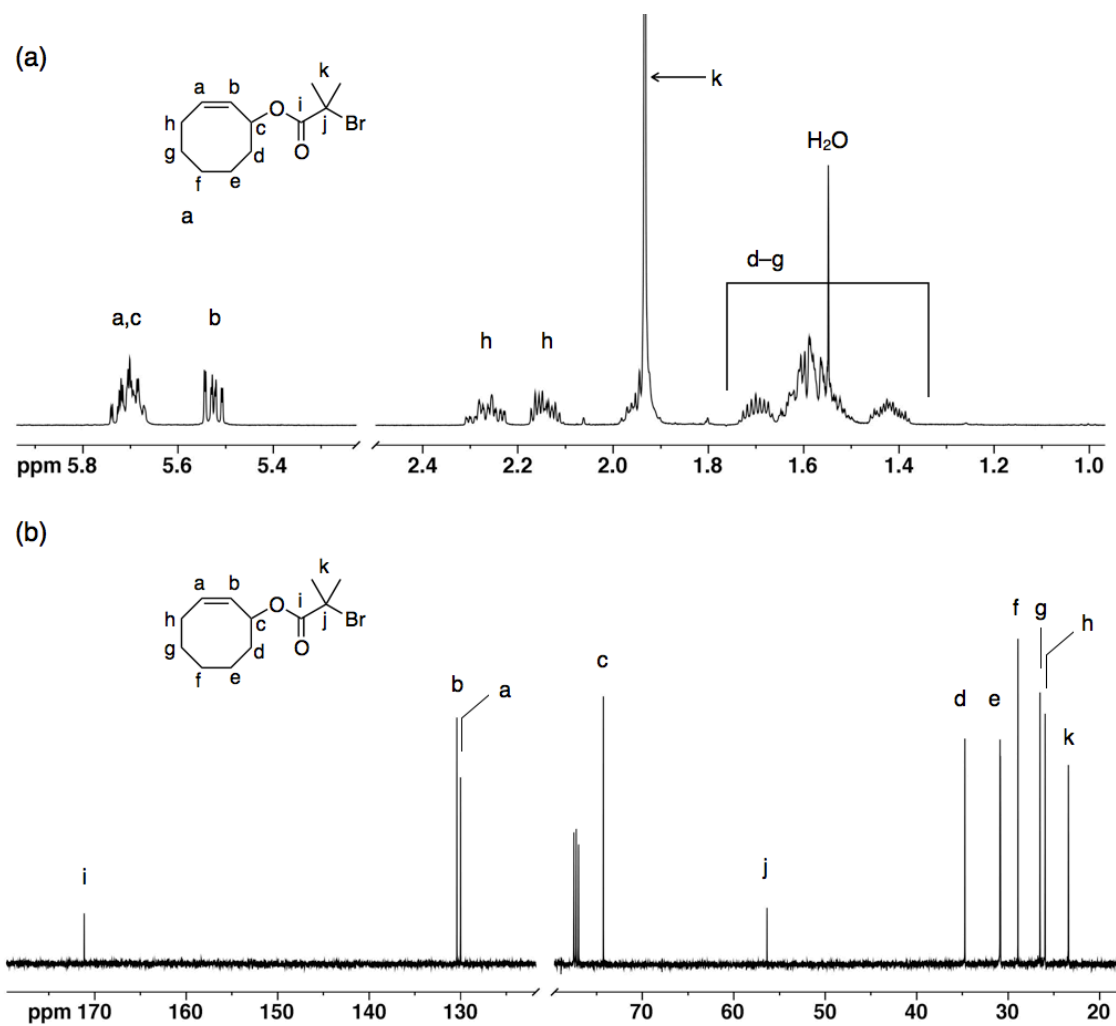


The monomer 3-(2-bromo-2-methyl propionate)-cyclooct-1-ene was synthesized by stirring 1.0 g of 3-hydroxycyclooct-1-ene (7.9 mmol) and 2.2 mL of  $\text{NEt}_3$  ( $\approx 1.6$  g; 15.8 mmol) in 20 mL of  $\text{CH}_2\text{Cl}_2$  before adding dropwise a solution of 2-bromo-2-methylpropionyl bromide in 20 mL of  $\text{CH}_2\text{Cl}_2$  at  $0\text{ }^\circ\text{C}$ . The bromide solution was added over a 1 h period, and the reaction mixture was stirred, allowing to warm slowly to ambient temperature over 18 h. The resulting yellow solution was diluted with  $\text{CH}_2\text{Cl}_2$  and washed consecutively with saturated solutions of  $\text{NaHCO}_3(\text{aq})$ , and  $\text{NaCl}$ . The solution was dried over  $\text{MgSO}_4$  and filtered, followed by purification using column chromatography (80/20 hexanes/ethyl acetate).

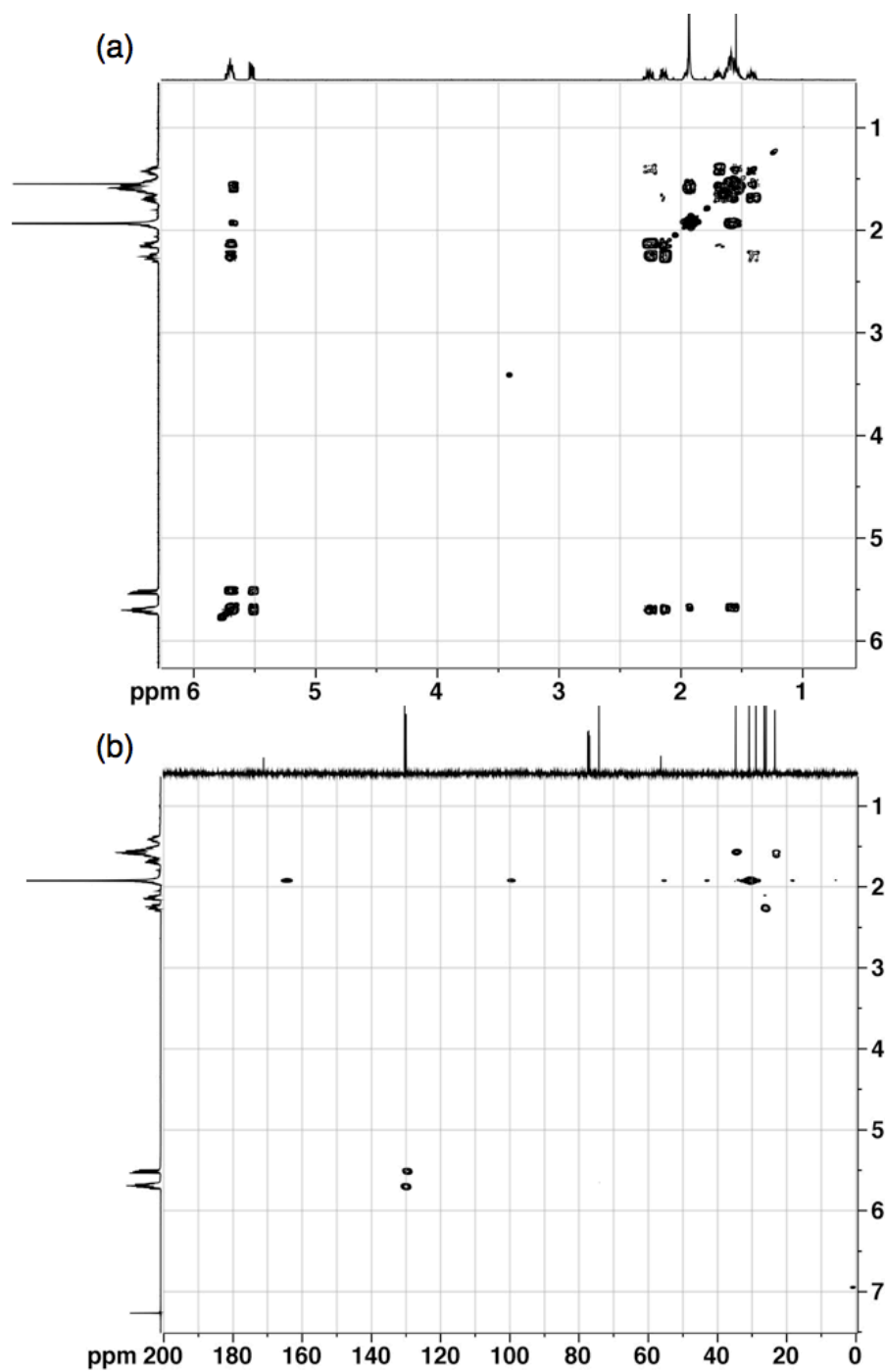


$^1\text{H NMR}$  ( $\text{CDCl}_3$ ):  $\delta$  (ppm) = 5.70 [**a**, m, 1H]; 5.67 [**c**, m, 1H]; 5.55 [**b**, m, 1H]; 2.25 [**h**, m, 1H]; 2.15 [**h**, m, 1H]; 1.90 [**d**, m, 2H]; 1.90 [**k**, s, 6H]; 1.65 [**f**, m, 2H]; 1.62 [**e**, m, 2H]; 1.55 [**g**, m, 2H]; 1.40 [**f**, m, 2H].

$^{13}\text{C NMR}$  ( $\text{CDCl}_3$ ):  $\delta$  (ppm) = 171.2 [**i**]; 130.4 [**b**]; 130.0 [**a**]; 74.3 [**c**]; 56.4 [**j**]; 34.7 [**d**]; 30.9 [**e**]; 28.9 [**f**]; 26.5 [**g**]; 26.0 [**h**]; 23.4 [**k**].

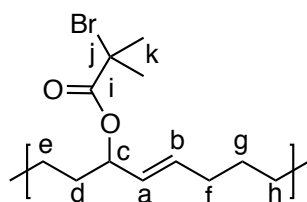
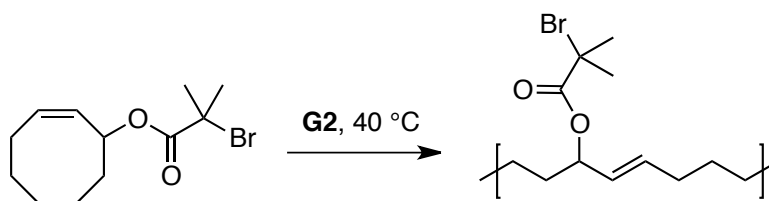
**Figure B.13**

Characterization of *cis*-3-(2-bromo-2-methylpropionyl)cyclooct-1-ene (3BrPrCOE) monomer by (a)  $^1\text{H}$  NMR spectroscopy and (b)  $^{13}\text{C}$  NMR spectroscopy.

**Figure B.14**

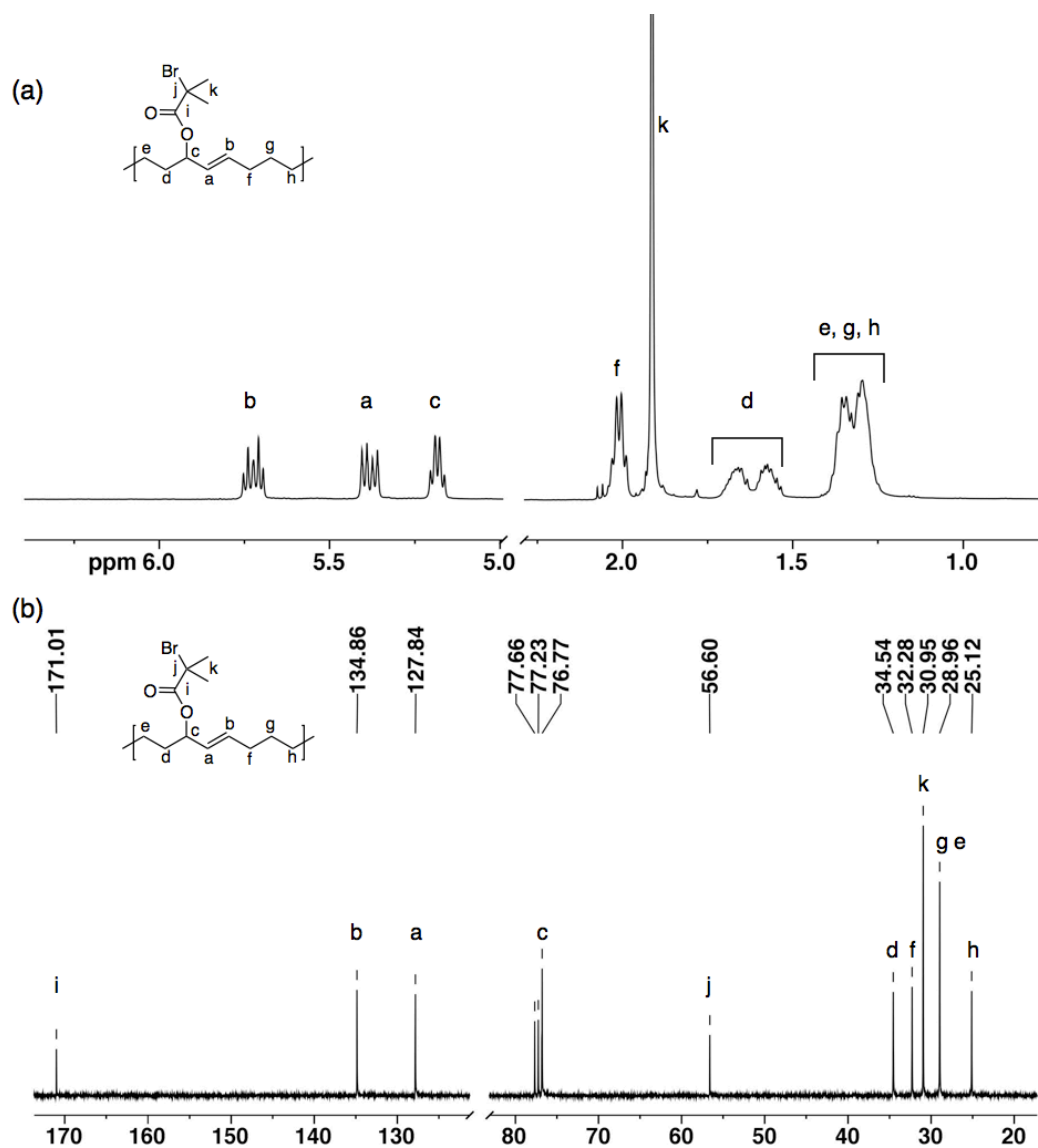
Characterization of *cis*-3-(2-bromo-2-methylpropionyl)cyclooct-1-ene (3BrPrCOE) monomer by (a)  $^1\text{H}$ - $^1\text{H}$  correlated NMR spectroscopy and (b)  $^1\text{H}$ - $^{13}\text{C}$  NMR spectroscopy.

## Polymerization of 3-(2-bromo-2-methylpropionate)-cyclooct-1-ene



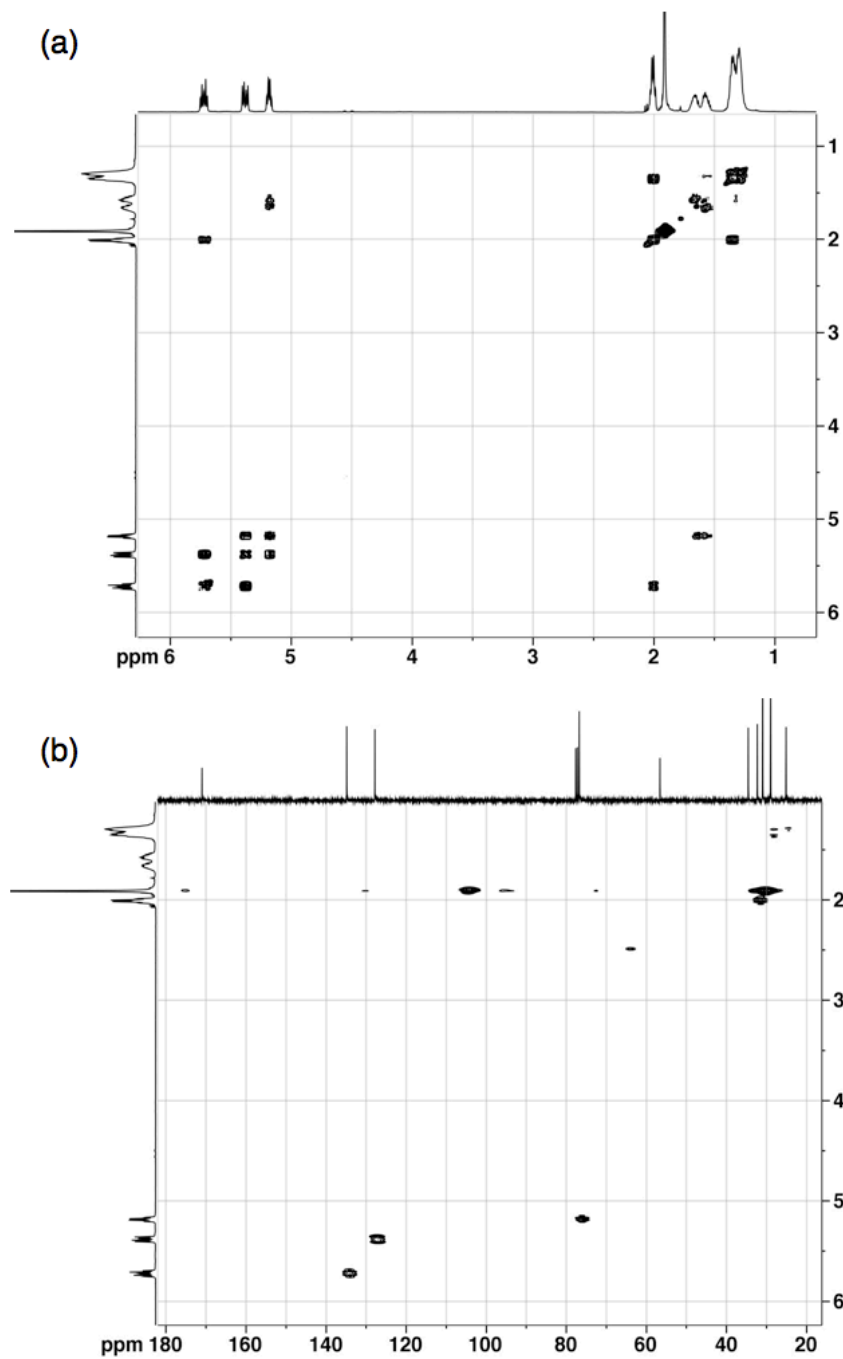
$^1\text{H}$  NMR ( $\text{CDCl}_3$ ):  $\delta$  (ppm) = 5.72 [**b**, dt, 1H,  $J$  = 14.8, 7.2 Hz]; 5.38 [**a**, dd, 1H, 15.4, 7.3 Hz]; 5.19 [**c**, q, 1H, 6.69 Hz]; 2.01 [**f**, m, 2H]; 1.91 [**k**, s, 6H]; 1.66, 1.57 [**d**, m, 2H]; 1.30–1.35 [**e**, **g**, **h**, m, 6H].

$^{13}\text{C}$  NMR ( $\text{CDCl}_3$ ):  $\delta$  (ppm) = 171.0 [**i**]; 134.9 [**b**]; 127.8 [**a**]; 76.8 [**c**]; 56.6 [**j**]; 34.5 [**d**]; 32.3 [**f**]; 30.9 [**k**]; 28.9 [**e,g**]; 25.1 [**h**].

**Figure B.15**

Characterization of poly(*cis*-3-(2-bromo-2-methylpropionyl)cyclooct-1-ene) (poly3BrPrCOE) monomer by (a)  $^1\text{H}$  NMR spectroscopy and (b)  $^{13}\text{C}$  NMR spectroscopy.



**Figure B.16**

Characterization of poly(*cis*-3-(2-bromo-2-methylpropionyl)cyclooct-1-ene) (poly3BrPrCOE) monomer by (a)  $^1\text{H}$ - $^1\text{H}$  correlated NMR spectroscopy and (b)  $^1\text{H}$ - $^{13}\text{C}$  NMR spectroscopy.